# Targeting The REF1/STAT3 Axis To Treat Tuberous Sclerosis

A thesis submitted in candidature for the degree of Doctor of Philosophy (PhD)

2023

**Jesse Champion**

Division of Cancer and Genetics

Cardiff University


Supervisors

Prof. Andrew Tee

Prof. Ann Ager

Prof. David Davies

# Abstract

Mammalian target of rapamycin complex 1 (mTORC1) inhibitors have provided clear clinical benefit to tuberous sclerosis complex (TSC) patients. However, not all patients respond to mTORC1 inhibitors. Alternatives to mTORC1 inhibitors remains a significant unmet clinical need for the management of TSC.

Elevated expression and activity of the transcription factors Hypoxia inducible factor 1 (HIF-1α) and Signal transducer and activator of transcription 3 (STAT3) has been observed in TSC. The redox signalling protein Reduction-oxidation factor 1 (Ref-1) acts upstream of both STAT3 and HIF-1α to induce their transcriptional activity. This thesis seeks to investigate the efficacy of drug inhibition of the Ref-1/HIF-1α/STAT3 within TSC model cells and expand current knowledge of HIF-1α and STAT3 signalling within TSC.

Research within this thesis identified drug blockade of Ref-1/HIF-1α/STAT3 activity reduced scores of tumorigenicity within *TSC2* deficient cells. Additionally, inhibitors of Ref-1 and STAT3 were found to be effective at decreasing HIF-1α activity and pro-angiogenic factor expression within *TSC2* deficient cells. The present work also developed the list of known STAT3 and HIF-1α targets dysregulated in cells upon the loss of *TSC2,* with analysis of their potential clinical relevance through comparison to data from TSC associated lesions. Mechanisms which lead to dysregulated STAT3 signalling were also elucidated within this work. Markers of oxidative stress were found to be elevated within TSC model cells, and the redox environment of TSC cells was shown to modulate markers of both HIF-1α and STAT3 activity. Finally, this thesis identifies the drug C188-9 as a potential therapeutic agent for the treatment of TSC. As C188-9 effectively repressed markers of STAT3 and mTORC1 activity within *TSC2* deficient cell lines.

Overall, this thesis provides a more developed understanding of mTORC1 and Ref-1/HIF-1α/STAT3 signalling within the context of TSC, which hopefully will lead better therapeutic interventions for TSC patients.

**Word Count: 78,893**

# Acknowledgements

Undertaking a PhD has been both challenging and rewarding in equal measure. I feel fortunate to have been able to undertake my PhD within the Tee lab and within the kind and supporting research environment within the School of Medicine at Cardiff University. During the course of this project, I have received invaluable support from multiple people.

Firstly, I would like to thank my supervisors Prof. Andrew Tee, Prof. Ann Ager and Prof. David Davies for the opportunity to undertake this research and for their support and guidance throughout the course of my PhD. I would especially like to thank Prof. Andrew Tee for his support and for the many helpful and interesting discussions we've had. His mentorship, encouragement and friendship have been invaluable and well beyond what I believe was required of him as a supervisor.

I would also like to thank the Tuberous Sclerosis Association for funding this research, being so understanding of the difficulties arising from the COVID-19 pandemic and the great work they do to raise awareness and support of TSC research.

I am very grateful for the help, guidance, and friendship of my colleagues within the Tee lab and Cancer Genetics Building. It has been a pleasure working and researching with them. They have helped me keep my sanity during the difficult and low points of my studies. I would especially like to thank Dr Elaine Dunlop. Despite not being one my official supervisors, she has always been willing to listen to my questions and take the time to provide guidance during the course of my research.

I would like to acknowledge and thank Prof. Mark Kelley for providing the Ref-1 inhibitors for my research and giving instruction in their use and Prof. Jeffrey MacKeigan for giving me access to sequencing data from TSC lesions, which was both fascinating and tremendously helpful to my research.

I would like to thank Dr Tracey Martin and Prof. Alan Parker for acting as my thesis review panel throughout my PhD, as well as Prof. Aled Clayton and Dr. Benjamin Housden, who both kindly agreed to act as my internal and external examiners.

On a personal note, I owe tremendous thanks to my partner Talfan, whose patience, love and encouragement has meant a great deal to me and without I would have been unable to complete my thesis. Finally, I would also like to acknowledge the unconditional love and support I have received from my family, not just during the course of my PhD but throughout my entire education

# Publications

The publication arising from the research contained in this thesis was:

Champion, J.D., Dodd, K.M., Lam, H.C., Alzahrani, M.A., Seifan, S., Rad, E., Scourfield, D.O., Fishel, M.L., Calver, B.L., Ager, A. and Henske, E.P. (2022). Drug inhibition of redox factor-1 restores hypoxia-driven changes in tuberous sclerosis complex 2 deficient cells. *Cancers*, **14**: 6195.

As of the date of submission of this thesis, data generated from this thesis will also contribute to two more publications which are currently in the stages of being drafted.

# Abbreviations

**Table 1.** Abbreviations Used Within This Thesis

| Abbr. | Full Name | Abbr. | Full Name |
|---|---|---|---|
| 3’ | 3 prime end | cDNA | Complementary DNA |
| 4E-BP1 | Eukaryotic translation initiation factor 4E-binding protein 1 | ChIP Seq. | Chromatin immunoprecipitation Sequencing |
| 5’ | 5 prime end | CKI | Cyclin-dependent kinase inhibitor |
| ADP | Adenosine Diphosphate | c-MYC | c-MYC proto-oncogene, bHLH transcription factor |
| AIFM2 | Apoptosis-inducing factor 2 | CO2 | Carbon Dioxide |
| AKT | AKT serine/threonine kinase 1 | Cryo-EM | Cryogenic electron microscopy |
| AML | Angiomyolipoma | c-Src | Proto-oncogene tyrosine-protein kinase Src |
| AMP | Adenosine Monophosphate | CTD | C-terminal Domain |
| ANGPTL4 | Angiopoietin Like 4 | DEG | Differential gene expression |
| ANOVA | Analysis of variance | DEPTOR | DEP Domain Containing MTOR Interacting Protein |
| AO/PI | Acridine Orange/Propidium Iodide | DMEM | Dulbecco's Modified Eagle Medium |
| ARE | Antioxidant response element | DMNQ | 2,3-dimethoxy-1,4-naphthalenedione |
| ATF4 | Activating Transcription Factor 4 | DMSO | Dimethyl sulfoxide |
| ATG13 | Autophagy Related 13 | DNA | Deoxyribonucleic acid |
| ATP | Adenosine Triphosphate | Dsh | Dishevelled |
| BER | Base excision repair | eEF2 | Eukaryotic translation elongation factor 2 |
| bFGF | Basic Fibroblast Growth Factor | eEF2K | Eukaryotic elongation factor 2 kinase |
| bHLH | Basic helix–loop–helix | EGF | Epidermal growth factor |
| BNIP3 | Bcl-2 interacting protein 3 | eIF4A | Eukaryotic initiation factor-4A |
| CA9 | Carbonic Anhydrase 9 | eIF4B | Eukaryotic initiation factor-4B |
| CAD | Carbamoyl-phosphate synthetase 2 | eIF4E | Eukaryotic initiation factor-4E |
| CAT | Catalase | eIF4F | Eukaryotic initiation factor-4F |
| CBP | CREB-binding protein | eIF4G | Eukaryotic initiation factor-4G |
| CCL5 | C-C motif chemokine ligand 5 | ELISA | Enzyme-linked immunosorbent assay |
| CDK | Cyclin-dependent kinases | ERK | Extracellular signal-regulated kinase |

| | |
|---|---|
| EZH2 | Enhancer of zeste homolog 2 |
| FAD | Flavin adenine dinucleotide |
| FAT | Focal adhesion targeting |
| FBS | Foetal Bovine Serum |
| FBW7 | F-box/WD repeat-containing protein 7 |
| FDR | False discover rate |
| FIH | Factor Inhibiting HIF-1α |
| FKBP12 | FKBP-type peptidyl-prolyl cis-trans isomerase |
| FPKM | Fragments Per Kilobase of transcript per Million mapped reads |
| FSP1 | Ferroptosis Suppressor Protein 1 |
| FTH1 | Ferritin Heavy Chain 1 |
| GAP | GTPase-activating protein |
| GAS | Gamma interferon activation site |
| GCLC | Glutamate-cysteine ligase, catalytic subunit |
| GDP | Guanosine diphosphate |
| GEF | Guanine nucleotide exchange factor |
| GLUT1 | Glucose transporter protein type 1 |
| gp130 | Glycoprotein 130 |
| GPX4 | Glutathione peroxidase 4 |
| GPX8 | Glutathione peroxidase 8 |
| GRB2 | Growth factor receptor-bound protein 2 |
| GSH | Glutathione |
| GSK3 | Glycogen synthase kinase 3 |
| GTP | Guanosine Triphosphate |
| h | hour |
| H2O2 | Hydrogen peroxide |
| HEAT | Huntington, EF3A, ATM, TOR repeat |
| HEK293 | Human embryonic kidney 293 |
| HGF | Hepatocyte growth factor |
| HIF | Hypoxia-inducible factor |
| HIF-1α | Hypoxia-inducible factor 1 alpha |
| HIF-1β | Hypoxia-inducible factor 1 beta |
| HK2 | Human kidney 2 |
| HMBS | Hydroxymethylbilane Synthase |
| HMOX | Heme oxygenase 1 gene |
| HRE | Hypoxia-response elements |
| HSPE1 | Heat Shock Protein Family E Member |
| IL-6 | Interleukin 6 |
| IL-6Rα | Interleukin 6 Receptor alpha |
| IPO8 | Importin 8 |
| IRS1 | Insulin receptor substrate 1 |
| JAK | Janus kinase |
| JNK-1 | c-Jun N-terminal kinase 1 |
| kDa | kilo Daltons |
| Keap1 | kelch like ECH associated protein 1 |
| Km | Michaelis constant |
| KU | Ku-0063794 |
| LAM | Lymphangioleiomyomatosis |
| LKB1 | Liver kinase B1 |
| LOH | Loss of heterozygosity |
| M | Molar |
| MAPK | Mitogen-activated protein kinase |
| MEF | Mouse embryonic fibroblast |
| MEK | Mitogen-activated protein kinase |
| MEKK1 | MEK kinase 1 |
| MGST1 | Microsomal glutathione transferase 1 |

| | |
|---|---|
| min | Minute |
| mLST8 | Mammalian lethal with SEC13 protein 8 |
| MMP | Matrix metalloproteinase |
| MNK | MAPK interacting protein kinases |
| mRNA | Messenger RNA |
| mSIN | Mammalian stress-activated protein kinase interacting protein 1 |
| MTHFD2 | Methylenetetrahydrofolate dehydrogenase |
| mTOR | Mammalian target of rapamycin |
| mTORC1 | Mammalian target of rapamycin complex 1 |
| mTORC2 | Mammalian target of rapamycin complex 2 |
| NAC | N-acetyl cysteine |
| NADP | Nicotinamide adenine dinucleotide phosphate (Oxidised) |
| NADPH | Nicotinamide adenine dinucleotide phosphate (Reduced) |
| NB | Normal Brain |
| NF-κB | Nuclear factor kappa-light-chain-enhancer of activated B cells |
| NK | Normal Kidney |
| Nrf2 | Nuclear factor erythroid 2-related factor 2 |
| NTD | N-terminal domain |
| O2 | Oxygen |
| ODDD | Oxygen Dependent Degradation Domain |
| p300 | Histone acetyltransferase p300 |
| p62 | Sequestosome 1 |
| Padj | Adjusted p value |
| PAS | Per-Arnt-Sim domain |
| PBS | Phosphate-buffered saline |
| PCAF | P300/CBP-associated factor |
| PCR | Polymerase chain reaction |
| PDCD4 | Programmed cell death protein 4 |
| PDK | Pyruvate dehydrogenase kinase |
| PECAM-1 | Platelet endothelial cell adhesion molecule-1 |
| Pen-Strep | Penicillin-Streptomycin |
| PGC1α | Peroxisome proliferator-activated receptor gamma coactivator 1-alpha |
| PHD | HIF prolyl hydroxylase |
| PI3K | Phosphoinositide 3-kinases |
| PIAS3 | Protein inhibitor of activated STAT 3 |
| PIKK | Phosphatidylinositol 3-kinase-related kinases |
| PIP2 | Phosphatidylinositol 4,5-bisphosphate |
| PIP3 | Phosphatidylinositol (3,4,5)-trisphosphate |
| PML | Promyelocytic leukemia protein |
| PP2A | Protein phosphatase 2 A |
| PRAS40 | Proline-rich AKT substrate of 40 kDa |
| PROTOR | Protein observed with Rictor |
| PTM | Post-translational modification |
| PTP | Protein tyrosine phosphatase |
| PTP1B | Protein Tyrosine Phosphatase 1B |
| pVHL | Von Hippel–Lindau tumor suppressor |

| | |
|---|---|
| qPCR | Quantitative polymerase chain reaction |
| Raf | Rapidly accelerated fibrosarcoma |
| RAP | Rapamycin |
| RAPTOR | Regulatory-associated protein of mTOR |
| Ras | Rat sarcoma virus protein |
| REDD1 | Regulated in development and DNA damage responses 1 |
| Ref-1 | Reduction-oxidation factor 1 |
| RELA | RELA Proto-Oncogene, |
| Rheb | Ras homolog enriched in brain |
| RhoA | Ras homolog family member A |
| RICTOR | Rapamycin-insensitive companion of mammalian target of rapamycin |
| RNA | Ribonucleic acid |
| RNA seq. | Ribonucleic acid sequencing |
| ROCK | Rho-associated protein kinase |
| ROS | Reactive oxygen species |
| RPKM | Reads per kilobase of exon per million reads mapped |
| rpm | rotations per minute |
| rpS6 | Ribosomal Protein S6 |
| rRNA | Ribosomal Ribonucleic acid |
| RSK | 90 kDa ribosomal S6 kinase |
| RSL3 | RAS-selective lethal 3 |
| RTK | Receptor tyrosine kinase |
| s | second |
| S6K1 | Ribosomal protein S6 kinase beta-1 |
| SEGA | Subependymal giant cell astrocytoma |
| SEN | Subependymal nodules |
| SET9 | Histone lysine methyltransferase Set9 |
| SH2 | Src Homology 2 domain |
| SHP | Src homology region 2 domain-containing phosphatase |
| SIRT1 | Sirtuin 1 |
| SLC7A11 | Solute Carrier Family 7 Member 11 |
| SOCS3 | Suppressor of cytokine signaling 3 |
| SOD3 | Super Oxide Dismutase |
| SOS | Son of Sevenless |
| Src | Proto-oncogene c-Src kinase |
| SREBP | Sterol regulatory element binding protein |
| STAT3 | Signal transducer and activator of transcription 3 |
| TAND | TSC-Associated Neuropsychiatric Disorders |
| TCA | Tricarboxylic acid cycle |
| TD | Transactivation domain |
| TELO2 | Telomere Maintenance 2 |
| TFEB | Transcription Factor EB |
| TNFRSF1A | TNF receptor superfamily member 1A |
| TOP | 5'terminal oligopyrimidine tract |
| TOS | TOR signalling motif |
| TRX1 | Thioredoxin 1 |

| | | | |
|---|---|---|---|
| TRXR1 | Thioredoxin reductase 1 | ULK1 | Unc-51 like autophagy activating kinase 1 |
| TSC | Tuberous Sclerosis Complex | U-STAT3 | Unphosphorylated-STAT3 |
| TSC1 | Tuberous Sclerosis Complex 1 (Hamartin) | UTR | Untranslated region |
| TSC2 | Tuberous Sclerosis Complex 2 (Tuberin) | v/v | volume/voulme |
| TTI1 | TELO2 Interacting Protein 1 | VEGFA | Vascular endothelial growth factor A |
| TUB | Cortical Tuber | w/v | weight/volume |
| TYK2 | Non-receptor tyrosine-protein kinase 2 | ULK1 | Unc-51 like autophagy activating kinase 1 |

# Contents

# List of Figures

# List of Tables

# Chapter 1: General Introduction

## 1.1 – Tuberous Sclerosis Complex and its human-impact

Tuberous Sclerosis Complex (TSC) is a rare autosomal dominant genetic disease affecting approximately 1 in 6,000 live births (O'Callaghan *et al.* 1998). First described over 160 years ago (Von Recklinghausen, 1862), it wasn't until relatively recently that the genetic cause of TSC was identified. That is the mapping of TSC to two genetic loci, *TSC1* which encodes hamartin (van Slegtenhorst *et al.*, 1997) and *TSC2* which encodes tuberin (European Chromosome 16 Tuberous Sclerosis Consortium, 1993). Loss of function of either *TSC1* or *TSC2* result in a person's diagnosis with TSC. And despite being a rare heritable disease, TSC is not only of relevance to families with a history of the disease as *de novo* germline mutations in either *TSC1* or *TSC2* constitute over 70% of all TSC diagnoses (Peron *et al.* 2018a).

At the cellular level the functional consequence of the loss of function of either the *TSC1* or *TSC2* genes, is the loss of the regulatory complex the protein products of these genes (hamartin and tuberin respectively) form. The TSC complex regulates mammalian target of rapamycin complex 1 (mTORC1), a protein complex itself that functions as a master regulator of cell growth and proliferation (Kwiatkowski, 2003). The functional consequence of a TSC diagnosis on an individual patient health outcomes can vary, but TSC carries a multitude of clinical manifestations that are a significant cause of morbidity and mortality (Zöllner *et al.* 2020). For example, one of the hallmarks of TSC is the growth of numerous benign lesions in multiple organs (Northrup *et al*. 2013). Including in the brains of patients, such as sub-ependymal giant astrocytomas (SEGAs) and cortical tubers, the kidneys of patients, in the form of angiomyolipomas (AMLs) and on the skin of patients. Whilst these lesions are benign, they still can, and often do, result in adverse health outcomes for patients. Including aneurysm of renal AML blood vessels, destruction of tissue patterning and in the case of brain lesions obstructive hydrocephalus. And while the formation of benign growths on the skin of patients don't typically lead to severe medical complications (Ebrahimi-Fakhari *et al.* 2017). They are a very frequent manifestation of TSC common to patients and associated with high psychological stress resulting from the disfiguring appearance these lesions can have. Lesions are not the source of adverse outcomes. Lymphangioleiomyomatosis (LAM) is a pulmonary manifestation of the disease that results in cystic destruction of the lungs that can lead to respiratory failure. Being the leading cause of mortality for adult female TSC patients (Zak *et al.* 2019). Furthermore, early onset epilepsy, which is the second highest source of morbidity and mortality for TSC patients (Zöllner *et al*. 2020), is also incredibly prevalent in the TSC patient population. As is a host of neuropsychiatric disorders, such as autism spectrum

disorder and intellectual disability (Kingswood *et al*. 2017). Altogether, the clinical manifestations of TSC can not only present patients with a substantial burden of illness, but also a substantial of care on the families and carers of TSC patients. Meaning the development of effective treatments for TSC, will not only benefit patients but their families as well.

The primary drug based therapy approved for TSC are the 1st generation mTORC1 inhibitors (Zheng and Jiang, 2015). Based around the structure of rapamycin, these so termed 'rapalogues' have provided clear clinical benefit to patients. With the most recent iteration approved for therapy found to shrink TSC associated lesions (Franz *et al.* 2013 and Bissler *et al.* 2017) and provide a modest reduction in epileptic seizure frequency (Bissler *et al.* 2017). These mTORC1 inhibitors however are not effective at targeting the clinical manifestations of TSC for a significant proportion of TSC patients. Additionally, these drugs help manage the symptoms of TSC, they are not curative, thus patients who take mTORC1 inhibitors must remain on them for the rest of their lives. Very recently, cannabidiol (brand name Epidyolex) was approved for use by the National Health Service (NHS) England for the treatment of seizures in TSC (National Institute for Health and Care Excellence, 2023), after showing efficacy in reducing treatment resistant epileptic seizure frequency (Thiele *et al.* 2021 and Thiele *et al.* 2022). Mechanistically, how cannabidiol exerts therapeutic effects is yet to be fully elucidated. But highlights that drugs other than direct mTORC1 inhibitors can provide clinical benefit for TSC patients. However, as with mTORC1 inhibitors, cannabidiol treatment was not completely effective in reducing seizure frequencies for all patients within the clinical trial cohorts. Therefore, to expand treatment options TSC patients, more research is needed into the molecular aetiology of TSC. Especially the cell signalling pathways perturbed on the loss of either *TSC1* or *TSC2* that are independent of/not wholly reliant on mTORC1 hyperactivity. Such research could also have a positive impact outside of TSC.

Multiple cancers show activation of the PI3K/Akt/mTORC1 pathway (Polivka and Janku, 2014), with *TSC1* and *TSC2* being tumour-suppressor genes frequently mutated in many cancers, including lung (Lee *et al.* 2019), kidney (Kwiatkowski *et al*. 2016), breast (Kurian *et al.* 2019) and liver (Ho *et al.* 2017). Yet while mTORC1 inhibitors have shown great pre-clinical indications for cancer treatment, these inhibitor often have shown marginal benefit in clinical trials (Naing *et al.* 2012, Carlo *et al.* 2016, Powles *et al.* 2016 and Graham *et al.* 2018). Research into the aberrant cell signalling pathways dysregulated on the loss of either *TSC1* or *TSC2*, and whether they are reliant, independent of or interlinked with hyperactive mTORC1 signalling could provide new druggable targets for cancers with mutations in the PI3K/Akt/mTORC1 pathway. Additionally, TSC and the TSC model cells used with this work

represent a “purer” model to elucidate the cellular consequences of loss of *TSC2*, as genomic instability is a hall mark of many carcinomas (Hanahan and Weinberg, 2011), whilst TSC associated lesions have been found to show relatively low somatic mutational burden (Martin *et al.* 2017).

The work contained within this thesis is a continuation of the research into the molecular aetiology of TSC. Aiming to further expand our knowledge of both mTORC1 signalling and other signalling pathways perturbed by the loss of *TSC2*, in order to contribute towards the development of better therapies for TSC patients.

### 1.1.1 Incidence of TSC

Considered to be a rare disorder, the incidence of TSC is estimated to be approximately 1 in 6,000 live births (O'Callaghan *et al.* 1998), with equal frequency among sexes and ethnicities. Epidemiological studies are limited, but those reviewed report the prevalence of TSC in the population as varying between 1.58 to 8.80 in 100,000 people (Hong *et al.* 2016, Shepherd *et al.* 1991a, Morrison *et al.* 1998 and O'Callaghan *et al.* 1998). The variation reported in incidence is in part due to high phenotypic variability of this disease. Clinical presentation of symptoms can not only vary in onset throughout the life of a patient, but also between patients (Northrup *et al.* 2013); with some patients having a debilitating form of the condition, whilst others appear asymptomatic. The high heterogeneity in presentation and onset of symptoms increases the complexity of not only the TSC patient population, but also in making a diagnosis. Coupled with that current conventional genetic testing yields a positive result (i.e., a clearly pathogenic mutation), for between 75-90% of TSC affected individuals, the actual incidence of TSC could be underestimated. Clinicians’ inexperience with the condition likely exasperates underreporting of TSC in the general population.

## 1.2 Genetics of TSC

Before describing in detail, the many and varied clinical of manifestations of TSC that impact patients’ lives, it is first worth describing the root cause of this disease. TSC is a genetic disease resulting from inactivating mutations to either *TSC1* located on chromosome 9q34 (van Slegtenhorst *et al*. 1997) or *TSC2* on chromosome 16p13 (European Chromosome 16 Tuberous Sclerosis Consortium, 1993). The protein products of these genes function in the same complex, thus losing the function of either will lead to TSC. Despite being heritable, *de novo* germline mutations constitute ~ 70% of all TSC diagnoses (Peron *et al.* 2018a). For familial cases, TSC is typically inherited in an autosomal dominant fashion irrespective of

which gene is affected. However, pathogenic mutations are not evenly distributed between the two loci and are reported with far greater frequency in *TSC2* than in *TSC1*; at a ratio of around 3:1. For those patients who have no mutation identified (NMI) by conventional genetic testing, Tyburczy *et al*. (2015) demonstrated these likely represent cases of mosaicism and intronic pathogenic variants. Mutations were identified in 85% of their NMI patient cohort by using in depth next generation sequencing with full gene coverage of *TSC1 & TSC2.* Martin *et al*. (2017) identified *TSC1*/*TSC2* mutations for 97% of patients by sequencing genomic DNA that was extracted from TSC-associated lesions. Regardless of which gene is affected, the penetrance of this disease is remarkably high, approaching 95% (Peron *et al.* 2018a). The potential severity of the disease is influenced by whether a patient has inactivating mutations within either *TSC1* or *TSC2*, which represents one of the only major genotype-phenotype correlations known for the disease. Pathogenic mutations in *TSC2* typically present with more severe symptoms than those patients with *TSC1* pathogenic mutations or those identified as NMI (Sancak *et al.* 2005, Au *et al.* 2007 and Camposano *et al.* 2009). Associations upheld by more recent studies with smaller cohorts (Avgeris *et al.* 2017, Rosset *et al.* 2017b, Peron *et al.* 2018b and Ding *et al.* 2020). Family members with the same inherited mutation often have variability in the symptoms they present (Peron *et al.* 2018a), A good example of this variability was described in two case studies of monozygotic twins (Martin *et al.* 2003 and Rok *et al.* 2005) who presented marked variability in symptoms despite sharing identical *TSC2* mutations. What all this information means in context, is that regardless of whether TSC patients have a mutation in *TSC1* or *TSC2*, and they will likely present with at least some manifestation of the disease. But on an individual level, the causative genetic mutation for a patient is a poor predictor of disease severity and clinical outcomes.

## 1.3. Clinical manifestations of TSC

Before discussing what is currently known about the cause of TSC, it is worth describing in detail how TSC can adversely impact patients, to contextualise why more research is necessary to develop better treatments for the disease.

### 1.3.1 TSC associated lesions.

The hallmark of TSC is the formation of hamartomas in multiple organs (Northrup *et al*. 2013). These hamartomas are benign malformations, formed due to an overgrowth of aberrant cells. As listed in table 1, there are many TSC associated hamartomas, occurring at different frequencies within patients. Tumour formation in TSC largely conforms to the Knudson's two hit model (Peron *et al.* 2018a), where loss of heterozygosity (LOH) is required via a second somatic hit to the remaining functional allele of either *TSC1* or *TSC2*. In depth sequencing of

TSC-associated lesions by Martin *et al.* (2017) confirmed this is often the case for renal angiomyolipomas (AMLs), subependymal nodules (SENs) and subependymal giant astrocytomas (SEGAs), but not cortical tubers. The authors showed a low somatic mutational burden in TSC associated lesions when compared to lesions from other human carcinomas. These findings are consistent with work by Giannikou *et al.* (2016), finding biallelic loss of *TSC1* or *TSC2* as the primary driver of AML development.

Dermatological lesions are also commonly reported in TSC (Northrup *et al.* 2013 and Kingswood *et al.* 2017). These lesions don't often result in severe medical complications (Ebrahimi-Fakhari *et al.* 2017), but can be disfiguring and result in psychological stress for patients. Renal and brain lesions present more severe adverse outcomes for patients. Renal AMLs are highly vascularised lesions with thick and elastin-poor blood vessel walls that are prone to aneurysm (Yamakado *et al*. 2002). Consequent rupture of these abnormal vessels can lead to haemorrhaging within patients, which can be severe enough to cause death. Long-term, formation of AMLs disrupts the normal renal parenchyma, decreasing kidney function (Eijkemans *et al.* 2015). The size and number of AMLs is positively correlated with age in TSC. If left without medical intervention then kidney failure becomes more likely, potentially progressing to end-stage renal disease (Sarraf *et al.* 2009). Renal complications represent one of the most common causes of mortality in patients (Shepherd *et al*. 1991b, Amin *et al*. 2017 and Zöllner *et al.* 2020), despite improvements in surveillance and treatment. Brain lesions are another significant source of mortality for TSC patients. As outlined in table 1, there are three main types of brain lesions within TSC. Cortical tubers are focal malformations of abnormal cells (Curatolo *et al.* 2015) believed to contribute to epileptogenic foci (small regions of the brain where seizures originate), but this is disputed however. SEGAs represent a more direct cause of mortality than tubers (Zöllner *et al.* 2020). Thought to potentially originate from SENs (Curatolo *et al.* 2015), SEGA's location and tendency to grow can lead to obstruction of cerebral-spinal fluid, increasing intra-cranial pressure and leading to hydrocephalus.

**Table 1.1 Major TSC associated lesions by organ, as outlined in the updated clinical diagnostic criteria for TSC 2012.** Reported lesion frequencies are from: [1] data collated in the TSC diagnostic criteria update (Northrup *et al.* 2013) and [2] from baseline data held 'TOSCA' a large registry of patient data (Kingswood *et al.* 2017).

| **Cardiovascular** | | |
|---|---|---|
| Lesion | Description | Frequency |
| Cardiac rhabdomyomas | Seldom seen in non-TSC affected individuals, these are benign tumour of the heart typically located on the ventricles. Usually regress by adulthood and associated with cardiac arrhythmias. | 34.3% [2] |
| **Dermatological** | | |
| Lesion | Description | Frequency |
| Hypomelanotic macules | Small lesions (~5-mm or larger) lacking pigment which are typically present from birth or infancy. Numerous in TSC patients. | 66.8% [2], 90% [1] |
| Angiofibromas | Small (1-3mm) fibrous papules of vascular and connective tissue. They onset from early infancy and often grow and become more numerous in adolescence. | 57.3%[2], 75.0% [1] |
| Peri-ungual and ungual fibromas | Also termed Koenen tumours, these smooth and nodular like lesions occur around or under the nails. Onset is typically latest of TSC associated dermatological lesions. | 16.7%[2], 20.0% [1] |
| Shagreen patch | These lesions generally present as large collagen rich plaques that have an uneven surface. They usually appear within first decade of life. | 27.4% [2], 50% [1] |
| Confetti skin lesions | Similar to hypomelanotic macules, these lesions are also hypo-pigmented but smaller (1-3mm) and more numerous. | 8.6%[2], 58% [1] |
| **Ophthalmologic** | | |
| Lesion | Description | Frequency |
| Multiple retinal hamartomas | Benign retinal tumours composed of abnormal glial cells with a similar histological profile to tuber within the brain of some TSC patients. Typically do not result in visual problems. | 14.0% [2], 30-50% [1] |
| **Renal** | | |
| Lesion | Description | Frequency |
| Angiomyolipoma (AML) | These tumours are composed of abnormal vascular, smooth muscle and adipose tissue. These lesions often occur bilaterally in the kidney, but can also appear in other organs; namely the lungs. Growth of these lesions can seriously disrupt kidney function and increase a patients risk of haemorrhage due increased aneurysms within AMLs. | 47.2% [2], 80% [1] |
| **Neurological** | | |
| Lesion | Description | Frequency |
| Subependymal nodules (SENs) | SENs are benign growths in the brain of patients that typically arise along the wall of the lateral and third cerebral ventricles. Often asymptomatic but may grow and become calcified. | 78.2% [2], 80% [1] |
| Subependymal giant cell astrocytoma (SEGA) | SEGAs are slow growing tumours composed of multiple cell lineages that are thought to arise from SENs, especially near the foramen of Monro. These lesions location and tendency to grow can lead to blockage of cerebral fluid, causing obstructive hydrocephalus. | 24.4% [2], 5-15% [1] |
| Cortical tuber | A type of focal cortical dysplasia were small areas of the cerebral cortex do not develop properly during pregnancy. These malformations disrupt proper cortical lamination. | 82.2% [2], 90%[1] |

### 1.3.2 Pulmonary lymphangioleiomyomatosis

The major pulmonary manifestation of TSC is pulmonary lymphangioleiomyomatosis (LAM). LAM is characterised by the interstitial proliferation of abnormal smooth muscle cells which eventually invade all lung structures (von Ranke *et al.* 2015), and the hallmark of this condition is formation of diffuse and thin-walled cysts bilaterally. LAM is a progressive condition, such that lung function declines eventually leading to respiratory failure. Within TSC, LAM almost exclusively affects woman of childbearing age (Kingswood *et al.* 2017). LAM contributes substantially to mortality associated with TSC. Zak *et al.* (2019) found that LAM was the leading cause of death in adult women TSC patients.

### 1.3.3 Epilepsy and neuropsychiatric disorders

Epilepsy is a major source of morbidity and mortality for TSC patients; second only to renal complications (Zöllner *et al.* 2020). Onset of epilepsy occurs early in most TSC patients and seizures can be of multiple types (Curatolo *et al.* 2015), often developing into refractory epilepsy where seizures cannot be controlled through anticonvulsants. The origin of epilepsy within TSC is disputed and still an active area of research. Cyst-like cortical tubers and other cortical malformations (e.g., white matter migration lines) are thought to provide a 'structural' cause of epilepsy (Chu-Shore *et al.* 2009). However, this notion has been challenged. *Tsc1* knockout mice (Zeng *et al.* 2008) that are tuber-free still develop spontaneous and progressive epilepsy; suggesting dysregulated mTORC1 signalling alone may be sufficient to drive epilepsy. Increasingly in models of epilepsy, neuroinflammation is seen to have a causative role in epileptogenesis (Barker-Haliski *et al.* 2017) and may in turn play a role in TSC patient epilepsy. As outlined in table 2, TSC is also associated with a wide range of neuropsychiatric disorders, collectively known as TANDs, which represent a significant burden of illness for TSC patients.

**Table 1.2. Non-lesion neurological TSC associated disorders.** Reported frequencies are from baseline data held in 'TOSCA' a large registry of patient data (Kingswood *et al*. 2017). Note in TOSCA documentation of TANDs was reported as poor, thus frequencies are for the subset of patients in which TAND checklist was used.

| Neurological | | |
|---|---|---|
| Symptom | Description | Frequency |
| Epilepsy | Epilepsy is extremely common in TSC patients and is typically early onset. TSC patients can present with multiple seizure types (e.g. tonic, atonic, tonic-clonic) and seizure frequency can be very high. | 83.5% |
| **TSC associated neuropsychiatric disorders (TANDs)** | | |
| Symptom | Description | Frequency |
| Autism spectrum disorder (ASD) | ASD is strongly associated with TSC patients, and is a group of neurodevelopmental disorders characterised in sufferers by problems in social communication and interaction, presenting restrictive or repetitive behaviours. | 20.7% |
| Attention deficit hyperactivity disorder (ADHD) | Also common in TSC patients, ADHD like ASD is a neurodevelopmental disorder characterised generally by inattention and hyperactivity along with disruptive and impulsive behaviour. | 19.6% |
| Anxiety disorder | Typically identified in adolescent to early adult patients, anxiety disorders are a group of mental illnesses generally characterised by the presence of significant and persistent anxiety and fear responses. | 9.1% |
| Depressive disorder | Like anxiety, typically diagnosed in adolescent to early adult patients. This mental disorder is characterised by a very low mood, low self-esteem and lack of interest which pervades all areas of life. | 6.1% |
| Behavioural difficulties | Several behavioural problems have been reported in TSC patients and include severe aggression, sleep difficulties, anxiety, low mood, self-injury and deficits in social behaviour and attention. | 35.6% - reported at least one behavioural problem |
| Intellectual disability | Over half of TSC patients will present with intellectual difficulties, the severity of which can range from mild to profound intellectual difficulties. | 54.9% |
| Academic difficulties | A substantial fraction of school age TSC patients are reported to have academic difficulties and can occur despite normal intellectual ability. | 57.8% |

## 1.4 Current treatments for TSC

### 1.4.1 Rapamycin and its derivative (rapalogues)

Currently, efficacious and approved therapeutic drugs for the management of TSC are lacking and largely based around the compound rapamycin. Rapamycin was first developed and approved for use as an immunosuppressant to prevent transplant rejection (Zheng and Jiang, 2015). Work with this drug led to the discovery of its target, the serine/threonine protein kinase mTOR (mammalian target of rapamycin) (Sabatini *et al.* 1994 and Sabers *et al.* 1995). The identification of which would provide the basis for understanding the regulatory role function

of TSC1 and TSC2 on the mTORC1 complex; of which mTOR is a constituent (Kwiatkowski, 2003). What this meant for patients is that a major molecular pathology of TSC was identified and mTOR inhibition became a potential avenue for therapy.

Rapamycin (or sirolimus) and rapalogues are classed as first generation mTOR inhibitors (Zheng and Jiang, 2015). These drugs contain two binding moieties essential for its mechanism of action, one moiety binds the cytosolic protein FKBP12 which facilitates binding of mTOR at the other moiety. Formation of this ternary complex is thought to inhibit mTOR allosterically, preventing the binding of substrates to mTOR rather than inhibiting the kinase activity directly. Structural analogues of rapamycin (rapalogues) have since been developed to improve pharmacokinetics (Zheng and Jiang, 2015). The 'EXIST' studies, were three multi-centre, randomised, placebo controlled phase 3 trials that assessed the efficacy and safety of Everolimus (a rapalogue) in treating SEGAs, AMLs and as an adjuvant therapy for treatment resistant seizures. In the EXIST-1 trial, 35% of patients receiving everolimus had a reduction in SEGA volume by 50%, compared to none in the placebo group by data cut-off (Franz *et al.* 2013). Everolimus was also effective at reducing tumour volume of AMLs, as shown in the EXIST-2 trial in which 42% of patients receiving Everolimus had a reduction in tumour volume of at least 50%, compared to none in the placebo group by data cut-off (Bissler *et al.* 2017). Finally, the EXIST-3 trial found that in patients with treatment-resistant focal-onset seizures already receiving anti-epileptic drugs, low and high doses of Everolimus resulted in a 50% or greater reduction in seizure frequency for 28% and 40% of patients respectively (French *et al.* 2016). The EXIST studies demonstrate efficacy of Everolimus as a therapy for major causes of mortality within TSC. Furthermore, as everolimus benefits multiple TSC manifestations, treatment for one symptom has been observed to improve outcome for others (Curatolo *et al.* 2016).

What should be noted from the EXIST studies however, is that a substantial fraction of patients do not respond to Everolimus. This incomplete response highlights not only the limitations of mTOR inhibition for the treatment of TSC but also that hyperactive mTORC1 signalling is likely not the sole driver of TSC pathology. mTOR inhibitors also possess significant toxicities and can produce adverse effects which include increased immunosuppression resulting in infection, decreased renal function, inflammation and ulceration of the mouth, skin complaints and hypercholesterolaemia; as were observed in the EXIST studies (Franz *et al.* 2013, Bissler *et al.* 2017 and French *et al.* 2016). Lastly, mTOR inhibitors have a cytostatic effect, not a cytotoxic one, thus if withdrawn for any reason then lesions will regrow rapidly, as observed with sirolimus (Bissler *et al.* 2008). Aforementioned toxicities and adverse events might be further compounded by the extended duration of treatment.

### 1.4.2 Cannabidiol

Treatment resistant epilepsy is a clinical manifestation of TSC frequently reported in patients (Kingswood *et al.* 2017) and remains to date a leading cause of mortality for the disease (Zöllner *et al.* 2020 and Parthasarathy *et al.* 2021). Very recently, the *Cannabis sativa* derivative cannabidiol (brand name Epidyolex) was approved for use by the NHS in the treatment of seizures in TSC (National Institute for Health and Care Excellence, 2023). Over the past decade Cannabidiol has shown promise in treating epilepsy resistant to treatment by conventional anti-convulsants associated with other human disorders (Silvestro *et al.* 2019 and Abu-Sawwa *et al.* 2020). Similarly recent clinical trials have shown the promising therapeutic potential of cannabidiol in managing epilepsy associated with TSC. A placebo controlled clinical trial by Thiele *et al.* (2020) found trial participants receiving either 25 mg/kg or 50 mg/kg of cannabidiol a day saw a reduction in seizure frequency of 48.6% and 47.5% respectively compared to 26.5% in the placebo group. A long term randomised, placebo controlled phase 3 trial by Thiele *et al.* (2022) found over the course of the trial (~ 48 weeks, median treatment time 38 weeks) that cannabidiol was well tolerated and crucially the median percentage reductions in seizure frequency for the patient cohort was 54% – 68%. Both of these clinical trials highlight that cannabidiol can be a potent therapeutic option for TSC patients suffering epilepsy alone or in combination with currently approved mTORC1 inhibitors. However, information regarding whether drug-drug interactions between cannabidiol and rapalogues is currently lacking. With a recent study finding such drug-drug interactions may be unfavourable and could lead to adverse effects (Ebrahimi-Fakhari *et al.* 2020). The authors found for patients treated with both cannabidiol and either everolimus or sirolimus, cannabidiol resulted in increased serum levels of everolimus or sirolimus, in some cases resulting in clinical toxicity.

The mechanism of action of how cannabidiol mediates is anticonvulsive effects is yet to be fully elucidated. Presently, the most current hypothesis is that cannabidiol reduces excitatory neurotransmission at the synaptic level through three possible mechanisms, inhibition of the adenosine reuptake pump ENT1, inhibiting activation of the GPR55 cannabinoid receptor and/or desensitising TRPV1 ion channels (Aronica *et al.* 2023). Evidence from a zebra fish model of TSC also found cannabidiol suppressed rpS6 phosphorylation in the larval brains of *tsc2* −/− zebra fish (Serra *et al.* 2019). Suggesting another way in which cannabidiol exerts its anticonvulsive effects, with particular relevance to TSC, is through repression of mTORC1

signalling. Supporting this notion is a study by Zeng *et al.* (2008), who found that rapamycin suppressed seizures in mice with *Tsc1* conditional knock out in the glia.

### 1.4.3 Other treatments

Despite the efficacy of mTOR inhibition, surgical intervention remains an effective treatment for TSC associated lesions. Surgical goals for renal AMLs centre around preventing acute events, especially haemorrhaging. This often involves elective resection and embolization of renal AMLs that are particularly large, growing and/or resistant to mTOR inhibition (Eijkemans *et al.* 2015). Resection remains the treatment of choice for acutely symptomatic SEGAs (Curatolo *et al.* 2015), with mTOR inhibition preferred for treating SEGAs that are growing but asymptomatic or SEGAs that aren't amenable to surgery; such as multiple bilateral SEGAs. It should be noted that resection of SEGAs carry significant risks and potential for complications (Kotulska *et al.* 2014). Lastly, surgery is also an option in the treatment of epilepsy associated with TSC if epileptogenic foci can be located. A meta-analysis of seizure outcomes after surgery by Zhang *et al.* (2013a) reported 59% of patients no longer experienced seizures. However, the percentage of seizure free cases has been found to decrease over time from surgery (Liang *et al.* 2017).

## 1.5 mammalian target of rapamycin (mTOR)

The action of the mammalian target of rapamycin (mTOR) protein is central to what we currently know about TSC. Therefore, an appreciation of mTOR's complexes, their regulation and downstream signalling are necessary to understand the molecular/cellular aetiology of TSC, and by and large why they have been the main target for therapeutic intervention

### 1.5.1 mTOR complexes

Mammalian target of rapamycin (mTOR), as its name implies was first described after the discovery of rapamycin and identification of the TOR genes in *S. cerevisiae* (Heitman *et al.*1991 and Kunz *et al.* 1993). Mammals possess one orthologue of *TOR1* and *TOR2*, *MTOR* (Sabatini *et al.* 1994 and Sabers *et al*. 1995), the product of which instead functions as part of two separate multi-protein kinase complexes; mTORC1 and mTORC2 (Kim and Guan, 2019). As described in figure 1.1, the two mTOR complexes differ in overall composition. mTORC1 is comprised of the core subunits mTOR, RAPTOR, mLST8 and also the non-core subunits PRAS40 and DEPTOR when in an unstimulated state (Yang *et al.* 2016a). mTORC2 retains the mTOR and mLST8 core subunits, but has RICTOR instead of RAPTOR (Chen *et al.* 2018).

The mTORC2 complex also contains mSIN1 as a core subunit and the non-core subunits DEPTOR and PROTOR. In addition to be structurally distinct, the two complexes are functionally distinct, with RAPTOR and RICTOR recruiting different substrates and regulators to mTORC1 and mTORC2 respectively. As described in figure 1.1, mTORC1 acts to positively regulate cell growth, proliferation and metabolism by stimulating anabolic processes whilst inhibiting those that are catabolic (Kim and Guan, 2019). mTORC2 however principally regulates cell survival, cell motility and cytoskeletal rearrangement. Lastly, mTORC1 and mTORC2 can also be distinguished by their sensitivity to rapamycin. mTORC1 is acutely sensitive to rapamycin treatment, with the rapamcyin-FKBP12 complex directly binding to mTOR and inhibiting mTORC1 activity allosterically (Chen *et al.* 1995). mTORC2 isn't acutely inhibited by rapamycin, thought to be due to steric hinderance generated by RICTOR and mSIN1 preventing rapamcyin-FKBP12 binding to mTOR (Chen *et al.* 2018). Long term, rapamycin treatment will inhibit mTORC2 (Sarbassov *et al.* 2006), which is thought to be due to rapamycin binding newly synthesised/unbound mTOR.

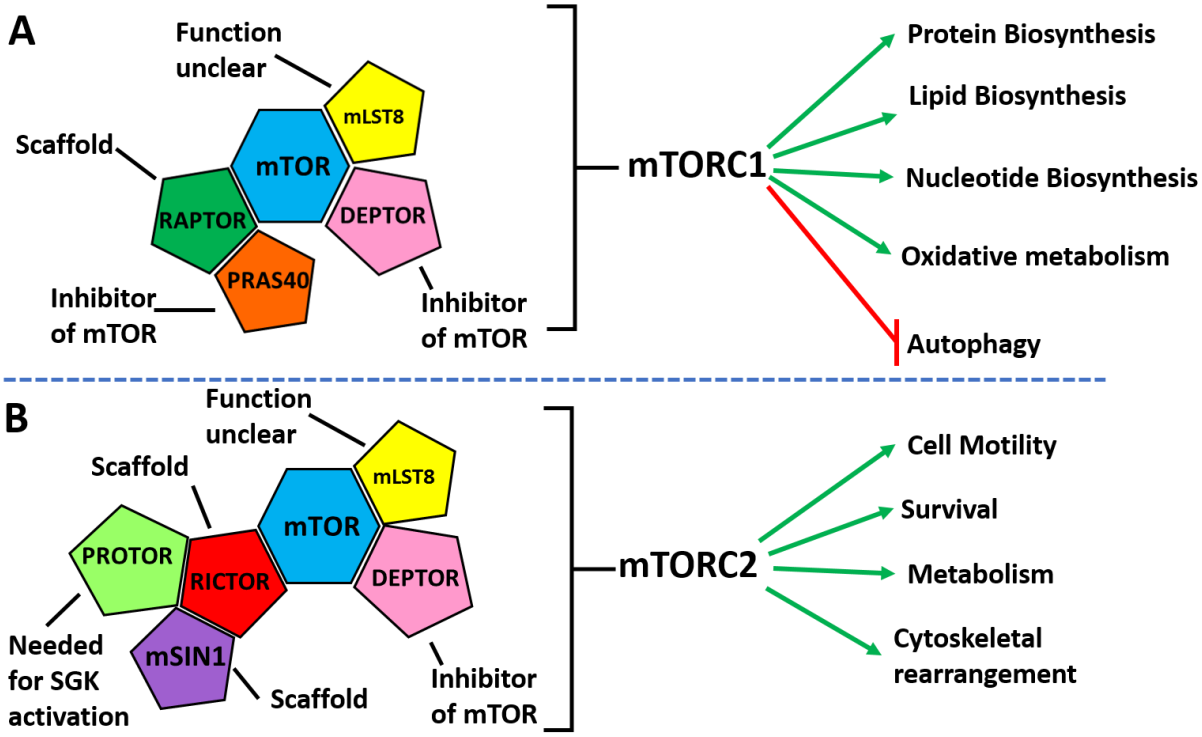


**Figure 1.1 The differing components and functions of the mTOR complexes. A**: The core components of mTORC1 are the kinase mTOR, RAPTOR and mLST8. In the absence of stimulation, the inhibitory proteins DEPTOR and PRAS40 also form part of mTORC1. **B**: mTORC2 is also comprised of mTOR, mLST8 and DEPTOR, but also contains RICTOR, PROTOR and mSIN1. RAPTOR= regulatory-associated protein of mTOR, mLST8= mammalian lethal with Sec13 protein 8, DEPTOR= Dishevelled, Egl-10, and Pleckstrin domain-containing mTOR-interacting protein, PRAS40= proline-rich AKT substrate 40 kDa, RICTOR= rapamycin-insensitive companion of mTOR, PROTOR= protein observed with Rictor, mSIN1= mammalian stress-activated protein kinase interacting protein 1.

### 1.5.2 mTORC1 Structure

**Core mTORC1 Subunits: mTOR, RAPTOR and mLST8.**

Cryo-EM structures of a high resolution have been resolved for the core mTORC1 complex and also with accessory proteins (RHEB and PRAS40) (Yang *et al.* 2013a, Yang *et al.* 2016a and Yang *et al.* 2017a). According to the structure resolved by Yang *et al.* (2016a), mTORC1 forms a symmetric dimer of the hetero-trimer mTOR/RAPTOR/mLST8 mediated by the two mTOR monomers and stabilised by the RAPTOR subunits binding across both mTOR monomers.

mTOR is a serine/threonine protein kinase that belongs to the phosphoinositide 3-kinase (PI3K)-related kinase (PIKK) family. mTOR's conserved domains are schematically represented in figure 1.2. mTOR's N-terminal domain, consists primarily of tandem HEAT repeats (Yang *et al*. 2016a), which provide surfaces for protein-protein interactions, including between HEAT repeats in different monomers (Yoshimura and Hirano, 2016). In the case of mTORC1, HEAT repeats within mTOR and RAPTOR mediate their interaction with one another, and with downstream substrates of the mTORC1 complex (Yang *et al.* 2016a). The C-terminal domain of mTOR forms a compact core, with the C shaped FAT domain wrapping around the kinase domain, so that FRB domain (where rapamycin binds) protrudes out. The kinase domain of mTOR, adopts a two-lobe structure characteristic of a PI3K kinase (Walker *et al.* 1999).

RAPTOR was identified by two groups, to be a mTOR binding protein able to interact with mTOR substrates (Hara *et al*. 2002 and Kim *et al.* 2002). RAPTOR is thought to function primarily as a scaffold protein, important for the recruitment of substrates such as S6K1 and 4E-BP1 to mTORC1 via their TOS (TOR signalling) motif (Nojima *et al.* 2003). Substrate recruitment of RAPTOR is thought to occur vis its RNC domain (Dunlop *et al.* 2009). RAPTOR is also a target for phosphorylation that regulates the overall activity of mTORC1. Foster *et al.* (2010) and Carriere *et al.* (2011) demonstrated that mTORC1 activation resulted in mTOR directed multi-site phosphorylation of RAPTOR, with mTORC1 containing phosphorylation defective RAPTOR mutants showing decreased kinase activity towards substrates. Conversely, Dunlop *et al.* (2011) demonstrated ULK1, itself a substrate of mTORC1, phosphorylated RAPTOR at multiple sites to decrease kinase activity towards substrates. The exact function of mLST8 in both the mTORC1 and mTORC2 complexes remains unclear (Yang *et al.* 2018), but is known to stabilise the interaction of mTORC1 and RAPTOR and increase the kinase activity of mTOR.

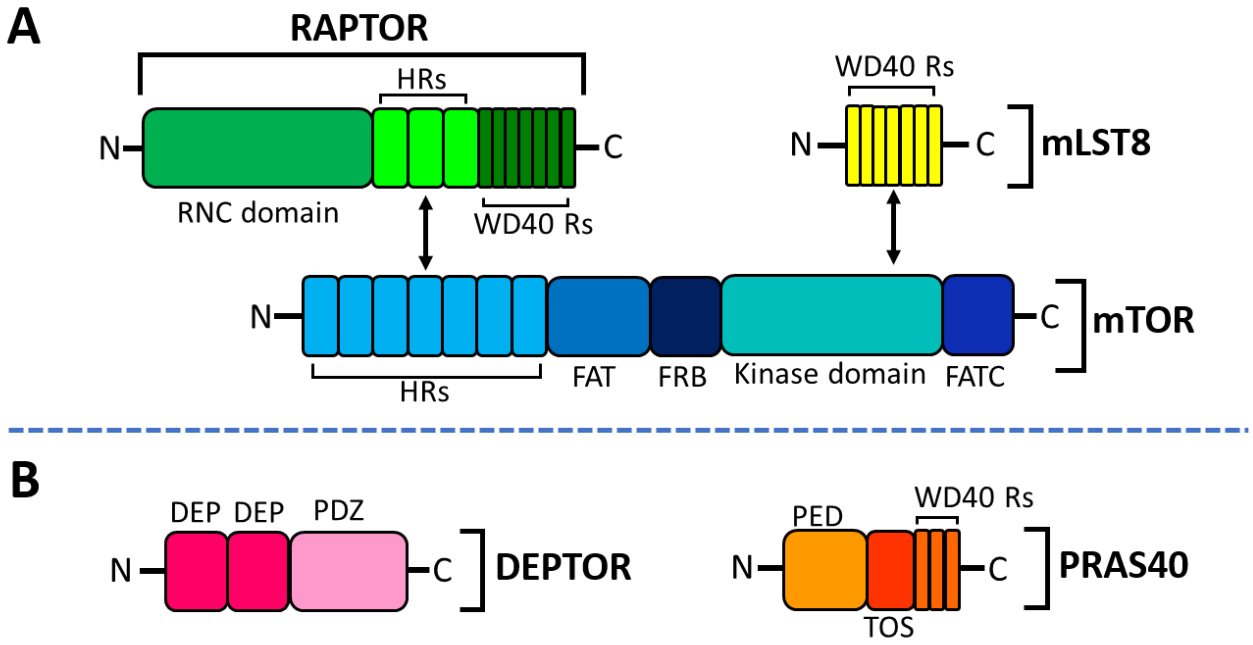


**Figure 1.2 Components of the mTORC1 signalling complex and their structural domains. A**: Conserved domains of the core mTORC1 components**.** mTORs conserved domains include N-terminus tandem HEAT repeats, FAT domain, FRB domain, kinase domain and a smaller FAT domain at the C-terminus (FATC). Raptor contains an N-terminal domain, three HEAT repeats and seven WD40 repeats. mLST8 is primarily comprised of seven WD40 repeats (Rs). Arrows represent respective binding domains between proteins. **B**: Conserved domains of the inhibitory mTORC1 proteins. DEPTOR contains two tandem N-terminal DEP domains and towards the C terminus a PDZ domain. PRAS40s conserved domains include a PED, a TOR signalling motif (TOS) and WD40 repeats (Rs). Protein domain schematics are not scaled. HEAT= Huntington, EF3A, ATM, TOR, FAT= FRAP–ATM–TTRAP, FRB= FKBP12/rapamycin binding, RNC= Raptor N-terminal conserved, DEP= dishevelled, egl-10, and pleckstrin, PDZ= postsynaptic density 95, disks large, zonula occludens-1, PED= proline enriched domain.

### PRAS40 and DEPTOR

PRAS40 and DEPTOR are negative regulators associated with the mTORC1 complex when it is in an unstimulated state. Identified as an insulin regulated inhibitor of mTORC1 by multiple groups (Sancak *et al.* 2007, Vander Haar *et al.* 2007 and Wang *et al.* 2007a), PRAS40 contains a variant TOS motif and acts as competitive substrate for mTOR (Oshiro *et al.* 2007). A recent cryo-EM structure of mTOR-mLST8-PRAS40 revealed PRAS40 binds with a higher affinity to substrate binding sites at the FRB domain (see figure 1.2 for schematic) thus inhibiting mTORC1 by competitively blocking substrate recruitment (Yang *et al.* 2017a). Stimulation of mTORC1 results in the phosphorylation of PRAS40, through PI3K activated AKT (Kovacina *et al.* 2003 and Vander Haar *et al.* 2007) and through Rheb stimulated mTOR (Oshiro *et al.* 2007). Phosphorylation of PRAS40 at multiple sites results its dissociation and sequestering by 14-3-3 proteins (Nascimento *et al.* 2010), allowing full activation of mTORC1. DEPTOR is another mTOR inhibitor (Peterson *et al.* 2009) which associates with mTORC1

through interaction of its PDZ domain (see figure 1.2) and mTORs' FAT domain. The exact mechanism of DEPTORs' inhibitory effect on mTOR isn't known, but loss of DEPTOR increases phosphorylation of mTORC1 substrates. DEPTOR is a substrate of mTOR (Gao *et al.* 2011), and increased mTOR activity results in phosphorylation of DEPTOR and its eventual degradation through the ubiquitin-proteasomal pathway.

**Rheb**

Whilst not part of the core complex, the protein Rheb (Ras homolog enriched in brain) is crucial to the activity of mTORC1 (Patel *et al.* 2003). Rheb is a small GTPase and like all small GTPases cycles between a GTP and GDP bound state, which affects the conformation and ultimately function of the GTPase (Cherfils and Zeghouf, 2013). Cycling of GTPases between GTP and GDP bound forms is regulated by GAPs (GTPase activating proteins) which promote hydrolysis of bound GTP to GDP and GEFs (Guanine nucleotide exchange factors) which promote the release of bound GDP and reloading of GTP. Binding of GTP-bound Rheb (but not GDP-bound Rheb) strongly stimulates the kinase activity of mTORC1 (Long *et al.* 2005 and Sato *et al.* 2009). The TSC1/TSC2 complex acts as a GAP for Rheb, and is key to the regulation of mTORC1 signalling. Rheb binds mTOR distally from the kinase site at the HEAT and FAT domains (see figure 1.2) producing a global conformational change that re-algins the active site residues to allosterically improve catalysis (Yang *et al.* 2017a).

### 1.5.3 Activation and Regulation of mTORC1 Signalling

mTORC1 acts as a major signalling node, integrating various intracellular and extracellular signals about the nutrient and energy status of the cell in order to regulate the growth and proliferation of the cell. The activation and regulation of this complex happens at multiple levels, affecting the activity and sub-cellular location of both the complex itself and its regulators.

**The TSC1/TSC2 complex and Rheb**

The small GTPase protein Rheb is key for mTORC1 activity; with the complex showing little kinase activity *in vitro* without the GTP-bound form (Long *et al.* 2005). The nucleotide bound status of Rheb is in turn controlled by the TSC1/2 complex (Inoki *et al.* 2003a), and thus through Rheb, TSC1/TSC2 negatively regulates mTORC1 signalling (Tee *et al.* 2002 and

Garami *et al.* 2003). Whilst a GTPase protein, Rheb exhibit low intrinsic GTPase activity itself (Yu *et al.* 2005) and thus favours its active state.

Therefore, the GAP activity of the TSC1/2 complex is key for the acute switch to revert Rheb-GTP to Rheb-GDP and thus inhibit mTORC1 (Mazhab-Jafari *et al.* 2012). The TSC complex itself is composed of three subunits: TSC1, TSC2 and also TBC1D7 (Dibble *et al.* 2012). TSC2 is the actual GAP protein for Rheb, containing the GAP domain (Tee *et al.* 2003a). TSC1 is essential for the proper functioning of the complex, as it acts to stabilise TSC2 which is unstable when unbound and is prone to ubiquitin mediated degradation (Benvenuto *et al.* 2000). So effective is TSC1/2s' regulation of mTORC1 through Rheb, that many of the pathways that signal mTORC1 do so by regulating the activity of TSC1 and TSC2 (Huang and Manning, 2008). As highlighted in figure 1.3, TSC1 and TSC2 contain sites subject to post translational modifications (PTM) which alter the activity, stability or localisation of the TSC1/2 complex, and hence the activity of mTORC1.

**Spatial regulation of the mTORC1 complex**

Spatial regulation of mTORC1 components happens at the cytoplasmic face of the lysosome (Menon *et al.* 2014). Sub-populations of Rheb have been found at the lysosome, tethering to the lysosomal membrane (Saito *et al.* 2005 and Menon *et al.* 2014). Through growth factor induced PI3K signalling colocalization of TSC1/2 complex at the lysosome is modulated. Activated AKT phosphorylates TSC2 at multiple sites (see figure 1.3), causing dissociation of the TSC1/TSC2 complex at the lysosome and partitioning of TSC2 to the cytoplasm (Cai *et al.* 2006). Amino acid signalling through a complex mechanism involving many proteins co-localises mTORC1 with active Rag GTPases at the lysosome (Sancak *et al.* 2008), thereby bringing the complex into closer proximity with its activator Rheb.

**Growth Factor Signalling through PI3K/AKT and MAPK Pathways**

Growth factors signal mTORC1 primarily through two well characterised signalling cascades, the PI3K/AKT pathway and the Ras pathway (Saxton and Sabatini, 2017). As highlighted in figure 1.4, binding of growth factors, like insulin, to cognate receptors, results in the recruitment of adaptor proteins to the activated receptor tyrosine kinase (RTK) (Dibble and Cantley, 2015). In the case of PI3K/AKT signalling, activation of PI3K results in the conversion of PIP2 (phosphatidylinositol (4,5)-bisphosphate) to PIP3 (phosphatidylinositol (3,5)-triphosphate). PIP3 in turn recruits AKT and PDK1, promoting the activation of AKT and also the phosphorylation of AKT by PDK1. PIP3 can activate mTORC2, which in turn phosphorylates AKT to further boost its activity. Activated AKT inhibits TSC2 as discussed in section 1.5.3 and

also via phosphorylation of PRAS40; resulting in its dissociation from mTORC1 (Sancak *et al.* 2007). RTK dependent Ras signalling also regulates mTORC1 through converging on TSC2. In this instance, the activated MAPK kinase ERK and its effector RSK1 phosphorylate TSC2 (Ma *et al.* 2005 and Roux *et al.* 2004) to inhibit the TSC1/TSC2 complex. Wnt signalling also stimulates mTORC1 signalling (Inoki *et al.* 2006) through TSC2 by inhibiting GSK3 (glycogen synthase kinase 3). Phosphorylation of TSC2 by GSK3 acts to promote activity of the TSC1/2 complex.

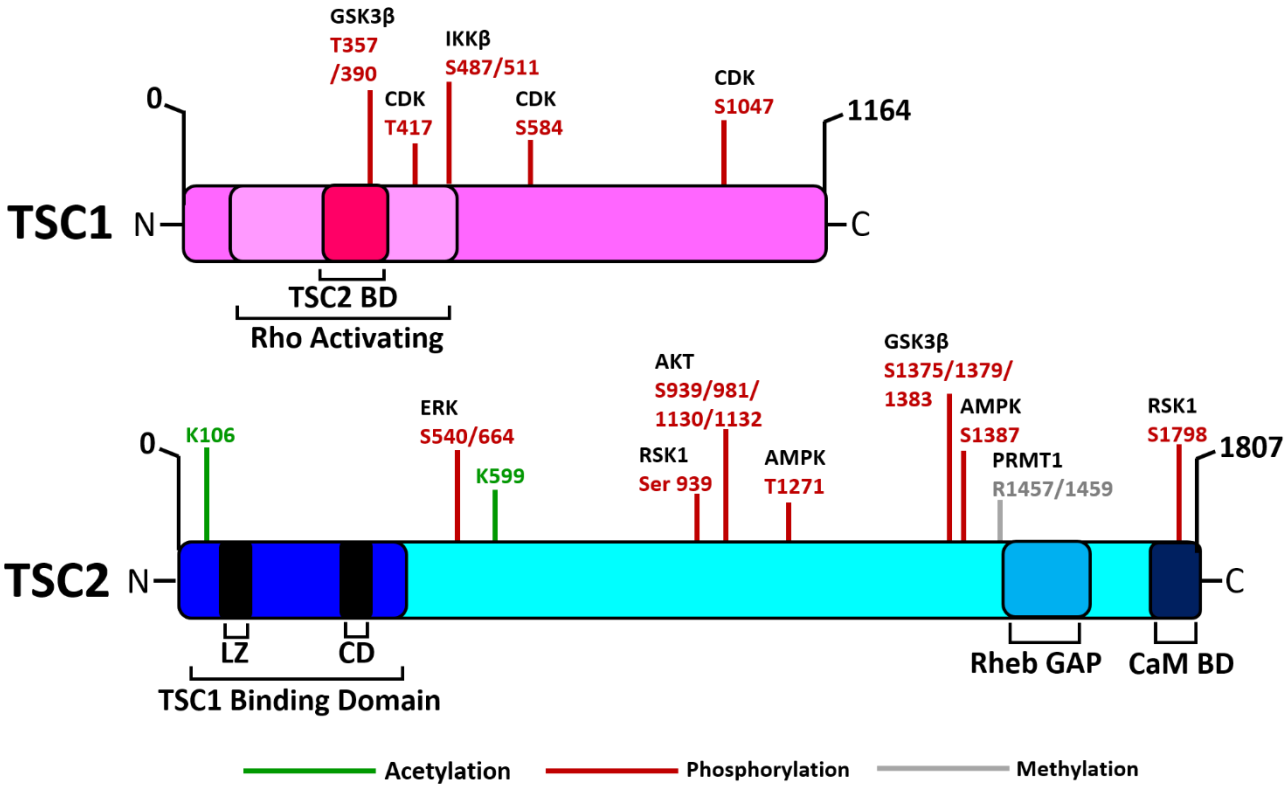


**Figure 1.3. Schematic representation of TSC1 and TSC2 protein structure and their regulatory post translation modifications.** Both TSC1 and TSC2 proteins are subject to multiple regulatory post-translation modifications (PTMs) that either positively or negatively affect their activity. Residue numbers subject to PTMs are annotated with the protein responsible for each PTM, if known, annotated above. BD= binding domain, LZ= leucine zipper domain, CD= coiled domain, CaM BD= calmodulin binding domain, Rheb Rheb GAP= GTPase-activating protein domain.

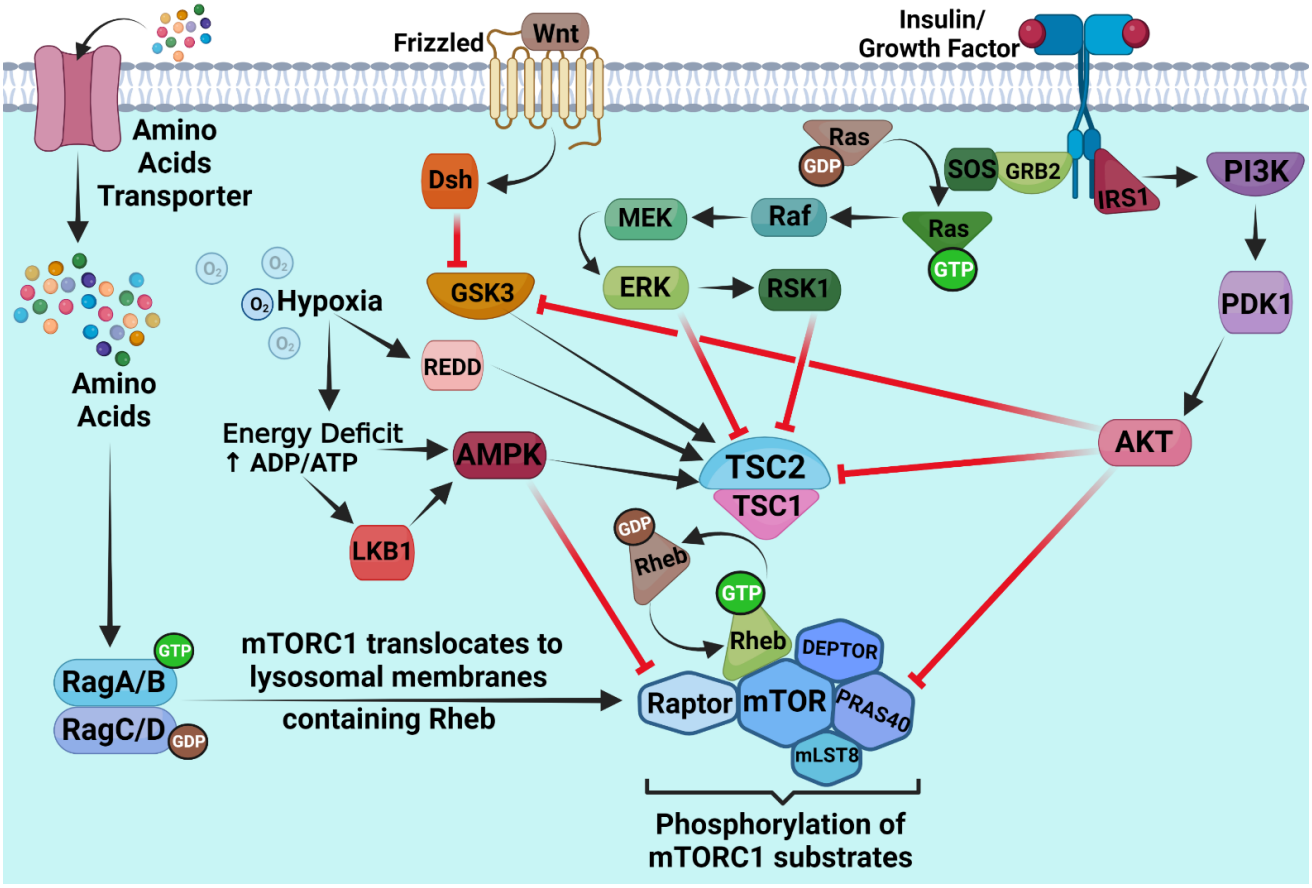


**Figure 1.4. Activation and regulation of the mTORC1 complex.** The activation and regulation of mTORC1 occurs not only through alteration of the complex itself, but also through altering the activity of its principal negative regulator, the TSC1/TSC2 complex. Activation of growth factor/insulin receptors increase mTORC1 activity through canonical RAS and PI3K signalling. With effectors kinases ERK, RSK1 and AKT mediating inhibitory phosphorylation of mTORC1 inhibitors TSC2, GSK3 or PRAS40. Low energy status (increased ATP/ADP ratio) is communicated to mTORC1 through AMPK. AMPK increases the GAP activity of TSC2 towards mTORC1s positive regulator Rheb and inhibits mTORC1 directly through phosphorylating RAPTOR. Hypoxia reduces ATP generation through decreased oxidative phosphorylation and thus feeds into AMPK. Hypoxia also upregulates the expression of REDD1, which competes with TSC2 for binding to inhibitory 14-3-3 proteins. Amino acids are a strong stimulator of mTORC1 activity independently of TSC1/TSC2. The mechanism of amino acid activation of mTORC1 involves many proteins. In general, when the local presence of amino acids increases, Rag protein heterodimers adopt their active configuration (Rag A/B bound to GTP and Rag A/C bound to GDP). Active Rag complex binds and colocalises mTORC1 at the lysosome. Bringing mTORC1 in closer proximity within the cell to Rheb. Figure was created through the use of Biorender.

### Energy and Oxygen Availability

In direct contrast to growth factor signalling through PI3K and Ras pathways, decrease in the energy status (e.g., drop in available glucose) of the cell acts to stimulate the activity of the TSC1/2 complex, thereby inhibiting mTORC1 signalling (Inoki *et al.* 2003b). AMPK largely governs this response. AMPK senses the ratios of AMP and ADP to ATP directly. Consequently, decreases in the ratio of ATP:ADP/AMP lead to AMPK activation (Hardie *et al.*

2012). AMPK inhibits mTORC1 through AMPK mediated phosphorylation of TSC2, increasing its GAP activity towards Rheb (Inoki *et al.* 2003b). Activated AMPK also inhibits mTORC1 directly, via AMPK phosphorylating RAPTOR (Gwinn *et al.* 2008), which induces RAPTOR to bind to 14-3-3 proteins, dissociating RAPTOR from the mTORC1 complex.

As with nutrient availability, oxygen status is communicated to mTORC1 to ensure growth and proliferation is enhanced only under optimal conditions. As detailed in figure 1.4, hypoxia is able to downregulate mTORC1 signalling through multiple mechanisms. Hypoxia feeds into AMPK activity, as hypoxic conditions decrease the rate of oxidative phosphorylation, reducing mitochondrial generation of ATP. The resulting concomitant decrease in available ATP activates AMPK as previously described. Hypoxia transcriptionally regulates the *REDD1* gene. Upregulation of REDD1 protein levels inhibits mTORC1 signalling through TSC2 (Brugarolas *et al.* 2004). REDD1 releases TSC2 from its association with inhibitory 14-3-3 proteins (DeYoung *et al.* 2008), increasing the amount of TSC2 available to form active TSC1/2 complexes. Lastly, the hypoxic response proteins BNIP3 and PML also negatively regulate mTORC1 signalling by binding mTOR and Rheb respectively (Bernardi *et al.* 2006 and Li *et al.* 2007), disrupting the association of mTOR with Rheb to decrease activity of the entire complex.

**Amino Acids**

As mTORC1 is a master regulator of protein synthesis, activity of the complex is coupled to intracellular concentrations of amino acids. Amino acid availability represents a potent activator of mTORC1, as even cells lacking functional TSC1 or TSC2 show decreased mTORC1 signalling on amino acid starvation (Nobukuni *et al.* 2005 and Roccio *et al.* 2006). Regulation of mTORC1 through amino acids has thus been viewed as largely independent of the TSC1/2 complex. The mechanisms by which amino acids regulate mTORC1 are complicated, and beyond the scope of this work. Simplified however, amino acid concentrations affect the nucleotide bound status of the Rag GTPases (Sekiguchi *et al.* 2001 and Sancak *et al.* 2008). In the presence of sufficient amino acids, these Rag GTPases adopt their active conformation (see figure 1.4) and then bind RAPTOR on mTORC1. Rag bound RAPTOR localises mTORC1 at the lysosome (Kim *et al.* 2008a) where Rheb also resides, thus acting to concentrate mTORC1 signalling components and regulators. Spatial regulation of mTORC1 and TSC1/2 by amino acid and growth factor signalling respectively couples these two modes of regulation; ensuring maximal mTORC1 activity only when conditions for growth and proliferation are optimal.

As highlighted by sections 1.5.2 and 1.5.3, mTORC1 is subject to regulation at multiple levels to ensure proper activation. And that much of that regulation is through the modulation of

activity of the TSC1/TSC2 complex. Which is why in the cells of TSC patients, loss of either *TSC1* or *TSC2* leads to run away hyperactivity of mTORC1.

### 1.5.4. mTORC1 Complex Regulated Processes

To understand how mTORC1 hyperactivity produces aberrant cell signalling and phenotypes, first the role of mTORC1 in healthy cells with functioning TSC1 and TSC2 must be described.

#### Protein Synthesis

Protein synthesis is the most energetically demanding process within a cell (Buttgereit and Brand, 1995) and is highly regulated to maintain cell homeostasis. mTORC1 positively regulates proteins synthesis through upregulating mRNA translation (Saxton and Sabatini, 2017). mTORC1 coordinates mRNA translation primarily through modulating the activity of two key effectors, 4E-BP1 (eIF4E binding protein) and (p70S6 kinase 1). As its name implies, 4E-BP1 is a binding protein that sequesters and inhibits translation initiation factor eIF4E. eIF4E binds the 5'-mRNA cap moiety present on all eukaryotic mRNAs and is part of the heterotrimeric eIF4F protein complex that recruits ribosomes and promotes translation initiation (Gingras *et al.* 1999a). Activated mTORC1 phosphorylates 4E-BP1 at multiple sites resulting in the dissociation of 4E-BP1 from eIF4E (Brunn *et al.* 1999 and Gingras *et al.* 1999b), promoting cap-dependent translation of mRNAs.

mTORC1 phosphorylation of S6K1 is stimulatory and increases this kinases activity (Magnuson *et al.* 2012). As detailed in figure 1.5, activated S6K1 phosphorylates a number of protein substrates that in turn regulate aspects of protein translation. S6K1 promotes cap-dependent translation through indirect activation of the eIF4A helicase, another member of the eIF4F complex responsible for unwinding secondary structures in the 5' untranslated region (Gingras et al. 1999a). S6K1 phosphorylates PDCD4, an inhibitor of eIF4A, there by promoting the degradation of PDCD4 (Dorello *et al.* 2006). S6K1 also stimulates the activity of eIF4B, a cofactor for eIF4A that promotes its helicase activity (Shahbazian *et al.* 2006). Aside from translation initiation, S6K1 has been shown to promote translation elongation through inhibitory phosphorylation of eEF2K; itself an inhibitor of the translation elongation factor eEF2 (Wang *et al.* 2001). Lastly, activated S6K1 and mTORC1 itself can promote the production of ribosomes by activating and inhibiting ribosomal protein S6 (rpS6) and PP2A respectively (Saxton and Sabatini, 2017). Thus, by affecting multiple components of the translation machinery, mTORC1 is able to greatly increase protein synthesis.

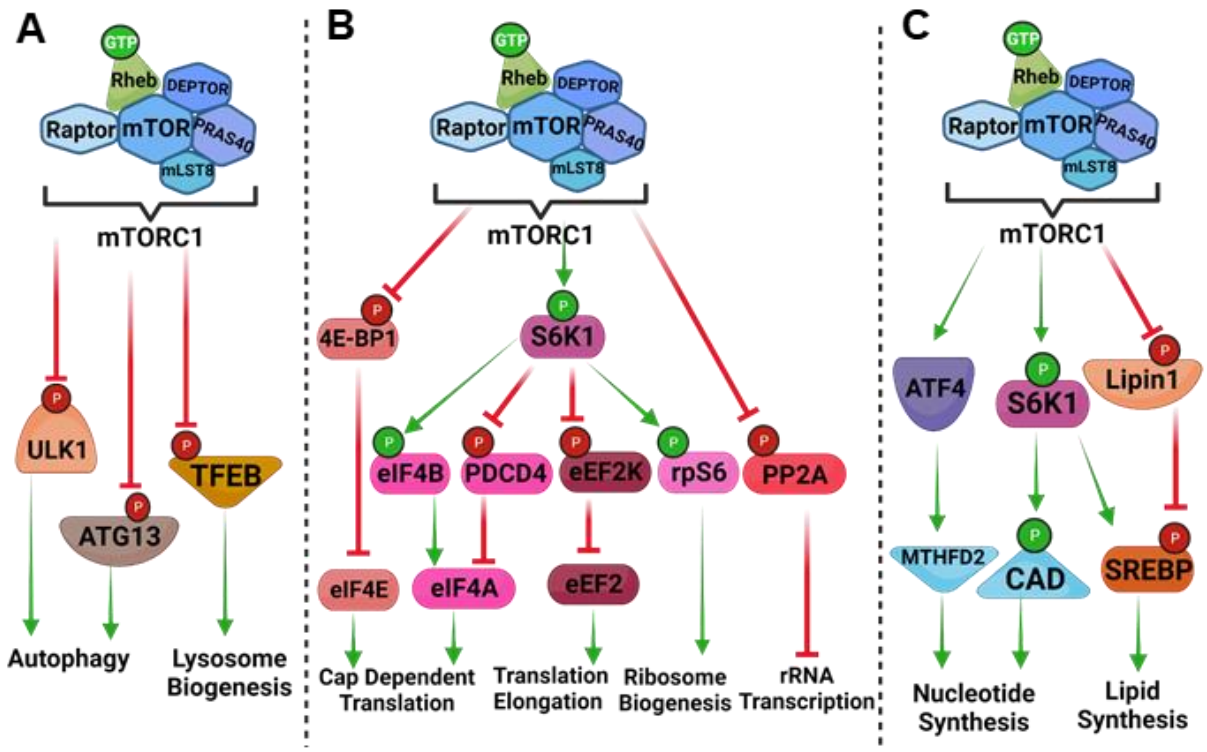


**Figure 1.5. mTORC1 mediated phosphorylation of targets and their downstream effectors.** Upon activation by upstream signalling, mTORC1 mediates activatory (green) or inhibitory (red) phosphorylation of downstream target proteins. Downstream signalling resulting from activated or inhibited mTORC1 substrates results in the upregulation of anabolic processes such as protein biosynthesis (**B**), nucleotide and lipid biosynthesis (**C**) and the downregulation of catabolic processes such as autophagy (**A**).

### Nucleotide and Lipid Biosynthesis

mTORC1 doesn't just drive protein synthesis, but also upregulates the activity of other anabolic pathways (figure 1.5). *De novo* synthesis of lipids is key to the growth and proliferation of cells, as it provides the materials for the generation of new membranes. mTORC1 activation of S6K1 promotes lipids synthesis through the activation of SREBP (sterol responsive element binding protein) transcription factors (Düvel *et al.* 2010) and inhibition of Lipin-1 an inhibitor of SREBPs (Peterson *et al.* 2011). mTORC1 also stimulates the *de novo* synthesis of nucleotides through S6K1 activation of CAD (carbamoyl-phosphate synthetase) (Ben-Sahra *et al.* 2013) and upregulating the expression of MTHFD2 (Ben-Sahra, *et al.* 2016).

### Autophagy

mTORC1 signalling also supports cell growth by inhibiting catabolic processes (figure 1.5), such as autophagy. mTORC1 directly phosphorylates and inhibits ULK1 and ATG13 (Jung *et al.* 2009), both of which function within the same multiprotein complex that drives early

autophagosome formation (Wirth *et al*. 2013). mTORC1 directed phosphorylation of ULK1 is a signalling mechanism by which mTORC1 can turn off autophagy. Phosphorylation of ULK1 by mTORC1 prevents its activation through AMPK (Kim *et al.* 2011a), which is a driver of autophagy under starvation conditions. Phosphorylation of ATG13 by mTORC1, prevents it binding and stabilising ULK1. Lastly, mTORC1 is able to inhibit autophagy transcriptionally, by phosphorylating TFEB (Martina *et al.* 2012), preventing TFEBs nuclear localisation. TFEB is a transcription factor that drives expression of autophagy and lysosomal genes.

### 1.5.5 Dysregulation of mTORC1 signalling in TSC.

The significance of the loss of *TSC1* or *TSC2* in patients is that loss of functional TSC1/2 complex equates to a loss of much of the regulation of mTORC1. As stated previously and highlighted in figures 1.3 and 1.4, many of the effector kinases of different signalling cascades modulate mTORC1 signalling through affecting the stability and activity of the TSC1/2 complex. Without the TSC1/2 complex, mTORC1 is rendered mostly insensitive to growth factor signalling, starvation signalling through AMPK and some forms of hypoxic regulation. Without TSC1/2 to effectively control the activity of Rheb, mTORC1 is rendered permanently active and promotes improper growth and proliferation through affecting the catabolic/anabolic processes previously discussed. The contribution of hyperactive mTORC1 signalling to improper growth/proliferation can be seen within cancers. Cancer cells are fundamentally characterised by their sustained proliferation despite the absence of growth promoting signals and presence of growth suppressing signals (Hanahan and Weinberg, 2011). This abnormal proliferative drive is in part achieved through aberrant mTORC1 activation, as highlighted by the finding that pathogenic mutations within oncogenes and tumour suppressor genes of the mTORC1 pathway and the upstream Ras and PI3K/Akt signalling pathways are detected in up to 80% of human cancers (Menon and Manning, 2008). Whilst TSC lesions show low metastatic potential, as discussed in section 1 their formation alone contributes significantly to the morbidity and mortality of patients. Clearly, mTORC1 is a major disease facet of TSC.

## 1.6 mTORC2 signalling.

### 1.6.1 mTORC2 signalling and regulation.

Regulation of mTORC2 and mTORC2 regulated processes were beyond the scope of this work, and comparatively is less understood relative to mTORC1. However, given there is signalling cross talk between the two mTOR complexes, the function of mTORC2 signalling is worth briefly summarising here. As with mTORC1, mTORC2 largely mediates complex activity through phosphorylation of downstream effectors. mTORC2 can promote cell survival and

growth through activating Akt signalling. mTORC2 can phosphorylate Akt at several sites, the best defined being at S473 (Hresko *et al.* 2005), but also at S477 and T479 (Liu *et al.* 2014a and Liu *et al.* 2014b). How phosphorylation of Akt at the S473 site effects Akt activity is context dependent (Hagiwara *et al.* 2012 and Tang *et al.* 2016), whereas the S477 and T479 site are thought to be crucial for Akt activity under growth stimulating conditions (Liu *et al.* 2014a and Liu *et al.* 2014b). Activation of mTORC2 by growth factors is thought to occur through occur through PI3K signalling (Gan *et al.* 2011 and Zinzalla *et al.* 2011). mTORC2 also functions in regulating the actin cytoskeleton (Jacinto *et al.* 2004), regulating actin polymerisation through phosphorylation of PKCα (Sarbassov *et al.* 2004). Not all signalling to Akt and PKCα by mTORC2 is growth factor dependent, as evidenced by the mTORC2 regulated phosphorylation sites T450 of Akt and T638 of PKCα being found unresponsive to growth factor stimulation and starvation conditions (Facchinetti *et al*. 2008 and Ikenoue *et al.* 2008). Other modes of growth factor independent activation of mTORC2 include the lipid species phosphatidic acids (Toschi *et al.* 2009 and Menon *et al.* 2017) and exercise (García-Martínez and Alessi, 2008 and Kleinert *et al.* 2017). mTORC2 also regulates cell growth and ion transport across cells through phosphorylation of its downstream substrate S6K1 (García-Martínez and Alessi, 2008 and Lu *et al.* 2011).

The components mTORC2 are subject to a number of posttranslational modifications which affect the activity of the overall complex, as with mTORC1. For example, p300 mediated acetylation of Rictor increases mTORC2 kinase activity towards Akt (Masui *et al.* 2015). Conversely phosphorylation of mSIN1 by Akt or S6K promotes mSIN1 dissociation from mTORC2, decreasing the complexes overall activity (Liu *et al.* 2013). As the case with the spatial regulation mTORC1 signalling components (Sancak *et al.* 2008 and Menon *et al.* 2014), how localisation of mTORC2 complex is tied to mTORC2 function is still an active area of research. mTORC2 has been observed to localise to many different subcellular locations, including the nucleus, cytoplasm, plasma membrane, endoplasmic reticulum and more (Betz and Hall, 2013). Studies have reported in response to growth factors, mTORC2 localises to the mitochondrial associated endoplasmic reticulum membrane (Betz *et al.* 2013) and associates with ribosomes (Zinzalla *et al.* 2011).

### 1.6.2 Cross talk between mTORC2 and mTORC1 signalling.

Signalling feedback loops exist between the two mTOR complexes. mTORC1 signalling can negatively regulate mTORC2 activity through a number of mechanisms. Activation of S6K1 by mTORC1 activity decreases mTORC2 activity by downregulating insulin-PI3K signalling through both inhibitory phosphorylation of insulin receptor substrate 1 (IRS1) and decreasing IRS1 protein expression (Shah *et al.* 2004 and Harrington *et al.* 2004). Furthermore, S6K1

can phosphorylate mSIN1 to decrease mTORC2 complex integrity (Liu *et al.* 2014c). In normal cells, mTORC2 signalling can promote mTORC1 signalling through increasing the activity of Akt1 (Hresko *et al.* 2005), which in turn can inhibit the function of the TSC1/TSC2 complex thereby relieving inhibition of mTORC1 (Cai *et al.* 2006). A study by of a related kinase, Akt2, found mutation of S474 (the homologous residue to S473 in Akt1) decreased Akt2 kinase activity for TSC2 by ~50% (Kearney *et al.* 2019). However, in TSC, Akt1's effect on mTORC1 through TSC2 is rendered non-functional due these cells lacking either functional TSC1 or TSC2.

### 1.6.3 mTORC2 signalling within TSC and its potential role in TSC pathogenesis.

Pharmacological intervention and study of the molecular aetiology of TSC has largely focused on mTORC1 signalling, however there is a growing appreciation that mTORC2 signalling may also contribute to TSC pathology. As mTORC1 hyperactivity is observed upon loss of either *TSC1* or *TSC2*, in contrast, mTORC2 signalling appears decreased in TSC cells (Huang *et al.* 2009 and Carson *et al.* 2012) and TSC associated lesions (Ruppe *et al.* 2014). This is in large part due to mTORC1 activity downregulating PI3K signalling (Shah *et al.* 2004 and Harrington *et al.* 2004), as previously describe in subsection 1.6.2. However, Huang *et al.* (2009) showed that the TSC1/TSC2 complex is able to stimulate the kinase activity of mTORC2 *in vitro*. Therefore, loss of function of the TSC1/TSC2 complex likely directly contributes to decreased mTORC2 activity observed in TSC cells. It should be noted that findings from a study by Yang *et al.* (2015) conflicted with previous reports of repressed mTORC2 activity in TSC cells. The authors found by immunohistochemical analysis of renal tumours of a *Tsc2* +/− mouse model, that mTORC2 specific Akt and PKCα phosphorylation sites were elevated. In a similar vein, there is conflict between the findings of studies into the role of mTORC2 in driving TSC pathology. *Rictor* conditional knockout mice showed disrupted brain and neurological features (Carson *et al.* 2013). Karalis *et al.* (2022) however observed that depletion of the mTORC1 component Raptor, but not the mTORC2 component Rictor in a murine TSC model, rebalanced perturbed mTOR signalling in *Tsc1* knockout neuronal cells and improved several pathology phenotypes associated with TSC, such as impaired myelination, neuronal hypertrophy, and premature mortality. Other studies have supported a role for mTORC2 activity in TSC pathogenesis. Goncharova *et al.* (2011) found that siRNA downregulation of *Rictor* repressed proliferation of *Tsc2* deficient cells. While Zordan *et al.* (2018) reported that sustained activation of Akt and mTORC2, concomitant with mTORC1 hyperactivity, was necessary for the induction of SENs and SEGAs in a murine TSC model. In summary, whilst there is conflict in the literature about whether mTORC2 activity is elevated or repressed in TSC model cells and TSC associated lesions, the role of mTORC2 signalling in TSC pathology

is not settled and may contribute towards aberrant signalling pathways explored within this thesis.

## 1.7 Angiogenesis within TSC

Whilst improper growth and proliferation through hyperactive mTORC1 signalling is the best defined aetiology for TSC, it is increasingly being shown not to be the sole driver of pathology. For example, increased angiogenesis within TSC lesions is an established consequence of loss of *TSC1*/*TSC2*. Angiogenesis is the process by which new blood vessels are formed from pre-existing vessels and is regulated by a number of secreted factors that activate many cellular pathways (Teleanu *et al.* 2019). Dysregulated angiogenesis is implicated in the pathogenesis of multiple diseases, and is necessary for the growth of solid tumours above the size of a few mm (McDougall *et al.* 2006). As without a dedicated blood supply to provide oxygen and nutrients the growth of the lesion would be severely restricted. TSC lesions are highly vascularised and display many characteristics that indicate pathological angiogenic signalling. For example, renal angiomyolipomas show extensive and irregular vasculature with elastic poor walls that are prone to aneurysm (Yamakado *et al.* 2002). While the stroma of the SEGA brain lesions is vasculature rich (Grajkowska *et al*. 2010).

In addition to the histological features of these lesions, immunohistochemical analysis of TSC associated lesions by multiple papers further identifies them as angiogenic neoplasms. For instance, increased staining for PECAM-1, a specific marker of vascular endothelium, in kidney, brain and skin lesions of TSC was observed by Arbisler *et al.* (2002). While Papakonstantinou *et al.* (2004) found protein expression of matrix metalloproteinases (MMP) was enhanced in TSC associated lesions, whilst conversely finding expression of endogenous MMP inhibitors was decreased. An environment which favours remodelling of the extracellular matrix, itself an important process in angiogenesis. Lastly, elevated levels of several pro-angiogenic factors, including hepatocyte growth factor (HGF), vascular endothelial growth factor-A (VEGFA), EGF (epidermal growth factor) and bFGF (basic fibroblast growth factor) were detected in TSC lesions by Parker *et al.* (2011) and Nguyen-Vu *et al.* (2001).

Aberrant angiogenesis can be described as resulting from the imbalance between such pro-angiogenic factors as mentioned above and endogenous anti-angiogenic factors. For example, pro-angiogenic factors whose expression was found to be elevated in TSC lesions, such as VEGF and HGF, have been found to promote aberrant angiogenesis within tumours. VEGF and HGF stimulate key steps in angiogenesis, including epithelial/endothelial cell migration, proliferation and vessel branching (Vimalraj, 2022). Increased expression and/or secretion of the pro-angiogenic VEGF has been described for numerous cancers (Kajdaniuk

*et al.* 2011). With cells from angiogenic tumours being found to secrete far more VEGF than cells derived from non-angiogenic tumours (Naumov *et al.* 2006). While elevated expression of HGF and its cognate receptor MET are frequently reported in cancers (Moosavi *et al.* 2019), with targeting of either being shown to have good efficacy in decreasing scores of angiogenesis in multiple cancer cell lines (Maemondo *et al.* 2002, Jiao *et al*. 2016 and Li *et al.* 2018a)

### 1.7.1 mTORC1/HIF-1α mediated Angiogenesis

Hyperactive mTORC1 signalling is not a hallmark of only TSC cells. Hyperactivity of the PI3K/AKT/mTORC1 cell signalling pathway is a common feature in human cancers (Polivka and Janku, 2014), promoting numerous perturbed cellular processes that drive tumorigenesis, angiogenesis being one of them (Karar and Maity, 2011). Indeed, within solid tumours, inhibitors which target mTORC1 have shown good antiangiogenic effects. For example, targeting mTORC1 directly, through rapamycin, suppressed enhanced PI3K/mTORC1/HIF-1α mediated expression of VEGF (Guba *et al*. 2002, Marimpietri *et al.* 2007, Falcon *et al.* 2011 and Frost *et al.* 2013). While curcumin was found to inhibit HGF induced angiogenic signalling through preventing c-Met phosphorylation and downstream activation of PI3K/Akt/mTOR signalling in lung cancer cell lines (Jiao *et al.* 2016). In regard to TSC, rapalogues have been shown to be efficacious anti-angiogenic drugs in their own right. Within a TSC mouse model co-treatment with the rapalog everolimus in addition to sorafenib, an angiogenesis inhibitor which inhibits protein kinases including VEGF receptors, was found to be more effective in decreasing kidney tumour size and number than either inhibitor alone (Yang *et al.* 2017b). While rapamycin was found to be more effective than a panel of angiogenesis inhibitors administered as single agents in increasing median survival in mouse models of TSC associated renal lesions (Woodrum *et al.* 2010).

In both cancers and TSC, stabilisation of HIF-1α by mTORC1 (Land and Tee, 2007) is thought to be one of the primary mechanisms by which mTORC1 hyperactivity promotes angiogenesis. A detailed description of HIF-1α signalling and regulation can be found later in this chapter (section 1.7). But in brief, HIF-1α is one part of the dimeric transcription factor complex HIF-1 (Majmundar *et al.* 2010). Through affecting target gene expression, HIF-1 regulates adaptive responses to hypoxia, including promoting expression of pro-angiogenic factors such as VEGFA. HIF-1α is the liable subunit of HIF-1, whose degradation is promoted under higher physiological oxygen concentrations (Wang *et al.* 1995a). But mTORC1 hyperactivity can lead to stabilisation of HIF-1α even under conditions of plentiful oxygen (Land and Tee, 2007), primarily through increasing preferential translation of *HIF1A* mRNA.

In murine cell models of TSC, Brugarolas *et al*. (2003) and Düvel *et al.* (2010) showed HIF-1α protein expression, and HIF-1α target gene expression was elevated on the loss of either *Tsc1* or *Tsc2*. And that rapamycin was effective at suppressing HIF-1α expression. Additionally, El-Hashemite *et al.* (2013) found mTORC1 hyperactivity in *Tsc1* and *Tsc2* deficient fibroblasts drove elevated VEGF expression, which could be normalised with rapamycin treatment. However, despite previously mentioned studies highlighting the ability of rapamycin to suppress HIF-1α expression, other studies have shown mixed results in the ability of mTORC1 inhibitors to decrease proangiogenic factor expression. For example, Brugarolas *et al*. (2003) reported that whilst HIF-1α expression was effectively normalised by rapamycin treatment within *Tsc2* −/− MEF cells, VEGF expression was relatively insensitive. A finding later confirmed in a TSC mouse model by Dodd *et al.* (2015). Additionally, other pro-angiogenic factors whose expression is elevated in *TSC1* and *TSC2* deficient cells, such as MMP2, have also been found to be insensitive to rapamycin (Lee *et al.* 2010). In TSC patients, Franz *et al.* (2012) found in an analysis of patient sera from two phase 3 clinical trials into the efficacy of everolimus, that while levels of many pro-angiogenic factors were lower in patients receiving everolimus, serum levels of VEGF-A were higher than in sera of patients receiving placebo. Furthermore, serum levels of several pro-angiogenic markers assayed in the sera of patients receiving everolimus were no different than levels in sera from patients receiving a placebo. Overall, the insensitivity of some of the pro-angiogenic factors (including VEGF) known to be elevated in TSC to rapamycin, highlighted by these studies suggest proangiogenic factor expression and hence angiogenesis is likely regulated by other dysregulated signalling pathways in addition to mTORC1/HIF-1α signalling.

### 1.7.2 STAT3 Mediated Angiogenesis

Relevant to the present work is the observation that the action of HIF-1α isn't the only factor promoting aberrant angiogenesis within disease, and likely within TSC. Dysregulated STAT3 activity may be driving pro-angiogenic factor expression within TSC. STAT3 is downstream of many tyrosine kinases, such as EGF-R (EGF-receptor) and Src, that promote angiogenesis. Early work by Niu *et al.* (2002) found STAT3 activity was correlated with VEGF expression in a set of diverse cancer cell lines. And since then, constitutive STAT3 activity has been found to drive tumorigenesis through enhancing pro-angiogenic factor expression in multiple types of cancer (Wei *et al.* 2003, Zhao *et al.* 2011, Yang *et al.* 2013b and Zhao *et al.* 2018). Furthermore, cross talk between dysregulated HIF-1α and STAT3 signalling within cancers has been shown to drive pathogenesis. Xu *et al.* (2005) found in breast, prostate and melanoma cancer cell lines, inhibiting STAT3 decreased HIF-1α and VEGF expression. Gray *et al.* (2005) found STAT3 and HIF-1α both bound at the *VEGF* promoter and co-operatively

drove VEGF expression in pancreatic and prostate cancer cell lines. Similar findings were observed in a triple negative breast cancer and renal clear cell carcinoma cell line by Pawlus *et al.* (2013) in which STAT3 and HIF-1α were found to cooperatively drive HIF-1α target gene expression. Lastly, focussing on TSC, Dodd *et al.* (2015) found that mTORC1 and STAT3 co-operate to drive HIF-1α expression at the protein and mRNA level. Although STAT3 regulation of *HIF1A* transcription was determined from HEK293 cells, not TSC model cells.

Within TSC cells dysregulated STAT3 activity alone, or in co-operation with hyperactive mTORC1/HIF-1α signalling, may be driving angiogenesis and cell proliferation. If true, then STAT3 inhibition may also normalise the expression of rapamycin resistant pro-angiogenic factor expression previously discussed. Given the requirement of lesions to co-opt angiogenic signalling pathways for growth above a certain size, and the mortality/morbidity arising from aneurysms of irregular vessels of TSC lesions (Yamakado *et al.* 2002 and Chihi *et al.* 2019), inhibitors of angiogenic pathways would have a clear clinical benefit for TSC patients.

## 1.8 HIF-1α Signalling.

As previously mentioned, TSC associated lesions are angiogenic lesions, whose abnormal vasculature and increased angiogenic signalling contribute to the morbidity and mortality these tumours incur on TSC patients. HIF-1α signalling is a key mediator of angiogenic signalling. Given that HIF-1α expression is elevated in TSC model cells and TSC associated lesions, further research into the ways increased HIF-1α signalling does and does not contribute to pro-angiogenic signalling within TSC is needed. Including whether there are better therapeutic agents than rapalogues which can target HIF-1α expression. In this regard, HIF-1α signalling and regulation are described below.

### 1.8.1 HIF

Molecular oxygen is indispensable for many cellular pathways, especially in the final step of synthesis of ATP through oxidative phosphorylation (Semenza *et al.* 2000). A decrease in oxygen levels below a certain point subjects' cells to hypoxia, creating significant stress, in part through impaired aerobic respiration. Therefore, to mitigate hypoxic stressors, cells activate a number of adaptive responses to maintain oxygen homeostasis, including cell cycle arrest, pro-angiogenic and cell survival factor secretion and increasing the oxygen independent glycolytic pathway for ATP production (Majmundar *et al.* 2010). The coordination of these adaptive responses to hypoxia are mediated through multiple cellular pathways,

including through the hypoxia inducible factor (HIF) family of transcription factors. HIFs were first described as nuclear factors which promote erythropoietin gene transcription (Semenza and Wang, 1992). HIF transcription factors function as obligate heterodimeric DNA binding complexes, composed of an oxygen labile α subunit (HIF-1/2/3α) and a stable constitutively expressed β subunit (HIF-1β) (Wang *et al.* 1995b and Wang and Semenza 1995). Cells continuously synthesis new HIF-1α subunits, but under conditions of plentiful oxygen (normoxia) HIF-1α subunits have a short half-life (Jewell *et al.* 2001). Stabilisation of HIF-1α leads to its heterodimerisation with HIF-1β via their bHLH/PAS domains to form the transcriptionally active dimer able to bind DNA at hypoxia response elements (HREs) within target genes (Wenger *et al.* 2005). HIFs bound to HREs then, through their C-terminal transactivation domain, recruit transcriptional co-activators, like p300/CBP, to regulate target gene expression.

Whilst the present work focuses on HIF-1α, two other HIF-α subunits have been described in humans, HIF-2α and HIF-3α (Majmundar *et al.* 2010). HIF-1α and HIF-2α are the best characterised HIF-α proteins. And while both isoforms are able to bind the same HRE, Mole *et al.* (2009) found in response to acute hypoxia, there was both overlap in promoters bound by HIF-1α and HIF-2α, and distinct promoter sites bound between the two HIF-α isoforms across the human genome. And while the stability of HIF-1α and HIF-2α are regulated by the same oxygen-dependent hydroxylation mechanisms (Ivan *et al.* 2001 and Lando *et al.* 2002), they differ in other post translation modifications (Keith *et al.* 2012), mRNA translation regulation through the mTOR complexes (Toschi *et al.* 2008) and sub-nuclear localisation and diffusion (Taylor *et al.* 2016).

### 1.8.2 mTORC1 Regulation of HIF-1α Activity

As discussed briefly in section 1.7.1 of this chapter, mTORC1 activity drives HIF-1α expression and therefore in the context of TSC an important driver of dysregulated signalling, including pro-angiogenic signalling. As seen in figure 1.6, growth factor/insulin signalling leads to activation of mTORC1 and Ras/ERK/MNK signalling. These signalling pathways drive the protein expression of HIF-1α through activation of protein biosynthesis machinery and factors that lead to enhanced *HIF1A* mRNA translation. mTORC1 activity promotes the preferential enhanced translation efficiency of a subset of mRNAs, of which HIF-1α is one, with long structured 5' untranslated regions (UTR). This is achieved through promoting formation of the eIF4F complex (Fonseca *et al.* 2014). Stable secondary structures with the 5' untranslated region (UTR) of mRNA impair translation efficiency (Jackson *et al.* 1997) and need to be linearised before initial 40S ribosome binding and scanning towards the translation initiation codon (Gebauer and Hentze 2004). Linearisation of this secondary structure is achieved by

the RNA helicase activity of eIF4A (Rogers Jr *et al.* 2002). mTORC1 promotes the activity of this helicase, and hence HIF-1α mRNA translation efficiency, through phosphorylation of multiple downstream substrates. Inhibition of 4E-BP1 relieves its inhibitory effect on eIF4E, allowing recruitment of eIF4G and in turn eIF4A to the 5′ end of an mRNA (Hara *et al.* 1997). eIF4A RNA helicase activity is elevated by eIF4B and inhibited by PDCD4. mTORC1 activation of S6K1, leads to activatory phosphorylation of eIF4B (Raught *et al.* 2004) and inhibition of PDCD4 (Dorrello *et al.* 2006). Additionally, work by Wang *et al.* (2022) identified that the 5' UTR of *HIF1A*, contained high affinity eIF4A binding motifs. Further indicating translation of *HIF1A* mRNA is particularly sensitive to mTORC1 activity. Additionally, the mRNAs whose translation is upregulated by mTOR/eIF4F activity have been found to almost entirely consist of transcripts containing 5' terminal oligopyrimidine (TOP) motifs (Hsieh *et al*. 2012 and Thoreen *et al.* 2012). These 5' TOP containing mRNAs have long been known to be rapamycin sensitive (Jefferies *et al.* 1994 and Terada *et al*. 1994). These TOP motifs are found at the 5' end of mRNAs encoding all ribosomal proteins, elongation factors and a number of initiation factors (Meyuhas, 2000). Therefore, preferential translation of these mRNAs through mTORC1 activity allows tight control of the biosynthesis of these translation components in line with energy and nutrient availability within the cell. Interestingly, TOPs have been identified in the 5'UTR region of *HIF1A* (Laughner *et al.* 2001 and Thomas *et al.* 2006), again highlighting HIF-1α translation is tightly coupled to mTORC1 activity. Hyperactivity of mTORC1 within the context of TSC, drives HIF-1α accumulation in disproportion to PHDs (prolyl hydroxylases), stabilising HIF-1α. Besides mTORC1's role in driving HIF-1α protein expression, mTORC1 activity has been found to promote transcriptional activity of HIF-1α. An mTORC1 signalling motif (TOS) in the N-terminal domain of HIF-1α is bound by Raptor, to promote p300/CBP binding (Land and Tee, 2007). HIF-1α mutants lacking this TOS motif, showed impaired HIF-1α transcription under hypoxia and p300/CBP binding.

It is also worth noting that feedback inhibition of mTORC1 by increased HIF-1α activity is impaired in TSC. Stabilisation of HIF-1α leads to increased HIF-1α target gene expression, including that of *REDD1* (Brugarolas *et al.* 2004). REDD1 inhibits mTORC1 signalling by releasing TSC2 from its inhibitory association with 14-3-3 proteins (DeYoung *et al.* 2008). Given that TSC patients lack functional TSC1/TSC2 complex, this feedback inhibition of mTORC1 signalling by HIF-1α activity is rendered unfunctional. In conclusion, within TSC cells, HIF-1α expression and activity are dysregulated at multiple levels through the loss of either *TSC1* or *TSC2*.

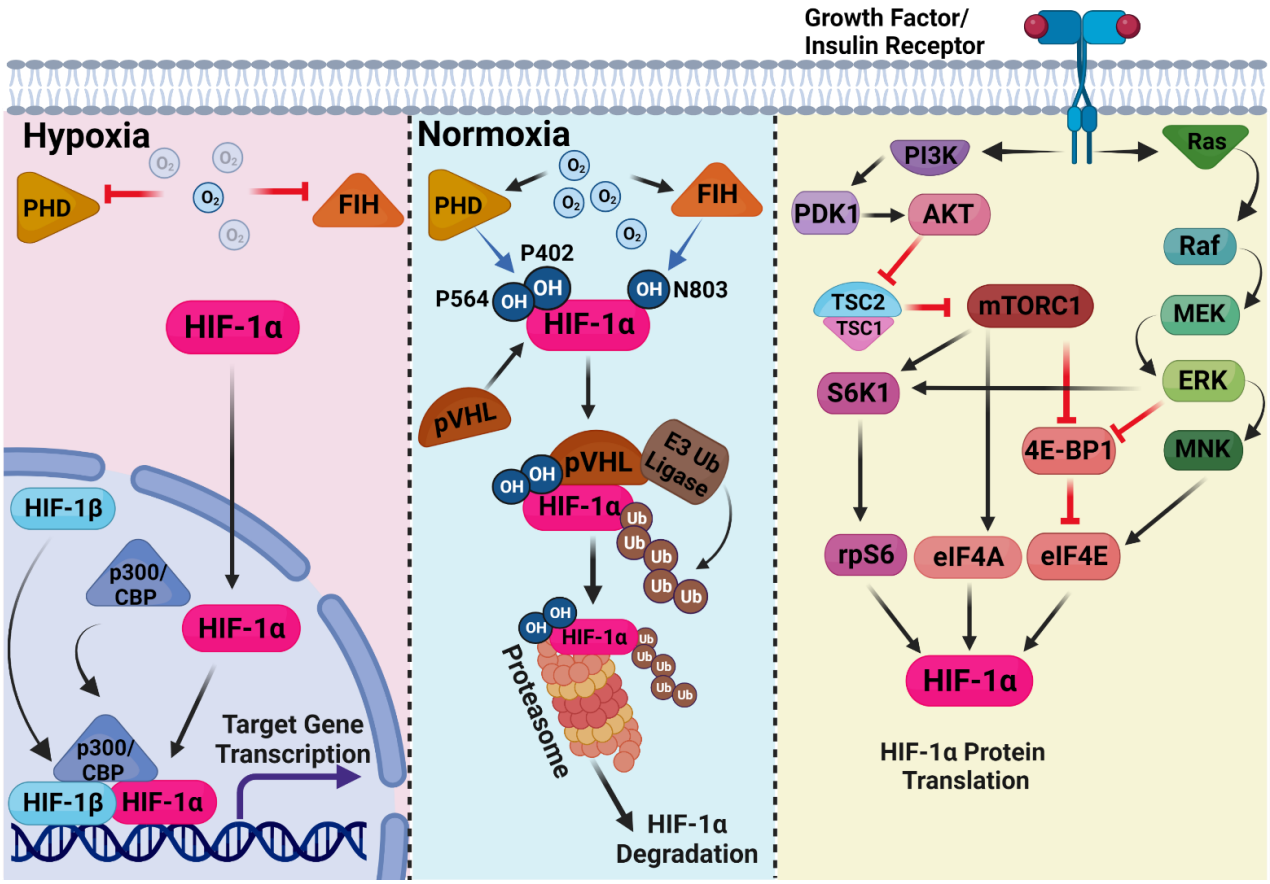


**Figure 1.6. HIF-1α protein regulation occurs through mTORC1 and Ras/Raf/MEK/ERK signalling mediated increase in protein synthesis and oxygen dependent proteasomal degradation.** Activation of growth factor/insulin receptors increases the activity of both mTORC1, through the PI3K/AKT pathway, and of ERK and MNK kinases, through the Ras/Raf/MEK pathway. mTORC1, ERK and MNK phosphorylate downstream effectors that act through multiple mechanisms to increase the translation of HIF-1α mRNA. Under conditions of plentiful oxygen (normoxia) newly synthesised HIF-1α is degraded through the ubiquitin-proteasome pathway. Oxygen dependent prolyl hydroxylases (PHDs) hydroxylate HIF-1α at P402 and P564, which in turn allows pVHL to bind HIF-1α. pVHL bound HIF-1α is polyubiquitinated by an E3 ubiquitin ligase complex which marks HIF-1α for degradation by the proteasome complex. Oxygen dependent hydroxylation of HIF-1α by FIH blocks HIF-1α associating with the transcriptional activator p300/CBP at target gene promoters. Repressing HIF-1α mediated transcription. Under conditions of low oxygen (hypoxia), the inhibitory activity of PHD and FIH hydroxylases is inhibited. Therefore HIF-1α is free to translocate to the nucleus, bind with HIF-1β into the transcriptionally active HIF1 heterodimer. HIF1 binds DNA at hypoxic response elements in a complex with transcriptional co-activators, such as p300/CBP, to regulate target gene transcription. Figure was created through the use of Biorender.

### 1.8.3 Canonical Regulation of HIF-1α through Oxygen Dependent Hydroxylation

Understanding how physiological oxygen concentrations regulate HIF-1α is necessary to contextualise the research presented in this thesis. As this thesis proposes there is a hypoxic element to the dysregulated signalling pathways observed upon the loss of *TSC2*, including for HIF-1α signalling.

To ensure proper activation of HIF-1 during periods of hypoxia, HIF-1α subunit stability is regulated by oxygen dependent enzymes that ultimately lead to degradation of HIF-1α through the ubiquitin mediated proteasomal degradation (Salceda and Caro, 1997). As illustrated in figure 1.6. These HIF-1α regulatory enzymes are prolyl hydroxylases (PHD) and Factor-Inhibiting HIF (FIH). PHDs, hydroxylate HIF-1α on two conserved proline residues (P402 and P564) within the oxygen dependent degradation domain (ODDD) (Maxwell *et al.* 1999 and Masson *et al.* 2001). Hydroxylation of these proline residues allows HIF-1α to be bound by von-Hippel-Lindau protein (pVHL) (Maxwell *et al.* 1999 and Ohh *et al*. 2000). pVHL acts as a substrate recognition subunit within an E3 ubiquitin ligase complex, on HIF-1α binding pVHL will poly-ubiquitinate HIF1-α at K532, K538 and K567 (Paltoglou and Roberts, 2007). Poly-ubiquitinated HIF-1α is then degraded by the 26S proteasome (Ivan *et al.* 2001).

HIF-1α hydroxylation is also mediated by the asparaginyl hydroxylase FIH in an oxygen dependent manner (Lando *et al.* 2002). FIH hydroxylates asparagine 803 within the C-terminal transactivation domain of HIF-1α. Rather than affecting protein stability, this PTM regulates HIF-1α's transcriptional activity by preventing association with transcriptional coactivators p300/CBP, which is necessary for HIF-1α to mediate hypoxic induced gene expression (Arany *et al.* 1996). The Km, substrate concentration permitting half maximum rate of enzymatic reaction, of FIH is lower than PHDs (Bracken *et al.* 2006). Meaning even on stabilisation of HIF-1α protein at lower intracellular oxygen concentrations, FIH may negatively regulate HIF-1α activity. As oxygen is a necessary substrate for FIH and PHD hydroxylation, under hypoxia the action of these enzymes is inhibited, and thus HIF-1α protein stability and transcriptional co-activator binding is increased. HIF-1α is then free to associate with HIF-1β, bind HRE containing genes and drive their expression. PHDs are also regulated by intermediates of the tricarboxylic acid (TCA) cycle. Both PHDs and FIH rely on α-ketoglutarate as a substrate for their hydroxylation reactions and have been shown to be inhibited by TCA cycle intermediates, for example succinate and fumarate (Koivunen *et al.* 2007). This mode of regulation of PHDs and FIHs likely has functional significance to TSC pathology as TSC cells show a disturbed metabolism. For example, mTORC1 hyperactivity, through upregulating HIF-1α (Düvel *et al.* 2010) and c-Myc (West *et al.* 1998) activity, promotes glycolysis within TSC cells.

### 1.8.4 Other Post-Translational Modifications Which Regulate HIF-1α Stability and Activity.

As can be seen from figure 1.7, aside from hydroxylation, HIF-1α is subject to many regulatory PTMs that modulate its activity. Some of which have particular relevance to TSC. Aside from GSK3's role in regulating mTORC1 signalling through the TSC1/TSC2 complex, GSK3 has been found to regulate HIF-1 activity. GSK3β has been found to phosphorylate serines 551 and 589 and threonine 555 within the N-terminal transactivation domain of HIF-1α (Flügel *et al.* 2007). Phosphorylation of HIF-1α by GSK3β leads to pVHL independent proteasomal degradation of HIF-1α through FBW7-E3 ubiquitin ligase (Cassavaugh *et al.* 2011). GSK3β activity is repressed within TSC cells, owing to hyperactive mTORC1 signalling through S6K1 activity (Zhang *et al.* 2006a and Pal *et al.* 2017). Additionally, Wnt signalling leads to GSK3 inhibition. Mak *et al.* (2005) and Jozwiak *et al.* (2007) both found elevated markers of Wnt signalling within TSC associated renal and brain lesions. Therefore, GSK3β mediated regulation of HIF-1α protein stability is impaired within TSC cells (Bhaskar *et al.* 2009). Mak *et al.* (2005) and Jozwiak *et al.* (2007) also observed elevated levels of β-catenin within TSC associated renal and brain lesions. β-catenin has been found to associate with HIF-1α at the promoter of HIF-1α target genes and promote their expression (Kaidi *et al.* 2007). Not all PTMs negatively regulate HIF-1α. Cyclin dependent kinase's (CDK) phosphorylation of HIF-1α increases HIF-1α stability. CDK1 directly interacts with and phosphorylates HIF-1α at serine 668 (Warfel *et al.* 2013), decreasing proteasomal degradation. Acetylation of HIF-1α can also positively regulate HIF-1α activity. For example, acetylation of lysine 674 by PCAF promotes HIF-1α's association with p300/CBP (Lim *et al.* 2010).

PTMs under redox control have also been found to modulate HIF-1α activity. Hypoxia and elevated reactive oxygen species promote the s-glutathionylation (addition of glutathione to cysteine residues) of HIF-1α at cysteine 520 (Watanabe *et al*. 2016). S-glutathionylation, through increased intracellular oxidised glutathione, has been found to promote HIF-1α protein stability (Jeon *et al*. 2018) and HIF-1 dependent promoter activity (Tajima *et al.* 2009). Additionally, a cysteine (C824) within the C-terminal transactivation domain of HIF-1α (Shah *et al.* 2017), when oxidised, is targeted for reduction by the redox signalling protein Ref-1 (Lando *et al.* 2000). Which increases the DNA binding affinity of HIF-1. Inhibition of Ref-1 decreased HIF-1α driven luciferase reporter activity within pancreatic cancer cell lines (Fishel *et al.* 2011 and Logsdon *et al.* 2016). These studies highlight that inhibition of Ref-1 may be an efficacious strategy for targeting HIF-1α mediated pro-angiogenic signalling within TSC.

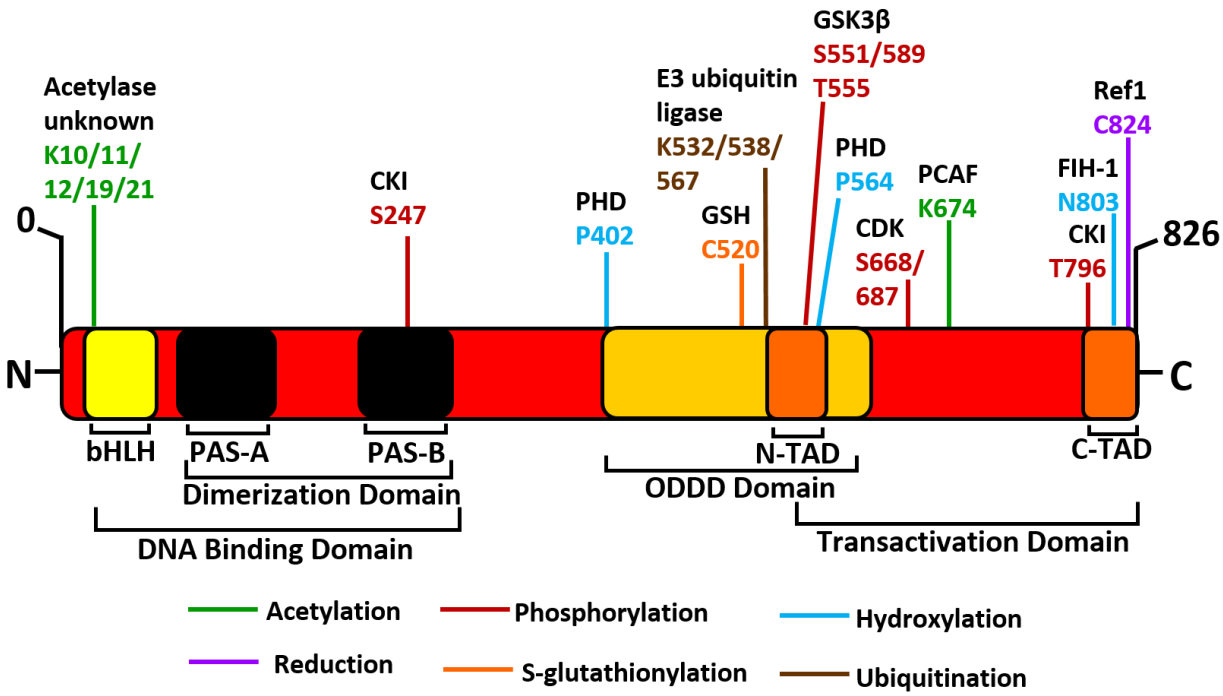


**Figure 1.7. Schematic representation of HIF-1α protein structure and its regulatory post translation modifications.** Post-translational modifications of HIF-1α across its protein structure regulate its activity at the level of protein stability and ability to bind transcriptional co-activators. Residue numbers subject to PTMs are annotated with the protein responsible for each PTM, if known, annotated above. bHLH= basic helix–loop–helix motif, PAS= Per-Arnt-Sim (PAS) domain, ODDD= oxygen dependent degradation domain, N-TAD= N-terminal transactivation domain, C-TAD= C-terminal transactivation domain.

### 1.8.5 Transcriptional Regulation of HIF-1α

Whilst post-translational modifications affecting HIF-1α stability and transcriptional activity ensure rapid and appropriate modulation of HIF-1α activity, mRNA expression of the *HIF1A* gene is also subject to regulation. Hypoxia has been found to induce *HIF1A* mRNA expression in multiple cell lines (reviewed in Gorlach, 2009). In addition, exposure of mice or rats to hypoxic conditions was found to elevate *HIF1A* mRNA expression within tissue samples from kidney, brain, and lung (Wiener *et al.* 1996). All organs predominantly affected by the clinical manifestations of TSC (Northrup *et al.* 2013) and have oxygen gradients across them as part of their normal functioning. Aside from hypoxia, *HIF1A* mRNA expression has been shown to be regulated by transcription factors, including nuclear factor kappa-light-chain-enhancer of activated B cells (NF-κB) and STAT3. Whilst the role of NF-κB signalling in TSC pathogenesis to date has been understudied, limited evidence has found elevated activity of this transcription factor within TSC brain lesions (Boer *et al.* 2008 and Dombkowski *et al.* 2019) and *TSC2* mutant cancer cells (Gao *et al.* 2015). Induction of NF-κB activity has been found

to increase *HIF1A* mRNA expression (van Uden *et al.* 2008). Additionally, NF-κB subunits p65 and p50 have been observed to directly interact with HIF-1α at a NF-κB consensus site within the *HIF1A* promoter upon increased hypoxia and ROS (BelAiba *et al.* 2007 and Bonello *et al.* 2007). STAT3 stimulatory cytokines have been found to increase *HIF1A* mRNA expression in multiple cell lines, in part through increased JAK signalling (Argaw *et al.* 2006, Gerber and Pober, 2008 and Vollmer *et al.* 2009). And Niu *et al.* (2008) found in myeloid derived cells, under hypoxia and growth stimulating conditions, STAT3 bound the *HIF1A* promoter and increased *HIF1A* mRNA levels (Niu *et al.* 2008). Lastly, in the context of TSC, Dodd *et al.* (2015) found that mTORC1 and STAT3 cooperate to drive *HIF1A* mRNA expression, through mTORC1 stimulating STAT3 transcriptional activity through phosphorylating STAT3 at S727. What these studies highlight is that within TSC, there are potentially several effectors, whose activity themselves has been found to be elevated in TSC, that could be driving aberrant *HIF1A* mRNA expression.

## 1.9 STAT3 Signalling

### 1.9.1 STAT3 and TSC

STAT3 belongs to the signal transducer and activator of transcription (STAT) family of proteins, that mainly function as transcription factors (Turkson *et al.* 2004) downstream of receptors activated by cytokines and growth factors. STAT3 is pleiotropic transcription factor, responsible for, through its transcription of target genes, regulating a wide spectrum of biological processes. Including cell proliferation, differentiation, survival, chemotaxis, inflammation, and angiogenesis (Roca Suarez *et al.* 2018). Aberrant STAT3 activity is a driver of tumorigenesis common to many cancers, with constitutive STAT3 activation reported in 70% of solid tumours (Diallo and Herrera, 2022). Constitutively activated STAT3 has been descried in multiple TSC associated lesions and model cell lines (El-Hashemite and Kwiatkowski, 2005, Chan *et al.* 2004 and Goncharova *et al.* 2009). Dodd *et al.* (2015) found that mTORC1 activity co-operates with STAT3 to drive HIF-1α expression through increasing S727 phosphorylation of STAT3. Presently however, knowledge of how STAT3 is constitutively activated within TSC and drives the pathogenesis of TSC remains unclear. STAT3 signalling and its regulation relevant to the present work is described below.

### 1.9.2 Canonical STAT3 Signalling

STAT3 activation can be initiated by a broad range of cytokines, including but not limited to interleukin 6 (IL-6) family members (Heinrich *et al.* 1998), and growth factors such as epidermal growth factor (Zhong *et al* 1994) and fibroblast growth factor (Megeney *et al.* 1996).

Some of which have been found to be elevated in *TSC1* and *TSC2* deficient cells (Parker *et al.* 2011 and Wang *et al.* 2021a). This broad range of activatory ligands for STAT3, in part, explains the many processes regulated by this protein. In canonical STAT3 signalling, STAT3 exists as a latent unphosphorylated cytoplasmic monomer until STAT3 stimulatory ligands bind their cognate receptors. As exemplified by the signalling schematic in figure 1.8, these receptors largely lack intrinsic tyrosine kinase activity, with the exception of receptor tyrosine kinases. Therefore, must recruit adaptor kinases such as JAK family members or Src.

Using IL-6 as an example for IL-6 family member cytokine activation, canonical STAT3 signalling proceeds as follows. Ligand binding to the IL-6 receptor (IL-6Rα) results in IL-6Rα associating with gp130 (the common shared chain of the IL-6 family of cytokines), and this hetero-tetramer then associates with another to form a hexameric signalling complex (Boulanger *et al.* 2003). Multimerization of receptor components brings receptor associated JAK family adaptor kinases into proximity, inducing autoactivation of the JAKs by transphosphorylation, whereby one JAK protein phosphorylates specific tyrosine residues within the activation loop of the other and vice versa (Feng *et al.* 1997). Activated JAK kinases now have their active site exposed, allowing substrate and ATP binding (Hubbard, 1997). Activated JAKs proceed to phosphorylate specific tyrosine residues within the cytoplasmic domain of gp130, creating binding sites for STAT3 to associate with the receptor complex via its Src Homology 2 (SH2) domain (Hemmann *et al.* 1996). Recruited STAT3 is then phosphorylated at Y705 through the kinase activity of JAKs (Kaptein *et al.* 1996), and Y705 phosphorylated STAT3 monomers dimerise with each other or other tyrosine phosphorylated STAT family members through their SH2 domain (Shuai *et al.* 1994). Tyrosine phosphorylated STAT3 dimers then translocate to the nucleus (Liu *et al.* 2005) where they preferentially bind to gamma interferon activation site (GAS) sequences (Raz *et al.* 1994 and Becker *et al.* 1998) and drive transcription of target genes. Aside from cytokine and growth factor receptor signalling, G-protein coupled receptors have been found to activate STAT3 through recruitment of JAK and Src adaptor kinases (reviewed in Yu *et al.* 2014).

### 1.9.3 Phosphorylation of STAT3 at S727

Aside from Y705 phosphorylation, phosphorylation of STAT3 at serine 727 (S727) is the other surrogate marker used to assess STAT3 activation or inhibition within the present work. Phosphorylation of STAT3 at S727 has also been shown to be constitutively high in TSC model cells (Onda *et al.* 2002), but it's function in regard to modulating STAT3 activity is more controversial than phosphorylation at Y705. Therefore, the role of this PTM will be discussed in the present section. First identified by Zhang *et al.* (1995), the S727 site is located within the C-terminal transactivation domain of STAT3 and has been reported to be phosphorylated

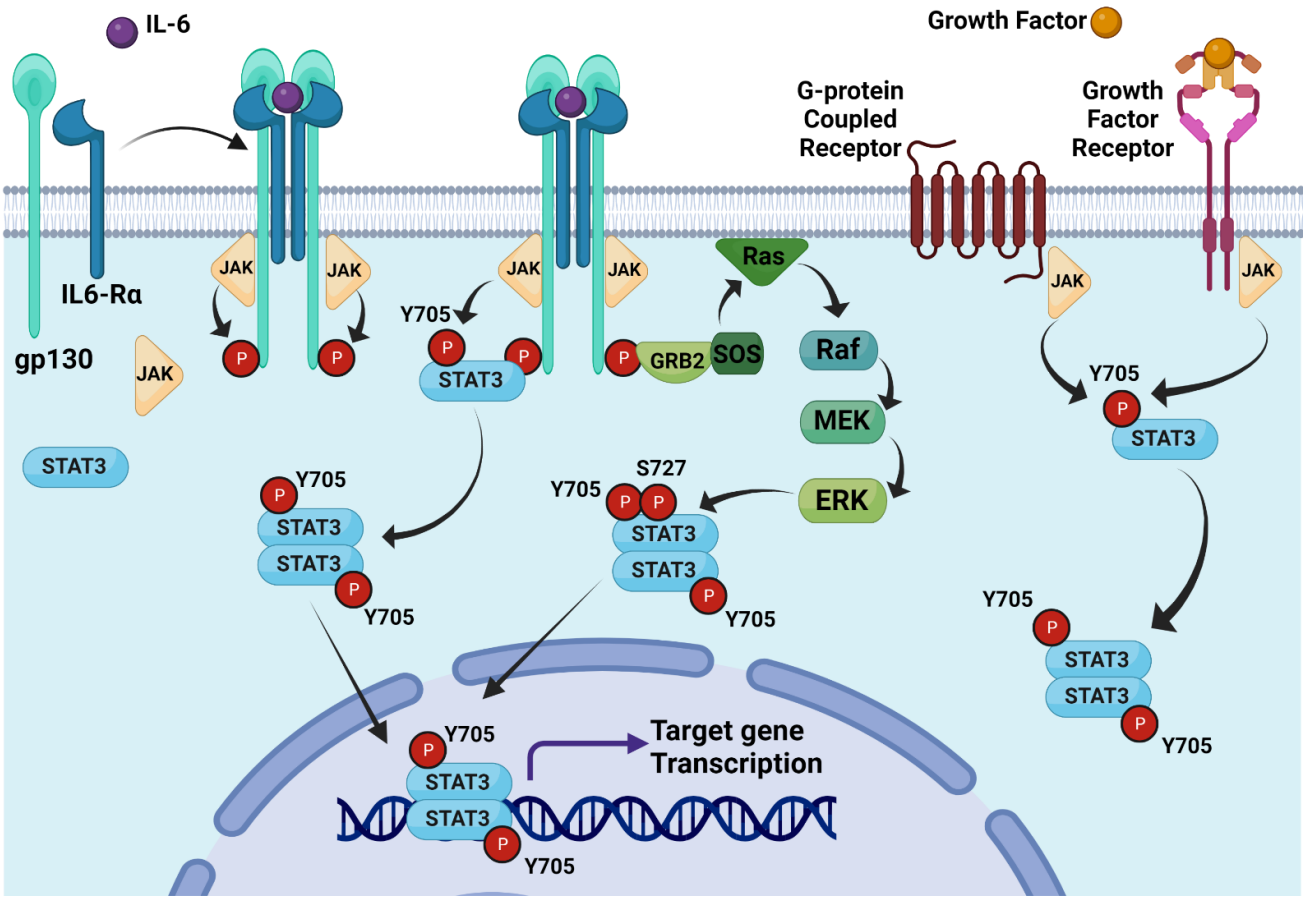


**Figure 1.8. Canonical STAT3 signalling.** Many cytokines and growth factors can activate canonical STAT3 signalling. In the case of an IL-6 family cytokine binding its cognate receptor, that receptor forms a heteromeric complex with the common gp130 receptor subunit. Adaptor kinases of the JAK family bound to the activated receptor complex autoactivate one another before phosphorylating specific tyrosine residues within gp130 to create binding sites for SH2 domain containing proteins. STAT3 is recruited to the receptor complex and is phosphorylated at Y705 by receptor bound JAK kinases. Activation of G-coupled receptors and growth factor receptors can also lead to phosphorylation of STAT3 at Y705 through recruited JAK family kinases. STAT3 monomers phosphorylated at Y705 dimerise through their SH2 domains. STAT3 dimers translocate to the nucleus where they bind to gene promoters with canonical GAS sequences and drive target gene expression. Activation of cytokines receptors can also lead to phosphorylation of STAT3 at S727. GRB2 binds JAK phosphorylated gp130. SOS bound to GRB2 activates Ras/Raf/MEK/ERK signalling, leading to ERK mediated phosphorylation of STAT3 at S727. Serine/threonine kinases activated through other pathways, not shown, can also phosphorylate STAT3 at S727. Such as MEKK1, JNK-1 and mTOR. Figure was created through the use of Biorender.

by multiple serine/threonine kinases in response to cytokine or growth factor stimulation. These include: JNK-1 (Lim and Cao, 1999), MEKK1 (Lim and Cao, 2001), ERK (Kuroki and O'Flaherty, 1999) and mTOR (Yokogami *et al.* 2000, Kim *et al.* 2008b and Dodd *et al.* 2015). Erk mediated phosphorylation of STAT3 at S727 on cytokine stimulation can be visualised in figure 1.8. However, the role of this phosphorylation site in modulating STAT3 activity is less clear than the function of the Y705 site. Initially this site proposed to increase STAT3 transcriptional activity. Wen *et al.* (1995) found through transfecting cells, showing low endogenous expression of STAT3, with wildtype STAT3 or a mutant STAT3 in which the S727

had been substituted for an alanine (S727A), phosphorylation of both the S727 and Y705 site was necessary for the maximal transcriptional activity of STAT3. Whilst the authors found by way of an electromobility shift assay that there was no difference in the DNA binding ability of Y705 phosphorylated wildtype STAT3 and S727A STAT3. Wildtype STAT3 however induced a luciferase reporter gene, driven by STAT3 binding sites, many fold higher than S727A STAT3.

Later work however challenged the findings of Wen *et al.* (1995). Kim and Baumann (1997) observed no difference in activation of the haptoglobin acute phase promoter between HepG2 cells overexpressing either wildtype STAT3 or the S727A STAT3 mutant. With other studies suggesting the S727 site negatively regulated Y705 phosphorylation of STAT3. Lim and Cao, (1999) found JNK1 mediated phosphorylation of STAT3 at S727 on EGF stimulation of COS-1 cells, which negatively regulated the Y705 phosphorylation and transcriptional activity of STAT3. Chung *et al.* (1997) performed phospho-amino acid analyses of immunoprecipitated proteins purified from $^{32}$P-labelled COS cells expressing either wild-type STAT3 or the S727A STAT3 mutant. The authors found tyrosine phosphorylation was elevated in the S727A STAT3 expressing cells. These findings are supported by findings on STAT3-β, an endogenous isoform of STAT3 which lacks the C-terminal S727 site (through alternative splicing). STAT3-β has been observed to be phosphorylated at Y705 even in the absence of stimulation (Caldenhoven *et al.* 1996 and Schaefer *et al.* 1995). Furthermore, Y705 phosphorylation of STAT3-β, induced by cytokine treatment, is sustained as opposed to the transient Y705 phosphorylation of typical STAT3 (STAT3α) (Bharadwaj *et al.* 2014). However, the longer half-life of phosphorylated Y705 of STAT3-β may be due to other factors outside the missing S727 site. Subsequent studies have supported the original findings of Wen *et al.* (1995) that the S727 site phosphorylation, in addition to Y705 site is necessary for full STAT3 transcriptional activation. Schuringa *et al*. (2001) observed in COS-7 cells, overexpression of the STAT3 S727A mutant or STAT3-β, resulted in lower STAT3 driven reporter activation on IL-6 treatment compared to overexpressing wildtype STAT3. While Shen *et al.* (2004) observed on IL-6 stimulation in MEF cells, generated from mice with the S727A mutation introduced into the STAT3 gene itself, lower STAT3 driven luciferase reporter activity than MEF cells with wildtype STAT3. Additionally, phosphorylation of the S727 site has been reported to promote association of STAT3 with the transcriptional co-activator p300/CBP (Schuringa *et al.* 2001). Therefore, S727 phosphorylation may promote STAT3 transcriptional activity despite reports this site attenuates Y705 phosphorylation. The conflicting results of the aforementioned studies, highlights that whether the S727 site is inhibitory or stimulatory to overall STAT3 activity is likely context and cell type specific.

Regardless of the exact role of S727 phosphorylation in modulating STAT3 activity, it appears indispensable for proper STAT3 function. Highlighted by Shen *et al.* (2004), who found mice heterozygous for wildtype STAT3 and S727A mutation remain viable during embryonic development, but ~75 % die shortly after birth. Improper S727 phosphorylation of STAT3 is also implicated in cancer pathogenesis. Overexpression of the S727A mutant in breast cancer cell lines was observed to decrease cell proliferation (Tkach *et al.* 2013). While constitutive phosphorylation of the S727 site has been found to promote tumorigenesis, independent of the Y705 site, in both prostate cancer and chronic lymphocytic leukemia (Qin *et al*. 2008 and Hazan-Halevy *et al.* 2010).

### 1.9.4 Other Post Translation Modifications of STAT3.

For the present work, it is an important consideration that STAT3 undergoes other post-translational modifications (PTMs) other than those already described. Phosphorylation of both the Y705 and S727 sites within the transactivation domain of STAT3 are considered the master regulators of STAT3 activity, as they regulate dimerization, subcellular location, and canonical transcriptional regulation by STAT3. And whilst both Y705 and S727 sites are the PTMs chosen in this work to assess STAT3 activity. STAT3, across its protein structure, is subject to a host of other PTMs which act to modulate its activity. A literature search did not find studies assaying these PTMs within TSC cell models. However, aberrant induction or repression of these PTMs are increasingly being shown to be critical regulators of STAT3 mediated pathogenesis, sometimes independent of Y705 phosphorylation.

As visualised by figure 1.9, STAT3 is subject to several other PTMs. STAT3 can be acetylated at multiple sites in its N-terminal and SH2 domain by the transcriptional co-activator p300 in response to IL-6 family cytokine stimulation (Wang *et al.* 2005a, Yuan *et al*. 2005, Ray *et a*l. 2005 and Ohbayashi *et al.* 2007). Acetylation of K49 and K87 appears to have an activatory effect on STAT3 mediated transcription. As mutation of these lysine residues to arginine's decreases STAT3 transcriptional activity, but through weaker association with p300 (Ray *et al.* 2005 and Hou *et al.* 2008) thereby destabilising enhanceosome formation. Acetylation of K685 on STAT3 by p300 is mediated through a PI3K/AKT dependent mechanism (Ohbayashi *et al.* 2007). The consequences of this PTM for STAT3 activity however is under debate, with reports finding acetylation of this residue promoting (Yuan *et al*. 2005) or inhibiting STAT3 transcriptional activity. STAT3 can also be subject to methylation in the N-terminal and coiled-coiled domain. Di-methylation of K49 or methylation of K180 by the histone modifying methyl transferase EZH2, has been observed to promote STAT3 mediated transcription (Kim *et al.* 2013 and Dasgupta *et al*. 2014). As mutating these residues or targeting EZH2 was found to downregulate expression of STAT3 regulated genes. Di-methylation of K140 by SET9 on the

other hand was reported to negatively regulate transcription, with Yang *et al*. (2010) reporting a subset of STAT3 genes were differentially expressed in cells expressing a K140R mutant of STAT3.

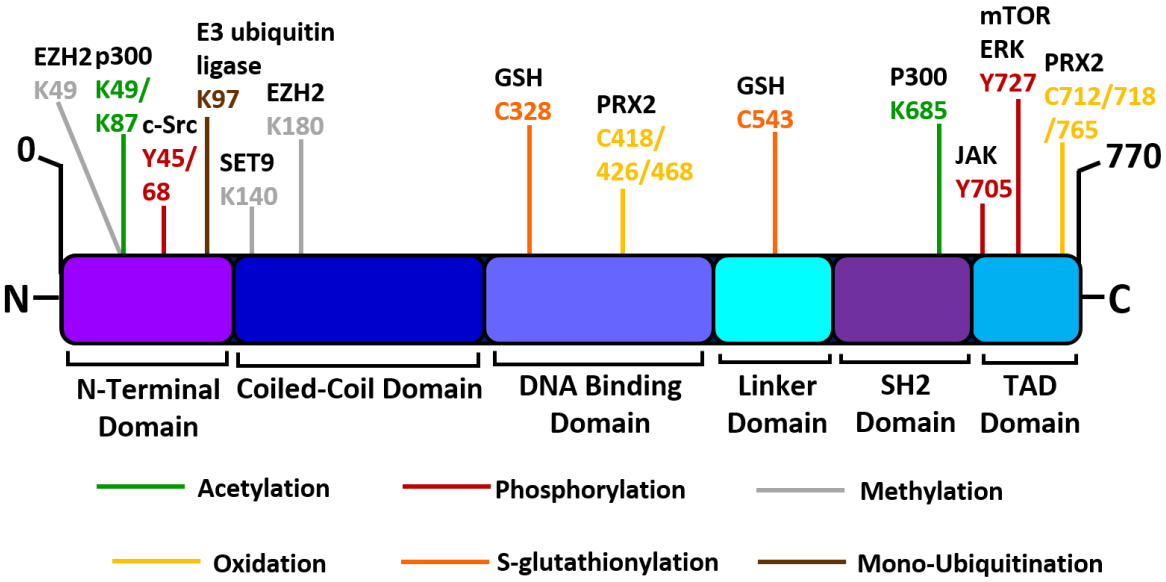


**Figure 1.9. Schematic representation of STAT3 protein structure and its regulatory post translation modifications.** Apart from phosphorylation of STAT3 at Y705 and S727, STAT3 is subject to multiple forms of post translation modification across its protein structure that modulate its activity. Residue numbers subject to PTMs are annotated with the protein responsible for each PTM, if known, annotated above. SH2 = Src Homology 2 and TAD= transactivation domain.

STAT3 is subject to redox control. Moderate ROS production can enhance JAK activity, STAT3 phosphorylation and nuclear activity (Simon *et al.* 1997, Lee *et al.* 2007, Yoon *et al.* 2010 and Kwon *et al.* 2016). However high intracellular ROS under conditions of oxidative stress can impair STAT3 transcriptional activity through s-glutathionylation or oxidation of specific cysteine residues (Kurdi and Booz, 2007, Xie *et al.* 2009, Li *et al*. 2010 and Sobotta *et al.* 2015). STAT3 cysteine oxidation can occur downstream of peroxiredoxin-2 (Prx2), a scavenger of $H_2O_2$. On $H_2O_2$ or IL-6 treatment, Prx2 oxidises cysteines located in the DNA binding domain and transactivation domain of STAT3 (Sobotta *et al*. 2015). This cysteine oxidation could be reversed through the treatment with thioredoxin-1 (Trx1), a protein which reduces oxidised cysteines on proteins. A recent study by Busker *et al*. (2020) highlighted the importance of Trx1's action in keeping STAT3 transcriptionally active within multiple cancer cell lines. The authors found irreversible inhibition of Trx1 repressed STAT3 transcription, an effect mediated by increased cysteine oxidation of STAT3 by Prx2. Expression of a redox insensitive STAT3 mutant, in which the aforementioned cysteines are substituted for serine residues, rendered STAT3 insensitive to $H_2O_2$ mediated repression of STAT3 activity and

increased proliferation of breast cancer cell lines (Li *et al*. 2010). Cysteine residues within STAT3 protein domains can also undergo s-glutathionylation through glutathione. This form of PTM has found to be inhibitory to STAT3 transcriptional activity, nuclear translocation and Y705 phosphorylation (Xie *et al.* 2009, Butturini *et al.* 2014 and Heiss *et al*. 2016). One of the aims of the present work is to evaluate the efficacy of inhibiting the redox signalling protein Ref-1 in normalising dysregulated signalling of *TSC2* deficient cells. STAT3 is a target of Ref-1 and these studies highlight that redox regulation of STAT3 play an important role in hyperactive STAT3 signalling observed in TSC cells.

### 1.9.5 Unphosphorylated STAT3

As summarised above, canonical STAT3 signalling is described by tyrosine phosphorylation of STAT3 inducing active dimer formation. However, it is important to note that assuming STAT3, which is not phosphorylated at Y705, does not have activity is incorrect. It has long been known that unphosphorylated STAT3 (U-STAT3) can associate into dimers prior to "activation" by JAK family kinases (Haan *et al.* 2000 and Braunstein *et al.* 2003), is capable of nuclear-cytoplasmic shuttling (Cimica *et al.* 2011) and binding to DNA (Nkansah *et al.* 2013). Dimer formation on Y705 phosphorylation is explained by the interaction of the SH2 domains of phosphorylated STAT3 monomers. However, U-STAT3 dimer formation is thought to be mediated via N-terminal domain (NTD) interaction (Braunstein *et al.* 2003 and Vogt *et al.* 2011). The important functional consequence of U-STAT3 is that a specific sub-set of STAT3 target genes are preferentially transcribed by U-STAT3, as first described by Yang *et al.* 2005 and confirmed by later studies (Yang *et al.* 2007 and Dasgupta *et al.* 2014). Whilst U-STAT3 can bind the canonical GAS sequences, U-STAT3 also binds to AT-rich DNA sequences and specific DNA secondary structures (Timofeeva *et al*. 2012), which is likely how U-STAT3 preferentially regulates a distinct subset of STAT3 target genes than those regulated by Y705 phosphorylated STAT3. It should be clarified that whilst U-STAT3 is not phosphorylated at Y705, it may still be subject to PTMs previously mentioned which affect activity. Indeed, Dasgupta *et al.* (2014) found acetylation of the K685 site on STAT3 was necessary for expression of the majority of U-STAT3 genes assayed. As with constitutively phosphorylated STAT3, U-STAT3 may have a pathogenic function in disease. Higher levels of nuclear U-STAT3 were correlated with the malignancy and lower survival within glioblastoma patients (Rodrigues *et al.* 2016).

### 1.9.6 Endogenous Inhibitors of the STAT3 signalling pathways.

Under normal physiological conditions STAT3 activation is typically transient and tightly controlled by negative regulators of the STAT3 pathway. Which include SOCS3, PIAS3 and protein phosphatases. *SOCS3* is a STAT3 target gene (Auernhammer *et al.* 1999) and on STAT3 activation through JAK family kinases, *SOCS3* mRNA expression is strongly induced. SOCS3 acts to inhibit further STAT3 activation through IL-6 family cytokines (Lang *et al.* 2003). SOCS3 binds strongly to gp130 that has been phosphorylated, by JAKs as part of the upstream STAT3/JAK signalling cascade, through SOCS3's SH2 domain (Nicholson *et al.* 2000). Binding of SOCS3 with gp130 is sufficient to inhibit subsequent MAPK/ERK pathway activation (Lang *et al.* 2003), SOCS3 mediated inhibition of JAK/STAT3 relies on gp130 bound SOCS3 occluding the substrate binding site on the JAK kinase (Sasaki *et al.* 1999). The inhibitory effect of PIAS3 on JAK/STAT3 signalling on the other hand works downstream of the activated receptor/JAK complex. PIAS3 binds to the DNA binding domain of Y705 phosphorylated STAT3 dimers, preventing STAT3 from binding to target DNA (Chung *et al.* 1999). Lastly, phosphorylation status of STAT3 can be regulated by protein tyrosine phosphatases (PTP). PTPs, such as SHP-1, SHP-2 and PTP1B dephosphorylate STAT3 and counteract JAK activity (Kim *et al.* 2018). There is a lack of information on these endogenous negative regulators of the JAK/STAT3 pathway within TSC and how they may contribute to dysregulated STAT3 activity. The importance of these negative regulators however in proper control of JAK/STAT3 signalling is highlighted by findings that impaired negative regulation of JAK/STAT3 has been shown to drive tumorigenesis. Decreased expression of both SOCS3 and PIAS3 have been found to promote chronic STAT3 activity within cancer cell lines (Zhang *et al.* 2002 and Yu *et al.* 2015a), while genes encoding PTPs are frequently inactivated across multiple cancers (Kim *et al.* 2018). Therefore, assaying expression and activity of the endogenous inhibitors of the JAK/STAT3 pathway, would elucidate whether similar mechanisms contribute to the enhanced activity of STAT3 within TSC.

## 1.10 Reduction-oxidation factor 1

Both HIF-1α and STAT3 are among the target transcription factors of Reduction-oxidation factor 1 (Ref-1) (Shah *et al.* 2017), and therefore represent a potential druggable target through which activity of these transcription factors could be normalised in TSC. Ref-1 is a dual function protein. Originally identified for its DNA repair role within the base excision repair pathway (Demple *et al.* 1991), a secondary function of Ref-1 as a redox sensitive regulator of transcription factor activation was defined shortly after (Xanthoudakis *et al.* 1992). The redox signalling and DNA repair activities of Ref-1 are functionally distinct and encoded by distinct and non-overlapping domains of the protein (Xanthoudakis *et al.* 1994). As well as HIF-1α and

STAT3, so far Ref-1's redox signalling activity has been found to regulate the activity of numerous transcription factors, including NF-κβ (Nishi *et al.* 2002), p53 (Jayaraman *et al.* 1997), nuclear factor erythroid 2-related factor 2 (Nrf2) (Fishel *et al.* 2015) and others.

As highlighted in the schematic in figure 1.10, Ref-1 reduces oxidised cysteine residues in specific transcription factors, generally enhancing their transcriptional activity. As discussed previously within the sections concerning HIF-1α and STAT3, oxidation of cysteines within the transactivation domain of transcription factors is in general inhibitory to their transcriptional activity. The redox ability of Ref-1 is thought to be mediated by key cysteine residues. Within mammalian Ref-1, seven cysteine (C) residues are conserved, three of them (C65, C93 and C99) considered important for Ref-1's redox signalling function (Luo *et al.* 2012). With analysis of cysteine to alanine Ref-1 mutants by Walker *et al.* (1993) identifying C65 as essential for redox activity. Mechanistically, how Ref-1 reduces target transcription factors is still being determined. But occurs through a thiol exchange reaction, whereby reduced cysteines on Ref-1 mediate a nucleophilic attack on the disulphide bond (oxidised cysteines) on the target transcription factor. This leads to the target cysteines on the transcription factor becoming reduced and the catalytic cysteines on Ref-1 becoming oxidised. Oxidation of Ref-1 significantly impairs its ability to stimulate subsequent reduction of target transcription factors (Xanthoudakis *et al.* 1992). Therefore Ref-1 must be reduced to become fully active again. Regeneration of reduced Ref-1 is mediated by the thioredoxin system, as outlined by figure 1.10. Reduced C32 and C35 of Thioredoxin (Trx1) mediates a nucleophilic attack on the oxidised cysteines within Ref-1 (Walker *et al.* 1993 and Qin *et al.* 1996) and resolves to form a disulphide bond in Trx1 and reduced cysteines within Ref-1. Oxidised Trx1 in turn is regenerated by thioredoxin reductase (TrxR1), whereby electrons from NADPH are transferred, through FAD co-enzyme bound to TrxR1, to a selenenylsulphide group within TrxR1, before regenerating reduced Trx1 (Zhong *et al.* 2000a and Cheng *et al.* 2009).

The contribution of dysregulated Ref-1 signalling to pathogenesis is highlighted by the observation that enhanced Ref-1 expression has been reported in numerous cancers (Thakur *et al.* 2014) and has been correlated with poor prognosis and resistance to chemo-/radiotherapy in multiple cancers (Yang *et al.* 2013b, Mahjabeen *et al.* 2013 and Cao *et al.* 2020). The redox function of Ref-1 is likely key within many cancers to maintain the activity of transcription factors driving tumorigenesis. As intracellular ROS is often elevated in cancer cells, and is in turn relied upon by cancer cells to enhance cell proliferation, cell survival and metabolic adaptation (Weinberg *et al.* 2010). Indeed, drug inhibition of Ref-1's redox inhibition has shown good efficacy in inhibiting dysregulated transcription factor activity within cancer cell lines. Including STAT3 (Cardoso *et al.* 2012 and Caston *et al.* 2021), HIF-1α (Fishel *et al.*

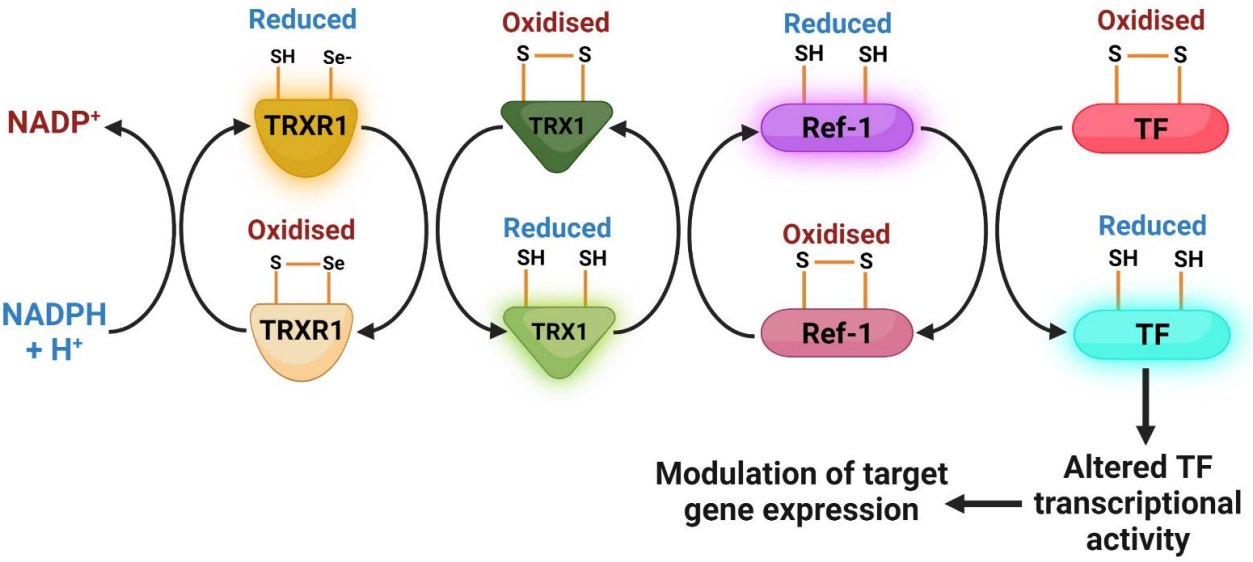


**Figure 1.10. The redox regulation of target transcription factors by Ref-1 relies on the thioredoxin antioxidant system.** Ref-1 reduces oxidised cysteine residues typically residing in the transactivation domain of target transcription factors. Ref-1 mediated reduction of TFs usually transactivates them, enhancing their DNA binding ability. Oxidised cysteines within Ref-1's active site must be reduced in turn for Ref-1 activity to be restored. This is achieved through a redox relay involving thioredoxin 1 (TRX1) and thioredoxin reductase 1 (TRXR1), which transfer electrons from NADPH to oxidised Ref-1 cysteines. Activity of the thioredoxin antioxidant system itself is affected by redox status (i.e., oxidative stress) within the cell, which will in turn modulate Ref-1 activity through the mechanism just highlighted. Figure was created through the use of Biorender.

2011 and Logsdon *et al*. 2016) and NF-κB (Nishi *et al.* 2002). The Ref-1 inhibitors used within these studies, crucially represses Ref-1's redox function without compromising Ref-1's DNA repair function (Shah *et al.* 2017). And authors saw either downregulated STAT3/HIF-1α/NF-κB driven luciferase activity or target gene expression. Within these studies Ref-1 inhibition resulted in repressed cancer cell proliferation and cell survival. Additionally inhibiting the thioredoxin system, which as described regenerates active Ref-1, has shown good efficacy in inhibiting STAT3 within cancer cell lines (Busker *et al.* 2020). Aside from stimulating HIF-1α and STAT3 activity by reducing oxidised cysteines within the transcription factors transactivating domains. Ref-1 has been shown to meditate recruitment of the transcriptional co-activators p300/CBP to HIF-1α and STAT3 target gene promoters (Ema *et al.* 1999, Carrero *et al.* 2000 and Gray *et al*. 2005). Therefore, targeting HIF-1α and STAT3 upstream by targeting Ref-1's redox function, may be effective within TSC model cells at inhibiting these transcription factor's dysregulated activity, downstream target gene expression and may decrease cell proliferation and cell survival.

## 1.11 Hypoxia

As previously mentioned, tissues predominantly affected by TSC have hypoxic gradients across them as part of their typical functioning (Northrup *et al.* 2013). Hypoxia may have several important functional consequences for TSC pathology, especially for the signalling pathways explored within this work. As described, hypoxia stabilises HIF1-α protein (Majmundar *et al.* 2010), but also has been found to be drive HIF-1α mediated transcription involving Ref-1 and STAT3 (Ziel *et al.* 2004, Gray *et al.* 2005, Logsdon *et* al. 2016 and Kobayashi *et al.* 2021). Similarly, within cancer cell lines, hypoxia has been found to stimulate STAT3 activity (Gray *et al.* 2005, Pawlus *et al.* 2014 and Soleymani Abyaneh *et al.* 2017). Hypoxia may also impact Ref-1 function within TSC cells. Ref-1 mRNA expression within colon cancer cells has been shown to be elevated under hypoxia (Yao *et al.* 1994). Additionally, ROS has been found to modulate Ref-1 expression (reviewed within Bhakat *et al.* 2009) and Ref-1s nuclear translocation (Tell *et al*. 2000 and Chen *et al.* 2010). While hypoxia has been observed to elevate levels of intracellular ROS through multiple pathways (Wang *et al.* 2007b and Kondoh *et al.* 2013), which may in turn stimulate Ref-1 activity through ROS production within TSC model cells. A stimulatory effect by hypoxia on HIF-1α, STAT3 and Ref-1 may further enhance pathogenic signalling within the context of TSC. Therefore, within this work, the effect of hypoxia on measurable tumorigenic outputs of TSC cells will be assayed, as will hypoxias effect on HIF-1α and STAT3 signalling.

## 1.12 improving therapies for TSC patients.

To better contextualise the present work, it is worth considering the research conducted so far in either improving mTORC1 inhibitors or identifying novel vulnerabilities of TSC cells that can be targeted independently or in concert with mTORC1 inhibition.

### 1.12.1 Improving efficacy of mTOR inhibitor based therapies.

Over the years, newer more potent mTOR inhibitors have been developed in the hope to provide better treatments for TSC patients and cancer where PI3K/AKT/mTORC1 signalling drives tumorigenesis. Several ATP-competitive mTOR inhibitors have been developed, which can inhibit both mTORC1 and mTORC2 complexes and overcome the overcome the incomplete inhibition of mTORC1 by rapalogues (Cho *et al*. 2008 and Thoreen and Sabatini, 2009). However, whilst pre-clinical studies of these 2$^{nd}$ generation mTOR inhibitors showed promising drug indications, in later clinical trials these inhibitors often showed only marginal benefit and significant toxicity (Naing *et al.* 2012, Carlo *et al.* 2016, Powles *et al.* 2016 and Graham *et al.* 2018).

Other research studies have instead focused on compensating for undesirable pro-survival effects that can be induced by rapalogue based mTORC1 inhibitors, as part of the therapeutic strategy to potentiate the efficacy of rapalogues. For example, in cells with chronically active mTORC1 signalling, such as those lacking functional *TSC1* or *TSC2*, Akt signalling is constitutively inhibited (Zhang *et al.* 2003). Akt activation promotes cell survival and resistance to apoptosis. Therefore, the fact that rapamycin induces Akt activation (Wan *et al.* 2007), attenuates mTORC1 inhibitor's therapeutic potential in targeting *TSC1* or *TSC2* deficient cells. Therefore, dual inhibition of both mTORC1 and Akt has been proposed as a strategy to improve the efficacy of mTORC1 inhibitors in treating TSC. Ji *et al.* (2017) found that combinatorial treatment of rapamycin and the Akt inhibitor MK-2206 repressed *Tsc1* and *Tsc2* null MEF cell proliferation further than either drug alone, in addition to inducing apoptosis in these cell lines. Furthermore, combinatorial treatment of rapamycin and MK-2206 decreased tumour size in a *Tsc1* null MEF xenograft tumour mouse model further than either rapamycin or MK-2206 alone. Similarly, Govindarajan *et al.* (2012) found combinatorial treatment with rapamycin and the tyrosine kinase inhibitor Imatinib (targets PDGFRβ signalling to Akt), suppressed Akt activation and substantially decreased tumour volume in a mouse TSC xenograft model further than either rapamycin or Imatinib treatment alone. Rapamycin treatment has also been shown to promote activation of the pro-survival ERK/MAPK signalling pathway by relieving mTORC1 mediated suppression of this signalling pathway (Carracedo *et al.* 2008). Similarly, to the dual targeting of Akt and mTORC1 signalling, combinatorial treatment of rapamycin and the MEK1/2 (constituent of the ERK/MAPK pathway) inhibitor PD98059 suppressed *Tsc2* −/− MEF proliferation to a greater extent than rapamycin or PD98059 alone (Mi *et al.* 2009). Lastly, as briefly described in section 1.5.4 of this chapter, mTORC1 signalling represses autophagy by inhibiting ULK1 and ATG13 (Jung *et al.* 2009). Consequently, rapalogue inhibition of mTORC1 leads to induction of autophagy, which has been shown to promote survival of TSC cells (Parkhitko *et al.* 2011). The addition of autophagy inhibitors to rapamycin treatment has been shown to preferentially promote apoptosis in *Tsc2* −/− MEF and *TSC2* deficient AML cells relative to *TSC2* competent control cells (Alayev *et al.* 2014) and to be more effective at decreasing the growth of *TSC2*-null xenograft tumours in mice compared to rapamycin or autophagy inhibitor alone (Parkhitko *et al.* 2011).

### 1.12.2 The search for alternative therapies to mTOR inhibition.

In the search for better therapies for TSC patients, a number of studies have attempted to exploit vulnerabilities of TSC diseased cells that do not rely on inhibition of mTORC1. Instead, many studies have focused on targeting the many facets of TSC cells imbalanced cell homeostasis to find alternate therapeutic strategies. For instance, as mTORC1 is a master

regulator of cell growth and proliferation in response to the energy and nutrient status of the cell (Kim and Guan, 2019), hyperactivity of the mTORC1 pathway leads to perturbations in the metabolism of TSC cells which can be exploited for potential therapies. For example, mTORC1 hyperactivity promotes glucose and glutamine addiction in *Tsc2* −/− MEF cells by upregulating glycolytic (Choo *et al.* 2010 and Düvel *et al.* 2010) and glutaminolysis pathways (Csibi *et al.* 2013). Jones *et al.* (2019) showed in *Tsc2* +/− mice that long term drug inhibition of both glycolysis and glutaminolysis reduced both size and number of renal lesions. While Csibi *et al.* (2013) found pharmacologic inhibition of both glycolysis and glutaminolysis resulted in significant and selective cell death in *Tsc2* −/− MEF cells. Other studies have focused on the elevated endoplasmic reticulum (ER) stress present in TSC cells, the result of the accumulation of unfolded protein in response to mTORC1 hyperactivity potently upregulating global protein synthesis, whilst simultaneously repressing autophagy (Appenzeller-Herzog and Hall, 2012). Enhancing ER stress, whilst inhibiting autophagy was shown to promote selective cell death in *Tsc2* deficient cell lines (Johnson *et al.* 2015 and McCann *et al.* 2018). TSC cells are thought to maintain proteostasis and prevent cell death in the absence of typical autophagy by upregulating proteasome activity through mTORC1 (Zhang *et al.* 2014a). Johnson *et al.* (2018a) found enhancing ER stress through nelfinavir treatment while simultaneously inhibiting the proteasomal degradation pathway through bortezomib treatment potently and selectively killed *Tsc2* deficient cells with minimal toxicity in *Tsc2* competent control cells. Another facet of TSC cells warped homeostasis found to be a potential avenue that could be exploited pharmacologically is redox homeostasis. Increasing evidence indicates loss of either *TSC1* or *TSC2* disrupts redox homeostasis and elevates oxidative stress in cells (Chen *et al*. 2008, Suzuki *et al.* 2008 and Di Nardo *et al.* 2009). As found with drugs which elevated metabolic and proteostatic stress in the aforementioned studies, enhancing oxidative stress further in *TSC2* deficient cells was found to show promising therapeutic effects. Drugs which reduced the antioxidant capacity of cells, such as chelerythrine (Medvetz *et al.* 2015) or glutaminase inhibitors (Li *et al.* 2015a) selectively induced cell death in multiple *TSC2* deficient cell lines. While Malik *et al.* (2015) found drug inhibition of glutamate-cysteine ligase catalytic subunit, a key enzyme in the biosynthesis of the cellular antioxidant glutathione, arrested growth and induced cell death in cells derived from SEGAs.

An increasing number of studies indicate that loss of *TSC1* or *TSC2* promotes a dysregulated inflammatory response (Boorjian *et al.* 2009, Makovski *et al.* 2014, Prabowo *et al.* 2013, Grabole *et al.* 2016 and Martin *et al.* 2017). Therefore, immunotherapy based treatments have also been explored *in vitro* and in animal models as a potential avenue of treatment for TSC. For example, as described in section 1.8 of this chapter, hyperactivity of the JAK/STAT3 pathway has been described in both TSC model cells and TSC associated lesions (Onda *et*

*al.* 2002, El-Hashemite and Kwiatkowski, 2005 and Goncharova *et al.* 2009), as has elevated production of IL-6 (Goncharova *et al.* 2012 and Lesma *et al*. 2014). Among STAT3 signalling's pleiotropic effects is the regulation of inflammation. Wang *et al.* (2021a) found blockade of IL-6 signalling through an anti-IL-6 neutralising antibody suppressed *TSC2* deficient cell proliferation and reduced the renal tumour burden in *Tsc2* +/− mice. A similar strategy of targeting cytokine/growth factor signalling was shown to be effective by Lesma *et al.* (2015). The authors previously found that proliferation and survival of cells isolated from a LAM/TSC patient were dependent on epidermal growth factor (EGF) signalling (Lesma *et al.* 2008). Repressing EGF signalling through a EGF receptor antagonising antibody, decreased the number and size of lung nodules in a LAM/TSC nude mouse model (Lesma *et al.* 2015). Other immunotherapy based strategies that have shown good therapeutic potential involve immune checkpoint blockade. That is reactivating suppressed activity of immune cells (such as T-cells) to mediate antitumour effects, typically by inhibiting/blocking expression of coinhibitory immune checkpoint receptors on T cells (Wei *et al.* 2018). One such coinhibitory immune checkpoint receptor that suppresses T-cell activity is programmed cell death protein 1 (PD-1). Liu *et al*. (2018) observed levels of T-cells are ~8 fold higher in AMLs relative to normal kidney tissue. With Liu *et al.* (2018) reporting elevated expression of PD-1 in those T-cells, and Maisel *et al.* (2018) finding elevated expression of PD-1's coinhibitory ligand PD-L1 in nodules from human LAM patients. Anti-PD1 blocking antibody treatments substantially suppressed tumour growth in a *Tsc2* deficient mouse model (Liu *et al.* 2018), with 37% of the mice showing complete tumour rejection 100 days after treatment.

Whilst pre-clinical, collectively these studies highlight that alternative therapies which target aberrant cell signalling pathways other than mTORC1 could lead to better treatments for TSC patients. The work contained within the present thesis is a contribution to this body of research, aiming to better elucidate mTORC1 dependent and independent signalling processes that contribute to TSC pathology and evaluate the efficacy of drug inhibition of such pathways against conventional mTORC1 inhibitors.

## 1.13 Central Hypothesis and Aims of This Project

Whilst rapamycin based drugs show clear clinical benefit for TSC patients, they do not normalise all signalling pathways that have been observed to be dysregulated upon loss of either *TSC1* or *TSC2*. To provide better therapies for TSC patients that can be used as single agents or in adjunct therapy with mTORC1 inhibitors, the mechanisms driving TSC pathology need to better defined. Especially those independent or not wholly reliant on mTORC1 signalling.

The main hypothesis of the present work is that tumorigenic and pro-angiogenic signalling observed within TSC is in part mediated through a signalling axis involving Ref-1, STAT3 and HIF-1α, with potential input from mTORC1 activity. The central objective of this work is to better characterise the Ref-1/STAT3/HIF-1α signalling axis and to assay whether drug inhibition of this axis shows desirable therapeutic effects *in vitro* within TSC model cell lines.

The main aims of this work were as follows:

1. Assess the efficacy of inhibitors targeting Ref-1, STAT3, HIF-1α or NF-κB in decreasing measurable tumorigenic outputs of *TSC2* deficient cells against efficacy of mTORC1 inhibitors.

2. Further characterise dysregulated HIF-1α and proangiogenic signalling within *TSC2* deficient cells and contrast the ability of Ref-1, STAT3 and mTORC1 inhibitors at normalising aberrant HIF-1α and proangiogenic signalling.

3. Better characterise mechanisms and outputs of dysregulated STAT3 signalling within *TSC2* deficient cells.

4. Further define the relationship between mTORC1 and STAT3 activity within *TSC2* deficient cells.

5. Briefly assess response of *TSC2* deficient cells to oxidative stress and it's input into HIF-1α and STAT3 signalling.

# Chapter 2. Materials and Methods

In general, experimental procedures were performed following standard protocols of the Tee lab. When procedures and kits were individualised, changes are indicated.

## 2.1 Materials

Reagents, kits, and equipment used for the research within this thesis are listed in the tables below. Reagents, kits and equipment and their supplier used for the outsourced mRNA sequencing are mentioned in the main text instead.

**Table 2.1 Reagents**

| Name | Supplier | Catalogue Number |
|---|---|---|
| ABsolute qPCR Plate Seals | Thermo Scientific | AB1170 |
| Acetic acid | Sigma-Aldrich | 695092 |
| Acridine Orange/Propidium Iodide Stain | Logos Biosystems | F23001 |
| Agarose (Low-EEO/Multi-Purpose/Molecular Biology Grade) | Fisher Scientific | BP160500 |
| Amersham ECL Select Western Blotting Detection Reagent | Cytiva | RPN2235 |
| Antipain dihydrochloride from microbial source | Sigma-Aldrich | A6191 |
| Anti-rabbit IgG, HRP-linked Antibody | CST | 7074 |
| Anti-mouse IgG, HRP-linked Antibody | CST | 7076 |
| Benzamidine | Sigma-Aldrich | 12072 |
| Bovine Serum Albumin | Sigma-Aldrich | A7906 |
| Bradford Reagent | Sigma-Aldrich | B6916 |
| Bromophenol Blue | Sigma-Aldrich | B0126 |
| DIFCO Noble Agar | BD | 214230 |
| Dimethyl sulfoxide | Sigma-Aldrich | D2650 |
| DL-Dithiothreitol | Roche | DTT-RO |
| Ethanol | Fisher Scientific | E/0600DF/17 |
| Ethylenediaminetetraacetic Acid, Di Na Salt Dihydr. | Fisher Scientific | BP120-1 |
| Flag-TSC2/pcDNA3.1 | Gifted by Prof. Cheryl Walker (Baylor College of Medicine) | |
| GelRed Nucleic Acid Gel Stain | Biotium | 41002 |
| Glycerol | Sigma-Aldrich | G6279 |
| Goat IgG HRP-conjugated Antibody | R&D Systems | HAF017 |
| HIF1 Luciferase Reporter Vector | Affymetrix | LR0128 |
| Hydrochloric Acid (~37%) | Fisher Scientific | H/1150/PB17 |
| Immobilon-P PVDF Transfer Membrane | Millipore | IPVH00010 |
| NuPAGE MES SDS Running Buffer (20X) | Invitrogen | NP0002 |
| NuPAGE Tris-Acetate SDS Running Buffer (20X) | Invitrogen | LA0041 |
| Ionic Detergent Compatibility Reagent | Thermo Scientific | 22663 |
| Leupeptin | Sigma-Aldrich | L8511 |

| | | |
|---|---|---|
| Matrigel Basement Membrane Matrix, LDEV-free | Corning | 354234 |
| Methanol | Sigma-Aldrich | M/4000/17 |
| MicroAmp Optical 96-Well Reaction Plate | Applied Biosystems | N8010560 |
| Nuclease free water | Invitrogen | AM9937 |
| NuPAGE 3 to 8%, Tris-Acetate, 1.0 mm, Mini Protein Gels | Invitrogen | 12085655 |
| NuPAGE 4 to 12%, Bis-Tris, 1.0 mm, Mini Protein Gels | Invitrogen | 10247002 |
| Orange G | Sigma-Aldrich | O3756 |
| pcDNA3.1 | Gifted by Prof. John Blenis (Harvard University) | |
| Pepstatin A | Sigma-Aldrich | P5318 |
| Phenylmethylsulfonyl fluoride | Sigma-Aldrich | PMSF-RO |
| Phosphate buffered saline | Sigma-Aldrich | P4417 |
| Pierce™ 660nm Protein Assay Reagent | Thermo Scientific | 22660 |
| Prestained Protein Ladder – Broad molecular weight (10-245 kDa) | Abcam | ab116028 |
| pRL Renilla Luciferase Control Reporter Vector | Promega | E2231 |
| Quantitative PCR Human Reference Total RNA | Agilent | 750500 |
| RNAprotect Cell Reagent | QIAGEN | 76526 |
| Skimmed Milk Powder | Millipore | 70166 |
| Sodium Chloride | Sigma-Aldrich | S7653 |
| Sodium deoxycholate | Sigma-Aldrich | 30970 |
| Sodium dodecyl sulfate | Sigma-Aldrich | L4390 |
| Sodium Hydroxide | Sigma-Aldrich | S8045 |
| Sodium orthovanadate | Sigma-Aldrich | S6508 |
| Sucrose | Sigma-Aldrich | 84100 |
| Triton X-100 | Sigma-Aldrich | X100 |
| Trizma base | Sigma-Aldrich | T1503 |
| Trizma hydrochloride | Sigma-Aldrich | T3253 |
| TWEEN 20 | Sigma-Aldrich | P1379 |
| Whatman Paper | Cytiva | 3030-917 |
| β-Mercaptoethanol | Sigma-Aldrich | M3148 |

**Table 2.2 Kits**

| Name | Supplier | Catalogue Number |
|---|---|---|
| CyQUANT Cell Proliferation Assay | Invitrogen | C7026 |
| Dual-Luciferase Reporter Assay System | Promega | E1960 |
| DuoSet ELISA Ancillary Reagent Kit 2 | R&D Systems | DY008B |
| GoldStar PCR Mix | Eurogentec | PK-0064-02 |
| Human HGF DuoSet ELISA | R&D Systems | DY294 |
| Human IL-6 DuoSet ELISA | R&D Systems | DY206 |

| | | |
|---|---|---|
| Human IL-6/IL-6R alpha Complex DuoSet ELISA | R&D Systems | DY8139 |
| Human VEGF DuoSet ELISA | R&D Systems | DY293B |
| jetPEI HTS DNA transfection reagent | VWR | 101000053 |
| Nuclear Extract Kit | Active Motif | 40010 |
| QIAshredder | QIAGEN | 79656 |
| Qubit RNA Broad Range Assay Kit | Invitrogen | Q10210 |
| Reverse Transcriptase Core kit | Eurogentec | RT-RTCK-03 |
| RNeasy Plus Mini Kit | QIAGEN | 74134 |
| Takyon ROX SYBR 2X MasterMix dTTP blue | Eurogentec | UF-RSMT-B0701 |
| TransAM STAT3 Transcription Factor ELISA Kit | Active Motif | 45196 |

**Table 2.3 Equipment**

| Name | Supplier |
|---|---|
| 7500 Real time PCR Systems | Applied Biosystems |
| Amersham ImageQuant 800 | Cytiva |
| Binder CB150 hypoxic chamber | BINDER |
| BioDoc-It Imaging Sytem | UVP |
| Bioruptor | Diagenode |
| Corning CoolCell Cell Freezing Container | Corning |
| Cytation 3 plate reader | BioTek |
| EVOSXL Core Imaging System - Microscope | Life Technologies |
| G-Storm Thermal Cycler | LabTech |
| Hoefer Blot Module for MiniVE Mini Vertical Electrophoresis Unit | Hoefer |
| Jenway 3510 benchtop pH meter | Jenway |
| Qubit 2.0 Fluorometer | Invitrogen |
| SE300 miniVE Integrated Vertical Protein Electrophoresis and Blotting Unit | Hoefer |
| TR717 Microplate Luminometer | Applied Biosystems |
| XCell SureLock Mini-Cell Electrophoresis System | Invitrogen |

**Table 2.4 Drugs, Antioxidants and Cytokines**

| Name | Supplier | Catalogue Number | Solvent |
|---|---|---|---|
| 1S,3R-RSL 3 | Sigma-Aldrich | SML2234 | DMSO |
| APX2009 | Gifted by Professor Mark Kelley (Indiana University) | | DMSO |
| APX2014 | Gifted by Professor Mark Kelley (Indiana University) | | DMSO |
| APX3330 | Gifted by Professor Mark Kelley (Indiana University) | | DMSO |
| DMNQ, non-alkyiating redox cycling quinone | Abcam | ab144626 | DMSO |
| Etoposide (VP-16) | Selleckchem | S1225 | DMSO |
| FLLL31 | Sigma-Aldrich | F9057 | DMSO |
| Glutathione reduced ethyl ester | Sigma-Aldrich | G1404 | Water |
| JSH-23 | Sigma-Aldrich | J4455 | DMSO |
| KU0063794 | Selleckchem | S1226 | DMSO |
| ML 385 | Bio-Techne | 6243 | DMSO |
| N-Acetyl-L-cysteine | Sigma-Aldrich | A7250 | DMEM |
| Rapamycin | Sigma-Aldrich | R8781 | DMSO |
| Recombinant human IL-6 protein | Abcam | ab198571 | Water |
| Rotenone | Sigma-Aldrich | R8875 | DMSO |
| STAT3 Inhibitor XIII, C188-9 | Sigma-Aldrich | 573128 | DMSO |
| Trolox | Tocris | 6002 | Ethanol |

**Table 2.5 General Cell Culture**

| Name | Supplier | Catalogue Number |
|---|---|---|
| 96-well Flat Clear Bottom Black Polystyrene TC-treated Microplates (Sterile) | Corning | 3603 |
| Dulbecco′s Modified Eagle′s Medium - high glucose | Sigma-Aldrich | D6429 |
| Trypsin-EDTA (0.25%), phenol red | Gibco | 25200056 |
| Fetal Bovine Serum | Sigma-Aldrich | F7524 |
| Penicillin-Streptomycin | Sigma-Aldrich | P0781 |
| Opti-MEM I Reduced Serum Medium | Thermo Scientific | 31985070 |
| Recovery Cell Culture Freezing Medium | Gibco | 12648010 |
| 6-well Tissue Culture Plate | TPP | 92006 |
| 12-well Tissue Culture Plate | TPP | 92012 |
| 24-well Tissue Culture Plate | TPP | 92024 |
| 75cm2 Tissue Culture Flask | TPP | 90076 |
| 300cm2 Tissue Culture Flask | TPP | 90301 |
| 40mm Tissue Culture Plate | TPP | 93040 |
| 60mm Tissue Culture Plate | TPP | 93060 |
| 100mm Tissue Culture Plate | TPP | 93100 |

**Table 2.6 Antibodies**

| Target | Company | Catalogue number | Dilution used (v/v) | Predicted Band Size (kDa) |
|---|---|---|---|---|
| β-Actin | CST | 4970 | 1/5000 | 45 |
| AIFM2/FSP | Protein Tech | 20886-1-AP | 1/2000 | 41 |
| ANGPTL4 | Abcam | ab115798 | 1/1000 | 45 |
| APE1/Ref-1 | Novus Bio | NB100-116 | 1/1000 | 37 |
| BNIP3 | Novus Bio | NBP2-67192 | 1/2000 | 21 |
| Catalase | R&D Systems | AF3398 | 1/500 | 64 |
| GPX8 | Protein Tech | 16846-1-AP | 1/2000 | 24 |
| HIF1-α | BD Biosciences | 610959 | 1/750 | 120 |
| HIF1-α | CST | 14179 | 1/1000 | 120 |
| HMOX1 | Abcam | Ab68477 | 1/4000 | 33 |
| JAK2 | CST | 3230 | 1/1000 | 125 |
| p-JAK2 (Y1007/1008) | CST | 3776 | 1/1000 | 125 |
| NRF2 | Novus Bio | NBP1-32822 | 1/1000 | 68 |
| NF-κB/RelA | CST | 8242 | 1/1000 | 65 |
| NF-κB/p-RelA (S536) | CST | 3033 | 1/1000 | 65 |
| rpS6 | CST | 2317 | 1/4000 | 32 |
| p-rpS6 (S235/236) | CST | 2211 | 1/4000 | 32 |
| SirT1 | CST | 9475 | 1/1000 | 120 |
| SOCS3 | Abcam | ab16030 | 1/2000 | 24 |
| STAT3 | CST | 9139 | 1/2000 | 86 |
| p-STAT3 (S727) | CST | 9134 | 1/1000 | 86 |
| p-STAT3 (Y705) | CST | 9145 | 1/2000 | 86 |
| Thioredoxin 1 | R&D Systems | AF1970 | 1/500 | 12 |
| Thioredoxin 2 | R&D Systems | AF3254 | 1/500 | 12 |
| Tuberin/TSC2 | CST | 4308 | 1/1000 | 200 |
| p-4E-BP1 (P65) | CST | 9451 | 1/1000 | 20 |
| p-4E-BP1 (T37/40) | CST | 9459 | 1/1000 | 20 |

## 2.2. Buffers

Buffers used for research within this thesis and their composition are listed in the tables below. Double-distilled water was used in the preparation of buffers unless otherwise stated. Hydrochloric acid and sodium hydroxide solution were used to adjust buffer pH as needed.

| Western Blotting – Transfer Buffer - 10X | |
|---|---|
| **Component** | **Concentration** |
| Trizma base | 250 mM |
| Glycine | 1.92 M |
| Sodium dodecyl sulphate (SDS) | 6.94 mM |

| Tris-Buffered Saline (TBS) - 10X | |
|---|---|
| **Component** | **Concentration** |
| Trizma base | 200 mM |
| Sodium Chloride | 1.37 |

- pH of TBS buffer is adjusted to 7.6.
- To make TBS-TWEEN (TBS-T), TWEEN-20 is added at 0.1% v/v to 1X TBS.

| Tris base, Acetic acid and EDTA (TAE) Buffer - 10X | |
|---|---|
| **Component** | **Concentration** |
| Trizma base | 400 mM |
| Acetic Acid | 200 mM |
| Ethylenediaminetetraacetic Acid (EDTA) | 10 mM |

| Laemmli Sample Buffer | |
|---|---|
| **Component** | **Concentration** |
| Trizma hydrochloride | 62.5 mM |
| SDS | 2% w/v |
| Glycerol | 10% v/v |
| DL-Dithiothreitol (DTT) | 50 mM |

- pH of Laemmli Sample Buffer is adjusted to 7.6 before SDS is added.
- DTT is added fresh before lysis and protein lysates standardisation.

| RIPA Buffer | |
|---|---|
| **Component** | **Concentration** |
| Trizma hydrochloride | 50 mM |
| TritonX-100 | 1% v/v |
| Sodium Chloride | 150 mM |
| Sodium Deoxycholate | 0.5% w/v |
| SDS | 0.1% w/v |

- pH of RIPA is adjusted to 7.6 before SDS is added.

| Orange G Loading Buffer – 5X (50 mL) | |
|---|---|
| **Component** | **Amount** |
| Sucrose | 8 g |
| EDTA (0.5 M) | 5 mL |
| Orange G | Spatula tip |

## 2.3. Methodology

### 2.3.1 General Cell Culture

The human TSC model cell lines used within this work were the *TSC2* deficient angiomyolipoma (AML) 621-102 cells and *TSC2* re-expressed (RE) AML 621-103 cells, both of which were a kind gift from Dr. L. Henske (Harvard University). The AML cell lines had previously been established by other groups as follows. Single cell cultures were established from patient derived angiomyolipoma tissue through collagenase digestion as described in Yu *et al.* (2004). Hong *et al.* (2008) generated the 621-102 and the 621-103 AML cells lines. The authors generated the stable AML 621-102 (previously termed TRI102) cell line from primary cultures of *TSC2* null human AML cells (Yu *et al.* 2004) through transfection of these cells with E6/E7 (pLXSN 16E6E7-neo) and human telomerase (pLXSN hTERT-hyg) plasmids. The 621-103 AML cell line (previously termed TRI102) was generated through stable transfection of the 621-102 AML cell line with wild-type TSC2 (pcDNA3.1 TSC2-zeo). The murine TSC model cell lines used within this work were the *Tsc2* −/− (*Tp53*−/−) mouse embryonic fibroblasts (MEFs) and the *Tsc2* +/+ (wildtype) (*Tp53*−/−) MEFs, which were a kind gift from Prof. D. Kwaitowski (Harvard University). Both MEF cell lines were established by Zhang *et al.* (2003) by littermate pair crossings. Both MEF cell lines were null for *Tp53* as authors found MEF cells

null for *Tsc2* alone showed early senescence. Therefore, Zhang *et al.* (2003) interbred *Tsc2*+/− mice with *Tp53*−/− mice to generate *Tsc2*+/− *Tp53*−/− mice, which in turn were interbred to generate *Tsc2* −/− *Tp53*−/− embryonic fibroblasts. *Tp53* loss rescued *Tsc2* loss induced senescence. *Tsc2* +/+ *Tp53*−/− embryonic fibroblasts were generated in the same manner. The human non-TSC cells used within this work were the human kidney 2 (HK2) cell line and the human embryonic kidney 293 (HEK-293) cell line. The HK2 cell line were a kind gift from Dr. S. Land (Dundee University) while the HEK-293 cell line was a kind gift from Prof. J. Blenis (Cornell University), with both cell lines originally purchased from ATCC. The HK2 cell line was originally immortalised through viral transduction of primary cells with the human papilloma virus (HPV 16) E6/E7 genes (Ryan *et al.* 1994). The HEK-293 cell line was originally generated through transformation of primary HEK cells with sheared fragments of human adenovirus 5 DNA (Graham *et al*. 1997).

Unless otherwise stated, AML cells lines were grown in Dulbecco′s modified Eagle′s medium (DMEM) supplemented with 15% (v/v) foetal bovine serum and 1% v/v penicillin streptomycin (Pen-Strep). Unless otherwise stated MEF, HEK-293 and HK2 cells were cultured in DMEM supplemented with 10% (v/v) foetal bovine serum and 1% v/v Pen-Strep. Cell lines were incubated in a humidified incubator with 5% $CO_2$ and 21% $O_2$ (normoxia) at 37$^{o}$C, unless otherwise stated, and split when confluent. For hypoxic (hypoxia) culture conditions, cells were incubated in a humidified Binder CB150 hypoxic chamber with 5% $CO_2$ and 1% $O_2$ at 37 $^{o}$C. Adherent cells were dissociated from tissue culture plastic through two sequential washes with trypsin-EDTA, which was aspirated off before incubation for 3 – 5 minutes at 37 $^{o}$C.

For long-term cell storage, cells were first trypsinised as previously described before resuspension in DMEM. Cells were then spun down at 5 min at 2000 rpm. Pelleted cells were then resuspended in 1 mL of recovery cell culture medium before being transferred to cryogenic vials that were initially frozen in a cell freezing container. Cryogenic vials were then transferred and kept in liquid nitrogen storage.

#### 2.3.1.1 Cell Treatments

Prior to generating RNA and protein lysates, all cell lines were cultured in DMEM (supplemented with 1% v/v Pen-Strep and 10% v/v FBS unless otherwise stated) with no drug, DMSO or the specified drug/antioxidant/cytokine for the time specified in the appropriate figure. Treated/untreated cells were then grown either under hypoxia or normoxia as previously described. Before any treatment cells were allowed to grow to a minimum of 70% confluency.

#### 2.3.1.2 Conditioned Media Treatments

To generate conditioned media for treatment of cells, either the AML or MEF cell lines were seeded at equal numbers in 100 mm tissue culture plates in DMEM and grown to confluency in a humidified incubator with 5% $CO_2$ and 21% $O_2$. Cells were then washed with serum free DMEM before equal volumes of fresh DMEM (supplemented with 1% v/v Pen-Strep and 10% v/v FBS unless otherwise stated) were applied and cells were incubated either under normoxia or hypoxia for 24 h. Conditioned media was then collected, and dead/floating cells were removed through centrifugation at 2500 rpm. Generated conditioned media was then used to treat confluent cells, washed with serum free DMEM, for the time specified in the appropriate figure.

#### 2.3.1.3 Drug Concentrations

Selectivity experiments (chapters 3 and 6) within this work informed the maximum dose of drugs used before cytotoxicity was observed.

Concentrations of the Ref-1 inhibitors (APX3330, APX2009 and APX2014) used within the present work were informed by guidance from the provider of these drugs, and expert in the field of Ref-1 signalling and drug inhibition, Prof. Mark Kelley. Drug concentrations of Ref-1 inhibitors used were the same or close to drug concentrations found to show desirable drug effects, e.g., inhibition of Ref-1's target transcription factors activity, in both pancreatic cancer cell lines (Fishel *et al.* 2011, Cardoso *et al.* 2012, Logsdon *et al.* 2016 and Logsdon *et al.* 2018) and prostate cancer cell lines (McIlwain *et al.* 2018). Furthermore, Champion *et al.* (2022) (a paper which this thesis contributed to) found in the *Tsc2* −/− MEF cell line, the same concentrations of APX3330 and APX2009 used within this thesis were sufficient to block activity of the Ref-1 target transcription factors HIF-1α, STAT3 and NF-κB, as assessed by luciferase assay.

Concentrations of mTOR inhibitors used for drug treatments were informed by the large body of research within the TSC model cell lines by the Tee lab and the wider TSC research community. 50 nm was the concentration of rapamycin used within this work, which has been shown to be sufficient to inhibit phosphorylation of downstream mTORC1 substrates (Dodd *et al.* 2015, Brugarolas *et al.* 2004, Land and Tee, 2007 and Tee *et al.* 2003b). 1 μM was the concentration of Ku-0063794 used within this work as García-Martínez *et al.* (2009) found 1 μM was able to completely suppress mTORC1 and mTORC2 activity without suppressing activity of 76 other kinases the authors tested.

FLLL31 concentrations used (largely 5 µM and 10 µM) were informed by a previous publication by the Tee lab (Dodd *et al*. 2015) in which FLLL31 repressed STAT3 mediated HIF-1α expression. Additionally, the paper initially characterising the efficacy of FLLL31 to inhibit STAT3 phosphorylation, found 5 µM of FLLL31 was sufficient to potently suppress JAK2 kinase activity and phosphorylation of STAT3 at Y705 in both pancreatic and breast cancer cell lines (Lin *et al.* 2010). Initial concentration range of C188-9 chosen was based on the paper initially characterising the efficacy of C188-9 in inhibiting STAT3 compared to the parent compound C188 (Bharadwaj *et al.* 2016). The authors found the $IC_{50}$ range for inhibiting constitutive STAT3 phosphorylation in four head and neck squamous cell carcinoma cell lines was between 10.6 µM and 22.8 µM. Early into the research contained in this thesis, a range of C188-9 concentrations were tested (1.875 – 60 µM) to inhibit constitutive STAT3 phosphorylation in *Tsc2* −/− MEF cells and reduce HIF-1α transcriptional activity (by way of luciferase assay) in *Tsc2* −/− MEF cells (see chapter 2, figure 4.7). Based on this work the primary C188-9 concentrations selected for treatment were primarily 15 and 30 µM.

Concentrations of the NF-κB inhibitor JSH23 chosen for this work, typically 10 and 20 µM, was based on the paper initially characterising efficacy of this compound to inhibit lipopolysaccharide (LPS) induced NF-κB nuclear translocation (Shin *et al.* 2004). Authors found 10 µM of JSH23 reduced NF-κB transcriptional activity by ~68% in LPS stimulated RAW 264.7 macrophage cells, as assessed by NF-κB reporter gene expression. Additionally, 10 µM of JSH23 has been shown to effective in reducing NF-κB target gene expression in other non-TSC cell lines (Gaultier *et al.* 2008, Zhang *et al.* 2016 and Li *et al.* 2018).

The initial concentration range of the Nrf2 inhibitor ML385 (1.25 – 20 µM) selected for this work was based on the paper initially characterising efficacy of this compound at inhibiting Nrf2 activity in the lung cancer cell line A549, which showed elevated Nrf2 activity due to a loss of function mutation in *KEAP1* a negative regulator of Nrf2 (Singh *et al.* 2016). The authors found 5 – 10 µM of ML385 was effective at reducing Nrf2 mediated transcription, decreasing the intracellular glutathione pool and total antioxidant capacity in A549 cells. 20 µM of ML385 was then selected for treatment of *TSC2* deficient AML and *Tsc2* −/− MEF cells, as little decrease in cell viability was observed for upper limit of initial concentration range tested for cytotoxicity (see supplemental figure S.6.6). The main purpose of treating AML and MEF cell lines with the ROS inducing drugs DMNQ, rotenone and RSL3, were to induce cell death in order to observe if there was selective cell death between *TSC2* deficient and competent cells in response to ROS induction. Therefore, a broad range of concentrations of DMNQ, rotenone and RSL3, were initially tested to narrow down cytotoxic concentration ranges of these drugs used within this work.

For experiments where etoposide was used as a positive control for a decrease in cell viability, a concentration in excess was used in order to induce cell death.

### 2.3.2 Tissue culture assays

#### 2.3.2.1 Anchorage Independent Growth Assay

Two-layered anchorage independent growth (soft agar) assays were performed in 6-well tissue culture plates. The initial layer consisted of 1.5mL melted 0.6% (w/v) agar in phosphate-buffered saline (PBS). After setting of the first layer, either AML (12,000 cells) or MEF (50,000 cells) were suspended in a second layer of 2 mL melted 0.3 % agar in PBS with DMEM (50% v/v). The top agar/cell layer was then set at 37 $^{o}$C within a tissue culture incubator before 2 mL of DMEM (supplemented with 10% v/v FBS and 1% v/v Pen-Strep for both cell lines) with working concentrations of each drug or DMSO. Colonies of AML and MEF cells were cultured for 4 weeks, with drugged media changed twice weekly. Pictures were then taken using an EVOSXL core microscope. Colonies were scored and colony diameter determined using ImageJ (v.50).

#### 2.3.2.2 Tumour Spheroid Growth Assay

To the bottom of each well of a clear bottomed 96 well tissue culture plate 70 µL of melted 1.5% (w/v) agarose in PBS was added to create a non-adherent surface for coalescing of cells into spheroids. On top of this agarose layer, either 5,000 *TSC2* deficient AML cells or 1,000 *Tsc2* −/− MEF cells were seeded in DMEM (supplemented with 10% v/v FBS and 1% v/v Pen-Strep). Optimal seeding densities for sustained spheroid growth was determined for AML and MEF cells by seeding density calibration experiments (see supplemental figures S.3.1 and S.3.2). Seeded cells were allowed to coalesce into spheroids in an incubator for 3 days, before treatment with specified drug or DMSO (day 0). Pictures were then taken using an EVOSXL core microscope at day 0, 4, 7, 11 and 14. With half of cell media being replaced with fresh drugged media at each time point. Area of spheroids was determined using ImageJ (v.50).

#### 2.3.2.3 Tumour Spheroid Outgrowth assay

Tumour spheroids after the end time point of the tumour spheroid growth assay (day 14) were transferred to separate wells of a 24-well tissue culture plate in drug free DMEM (supplemented with 10% v/v FBS and 1% v/v Pen-Strep). Transplanted MEF tumour spheroids were then incubated for 3 days, whereas transplanted AML tumour spheroids were incubated

for 6 days with 5% $CO_2$ and 21% $O_2$ (normoxia). Pictures were then taken using an EVOSXL core microscope to assess viability and outgrowth of spheroids after long-term treatment with specified drug or DMSO.

#### 2.3.2.4 Vasculature Mimicry Assay

To the bottom of each well of a clear bottomed 96 well tissue culture plate 50 µl of chilled Matrigel basement membrane matrix was added and allowed to set at room temperature. On top of this matrigel layer, either 50,000 *TSC2* deficient AML cells or 30,000 *Tsc2* −/− MEF cells were seeded in Optimem reduced serum media and treated with specified drug or DMSO control. Tissue culture plates were then incubated overnight for 16 h in a humidified Binder CB150 hypoxic chamber with 5% $CO_2$ and 1% $O_2$ (hypoxia) at 37 $^oC$. Pictures of each well were then taken using an EVOSXL core microscope and analysed using AngioTool software (v.0.6a) (Zudaire *et al.* 2011).

#### 2.3.2.5 Acridine Orange/Propidium Iodide (AO/PI) Cell Viability Assay

Plates of *TSC2* deficient AML cells or *Tsc2* −/− MEF cells at a minimum of 70% confluency were treated with the specified drug or DMSO in DMEM, supplemented with 1% v/v Pen-Strep and either 2.5% v/v FBS in the case of the viability assay in chapter 3 and 10% v/v FBS in the case of the viability assay in chapter 6. Cells were then incubated for 24 h under in a humidified incubator with 5% $CO_2$ and either 21% $O_2$ or 1% $O_2$ (see specific figure). Cells were then trypsinised and collected, retaining original drugged media and trypsin washes, before being spun down at 2000 rpm. Cell pellets were then resuspended in 1 mL of fresh media. 18 µL of each cell suspension was mixed with 2 µL of AO/PI before being analysed on a LUNA-FL Dual Fluorescence Cell Counter to assay cell viability.

#### 2.3.2.6 CyQuant Cell Proliferation Assay

Either 5,000 cells for the AML lines or 2,500 cells for the MEF lines were seeded into the wells of a 96-well clear bottoms opaque walled tissue culture plate. Cells were allowed to adhere for 24 h in a humidified incubator at 5% $CO_2$ and 21% $O_2$, before fresh DMEM (supplemented with 1% v/v Pen-Strep and either 15% v/v FBS for AML lines or 10% FBS for MEF lines) alone or with specified drug, was added to each well. Cells were cultured for the specified time before being assayed for cell number using the CyQuant Cell Proliferation Assay Kit according to manufacturer's instructions. Fluorescence was assayed on a Cytation 3 plate reader.

Fluorescence was converted to cell number using cell line specific standard curves of cell number.

#### 2.3.2.7 Scratch Wound Healing Assay

*Tsc2* −/− MEF cells were seeded in 60 mm tissue culture plates with DMEM (supplemented with 1% v/v Pen-Strep and 10% FBS) and cultured to 100% confluency in in a humidified incubator at 5% $CO_2$ and 21% $O_2$. Confluent cell monolater was then 'wounded' using a pipette tip and dead/floating cells were removed through washes with fresh serum-free DMEM. Fresh serum-free DMEM with either DMSO or specified drug was then added to tissue culture plates. Pictures were then taken 24 h after treatment using an EVOSXL core microscope.

### 2.3.3 Cell Lysis

#### 2.3.3.1 In Laemmli Sample Buffer

Cells were lysed Laemmli sample buffer, after specified treatment and/or culture conditions, for analysis by western blotting. Treated/untreated cells were first washed in 1 mL of chilled PBS. Unless cells were cultured under hypoxia, in which they were lysed immediately to limit re-oxygenation of cells. Cells were then lysed in Laemmli sample buffer, before being sonicated for 3 x 30 s cycles on full power (30 microns) using a Bioruptor. Lysates were then centrifuged at 13,000 rpm for 8 minutes at room temperature before being stored at −80 $^{o}$C.

#### 2.3.3.2 In RIPA Buffer

Cells were lysed in RIPA buffer, after specified treatment and/or culture conditions, to generate whole cell lysates for analysis by ELISA (chapter 4). Cells were washed in 1 mL of chilled PBS before being lysed in RIPA buffer supplemented with protease inhibitors: 2 µM of antipain, 1 mM of benzamidine, 10 µM of leupeptin, 1 mM of Sodium orthovanadate, 1µg/mL of pepstatin and 100 µM of Phenylmethylsulfonyl fluoride. Lysed cells were sonicated for 3 x 30 s cycles on full power (30 microns) using a Bioruptor and then centrifuged at 13,000 rpm for 8 minutes at 4 $^{o}$C before use in ELISAs.

#### 2.3.3.3 In RNA Protect Cell Reagent

Cells for mRNA extraction were first washed in in 1 mL of chilled PBS before being lysed in RNA Protect Cell Reagent. These lysates were stored at −80 $^{o}$C until mRNA extraction.

### 2.3.4 Western Blot

#### 2.3.4.1 Protein Quantification

The protein concentration of lysates was determined through using either Pierce 660nm or Bradford reagent in the microplate format according to the manufacturer's instructions. For protein quantification of lysates generated with Laemmli sample buffer, Pierce 660nm reagent was supplemented with Ionic Detergent Compatibility Reagent according to manufacturer's instructions. 96-well microplates were analysed on a Cytation 3 plate reader. Absorbance readings were converted into protein concentrations utilising standard curves generated from bovine serum albumin (BSA) serially diluted into the appropriate lysis buffer. Ascertained protein concentration values were then used to standardise protein concentration of lysates, with bromophenol blue added to standardised lysates generated with Laemmli sample buffer after protein quantification to avoid interference with measurement.

#### 2.3.4.2 SDS – Polyacrylamide Gel Electrophoresis

Electrophoresis was carried out using Invitrogen NuPAGE gel Novex gel system according to manufacturer's protocol. Lysates previously standardised for protein concentration were loaded first heated to 90 $^{o}$C for 10 mins before being centrifuged for 1 min at 13,000 rpm. Lysates were then loaded into the wells of pre-cast NuPAGE gels, with the first well being loaded with pre-stained protein ladder. Typically, 3-8% Tris-acetate gels were used to separate larger weight (kDa) proteins and 4-12% Bis-Tris gels were used to separate small to medium weight proteins. 3-8% gels were run in Tris-Acetate SDS running buffer, whereas 4-12% gels were run in MES SDS running buffer. Gels were initially run at 200 V for 10 min and then at 120 V until appropriate separation of the protein ladder was achieved.

#### 2.3.4.3 Electro-transfer

After electrophoresis, separated proteins on gels were transferred to polyvinylidene difluoride (PVDF) membranes using a Hoefer miniVE vertical electrophoresis system according to manufacturer's protocol. Before electro-transfer, PVDF membranes were pre-treated with methanol for 1 min before washing with in 1X transfer buffer. PDVF membrane and gel were sandwiched between Whatman paper. Electro-transfer was run in transfer buffer at 5 V overnight (~ 18 h).

#### 2.3.4.4 Western Blot Analysis

Membranes with transferred protein were blocked in 10 mL of TBS-T with 5% (w/v) skimmed milk powder for 2 h minimum. After blocking, membranes were washed in TBS-T for 3 min twice before incubation overnight at 4 $^{o}$C with primary antibody diluted in TBS-T supplemented with 2% (w/v) of BSA. Primary antibody sourcing and dilutions used can be found in table 2.6. The next day, membranes were washed twice in TBS-T for 3 min, before incubation at room temperature with the appropriate secondary horse radish peroxidase-conjugated antibody diluted (1/10,000 v/v) in 10 mL of TBS-T with 5% (w/v) skimmed milk powder. Membranes were the washed for 3 mins in TBS-T four times before incubation in Amersham ECL Select Western Blotting Detection Reagent for 1 min. Chemiluminescence analysis of blots was performed using the Amersham ImageQuant 800. Predicted resolving band sizes (kDa) for the protein targets detected by specific antibodies are listed in table 2.6.

#### 2.3.4.5 Densitometry Analysis of Western Blots

Densitometry analysis is semi-quantitative and has been considered unreliable (Butler *et al.* 2019) but is used within the present work to elucidate trends and differences in protein expression that can be statistically tested. Densitometry analysis of western blots was performed using plot profile function on ImageJ software (v.50). Resulting values for protein bands were typically normalised to values obtained for β-actin or total protein bands. Resulting ratios for experimental conditions were often expressed as a foldchange to a designated control sample (see appropriate figure legend).

### 2.3.5 Polymerase Chain Reaction (PCR)

#### 2.3.5.1 mRNA purification

Cells previously stored in RNA Protect Cell Reagent were thawed and then centrifuged for 5 min at 5,000 rpm. Supernatant was discarded and mRNA was purified from cell pellets using RNeasy Plus Mini Kit according to manufacturer's instructions. 10 µL of β-mercaptoethanol was added per 1 mL of RLT lysis buffer used. Cell lysates were homogenized using QIAshredders. Purified RNA was stored at −80 $^{o}$C until use.

#### 2.3.5.2 Complementary DNA (cDNA) Synthesis

Previously purified RNA was quantified using Qubit RNA Broad Range Assay Kit according to manufacturer's instructions on a Qubit 2.0 fluorometer. cDNA was synthesised from purified RNA using the Reverse Transcriptase Core kit according to manufacturer's instructions on a

G-Storm Thermal Cycler. Random nonamers, part of the kit, were used as reverse transcription primers. 200 ng per reaction volume (10 µL) for each sample, generating cDNA at 20 ng/µL (assuming 1:1 conversion of RNA to cDNA). cDNA was stored at −80 °C until use.

| cDNA synthesis cycling conditions | | |
|---|---|---|
| **Step** | **Time (min)** | **Temperature (°C)** |
| Initial Step | 10 | 25 |
| Reverse Transcription Step | 30 | 48 |
| Inactivation of RT Enzyme | 5 | 95 |

#### 2.3.5.3 Quantitative Real-Time PCR (qPCR)

For qPCR, Takyon ROX SYBR 2X MasterMix dTTP blue was used according to manufacturer's instructions. As part of this master mix, SYBR green dye is used for detection of double stranded PCR products, whilst ROX acts as the passive reference dye. qPCR reactions were set up within MicroAmp Optical 96-Well Reaction Plates. Per reaction, 25 ng of cDNA was added, as well as 100-200 nM of both forward and reverse primer. Plates were sealed with optically clear plate seals. qPCR reactions were run on a 7500 Real time PCR System with the cycling conditions below. A no template control was run for each primer pair for each qPCR ran to check for contamination.

| qPCR cycling conditions | | | |
|---|---|---|---|
| **Step** | | **Time** | **Temperature (°C)** |
| Takyon Activation | | 3 min | 95 |
| 40 cycles of | Denaturation | 10 s | 95 |
| | Annealing | 20 s | Optimal primer annealing temp. |
| | Extension | 40 s | 72 |

To ensure primer specificity, i.e., only one PCR product was formed per primer pair, a dissociation step was performed following each qPCR for melt curve analysis. Gene expression analysis was performed using the Pfaffl method (Pfaffl, 2001), which allows for differing primer efficiencies (E). In short, for target gene and the housekeeping gene, first $C_T$ values of technical repeats were averaged and $\Delta C_T$ between condition and reference condition (e.g., DMSO) calculated. Then $E^{\Delta C_T}$ of target gene was divided by $E^{\Delta C_T}$ of the house keeping gene to calculate normalised gene expression values. Either *HMBS* or *IPO8* were utilised as housekeeping genes. Annealing temperature and efficiencies of primer pairs were previously assayed. All primers can be found in the appendix, tables 1 and 2.

#### 2.3.5.4 Primer Design

The Primer3 online tool (Rozen and Skaletsky, 2000) and exonic gene sequences sourced from Ensembl (Cunningham *et al.* 2022) were used to design custom primers for qPCR. Primer specificity and correct gene mRNA targeting were assessed using in silico PCR (Kent *et al.* 2002) and Primer-BLAST (Ye *et al.* 2012) online tools. Pre-designed KiCqStart SYBR Green Primers were also purchased. Primer sequence, sourcing and optimisation information can be found in the appendix, tables 1 and 2.

#### 2.3.5.5 Annealing Temperature Optimization

Before use in qPCR, primers optimal annealing temperatures were first determined by endpoint PCR using GoldStar PCR Mix according to manufacturer's instructions. Annealing temperature was run at a temperature gradient (50 – 65 $^{o}$C) on a G-Storm Thermal Cycler. Template DNA used was cDNA reverse transcribed (as previously described) from Quantitative PCR Human Reference Total RNA.

| PCR cycling conditions | | | |
|---|---|---|---|
| **Step** | | **Time** | **Temperature ($^{o}$C)** |
| Initial Denaturation | | 5 min | 94 |
| 35 cycles of | Denaturation | 30 s | 94 |
| | Annealing | 30 s | 50 – 65 |
| | Extension | 30 s | 72 |
| Final Elongation | | 5 min | 72 |

PCR products were then mixed in equal volume with orange G loading dye and electrophoretically separated on a 1.2% (w/v) agarose gel (agarose melted in 1X TAE buffer with 1% v/v gel red) in 1X TAE buffer. Bands of PCR products were then visualised under UV light on a BioDoc-It Imaging System. Annealing temperatures for primer pairs that produced single bands and highest amount of product were determined using plot profile function of ImageJ (v.50).

#### 2.3.5.6 Primer Efficiency Determination

Prior to experimental qPCR amplification efficiency of primer pairs was determined by qPCR, using Takyon ROX SYBR 2X MasterMix dTTP blue and cycling conditions previously outlined on a 7500 Real time PCR System. This time template DNA (cDNA reverse transcribed from

Quantitative PCR Human Reference Total RNA) was run at a gradient (50, 25, 10, 5, 2 ,1, 0.4 ng). For each primer pair $C_T$ values of technical repeats were averaged and plotted against the log concentration of template. The slope of the line was converted into an efficiency value by efficiency (%) = (10^(-1/slope)-1)*100. For gene expression analysis using the Pfaffl method, efficiency values were converted by E = (primer effiency (%)/100) + 1.

### 2.3.6 mRNA Sequencing Data

Within the present work, differentially expressed gene (DEG) analyses of four different RNA sequencing data sets were utilised. Two RNA sequencing data sets were generated during the research contained with this thesis: *TSC2* deficient AML versus *TSC2* re-expressed AML cells cultured under normoxia or hypoxia and *TSC2* deficient AML cells treated with either DMSO, rapamycin or C188-9. The other two RNA sequencing data sets were generated prior to the research contained within this thesis. The first was conducted by another research group (see Martin *et al.* 2017) and compared TSC associated lesions to non-TSC tissue. The second was conducted in the Tee lab (Johnson *et al*. 2018a) and compared *Tsc2* −/− MEF and *Tsc2* +/+ MEF cells. Methods and materials for sample collection, mRNA extractions, sequencing library preparation, sequencing platform, sequencing data quality control and differential expression analysis are described individually for each data set in the following subsections. Company or institution who performed the sequencing and differential expression analysis are noted also.

#### 2.3.6.1 *TSC2* deficient AML versus *TSC2* re-expressed AML cells cultured under normoxia or hypoxia RNA sequencing data set.

This RNA sequencing data set compared *TSC2* deficient or *TSC2* re-expressed AML cells cultured under either normoxia or hypoxia. Six biological repeats per cell line per condition (normoxia or hypoxia) were included within the analysis. Sequencing data was generated during the research contained within this thesis and is currently unpublished. Cell culture and sample preparation was undertaken within the Tee lab, the library preparation, RNA sequencing itself and subsequent DEG analyses was outsourced to Wales Gene Park (Cardiff University).

**Sample Collection**

The cell lines used for this RNA sequencing data set were the AML 621-102 (*TSC2* deficient) and the AML 621-103 (*TSC2* re-expressed) cell lines, whose features, origin, and culture are described in section 2.3.1 within this chapter. AML cell lines were plated onto 6cm$^2$ tissue

culture plates and allowed to adhere overnight. AML cell lines were then cultured for 24 h in DMEM supplemented with 15% (v/v) foetal bovine serum and 1% v/v Pen-Strep at 37 °C, 5% (v/v) $CO_2$ under either normoxia (21% $O_2$) or hypoxia (1% $O_2$).

**mRNA extraction and quality control**

AML cells were washed in PBS before lysis with RNAprotect cell reagent (Qiagen). Lysates were homogenised using Qiashredders (Qiagen) and RNA was purified from homogenised lysates as described in section 2.3.5.1 of this chapter. Before sequencing, isolated RNA integrity and concentration was determined by Wales Gene Park using an Agilent 4200 TapeStation and RNA screenTapes (Agilent Technologies). Only samples with a high RNA integrity number (RIN) (> 7) were taken forward for library preparation.

**Sequencing Library Preparation and Sequencing Platform**

Library preparation was conducted by Wales Gene Park as follows. From 50 ng of input RNA per sample, mRNA was isolated using the NEBNext® Poly(A) mRNA magnetic isolation module (New England BioLabs) according to the manufacturer's instructions. Sequencing libraries were generated using the NEB® Ultra™ II Directional RNA Library Prep Kit for Illumina (New England BioLabs). Manufacturer's instructions were followed, for the following stages: ribosomal RNA depletion, mRNA purification from input RNA, first strand cDNA synthesis, second strand cDNA synthesis, adenylation of DNA fragment 3' ends, adapter ligation (1:80 dilution) and PCR amplification (14 cycles). For purification of double-stranded cDNA after second strand cDNA synthesis AMPure XP beads (Beckman Coulter®) were used instead of SPRIselect Beads or NEBNext Sample Purification Beads part of the NEB® Ultra™ II Directional RNA Library Prep Kit. Amplified and purified libraries were both validated and insert size was determined using the Agilent 4200 TapeStation and hsD1000 ScreenTapes (Agilent Technologies). Fluorometric quantification of libraries were performed using a Qubit (Thermo Fisher Scientific). Validated and quantified libraries were normalised to 4 nM, pooled together, and sequenced with 1% PhiX spike-in, on an S1 (200 cycle) flow cell (v1.0) using a 2x100 bp paired end strategy on an Illumina NovaSeq6000 sequencing system.

**Quality Control, read Quantification and differential expression (DEG) analysis.**

Raw sequencing reads were processed by Wales Gene Park's in-house scripts to clean paired end reads. Quality control checks of data were undertaken using FastQC. Paired-end clean reads were mapped to the UCSC human GRCh38 reference genome using Tophat and Bowtie

software. Read numbers mapped to genes or exons in the reference genome were counted and normalised RPKM (fragments per kilobase of exon per million mapped fragments) values calculated. Differential expression analysis of normalised count data between conditions was performed by Wales Gene Park on R software using DESeq2 R package. Resulting p-values were adjusted using Benjamini and Hochberg's procedure (Benjamini and Hochberg, 1995) for controlling the False Discovery Rate (FDR).

#### 2.3.6.2 *TSC2* deficient AML cells DMSO versus Rap versus C188-9 treatment RNA sequencing data set.

This RNA sequencing data set compared *TSC2* deficient AML cells cultured under hypoxia treated with either DMSO, rapamycin or C188-9. Eight biological repeats per treatment condition were included within the analysis. Sequencing data was generated during the research contained within this thesis and is currently unpublished. Cell culture and sample preparation was undertaken within the Tee lab, the library preparation, RNA sequencing itself and subsequent DEG analyses was outsourced to Novogene (Cambridge, UK).

**Sample Collection**

The cell line used for this RNA sequencing data set were the AML 621-102 (*TSC2* deficient) cells, whose features, origin, and culture are described in section 2.3.1 within this chapter. AML cell lines were plated onto 6cm$^2$ tissue culture plates, initially cultured in DMEM supplemented with 15% (v/v) foetal bovine serum and 1% v/v Pen-Strep and allowed to adhere overnight at 37 °C, 5% (v/v) $CO_2$ before treatment. AML cells were then cultured in DMEM supplemented with 10% (v/v) foetal bovine serum and 1% v/v Pen-Strep under hypoxia (1% $O_2$) for 8 h in the presence of either DMSO, rapamycin at 50 nM or C188-9 at 15 µM. Lower concentration of 15 µM C188-9 rather than 30 µM was used for these treatments to limit potential apoptotic pathways from being activated. The volume of DMSO between treatments was kept consistent.

**mRNA extraction and quality control**

After 8 h treatment, AML cells were washed in PBS before lysis with RNAprotect cell reagent (Qiagen). Lysates were homogenised using Qiashredders (Qiagen) and RNA was purified from homogenised lysates as described in section 2.3.5.1 of this chapter. Before sending samples for sequencing with Novogene, isolated RNA integrity and concentration was determined using an Agilent 4200 TapeStation and RNA screenTapes (Agilent Technologies)

by Wales Gene Park (Cardiff University). Only samples with a high RNA integrity number (RIN) (> 8) were taken forward for sequencing.

**Sequencing Library Preparation and Sequencing Platform**

RNA sequencing, library preparation by Novogene was as follows. Sequencing libraries were generated using NEBNext® UltraTM RNA Library Prep Kit for Illumina® (NEB). Manufacturer's instructions were followed, for the following stages: ribosomal RNA depletion, mRNA purification from input RNA, RNA fragmentation, first strand cDNA synthesis, second strand cDNA synthesis, blunting of overhangs, adenylation of DNA fragment 3' ends and adaptor ligation with NEBNEXT Adaptors. AMPure XP system (Beckman Coulter) was used for selection of cDNA fragments preferentially of 150 – 200 bp length. Amplification PCR was performed with Phusion High-Fidelity DNA polymerase (NEB), Universal PCR Primers (NEB), Index (X) Primers (NEB) and adaptor ligated and size selected cDNA. Subsequent PCR products were purified using the AMPure XP system (NEB) and library quality was then validated using an Agilent Bioanalyzer 2100 system. Following library preparation, RNA concentration normalised samples were clustered on a cBot$^{TM}$ Cluster Generation System according to the manufacturer's instructions. Library preparations were then sequenced using a 150 bp paired-end strategy on an Illumina NovaSeq 6000 platform.

**Quality Control, read Quantification and differential expression (DEG) analysis.**

Raw sequencing reads were processed by Novogene's in-house scripts to produce clean data. Paired-end clean reads were mapped to the UCSC human GRCh38 reference genome using HISAT2 software. Read numbers mapped to genes or exons in the reference genome were counted and FPKM (fragments per kilobase of exon per million mapped fragments) calculated. FPKM, used over RPKM for paired-end RNA-seq, considers sequencing depth and a genes length on counting fragments. Differential expression analysis of normalised FPKM values for genes between treatment conditions was performed by Novogene on R software using DESeq2 R package. Resulting p-values were adjusted using Benjamini and Hochberg's procedure (Benjamini and Hochberg, 1995) for controlling the False Discovery Rate (FDR).

#### 2.3.6.3 TSC lesion versus non-TSC tissue RNA sequencing data set.

This RNA sequencing data set compared the TSC associated lesions to non-TSC tissue. Brain TSC associated lesions subependymal nodule/subependymal giant cell astrocytomas (SEN/SEGA) and cortical tubers (TUB) to non-TSC brain tissue (NB). And renal TSC associated angiomyolipomas (RA) to non-TSC kidney tissue (NK). Sample repeat numbers included in the final analysis were 15 for SENSEGA, 15 for TUB, 8 for NB, 11 for RA and 3 for NK. Sequencing data was generated prior to the research contained in this thesis by a different research group (see Martin *et al.* 2017) and access to the data was kindly provided by Prof. Jeffrey MacKeigan (Michigan State University).

**Sample Collection**

The authors acquired TSC lesion or non-TSC tissue samples from TSC patients or non-TSC organ donors respectively through tissue banks and medical schools referenced in Martin *et al.* (2017). Tissue samples used for the generation of these RNA sequencing data sets were fresh-frozen at the time of surgery or post-mortem. Before subsequent workflow, tissue type and sample integrity were confirmed by a clinical pathologist. Samples with inconsistent/unclear diagnoses of tissue type were excluded from the study. For all participants providing samples for this study written informed consent was obtained. Detailed information about individual sample and patients/donors can be found in the supplementary information section in Martin *et al.* (2017).

**mRNA extraction and quality control**

Authors isolated RNA from frozen tissue samples using an altered version of the method described in Peña-Llopis and Brugarolas (2013). Tissue samples were disrupted and homogenised with mirVana kit lysis buffer (Ambion), micropestle and QIAshredder columns (Qiagen). Homogenised lysates were then run through AllPrep coulmns (Qiagen), with acid phenol–chloroform extraction and the mirVana kit (Ambion) used to isolate RNA from column flowthroughs. Before sequencing, RNA extractions from tissue samples were assayed using a BioAnalyser 2100 (Agilent Technologies) for RNA integrity.

**Sequencing Library Preparation and Sequencing Platform**

RNA isolated from TSC lesion and non-tissue samples was sequenced by HudsonAlpha Institute for Biotechnology Genomic Services Laboratory. Ribosomal RNA depletion and mRNA libraries were prepared for RNA sequencing using NEBNext reagents (New England

BioLabs) according to the manufacturer's instructions. mRNA library preparations were sequenced using a directional 100 bp paired-end read strategy on the Illumina HiSeq 2500 sequencing system.

**Quality Control, read Quantification and differential expression (DEG) analysis.**

Raw sequencing reads were quality filtered and clean paired end reads were mapped to the hg19 reference genome through Subread. Raw read counts were then obtained using FeatureCounts software. Differential expression analysis was undertaken using limma from raw read counts imported into R software. Counts per million were calculated and log2-transformed through voom and then normalised through trimmed mean of M-values normalisation method. Resulting p values of differential expression analysis were corrected using the FDR method.

#### 2.3.6.4 *Tsc2* −/− MEF versus *Tsc2* +/+ MEF cell RNA sequencing data set.

This RNA sequencing data set compared *Tsc2* +/+ MEF and *Tsc2* −/− MEF cell lines. Three biological repeats per cell line were included within the final analysis. Sequencing data was generated prior to the research contained within this thesis by the Tee lab and published in Johnson *et al*. (2018). Cell culture and sample preparation was undertaken within the Tee lab, the library preparation, RNA sequencing itself and subsequent DEG analyses was outsourced to Wales Gene Park (Cardiff University).

**Sample Collection**

The cell lines used for this RNA sequencing data set were the *Tsc2* +/+ *Tp53* −/− MEF and *Tsc2* −/− *Tp53* −/− MEF cell lines, whose features, origin, and culture are described in section 2.3.1 within this chapter. MEF cell lines were plated onto 6cm$^2$ tissue culture plates, cultured in DMEM supplemented with 10% (v/v) foetal bovine serum and 1% v/v Pen-Strep and allowed to adhere overnight at 37 °C, 5% (v/v) $CO_2$ before treatment with DMSO. MEF cells were treated with DMSO as these samples were vehicle only controls for other samples in the whole original RNA sequencing data experiment that were treated with Nelfinavir mesylate hydrate (Sigma-Aldrich, PZ0013) and Bortezomib (Merck, CAS 179324-69-7). DEG analyses of Nelfinavir mesylate hydrate & Bortezomib treated MEF cell lines was excluded from bioinformatic analysis for the purpose of this work.

**mRNA extraction and quality control**

DMSO treated MEF cells were washed in PBS before lysis with RNAprotect cell reagent (Qiagen). Lysates were homogenised using Qiashredders (Qiagen) and RNA was purified from homogenised lysates as described in section 2.3.5.1 of this chapter. Before sequencing, isolated RNA integrity and concentration was determined using an Agilent 2100 Bioanalyser and an RNA Nano 6000 kit (Agilent Technologies).

**Sequencing Library Preparation and Sequencing Platform**

Library preparation was conducted by Wales Gene Park as follows. Between 100 and 900 ng of total RNA with an RNA integrity number (RIN) value of > 8 was depleted of ribosomal RNA with Ribo-Zero Gold kit (Illumina) according to the manufacturer's instructions except the clean-up stage after the ribosomal RNA depletion, where instead AmpureXP beads (Beckman Coulter) and 80% ethanol were used. Following ribosomal RNA depletion and cleanup samples were then used to prepare sequencing libraries using the Illumina TruSeq Stranded total RNA kit (Illumina) according to the manufacturer's instructions. Library preparation stages included: RNA fragmentation, first strand cDNA synthesis, second strand cDNA synthesis, adenylation of DNA fragment 3' ends, adapter ligation, library amplification by PCR. Libraries were cleaned up according to Illumina TruSeq Stranded total RNA kit instructions. Amplified and cleaned libraries were validated on a 2100 Bioanalyser with a high-sensitivity kit (Agilent Technologies) in order to determine insert size. Validated library preparations were quantified using a Qubit (Thermo Fisher Scientific) and then normalised to 4nM and clustered on a cBot™ 2 Cluster Generation System according to the manufacturer's instructions. RNA library preparations were then sequenced using a 75 bp paired end dual index read strategy on an Illumina HiSeq 2500 sequencing system (high-output mode).

**Quality Control, read Quantification and differential expression (DEG) analysis.**

Raw sequencing reads were processed by Wales Gene Park's in-house scripts to clean paired end reads. Quality control checks of data were undertaken using FastQC. Paired-end clean reads were then mapped to the UCSC mouse mm10 reference genome using Tophat and Bowtie software. Read numbers mapped to genes or exons in the reference genome were counted and RPKM (fragments per kilobase of exon per million mapped fragments) calculated. Differential expression analysis of normalised count data between conditions was performed on R software by Wales Gene Park using DESeq2 R package. Resulting p-values were adjusted using Benjamini and Hochberg's procedure (Benjamini and Hochberg, 1995) for controlling the False Discovery Rate (FDR).

#### 2.3.6.5 Compilation of Gene Sets

The gene sets used for the present work, to generate volcano plots and heat maps were manually compiled. Genes chosen were experimentally validated in the literature. Gene sets used within this present work can be found in the appendix.

- **HIF1-α target gene set**: genes were collated from a meta-analysis of HIF1-α target genes in literature (Slemc *et al.* 2016), two papers utilising chromatin immunoprecipitation (ChIP) and genome profiling to identify HIF1 target genes (Mole *et al.* 2009 and Xia *et al.* 2009) and one review article (Wenger *et al.* 2005).

- **STAT3 target gene set**: genes were collated from a ChIP and microarray analysis of STAT3 DNA binding (Snyder *et al.* 2008), a study contrasting expression of STAT3 regulated genes in RNA-seq data from renal cell carcinoma subtypes (Robinson *et al.* 2019) and a review which listed experimentally validated STAT3 target genes relevant to human cancers (Carpenter and Lo, 2014).

- **The Nrf2 target gene set**: genes were collated mainly from the supplementary table of Nrf2 regulated genes in Ma (2013) and individual papers experimentally confirming Nrf2 mediated expression of genes within different cellular contexts.

- **Endogenous Antioxidant gene set**: genes were collated from the literature, including any genes found involved in the cells response to oxidative and xenobiotic induced stress.

Volcano plots and heatmaps were generated using R software with inbuilt packages and the following optional packages installed: ggplot2, ggrepel, RColorBrewer and gplots.

### 2.3.7 Enzyme-Linked Immunosorbent Assay (ELISA)

DUOSET ELISAs were used, according to manufacturer's instructions, to quantify protein concentration of VEGFA, HGF, IL6 or IL-6/IL6R complex in either the conditioned media or whole cell lysate of AML cell lines under oxygen and culture conditions listed in the appropriate figure legend. Whole cell lysates were generated using RIPA buffer as previously described. Conditioned media was diluted 1/5 into fresh DMEM to assay IL6 and VEGFA. ELISA plates were assayed for absorbance on a Cytation 3 plate reader. Absorbance values were converted into protein concentrations using standard curves generated from serially diluted protein standards provided in the DUOSET ELISA kits.

### 2.3.8 Assaying Nuclear Active STAT3

Nuclear lysates were generated from the AML and MEF cell lines using Active Motif's nuclear extract kit according to manufacturer's instructions. Nuclear lysates were assayed for protein concentration using Pierce 660nm reagent, as previously described. Active Motif STAT3 TransAM ELISA kits were used to assay active DNA binding STAT3 in nuclear lysates standardised for protein concentration. The wells of the TransAM ELISA plates are coated in immobilised oligonucleotides that contain STAT3 consensus sequences and therefore capture the STAT3 in nuclear lysates capable of binding DNA. TranAM ELISA plates were assayed for absorbance on a Cytation 3 plate reader.

### 2.3.9 Luciferase Assay

A Promega dual-luciferase reporter assay was utilised according to the manufacturer's instructions to assay transcriptional activity of HIF-1α. The HIF1-α luciferase reporter vector used contained multiple copies of HIF-1α cis-acting enhancer elements inserted upstream of a promoter which drives firefly luciferase expression. Thereby DNA binding of HIF-1α correlates to luciferase expression and is termed HIF-1α "transcriptional activity" within the present work.

HIF-1α sequence (5'-3'): GTGACTACGTGCTGCCTAGGTGACTACGTG
CTGCCTAGGTGACTACGTGCTGCCTAGGTGACTACGTGCTGCCTAG

A pRL Renilla luciferase control reporter vector was used as an internal transfection control, and it was assumed the Renilla luciferase reporter was constitutively expressed regardless of treatments within this work.

Before conducting luciferase assay sub-confluent *Tsc2* −/− MEFs cultured in 40mm tissue culture plates were transfected using jetPEI HTS DNA transfection reagent according to manufacturer's instructions. For *Tsc2* add back conditions, *Tsc2* −/− MEFs were transfected with Flag-TSC2/pcDNA3.1, under all other conditions *Tsc2* −/− MEFs were transfected with an empty vector (pcDNA3.1). Optimal ratio of HIF-1α luciferase reporter vector to additional vectors used was previously determined in the Tee lab and is summarised in the table below.

| **Optimal vector amount for transfection of one 40mm plate of *Tsc2* −/− MEFs** | |
|---|---|
| **DNA Construct** | **Amount of Construct (ng)** |
| HIF1 Luciferase Reporter Vector | 1200 |
| pRL Renilla Luciferase Control Reporter Vector | 400 |
| pcDNA3.1 (empty vector) **or** Flag-TSC2/pcDNA3.1 | 400 |

Plates were lysed in passive lysis buffer provided with the Promega dual-luciferase reporter assay system. 20 µL of protein lysates were added per well of an opaque walled clear bottomed 96-well plate. Luminescence was assayed using a TR717 Microplate Luminometer and luminescence values were adjusted to total protein concentrations of lysates determined by a Bradford assay, as previously described. To confirm repression of STAT3 phosphorylation at Y705 in the case of C188-9 treatment, equal parts luciferase lysate and 2X Laemmli sample buffer were mixed and then sonicated before being subject to western blotting procedure as previously described.

### 2.3.10 Statistical Analysis

All statistical analysis was performed using R software. Means between two groups of smaller data sets were compared for statistically significant differences by using either two sample t-tests, when the assumption of normal data distribution were met, or a Mann-Whitney U test when the assumption of normal data distribution were not met. To determine whether a t-test or Mann-Whitney U test was the appropriate statistical test for a data set, normality of data was tested using a Shapiro Wilks test and Q–Q plots. The type of t-test performed was either a student's t-test if variances of data were found equal, or a Welch's t test was performed if variances of data were found to be unequal. An F-test was used to determine whether variances of data sets were equal or not, and hence whether a student's t-test or a Welch's t test was the appropriate statistical test. Means of larger data sets were compared for statistically significant differences amongst multiple groups through the use of a one way analysis of variance (ANOVA) test. Normal distribution of data was determined by a Shapiro Wilks test and Q-Q plots on the standardised residuals of the ANOVA, to assess whether an ANOVA was the statistically appropriate test. If data was found to be normally distributed, then a Bartlett test was used to determine if whether variances of data sets were equal or not. If assumptions about normality or homogeneity of variances of data were not met, then a Kruskal–Wallis one-way ANOVA was performed. For statistical comparisons between all means amongst groups within the same large data set, a Tukey's post-hoc test was used. In incidences were the effect of two different categorical variables on one dependent variable was assessed, a two-way ANOVA was performed. Bioinformatics deriving p values and adjusted p values associated with DEG analysis of RNA sequencing data was undertaken out of house. The statistical test used to assess significance between groups of data is annotated in each appropriate figure legend.

# Chapter 3. Evaluating the efficacy of targeting the Ref-1/HIF-1α/STAT3/NF-κB signalling axis on measurable tumourigenic outputs of *TSC2* deficient cells against mTORC1 inhibitors.

## 3.1 Introduction

TSC associated lesions remain a significant burden of illness and represent a leading cause of mortality for TSC patients (Amin *et al*. 2017, Sheperd *et al.* 1991 and Zöllner *et al.* 2020). And whilst phase three clinical trials of Everolimus (rapamycin analogue) demonstrate that mTOR inhibition is effective at reducing tumour volume of brain and renal lesions (Bissler *et al.* 2013 and Franz *et al.* 2013), these trials also showed that a significant proportion of patients did not respond to treatment. This suggests, that on loss of *TSC1/TSC2*, other signalling pathways are dysregulated independently of mTORC1 hyperactivity and in turn may contribute towards tumourigenesis within TSC. Preliminary data (now published in Champion *et al*. 2022) that formed the basis of this research project identified a signalling axis upregulated in *Tsc2* −/− MEF cells; composed of Ref-1, HIF-1α, STAT3 and NF-κB. The preliminary data established that: Ref-1 protein expression and activity of HIF-1α, STAT3 and NF-κB (reported by luciferase assays) was elevated in *Tsc2* −/− MEFs compared to *Tsc2* +/+ MEFs. Crucially, it was also demonstrated that rapamycin treatment did not normalise HIF-1α or STAT3 activity in *Tsc2* −/− MEFs to a level equivalent to wild-type cells, but treatment with the 1$^{st}$ generation Ref-1 inhibitor APX3330 did. Based on the preliminary data and observations from clinical trials about the incomplete efficacy of mTOR inhibitors at reducing tumour burden in all TSC patients, the present work hypothesised that increased activity of the Ref-1/HIF-1α/STAT3/NF-κB axis drives increased cell growth and proliferation in *TSC2* deficient cells.

Aside from its function in the base-excision repair pathway (Demple *et al*. 1991), Ref-1 is a redox status signalling protein (Xanthoudakis *et a*l. 1992). In response to redox stress, Ref-1 upregulates the activity of its target transcription factors through oxidising specific cysteine residues (Shah *et al.* 2017); transactivating them. Ref-1 has been shown to increase the activity of HIF-1α (Logsdon *et al.* 2016), STAT3 (Cardoso *et al.* 2012) and NF-κB (Nishi *et al.* 2002). These transcription factors individually regulate a host of target genes involved in many diverse processes (Dengler *et al.* 2014, Snyder *et al.* 2008 and Oeckinghaus and Ghosh, 2009). Aside from activation by Ref-1, each of these transcription factors have well defined pathways and mechanisms through which their activity is regulated in response to stimulation. See the main introduction for activation and regulation of HIF-1α and STAT3. Cytokine activation of NF-κB canonically follows a mechanism whereby inhibitors of the inhibitory protein that sequester NF-κB in the cytoplasm are themselves phosphorylated (Oeckinghaus

and Ghosh, 2009), marking them for degradation. NF-κB subunits can also be subject to a number of post-translational modifications which alter their activity. For example, phosphorylation of S536, which is thought to increase NF-κB transactivation (Jiang *et al*. 2003) and may be important for translocation of NF-κB to the nucleus (Oakley *et al*. 2009).

Owing to its function as a master regulator of the hypoxic response (Majmundar *et al.* 2010), HIF-1a activity is elevated under low oxygen. STAT3 activity has also been shown to be elevated under hypoxia in a variety of human cancers (Pawlus *et al.* 2014 and Soleymani Abyaneh *et al.* 2017), whilst multiple mechanisms have been described for how hypoxia promotes NF-κB activity (Xie *et al.* 2015, Koong *et al.*1994 and Li *et al.* 2015b). Hypoxia also increases the production of cellular reactive oxygen species (ROS) (Kondoh *et al.* 2013 and Wang *et al.* 2007b). Kobayashi *et al*. (2021) recently demonstrated that increased ROS production under prolonged hypoxia induced Ref-1, in turn increasing HIF-1α activity. Given that in different contexts, hypoxia has been shown to increase the activity of Ref-1, HIF-1α, STAT3 and NF-κB, the present work hypothesised that hypoxia will further elevate the activity of the Ref-1/HIF-1α/STAT3/NF-κB signalling axis in TSC. Supported by the observation that the tissues predominantly effected by TSC, (namely skin, lungs, kidneys and brain) all have hypoxic gradients across them as part of their normal functioning (Northrup *et al.* 2013).

Whilst not metastatic in nature, growth of benign lesions in TSC still result in severe symptoms for patients (Northrup *et al.* 2013) and TSC lesions are also highly vascularised and prone to aneurysm (Yamakado *et al*. 2002). Therefore, delineating other modes of tumorigenesis and dysregulated angiogenesis in TSC is crucial for improving treatment. The present chapter therefore employed assays typically used to study effectiveness of drugs at targeting cancer cell lines *in vitro.* Namely, tumour spheroid growth, anchorage independent growth and tube formation (vasculature mimicry) assays. To assess the relative contribution of each component of the Ref-1/HIF-1α/STAT3/NF-κB axis, inhibitors which target Ref-1, STAT3 and NF-κB individually were used. Rapamycin was employed to also target HIF-1α, as mTOR inhibition has been demonstrated to reduce total HIF-1α protein in *TSC2* deficient cells (Land and Tee, 2007). Ref-1 inhibitors used were APX3330, APX2009, APX2014, which are highly selective at targeting the redox function of Ref-1 without compromising the proteins endonuclease activity (Shah *et al*. 2017). The STAT3 inhibitors used were FLLL31 and C188-9 (Lin *et al.* 2010 and Bharadwaj *et al.* 2016). The NF-κB inhibitor used was JSH23 (Shin *et al.* 2004). The second generation mTOR inhibitor Ku0063794, which more robustly inhibits the mTOR complexes (García-Martínez *et al.* 2009), was also used in the present work.

The TSC model cell lines used within this chapter, and all subsequent chapters, are the human *TSC2* deficient angiomyolipoma (AML) 621-102 and *TSC2* re-expressed (RE) AML 621-103

cells, and the murine *Tsc2* −/− (*Tp53*−/−) mouse embryonic fibroblasts (MEFs) and the *Tsc2* +/+ (wildtype) (*Tp53*−/−) MEFs. The AML 621-102 cell line were previously generated by Hong *et al.* (2008), where primary AML cells were immortalised through transfection with human papilloma virus E6/E7 and human telomerase plasmids. Hong *et al.* (2008) generated the AML 621-103 cell line by stably transfecting the AML 621-102 cell line with wildtype *TSC2*. Both MEF cell lines were generated by Zhang *et al.* (2003), through mice littermate pair crossings to generate embryonic fibroblasts which were *Tp53*−/− and either had *Tsc2* −/− or *Tsc2* +/+. MEFs null for *Tp53* were necessary to overcome the senescence associated with null *Tsc2*. More detail on cell lines and their culture can be found in chapter 2, section 2.3.1.

## 3.2 Results

### 3.2.1 Protein expression and activity of constituents of the Ref-1/HIF-1α/STAT3/NF-κB signalling axis is dysregulated in *TSC2* deficient cells.

Based on the findings from the preliminary data this chapter's first aim was twofold. First through western blotting to establish in the *Tsc2* −/− MEFs whether the luciferase assay data is reflected in the total protein expression of Ref-1, HIF-1α, STAT3, NF-κB and markers of their activity. Secondly to carry out the western blot analysis in the AML cells, to see if the findings within the murine TSC cell model is reflected in the human TSC cell model. The effect of normoxic and hypoxic culture conditions was also assayed. As illustrated within the blot panels in figures 3.1 (**A**) and 3.2 (**A**) both the *TSC2* deficient AML and MEF cell lines do not express TSC2 protein. Furthermore, re-expression of *TSC2* within the AML cells (*TSC2* RE) appears stable.

Both *TSC2* deficient AML cells and *Tsc2* −/− MEF cells cultured under normoxia show higher expression of HIF-1α compared to *TSC2* RE AML and *Tsc2* +/+ cells cultured under normoxia. A finding reported as significant by densitometry analysis (figures 3.1 **B** and 3.2 **B**). HIF-1α protein expression was elevated under hypoxic culture in all cell lines, with densitometry analysis reporting the enhanced foldchange in HIF-1α protein expression for each AML and MEF cell line under hypoxia as significant relative to their normoxia cultured equivalents. While blot panels indicate HIF-1α protein expression is higher in both *TSC2* deficient AML and *Tsc2* −/− MEF cells cultured under hypoxia than *TSC2* RE AML and *Tsc2* +/+ MEF cells respectively cultured under hypoxia, densitometry analysis did not report the differences in foldchange in HIF-1α expression as significant. However, protein expression of BNIP3, whose gene is a direct target of HIF-1α (Guo *et al.* 2001), is elevated substantially in both *TSC2* deficient AML

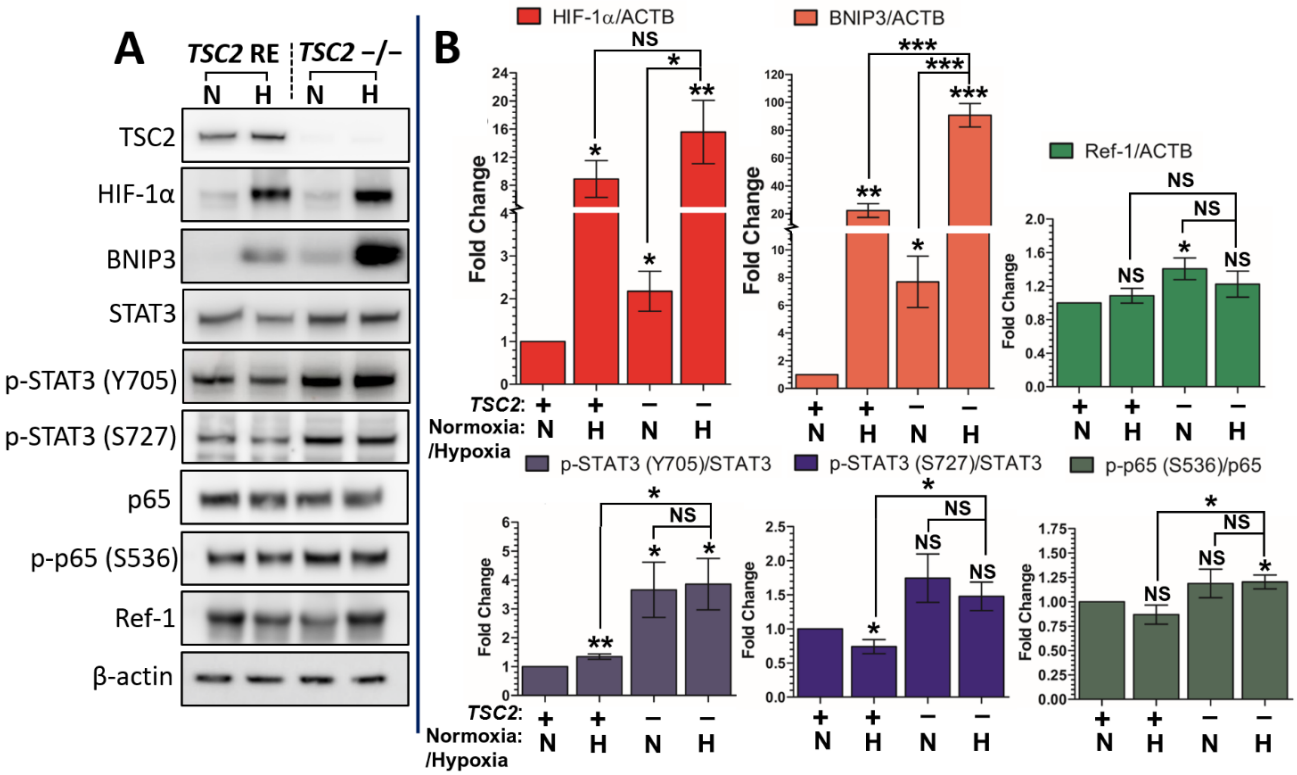


**Figure 3.1. Protein expression and markers of activity of constituents of the Ref-1/HIF-1α/STAT3/NF-κB signalling axis is upregulated upon loss of *TSC2* in AML cells.** *TSC2* deficient (−/−) and *TSC2* re-expressed (RE) AML cells were cultured overnight in either normoxic (N) or hypoxic (H) conditions. Cells were then lysed and protein expression of TSC2 and constituents of the Ref-1/HIF-1α/STAT3/NF-κB signalling axis were assayed by western blotting, with β-actin acting as a loading control. Panel **A** shows representative panel of the assayed protein targets in the AML cell lines (N=3 minimum). Panel **B** shows densitometry analysis of the resulting western blots (N=3 minimum). For densitometry analysis total proteins (HIF-1α, p65 (Rela) and Ref-1) were normalised to β-Actin and phosphorylated proteins were normalised to their respective total proteins. Resulting ratios were then expressed as fold changes compared to a designated control sample, in this case *TSC2* RE cells under normoxia. Statistical analysis of differences in foldchange was by student's t test. Significance annotations above each bar on graph indicates significance of difference in foldchange between each condition and *TSC2* RE cells under normoxia. Pairwise statistical comparisons between *TSC2* (−/−) cells under normoxia or hypoxia and between *TSC2* (−/−) and *TSC2* RE cells under hypoxia are also annotated. Significance denoted by: * = p <0.05, ** = p <0.01, *** = p< 0.001, NS = not significant. Bars represent standard error of the mean. Predicted running band size (kDa) of protein targets can be found in chapter 2, table 2.6.

and *Tsc2* −/− MEF cell lines cultured under hypoxia compared to *TSC2* RE AML and *Tsc2* +/+ MEF cells cultured under hypoxia. The difference in foldchange in HIF-1α between the *Tsc2* −/− MEF and *Tsc2* +/+ MEF cells under hypoxia was not reported as significant however (Figure 3.3 **B**). As the case with HIF-1α expression, significantly enhanced BNIP3 expression was observed under hypoxia in all cell lines relative to their normoxia cultured equivalents. Within *TSC2* deficient AML cells, BNIP3 expression was significantly enhanced under normoxia relative to the *TSC2* RE AML cells under normoxia (Figure 3.1 **A**). Observations that either HIF-1α and/or BNIP3 protein expression under normoxia is elevated on loss of *TSC2*, characterises *TSC2* deficient AML and MEF cells as 'psuedohypoxic', that is enhanced

hypoxic-like signalling by these cells is observed even when oxygen is plentiful (Hayashi *et al.* 2019).

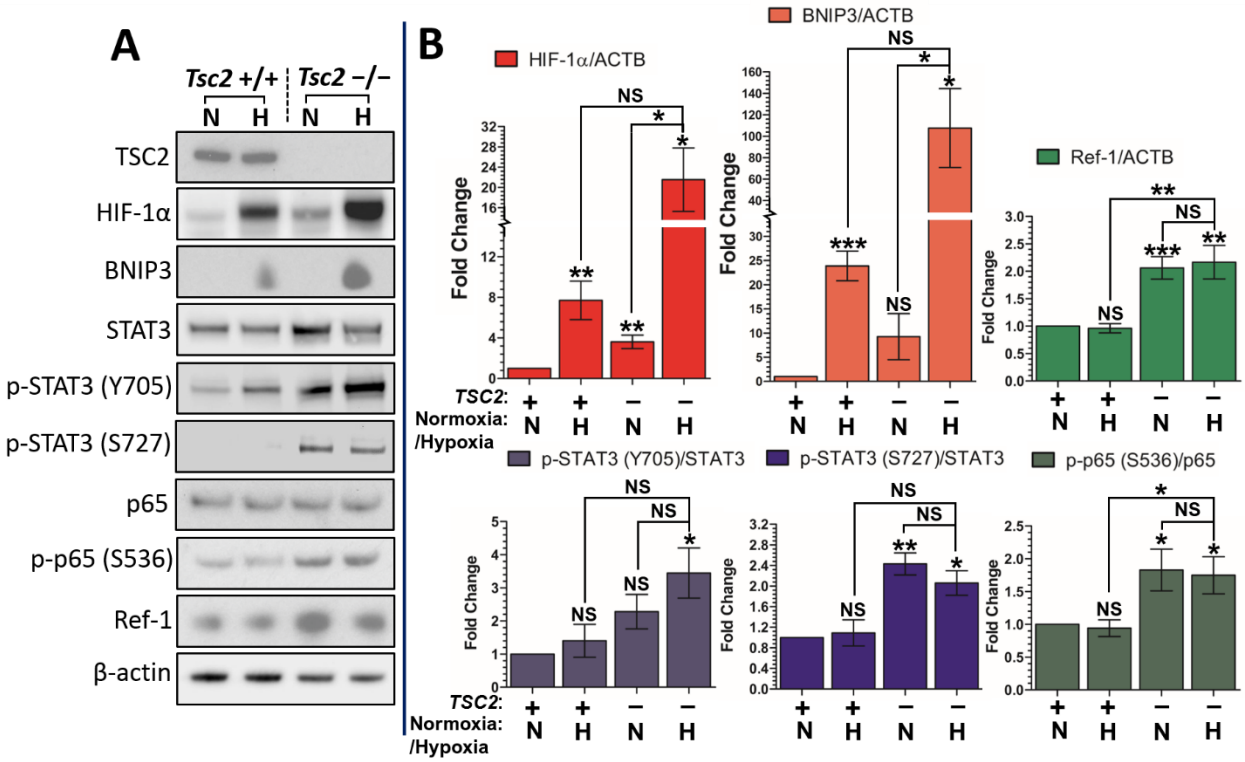


**Figure 3.2. Protein expression and markers of activity of constituents of the Ref-1/HIF-1α/STAT3/NF-κB signalling axis is upregulated upon loss of *Tsc2* in MEF cells.** *Tsc2* −/− and *Tsc2* +/+ MEF cells were cultured overnight in either normoxic (N) or hypoxic (H) conditions. Cells were then lysed and protein expression of TSC2 and constituents of the Ref-1/HIF-1α/STAT3/NF-κB signalling axis were assayed by western blotting, with β-actin acting as a loading control. Panel **A** shows the shows representative panel of the assayed protein targets in the MEF cell lines (N=3 minimum). Panel **B** shows densitometry analysis of the resulting western blots (N=3 minimum). For densitometry analysis total proteins (HIF-1α, p65 (Rela) and Ref-1) were normalised to β-Actin and phosphorylated proteins were normalised to their respective total proteins. Resulting ratios were then expressed as fold changes compared to a designated control sample, in this case *Tsc2* +/+ cells under normoxia. Statistical analysis of differences in foldchange was by student's t test. Significance annotations above each bar on graph indicates significance of difference in foldchange between each condition and *Tsc2* +/+ cells under normoxia. Pairwise statistical comparisons between *Tsc2* −/− cells under normoxia or hypoxia and between *Tsc2* −/− and *Tsc2* +/+ cells under hypoxia are also annotated. Significance denoted by: * = p <0.05, ** = p <0.01, *** = p< 0.001, NS = not significant. Bars represent standard error of the mean. Predicted running band size (kDa) of protein targets can be found in chapter 2, table 2.6.

Total STAT3 protein is elevated in both *TSC2* deficient cell lines. β-actin bands for *Tsc2* −/− MEF cells are less intense than those of *Tsc2* +/+ MEFs, therefore total STAT3 protein is likely to be more strongly expressed in *Tsc2* −/− MEFs than represented in figure 3.2. Analysis of the expression of total STAT3, within both AML and MEF lines will be more fully described in chapter 5, which focuses on characterising the STAT3 signalling pathway within these cells in more depth than the present chapter. In both *TSC2* deficient AML and MEF cell lines

phosphorylation markers of active STAT3, tyrosine 705 (Y705) and serine 727 (S727) (two post translation modifications that increase the transcriptional activity of STAT3, see main introduction), are elevated irrespective of normoxic/hypoxic culture conditions relative to *TSC2* RE AML and *Tsc2* +/+ MEF cells respectively (Figures 3.1 and 3.2). Although densitometry analysis did not find the increased foldchange in STAT3 phosphorylated at S727 in *TSC2* deficient AML cells relative to the *TSC2* RE AML cells significant, except when both cell lines had been cultured under hypoxia (Figure 3.1 **B**). While enhanced phosphorylation of STAT3, at either Y705 or S727, within hypoxic cultured *Tsc2* −/− MEF cells relative to hypoxic cultured *Tsc2* +/+ cells was not found to be significant by densitometry analysis (Figure 3.2 **B**). Whilst oxygen availability appeared to significantly affect the level of phosphorylation of STAT3 at Y705 and S727 within *TSC2* RE AML cells (figure 3.1 **B**), it did not have a significant effect in either *TSC2* deficient AML or *Tsc2* −/− MEF cells.

As can be seen from the blot panel and densitometry analysis in figure 3.1, Ref-1 protein expression appears only moderately elevated within *TSC2* deficient AML cells relative to *TSC2* RE AML cells. And only for *TSC2* deficient AML cells cultured under normoxia was the increased Ref-1 expression reported significant. Within *Tsc2* −/− MEF cells, Ref-1 expression is far more enhanced relative to *Tsc2* +/+ MEF cells (over 2 fold higher), irrespective of oxygen availability. Densitometry analysis found the higher Ref-1 expression of *Tsc2* −/− MEF cells under either normoxia or hypoxia as significant (figure 3.2 **B**). Oxygen availability did not significantly impact Ref-1 expression in the AML or MEF cell lines. It should be noted that the lack of substantial differences observed in Ref-1 expression between the AML cell lines does not truly reflect the activity of Ref-1 to promote redox driven transcription. This is because Ref-1 is activated by reactive oxygen species (ROS) and transactivates target transcription factors (Shah *et al.* 2017). However, the contrasting Ref-1 protein expression between the *TSC2* deficient AML and MEF cell lines could represent an important difference in Ref-1 cell signalling overall, and any perturbed signalling pathways Ref-1's activity factors in, between the human and murine model cells.

p65 (nuclear factor NF-kappa-B p65 subunit or RelA) is a key component of the transcriptionally active NF-κB dimer p50/p65 (Oeckinghaus and Ghosh, 2009). Therefore, p65 was chosen as the target indicator of NF-κB activity. Across all cell lines cultured under both normoxic and hypoxic conditions, total p65 protein appears expressed to a similar level (Figures 3.1 **A** and 3.2 **A**), although may be elevated within *Tsc2* −/− MEFs owing to the less intense β-actin bands. Phosphorylation of p65 at S536 by and large does not appear to be

enhanced within *TSC2* deficient AML cells relative to *TSC2* RE AML cells (Figure 3.1 **A**). Only the slight increase in phosphorylation of p65 at S536 within *TSC2* deficient AML cells cultured under hypoxia was found significant relative to *TSC2* RE AML cells cultured under either normoxia or hypoxia (Figure 3.1 **B**). Within the *Tsc2* −/− MEF cells however, phosphorylation of p65 at S536 appears enhanced to a much greater degree relative to the *Tsc2* +/+ MEF cells (figure 3.2 **A**). Densitometry analysis reported the increased phosphorylation of p65 at S536 within the *Tsc2* −/− MEF cells compared to the *Tsc2* +/+ MEF cells as significant, irrespective of oxygen availability (Figure 3.2 **B**). Normoxic vs hypoxic culture conditions however had no significant effect on phosphorylation of p65 at S536 in either MEF cell line. As the case with Ref-1 expression, discordance in the level of phosphorylation of p65 at S536 between both *TSC2* deficient AML and MEF cells may represent an important distinction in the aberrant signalling pathways that characterise these TSC model cells upon the loss of *TSC2.*

### 3.2.2 *APEX1*, *HIF1A* and *STAT3* are differentially expressed between *TSC2* re-expressed/+/+ and *TSC2* deficient AML and MEF cells.

As protein markers of Ref-1, HIF-1α, STAT3 and p65 (Rela) were found to be elevated upon loss of *TSC2* in AML and MEF cells (Figures 3.1 and 3.2), qPCR was utilised to assess whether gene expression of *APEX1* (Ref-1), *HIF1A*, *STAT3* and *RELA* was also dysregulated upon loss of *TSC2* in AML and MEF cells. With the effect of oxygen availability on mRNA expression also assessed. As shown in figure 3.3. expression of the *APEX1* gene appears to be downregulated in AML *TSC2* deficient cells under normoxia and hypoxia, having a fold change of 0.49 (p=0.0005) and 0.65 (p=0.0015) respectively relative to AML *TSC2* RE cells under normoxia. *APEX1* expression in AML cells appears to be sensitive to oxygen availability as the differences in *APEX1* fold change between cells under normoxia and hypoxia was significant for both cell lines (p=0.0103 between AML *TSC2* RE cells and p=0.0095 between AML *TSC2* deficient cells). Again, the trend for the expression of the *Apex1* gene appears to be downregulated in MEF *Tsc2* −/− cells. However, only the foldchange observed in the MEF *Tsc2* −/− cells (0.49 fold) was reported as being significant (p=0.0175). As with the AML cell lines, the expression of *Apex1* within between MEF *Tsc2* −/− cells cultured under either normoxia or hypoxia was significant (p=0.0278). However, in both *TSC2* deficient AML and *Tsc2* −/− cells cultured under hypoxia, *APEX1* expression was not found to be significantly different from their *TSC2* competent counterparts cultured under hypoxia.

As illustrated in figure 3.4. the mRNA expression of *HIF1A*, *STAT3* & *RELA* is elevated within both AML and MEF *TSC2* deficient cell lines and oxygen availability appears to have an input in the expression of each gene. Within AML *TSC2* deficient cells both *HIF1A* and *STAT3* are upregulated irrespective of oxygen availability. *HIF1A* was found to be expressed higher in

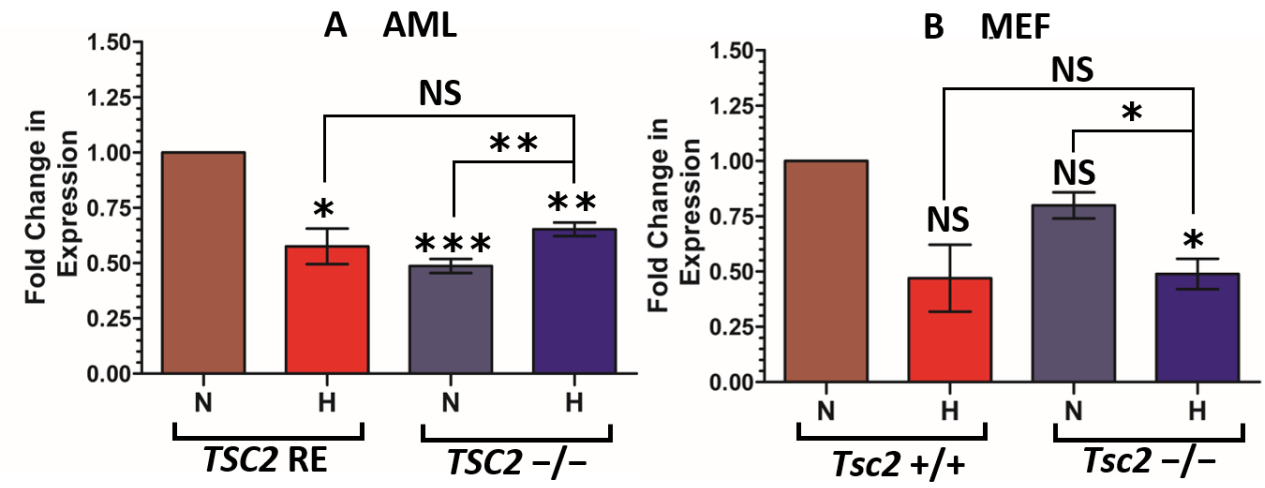


**Figure 3.3. mRNA expression of *APEX1* is downregulated upon loss of *TSC2* and is oxygen sensitive.** *TSC2* deficient and *TSC2* re-expressed (RE) AML cells or *Tsc2* −/− and *Tsc2* +/+ MEFs were cultured overnight in either normoxic (N) or hypoxic (H) conditions. Cells were then lysed and mRNA was purified from these cells and by qPCR mRNA expression of *APEX1* was quantified (N=3 minimum). mRNA levels were standardised to *HMBS* expression. For fold change calculations, AML *TSC2* RE under normoxia and MEF *Tsc2* +/+ under normoxia acted as reference samples. Statistical analysis of differences in foldchange between conditions was by way Welch's two sample t test. Significance annotations above each bar on graph indicates significance of difference in foldchange between each condition and the reference sample (AML: *TSC2* RE or MEF: *Tsc2* +/+ cells under normoxia). Pairwise statistical comparisons between *TSC2* deficient/*Tsc2* −/− cells under normoxia or hypoxia and between *TSC2* deficient/*Tsc2* −/− cells and *TSC2* RE/*Tsc2* +/+ cells under hypoxia are also annotated. Significance denoted by: * = p <0.05, ** = p <0.01, *** = p< 0.001, NS = not significant. Bars represent standard error of the mean.

AML *TSC2* deficient cells under either normoxia (3.75 fold, p=0.0126) and hypoxia (2.90 fold, p=0.0461) compared to AML *TSC2* RE cells under normoxia. However, the difference in *HIF1A* expression between AML *TSC2* deficient cells grown under normoxia or hypoxia was not reported as significant. The same expression pattern was found for *STAT3* in the AML cells. Fold changes in *STAT3* mRNA for AML *TSC2* deficient cells under normoxia (2.03 fold, p=0.0360) or hypoxia (2.79 fold, p=0.0111) was significantly different from AML *TSC2* RE cells under normoxia; but was not significantly different from each other. Additionally, the foldchange in *STAT3* mRNA between *TSC2* deficient and *TSC2* RE AML cells cultured under hypoxia (p= 0.00821).

Within the MEF cells, only the *Tsc2* −/− cells under hypoxia showed a significantly different fold change in *Hif1a* (3.12 fold, p= 0.0114) and *Stat3* mRNA (3.10 fold, p=0.0294) compared to the *Tsc2* +/+ cells under normoxia. Additionally, the difference in foldchange in *Hif1a* and *Stat3* mRNA between *Tsc2* −/− and *Tsc2* +/+ cells cultured under hypoxia was found to be significant (*Hif1a* p= 0.0027, *Stat3* p= 0.0162). Unlike what was observed in the AML cell lines, the difference between mRNA expression of *Hif1a* and *Stat3* between *Tsc2* −/− MEF cells cultured under normoxia or hypoxia was found significant (*Hif1a* p=0.0051, *Stat3* p=0.0397).

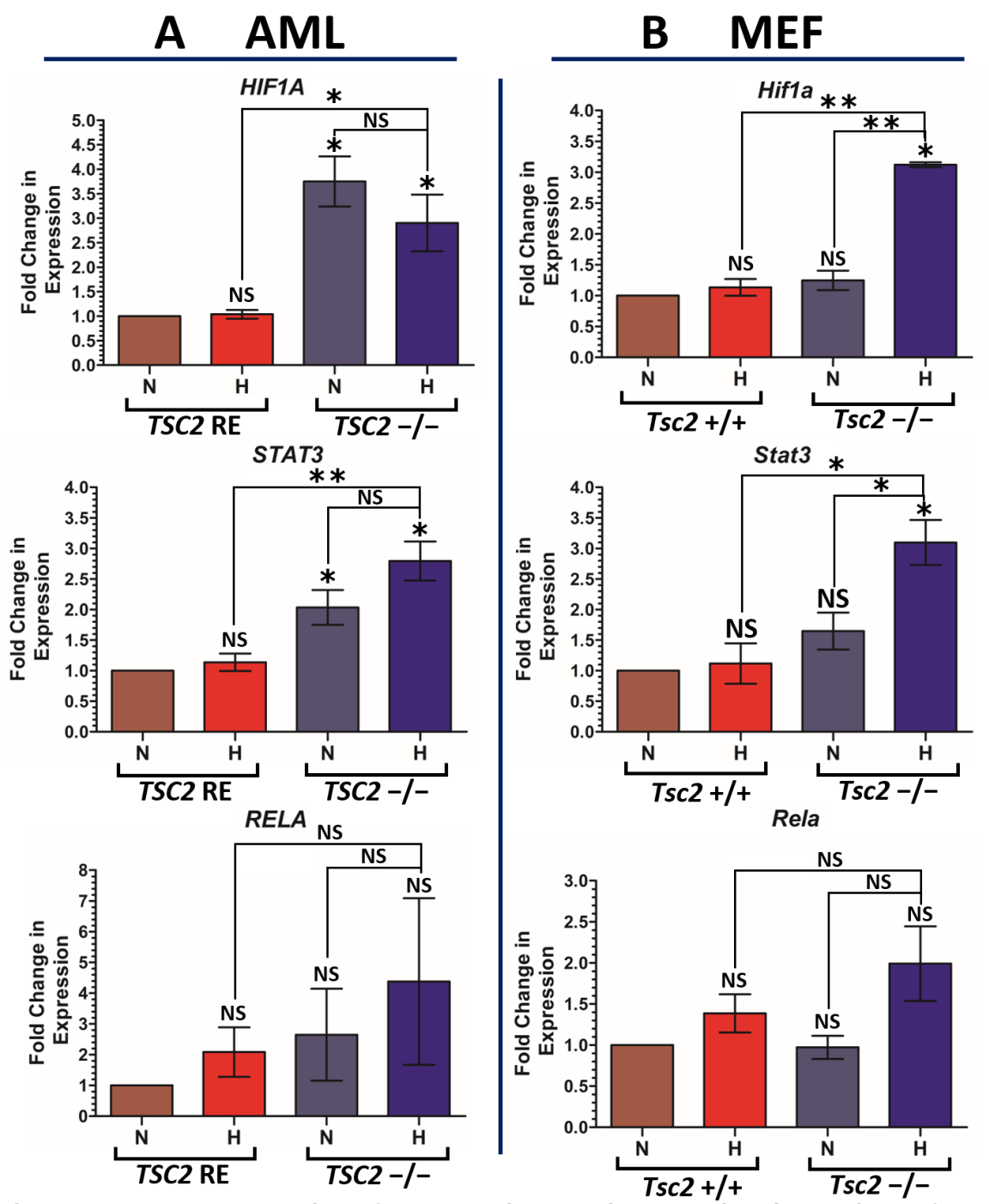


**Figure 3.4. mRNA expression of *HIF1A* and *STAT3* is upregulated upon loss of *TSC2* and is oxygen sensitive.** *TSC2* deficient and *TSC2* re-expressed (RE) AML cells or *Tsc2* −/− and *Tsc2* +/+ MEF cells were cultured overnight in either normoxic (N) or hypoxic (H) conditions. Cells were then lysed, and mRNA was purified from these cells and by qPCR *HIF1A*, *STAT3* and *RELA* mRNA expression was quantified (N=3 minimum). mRNA levels for each gene were standardised to *HMBS* expression. For fold change calculations, AML *TSC2* RE under normoxia and MEF *Tsc2* +/+ under normoxia acted as reference samples. Significance annotations above each bar on graph indicates significance of difference in foldchange between each condition and the reference sample (AML: *TSC2* RE or MEF: *Tsc2* +/+ cells under normoxia). Pairwise statistical comparisons between *TSC2* deficient/*Tsc2* −/− cells under normoxia or hypoxia and between *TSC2* deficient/*Tsc2* −/− cells and *TSC2* RE/*Tsc2* +/+ cells under hypoxia are also annotated. Statistical analysis was by way of Welch's two sample t test. Significance denoted by: * = p <0.05, ** = p <0.01, NS = not significant. Bars represent standard error of the mean.

Overall, this suggests hypoxia may play a more important role in the dysregulation of the *STAT3* and *HIF1A* genes with the murine model than the human model of TSC. When comparing mRNA expression of *RELA*, no differences in mRNA expression between either AML or MEF *TSC2* deficient cells and their controls, respective *TSC2* competent cells under normoxia, were reported as significant irrespective of oxygen availability.

### 3.2.3. Inhibition of Ref-1, HIF-1α, STAT3 or NF-κB alone or in combination with rapamycin was not selectively cytotoxic to *TSC2* deficient cells.

Whilst treatment with current mTOR inhibitors (rapamycin and its structural analogues) is effective at shrinking TSC lesions (Bissler *et al.* 2008), their drug effect is cytostatic, rather than cytotoxic. Therefore, the next aim of the present chapter was to assess whether a potential therapeutic benefit of targeting the Ref-1/HIF-1α/STAT3/NF-κB signalling axis would be induction of selective cytotoxicity in *TSC2* deficient cells but not the *TSC2* wildtype control cells. To develop this line of enquiry further, inhibitors of the Ref-1/HIF-1α/STAT3/NF-κB signalling axis were tested as single agents or in combination with rapamycin. To assess cell viability, acridine orange/propidium iodide (AO/PI) staining was utilised. AO/PI staining is a more robust viability assay when compared to trypan blue exclusion methods (Mascotti *et al*. 2000). It was first observed that the inhibitors used to target the Ref-1/HIF-1α/STAT3/NF-κB signalling axis were generally well tolerated at standard FBS concentrations used to culture both the AML and MEF cell lines. It is well established that albumin protein components in supplemented culture media reversibly bind many drugs and small molecule inhibitors (Epps *et al.* 1999), thereby effectively decreasing the active titre of drug. Therefore, FBS concentration was lowered to 2% (v/v) for these assays to increase potential sensitivity to the drug inhibitors used.

As visualised in figure 3.5 **A**, both concentrations of the Ref-1 inhibitors APX3330 and APX2009 and the lower concentration of APX2014 are well tolerated in both *TSC2* RE and *TSC2* deficient AML cells under normoxia or hypoxia. A one way analysis of variance (ANOVA), reported there was no significant difference in cell viability compared to the DMSO controls. Consistent with what is known about mTOR inhibition in TSC cells, rapamycin or the more potent mTOR inhibitor Ku0063794, caused no significant decrease in cell viability (as shown in figure 3.5 **B**). Additionally, both concentrations of APX3330 and APX2009, and the lower concentration of APX2014, in combination with rapamycin caused no significant change in cell viability compared to the DMSO controls. Furthermore, there was no significant difference in cell viability between cells treated with either of the three Ref-1 inhibitors at the

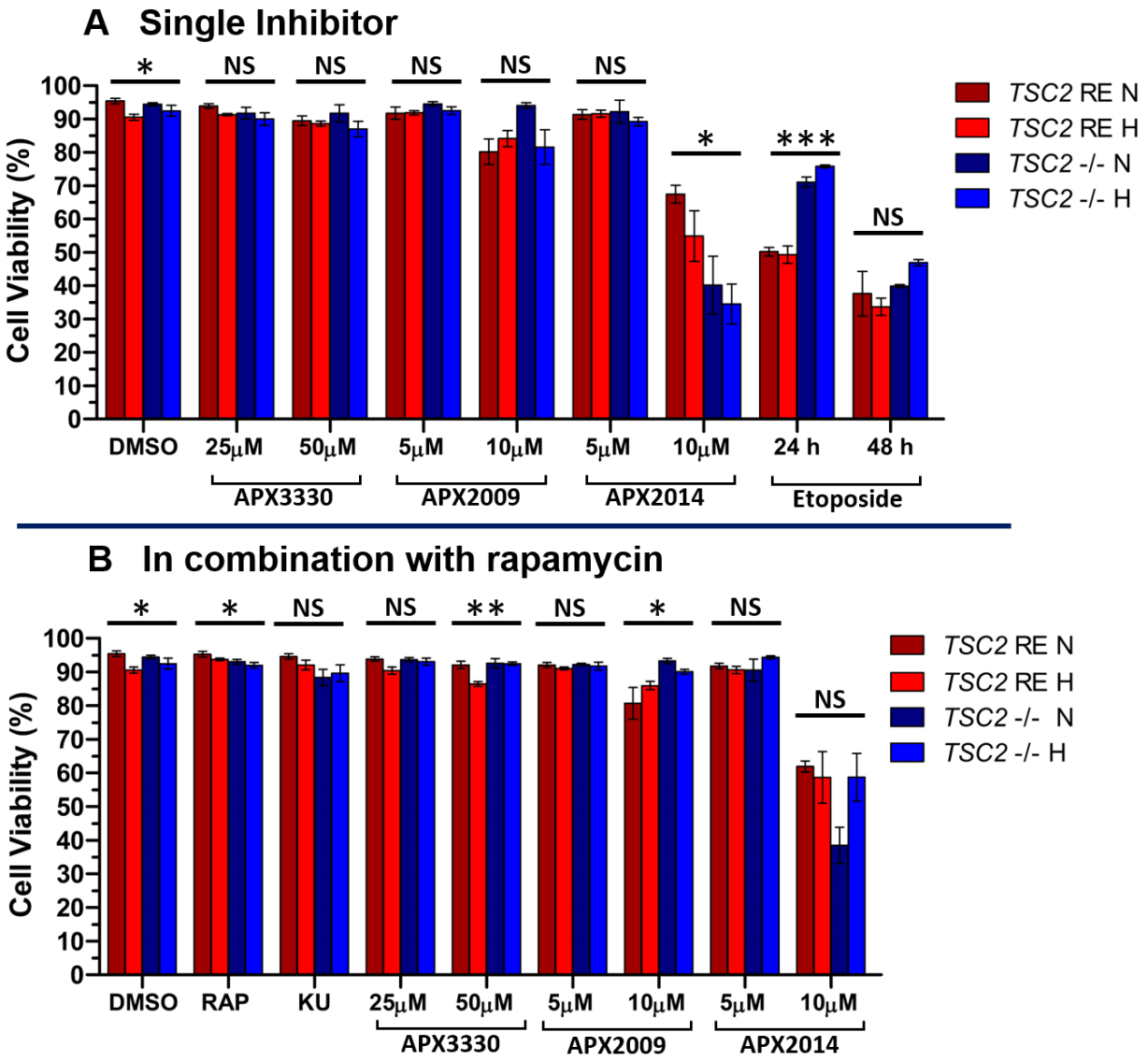


**Figure 3.5. Ref-1 inhibitors alone or in combination with rapamycin are not selectively cytotoxic to *TSC2* deficient AML cells**. *TSC2* RE or *TSC2* deficient (−/−) cells in tissue culture plates were grown to ~70-80% confluency. Cells were then treated with Ref-1 inhibitors (APX3330, APX2009, APX2014) either under normoxia (N) or hypoxia (H) for 24 h with either the specified inhibitor alone (Graph **A**) or in combination with rapamycin (Graph **B**) at 50 nM. Cells were then collected, retaining trypsin washes and original drugged media, spun down and resuspended. Cell suspensions were then mixed with AO/PI stain and viable/non-viable cells were assayed on a dual-fluorescence cell counter (N=4 minimum). Average percentage of viable cells are plotted on the above graphs. The significance between differences in percentage of viable cells for each cell line under each drug condition was determined through one-way ANOVA and annotated on each graph. Significance denoted by: * = p <0.05, ** = p <0.01, *** = p< 0.001, NS = not significant. Etoposide (100 μM) treatments represent positive controls for decrease in cell viability. Bars represent standard error of the mean.

aforementioned concentrations alone and in combination with rapamycin. For both AML cell lines under either normoxia or hypoxia, only APX2014 at the higher concentration caused a significant decrease in cell viability compared to DMSO controls (figure 3.5 **A**) (AML *TSC2* RE N = 67.5%, $p=5.0x10^{-6}$, AML *TSC2* RE H = 54.9% $p=2.9x10^{-5}$, AML *TSC2* −/− N = 40.8%

p=<1.0x10$^{-8}$, AML *TSC2* −/− H = 34.6% p=<1.0x10$^{-8}$). A two-way ANOVA found that the difference between cell viability on treatment with APX2014 at 10 μM between *TSC2* RE and *TSC2* deficient AML cells was significantly different (p=0.0026), but that oxygen availability made no significant difference. The addition of rapamycin with APX2014 at 10 μM treatment only significantly changed the cell viability for AML *TSC2* deficient cells under hypoxia (figure 3.5 **B**). Overall, these results indicate that under these conditions Ref-1 inhibition by and large is not selectively cytotoxic to AML *TSC2* deficient cells, as only treatment of APX2014 at 10 μM seemed to cause any decrease in viability compared to AML *TSC2* RE cells and this finding is not fully recapitulated when AML *TSC2* deficient cells were treated with rapamycin in combination with APX2014 at 10 μM.

As seen if figure 3.6 (**A** & **B**), treatment of MEFs with both concentrations of APX3330, APX2009 at 5 μM and APX2014 at 5 μM alone or in combination with rapamycin recapitulate the previous findings within the AML cell lines. With no significant difference in cell viability for *Tsc2* +/+ and *Tsc2* −/− MEF cells under either normoxia or hypoxia compared to DMSO controls. MEF cell lines appear to be more sensitive to APX2009 and APX2014 at 10 μM than the AML cells (figure 3.6 **A**). Additionally, the finding that APX2014 at 10 μM appears more selectively cytotoxic to *TSC2* deficient AMLs is not reproduced in the *Tsc2* −/− MEF cells. With differences in cell viability on treatment with APX2014 at 10 μM between *Tsc2* +/+ and *Tsc2* −/− MEF cells not being reported as significant, irrespective of oxygen availability or the addition of rapamycin (as reported by two-way ANOVAs).

As visualised in figure 3.7 (**A**), targeting STAT3 downstream of Ref-1 through either the FLLL31 or C188-9 inhibitors in AML cells does not appear to be selectively cytotoxic towards *TSC2* deficient AML cells. In fact, the trend appears to be a relative decrease in cell viability of *TSC2* RE AML cells. AML cell lines tolerate lower concentrations of FLLL31 and C188-9 well, with the exception of *TSC2* RE cells under normoxia, whose decrease in cell viability was found to be significantly different from relative DMSO controls when treated with FLLL31 at 5 μM (64.1% p=1.8x10$^{-7}$) or C188-9 at 15 μM (68.1% p=5.6x10$^{-6}$). Treatment of AML cell lines under normoxia or hypoxia at the higher concentrations of FLLL31 and C188-9, did cause a significant decrease in cell viability compared to DMSO controls (figure 3.7 **A**). Interestingly, treatment of *TSC2* deficient cells with 30 μM of C188-9 under hypoxia caused a significant decrease in cell viability compared to the same treatment under normoxia (normoxia=69.8%, hypoxia=41.3%, p=0.0010). This finding is repeated within *TSC2* deficient AML cells treated with C188-9 at 15 μM in combination with rapamycin (figure 3.7 **B**). As observed with the Ref-1 inhibitors, combinatory treatment of the STAT3 inhibitors with rapamycin had no significant effect on cell viability. Both the higher and lower concentrations of the NF-κB inhibitor JSH23

are well tolerated by both AML cells lines irrespective of oxygen availability, with no significant difference in cell viability compared to DMSO controls.

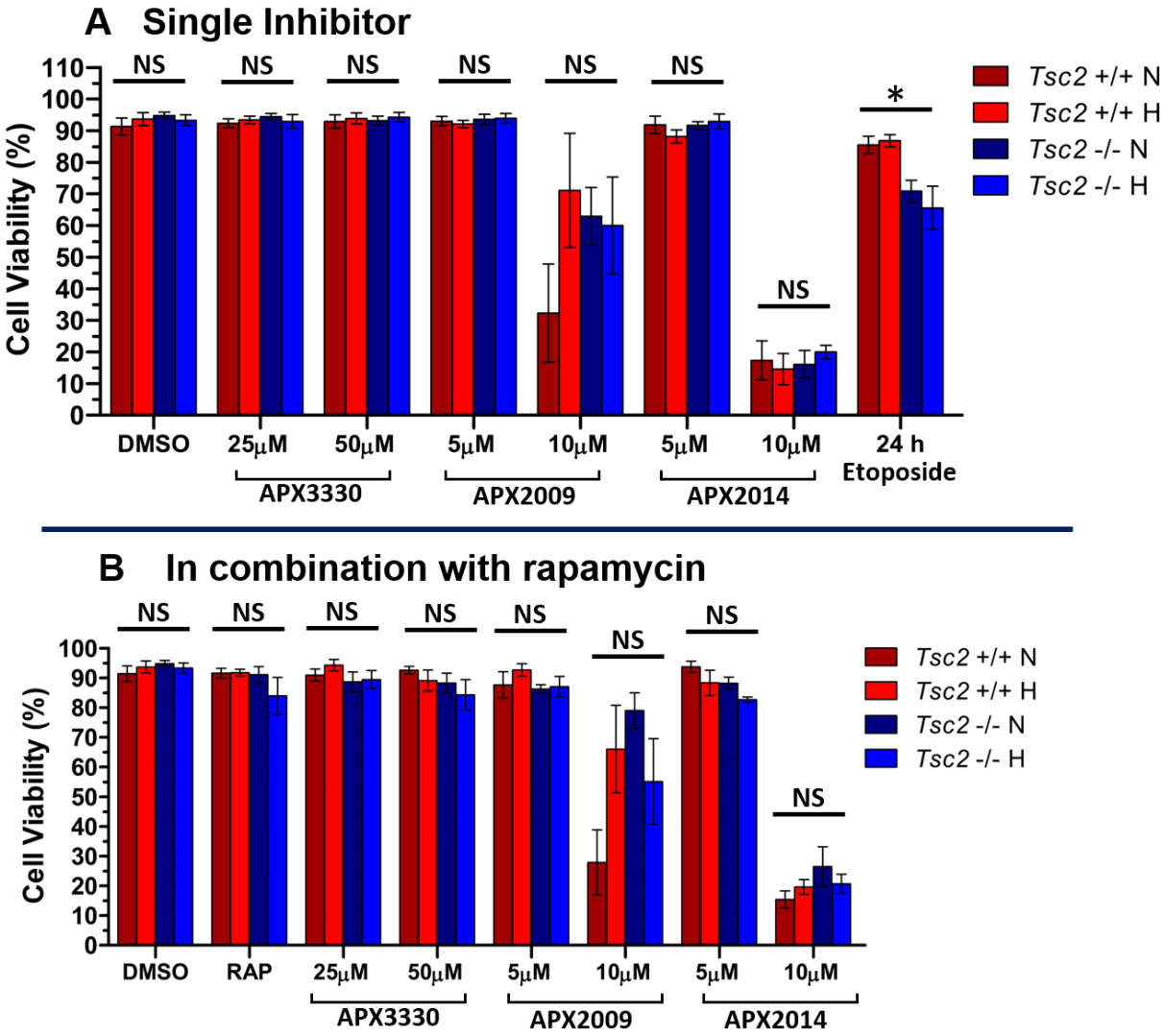


**Figure 3.6. Ref-1 inhibitors alone or in combination with rapamycin are not selectively cytotoxic to *Tsc2* −/− MEF cells**. *Tsc2* +/+ or *Tsc2* −/− MEF cells in tissue culture plates were grown to ~70-80% confluency. Cells were then treated with Ref-1 inhibitors (APX3330, APX2009, APX2014) either under normoxia (N) or hypoxia (H) for 24 h with either the specified inhibitor alone (Graph **A**) or in combination with rapamycin (Graph **B**) at 50 nM. Cells were then collected, retaining trypsin washes and original drugged media, spun down and resuspended. Cell suspensions were then mixed with AO/PI stain and viable/non-viable cells were assayed on a dual-fluorescence cell counter (N=4 minimum). Average percentage of viable cells are plotted on the above graphs. The significance between differences in percentage of viable cells for each cell line under each drug condition was determined through one-way ANOVA and annotated on each graph. Significance denoted by: * = p <0.05, ** = p <0.01, *** = p< 0.001, NS = not significant. Etoposide (100 μM) treatments represent positive controls for decrease in cell viability. Bars represent standard error of the mean.

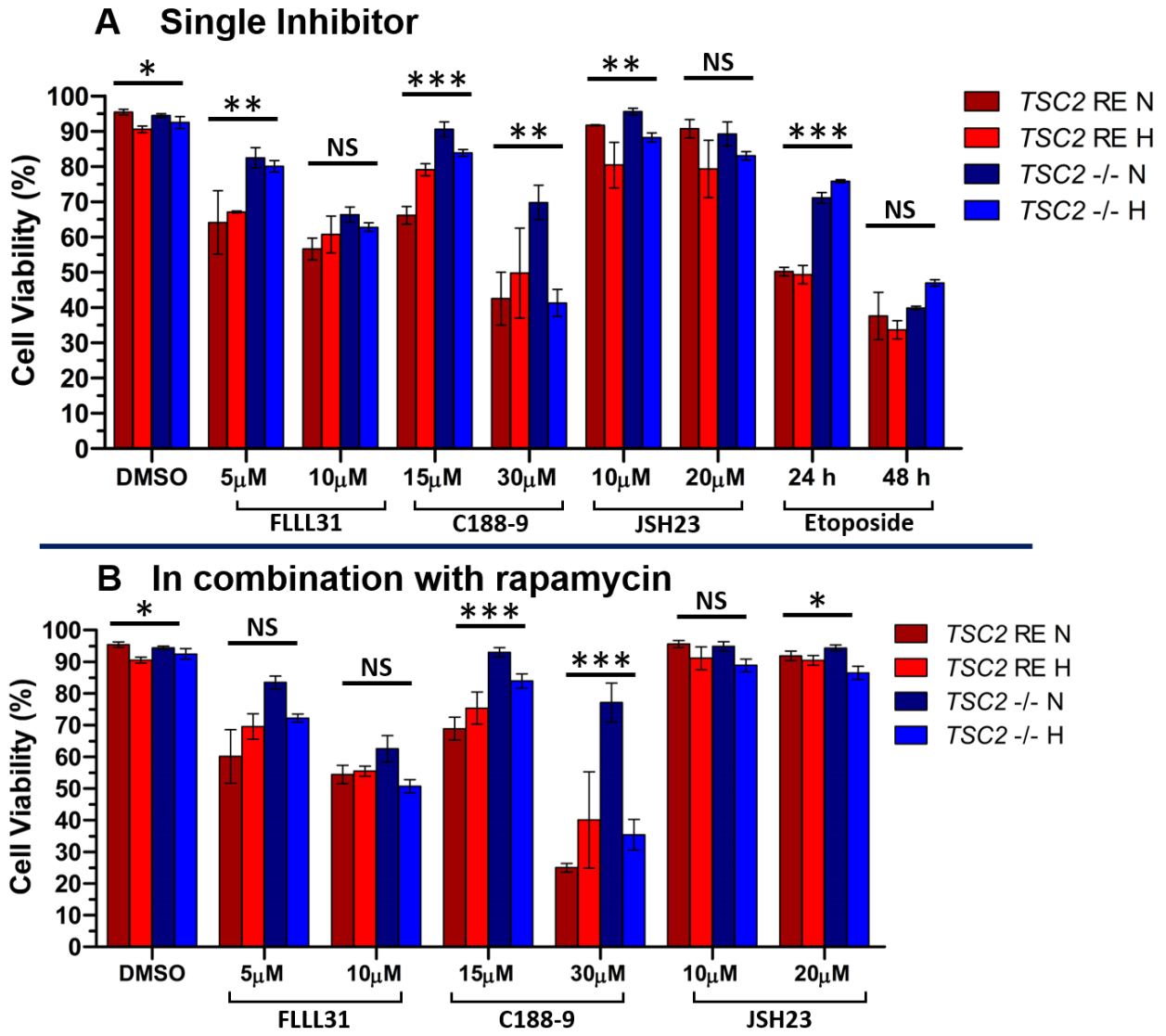


**Figure 3.7. Targeting STAT3 downstream of Ref-1 in AML cells is generally more cytotoxic than targeting Ref-1 but doesn't appear selective towards *TSC2* deficient AML cells.** *TSC2* RE or *TSC2* deficient (-/-) AML cells in tissue culture plates were grown to ~70-80% confluency. Cells were then treated with the STAT3 inhibitors (FLLL31 & C188-9)/NF-kB inhibitor (JSH23) either under normoxia (N) or hypoxia (H) for 24 h, with either the specified inhibitor alone (Graph **A**) or in combination with rapamycin (Graph **B**) at 50 nM. Cells were then collected, retaining trypsin washes and original drugged media, spun down and resuspended. Cell suspensions were then mixed with AO/PI stain and viable/non-viable cells were assayed on a dual-fluorescence cell counter (N=4 minimum). Average percentage of viable cells are plotted on the above graphs. The significance between differences in percentage of viable cells for each cell line under each drug condition was determined through one-way ANOVA and annotated on each graph. Significance denoted by: * = $p < 0.05$, ** = $p < 0.01$, *** = $p < 0.001$, NS = not significant. Etoposide (100 μM) treatments represent positive controls for decrease in cell viability. Bars represent standard error of the mean.

### 3.2.4. Effect of Ref-1 inhibition on the growth of *TSC2* deficient AML and MEF tumour spheroids.

Whilst Everolimus (rapamycin analogue) is effective at reducing tumour volume of brain and renal lesions (Bissler *et al.* 2013 and Franz *et al.* 2013), these inhibitors are not effective for all TSC patients. This clinical observation suggests that other dysregulated signalling pathways besides mTORC1 may contribute towards tumourigenesis in TSC. Therefore, the next aim of this chapter was to evaluate the efficacy of targeting the Ref-1/HIF-1α/STAT3/NF-κB axis in reducing the growth of tumour spheroids formed from *TSC2* deficient cells. Tumour spheroids are a more representative cell model for screening drug efficacy *in vitro,* as 3D-cell cultures recapitulate more features of lesions than 2D cell culture. Such as cell to cell contacts/signalling (Baker and Chen, 2012), oxygen gradients through tumours (Grimes and Currell, 2018) and factoring in drug penetrance (Minchinton and Tannock, 2006).

As seen by the growth curve in figure 3.8 (**A**), a one-way ANOVA found that the mean differences in spheroid area from time 0 days among all treatment conditions, at each timepoint, was significant. Treatment with either 50 µM or 100 µM of APX3330 does not significantly affect the growth of *TSC2* deficient AML spheroids compared to the DMSO control, with a Tukey post-hoc test finding at no time point was the difference in spheroid growth between DMSO and APX3330 treated spheroids significant. Spheroids treated with both concentrations of APX2009 (5 and 10 µM) and 5 µM of APX2014 showed decreased growth over time in culture compared to the DMSO control, as shown in figure 3.8 (**A**). However, the % change in spheroid area between 14 and 0 days in culture, the endpoint of the growth assay for statistical analysis, was only found to be significantly different for spheroids treated with 5 µM of APX2009 compared to DMSO (32.8% for APX2009 at 5 µM compared to 66.6% for DMSO) (Figure 5.8 **B**). At no time point before day 14 was there a significant difference between % change in spheroid area from time 0 days between DMSO and APX2009 treated spheroids, as determined by a Tukey post-hoc test. Strangely, higher concentrations of both APX3330 (100 µM) and APX2014 (10 µM) resulted in a higher % change in spheroid area between 14 and 0 days in culture, but again was not significantly different from spheroids treated with DMSO. Only at day 4 of treatment was the % change in spheroid area from time 0 days found to be significantly different between spheroids treated with either DMSO or APX2014 at 10 µM. By and large however, from treatment time 7 days a Tukey post-hoc test found that the difference between % change in spheroid area from time 0 days between APX2014 at 10 µM treated spheroids and spheroids treated with the other Ref-1 inhibitors was significant. Although a standard method, measuring the perimeter of spheroid cross section images may not be the best way to assess tumour growth. It was observed in the image panel in figure 3.9, that the treatment with these inhibitors resulted in cell

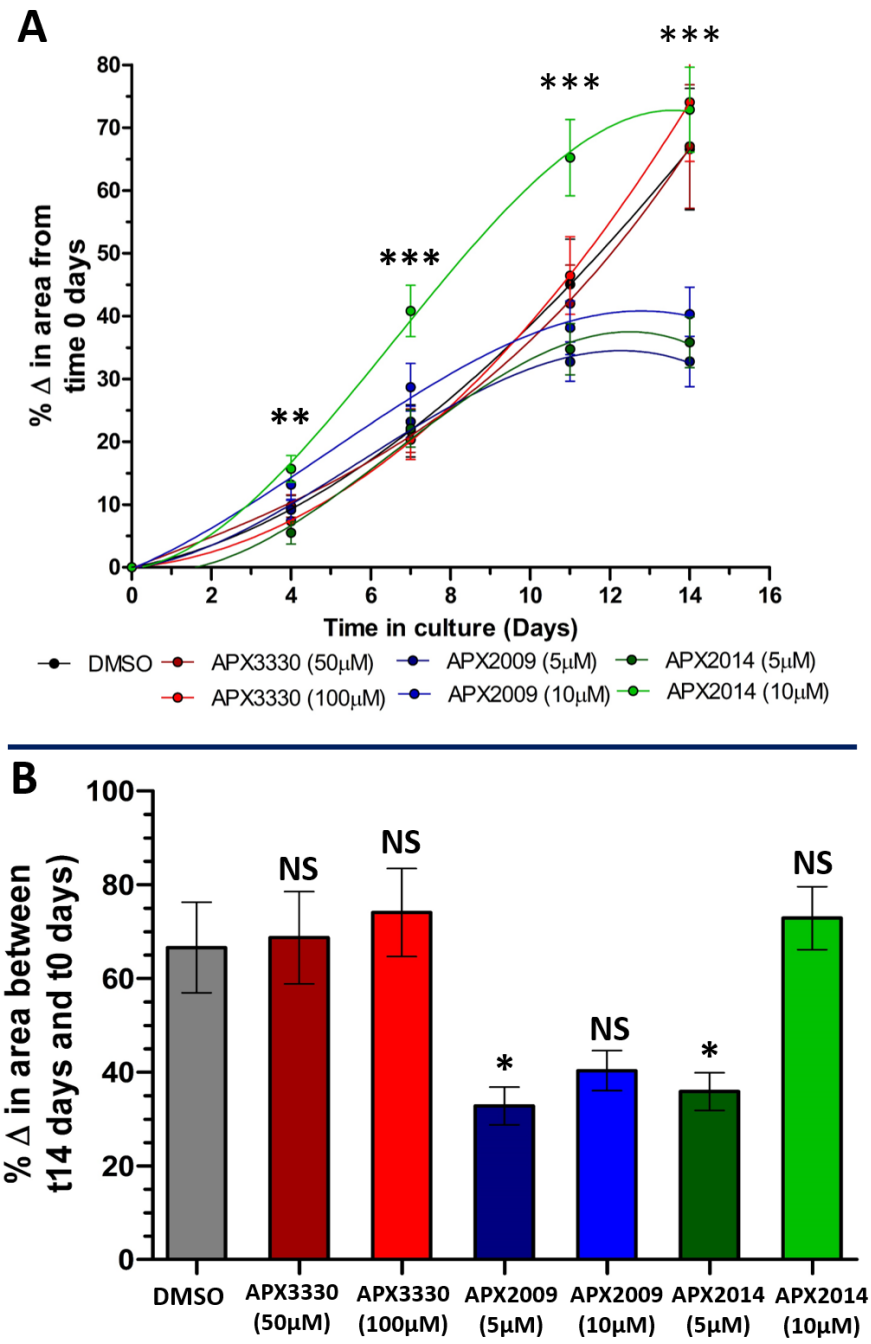


**Figure 3.8 Lower concentrations of APX2009 and APX2014 significantly affect *TSC2* deficient AML spheroid growth.** In the agarose coated wells of a clear-bottom 96-well plate, 5,000 cells were added per well and allowed to coalesce into spheroids for 3 days. After 3 days, spheroids were treated with either DMSO (vehicle) or the specified concentrations of Ref-1 inhibitors APX3330, APX2009 and APX2014. Pictures were taken from treatment at time = 0, 4, 7, 11, and 14 days, with half of media in each well changed for fresh drugged media at each time point. Area of spheroids at each time point was measured and change in area from time 0 days was calculated and plotted to generate a growth curve (graph **A**). Median number of spheroids scored per condition (N#) was 44. Significance of differences in change in area from time 0 days at each time point between all treatment conditions was determined by one-way ANOVA and annotated on graph. Change in area of spheroids between time 14 and 0 days was taken as the endpoint of the spheroid growth assay (graph **B**). Statistical analysis of differences in change in area from time 0 days and 14 days between DMSO and all other drug treatments was by one-way ANOVA with a Tukey post Hoc test and annotated on graph. Significance denoted by: * = $p < 0.05$, ** = $p < 0.01$, *** = $p < 0.001$, NS = not significant. Bars represent standard error of the mean.

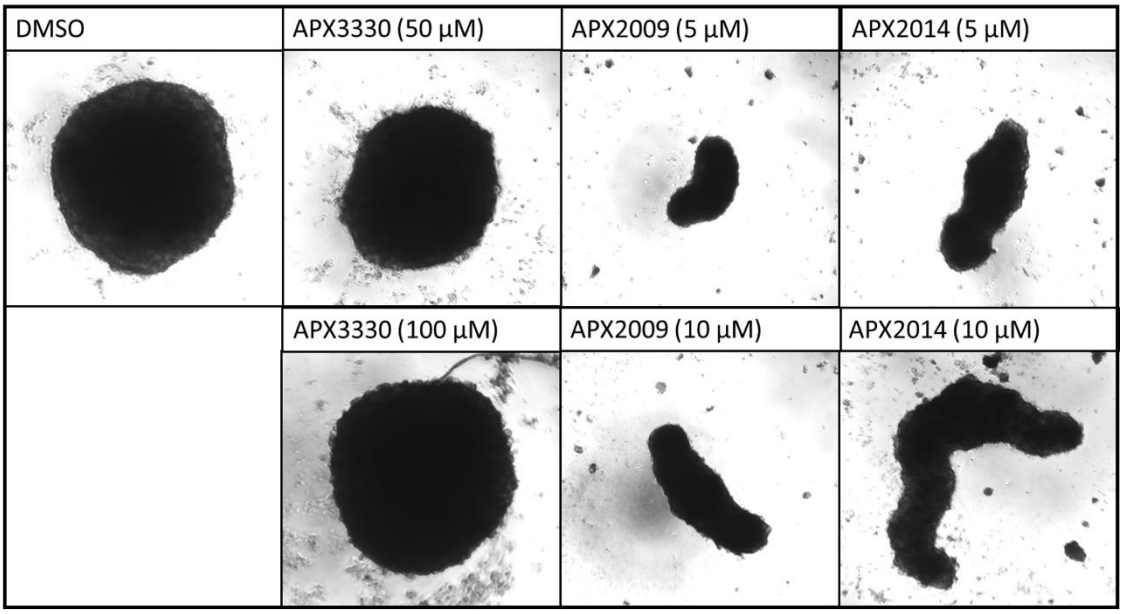


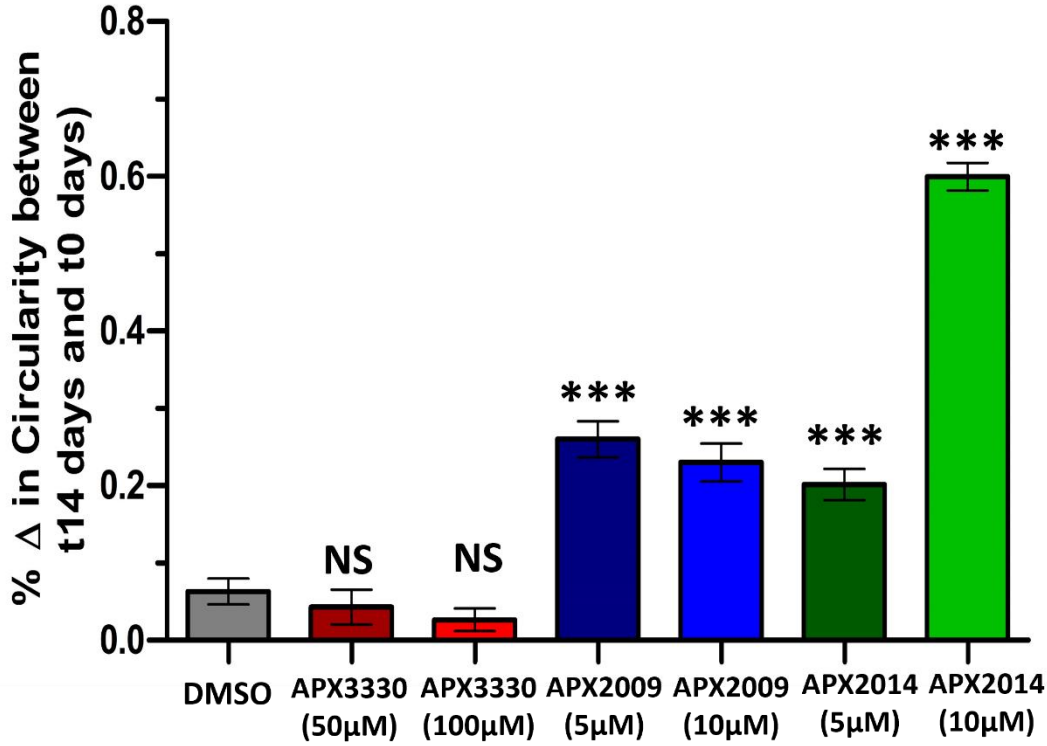


**Figure 3.9. AML *TSC2* deficient spheroids treated with 2nd generation Ref-1 inhibitors adopt irregular shapes, as reflected by their change in circularity.** The Image panel shows representative images of treated AML spheroids at time 14 days. As seen, treating *TSC2* deficient AML spheroids with the 2nd generation Ref-1 inhibitors APX2009 and APX2014 results in them adopting irregular more elongated shapes. This is reflected in the average change in the spheroid's circularity at time 14 days since time 0 days. Median number of spheroids scored per condition (N#) was 44. Significance of differences in change in circularity between t=14 days and 0 days between DMSO and all other drug treatments was by one-way ANOVA with a Tukey post Hoc test and annotated on graph. Significance denoted by: *** = p< 0.001 and NS = not significant. Bars represent standard error of the mean.

aggregations that adopted unusual and elongated cylinder shapes. This change in shape can be scored by the average % change in spheroid circularity between 14 and 0 days in culture. Circularity, defined by the equation $4\pi$ x (area/(perimeter$^2$)), is a measure of how much a shape conforms to that of a perfect circle. The lower a shape's circularity than 1, the less that shape conforms to a perfect circle. As shown in figure 3.9, DMSO treated AML spheroid's shape remains stable and show a small average change in circularity (0.06%). The average change in circularity for AML spheroids treated with APX2009 and APX2014 was much higher (APX2009 at 5 µM and 10 µM: 0.25% and 0.24% respectively, APX2014 at 5 µM and 10 µM: 0.20% and 0.60% respectively) and was found to be significantly different compared spheroids treated with DMSO. Linear regression analyses found strong negative correlations between spheroid area and circularity for spheroids treated with APX2009 and APX2014. This further suggests that area measurements for spheroids treated with APX2009 and APX2014 is influenced by their change in circularity and thus may not be directly comparable with DMSO spheroids.

As with *TSC2* deficient AML spheroids, the general trend for *Tsc2* −/− MEF cell spheroid growth on treatment with Ref-1 inhibitors is to decrease compared to the DMSO control. With a one-way ANOVA finding that the mean differences in spheroid area from time 0 days among all treatment conditions, at each time point, significant. As seen in figure 3.10 (**A**), treatment of MEF *Tsc2* −/− spheroids with 50 µM and 100 µM of APX3330 results in decreased growth compared to spheroids treated with DMSO. With a one way ANOVA reporting the % change in spheroid area between 14 and 0 days in culture for APX3330 treated spheroids (-4.4% at 50 µM, 8.7% at 100 µM) as significantly different from DMSO (31.6%) treated spheroids (APX3330 50 µM vs DMSO $p=3.16x10^{-6}$ and APX3330 100 µM vs DMSO p=0.0408) (figure 3.10 **B**). Interestingly, it was observed that at day 4 and 7, the lower concentration of APX3330 (50 µM) repressed spheroid growth relative to day 0 further than the higher concentration of APX3330 used (100 µM). With a Tukey post-hoc test finding that % change in spheroid area from time 0 days between spheroids treated with APX3330 at 50 µM and 100 µM significant. Why the lower concentration of APX3330 would repress the growth of *Tsc2* −/− MEF spheroids further than the higher concentration used is unclear. The lower % change in spheroid area between 14 and 0 days in culture for MEF spheroids treated with APX2009 at 5 µM (19.7%), APX2014 at 5 µM (21.7%) and 10 µM (9.5%) was not found to be significantly different from spheroids treated with DMSO. This is despite MEF spheroid shape remaining stable as seen in figure 3.11, and average % change in spheroid circularity between 14 and 0 days in culture not significantly different between MEF spheroids treated with DMSO or APX2009 and APX2014. Owing to high standard deviation in spheroid area at day 14 (figure 5.10), perhaps

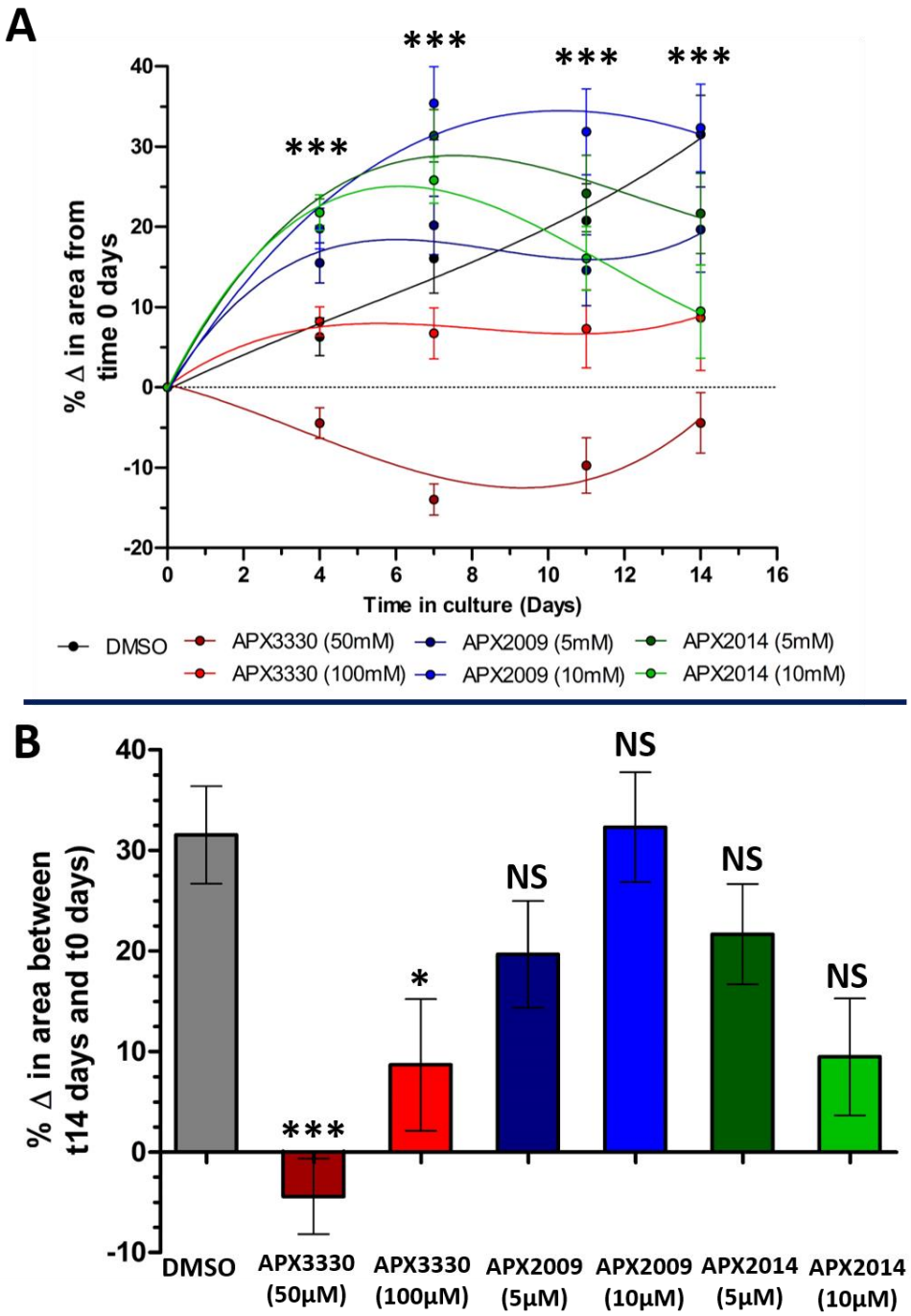


**Figure 3.10 APX3330 significantly decreases *Tsc2* −/− MEF spheroid growth.** In the agarose coated wells of a clear-bottom 96-well plate, 1,000 cells were added per well and allowed to coalesce into spheroids for 7 days. After 7 days, spheroids were treated with either DMSO (vehicle) or the specified concentrations of Ref-1 inhibitors APX3330, APX2009 and APX2014. Pictures were taken from treatment at time = 0, 4, 7, 11, and 14 days, with half of media in each well changed for fresh drugged media at each time point. Area of spheroids at each time point was measured and change in area from time 0 days was calculated and plotted to generate a growth curve (graph **A**). Median number of spheroids scored per condition (N#) was 37. Significance of differences in change in area from time 0 days at each time point between all treatment conditions was determined by one-way ANOVA and annotated on graph. Change in area of spheroids between time 14 and 0 days was taken as the endpoint of the spheroid growth assay (graph **B**). Statistical analysis of differences in change in area from time 0 days and 14 days between DMSO and all other drug treatments was by one-way ANOVA with a Tukey post Hoc test and annotated on graph. Significance denoted by: * = p <0.05, *** = p< 0.001, NS = not significant. Bars represent standard error of the mean.

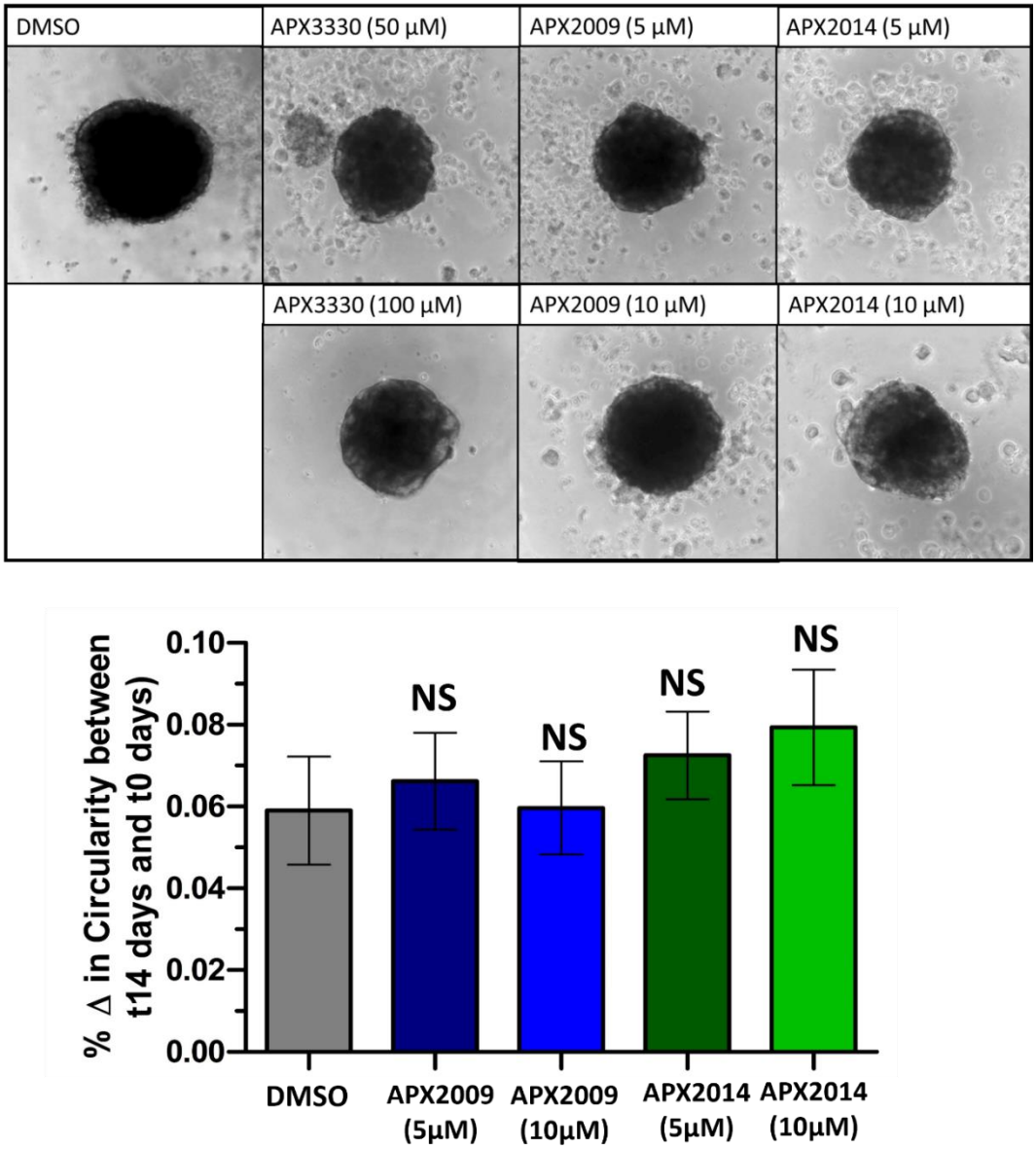


**Figure 3.11. MEF *Tsc2* −/− spheroids circularity remains stable when treated with 2nd generation Ref-1 inhibitors.** The Image panel shows representative images of treated MEF spheroids at time 14 days. As seen, *Tsc2* −/− MEF spheroids treated with the 2nd generation Ref-1 inhibitors APX2009 and APX2014 retain a spherical shape and does not result in significant changes to the spheroid's circularity at time 14 days since time 0 days. Median number of spheroids scored per condition (N#) was 37. Significance of differences in change in circularity between t=14 days and 0 days between DMSO and all other drug treatments was by one-way ANOVA with a Tukey post Hoc test and annotated on graph. Significance denoted by: NS = not significant. Bars represent standard error of the mean.

the experiment was not empowered enough to find the observed decrease in spheroid growth on treatment with APX2009 or APX2014 statistically significant, despite a median of 37 spheroids measured per condition at time 14 days. Looking at % change in spheroid area from time 0 days before the day 14 endpoint, a Tukey post-hoc test did find that at day 4 and day 7, all three Ref-1 inhibitors at least at one concentration used, resulted in a significant % change in spheroid area from time 0 days relative to the DMSO control. In order to check that decrease in spheroid growth was not due spheroids becoming non-viable in the presence of

Ref-1 inhibitors, tumour outgrowth was carried out. As demonstrated in the image panel in figure 3.12, both *TSC2* deficient AML and MEF spheroids treated with APX3330, APX2009 and APX2014 remained viable, showing cell outgrowth. The etoposide treated control spheroids however showed no outgrowth, as expected with this cytotoxic drug. Therefore, the drug action of the Ref-1 inhibitors to reduce tumour growth is likely cytostatic, as opposed to cytotoxic.

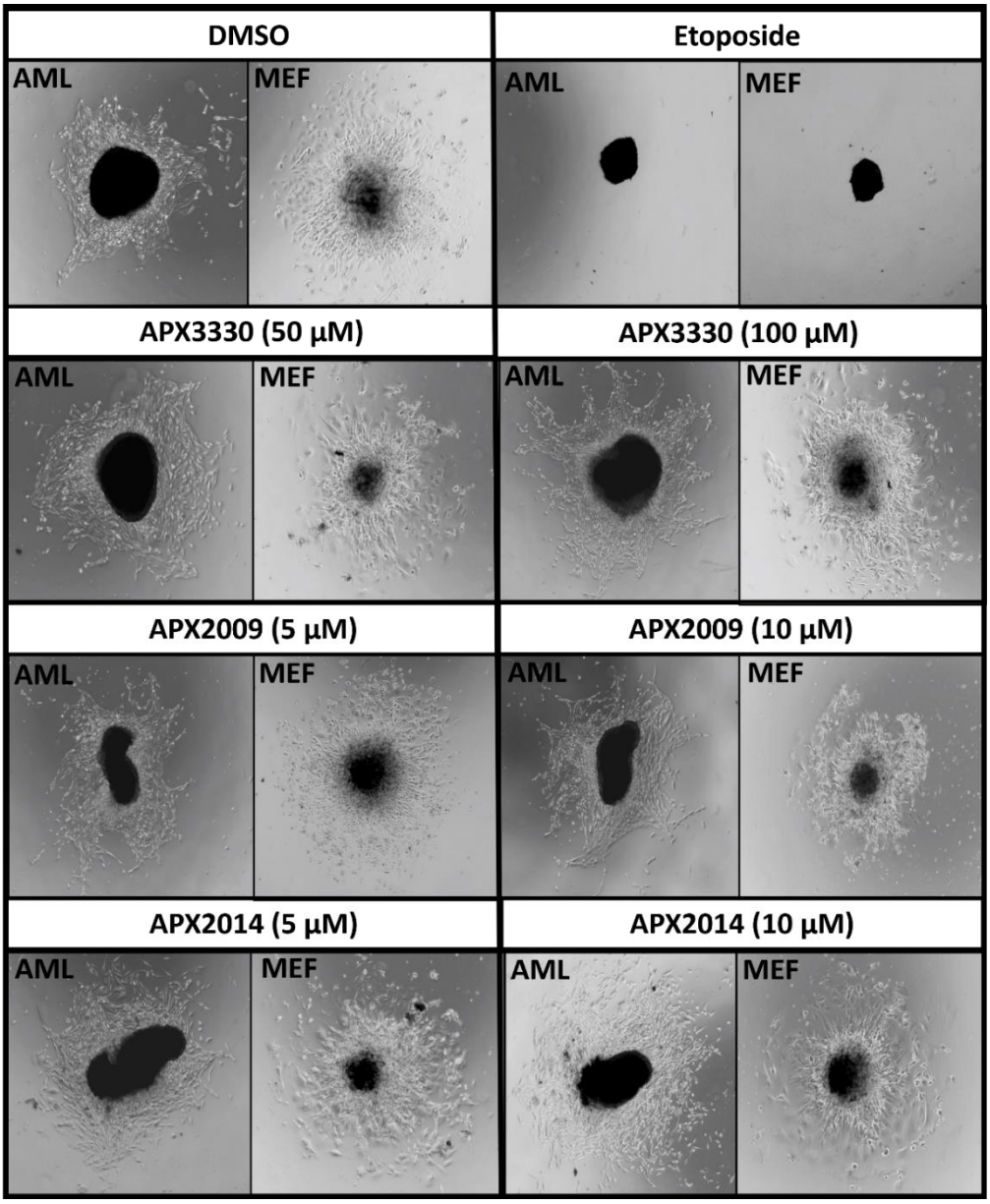


**Figure 3.12 Both *TSC2* deficient AML and MEF tumour spheroids remain viable after treatment with Ref-1 inhibitors.** At the end of tumour spheroid growth assays (t=14days), AML and MEF spheroids were transferred individually to the wells of a 24-well tissue culture plate, containing fresh drug free media. Tumour spheroids were allowed to outgrow to assess spheroid viability after treatment. Pictures were taken at time 6 days for AML spheroid and 3 days MEF spheroids. The above image panel shows representative images (N=6 spheroids per condition). After prolonged drug treatment with Ref-1 inhibitors, both *TSC2* deficient AML and MEF spheroids are able to outgrow. The inhibitor, at the defined concentration, the spheroids were cultured with is annotated above images. Etoposide (100 µM) control spheroids show no outgrowth.

### 3.2.5. Effect of STAT3 and NF-κB inhibition on the growth of AML and MEF *TSC2* deficient tumour spheroids.

The next aim of the present chapter was to assay whether targeting STAT3 or directly NF-κB reduced the growth of tumour spheroids formed from *TSC2* deficient cells, in comparison to mTORC1 inhibition. As seen by the growth curve in figure 3.13 (**A**), a one-way ANOVA found that the mean differences in spheroid area from time 0 days among all treatment conditions, at each timepoint, was significant. mTOR inhibition is the most effective at decreasing AML *TSC2* deficient spheroid growth, reducing spheroid area early into treatment and resulting in a negative % change in spheroid area over 0 and 14 days in culture when compared to DMSO treated spheroids (-10.1% vs 66.6% for Rapamycin $p=<1x10^{-8}$ and -2.56% vs 66.6% for Ku0063794 $p=<1x10^{-6}$) (figure 3.13 **B**). The negative decrease in % change in spheroid area from day 0 for spheroids treated with either rapamycin or Ku0063794 relative to DMSO treated spheroids was reported significant by a Tukey post-hoc test. Additionally, at every timepoint before day 14, the negative decrease in % change in spheroid area from day 0 was significantly larger for rapamycin and Ku0063794 treated spheroids than observed with any other inhibitor. As reported by a Tukey post-hoc test.

Compared to treatment with Ref-1 inhibitors, inhibiting STAT3 and NF-κB directly is far more effective at reducing AML spheroid growth. After the mTOR inhibitors, treatment with C188-9 results in the smallest % change in spheroid area between 14 and 0 days in culture compared to DMSO (2.1% vs 66.6%, $p=<1x10^{-8}$). FLLL31 treatment is the next most effective (13.2% vs 66.6% $p=<1x10^{-8}$), followed lastly by treatment with JSH23 (31.2% vs 66.6%, $p=1.9x10^{-6}$). A Tukey post hoc test found no significant difference between % change in spheroid area between 14 and 0 days in culture for AML spheroids treated with either STAT3 inhibitors (FLLL31 and C188-9) (figure 3.13 **B**). The difference between % change in spheroid area between 14 and 0 days in culture for AML spheroids treated with C188-9 and JSH23 was found to be significant ($p=1.5x10^{-4-}$). Suggesting inhibition of STAT3 is more effective at decreasing *TSC2* deficient AML spheroid growth than NF-κB inhibition. Looking more broadly at the whole treatment time course. Differences in % change in spheroid area from time 0 days for spheroids treated with either C188-9 or FLLL31 and DMSO treated spheroids, were reported significant at each timepoint by a Tukey post-hoc test. Additionally, at no time point was the % change in spheroid area from time 0 days between C188-9 and FLLL31 treated spheroids reported significant. Indicating both STAT3 inhibitors are equally as effective as one another in repressing *TSC2* deficient AML spheroid growth. Comparatively, only from day 11 of treatment was the % change in spheroid area from time 0 days between JSH23 and DMSO treated spheroids reported significant. Highlighting that across the whole treatment time course, STAT3 inhibition appears more effective at repressing *TSC2* deficient AML spheroid

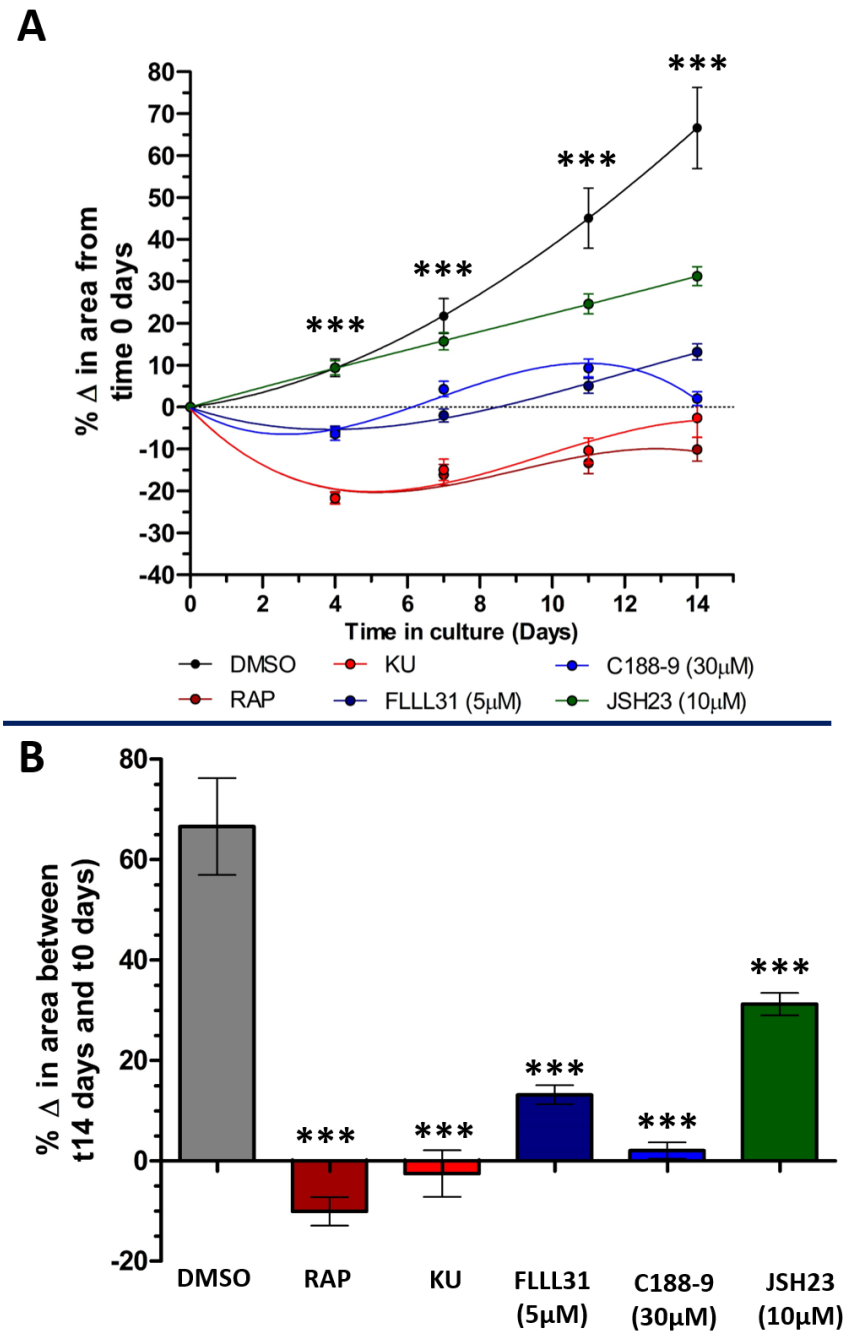


**Figure 3.13. Inhibition STAT3 or NF-kB directly significantly decreases *TSC2* deficient AML spheroid growth.** In the agarose coated wells of a clear-bottom 96-well plate, 5,000 cells were added per well and allowed to coalesce into spheroids for 3 days. After 3 days, spheroids were treated with either DMSO (vehicle) or the specified concentrations of mTORC1 inhibitors, rapamycin (50 nM) or Ku0063794 (1 μM), STAT3 inhibitors FLLL31 or C188-9 or the NF-kB inhibitor JSH23. Pictures were taken from treatment at time = 0, 4, 7, 11, and 14 days, with half of media in each well changed for fresh drugged media at each time point. Area of spheroids at each time point was measured and change in area from time 0 days was calculated and plotted to generate a growth curve (graph **A**). Median number of spheroids scored per condition (N#) was 41. Significance of differences in change in area from time 0 days at each time point between all treatment conditions was determined by one-way ANOVA and annotated on graph. Change in area of spheroids between time 14 and 0 days was taken as the endpoint of the spheroid growth assay (graph **B**). Statistical analysis of differences in change in area from time 0 days and 14 days between DMSO and all other drug treatments was by one-way ANOVA with a Tukey post Hoc test and annotated on graph. Significance denoted by: *** = p< 0.001, NS = not significant. Bars represent standard error of the mean. RAP = rapamycin, KU= Ku-0063794.

growth than NF-κB inhibition. Unlike treatment with the 2nd generation Ref-1 inhibitors APX2009 and APX2014 (figure 3.9), treating AML spheroids with rapamycin, Ku0063794, FLLL31, C188-9 or JSH23 did not significantly affect the average % change in spheroid circularity between 14 and 0 days in culture compared to AML spheroids treated with DMSO, as shown in figure 3.14.

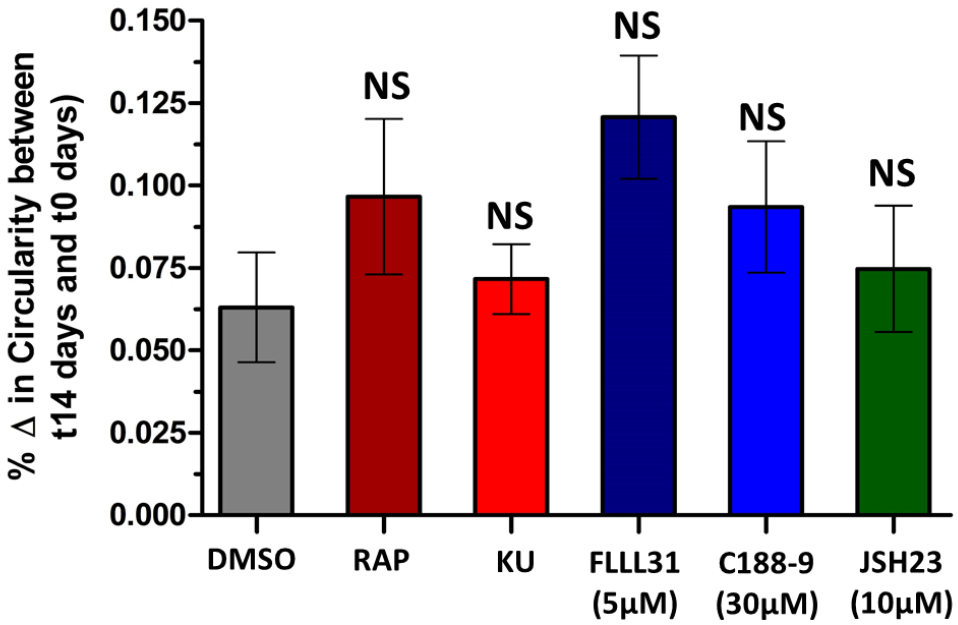


**Figure 3.14. Treatment of AML *TSC2* deficient spheroids with rapamycin, Ku0063794, FLLL31, C188-9 or JSH23 does not significantly change their circularity compared to DMSO control**. RAP = rapamycin (50 nM), KU= Ku-0063794 (1 μM). Median number of spheroids scored per condition (N#) was 41. Significance of differences in change in circularity between t=14 days and 0 days between DMSO and all other drug treatments was by one-way ANOVA with a Tukey post Hoc test and annotated on graph. Significance denoted by: *** = p< 0.001 and NS = not significant. Bars represent standard error of the mean.

As seen in figure 3.15 (**A**), a one-way ANOVA found that the mean differences in spheroid area from time 0 days among all treatment conditions, at each timepoint, was significant. The growth of *Tsc2* −/− MEF spheroids is far more effected by mTOR inhibition than the AML spheroids, and again mTOR inhibitors were the most effective at decreasing MEF *Tsc2* −/− spheroid growth, reducing spheroid area dramatically early into treatment and resulting in large negative % changes in spheroid area between 14 and 0 days in culture when compared to DMSO treated spheroids (-63.25% vs 31.6% for Rapamycin p=<$1x10^{-8}$ and -67.63% vs 66.6% for Ku0063794 p=<$1x10^{-8}$) (figure 3.15 **B**). As in the case of the AML spheroids, the negative decrease in % change in spheroid area from day 0 for spheroids treated with either rapamycin or Ku0063794 relative to DMSO treated spheroids was reported significant by a Tukey post-hoc test. At every timepoint before day 14, the substantial negative decrease in %

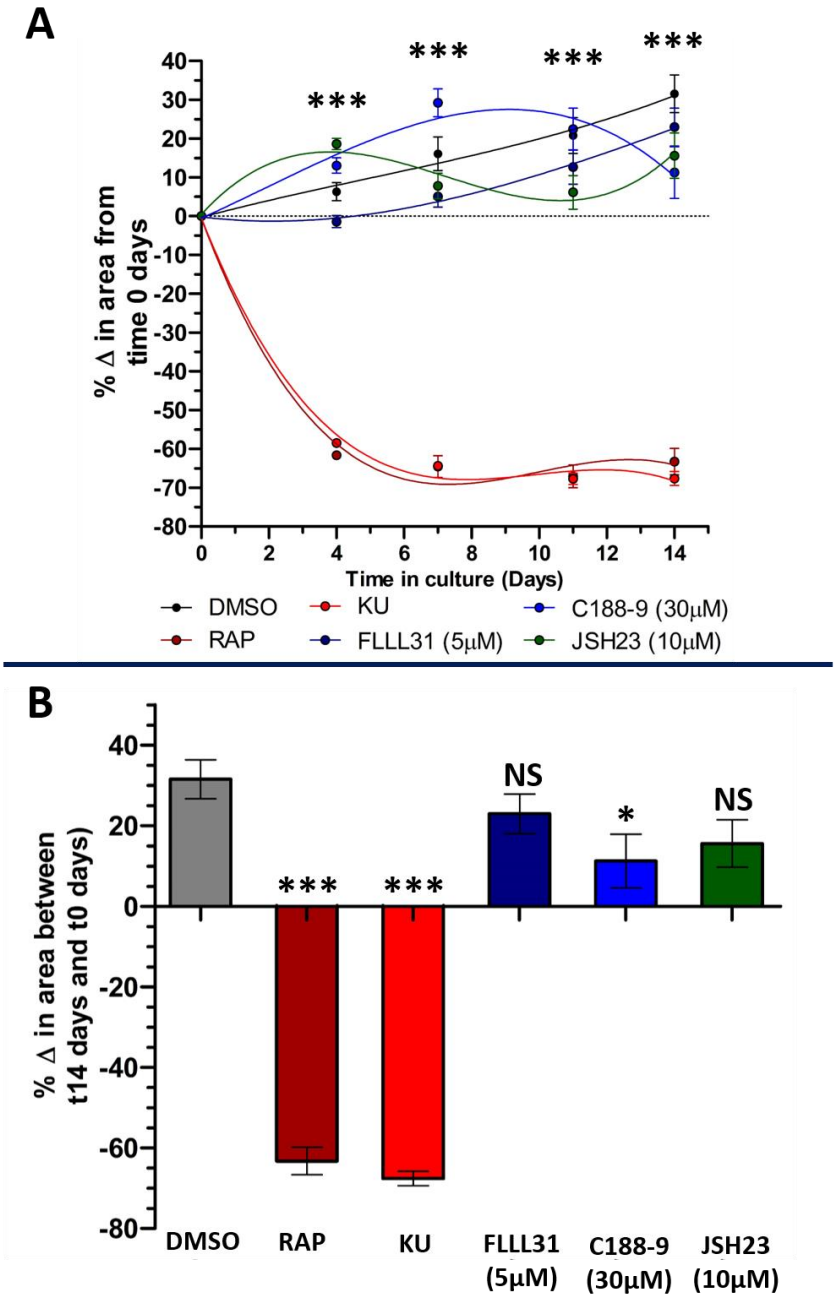


**Figure 3.15 Treatment with C188-9 significantly decreases *Tsc2* −/− MEF spheroid growth.** In the agarose coated wells of a clear-bottom 96-well plate, 1,000 cells were added per well and allowed to coalesce into spheroids for 7 days. After 7 days, spheroids were treated with either DMSO (vehicle) or the specified concentrations of mTORC1 inhibitors, rapamycin (50 nM) or Ku0063794 (1 μM), STAT3 inhibitors FLLL31 or C188-9 or the NF-kB inhibitor JSH23. Pictures were taken from treatment at time = 0, 4, 7, 11, and 14 days, with half of media in each well changed for fresh drugged media at each time point. Area of spheroids at each time point was measured and change in area from time 0 days was calculated and plotted to generate a growth curve (graph **A**). Change in area of spheroids between day 14 and day 0 was taken as the endpoint of the spheroid growth assay for statistical analysis (graph **B**). Median number of spheroids scored per condition (N#) was 37. Significance of differences in change in area from time 0 days at each time point between all treatment conditions was determined by one-way ANOVA and annotated on graph. Change in area of spheroids between time 14 and 0 days was taken as the endpoint of the spheroid growth assay (graph **B**). Statistical analysis of differences in change in area from time 0 days and 14 days between DMSO and all other drug treatments was by one-way ANOVA with a Tukey post Hoc test and annotated on graph. Significance denoted by: * = $p < 0.05$, *** = $p < 0.001$, NS = not significant. Bars represent standard error of the mean. RAP = rapamycin, KU= Ku-0063794.

change in spheroid area from day 0 was significantly larger for rapamycin and Ku0063794 treated spheroids than observed with any other inhibitor. As reported by a Tukey post-hoc test.

Inhibiting STAT3 or NF-κB directly is less effective at reducing growth in *Tsc2* −/− MEF spheroids than in the AML spheroids. With a Tukey post hoc test only finding C188-9 treatment causing a significantly lower % change in spheroid area over 14 and 0 days in culture compared to spheroids treated with DMSO (11.24 vs 31.6% p=0.0338). The % change in spheroid area over 14 and 0 days in culture for MEF spheroids treated with either FLLL31, C188-9 or JSH23 was not reported as significantly different from each other at day 14 (figure 3.15 **B**). Looking more broadly at the whole treatment time course. On day 4, 7 and 11 of treatment, neither FLLL31, C188-9 and JSH23, consistently resulted in % changes in spheroid area from day 0 that were reported as significantly different compared to DMSO treated spheroids. And only at day 4 of treatment did JSH23 or FLLL31 result in % changes in spheroid area from day 0 significantly different to DMSO treated spheroids. Highlighting that STAT3 and NF-κB inhibition are not particularly effective at repressing *Tsc2* −/− MEF spheroid growth and suggesting that mTORC1 hyperactivity may be a more critical driver of spheroid growth. As in the case for Ref-1 inhibitors, MEF and AML spheroids treated with rapamycin, Ku0063794, FLLL31, C188-9 or JSH23 remained viable after the treatment regime ended (see figure 3.16).

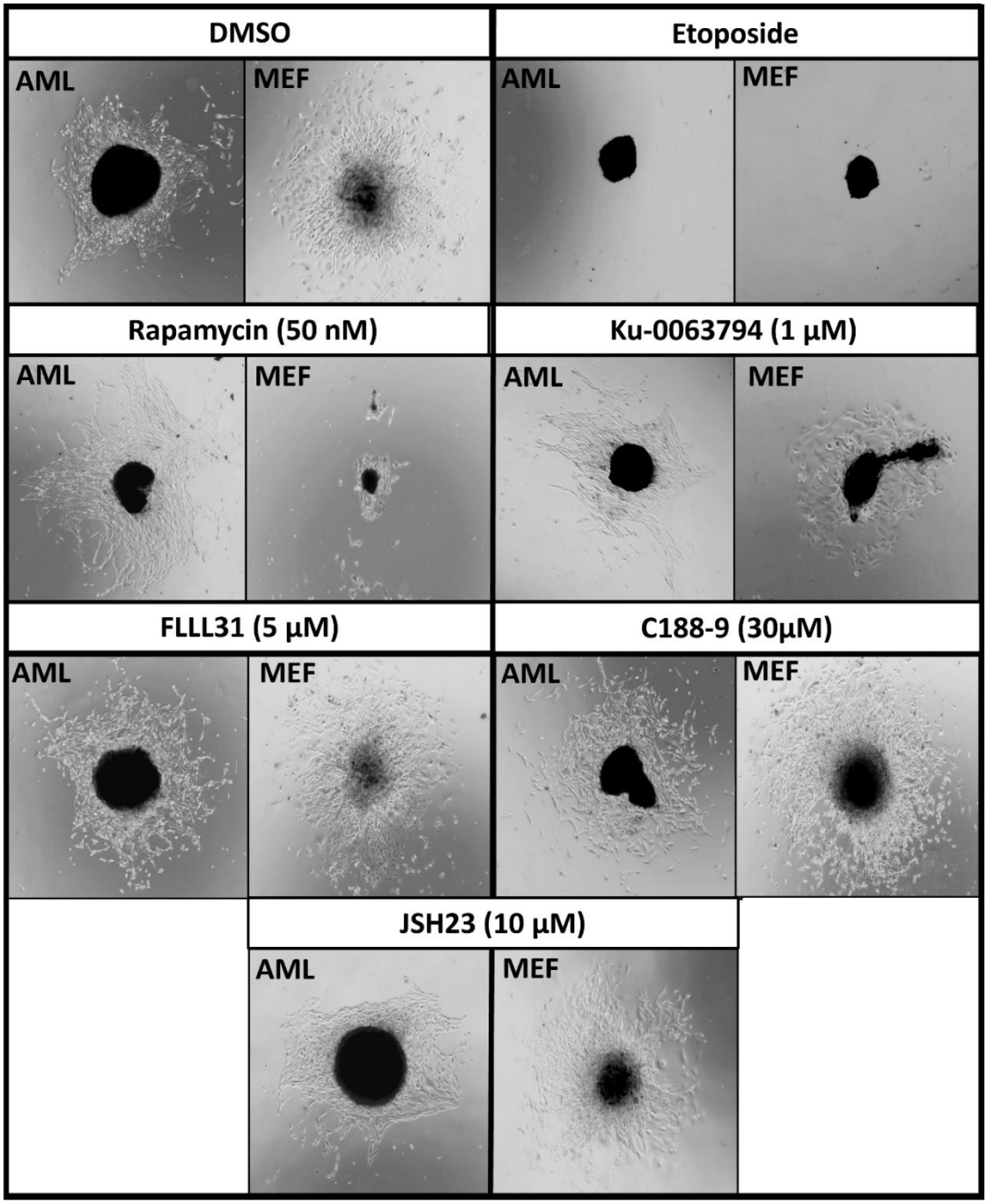


**Figure 3.16 Both *TSC2* deficient AML and MEF tumour spheroids remain viable after treatment with mTOR, STAT3 and NF-kB inhibitors.** At the end of tumour spheroid growth assays (t=14days), AML and MEF spheroids were transferred individually to the wells of a 24-well tissue culture plate, containing fresh drug free media. Tumour spheroids were allowed to outgrow to assess spheroid viability after treatment. Pictures were taken at time 6 days for AML spheroid and 3 days MEF spheroids. The above image panel shows representative images (N=6 spheroids per condition). After prolonged drug treatment with mTOR, STAT3 and NF-kB inhibitors, both *TSC2* deficient AML and MEF spheroids are able to outgrow. The inhibitor, at the defined concentration, the spheroids were cultured with is annotated above images. Etoposide (100 µM) control spheroids show no outgrowth.

### 3.2.6 Effect of targeting the Ref-1/HIF-1α/STAT3/NF-κB signalling axis on anchorage independent growth of *TSC2* deficient AML cells.

Anchorage-independent growth refers to the ability of cells to grow independently of surrounding extracellular matrix or a solid support (Borowicz *et al.* 2014). Non-transformed cells are prevented from growing when detached from the extracellular matrix by a form of programmed cell death, termed anoikis (Taddei *et al*. 2012). However, the increased capacity of tumorigenic cells from a variety of cancers for anchorage-independent growth is well established (Shin *et al.* 1975). Both murine and human *TSC2* deficient cells have been shown to display anchorage independent growth *in vitro* (Johnson *et al.* 2018a, Lam *et al.* 2017 and Lesma *et al.* 2014). Therefore, the efficacy of targeting the Ref-1/HIF-1α/STAT3/NF-κB axis as a strategy to reduce anchorage-independent growth was assessed.

Per condition, the diameter of up to 100 colonies per repeat number (n=3) were measured from up to 10 pictures per repeat. As can be seen from plots of the anchorage independent growth assay (figures 3.17, 3.18, 3.19 and 3.20), there is a large degree of heterogeneity in colony size. Therefore, in order to prevent the scoring of single cells and small cell aggregates as colonies, the lower colony diameter threshold for scored AML and MEF *TSC2* deficient colonies was set arbitrarily at 30 µm. As shown in the dot plot in figure 3.17., treatment of *TSC2* deficient AML cells with Ref-1 inhibitors does not completely prevent anchorage independent growth. As reported by a one-way ANOVA of aggregated colony diameters of all colonies scored across all 3 repeats, only the average colony diameter in the APX2014 at 10 µM treated condition is significantly different from DMSO control (41.0 µm vs 91.8 µm $p=4.40x10^{-4}$). Whilst colony diameter in the APX2014 at 5 µM appears lower compared to the DMSO control (66.2 µm vs 91.8 µm), this difference was not reported as significant. Large heterogeneity in colony size, as represented by the large standard deviation seen in figure 3.17., limits finding statistical significance. The more potent Ref-1 inhibitors, APX2009 and APX2014, do appear to affect the proportion of seeded cells able to undergo anchorage independent growth. As denoted by the number of colonies scored in each condition, the number of colonies above 30 µm is considerably lower In APX2009 and APX2014 treated conditions. Unfortunately, due to equipment failure, different microscopes had to be used for imaging across repeat numbers. Therefore, unlike the *Tsc2* −/− MEF cell anchorage independent growth assays, scoring colony number per image, was not able to be recorded accurately due to the different frame sizes of images taken on different microscopes. As shown in figure 3.18, mTOR inhibition, either through rapamycin or Ku0063794, was very effective at reducing both total colonies scored and significantly decreased the average colony diameter compared to DMSO (Rapamycin vs DMSO: 55.6 µm vs 98.6 µm $p=<1x10^{-8}$, Ku0063794 vs

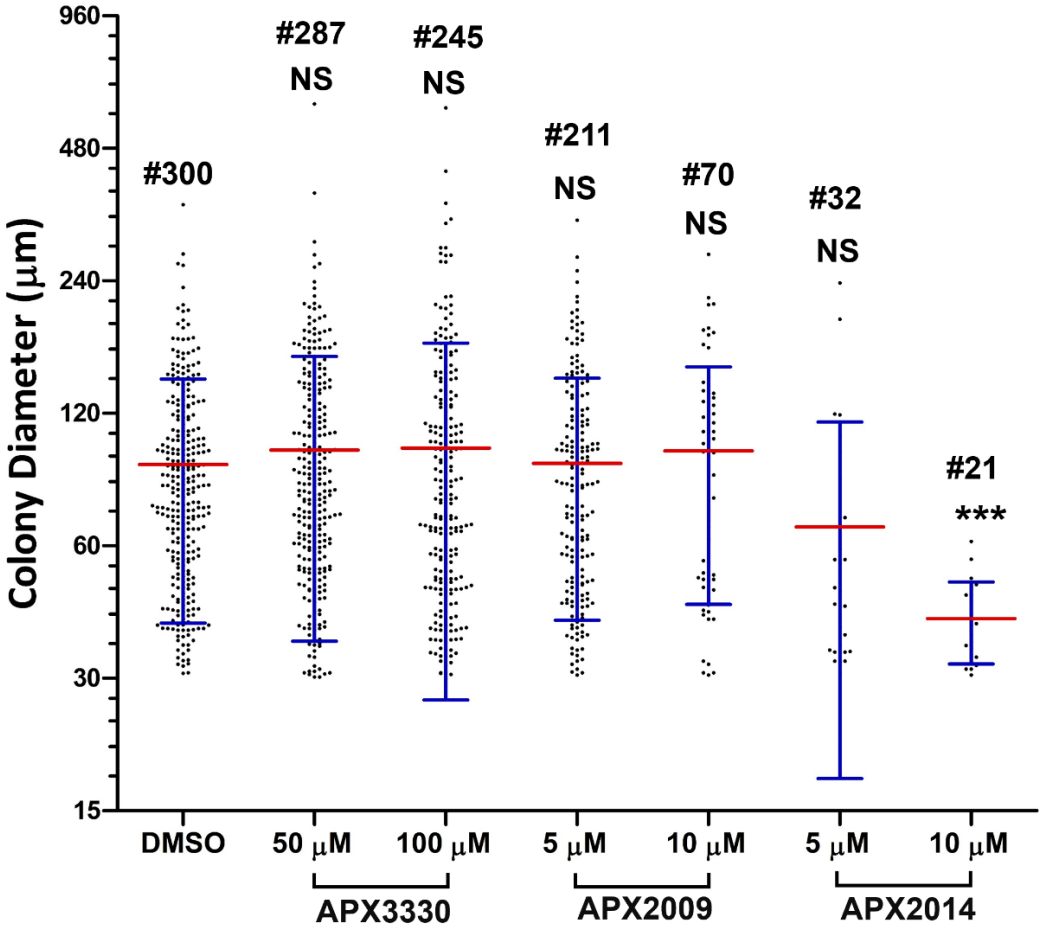


**Figure 3.17. Inhibition of Ref-1 effects colony formation of *TSC2* deficient AML cells, but only APX2014 at 10 µM significantly decreases colony diameter.** 12,000 *TSC2* deficient AML cells were seeded per well (six well plate) in a layer of 0.3% (w/v) agar/DMEM, with working concentration of defined drug. Drug treated media was added on top of this layer and replaced twice per week. After 4 weeks in culture, pictures were taken, and colony diameter scored. Lower diameter limit for colonies was set at 30 µM. Per condition up to 100 colonies per repeat number (N=3) were measured from up to 10 pictures per repeat number. Colony diameters across the three repeats were aggregated and plotted. # denotation above scatter plots indicate colony number up to 300. Y axis is scaled to Log2 colony diameter. Significance of differences in colony diameter between DMSO and all other drug treatments was determined by one way ANOVA with a Tukey Post Hoc test and annotated on graph. Significance denoted by: *** = p< 0.001 and NS = not significant. Bars represent standard deviation.

DMSO: 54.4 µm vs 98.6 µm p $2x10^{-8}$); as expected. STAT3 inhibition, through treatment with FLLL31 or C188-9, was able to significantly reduce colony diameter compared to DMSO (FLLL31 vs DMSO: 57.1µm vs 98.6 µm p=0.0123, C188-9 vs DMSO: 41.0 µm vs 98.6 µm p=$1x10^{-8}$). There was no significant difference between the average colony diameter recorded for FLLL31 and C188-9 treated AML cells. Nor was there a significant difference between the effect of mTOR inhibition vs STAT3 inhibition on average colony diameter. Interestingly, average colony diameter recorded for JSH23 treated AML cells was significantly higher than the DMSO control (JSH23 vs DMSO: 117.7 µm vs 98.6 µm p=<$1x10^{-8}$). Anchorage independent growth assay to record the effect of JSH23 treatment was set up at a different

time than the DMSO control. Therefore, whether the increase in colony diameter relative to DMSO control is a true effect of JSH23 treatment or whether it reflects a difference in the proliferative drive of the cells used for each set up is not known. Unlike AML cells treated with the Ref-1 inhibitors (figure 3.17), the number of cells seeded for the anchorage independent growth assay was different for the C188-9, JSH23 and etoposide treated conditions (figure 3.18), therefore firm conclusions about the proportion of seeded cells able to undergo anchorage independent growth in these conditions relative to the DMSO control cannot be made. Representative images of the anchorage independent growth assays can be seen in the supplementary data section (Figure S.3.3/4/5/6).

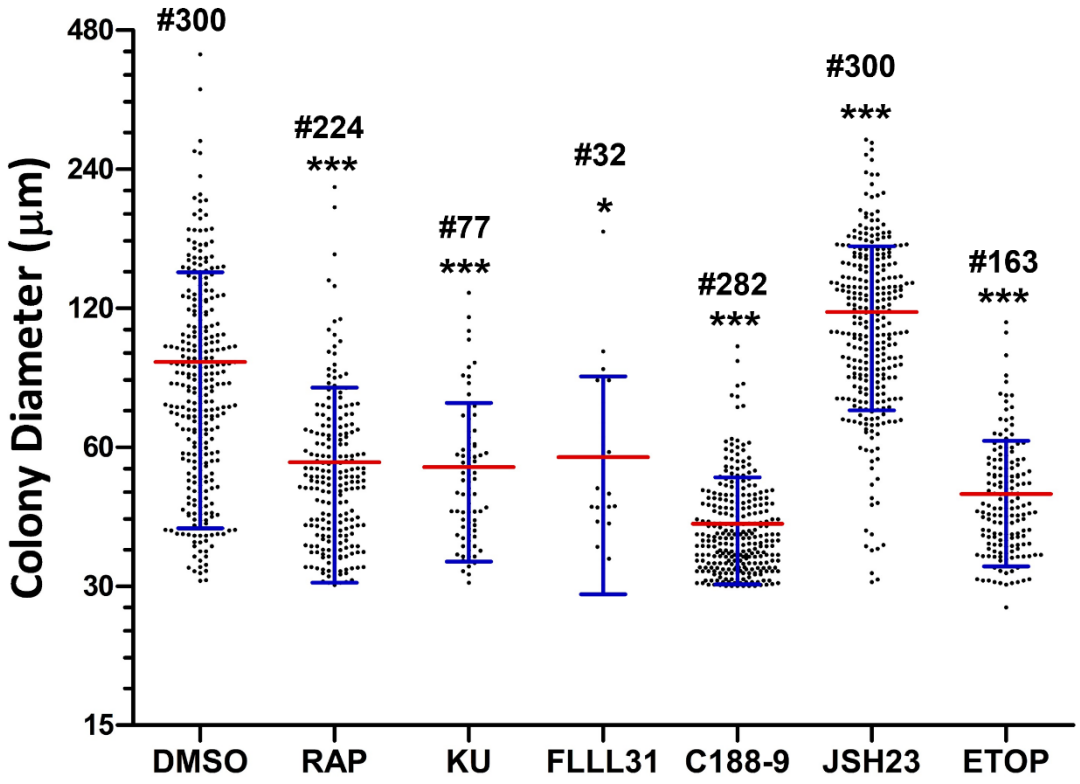


**Figure 3.18. Inhibition of STAT3 significantly decreases *TSC2* deficient AML colony diameter.** 12,000 *TSC2* deficient AML cells (40,000 cells for FLLL31, C188-9 and JSH23) were seeded per well (six well plate) in a layer of 0.3% (w/v) agar/DMEM, with working concentration of defined drug. Drug treated media was added on top of this layer and replaced twice per week. After 4 weeks in culture, pictures were taken, and colony diameter scored. Lower diameter limit for colonies was set at 30 µM. Per condition up to 100 colonies per repeat number (N=3) were measured from up to 10 pictures per repeat number. Colony diameters across the three repeats were aggregated and plotted. RAP= rapamycin (50 nM), KU=Ku-0063794 (1 µM), FLLL31 (5 µM), C188-9 (30 µM), JSH23 (10 µM) and ETOP= etoposide (100 µM). Y axis is scaled to Log2 colony diameter. # denotation above scatter plots indicate colony number up to 300. Significance of differences in colony diameter between DMSO and all other drug treatments was determined by one way ANOVA with a Tukey Post Hoc test and annotated on graph. Significance denoted by: * = $p < 0.05$, *** = $p < 0.001$ and NS = not significant. Bars represent standard deviation.

### 3.2.7 Effect of targeting the Ref-1/HIF-1α/STAT3/NF-κB signalling axis on anchorage independent growth of *Tsc2* −/− MEF cells.

Following the results of the anchorage independent growth assay in the *TSC2* deficient AML line, the same assay was set up in the murine TSC cell model. As seen by the recorded average colony diameter and total colonies scored, Ref-1 inhibition appears to be more effective at reducing anchorage independent growth in *Tsc2* −/− MEF cells (figure 3.19) compared to *TSC2* deficient AML cells (figure 3.17). APX3330 at either 50 µM or 100 µM does not significantly MEF colony diameter compared to the DMSO control. Treatment with APX2009 at 10 µM and both concentrations of APX2014 significantly reduces average colony diameter (figure 3.19). APX2009 at 10 µM vs DMSO: 46.4 µm vs 98.7 µm p=0.0253, APX2014 at 5 µM vs DMSO: 42.7 µm vs 98.7 µm $p=6.7x10^{-5}$ and APX2014 10 µM vs DMSO: 47.6 µm vs 98.7 µm $p=9.3x10^{-4}$. APX2009 and APX2014 at the aforementioned concentrations have a comparable effect on *Tsc2* −/− MEF anchorage independent growth, with average colony diameter not reported as significantly different from each other. As visualised in figure 3.20, treatment with the mTOR inhibitors rapamycin or Ku-0063794 was effective at reducing both total colonies scored and significantly decreased the average colony diameter compared to DMSO (rapamycin vs DMSO: 52.7 µm vs 98.7 µm $p=8x10^{-5}$, Ku0063794 vs DMSO: 47.5 µm vs 98.7 µm $p=3.6x10^{-4}$); as expected. Unlike with the *TSC2* deficient AML cells (figure 3.18), FLLL31 treatment seemed to significantly increase the colony diameter compared to the DMSO control (FLLL31 vs DMSO: 155.6 µm vs 98.7 µm $p=<1x10^{-8}$). C188-9 treatment however was significantly able to reduce average colony diameter compared to the DMSO control (C188-9 vs DMSO: 48.6 µm vs 98.7 µm p=0.0016) (figure 3.20). JSH23 treatment had no significant effect on average colony diameter compared to the DMSO control.

As pictures of anchorage independent growth assays of *Tsc2* −/− MEF cells were all taken using the same microscope, average number of colonies above 30 µm per picture (14,600 $mm^2$) could be accurately scored. As shown in figure 3.21, treatment with APX2009 at 10 µM, APX2014 at 5 µM and 10 µM and C188-9 were all as effective as mTOR inhibitors at reducing the proportion of seeded cells able to undergo anchorage independent growth (all p values=$<1x10^{-8}$). With a Tukey's post hoc test finding no significant difference in the average number of colonies per 14,600 $mm^2$ between these conditions. Whilst not significantly affecting colony diameter, APX3330 at 100 µM and APX2009 at 5 µM was able to significantly decrease the average number of colonies per 14,600 $mm^2$ compared to the DMSO control (both p values=$<1x10^{-8}$). Interestingly, treatment with 50 µM of APX3330 resulted in an almost twice as high average colony number per 14,600 $mm^2$ compared to the DMSO control (p=$<1x10^{-8}$)

(figure 3.21). JSH23 treatment had no significant effect on the average colony number per 14,600 $mm^2$ compared to the DMSO control.

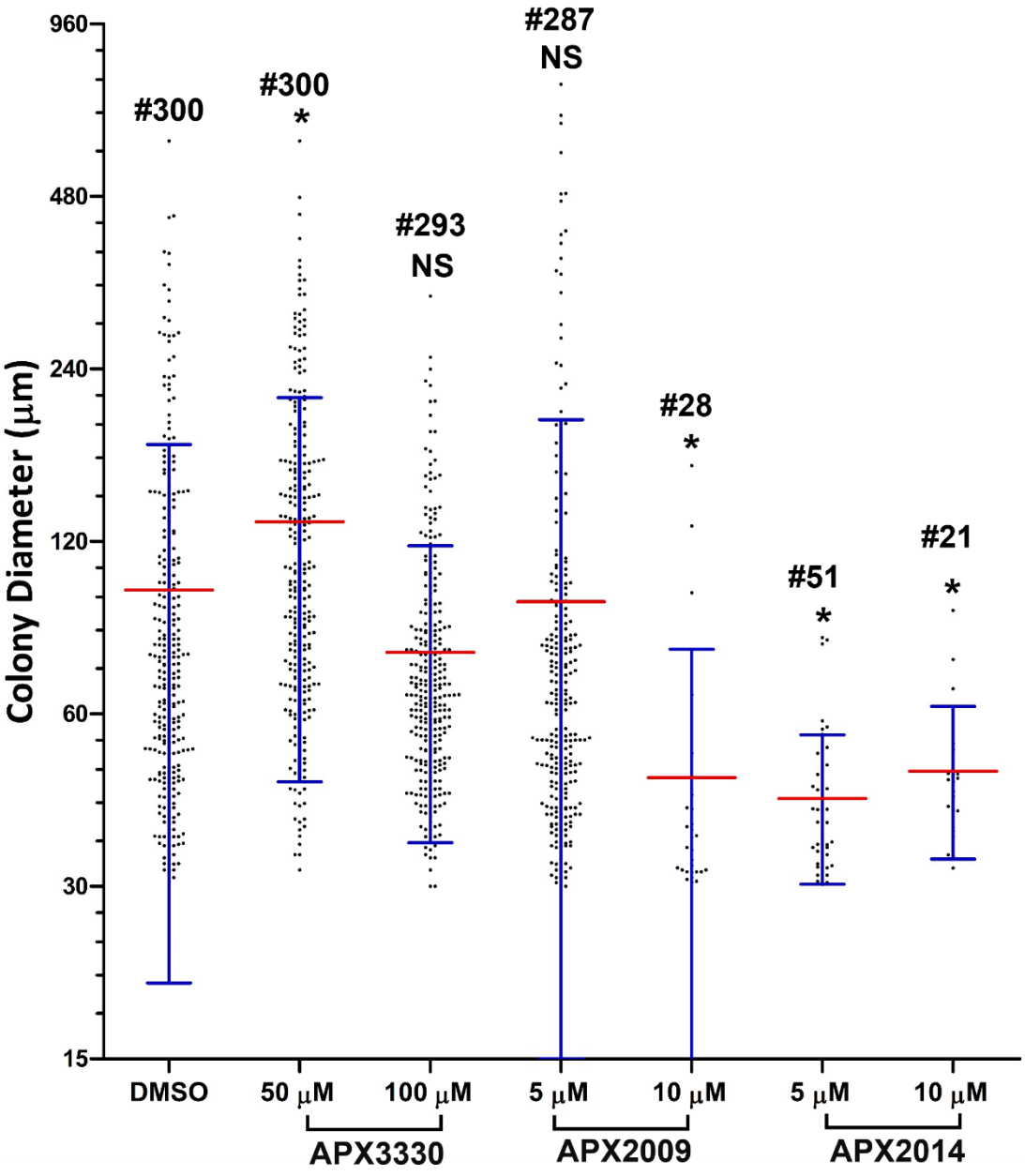


**Figure 3.19. The more potent Ref-1 inhibitors, APX2009 and APX2014, significantly decrease *Tsc2* −/− MEF colony diameter.** 40,000 *Tsc2* −/− MEF cells were seeded per well (six well plate) in a layer of 0.3% (w/v) agar/DMEM, with working concentration of defined drug. Drug treated media was added on top of this layer and replaced twice per week. After 4 weeks in culture, pictures were taken, and colony diameter scored. Lower diameter limit for colonies was set at 30 µM. Per condition up to 100 colonies per repeat number (N=3) were measured from up to 10 pictures per repeat number. Colony diameters across the three repeats were aggregated and plotted. Y axis is scaled to Log2 colony diameter. Number below each plot refers to concentration (µM). # denotation above scatter plots indicate colony number up to 300. Significance of differences in colony diameter between DMSO and all other drug treatments was determined by one way ANOVA with a Tukey Post Hoc test and annotated on graph. Significance denoted by: * = $p< 0.05$ and NS = not significant. Bars represent standard deviation.

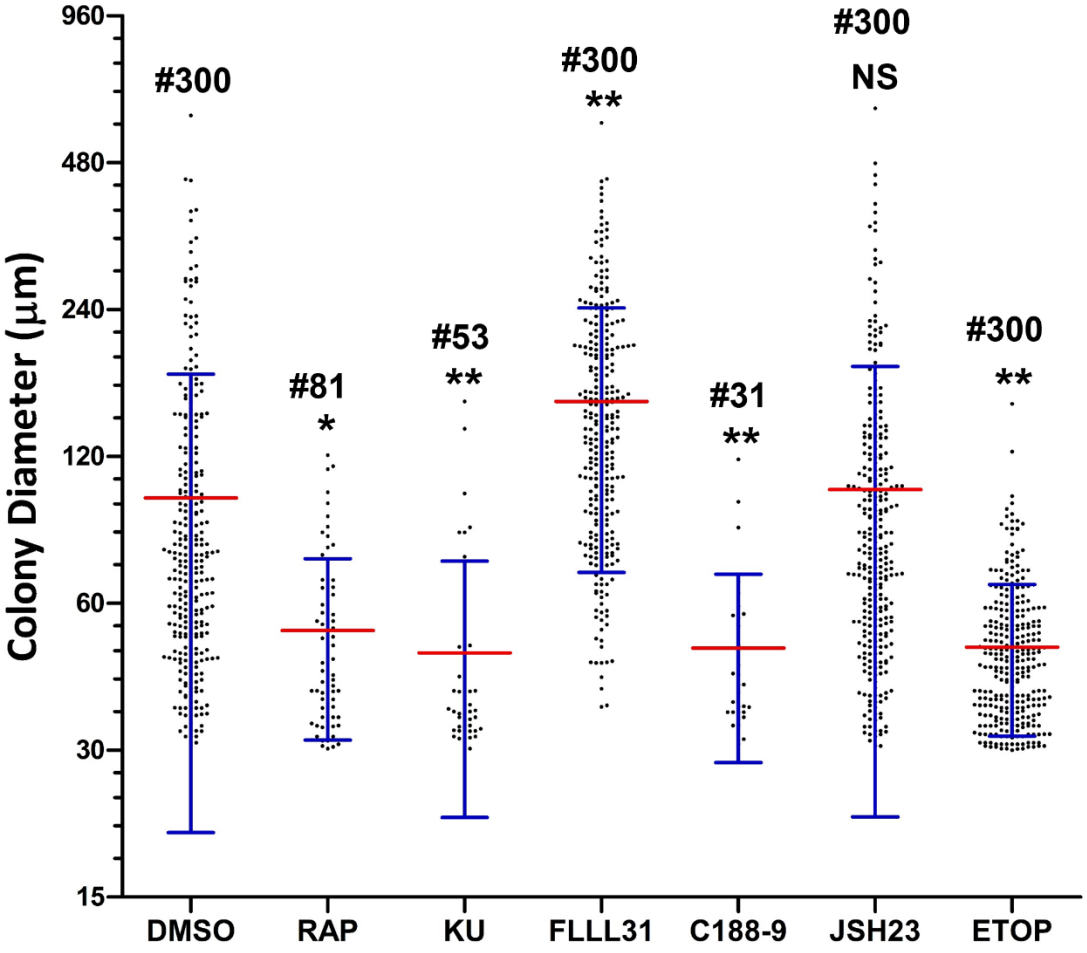


**Figure 3.20. Inhibition of STAT3 through C188-9, but not FLLL31, significantly decreases *Tsc2* −/− MEF colony diameter.** 40,000 *Tsc2* −/− MEF cells were seeded per well (six well plate) in a layer of 0.3% (w/v) agar/DMEM, with working concentration of defined drug. Drug treated media was added on top of this layer and replaced twice per week. After 4 weeks in culture, pictures were taken, and colony diameter scored. Lower diameter limit for colonies was set at 30 µM. Per condition up to 100 colonies per repeat number (N=3) were measured from up to 10 pictures per repeat number. Colony diameters across the three repeats were aggregated and plotted. RAP= rapamycin (50 nM), KU=Ku-0063794 (1 µM), FLLL31 (5 µM), C188-9 (30 µM), JSH23 (10 µM) and ETOP= etoposide (100 µM). Y axis is scaled to Log2 colony diameter. # denotation above scatter plots indicate colony number up to 300. Significance of differences in colony diameter between DMSO and all other drug treatments was determined by one way ANOVA with a Tukey Post Hoc test and annotated on graph. Significance denoted by: * = $p<0.05$, ** = $p< 0.01$ and NS = not significant. Bars represent standard deviation.

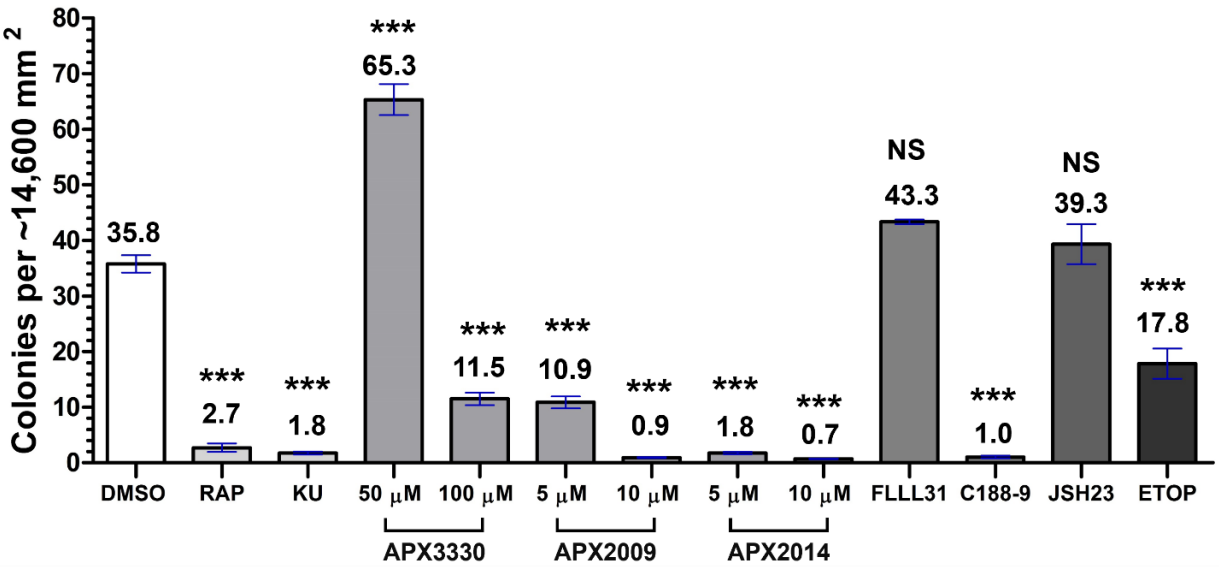


**Figure 3.21. Targeting Ref-1 and STAT3 is effective at significantly reducing *Tsc2* −/− MEF colony formation.** 40,000 *Tsc2* −/− MEF cells were seeded per well (six well plate) in a layer of 0.3% (w/v) agar/DMEM, with working concentration of defined drug. Drug treated media was added on top of this layer and replaced twice per week. After 4 weeks in culture, pictures were taken, and colony diameter scored. Lower diameter limit for colonies was set at 30 µM. Colonies above 30 µM per image (~14,600 $mm^2$) were counted, 10 pictures per repeat number (N=3). Number below each plot refers to concentration (µM). RAP= rapamycin (50 nM), KU=Ku-0063794 (1 µM), FLLL31 (5 µM), C188-9 (30 µM), JSH23 (10 µM) and ETOP= etoposide (100 µM). 14,600$mm^2$ represent area of each image taken. Average colony number per ~14,600$mm^2$ noted above each column. Significance of differences in colonies per ~14,600 $mm^2$ between DMSO and all other drug treatments was determined by one way ANOVA with a Tukey Post Hoc test and annotated on graph. Significance denoted by: *** = p< 0.001 and NS = not significant. Bars represent standard error of the mean.

### 3.2.8. *TSC2* deficient cell proliferation under hypoxia is increased relative to under normoxia.

As discussed in chapter 1, hypoxia has been shown to increase the activity of the signalling pathways of interest, namely HIF-1α, STAT3 and NF-κB cell signalling, in certain cancer cell lines. Therefore in order to assess if the Ref-1/HIF-1α/STAT3/NF-κB axis under hypoxia would increase proliferation of *TSC2* deficient cells further, a cell proliferation assays were performed. First the affect of normoxia or hypoxia on *TSC2* deficient cell proliferation was assayed. As represented in figure 3.22 (**A)**., *TSC2* deficient AML cell proliferation was increased compared to *TSC2* RE AML cells, as expected. With *TSC2* deficient AMLs having an average proliferation rate ((cell # at 72 h – cell # at 24 h)/2) of 12,511 cells/24 h under normoxia and 14,311 cells/24 h under hypoxia compared to 6,339 cells/24 h and 6,613 cells/24 h for *TSC2* RE AML under normoxia and hypoxia respectively. The average cell number at 72 h was significantly different between *TSC2* deficient AML cells grown under normoxia or hypoxia (41,896 vs 46,641 p= $1.9x10^{-9}$). Difference in the average cell number at 72 h between *TSC2* RE AML cells grown under normoxia or hypoxia was not reported as significant (figure

3.22 **A**). *Tsc2* −/− MEF cell proliferation was also found to be higher than *Tsc2* +/+ MEF cells (figure 2.22 **B**). With *Tsc2* −/− MEFs having an average proliferation rate of 6,814 cells/24 h under normoxia and 6,646 cells/24 h under hypoxia compared to -1,069 cells/24 h and 1,465 cells/24 h for *Tsc2* +/+ MEF under normoxia and hypoxia respectively. *Tsc2* +/+ MEFs under normoxia, showed a loss of cell number over time, suggesting the confluency they were plated at was not high enough to maintain cell viability under normoxia. The average cell number at 72 h was significantly different between *Tsc2* −/− MEF cells grown under normoxia or hypoxia (23,503 vs 27,680, p= 0.0203) (figure 2.22 **B**).

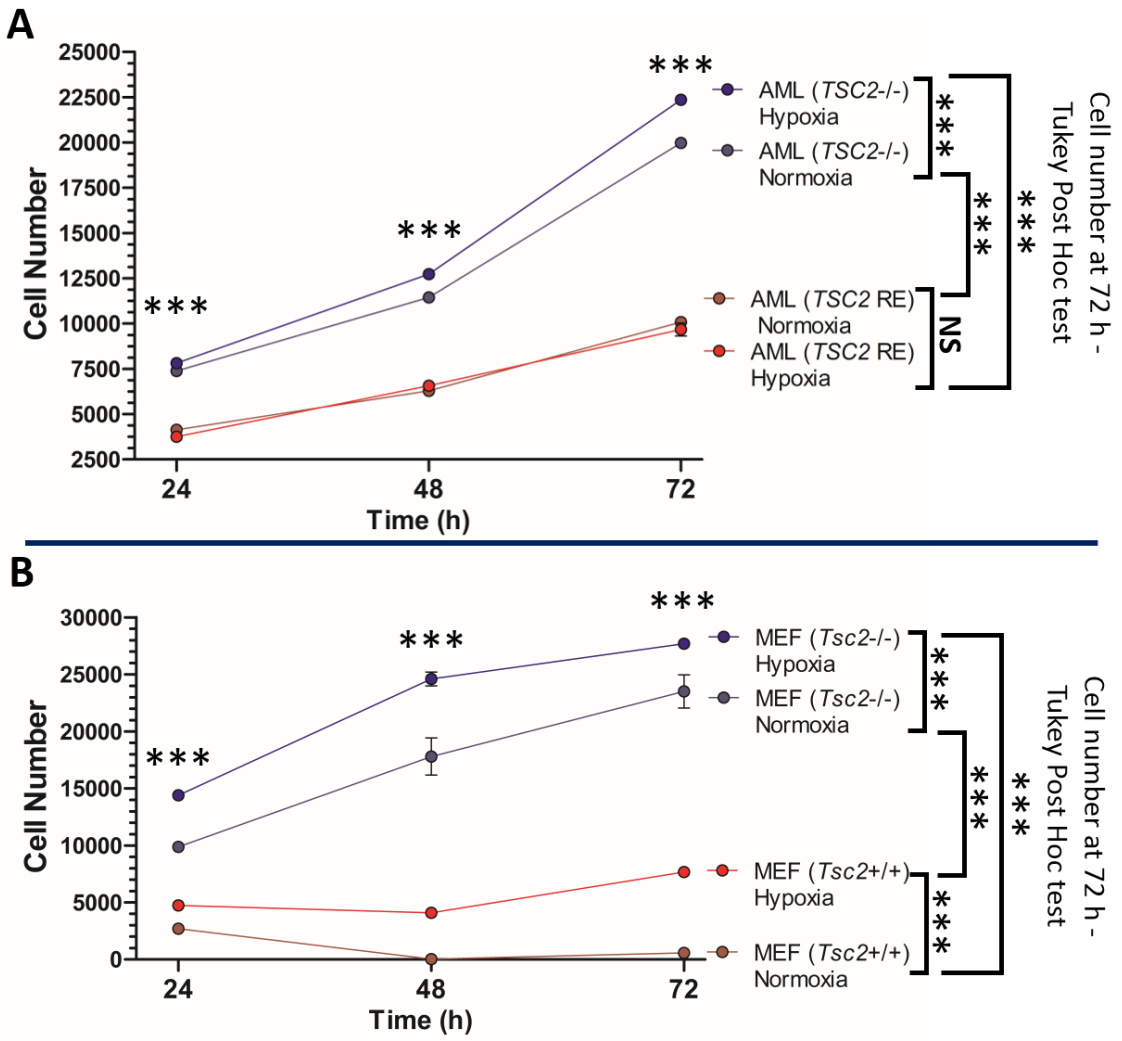


**Figure 3.22. Hypoxia increases *TSC2* deficient AML and MEF cell proliferation.** Either 2,500 MEF or 5,000 AML cells were seeded per well of a 96 well plate and 24 h after seeding, media was changed (time 0 days). Cells were grown for either for 24, 48 or 72 h under normoxia or hypoxia. At each time point 96-well plates were frozen and then cells were quantified using CyQuant Cell Proliferation Assay Kit and cell specific standard curves. Average AML cell number over time in culture is plotted on graph **A** (N=4) and average MEF cell number over time was plotted on graph **B** (N=5). Significance of differences in cell number at each timepoint between cell lines under either normoxia or hypoxia was determined by one-way ANOVA, with the significance of differences in cell number between conditions, as determined with a Tukey Post Hoc test, annotated also. Significance denoted by: *** = p< 0.001 and NS = not significant. Bars represent standard errors of the mean.

### 3.2.9 Targeting the Ref-1/HIF-1α/STAT3/NF-κB signalling axis under hypoxia is more effective at decreasing *TSC2* deficient AML cell proliferation than under normoxia.

As proliferation of both the *TSC2* deficient AML and *Tsc2* −/− MEF cells appeared increased under hypoxia, whether enhanced activity of the Ref-1/HIF-1α/STAT3/NF-κB signalling axis under hypoxia, in part, drove this elevated proliferation was assessed. Whilst the difference in the effect of Ref-1 inhibition on cell proliferation between *TSC2* deficient AML cells grown under normoxia or hypoxia cannot be easily distinguished by comparing the cell proliferation plots in figure 3.23 (**A** and **B**). The general trend is for cell number at time 72 h to be lower on treatment with APX3330, APX2009 and APX2014 under hypoxia (figure 3.23 **B**) compared to normoxia (figure 3.23 **A**) (APX3330 50 µM: 13,395 vs 15,575, APX3330 100 µM: 13,212 vs 14,927, APX2009 5 µM: 12,224 vs 14,417, APX2009: 10 µM 13,053 vs 17,246, APX2014 5 µM: 12,791 vs 17,246 and APX2014 10 µM: 9,536 vs 10,067). Only treatment with APX2014 at 10 µM treatment resulted in a significantly different cell number at time 72 h compared to the DMSO control for cells grown under normoxia (figure 3.23 **A**) (10,067 vs 14,718 p=0.0424). Conversely, under hypoxia cell number at time 72 h was also found to be significantly different between the lower concentrations of APX2009 and APX2014. DMSO vs APX2009 at 5 µM (14,869 vs 12,224 p=0.0278) and DMSO vs APX2014 at 5 µM (14,869 vs 9,536 $p=8x10^{-8}$) (figure 3.23 **B**) . If the proliferation assay was extended further, it is likely differences in cell number on Ref-1 treatment would be reported as significant.

Targeting STAT3 and NF-κB directly via C188-9 and JSH23 is far more effective at reducing *TSC2* deficient AML cell proliferation under hypoxia than Ref-1 inhibition. As shown in figure 3.24., whilst not as effective as mTOR inhibition, C188-9 and JSH23 treatment of *TSC2* deficient AML cells markedly decreases cell number at time 72 h. A one-way ANOVA found that cell number at time 72 h was significantly different between treatments with either concentration of C188-9 and JSH23 compared to DMSO under hypoxia (figure 3.24 **B**). C188-9 at 15 µM vs DMSO: 11,465 vs 14,718 p=0.0015, C188-9 at 30 µM vs DMSO: 12,310 vs 14,718 p=0.03786, JSH23 at 10 µM vs DMSO: 11,642 vs 14,718 p=0.0031 and JSH23 at 20 µM vs DMSO: 10,560 vs 14,718 $p=3.9x10^{-5}$). A Tukey post hoc test found no significant difference in the cell number at time 72 h between C188-9 and JSH23 conditions. Under normoxia, treatment with C188-9 or JSH23 did not significantly affect cell number at time 72 h (figure 3.24 **A**). Under both normoxia and hypoxia, FLLL31 treatment resulted in a net decrease in cell number over time, indicating the drug was killing the cells. As this drug is well tolerated in other assays, it is unclear why FLLL31 is cytotoxic in this assay format.

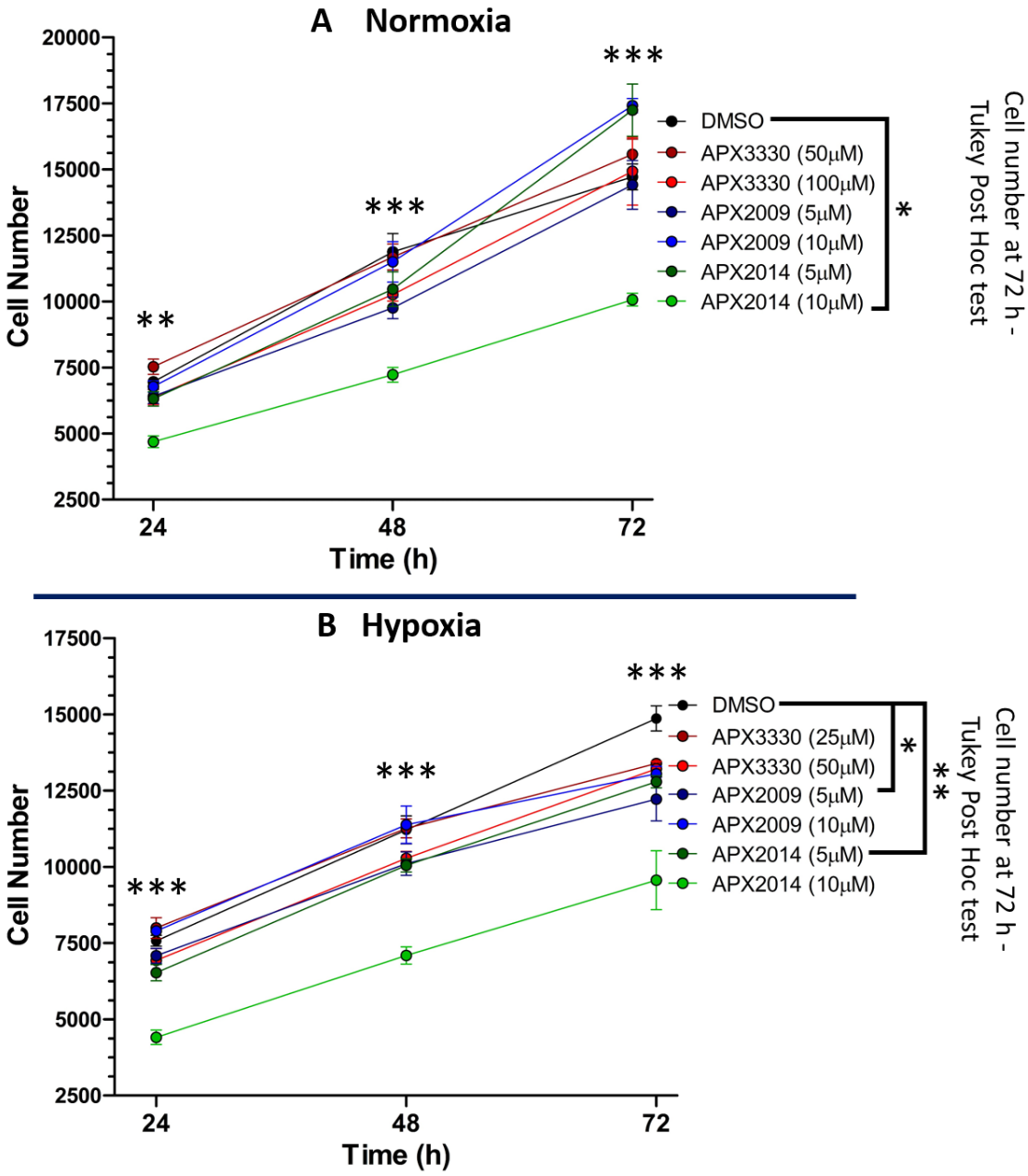


**Figure 3.23. Ref-1 inhibition is more effective at decreasing *TSC2* deficient AML cell proliferation under hypoxia than normoxia.** 5,000 AML cells were seeded per well of a 96 well plate and 24 h after seeding, media was changed, and cells were treated (time 0 days). Cells were grown under treatment for either for 24, 48 or 72 h under normoxia (**A**) or hypoxia (**B**). At each time point 96-well plates were frozen and then cells were quantified using CyQuant Cell Proliferation Assay Kit and cell specific standard curves. Effect of Ref-1 inhibitors on average AML cell number under normoxia (N=4) is shown on graph **A** and under hypoxia (N=4) is shown on graph **B**. Significance of differences in cell number at each timepoint between treatment conditions, under either normoxia or hypoxia, was determined by one-way ANOVA, with the significance of differences in cell number between conditions at t 72, as determined with a Tukey Post Hoc test, annotated also. Significance denoted by: * = $p < 0.05$, ** = $p < 0.01$, *** = $p < 0.001$. Bars represent standard errors of the mean.

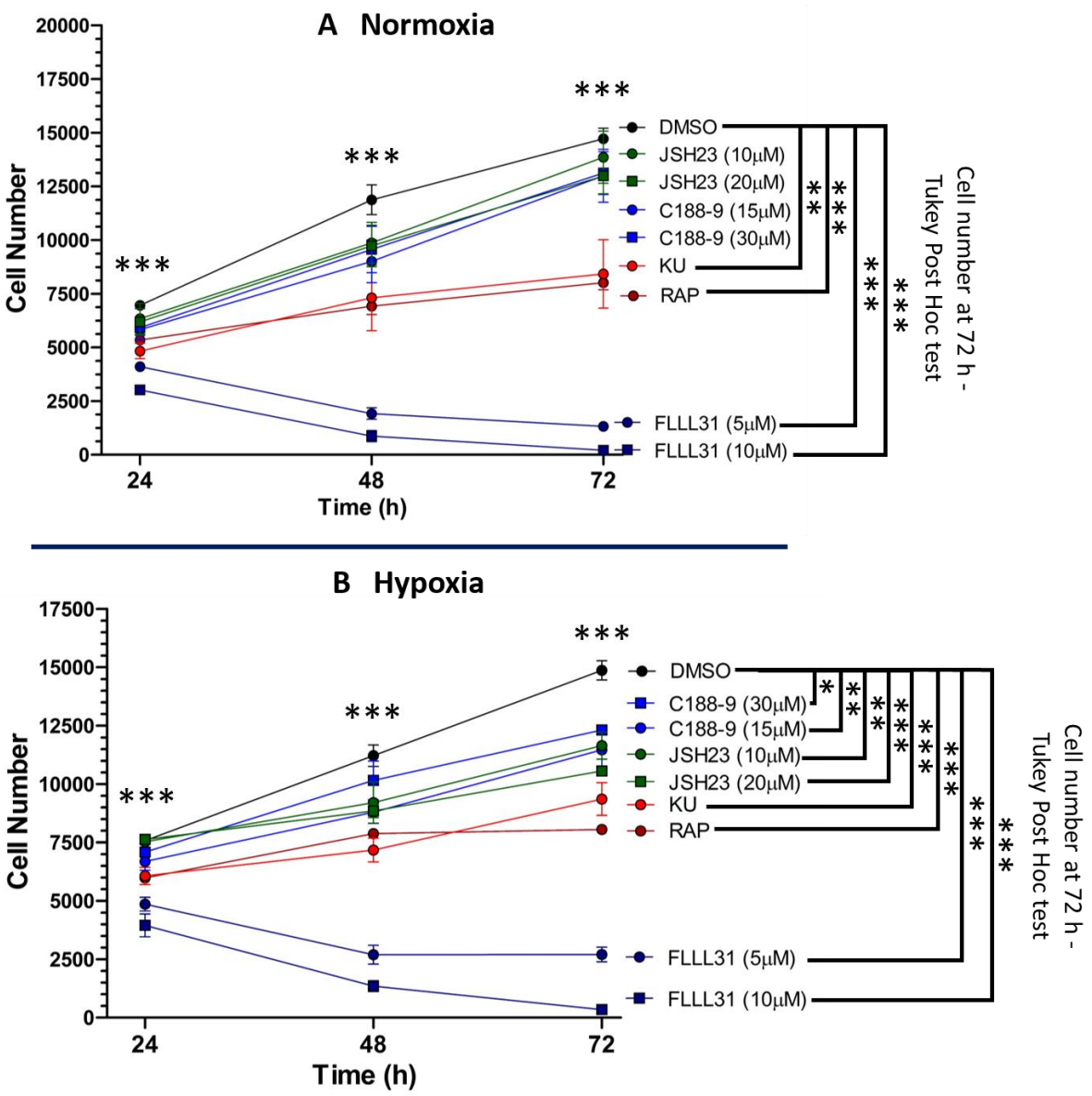


**Figure 3.24. STAT3 and NF-kB inhibitors are more effective at decreasing *TSC2* deficient AML proliferation under hypoxia than normoxia.** 5,000 AML cells were seeded per well of a 96 well plate and 24 h after seeding, media was changed and cells were treated (time 0 days). Cells were grown under treatment for either for 24, 48 or 72 h under normoxia or hypoxia. At each time point 96-well plates were frozen and then cells were quantified using CyQuant Cell Proliferation Assay Kit and cell specific standard curves. Effect of inhibitors on average AML cell number under normoxia (N=4) is shown on graph **A** and under hypoxia (N=4) is shown on graph **B**. RAP = rapamycin (50 nM) and KU = Ku0063794 (1 μM). Significance of differences in cell number at each timepoint between treatment conditions, under either normoxia or hypoxia, was determined by one-way ANOVA, with the significance of differences in cell number between conditions at t 72, as determined with a Tukey Post Hoc test, annotated also. Significance denoted by: * = p <0.05, ** = p <0.01, *** = p< 0.001. Bars represent standard errors of the mean.

### 3.2.10 Targeting the Ref-1/HIF-1α/STAT3/NF-κB signalling axis is not as effective at decreasing *Tsc2* −/− MEF cell proliferation than *TSC2* deficient AML cell proliferation.

For the CyQuant proliferation assay of *Tsc2* −/− MEFs, the end point was 48 h as these cells proliferate quickly to full confluency in the wells of a 96-well plate. As can be seen from figure 3.25. treating *Tsc2* −/− MEF cells with either Ref-1 inhibitors (figure 3.25 **A**), C188-9 or JSH23 (figure 3.25 **B**) was not very effective at reducing *Tsc2* −/− MEF cell proliferation. Apart from mTOR inhibitors, only APX2014 at 5 μM results in a significantly different cell number at time 48 h compared to DMSO (11,824 vs 25,014 under normoxia $p=<1x10^{-8}$, 25,082 vs 5,515 under hypoxia $p=<1x10^{-8}$) (figure 3.25 **A**). As can be seen in figure 3.25 (**A**), higher concentrations of APX2014 appears to be killing the cells, which was concluded as the cell number at time 48 h in the APX2014 10μM was lower than the number of cells that were seeded originally. FLLL31 appears to be effective at reducing *Tsc2* −/− MEF cell proliferation (figure 3.25 **B**). However, in 3D tissue culture cell proliferation experiments, FLLL31 was ineffective at significantly reducing spheroid growth (figure 3.15) or anchorage independent growth (figure 3.20) relative to DMSO controls. Why FLLL31 was effective at reducing cell proliferation in a 2D format (i.e., CyQuant proliferation assay) is unclear. It is possible FLLL31 is killing a proportion of the *Tsc2* −/− MEF cells over time in the CyQuant assay rather than reducing proliferation, as a limitation of such an assay is that non-adherent dead cells would not be measured by the CyQuant assay owing to them being washed off the tissue culture plates before measurement. Although it would be expected that if FLLL31 was significantly and substantially reducing *Tsc2* −/− MEF cell proliferation or killing all/a large fraction of *Tsc2* −/− cells, you would see under FLLL31 treatment spheroid growth plateau and or fewer colonies in the anchorage independent growth assays relative to DMSO. Confusing conclusions on FLLL31's efficacy in killing *Tsc2* −/− MEFs or reducing their proliferation is the differences in treatment time between assays. The *Tsc2* −/− MEF cells within the spheroid growth and anchorage independent growth assays were under FLLL31 treatment far longer (14 days and 4 weeks respectively) yet again, no significant decrease in spheroid growth or anchorage independent growth relative to DMSO was observed. Whilst *Tsc2* −/− MEF cells within the CyQuant proliferation assay were under treatment for the much shorter period of 48 h.

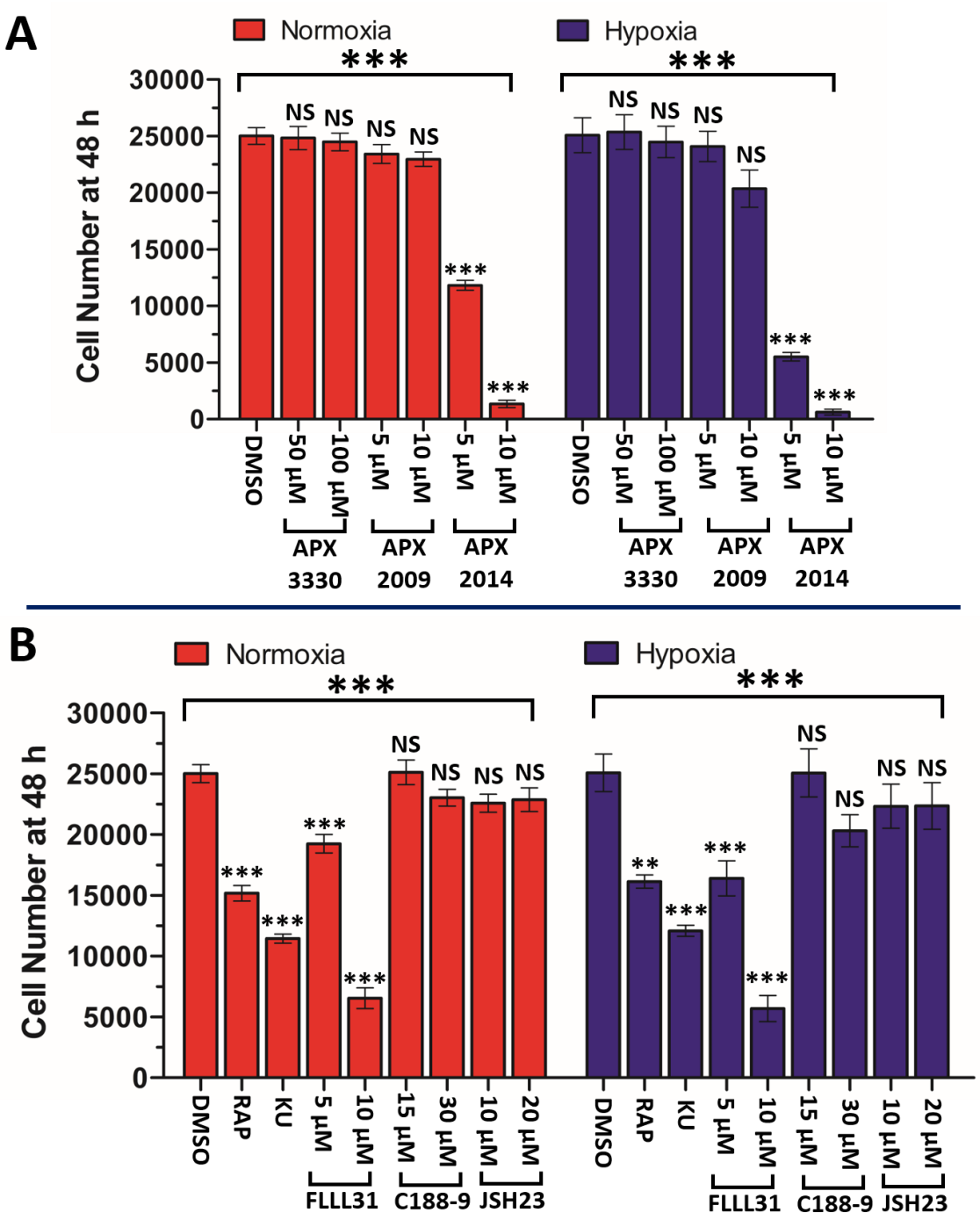


**Figure 3.25. Targeting the Ref-1/Hif-1α/STAT3/NF-kB axis is not effective at decreasing *Tsc2* −/− MEF proliferation in a 2D cell culture setting.** 2,500 MEF cells were seeded per well of a 96 well plate and 24 h after seeding, media was changed and cells were treated (time 0 days). Cells were grown under treatment for either for 48 h under normoxia or hypoxia. 96-well plates were then frozen and cell number was quantified using CyQuant Cell Proliferation Assay Kit and standard curves. Effect of Ref-1 inhibitors on MEF cell number under normoxia/hypoxia (N=9) is shown on graph **A** and effect mTOR, STAT3 and NF-kB inhibitors on MEF cell number (N=9) under normoxia/hypoxia is shown on graph **B**. Significance of overall differences in cell number between treatment conditions under normoxia or hypoxia was determined by one-way ANOVA and annotated above brackets. The significance of differences in cell number under normoxia or hypoxia between DMSO and other treatment conditions was determined with a Tukey Post Hoc test and is annotated above bars. Significance denoted by: * = p <0.05, ** = p <0.01, *** = p< 0.001 and NS = not significant. Bars represent standard errors of the mean.

### 3.2.11. Targeting the Ref-1/HIF-1α/STAT3/NF-κB signalling axis is effective at blocking vasculature mimicry in both *TSC2* deficient AML and MEF cells.

TSC associated lesions are highly vascularised (Yamakado *et al.* 2002) and are prone to aneurysm, representing a significant cause of morbidity and mortality to TSC patients (Amin *et al*. 2017, Sheperd *et al.* 1991 and Zöllner *et al.* 2020). Therefore, whether targeting the Ref-1/HIF-1α/STAT3/NF-κB had any efficacy in reducing *TSC2* deficient cells vasculature mimicry phenotype, observed when these cells are grown in a matrigel based tube formation assay (Francescone III *et al.* 2011), was tested.

Angio tool analysis measures a number of parameters that describe vasculature mimicry *in vitro*. The parameters chosen to assess the impact of targeting the Ref-1/HIF-1α/STAT3/NF-κB axis in this context were vessel density (the percentage of vessels inside the analysed image area), average vessel length (mean length of all vessels measured in the image) and total number of endpoints (the number of open-ended segments within the analysed image area). As shown in figure 3.26., mTOR inhibition through rapamycin has no significant effect on vessel density (VD), average vessel length (AVL) or total number of endpoints (TNE) compared to the DMSO control. The more potent Ref-1 inhibitors, APX2009 and APX2014, are effective at significantly reducing VD and AVL compared to the DMSO control (figure 3.26 **A** and **B**); as reported by a one-way ANOVA. Inhibition of STAT3, through FLLL31 or C188-9 treatment, also significantly decreases both VD and AVL compared to the DMSO control. A Tukey's post hoc test showed that effect of APX2014, FLLL31 and C188-9 on VD and AVL was not significantly different from each other. Inhibition of NF-κB, through JSH23 treatment, does not significantly affect VD or AVL. Treatment with APX2014, FLLL31 and C188-9 significantly increases the TNE, i.e., the number of open-ended vessels not networked with other vessels through junctions (figure 3.26 **C**). It should be noted however that analysis of the tube formation assay using Angio tool does not exactly score what can be observed from the images by eye. As seen in figure 3.27., *TSC2* deficient cells treated with APX2014, FLLL31 and C188-9, largely remain either as single cells or small aggregates of cells. And due to the slight convex shape of the Matrigel layer, slight blurring of the image leads Angio tool to detect these cell aggregates as small vessels. Therefore, as seen from the image panel in figure 3.27. treatment with APX2014, FLLL31 and C188-9 does appear to completely ablate vasculature mimicry of *TSC2* deficient AML cells.

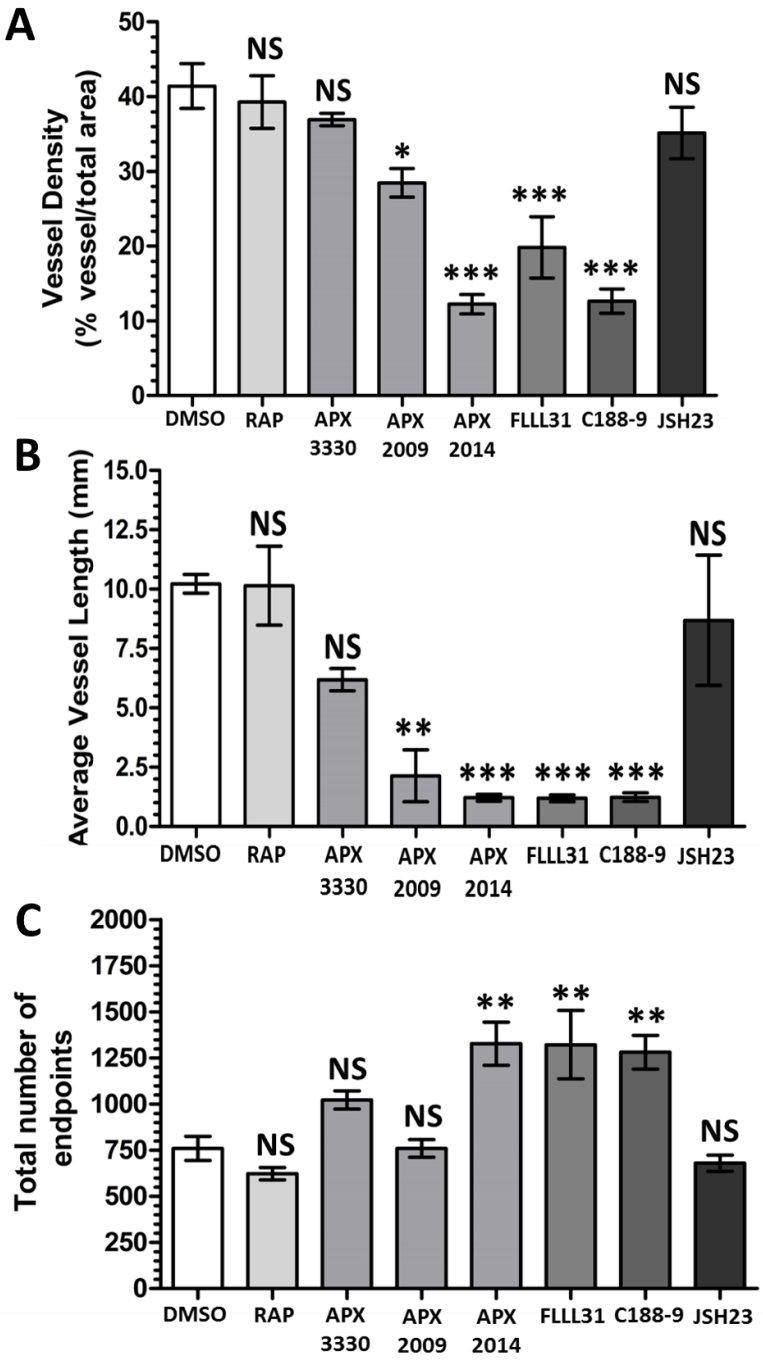


**Figure 3.26. Inhibition of Ref-1 and STAT3 is effective at blocking vasculature mimicry in *TSC2* deficient AML cells**. 50,000 *TSC2* deficient AML cells (in Optimem media) were seeded per matrigel basement membrane matrix coated well (96-well plate). Cells were incubated under hypoxia with either DMSO, rapamycin (RAP) at 50 nM, the Ref-1 inhibitors APX3330 (50 μM), APX2009 (5 μM) or APX2014 (5 μM), the STAT3 inhibitors FLLL31 (5 μM) or C188-9 (15 μM) or the NF-κB inhibitor JSH23 (10 μM). N=5. After 16 h in culture pictures were taken of wells. Pictures were analysed using Angio Tool software, which measures several parameters of network formation. Vessel density (**A**) is defined as the percentage of vessels inside the vessel containing area. Average vessel length (**B**) is defined as mean length of all vessels detected in the image. Total number of endpoints (**C**) is defined as total number of open-ended segments within the vessel containing area. Significance of differences in vessel density, average vessel length and total number of endpoints between DMSO and all other treatment conditions was by one-way ANOVA with a Tukey Post Hoc test. N=5. Significance denoted by: * = $p<0.05$, ** = $p< 0.01$, *** = $p< 0.001$ and NS = not significant. Bars represent standard error of the mean.

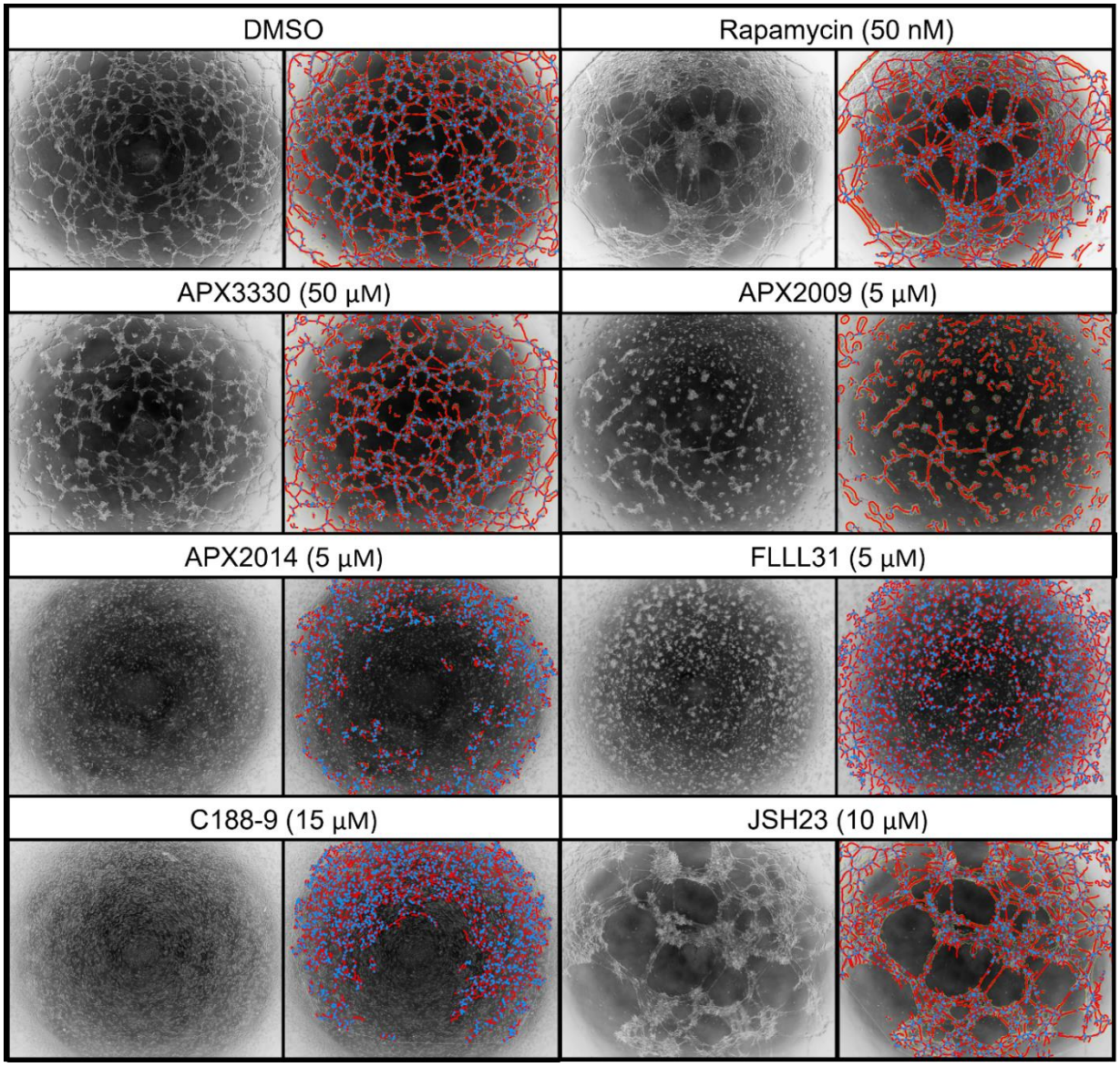


**Figure 3.27. Effect of mTOR, Ref-1, STAT3 and NF-kB inhibition on *TSC2* deficient AML cells is better visualised from an image panel of raw and analysed images.** 50,000 *TSC2* deficient AML cells (in Optimem media) were seeded per matrigel basement membrane matrix coated well (96-well plate). Cells were incubated under hypoxia with either DMSO or the inhibitor, at the defined concentration, annotated on image panel. After 16 h in culture pictures were taken of wells. Pictures were analysed using Angio Tool software, which measures several parameters of network formation. Vessel density is defined as the percentage of vessels inside the vessel containing area. Average vessel length is defined as mean length of all vessels detected in the image. Raw image and analysed images shown. Red lines represent detected vessels whilst blue dots represent vessel junctions.

Targeting the Ref-1/HIF-1α/STAT3/NF-κB axis was also effective at blocking vasculature mimicry in *Tsc2* −/− MEF cells, as shown in figure 3.38. As with the mTOR inhibition of the *TSC2* deficient AML cells, rapamycin treatment has no significant effect on vasculature mimicry in the *Tsc2* −/− MEF cells. As reported by a one-way ANOVA, Ref-1 inhibition, through APX3330, APX2009 and APX2014, significantly reduces VD and AVL compared to the DMSO control (figure 3.28 **A** and **B**). Lower concentrations of FLLL31, C188-9 and JSH23 were also included in the tube formation set up for the *Tsc2* −/− MEF cells, to see if a graded response to inhibitor concentration could be observed. Both concentrations of FLLL31, were effective at significantly reducing vessel density and average vessel length compared to the DMSO control. Only the difference in VD between both concentrations of FLLL31 was reported as significant ($p=1.4x10^{-4}$) (figure 3.28 **C**). Both concentrations of C188-9, decreased VD and AVL significantly. No significant graded response was reported between the two concentrations of C188-9. Unlike, *TSC2* deficient AML cells, JSH23 treatment is able to significantly block vasculature forming phenotype of *Tsc2* −/− MEF cells. Whilst not as effective as STAT3 inhibition, both concentrations of JSH23 significantly decrease VD compared to the DMSO control (figure 3.28 **B**). Only, JSH23 at the higher concentration of 10 μM significantly decreased AVL however. Unlike with *TSC2* deficient AML cells, only treatment of *Tsc2* −/− MEFs with APX2014 and C188-9 seemed to cause a significant increase in the total number of open-ended segments (figure 3.28 **C**). For the reasons highlighted earlier in this section, a clearer picture of how inhibitors targeting the Ref-1/HIF-1α/STAT3/NF-κB axis effect the vasculature mimicry phenotype of *Tsc2* −/− MEF cells, can be visualised in the image panel of figure 3.29.

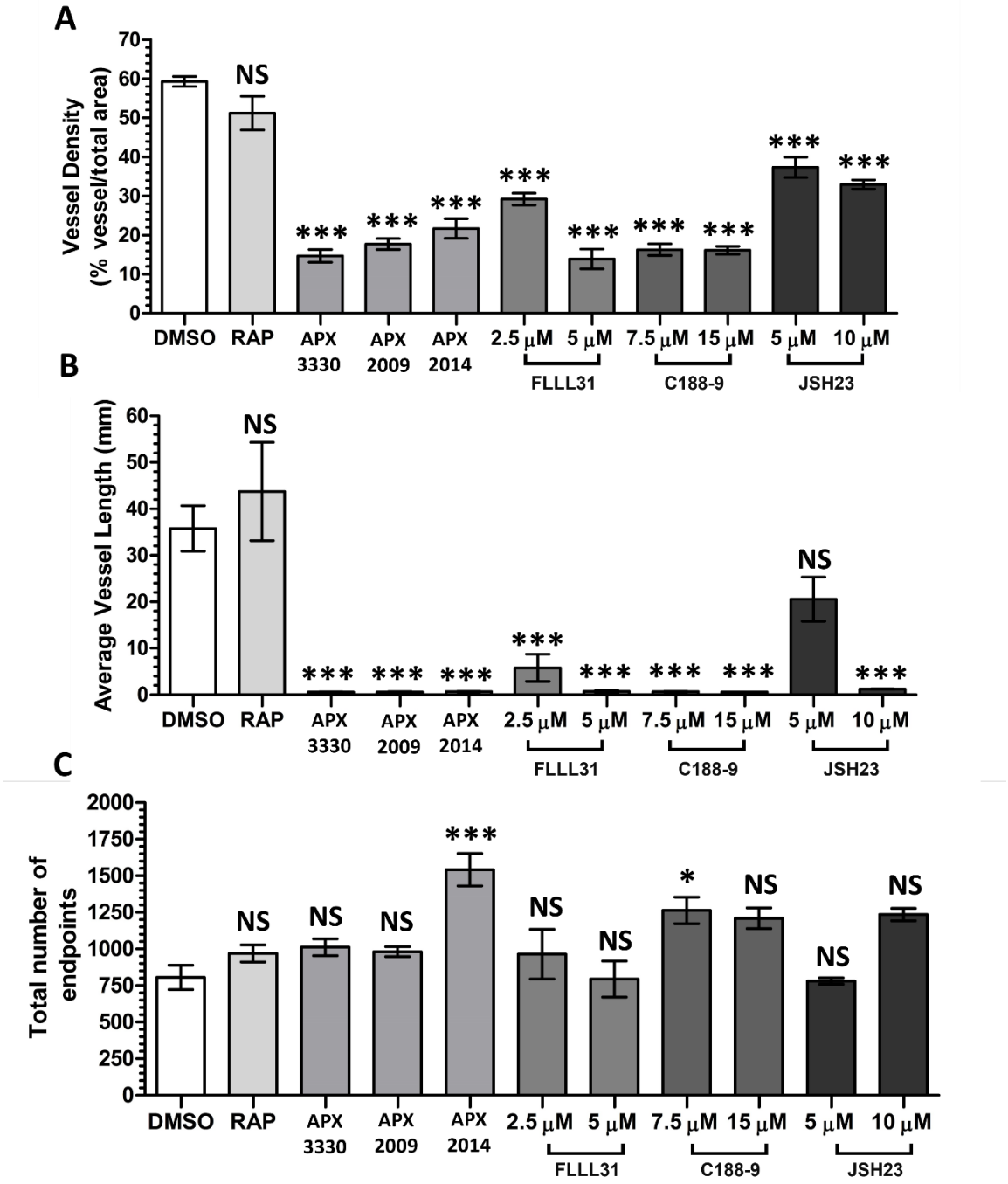


**Figure 3.28. Inhibition of Ref-1, STAT3 and NF-kB is effective at blocking vasculature mimicry in *Tsc2* −/− MEF cells**. 30,000 *Tsc2* −/− MEF cells (in Optimem media) were seeded per matrigel basement membrane matrix coated well. Cells were incubated under hypoxia with either DMSO, rapamycin (RAP) at 50 nM, the Ref-1 inhibitors APX3330 (50 μM), APX2009 (5 μM) or APX2014 (5 μM), the STAT3 inhibitors FLLL31 or C188-9 or the NF-κB inhibitor JSH23 (at the concentrations defined). N=9. After 16 h in culture pictures were taken of wells. Pictures were analysed using Angio Tool software, which measures several parameters of network formation. Vessel density (**A**) is defined as the percentage of vessels inside the vessel containing area. Average vessel length (**B**) is defined as mean length of all vessels detected in the image. Total number of endpoints (**C**) is defined as total number of open-ended segments within the vessel containing area. Significance of differences in vessel density, average vessel length and total number of endpoints between DMSO and all other treatment conditions was by one-way ANOVA with a Tukey Post Hoc test. N=9. Significance denoted by: * = $p<0.05$, *** = $p< 0.001$ and NS = not significant. Bars represent standard error of the mean.

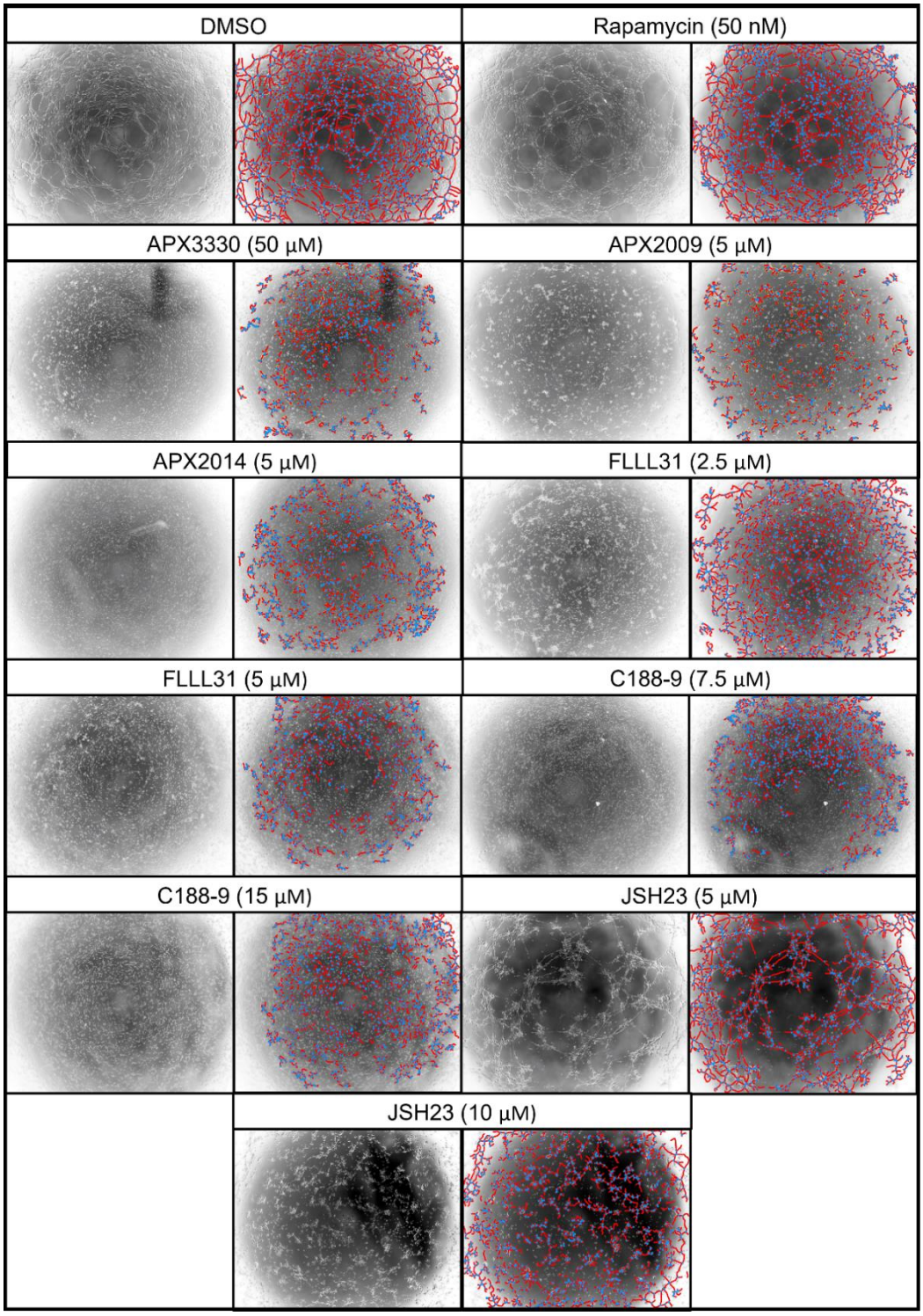


**Figure 3.29. Effect of mTOR, Ref-1, STAT3 and NF-kB inhibition on *Tsc2* −/− MEF cells is better visualised from an image panel of raw and analysed images.** 30,000 *Tsc2* −/− MEF cells (in Optimem media) were seeded per matrigel basement membrane matrix coated well. Cells were incubated under hypoxia with either DMSO or the inhibitor, at the defined concentration, annotated on image panel. After 16 h in culture pictures were taken of wells. After 16 h in culture pictures were taken of wells. Pictures were analysed using Angio Tool software, which measures several parameters of network formation. Vessel density is defined as the percentage of vessels inside the vessel containing area. Average vessel length is defined as mean length of all vessels detected in the image. Raw image and analysed images shown. Red lines represent detected vessels whilst blue dots represent vessel junctions.

### 3.2.12. Targeting the Ref-1/HIF-1α/STAT3/NF-κB signalling axis appears to reduce *Tsc2* −/− MEF cell migration in a wound healing assay.

Given the importance of cell migration in both typical angiogenesis (Lamalice *et al.* 2007) and to tumour vasculature mimicry (Dunleavey and Dudley 2012, Maes *et al.*2014 and Zhang *et al.* 2014b). It was hypothesised, that the action of Ref-1, STAT3 and NF-κB inhibitors to ablate vasculature mimicry in *TSC2* deficient cells, could in part be through blocking migration pathways. Preventing cells from reorganising into vasculature-like networks. Thus, a provisional cell migration assay was conducted to test this hypothesis.

Initially the scratch wound healing assay was set up with AML cells (both *TSC2* RE and *TSC2* deficient cells to assess differences in migratory capacity). However, serum starvation did not induce cell migration as can be seen in the supplementary data (Figure S.7). *Tsc2* −/− MEF cells were far more motile and closed the wound typically at the 24 h mark. As can be seen from the representative image panel in figure 3.30, DMSO and rapamycin treated *Tsc2* −/− MEF cells migrate into and close the wound by the 24 h. Though it is not very clear, Ref-1

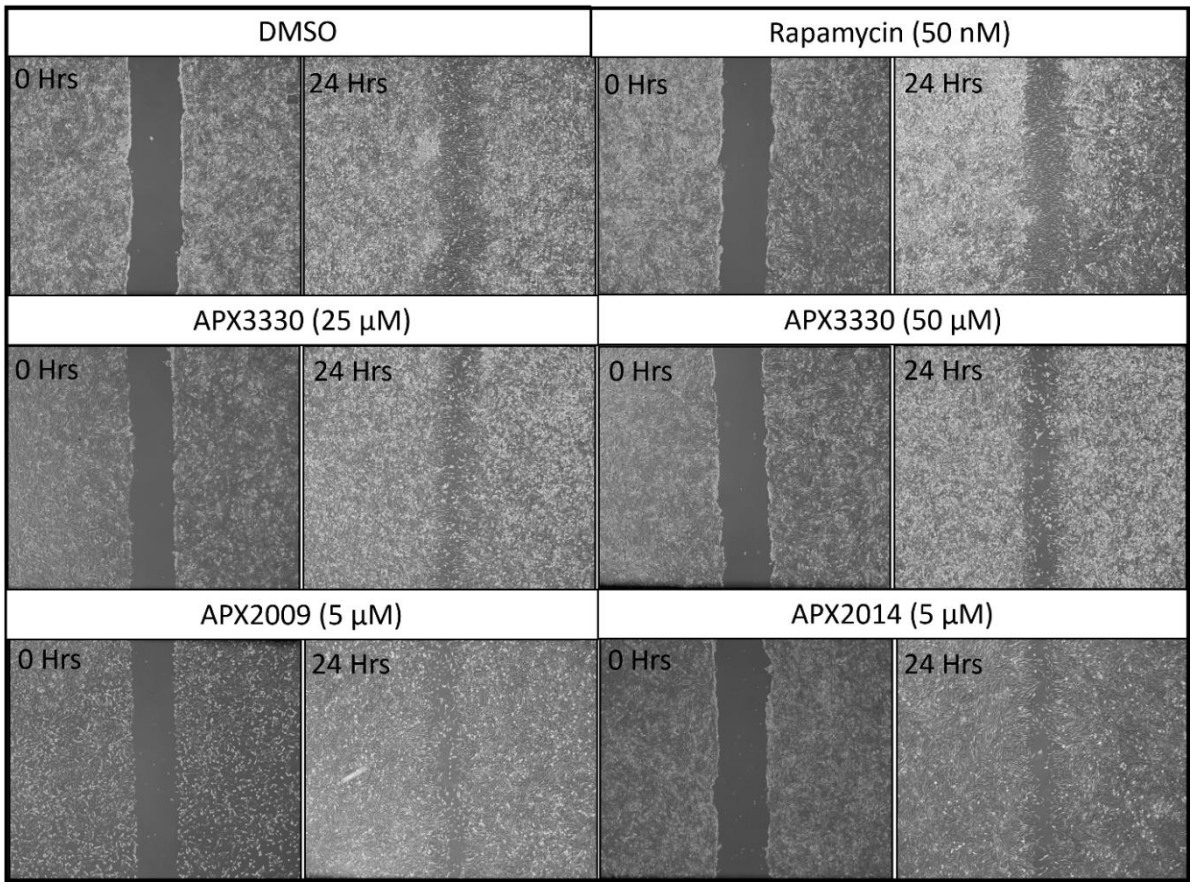


**Figure 3.30. Ref-1 inhibition appears to slightly reduce *Tsc2* −/− MEF cell migration.** MEF cells were seeded in 60 mm tissue culture plates and grown under normoxia until confluent. Cell monolayer was then 'scratched' using a pipette tip and plates were washed with 0% FBS (v/v) DMEM media. 0% (v/v) FBS DMEM with either DMSO, rapamycin or specified Ref-1 inhibitor at defined concentration was then added to the plates and pictures taken at time 0 h and then again at 24 h. N=2.

inhibition does appear to present full wound closure by the 24 h mark. Inhibiting STAT3 or NF-κB directly was far more effective at preventing wound closure (figure 3.31). With FLLL31, C188-9 and JSH23 all effective. Efficacy of these drugs aligns between both the vasculature mimicry assay and the migration assay utilising *Tsc2* −/− MEF cells. However, a more robust assay such as the Boyden chamber assay is needed to properly assess the effects of targeting the Ref-1/HIF-1α/STAT3/NF-κB axis on *TSC2* deficient cell migration.

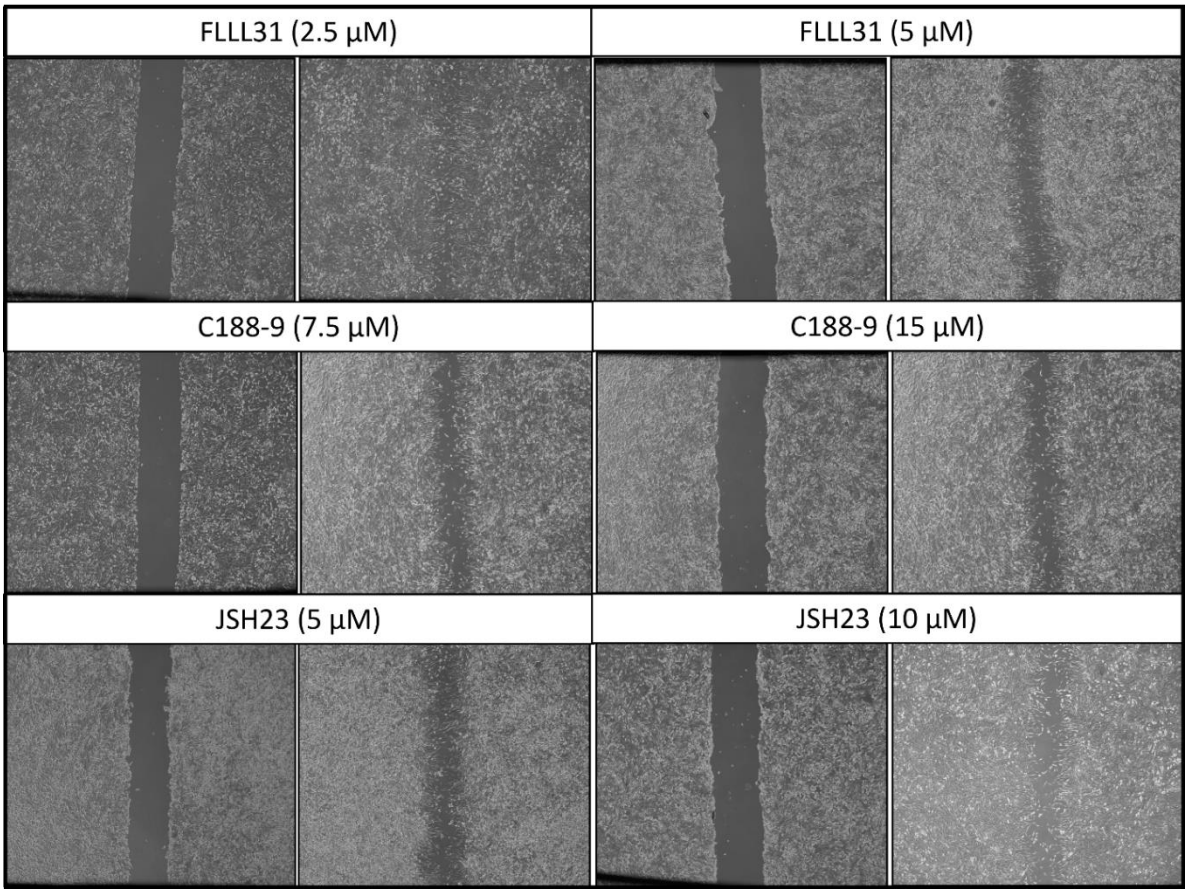


**Figure 3.31. Inhibiting STAT3 or NF-κB directly appears to be more effective at reducing *Tsc2* −/− MEF cell migration than mTOR or Ref-1 inhibition.** *Tsc2* −/− MEF cells were seeded in 60 mm tissue culture plates and grown under normoxia until confluent. Cell monolayer was then 'scratched' using a pipette tip and plates were washed with 0% (v/v) FBS DMEM media. 0% FBS (v/v) DMEM with either FLLL31, C188-9 or JSH23 at the defined concentration was then added to the plates and pictures taken at time 0 h and then again at 24 h. N=2.

## 3.3 Discussion

The results of the present chapter have indicated that at the protein and/or gene level, activity of the Ref-1/HIF-1α/STAT3/NF-κB signalling axis was elevated in at least one or both of the *TSC2* deficient AML and MEF cell lines relative to their *TSC2* competent counterparts. Whilst not cytotoxic in effect, drug blockade of the Ref-1/HIF-1α/STAT3/NF-κB signalling axis still showed favourable drug indications in reducing the tumourigenic phenotypes of *TSC2* deficient cells in multiple tissue culture assays.

The initial aim of this chapter was to analyse the protein and gene expression of components of the Ref-1/HIF-1α/STAT3/NF-κB signalling axis within TSC cell models. There is no great difference in the protein expression of Ref-1 between the two human AML cell lines (figure 3.1); while Ref-1 was overexpressed in *Tsc2* −/− MEF cells (figure 3.2). This is in contrast with other diseases were Ref-1 is dysregulated. Within cancer, *APEX1* (Ref-1) mRNA and protein is typically elevated and found to positively correlate with adverse prognostic and survival outcomes for patients (Mahjabeen *et al.* 2013, Cao *et al*. 2020 and Yang *et al.* 2010b). *APEX1* expression was unexpectedly downregulated in both *TSC2* deficient cell lines (figure 3.3). Increased ROS production has been reported to increase *APEX1* gene transcription and subsequent protein expression (Ramana *et al.* 1998 and Pines *et al.* 2005). However, more recent studies have found this is not always the case. Both Jiang *et al.* (2015) and Hu *et al.* (2021) found Ref-1 expression at the protein and mRNA level decreased with treatment of increasing concentrations of exogenous ROS (in the form of $H_2O_2$) within pancreatic cancer cell lines (SW-1990 and Panc-1) and cardiomyocytes. This suggests transcriptional control of the *APEX1* gene is more context dependent between different cell types than simply the levels of intracellular ROS; which may be the case within TSC. Furthermore, Ref-1 activity is not simply a function of its total protein copy number within a cell. Several studies have demonstrated that translocation of Ref-1 to the nucleus increases activity of its target transcription factors (Chen *et al.* 2010 and Tell *et al.* 2000). Therefore, the lack an observable difference in total Ref-1 protein between *TSC2* RE and *TSC2* deficient AML cells does not describe a lack of difference in the activity of Ref-1 between these two cell lines. Especially, when Ref-1 inhibitors are effective at significantly decreasing tumourigenic outputs within *TSC2* deficient cells. Within chapter 7, the effect of ROS inducing drugs and ROS quenchers on *APEX1* expression in *TSC2* deficient cells will be characterised.

Western blot analysis of *TSC2* wildtype/re-expressed and *TSC2* deficient cells (Figures 3.1 and 3.2) revealed that markers of HIF-1α, STAT3 and NF-κB (p65) activity were elevated upon loss of *TSC2*. Confirming increased activity of the Ref-1/HIF-1α/STAT3/NF-κB signalling axis with both the murine and human *TSC2* deficient cell lines. Ref-1 is not a kinase and transactivates HIF-1α, STAT3 and NF-κB by increasing their DNA binding affinity through

oxidising specific cysteine residues (Shah *et al.* 2017). Therefore, Ref-1 isn't expected to be directly responsible for increases in STAT3 phosphorylation at Y705 and S727 (Figures 3.1 and 3.2) or p65 phosphorylation at S536 (Figure 3.2). Instead, activity of STAT3, HIF-1α and NF-κB mediated through Ref-1, was hypothesised to result in a positive feedback loop in which STAT3, HIF-1α and NF-κB enhance each other's activity. Positive feedback on STAT3 activity through STAT3 increasing transcription of *IL6*, is well documented in STAT3 driven cancers (Chang *et al.* 2013). Elevated IL-6 has been observed within patients suffering from other genetic diseases and cancers where upregulated mTORC1 and STAT3 activity contribute to pathogenesis (Vella *et al.* 2020, Han *et al.* 2014 and Sanchez-Correa *et al.* 2013).

Cross talk between NF-κB and STAT3 is known to positively reinforce each other's activity (Ji *et al.* 2019, Wang *et al.* 2000 and Libermann and Baltimore 1990). Therefore, crosstalk between Ref-1 activated STAT3, HIF-1α and NF-κB was hypothesised to contribute towards the increased expression of their respective genes observed within human and murine *TSC2* deficient cells (Figure 3.4). This hypothesis will be tested for HIF-1α and STAT3 within chapters 4 and 5. Despite *HIF1A* being a target gene of both STAT3 and NF-κB (Nie *et al.* 2008 and Rius *et al.* 2008), the increased *HIF1A* expression (figures 3.1, 3.2 and 3.4) and activity (i.e., upregulation of BNIP3, figures 3.1 and 3.2) observed will not solely result from increased Ref-1 activity. As it is well documented that mTORC1 hyperactivity drives *HIF1A* translation (Dodd *et al.*2015) and transcription (Land and Tee, 2007). Dodd *et al.* (2015) also demonstrated mTORC1 upregulates *HIF1A* transcription through activating STAT3, by increasing phosphorylation at serine 727, which could be blocked by rapamycin treatment. Although the authors observed rapamycin treatment did not completely normalise *HIF1A* expression or alter the high level of STAT3 phosphorylated at tyrosine 705, suggesting upregulated STAT3 activity observed in *TSC2* deficient cells (figures 3.1 and 3.2) is not through mTORC1 hyperactivity alone. Whilst *RELA* (p65) expression appeared upregulated within *TSC2* deficient cells, this was not reported as significant (figure 3.4). Additionally, as phosphorylation of p65 at serine 536 (Figure 3.1) appeared only marginally higher in *TSC2* deficient AML cells compared to *TSC2* RE AML cells, the hypothesised contribution of NF-κB activity to pathogenesis within the human model of TSC is yet uncertain. As expected, hypoxia appeared to drive HIF-1α activity within *TSC2* deficient cells (BNIP3 blots, figures 3.1 and 3.2), but an effect was not observed for STAT3 or NF-κB, except at the transcriptional level (Figure 3.4). Given, that hypoxia has been shown to induce STAT3 activity within the cancer setting (Soleymani *et al.* 2017), chapter 5 will aim to quantify the effect of hypoxia on STAT3 signalling in the context of TSC. Overall, this initial work validated that the Ref-1/HIF-1α/STAT3/NF-κB signalling axis is upregulated at the protein and mRNA level within *TSC2* deficient cells and supports the strategy of targeting the Ref-1/HIF-1α/STAT3/NF-κB signalling axis within TSC.

Whilst rapamycin analogues have been shown to effectively reduce volume of both renal and brain lesions within TSC (Bissler *et al.* 2013 and Franz *et al.* 2013), their drug action is cytostatic rather than being cytotoxic (Bissler *et al.* 2008). Therefore, there would be a clear therapeutic benefit to drugs that are selectively cytotoxic to *TSC2* deficient cells. This has recently been demonstrated in the murine model of TSC with the drug combinations nelfinavir/bortezomib and nelfinavir/mefloquine within *Tsc2* −/− murine cells (Johnson *et al.* 2018a and McCann *et al.* 2018). The comprehensive cell viability assays show that the potential therapeutic benefit of targeting the Ref-1/HIF-1α/STAT3/NF-κB axis is not mediated through selective cytotoxicity towards *TSC2* deficient cells. Either as an adjunctive therapy with rapamycin or under differing oxygen availability. Only the Ref-1 inhibitor APX2014 at 10 μM resulted in a significant decrease in the viability of *TSC2* deficient AML cells compared to the *TSC2* RE AML controls (figure 3.5). This observed selective cytotoxicity was not recapitulated in the MEFs (figure 3.5). As the Ref-1 inhibitors APX3330, APX2009 and APX2014 differ in potency (Kelley *et al*. 2016), not how they target Ref-1, it is unlikely APX2014 would be selective for *TSC2* deficient cells. Supported by the observation that APX2009 at 10 μM caused a significant decrease in cell viability compared to the DMSO control, but was not selective for *Tsc2* −/− MEFs compared to *Tsc2* +/+ controls (figure 3.6). In addition, clinical trials of APX3330 show that even at high doses the drug is well tolerated with limited side effects (Shahda *et al.* 2019). Furthermore, Logsdon *et al.* (2018) and Kelley *et al.* (2016) showed APX2009 treatment decreased pancreatic cancer cell viability (PDAC) but not cancer associated fibroblasts in co-cultured spheroids.

The expected principal benefit of targeting the Ref-1/HIF-1α/STAT3/NF-κB signalling axis would be to normalise dysregulated angiogenesis and inflammation within TSC lesions (Arbiser *et al.* 2002, Parker *et al.* 2011 and Martin *et al.* 2017) by reducing expression of rapamycin insensitive biomarkers (Lee *et al*. 2010, and Dodd *et al.* 2015). However, as current rapamycin-based drugs do not reduce tumour volume within all patients (Bissler *et al.* 2013 and Franz *et al*. 2013), therapies which could reduce patient tumour volume and burden would be of clear clinical benefit. Tumour spheroid and anchorage independent growth assays are useful for assessing drug potential *in vitro*. Spheroids are a more representative model of lesions than 2D cultures, recapitulating more of the morphological and physiological traits of tumours (Edmonson *et al.* 2014). Anchorage independent growth assays are a useful approximation of tumour formation from a single cell, given that tumour formation in TSC largely conforms to Knudson's two hit hypothesis (somatic second hit to functional *TSC1* or *TSC2* allele) (Peron *et al.* 2018a). Whilst none of the inhibitors targeting components of the Ref-1/HIF-1α/STAT3/NF-κB axis were as effective as mTORC1 inhibition at reducing growth in a 2D or 3D *in vitro* setting, these assays demonstrate that drug inhibition of the Ref-1/HIF-

1α/STAT3/NF-κB signalling axis was able to reduce *Tsc2* −/− cell proliferation. There were some important distinctions between the murine and human cell lines. It should be noted here that inclusion of the competitive ATP inhibitor of mTOR, Ku-0063794 (Garcia *et al*. 2009), served as an important control. Ensuring a treated condition were the rapamycin insensitive functions of mTORC1 were also inhibited (Thoreen *et al.* 2009 and Feldman *et al.* 2009)

*Tsc2* −/− MEFs appear more sensitive to APX3330 than *TSC2* deficient AMLs, with APX3330 at both concentrations (50 and 100 μM) sufficient to decrease *Tsc2* −/− MEFs tumour spheroid growth (figure 3.10) and at 100 μM significantly reduce *Tsc2* −/− MEFs colony formation in the anchorage independent growth assays (figure 3.21). APX3330 at either concentration, had no significant effect on AMLs in these assays (figures 3.8 and 3.17). It is worth noting however that the apparent increased sensitivity of MEFs to APX3330 could be a result of the lower concentration of FBS used to culture MEFs in these assays compared to the AMLs (10% vs 15% v/v FBS). As albumin proteins in FBS supplemented media can reversibly bind many drugs, effectively decreasing the drugs pharmacological concentration (Epps *et al*. 1999). The effect of APX2009 and APX2014 on tumour spheroid growth is harder to define. For example, treatment with APX2014 at 10 μM (figure 3.8) appeared to have no effect on AML spheroid growth, despite APX2009 (at 5 μM and 10 μM) and APX2014 at 5 μM, appearing to decrease spheroid size. But APX2014 at 10 μM treated spheroids also showed the largest change in circularity (figure 3.9); which we found was positively correlated with spheroid area in this condition. Treatment of MEF spheroids with APX2014 (at 5 μM and 10 μM) and APX2009 (at 5 μM) appeared to reduce spheroid growth (figure 3.10). But likely due to the high standard deviations in spheroid area, these differences were not found to be significant. Comparing these results to the literature, APX3330, APX2009 and APX2014 have been found to decrease growth of spheroids formed from multiple cancer cell lines (Caston *et al.* 2021). APX2009 and APX2014 did however significantly impact anchorage independent growth of both MEF and AML cell line models (figures 3.17 and 3.19). Whist APX2009 and APX2014 treatment did not significantly affect *TSC2* deficient cell colony diameter (with exception of APX2014 at 10 μM), the number of scorable colonies was dramatically decreased. Within the *Tsc2* −/− MEF cells, APX2009 and APX2014 had an even greater effect on anchorage independent growth, decreasing both colony diameter significantly (figure 3.19) and colony formation (figure 3.21) relative to the DMSO controls. Studies investigating efficacy of inhibiting Ref-1 on reducing anchorage independent growth are scarce, however Yang *et al.* (2007) found that within the JB6 mouse cell model of tumour progression, knock-down of *APEX1* did inhibit 12-O-Tetradecanoylphorbol-13-acetate (TPA, a phorbol ester that is a potent carcinogen) induced anchorage independent growth.

These assays demonstrate that targeting STAT3 directly, rather than through Ref-1 appears to be more effective at decreasing measures of *TSC2* deficient AML cell growth. Apart from mTOR inhibition, STAT3 inhibition caused the largest decrease in growth of AML spheroids (figure 3.13). Caston *et al.* (2021) found that STAT3 inhibitor treatment of spheroids formed from multiple cancer cell lines also significantly decreased spheroid growth. Supporting the hypothesis that inhibition of STAT3 could decrease tumour growth in diseases like TSC, where STAT3 signalling is dysregulated. Both, STAT3 inhibitors were also effective at reducing scores of anchorage independent growth in *TSC2* deficient AML cells (figure 3.18), decreasing colony size significantly. Several studies implicate STAT3 hyperactivity in mediating anchorage independent growth within cancers (Cheng *et al.* 2008, Zhang *et al.* 2006b and Zong *et al.* 1998). Previous studies of cancer in which STAT3 contributes towards tumourigenesis, taken together with the present results, suggests dysregulation of STAT3 activity contributes towards tumour formation within TSC. *Tsc2* −/− MEF spheroid and anchorage independent growth was significantly decreased by treatment with C188-9, but not with FLLL31 (figures 3.15, 3.20 and 3.21). Both STAT3 inhibitors work through blocking formation of the active dimer through binding to the SH2 domain of STAT3 (Lin *et al.* 2010 and Bharadwaj *et al.* 2016). Therefore, why FLLL31 is ineffective is unclear. Potentially, the dissociation and inhibitor constants between FLLL31 and STAT3 are quite large. Otherwise, *TSC2* deficient AML cells may be more responsive to STAT3 inhibition. Lastly, whilst NF-κB inhibition has a significant impact of *TSC2* deficient AML spheroid growth (figure 3.13), it does not decrease anchorage independent growth of *TSC2* deficient AML cells (figure 3.18) or effect the growth of *Tsc2* −/− MEF cells in these assays. Taken with the protein analysis of NF-κB (p65) in *TSC2* deficient cells (Figures 3.1 & 3.2), these findings suggest NF-κB activity is not as an important driver of *TSC2* deficient cell proliferation as Ref-1 and STAT3.

Data gathered through CyQuant cell proliferation assays, supported the hypothesis that hypoxia increases *TSC2* deficient cell proliferation (figure 3.22). In this 2D format, Ref-1 inhibition under normoxia only caused a significant decrease in *TSC2* deficient AML cell number at time 72 h for the most potent Ref-1 inhibitor, APX2014, at the highest concentration (figure 3.23). Conversely, under hypoxia, the lower concentrations of APX2009 and both concentrations of APX2014 significantly decreased *TSC2* deficient AML cell number at time 72 h timepoint. Further supporting the hypothesis that hypoxia increases activity of the Ref-1/HIF-1α/STAT3/NF-κB signalling axis, which in turn drives tumorigenesis through increased cell proliferation. This idea is further supported by findings from treating *TSC2* deficient AML cells with direct STAT3 and NF-κB inhibitors. Under normoxia, C188-9 and JSH23 treatment did not significantly affect cell number at time 72 h compared to the DMSO control. However,

under hypoxia, both concentrations of C188-9 and JSH23 significantly decreased *TSC2* deficient cell proliferation (figure 3.24).

Importantly, between normoxia and hypoxia, there was no significant difference in cell number at time 72 h timepoint for rapamycin and Ku0063794 treated conditions. Suggesting that in this context, hypoxia is not increasing *TSC2* deficient AML cell proliferation through mTORC1 activity. These findings have relevance to the tumour spheroid data. Tumour spheroids recapitulate hypoxic gradients observed in solid tumours (Riffle and Hedge, 2017) and within the 3D context of both spheroids and tumours, has important implications for cell signalling. For example, HIF-1α and its target genes, *GLUT1* and *VEGFA*, are found expressed in the inner hypoxic area of spheroids (Menrad *et al.* 2010 and Shweiki *et al.* 1995) and are involved in spheroid growth. As described before, hypoxia has also been shown to drive STAT3 and NF-κB activity (Soleymani *et al.* 2017, Yokogami *et al.* 2013 and Xie *et al.* 2014). Therefore, increased hypoxia within *TSC2* deficient cell spheroid cores may promote spheroid growth in part through increasing activity of STAT3 and NF-κB; and explain why their respective inhibitors effectively reduce the growth of *TSC2* deficient AML spheroids. The CyQuant proliferation assay in the MEFs shows their proliferation in 2D culture is not significantly affected by C188-9 or JSH23 treatment. This data, along with the results of the other growth assays indicates a difference between *TSC2* deficient AML and MEF cells dependence on mTORC1 hyperactivity vs activity of the Ref-1/HIF-1α/STAT3/NF-κB signalling axis for proliferation. Overall, our data shows that unlike the *TSC2* deficient AML cells, *Tsc2* −/− MEF cells are more sensitive to mTORC1 inhibition than inhibitors targeting Ref-1, STAT3 or NF-κB. Given treatments which are deemed effective in mouse models do not always turn out as clinically viable within human patients (Gould *et al.* 2015), differences between the two models of TSC established in this chapter is an important consideration moving forward.

Lastly, our findings demonstrate that targeting the Ref-1/HIF-1α/STAT3/NF-κB signalling axis completely ablates the vascular mimicry phenotype of *TSC2* deficient cells grown on matrigel under hypoxia. With the *TSC2* deficient AML cells, targeting both Ref-1 and STAT3 substantially decreased the amount of vasculature and length of vessels within the tube formation assay (figure 3.26). Within the *Tsc2* −/− MEF cells, all inhibitors targeting Ref-1, STAT3 and NF-κB were effective at reducing the amount of vasculature and length of vessels (figure 3.28). NF-κB inhibition was not effective within AML cells however, potentially reflecting a difference in the signalling mechanisms that govern adoption of this phenotype between the murine and human cell lines. mTORC1 inhibition through rapamycin however had no significant impact on vessel density or vessel length. Given rapamycin's anti-angiogenic activity being well demonstrated in cancer (Guba *et al.* 2002 and Marimpietri *et al*. 2007), increased vasculature phenotype of *TSC2* deficient cells is not through typical angiogenic

pathways. And it is important to note this tube formation assay is not a representative model of angiogenesis. Instead, vasculature mimicry observed in cancers is a more useful model, as it describes the process were tumourigenic cells can dedifferentiate into a more endothelial like phenotype and form *de-novo* perfusable vasculature-like networks without pre-existing endothelial cells (Maniotis *et al.* 1999). Given the genetic stability of AML tumours (Martin *et al.* 2017), it is not expected that processes that govern vasculature mimicry in cancer to be reflected within TSC. However, useful comparisons can be made. The RhoA/ROCK pathway, which among processes can mediate cell migration, has been found to underpin vascular mimicry in a variety of human cancers (Xia *et al.* 2017, Xia *et al.* 2019 and Zhang *et al.* 2020); with STAT3 implicated in this process to (Li *et al.* 2018). Therefore, efficacy of drugs that target the Ref-1/HIF-1α/STAT3/NF-κB signalling axis in blocking vasculature mimicry within *TSC2* deficient cells could be through inhibiting cell migration. STAT3 inhibition alone and in combination with Ref-1 inhibitors has been observed to decrease pancreatic cancer cell migration (Bi *et al.* 2018 and Cardoso *et al.* 2012) and is implicated in upregulating the RhoA/ROCK pathway (Pan *et al.* 2018). A scratch wound healing assay of the *Tsc2* −/− MEFs demonstrated that inhibition of Ref-1, STAT3 and NF-κB reduced wound healing, compared to both the DMSO control and mTOR inhibition (figures 3.30 and 3.31). This is a relatively rudimentary assessment of *Tsc2* deficient cell migration however, and thus conclusions drawn are limited.

In summary, the results discussed in the present chapter demonstrate that the Ref-1/HIF-1α/STAT3/NF-κB signalling axis is upregulated in the both the human and murine cell models of TSC and that targeting this signalling axis could have clinical benefit in reducing growth of lesions and potentially abnormal vasculature in patients not responsive to mTOR inhibitors.

# Chapter 4: Targeting mTORC1, Ref-1 and STAT3 to normalise pro-angiogenic signalling within *TSC2* deficient cells

## 4.1 Introduction

The previous chapter demonstrated that inhibition of Ref-1 and STAT3 is effective at normalising measurable tumourigenic outputs in both murine and human *TSC2*-deficient cells. However, dysregulated cell growth and proliferation on loss of either *TSC1* or *TSC2* are not the only driver of pathology within TSC patients. As described within chapter 1, kidney, brain, and skin lesions associated with TSC are highly vascularised (Yamakado *et al.* 2002, Grajkowska *et al.* 2010 and Papakonstantinou *et al.* 2004). Immunohistochemical studies further identify TSC associated tumours as being angiogenic lesions. Furthermore, elevated protein expression of several pro-angiogenic factors, such as HGF, VEGFA, Epidermal growth factor (EGF) and fibroblast growth factor basic (bFGF) have been observed within patient brain and skin lesions (Parker *et al.* 2011 and Nguyen-Vu *et al.* 2001). Angiogenic protein expression observed within these lesions are also found within TSC model cell lines (El-Hashemite *et al.* 2003, Düvel *et al*. 2010 and Brugarolas *et al.* 2003) or cells with hyperactive mTORC1 activity (Land and Tee, 2007 and Dodd *et al.* 2015). Within multiple human cancers, both HIF-1α and STAT3 are known angiogenic drivers (Semenza *et al.* 2012 and Gao *et al.* 2017) whose activity is further promoted during hypoxia (Lee *et al*. 2006, Norman *et al.* 2009, Kang *et al*. 2010 and Pawlus *et al*. 2014). Elevated expression/activity of these transcription factors within TSC has long been described (Düvel *et al*. 2010, Brugarolas *et al.* 2003, Goncharova *et al.* 2009 and El-Hashemite and Kwiatkowski, 2005). Furthermore, the hypoxic nature of tumours and tissues predominantly affected by TSC (Northrup *et al.* 2013) likely contributes to dysregulated angiogenesis seen in TSC.

Within the context of TSC, targeting mTORC1 can normalise elevated angiogenic markers. Rapamycin has been shown to decrease both HIF-1α protein and target gene mRNA expression in murine *Tsc1*/*Tsc2*-deficient cell lines, (Düvel *et al*. 2010 and Brugarolas *et al.* 2003). In the phase 3 clinical trial examining efficacy of Everolimus (a structural analogue of rapamycin) in TSC patients, Franz *et al.* (2012) found a reduction in the plasma concentrations of a number of angiogenic markers. It was considered that adjunct therapy of rapamycin with inhibitors that also target HIF-1α and STAT3 maybe more effective than targeting mTORC1 alone at normalising aberrant angiogenic signalling observed upon loss of *TSC1*/*TSC2*. Studies within mice heterozygous for *TSC2* have shown angiogenesis inhibitors may have a therapeutic benefit when used alongside rapamycin (Woodrum *et al.* 2010 and Yang *et al.* 2017). Whilst within cancer cell lines, inhibitor blockade of both STAT3 and HIF-1α has been

shown to have a potent anti-angiogenic effect (Carbajo-Pescador *et al.* 2013 and Shin *et al.* 2011).

STAT3 and HIF-1α are among the redox-sensitive transcription factors that are transactivated by Ref-1, through Ref-1's reduction of specific oxidised cysteines found within their transcriptional activation domains (Shah *et al.* 2017). Ref-1 inhibitors used within the previous chapter inhibit Ref-1's redox function without affecting its function in the base excision repair (BER) pathway. Indeed, APX3330 treatment has been found to decrease angiogenesis in retinal vascular endothelial cells (Jiang *et al.* 2011), choroid endothelial cells (Li *et al.* 2014a), and retinal pigment epithelium cells (Li *et al.* 2014a). STAT3 phosphorylated at Y705 is considered transcriptionally active, able to form dimers with other STAT3 or STAT family members to enter the nucleus and drive transcription (Wen *et al.* 1995). *HIF1A* is reported as being a STAT3 target gene (Jung *et al.* 2005), while constitutively active STAT3 can stabilise HIF-1α protein (Jung *et al.* 2005 and Jung *et al.* 2008). STAT3 inhibition has been shown to decrease pro-angiogenic protein expression and scores of angiogenesis in multiple cancer cell lines (Leong *et al.* 2009, Laird *et al*. 2003, Kukawski *et al.* 2008 and Xu *et al*. 2005). Therefore, repression of STAT3 phosphorylation with STAT3 inhibitors previously used in the chapter 3, C188-9 and FLLL31, would likely reduce HIF-1α driven pro-angiogenic gene transcription. It should be noted however that STAT3 is not always found to be an upstream activator of HIF-1α. For instance, in multiple cancer cell lines where both HIF-1α and STAT3 are constitutively active, drug inhibition of STAT3 was not always associated with a repression of *HIF1A* mRNA and/or protein expression (Adachi *et al.* 2012, Bai *et al.* 2014 and Pawlus *et al.* 2014).

The aims of this chapter include expanding the list of HIF-1α target genes dysregulated on loss of *TSC2* within our cellular models of TSC, especially the patient-derived AML 621-102 line. Then to validate the potential clinical relevance of these differentially expressed genes using previously published RNA sequencing data comparing TSC associated lesions to non-TSC tissue (kindly given access to by Prof. Jeffrey MacKeigan). Secondly, a key aim is to assay protein expression of pro-angiogenic factors, some of which are already described within TSC lesions, within *TSC2* deficient cells. A third aim is to evaluate the efficacy of Ref-1 and STAT3 inhibitors alone or in combination with rapamycin to normalise mRNA and protein expression of identified pro-angiogenic factors. For the purpose of figures, *TSC2* deficient AML cells are referred to as *TSC2* −/− AMLs.

## 4.2 Results

### 4.2.1 The HIF-1α driven transcriptome is dysregulated in TSC lesions and upon loss of *TSC2* within AML and MEF cells.

Previous studies have established that loss of either *Tsc1* or *Tsc2* in murine models of TSC results in a higher expression of HIF-1α target genes. Through Northern blotting, Brugarolas *et al.* (2003) found elevated expression of *Vegfa, Glut1* and *Pgk1* mRNA in *Tsc2* −/− MEFs compared to *Tsc2* +/+ MEFs. Düvel *et al*. (2010) found within their gene expression array that the expression of HIF-1α target genes were elevated in both the *Tsc1* and *Tsc2* deficient MEFs compared to their respective wildtype controls. Chapter 3 demonstrated HIF-1α mRNA and protein expression is elevated in both human and murine *TSC2* deficient cells (figure 3.4). Given the key role that HIF-1α has in cancer in driving angiogenesis (Semenza *et al.* 2012), HIF-1α likely contributes to the highly vascular and angiogenic nature of TSC tumours (Nguyen-Vu *et al*. 2001 and Arbiser *et al.* 2002). The first aim of the present chapter was to identify and expand on known HIF-1α target genes that may more broadly contribute to TSC pathology on loss of *TSC2* in both the MEF cell lines and the more clinically relevant patient derived AML cell lines. For this purpose, differential expression (DEG) analyses of two RNA sequencing data set were utilised. The first compared *TSC2* deficient AML (621-102) to *TSC2* add back (621-103) cells cultured under normoxia (21% $O_2$) or hypoxia (1% $O_2$). This data set was generated during the course of research for this thesis by the Tee lab (sequencing itself by Wales Gene Park). The second RNA sequencing data compared *Tsc2* −/− MEF cells to *Tsc2* +/+ MEF cells and was generated within the Tee lab (sequencing itself by Wales Gene Park) but prior to course of research for this thesis (see Johnson *et al.* 2018a). To identify clinically relevant HIF-1α target genes, DEG of additional RNA sequencing data sets that were generated by another research group (see Martin *et al.* 2017) were used. Within these data sets, gene expression of TSC lesions (sub-ependymal nodules/subependymal giant cell astrocytomas, cortical tubers and renal angiomyolipomas) was compared to non-TSC tissue samples (normal brain or kidney). Access to these TSC lesions versus non-TSC tissue data sets was kindly given by Prof. J. Mackeigan. Full details of the sample origin and sequencing methodology for each RNA sequencing data set can be found in chapter 2, section 2.3.6.

The number of genes known to be regulated by the HIF family of transcription factors is substantial. An estimate based on studies utilising genome-wide chromatin immunoprecipitation (ChIP), DNA sequencing and mRNA microarrays, places the number of direct HIF target genes as greater than 800 (Semenza *et al.* 2012). In addition, HIF family members, such as HIF-1α and HIF-2α, show overlap in some target genes (Mole *et al.* 2009). Therefore, a large gene set of 181 HIF-1α target genes was compiled from ChIP sequencing studies (Xia *et al.* 2009 and Mole *et al.* 2009) and meta-analyses/reviews of experimentally

validated HIF-1α target genes within the literature (Slemc and Kunej, 2016 and Wenger *et al.* 2005), to better characterise the HIF-1α driven transcriptome within the TSC cell line model. See appendix for full HIF-1α target gene set.

For the RNA seq data set comparing TSC lesions to non-TSC tissue, DEG analysis revealed that many HIF-1α target genes were differentially expressed. As seen by the volcano plot in figure 4.1 (**A**), this was most pronounced in the SEN/SEGAs. Out of the 181 genes within the HIF-1α target gene set, 93 were significantly differentially expressed, with 62 genes that were upregulated and 31 that were downregulated compared to normal matched brain tissue. Comparing the other TSC lesions and non-TSC tissue, the number of significantly differentially expressed HIF-1α target genes was lower, as seen in the volcano plots in supplemental figure S.4.1 and by table 4.1. DEG analysis showed 32 genes that were significantly differentially expressed between the cortical tubers and normal matched brain tissue (24 upregulated and 8 downregulated). Whilst 42 genes are significantly differentially expressed between the renal angiomyolipomas and normal matched kidney tissue (22 upregulated and 20 downregulated). The lower number of differentially expressed HIF-1α genes in the kidney samples compared to SEN/SEGAs versus normal brain tissue is surprising. Renal AML lesions are highly vascularised with irregularly formed blood vessels (Yamakado *et al.* 2002), implying increased and aberrant angiogenesis. That being said, as can be seen from the volcano plots in supplemental figure S.4.1 a number of HIF-1α genes had $\log_2$ foldchange values < -1 or >1, but failed to meet the significance threshold. This is likely due to the lower empowerment within the renal AML vs normal kidney data set, with a smaller number of normal kidney samples when compared to brain tissue samples.

DEG analyses within the AML cell line RNA seq data set revealed that a majority of HIF-1α target genes were upregulated within *TSC2* deficient cells compared to *TSC2* re-expressed (RE) cells. As shown in figure 4.1 (**B**) and table 4.1, for the AML cell lines cultured under normoxia (21% $O_2$), 115 out of the 181 genes within the HIF-1α target gene set are significantly differentially expressed. With 77 and 38 genes significantly upregulated and downregulated, respectively, within the *TSC2* deficient cells compared to the *TSC2* RE cells. The greater HIF-1α transcriptional profile within the *TSC2* deficient AML cells, even under normal oxygen conditions (figure 4.1 **B**), could be a result of hyperactive mTORC1 signalling. Several studies have demonstrated that activation of mTORC1 can increase HIF-1α protein expression, mediated transcription and metabolic reprogramming within the context of TSC and cancers (Düvel *et al.* 2010, Hudson *et al.* 2002 and Zhong *et al.* 2000b). Under hypoxia (1% $O_2$), more HIF-1α target genes are significantly downregulated (53 genes) and less are significantly upregulated (67 genes) within the *TSC2* deficient cells compared to the *TSC2* RE cells (figure 4.1 **C** and table 4.1).

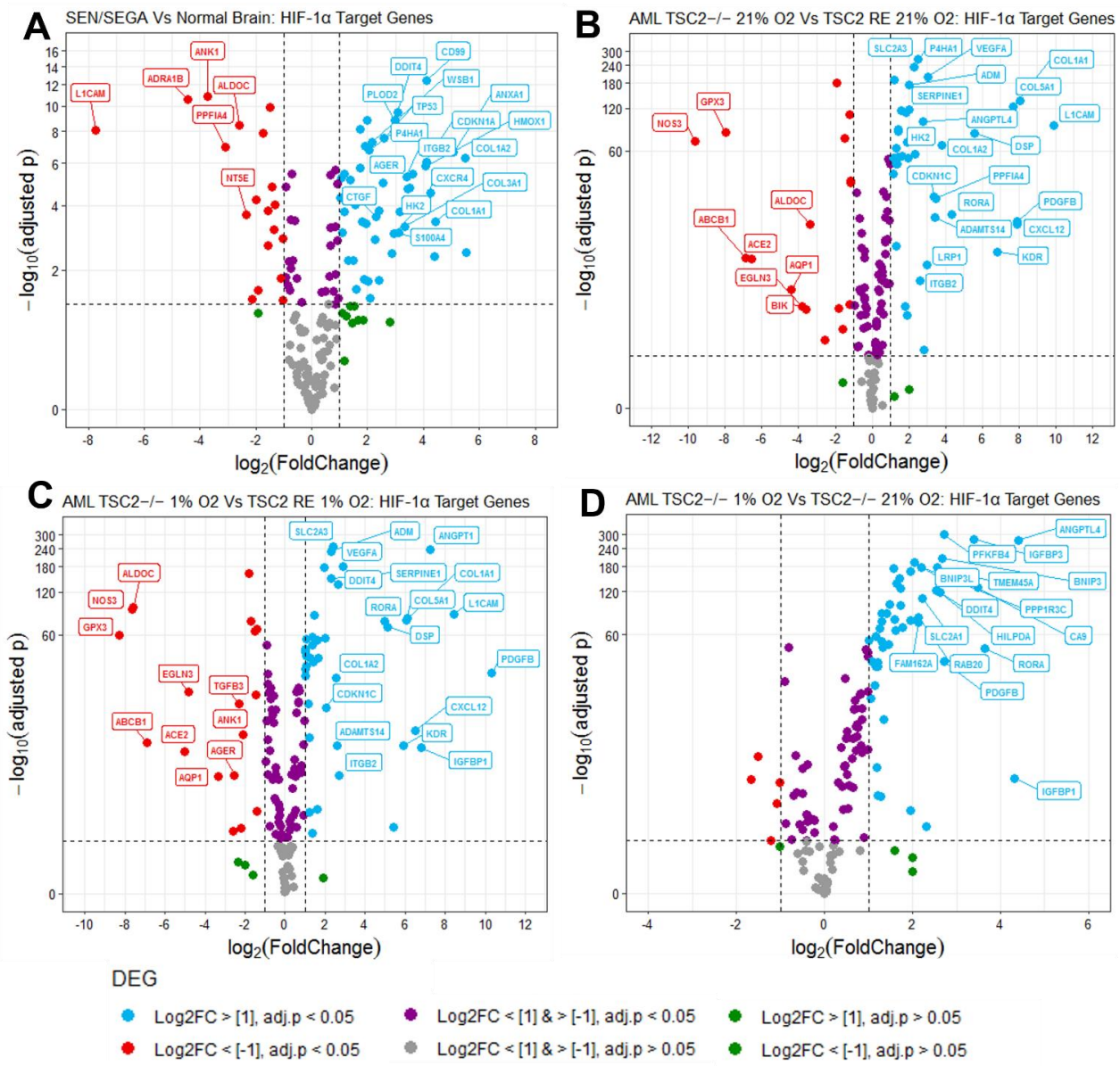


**Figure 4.1 HIF-1α target genes are dysregulated upon loss of *TSC2* within patient tumours and AML cells.** Differential gene expression (DEG) comparison is annotated above each plot. Volcano plot **A** was generated from previously published RNA sequencing data which Prof. Jeffrey MacKeigan gave access to. This data set compares gene expression of donated TSC patient tumours samples versus non-TSC healthy tissue samples. In this case SEN/SEGA (Subependymal nodules/ Subependymal giant cell astrocytomas) (N=15) versus normal brain (N=8). See Martin *et al*. (2017) for methods on sample collection, data collection and DEG analysis. Volcano plots **B**, **C** and **D** were generated from RNA sequencing data, comparing either AML *TSC2* deficient −/− and *TSC2* RE (re-expressed) cells cultured under either normoxia (21% $O_2$) or hypoxia (1% O2) (N=6). RNA sequencing was conducted through Wales Gene Park and expression levels were calculated and normalised from raw read counts as RPKM (Reads per Kilobase exon Model per million mapped reads) with DEG analysis generated through DEseq2 analysis and resulting p-values were corrected for multiple testing and false discovery by FDR method. For all volcano plots Log2 transformed fold change in expression of genes was plotted against their -log10 transformed FDR adjusted p-values. Dotted lines at x axis represent increase or decrease in foldchange of 2 or -2 respectively. Dotted line at y axis represents significance threshold of 0.05. Genes annotated had a Log2 fold change in expression greater or lower than 2 or -2 (i.e., fourfold higher or lower in expression) respectively and an -log10 adjusted p-value greater than 3 (i.e., below 0.001 significance threshold).

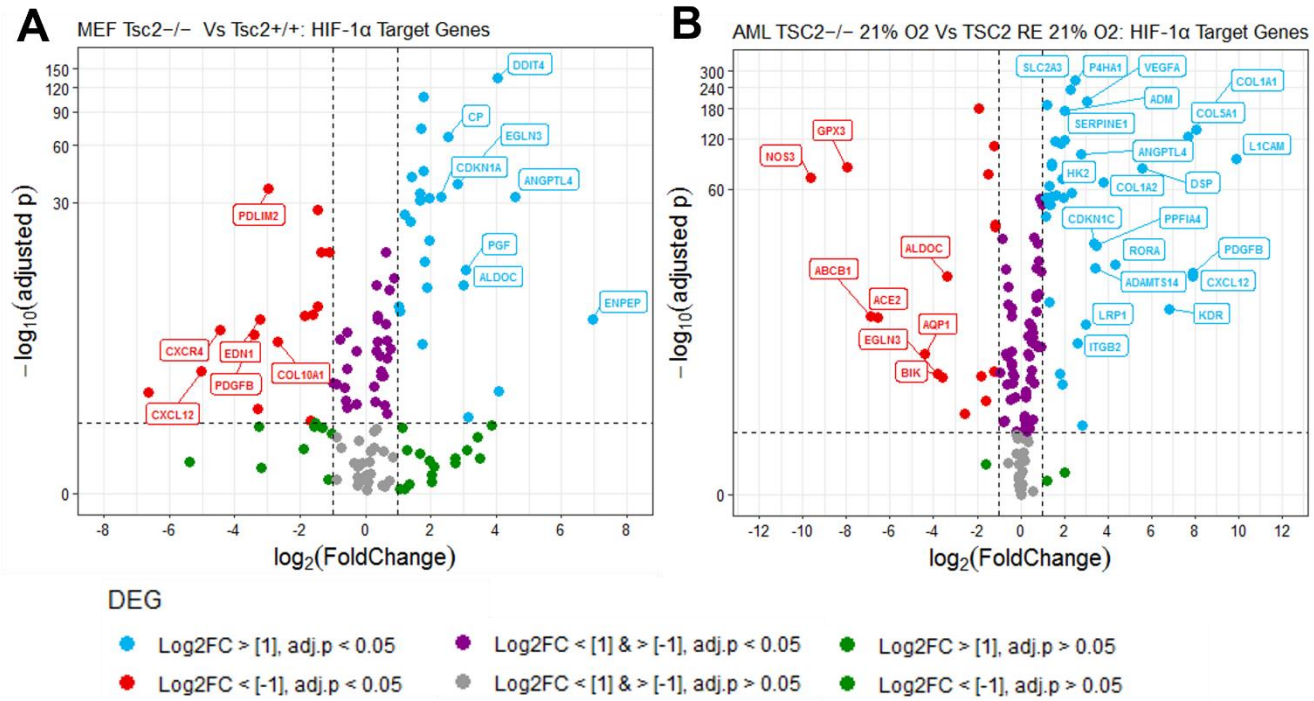


**Figure 4.2 HIF-1α target gene expression is dysregulated in both MEF and AML cell lines on loss of *TSC2*.** Differential gene expression (DEG) comparison is annotated above each plot. Two separate RNA sequencing experiments were conducted through Wales Gene Park, comparing either AML *TSC2* −/− and *TSC2* RE (re-expressed) (N=6) cells or MEF *Tsc2* −/− and *TSC2* WT cells (N=3). Expression levels were calculated and normalised from raw read counts as RPKM (Reads per Kilobase exon Model per million mapped reads) with DEG analysis generated through DEseq2 analysis and resulting p-values were corrected for multiple testing and false discovery by FDR method. Log2 transformed fold change in expression of genes (*TSC2* −/− cells against *TSC2* RE for AMLs or *TSC2* WT for MEFs) was plotted against their -log10 transformed FDR adjusted p-values. Dotted lines at x axis represent increase or decrease in foldchange of 2 or -2 respectively. Dotted line at y axis represents significance threshold of 0.05. Genes annotated had a Log2 fold change in expression greater or lower than 2 or -2 (i.e., fourfold higher or lower in expression) respectively and an -log10 adjusted p-value greater than 3 (i.e., below 0.001 significance threshold).

**Table 4.1 Comparison of HIF-1α target gene DEG analysis between RNA sequencing data of TSC lesions vs non-TSC tissue, *TSC2* deficient (−/−) AML vs TSC2 re-expressed (RE) AML cells and *Tsc2* −/− MEF vs *Tsc2* +/+ MEF cells**

| Comparison | Detectable genes (out of 181 genes) | Sig. differentially expressed genes | Sig. Upregulated (Log2FC = 0 – <1) | Sig. Upregulated (Log2FC = >1) | Sig. Downregulated (Log2 FC = >-1 – 0) | Sig. Downregulated (Log2 FC = <-1) |
|---|---|---|---|---|---|---|
| SEN/SEGA Vs normal brain | 167 | 93 | **12** | **19** | **14** | **48** |
| Cortical tuber Vs normal brain | 167 | 32 | **6** | **2** | **8** | **16** |
| Renal AML vs normal kidney | 167 | 42 | **3** | **19** | **2** | **18** |
| *TSC2* −/− AML vs *TSC2* RE AML 21% $O_2$ | 149 | 115 | **37** | **40** | **21** | **17** |
| *TSC2* −/− AML vs *TSC2* RE AML 1% $O_2$ | 151 | 121 | **26** | **42** | **35** | **18** |
| *TSC2* −/− AML 1% $O_2$ vs 21% $O_2$ | 146 | 113 | **39** | **50** | **19** | **5** |
| *TSC2* −/− MEF vs *TSC2* +/+ MEF 21% $O_2$ | 124 | 77 | **21** | **27** | **10** | **19** |

The effect of hypoxia still appears to be a relevant factor in driving HIF-1α transcriptional activity within *TSC2* deficient AML cells. As seen in figure 4.1 (**D**) and table 4.1, by and large HIF-1α target gene expression is elevated further in *TSC2* deficient AML cells cultured under hypoxia than normoxia (with 89 genes significantly upregulated). This observation is relevant within the context of TSC lesions, as the hypoxic nature of large lesions will likely drive HIF-1α activity further (Riffle and Hegde, 2017). As MEFs are the other cell model of TSC used in this work, whether loss of *Tsc2* within MEFs also resulted in a HIF-1α transcriptional signature, as would be expected from previous research (Düvel *et al*. 2010 and Brugarolas *et al.* 2003), was assessed. As seen from the volcano plot in figure 4.2 (**A**), 70 out of the 181 genes within the HIF-1α target gene set are significantly differentially expressed between *Tsc2* −/− and *Tsc2* +/+ MEFs. With 45 and 25 genes significantly upregulated and downregulated, respectively, within the *Tsc2* −/− MEFs compared to the *Tsc2* +/+ MEFs (table 4.1).

Contrasting RNA seq data sets, it is clear that the HIF-1α driven transcriptome is dysregulated on loss of *TSC2*, both in TSC lesions and in *TSC2*-deficient cell lines. As shown in the heat

map in figure 4.3, there was significant fold changes in HIF-1α target gene expression between *TSC2* deficient and *TSC2* RE AML cells (under either normoxia and hypoxia) and between at least one TSC lesion and their corresponding matched normal tissue, as shown in table 4.2. The number of differentially regulated genes is 96, representing more than half of the genes within the HIF-1α target gene set. The heatmap highlights similarities and differences in expression patterns of those genes between data sets. Firstly, it is clear there is a large variation in HIF-1α target gene expression between TSC lesion types relative to their non-TSC tissue controls. Secondly there is variation between which HIF-1α target genes are dysregulated between AML cell lines and the TSC lesions and normal tissue controls. Comparing the direction of fold changes (upregulated or downregulated) in HIF-1α target genes between the SEN/SEGA vs NB and *TSC2* −/− vs *TSC2* RE AML cells data sets. For AML cells grown under normoxia, 55 HIF-1α target genes are differentially expressed in the same direction (e.g., a gene upregulated in the *TSC2* −/− AML cells and SEGAs) and 41 in a different direction (e.g., a gene downregulated in the *TSC2* −/− AML cells but upregulated in SEGAs) between the two data sets. For AML cells grown under hypoxia, 52 HIF-1α target genes are differentially expressed in the same direction and 44 in a different direction between the two data sets. Lastly, when comparing the *Tsc2* −/− vs *Tsc2* +/+ MEF cells to the SEN/SEGA vs NB data set, 41 HIF-1α target genes are differentially expressed in the same direction and 47 in a different direction between the two data sets. These comparisons highlight that whilst HIF-1α driven transcriptome is dysregulated in both TSC lesions and TSC cell models, there are differences in individual HIF-1α target gene's expression between the cell models and lesions. For example, *VEGFA* is substantially upregulated within *TSC2* −/− AML cells, but far less so in SEN/SEGAs and actually downregulated within renal AMLs compared to normal kidney. This data contrasts with published studies were VEGFA protein and mRNA expression have been detected in TSC lesions (Nguyen-Vu *et al*. 2001 and Arbiser *et al.* 2002). Therefore, considering that neither the *TSC2* −/− AML or MEF cells are wholly representative of the HIF-1α driven transcriptome in patient lesions is an important consideration moving forward.

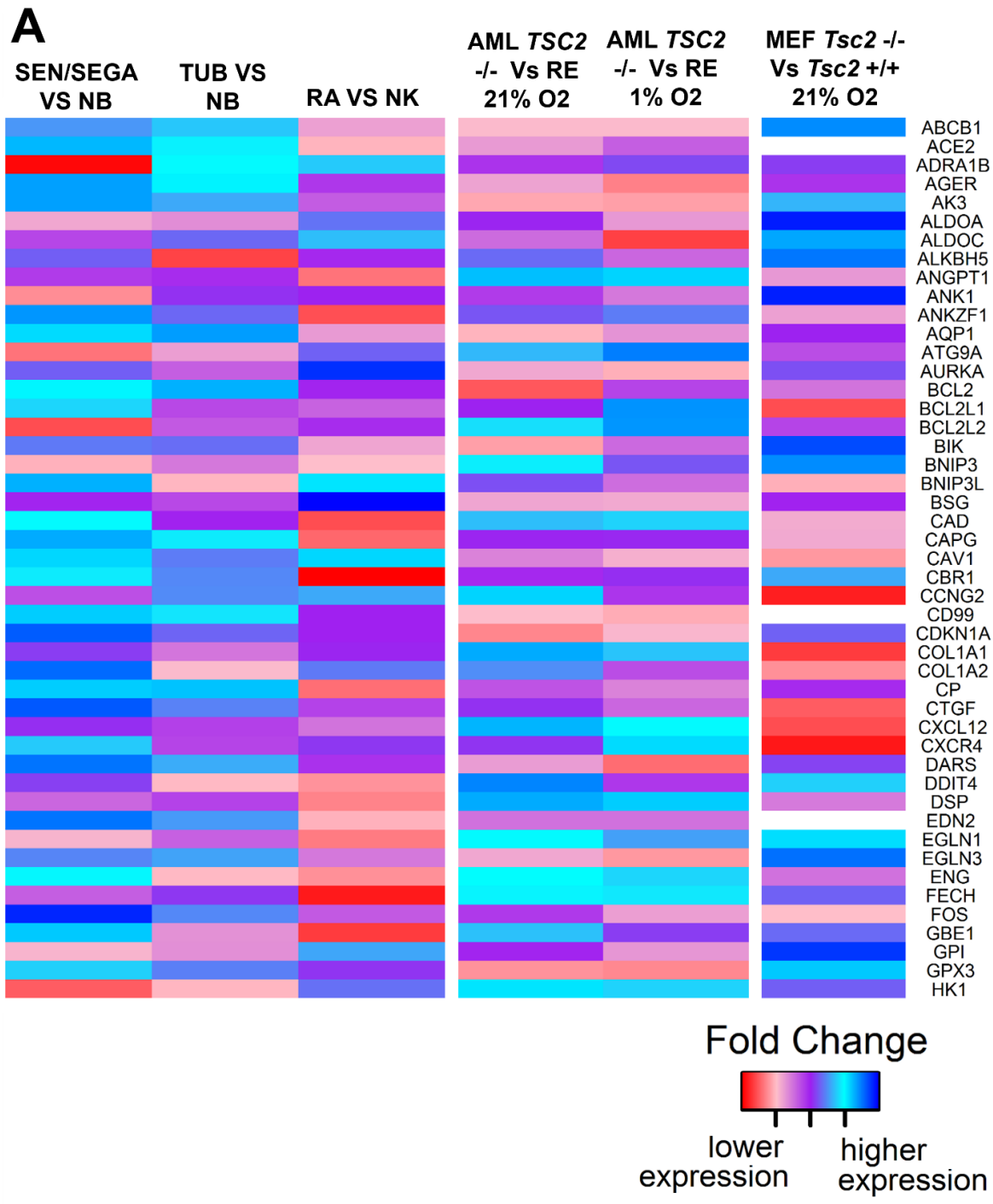
A
SEN/SEGA VS NB
TUB VS NB
RA VS NK
AML TSC2 -/- Vs RE 21% O2
AML TSC2 -/- Vs RE 1% O2
MEF Tsc2 -/- Vs Tsc2 +/+ 21% O2
ABCB1
ACE2
ADRA1B
AGER
AK3
ALDOA
ALDOC
ALKBH5
ANGPT1
ANK1
ANKZF1
AQP1
ATG9A
AURKA
BCL2
BCL2L1
BCL2L2
BIK
BNIP3
BNIP3L
BSG
CAD
CAPG
CAV1
CBR1
CCNG2
CD99
CDKN1A
COL1A1
COL1A2
CP
CTGF
CXCL12
CXCR4
DARS
DDIT4
DSP
EDN2
EGLN1
EGLN3
ENG
FECH
FOS
GBE1
GPI
GPX3
HK1
Fold Change
lower expression
higher expression

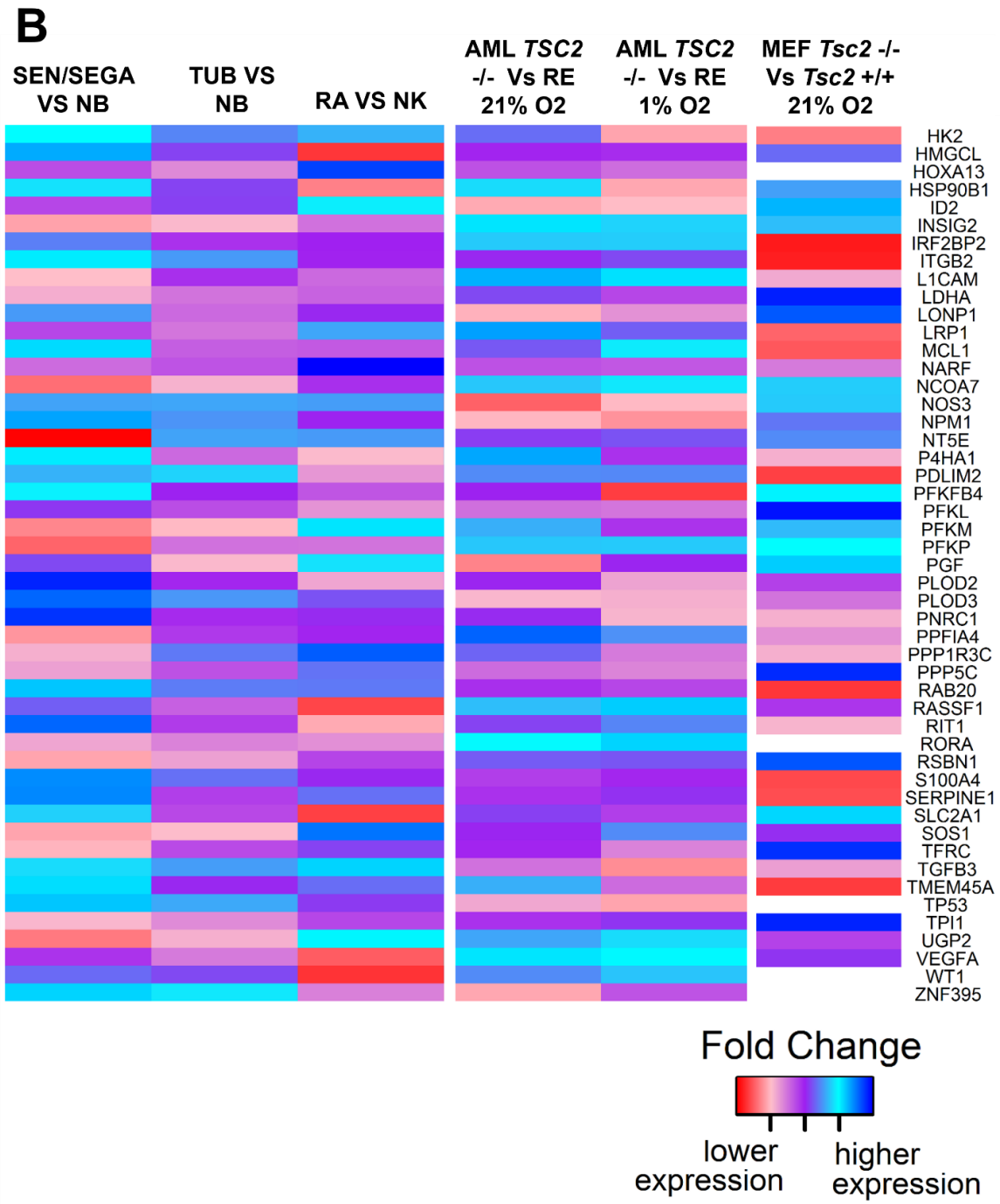


**Figure 4.3 HIF-1α target gene set is differentially expressed between TSC tumour types, human and murine cell models lines of TSC.** Panels **A** and **B** belong to the same heatmap comparing fold change in expression of HIF-1α target genes between either a TSC lesion and healthy tissue or a *TSC2* −/− cell line with a *TSC2* re-expressed (RE) (AML) or *TSC2* +/+ (MEF) cell line. HIF-1α target genes selected for the heatmap are those which are significantly differentially expressed between the *TSC2* −/− and *TSC2 RE* cell lines (under either oxygen conditions) and between at least one TSC lesion and healthy tissue. Differential gene expression (DEG) comparison is annotated above each column and the oxygen conditions, 21% $O_2$ (normoxia) or 1% $O_2$ (hypoxia), cell lines were cultured under is also denoted. White spaces within columns indicate that gene's expression was not detectable in that data set. Gene names are shown on the right of the heatmap. It should be noted these data sets are distinct, generated differently from one another (see methods and materials section). **SEN/SEGA** = subependymal nodule/Subependymal giant cell astrocytomas, **NB** = normal brain, **TUB** = TSC tuber, **RA** = renal angiomyolipoma, **NK** = normal kidney.

**Table 4.2. Many HIF-1α target genes expression is dysregulated in both TSC lesions and in *TSC2* deficient AML cells.** HIF-1α target genes below are those whose foldchange in expression between a lesion and its matched non-TSC tissue, or between *TSC2* deficient AML cells and *TSC2* expressed AML cells, were found significant.

| Dysregulated in TSC lesions only | | Dysregulated in cells only | | Dysregulated in both cells and at least one TSC lesion. | | | |
|---|---|---|---|---|---|---|---|
| *ALKBH5* | *NEU1* | *ABCG2* | *MET* | *ABCB1* | *CAV1* | *ID2* | *PPFIA4* |
| *ANGPT1* | *NOS2* | *ADAMTS14* | *MIF* | *ACE2* | *CCNG2* | *INSIG2* | *PPP1R3C* |
| *ARNT* | *NPPA* | *ADM* | *NOS3* | *ADRA1B* | *CD99* | *IRF2BP2* | *PPP5C* |
| *ATRIP* | *PCK1* | *ARNTL* | *NR4A1* | *AGER* | *CDKN1A* | *ITGB2* | *RAB20* |
| *BCL2L2* | *PFKL* | *BCKDHA* | *PDGFB* | *AK3* | *COL1A1* | *KDR* | *RASSF1* |
| *BHLHE41* | *PGF* | *BHLHE40* | *PFKFB3* | *ALDOA* | *COL1A2* | *L1CAM* | *RIT1* |
| *BNIP3L* | *SLC2A2* | *CA9* | *PFKM* | *ALDOC* | *CP* | *LDHA* | *RORA* |
| *CBR1* | *SOS1* | *CD274* | *PGAM1* | *ANGPTL4* | *CXCL12* | *LONP1* | *RSBN1* |
| *COL3A1* | *SOX9* | *CDKN1B* | *PKM* | *ANK1* | *DSP* | *LRP1* | *S100A4* |
| *CTGF* | *TF* | *CDKN1C* | *PMAIP1* | *ANKZF1* | *EDN2* | *MCL1* | *SERPINE1* |
| *CXCR4* | *TPI1* | *CITED2* | *PPP4R3B* | *ANXA1* | *EGLN1* | *NARF* | *SLC2A1* |
| *DARS* | *WSB1* | *COL5A1* | *RAPGEF1* | *AQP1* | *EGLN3* | *NCOA7* | *TFRC* |
| *DDIT4* | *WT1* | *EDN1* | *SLC2A3* | *ATG9A* | *ENG* | *NPM1* | *TGFB3* |
| *ENO1* | *ZNF395* | *ETS1* | | *AURKA* | *FECH* | *NT5E* | *TMEM45A* |
| *ENPEP* | | *FAM162A* | | *BCL2* | *FOS* | *P4HA1* | *TP53* |
| *FLT1* | | *GAPDH* | | *BCL2L1* | *GBE1* | *PDLIM2* | *UGP2* |
| *GCK* | | *GBE1* | | *BIK* | *GPX3* | *PFKFB4* | *VEGFA* |
| *GPI* | | *IGFBP1* | | *BNIP3* | *HK1* | *PFKP* | *ZNF395* |
| *HMOX1* | | *INHA* | | *BSG* | *HK2* | *PLOD2* | |
| *HOXA13* | | *KDM3A* | | *CAD* | *HMGCL* | *PLOD3* | |
| *MT1A* | | *KDM5B* | | *CAPG* | *HSP90B1* | *PNRC1* | |

### 4.2.2 Loss of *TSC2* upregulates expression of HIF-1α and STAT3 driven pro-angiogenic genes.

As well as HIF-1α, STAT3 and other transcription factors are known to regulate angiogenesis. In the previous results chapter (section 3.3.1, figures 3.1 and 3.2), markers of both HIF-1α and STAT3 activity were shown to be elevated within both *TSC2* deficient AML and MEF cell lines. Therefore, before assessing the efficacy of either mTORC1, Ref-1 or STAT3 inhibitors in normalising pro-angiogenic signalling. The next aim of this chapter was to assay, through qPCR, the expression of a panel of pro-angiogenic genes whose transcription is driven by either HIF-1α, STAT3 or both, between *TSC2* deficient and *TSC2* RE AML cells. Aberrant STAT3 signalling in multiple human cancers drives tumour angiogenesis (Wei *et al.* 2003, Yang *et al*. 2013b and Zhao *et al.* 2018). And in relation to TSC, a number of proangiogenic direct target genes of STAT3 have been found to be upregulated upon loss of *TSC1* or *TSC2*. For example, Parker *et al.* (2017) found mRNA expression of *HGF* and *VEGFA* was upregulated in *TSC1* knockout mouse cortex. Additionally, *HIF1A* itself is a STAT3 target gene (Niu *et al.* 2008 and Jung *et al.* 2005). Dodd *et al.* (2015) reported that mTORC1 directly phosphorylates STAT3 at S727, which promotes the STAT3 mediated transcription of *HIF1A*. The present chapter hypothesised that HIF-1α and STAT3 both likely orchestrate a pro-angiogenic transcriptional programme within TSC. Genes chosen for the pro-angiogenic gene panel were *HIF1A*, *HGF*, *TNFRSF1A*, *VEGFA*, *CCL5* and *ANGPTL4*. These genes were significantly differentially expressed between the two AML lines and between at least one TSC lesion and corresponding non-TSC tissue. As the AML cell line RNA sequencing data was not obtained before the following qPCR experiments were performed, selection of genes for the pro-angiogenic gene panel was not based an unbiased top-down bioinformatic approach.

As seen in figure 4.4, expression of *HIF1A*, *HGF*, *TNFRSF1A*, *VEGFA*, *CCL5* and *ANGPTL4* were all significantly upregulated within *TSC2* deficient AML cells cultured under either normoxia or hypoxia relative to the control sample (*TSC2* RE AML cells under normoxia). Additionally, aside from *HGF*, the difference in foldchange in mRNA of all proangiogenic genes assayed between *TSC2* deficient AML cells and *TSC2* RE AML cells cultured under hypoxia was found significant. Furthermore, only the difference in mRNA expression of *VEGFA* and *ANGPTL4* between *TSC2* deficient AML cells cultured either under normoxia or hypoxia was found to be significant (normoxia vs hypoxia *VEGFA* p=0.0441, *ANGPTL4* p=0.0024). This may be due to the increased stability and activity of the HIF-1α protein induced at low oxygen (Majmundar *et al.* 2010). The difference in *HIF1A* mRNA expression between *TSC2* deficient AML cells cultured under normoxia or hypoxia was not reported as significant. Therefore, increased expression of HIF-1α target genes within *TSC2* deficient AML cells cultured under hypoxia is not a function of increased transcription of the *HIF1A* gene itself under hypoxia. As

aside from *VEGFA,* hypoxia does not significantly upregulate the *STAT3* target genes *HIF1A, HGF, TNFRSF1A* and *CCL5* further within *TSC2* deficient AML cells. In contrast to the *TSC2* deficient cells, hypoxia only significantly increased the mRNA expression of *CCL5* within *TSC2* RE AML cells (p=0.0144).

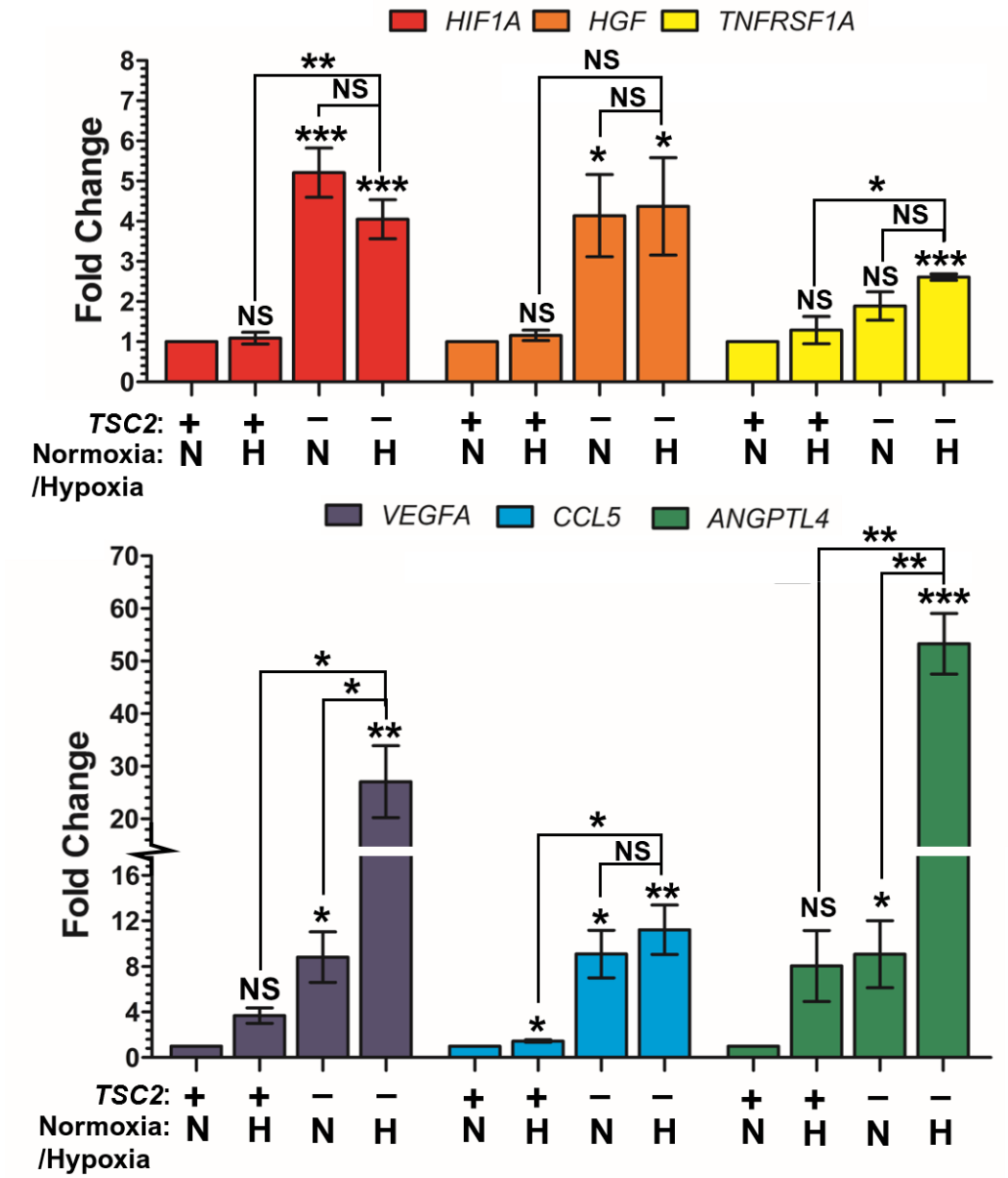


**Figure 4.4 Loss of *TSC2* in angiomyolipoma cells results in elevation of HIF-1α and STAT3 driven pro-angiogenic genes, some of which are further elevated under hypoxia.** Either under normoxia (**N**, 21% $O_2$) or hypoxia (**H**, 1% $O_2$), AML cells lacking *TSC2* (**TSC2 –** ) or with *TSC2* re-expressed (***TSC2* +**) were cultured overnight before being lysed. mRNA was purified from these lysates, converted to cDNA, and through qPCR the expression of target genes was quantified. Fold change in expression was calculated compared to a designated reference sample, in this case *TSC2* re-expressed under normoxia. Fold changes of target genes in samples were normalised to the housekeeping gene *HMBS*. Significance annotations above each bar on graph indicates significance of difference in foldchange between each condition and the reference sample (*TSC2* RE cells under normoxia). Pairwise statistical comparisons between *TSC2* deficient cells under normoxia or hypoxia and between *TSC2* deficient and *TSC2* RE cells under hypoxia are also annotated. Statistical analysis of differences in foldchange (N=3 minimum) was by student's t test. Significance denoted by: * = p <0.05, ** = p <0.01, *** = p< 0.001, NS = not significant. Bars represent standard error of the mean.

### 4.2.3 Elevated HIF-1α and STAT3 driven pro-angiogenic gene expression upon *TSC2* loss are regulated by STAT3 but not Ref-1 activity.

Given expression of the HIF-1α and STAT3 driven pro-angiogenic gene panel was elevated upon loss of *TSC2* in AML cells (figure 4.4), the next aim of the present chapter was to assess the efficacy of mTORC1, Ref-1 or STAT3 inhibitors at normalising the expression of the gene panel. Inhibition of either mTORC1, Ref-1 or STAT3 should in theory decrease transcription of the aforementioned genes. *In vitro,* inhibitors of these proteins/complexes have all been shown to have anti-angiogenic properties in cancer cell lines (Pang *et al.* 2010, Zou *et al.* 2009 and Leong *et al.* 2009). Both Düvel *et al.* (2010) and Brugarolas *et al.* (2003) found that inhibition of mTORC1 with rapamycin repressed the high levels of HIF-1α target gene expression in murine cell lines lacking either *Tsc1* or *Tsc2*. Dodd *et al.* (2015) demonstrated that mTORC1 activity promoted STAT3 driven transcription of *HIF1A* by directly phosphorylating S727 on STAT3. Ref-1 has been shown to transcriptionally activate both HIF-1α and STAT3 (Shah *et al.* 2017), which the Ref-1 inhibitor APX3330 was able to block in pancreatic cancer cell lines (Cardoso *et al.* 2012 and Logsdon *et al.* 2016). STAT3 is known to regulate its own gene expression (Ichiba *et al.* 1998 and Narimatsu *et al.* 2001), and to directly regulate the gene expression of *HIF1A* (Niu *et al.* 2008).

As shown in figure 4.5, mTORC1 inhibitors are effective at downregulating expression of *HGF*, *TNFRSF1A*, *VEGFA* and *ANGPTL4* relative to the DMSO control. mTORC1 inhibition resulted in a modest decrease in the expression of *TNFRSF1A* (KU: FC= 0.821 p=0.022) and *VEGFA* (RAP: FC=0.719 p=0.0289 and KU: FC= 0.748 p=0.0169). Of interest, mTORC1 inhibition, by either rapamycin or Ku-0063794, substantially decreased expression of *HGF* and *ANGPTL4.* Neither mTORC1 inhibitor treatment downregulated *HIF1A* expression. In fact, rapamycin treatment resulted in a slight but significant increase in the expression of *HIF1A*. Previous studies dispute this observation. Düvel *et al.* (2010) observed treating *Tsc2* null ($p53^{-/-}$) MEF cells (derived from littermate-pair crossings & described in Zhang *et al.* 2003) with rapamycin at 20 nM, a lower dose than used in this work, decreased expression of not only HIF-1α target genes, but the *Hif1a* gene itself. Whilst Dodd *et al*. (2015) found rapamycin treatment blocked the insulin mediated increase in *HIF1A* mRNA expression within HEK293 cells that had been transfected with an active mutant of mTOR. However, the caveat here is that Düvel *et al.* (2010) used a murine TSC cell model, whilst Dodd *et al*. (2015) used HEK293 cells transfected with an active mTOR mutant which would not fully recapitulate TSC pathology. The present qPCR data was collected from the AML 621-102 cell line. Ref-1 inhibitors however were completely ineffective at downregulating the expression of the HIF-1α/STAT3 driven pro-angiogenic gene panel. Two of the three Ref-1 inhibitors resulted in a significant increase in the expression of *ANGPTL4* relative to the control (APX3330: FC=8.045 p=0.0456, APX2014:

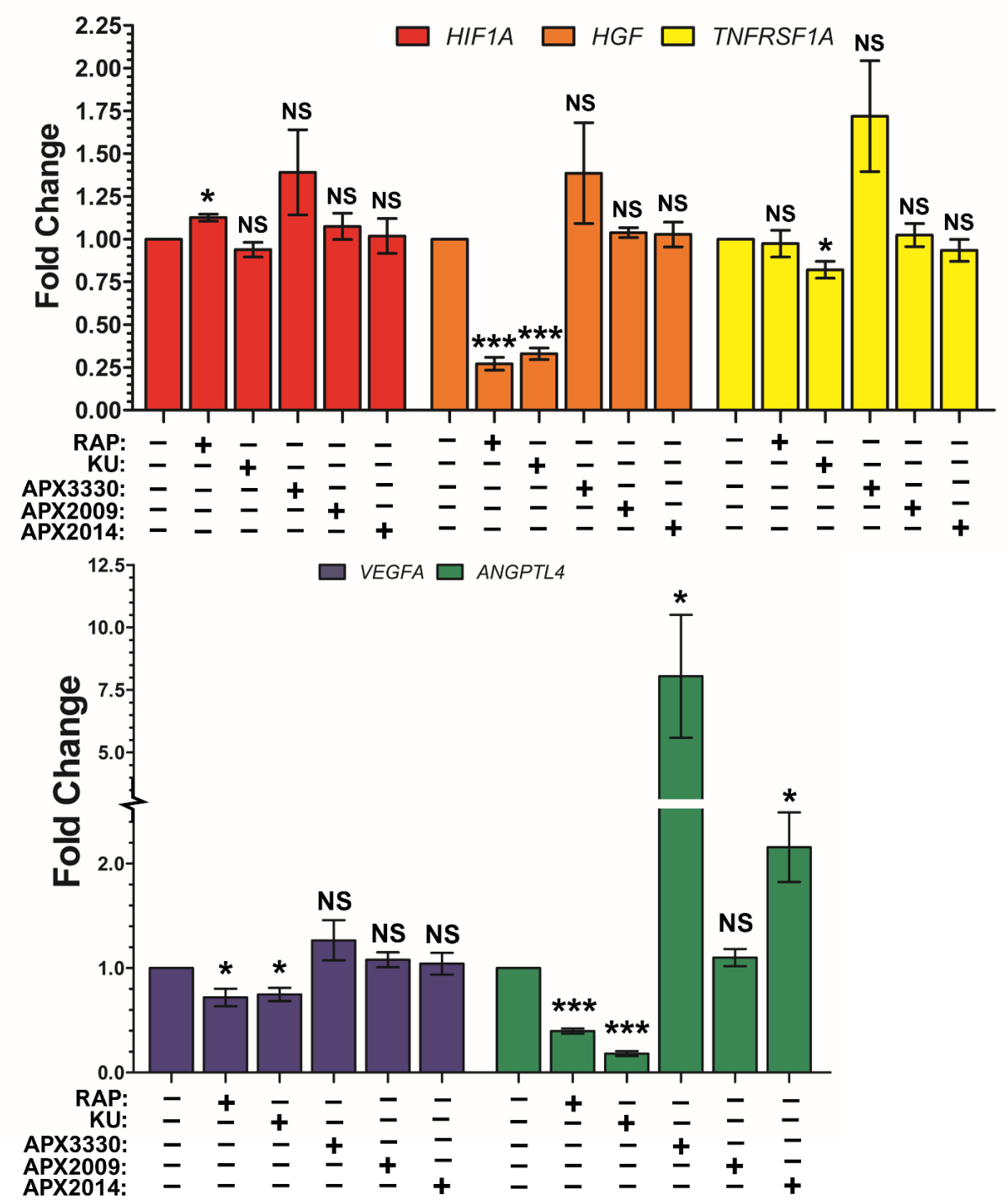


**Figure 4.5. qPCR analysis reveals Ref-1 inhibitors are ineffective at downregulating assayed HIF-1α and STAT3 driven proangiogenic genes in *TSC2* deficient AML cells.** *TSC2* deficient AML cells were cultured for 18 h in the presence of either DMSO, rapamycin (RAP) at 50 nM, APX3330 at 100 µM, APX2009 at 10 µM or APX2014 at 10 µM before being lysed. mRNA was purified from these lysates, converted to cDNA, and through qPCR the expression of target genes was quantified. Fold change in expression was calculated compared to a designated reference sample, in this case *TSC2* −/− cells treated with vehicle (DMSO). Fold changes of target genes in samples were normalised to the housekeeping gene *IPO8*. Significance annotations above each bar on graph indicates significance of difference in foldchange between each condition and the reference sample (DMSO). Statistical analysis of differences in foldchange (N=3 minimum) was by student's t test. Significance denoted by: * = p <0.05, ** = p <0.01, *** = p< 0.001, NS = not significant. Bars represent standard error of the mean.

FC=2.157 p=0.0255) (figure 4.5). This is despite HIF-1α and STAT3 being among the transcription factors known to be transactivated by Ref-1 protein (Shah *et al.* 2017). In pancreatic cancer cells, *in vitro* studies have demonstrated the efficacy of Ref-1 inhibition in decreasing transcriptional activity of HIF-1α and STAT3 (Cardoso *et al.* 2012 and Logsdon *et al.* 2016 and Fishel *et al.* 2011). The present findings suggest that Ref-1 isn't a key driver of HIF-1α and STAT3 regulated pro-angiogenic gene expression within TSC, at least for the genes assayed. Therefore, the potential effect of co-treatment of rapamycin and Ref-1 inhibitors on expression of the pro-angiogenic gene panel was not assayed.

STAT3 inhibitors were more effective at downregulating the expression of pro-angiogenic genes (figure 4.6). C188-9 treatment alone significantly downregulated the expression of *HGF*, *TNFRSF1A* and *VEGFA*. Whereas FLLL31 treatment alone only significantly downregulated *VEGFA* expression. Rapamycin treatment alone significantly downregulated the expression of *HGF*, *TNFRSF1A* and *ANGPTL4*. These findings are consistent with the effect of rapamycin in the previous qPCR data (figure 4.5), except in the case of *VEGFA*. Interestingly, STAT3 inhibition through C188-9 treatment alone, significantly upregulates the expression of *CCL5* and *ANGPTL4* relative to the DMSO control. *CCL5* is part of a subset of STAT3 target genes whose expression is more strongly induced by unphosphorylated STAT3 than STAT3 phosphorylated at tyrosine 705 (Yang *et al.* 2005 and Yang *et al.* 2007). *ANGPTL4* has also been identified as a STAT3 target gene in cancers (Avalle *et al.* 2022 and Yu-Ting *et al.* 2017). Combinatory treatment of rapamycin and C188-9 prevented the undesirable induced expression of *CCL5* and *ANGPTL4* that was observed by C188-9 treatment alone (RAP+C188-9 vs C188-9: *CCL5*: p= 0.0016 *ANGPTL4*: $1.0451 \times 10^{-5}$). The effect of combinatory treatment with rapamycin and C188-9 on the expression of *HIF1A, HGF, TNFRSF1A* and *VEGFA* was not markedly different to the effect observed with that of the single drug treatment conditions with either rapamycin or C188-9 (figure 4.6). This is despite Dodd *et al.* (2015) finding dual targeting of both the tyrosine 705 and serine 727 phosphorylation sites of STAT3, through FLLL31 and rapamycin treatment respectively, blocked the insulin induced mRNA expression of *HIF1A*. This data implies that in these AML cells, neither STAT3 or mTORC1 is driving the mRNA expression of *HIF1A* reported (figure 4.4).

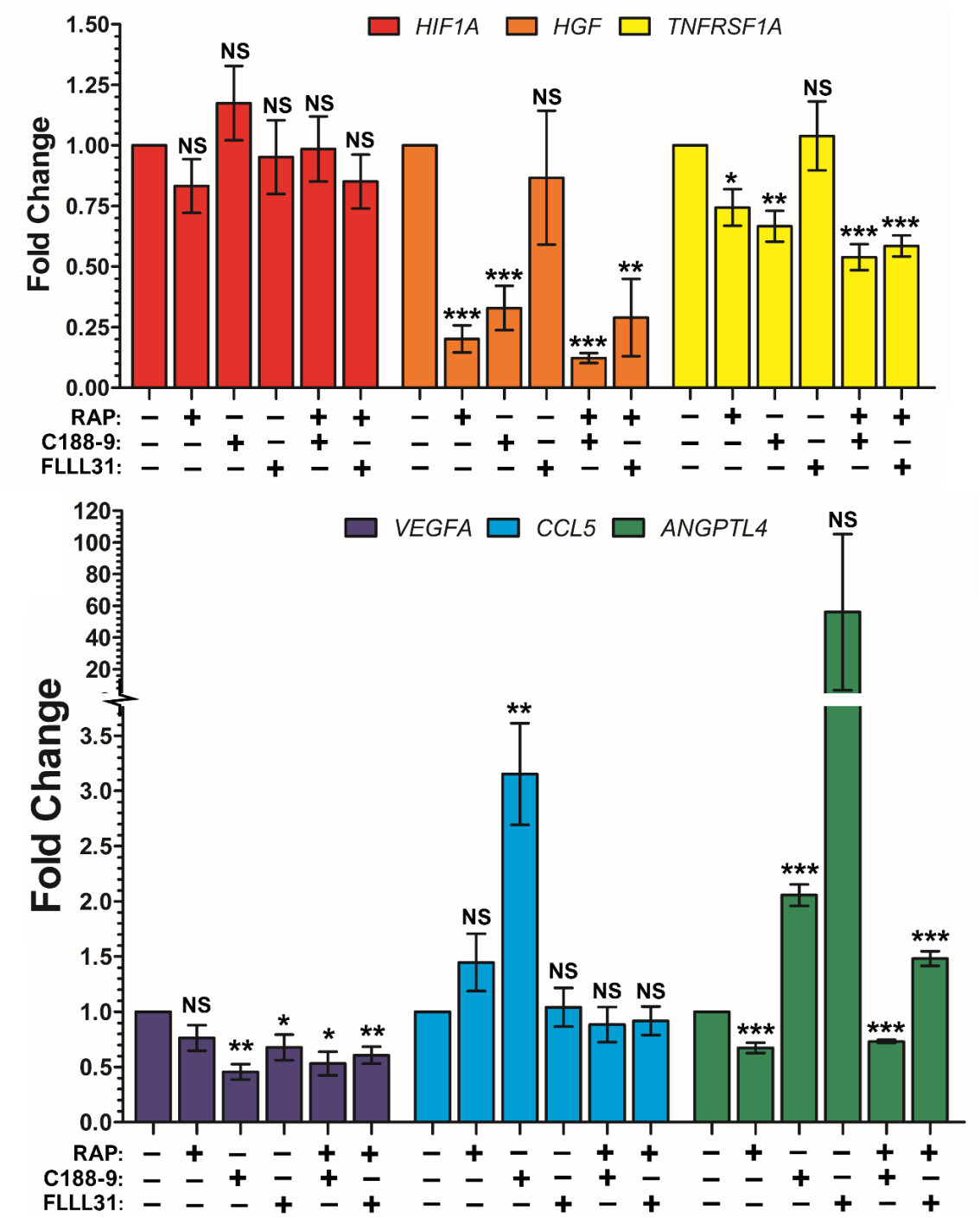


**Figure 4.6. qPCR analysis reveals rapamycin and C188-9 alone or in combination downregulates some of the assayed HIF-1α and STAT3 driven proangiogenic genes in *TSC2* deficient AML cells.** *TSC2* deficient AML cells were cultured for 18 h in the presence of either DMSO, rapamycin (RAP) at 50 nM, C188-9 at 30 μM or FLLL31 10 μM alone or in combination before being lysed. mRNA was purified from these lysates, converted to cDNA, and through qPCR the expression of target genes was quantified. Fold change in expression was calculated compared to a designated reference sample, in this case *TSC2* deficient AML cells treated with vehicle (DMSO). Fold changes of target genes in samples were normalised to the housekeeping gene *IPO8*. Significance annotations above each bar on graph indicates significance of difference in foldchange between each condition and the reference sample (DMSO). Statistical analysis of differences in foldchange (N=3 minimum) was by student's t test. Significance denoted by: * = p <0.05, ** = p <0.01, *** = p< 0.001, NS = not significant. Bars represent standard error of the mean.

### 4.2.4 Within *Tsc2* −/− MEFs, HIF-1α transcriptional activity decreases on C188-9 treatment and is concurrent with decreasing phosphorylation of STAT3.

Given that the STAT3 inhibitor C188-9 was able to modulate the expression of the assayed pro-angiogenic gene panel in figure 4.6 but did not affect transcription of *HIF1A*, the next aim of this results chapter was to confirm whether STAT3 inhibition within *Tsc2* −/− MEF cells could decrease the transcriptional activity of HIF-1α. For this purpose, HIF-1α luciferase reporter assays were utilised. The inducible luciferase reporter construct used contained multiple copies of cis-acting enhancer elements for HIF-1α (called HIF-1 response elements) inserted upstream of a promoter (for full details refer to chapter 2 section 2.3.9) which drives firefly luciferase production. In this assay, luminescence from firefly luciferase production is indicative of HIF-1α binding to HIF-1 response elements on DNA and driving target gene (luciferase) expression. Therefore, this assay measures the relative transcriptional activity of HIF-1α. *Tsc2* −/− MEFs cells were utilised for the luciferase assay, as *TSC2* −/− AML cells could not be successfully transfected despite testing multiple transfection reagents.

As seen in figure 4.7 (**A**), HIF-1α transcriptional activity is significantly elevated within *Tsc2* −/− MEF cells cultured under hypoxia compared to the same cells cultured under normoxia. Which is in line with what we'd expect about the stabilisation of HIF-1α protein under low oxygen (Majmundar *et al.* 2010). All drug treated conditions were undertaken under hypoxia, and average luminescence values for these conditions were compared to DMSO treated *Tsc2* −/− MEF cells cultured under hypoxia for the purpose of assessing statistical significance. As a whole, increasing concentrations of FLLL31 did not significantly lower the transcriptional activity of HIF-1α, bar 10 μM (luminescence FC = 199.3% p=0.0479), relative to *Tsc2* −/− MEF cells cultured under hypoxia (figure 4.7 **A**). This observation is in line with FLLL31's ineffectiveness at decreasing expression of the pro-angiogenic gene panel (bar *VEGFA*) in *TSC2* deficient AML cells (figure 4.6). C188-9 treatment however, was able to significantly repress the transcriptional activity of HIF-1α relative to DMSO treated *Tsc2* −/− MEFs cultured under hypoxia (figure 4.7 **A**). At 3.75 μM, C188-9 resulted in a significant decrease in the transcriptional activity of HIF-1α. Increasing concentrations of C188-9 further resulted in larger decreases in the transcriptional activity of HIF-1α. Higher concentrations above 15 μM of C188-9 resulted in a marked repression of HIF-1α transcriptional activity, with a >50% reduction when compared to DMSO treated *Tsc2* −/− MEFs cultured under hypoxia (C188-9 15 μM luminescence FC =136.7% vs 308.0% p=0.0041). At the highest concentration of C188-9 used, 60 μM, the transcriptional activity of HIF-1α was even lower than that observed in DMSO treated *Tsc2* −/− MEFs under normoxia (C188-9 60 μM luminescence FC =44.1% vs 100% $p=7.578x10^{-5}$).

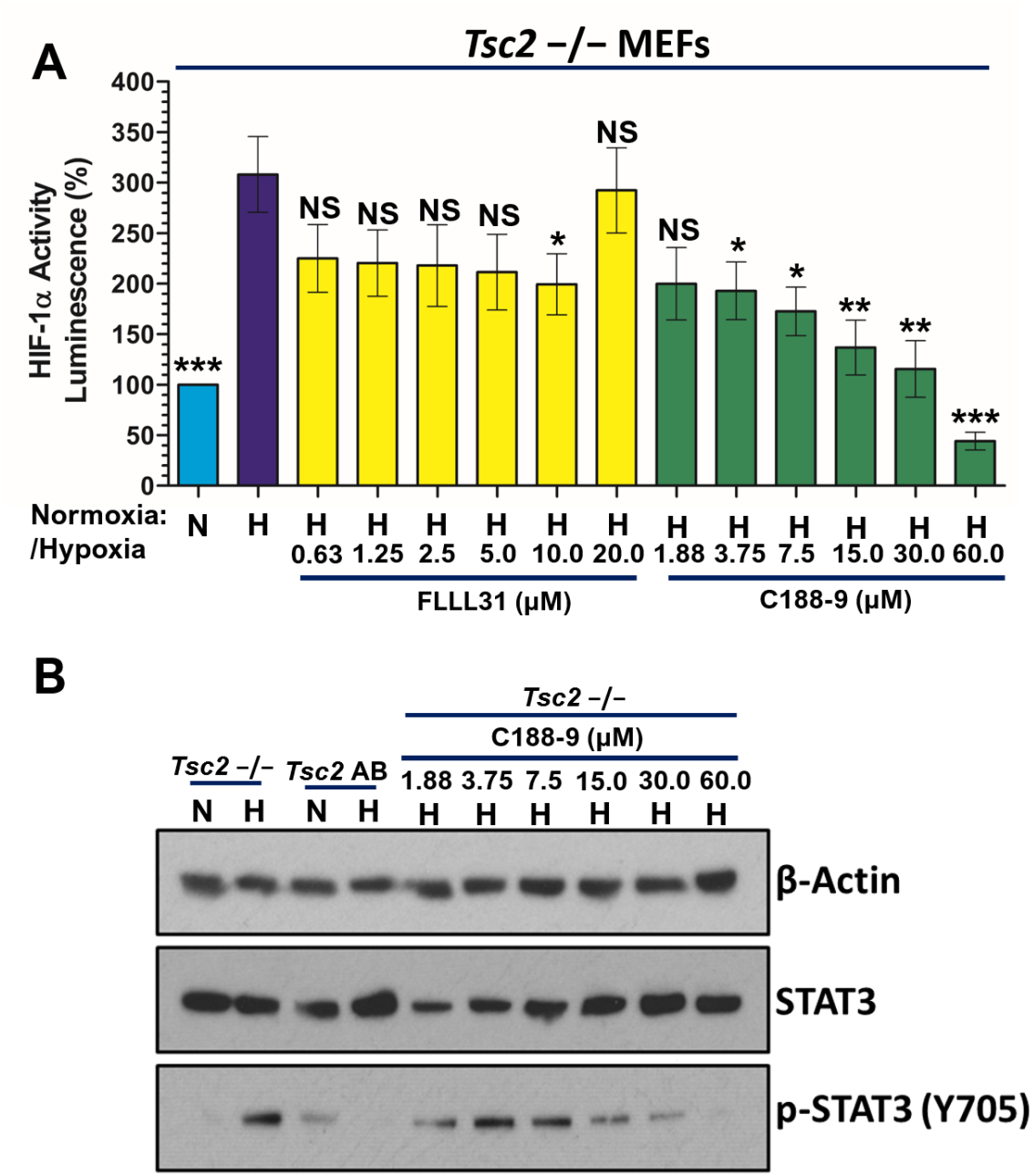


**Figure 4.7. Increasing concentrations of C188-9 decrease HIF-1α transcriptional activity and p-STAT3 (Y705) within *Tsc2* −/− MEF cells. A=** *Tsc2* −/− MEF cells transfected with an inducible HIF luciferase construct, renilla luciferase construct and a PcDNA3 empty vector or a *TSC2* construct for *TSC2* AB (add back) samples. After incubation with transfection reagents, cells were treated with either DMSO, FLLL31 or C188-9 at the indicated concentration for 18 h under normoxia (**N**) or hypoxia (**H**). Cells were the lysed and lysates were assayed for ratio of renilla to firefly luminescence (N=5 minimum). Resulting luminescence ratios for each sample was adjusted to total protein concentration. Normalised luminescence (i.e. HIF-1α activity) values were expressed as a fold change to a reference sample, *Tsc2* −/− MEF cells under normoxia and plotted. Statistical analysis of differences in foldchange in luminescence between MEF *Tsc2* −/− cells under hypoxia and all other conditions was by student's t test. Significance denoted by: * = p <0.05, ** = p <0.01, *** = p< 0.001, NS = not significant. Bars represent standard error or mean. **B** Lysates from luciferase assay were subject to harsher lysis buffers and analysed by western blotting to confirm inhibition of STAT3 phosphorylation at tyrosine (Y) 705. Representative blots, N=2 analysed.

Shown in figure 4.7 (**B**), western blotting of lysates used for the luciferase assay was then undertaken to examine STAT3. The phospho-marker of STAT3 activity, Y705, was shown to be markedly elevated in the *Tsc2* −/− MEF cells during hypoxia. This observation isn't consistently seen across experiments, where there is variation in the level of STAT3 phosphorylation observed. On the whole, increasing doses of C188-9 resulted in the repression of STAT3 phosphorylation at Y705. Taken together with the HIF-1α luciferase assay, this suggests that C188-9 treatment represses the transcriptional activity of HIF-1α via drug inhibition of STAT3 within the *Tsc2* −/− MEFs.

### 4.2.5 Pro-angiogenic factor protein expression is elevated upon loss of *TSC2* within both AML and MEF cells.

As previously described, cellular models of TSC and patient lesions are highly angiogenic in that they show elevated expression of proteins that promote formation of new vasculature. Therefore, the next aim of the present chapter was to first establish whether protein expression of pro-angiogenic HIF-1α, VEGFA, HGF and ANGPTL4 is elevated within *TSC2* deficient AML or MEF cells, as expected from the literature. Efficacy of Ref-1 or STAT3 inhibition, alone/in combination with rapamycin, at repressing expression of these proteins within *TSC2* deficient cells will then be assessed.

As seen in figure 4.8 (**A**), protein expression of HIF-1α and BNIP3, a direct HIF-1α target gene and surrogate marker to assay HIF-1α activity (Guo *et al.* 2001), is elevated within MEFs upon loss of *TSC2*. Additionally, HIF-1α expression within the *Tsc2* −/− MEF and *TSC2* deficient AML cells remained elevated relative to *Tsc2* +/+ MEF and *TSC2* RE AML cells, even under normoxia (previous densitometric quantification of HIF-1α and BNIP3 can be found in chapter 3, section 3.2.1, figures 3.1 and 3.2). BNIP3 expression is induced by hypoxia, which was observed in both the AML and MEF cell lines. Within the *TSC2* deficient AML line, BNIP3 was strongly expressed under hypoxia. But under normoxia, BNIP3 expression was detectable and was still noticeably higher in the *TSC2* deficient AML cells when compared to the *TSC2* RE AML cells (figure 4.8 **A**). ANGPTL4 expression was also elevated in the *TSC2* deficient AML cells (figure 4.8 **A**). Interestingly, ANGPTL4 protein expression appeared to be repressed by hypoxia, even though *ANGPTL4* mRNA expression was strongly induced by hypoxia within the AML lines (as seen in figure 4.4). Why this would be the case is unclear. Potentially ANGPTL4 protein is secreted, rather than retained within the cell, under hypoxia. However, ANGPTL4 secretion was not measured as part of this work. In the literature, *ANGPTL4* has been shown to be a hypoxia inducible gene (Le Jan *et al.* 2003) and several studies have shown mRNA and protein expression of *ANGPTL4* to be strongly elevated under hypoxia within multiple cancer cell lines (Baba *et al.* 2017 and Kim *et al.* 2011b).

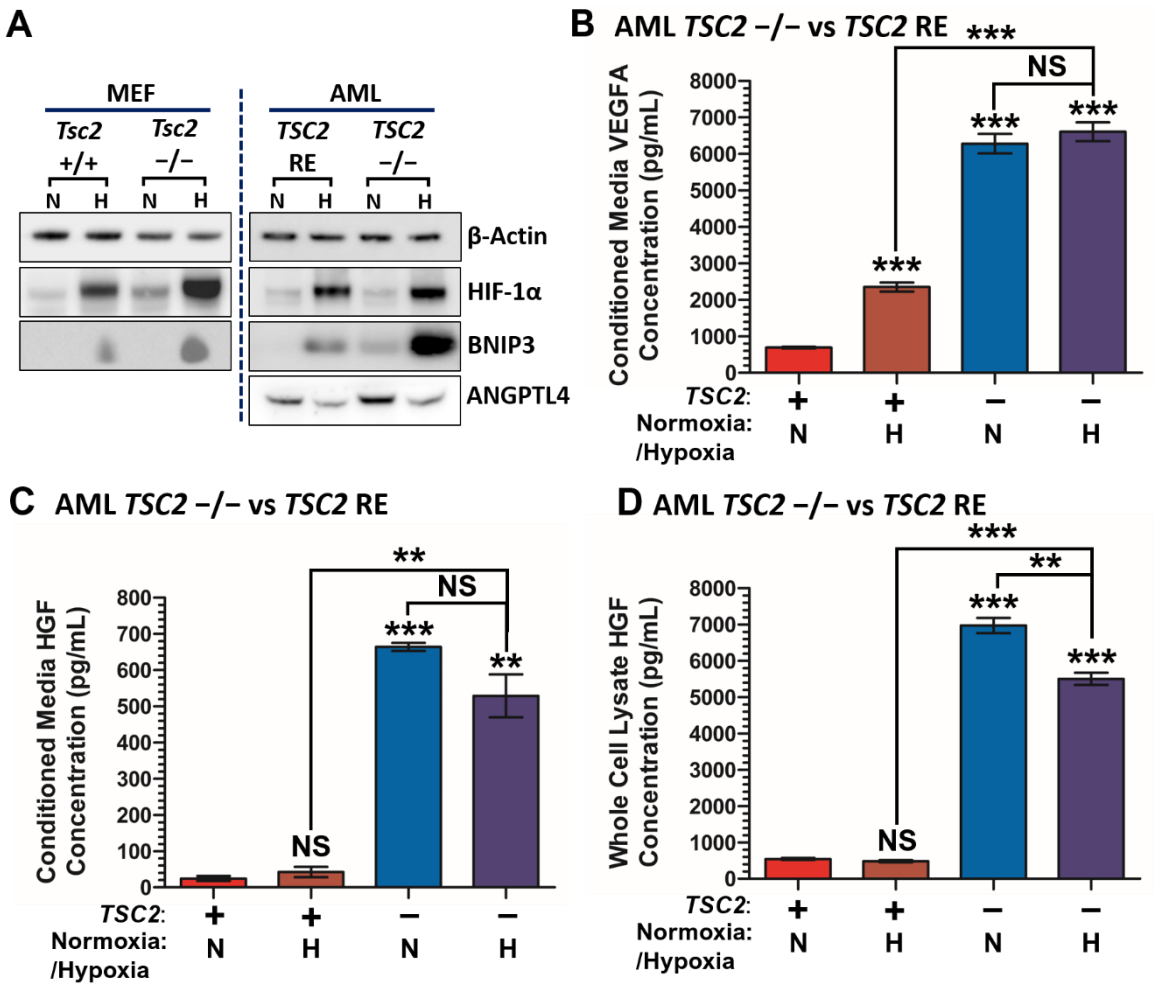


**Figure 4.8. Loss of *TSC2* leads to elevated protein expression of pro-angiogenic proteins within AML and MEF cell lines and soluble expression of VEGFA and HGF in AML cells. A=** Representative western blots (N=3). AML cells lacking *TSC2* (*TSC2* −/−) or with *TSC2* re-expressed (*TSC2* RE) and MEF cells lacking *Tsc2* (*Tsc2* −/− or with wild type *Tsc2* (*Tsc2*+/+), were cultured overnight under normoxia (**N**, 21% $O_2$) or hypoxia (**H**, 1% $O_2$) before being lysed. Through western blotting lysates were assayed for protein expression, with β-actin acting as a loading control (N=3 minimum). **B**, **C** and **D** = AML cells lacking *TSC2* (*TSC2* −/−) or with *TSC2* re-expressed (*TSC2* RE) were cultured overnight under normoxia (**N**, 21% $O_2$) or hypoxia (**H**, 1% $O_2$) before having conditioned media (**B** and **C**) analysed for VEGFA and HGF expression by way of ELISA (N=3) or lysed and whole cell lysates (**D**) analysed for HGF expression by way of ELISA (N=3). Significance annotations above each bar on graph indicates significance of difference in HGF/VEGFA concentration between each condition and the *TSC2* RE cells under normoxia. Pairwise statistical comparisons between *TSC2* deficient cells under normoxia or hypoxia and between *TSC2* deficient and *TSC2* RE cells under hypoxia are also annotated. Statistical analysis of differences in protein concentration was by student's t test. Significance denoted by: * = p <0.05, ** = p <0.01, *** = p< 0.001, NS = not significant. Bars represent standard error of the mean. Predicted running band size (kDa) of protein targets can be found in chapter 2, table 2.6.

As seen in the ELISA assays in figure 4.8 (**B**), protein expression of VEGFA is significantly higher for *TSC2* deficient AML cells under normoxia or hypoxia, remaining significantly higher than in *TSC2 RE* AML cells cultured under normoxia or hypoxia. This finding confirms that VEGFA expression is induced by mechanisms other than hypoxia within *TSC2* deficient cells. Unlike for the *VEGFA* gene, hypoxia doesn't significantly enhance VEGFA protein expression further within *TSC2* deficient AML cells, but does in *TSC2* RE AML cells. Which suggests VEGFA protein expression may be maximal within the *TSC2* deficient AML cells.

Due to the low expression of HGF in the conditioned media removed from *TSC2* RE, but not *TSC2* deficient, cultured AML cells, HGF protein expression was also assayed by way of ELISA in matched whole cell lysates. It should be noted that HGF is known to become tethered to cell membranes upon secretion as a pro-HGF isoform, which may explain why little free HGF was detected within the conditioned media. As seen from figure 4.8 **C** and **D**, protein expression of HGF within cells and into the conditioned media is significantly and substantially higher for *TSC2* deficient AML cells than *TSC2* RE AML cells, regardless of oxygen conditions. Which is consistent with elevated mRNA expression of *HGF* observed upon loss of *TSC2* within AML cells (figure 4.4). It was observed that oxygen availability only significantly affected HGF protein expression measured in lysates prepared from whole cell extracts (including any tethered membrane bound HGF) ($p=0.0055$).

### 4.2.6 Within *TSC2* deficient cells, next generation APX3330 Ref-1 inhibitor analogues were effective at decreasing HIF-1α, BNIP3 and ANGPTL4 protein expression, but were not effective at repressing either HGF or VEGFA.

The next aim of the present work was to assess the efficacy of Ref-1 or STAT3 drug inhibitors, at repressing angiogenic markers linked to TSC. Rapamycin has anti-angiogenic drug properties in diseases other than TSC (Guba *et al*. 2002, Huynh *et al*. 2009 and Miricescu *et al.* 2021) and in TSC (Düvel *et al.* 2010, Land and Tee *et al.* 2007, and Brugarolas *et al.* 2003). Therefore, the efficacy of Ref-1/STAT3 inhibitors alone and in combination with rapamycin was evaluated.

As seen in figures 4.9 and 4.10, rapamycin and Ku-0063794 ablated rpS6 phosphorylation at S235/236 (a surrogate marker of mTORC1 activity) indicating repression of mTORC1. The blot panels and accompanying densitometry graphs in figures 4.9 and 4.10 show that both rapamycin and Ku-0063794 were effective at repressing expression of HIF-1α and BNIP3 in both the *TSC2* deficient MEF and AML lines. mTORC1 inhibition was more effective in the *Tsc2* −/− MEFs, at reducing the expression of HIF-1α and BNIP3. In the *TSC2* deficient AML cells, the reduction was less apparent with drug treatment (figure 4.10). A greater reduction in

BNIP3 and HIF-1α protein expression was seen on treatment with Ku-0063794, when compared to rapamycin. This is likely due to the higher potency that Ku-0063794 has to inhibit mTORC1 (Garcia *et al.* 2009), where Ku-0063794 can also inhibit rapamycin resistant phosphorylation events of mTORC1. (Thoreen *et al.* 2020).

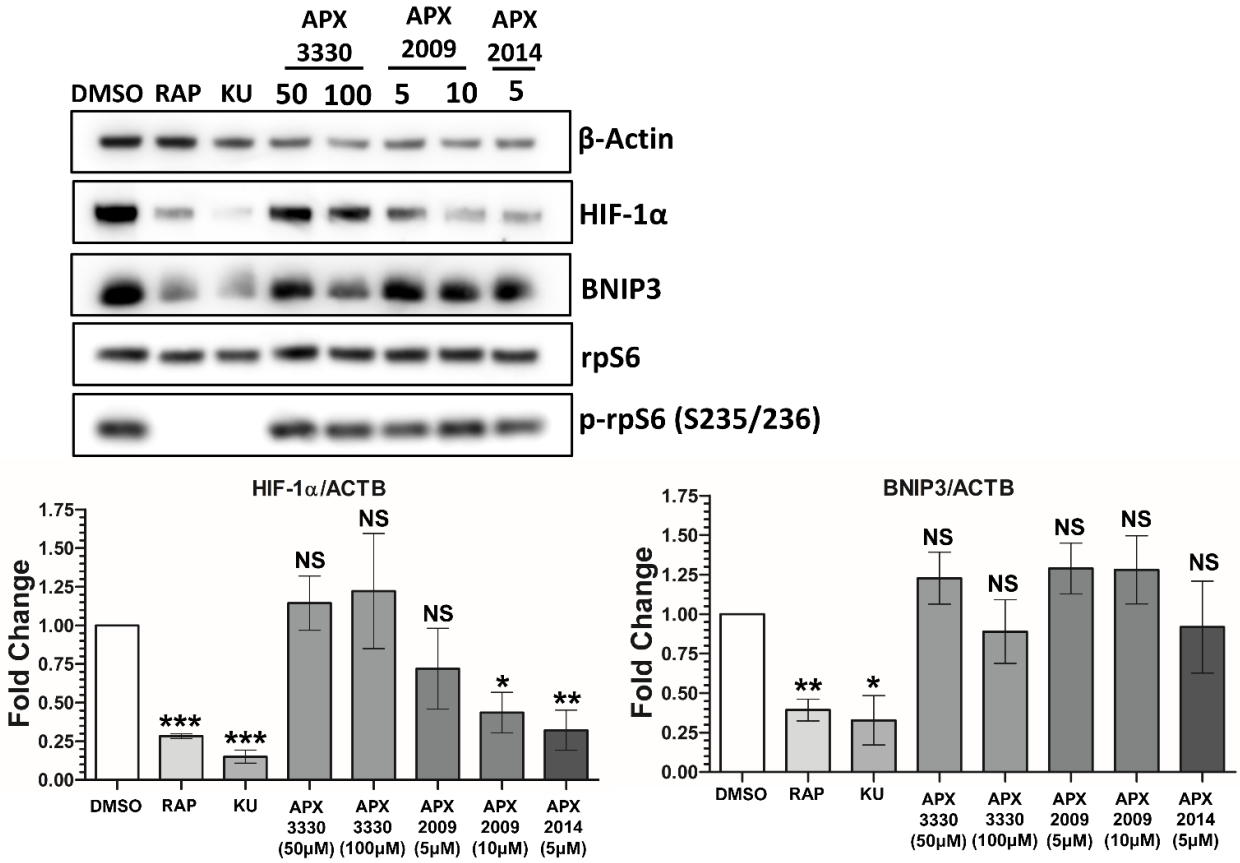


**Figure 4.9. Within *Tsc2* −/− MEF cells 2nd generation Ref-1 inhibitors are effective at significantly decreasing HIF-1α protein expression, but not that of HIF-1α's downstream target BNIP3.** Representative western blots (N=3). *Tsc2* **−/−** MEF cells were cultured under hypoxia (1% $O_2$) for 18 h in the presence of either DMSO, rapamycin (RAP) at 50 nM, Ku-0063794 (KU) at 1 μM, APX3330 at 50 μM or 100 μM, APX2009 at 5 μM or 10 μM or APX2014 at 5 μM. Through western blotting lysates were assayed for protein expression (N=3 minimum), with β-actin acting as a loading control. Densitometry analysis of resulting western blots (N=3 minimum) was performed, with HIF-1α and BNIP3 both being normalised to β-actin. Resulting ratios were then expressed as fold changes compared to control sample (DMSO) and plotted on graphs below blot panel. Significance annotations above each bar on graph indicates significance of difference in foldchange between each condition and the control sample (DMSO). Statistical analysis of differences in foldchange of normalised protein relative to control was by student's t test. Significance denoted by: * = p <0.05, ** = p <0.01, *** = p< 0.001, NS = not significant. Bars represent standard error of the mean. Predicted running band size (kDa) of protein targets can be found in chapter 2, table 2.6.

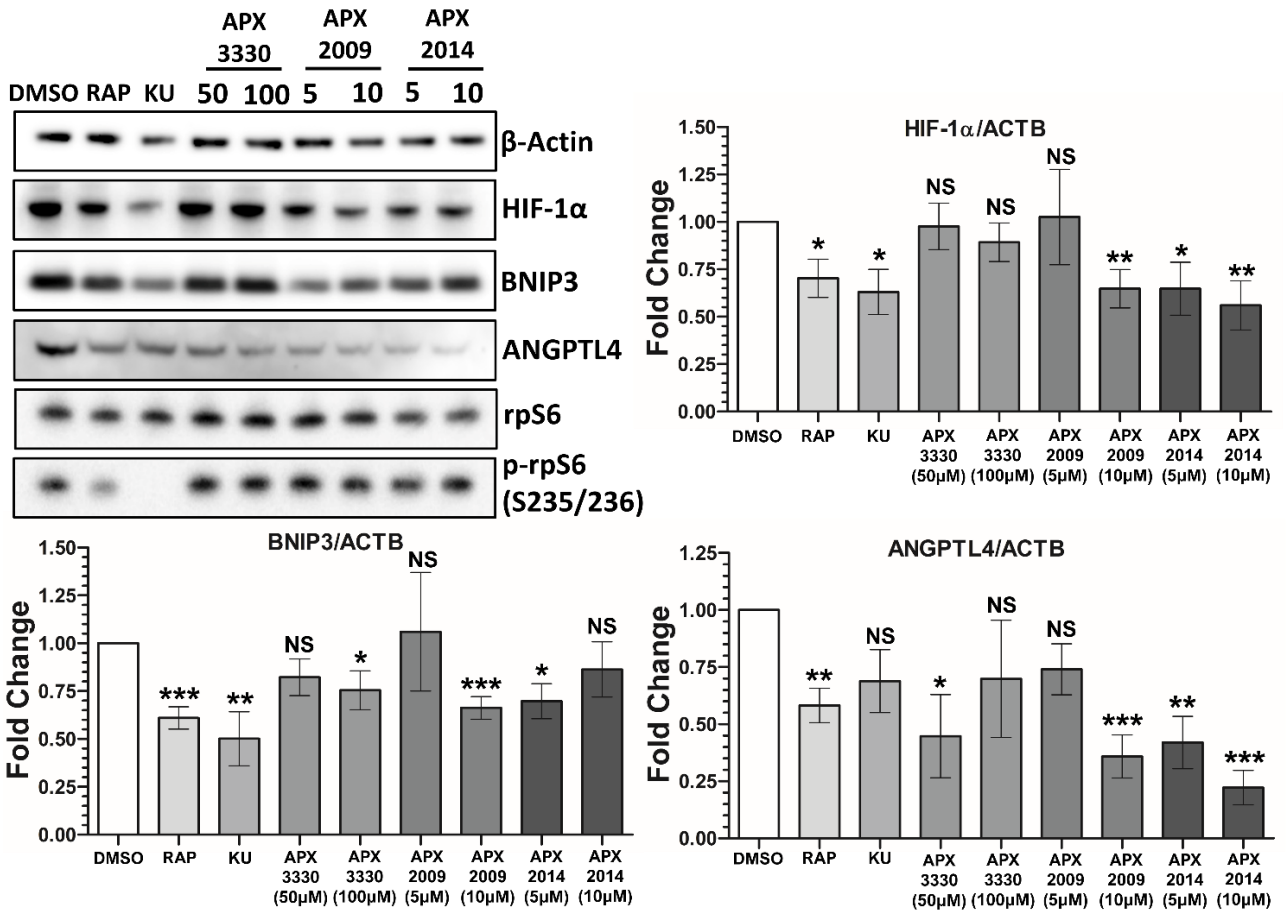


**Figure 4.10. Within *TSC2* deficient AML cells mTORC1 and Ref-1 inhibitors are effective at significantly decreasing HIF-1α protein expression, and that of HIF-1α's downstream targets BNIP3 and ANGPTL4.** Representative western blots (N=3 minimum). *TSC2* deficient AML cells were cultured under hypoxia (1% $O_2$) for 18 h in the presence of either DMSO, rapamycin (RAP) at 50 nM, Ku-0063794 (KU) at 1 μM, APX3330 at 50 μM or 100 μM, APX2009 at 5 μM or 10 μM or APX2014 at 5 μM or 10 μM. Through western blotting lysates were assayed for protein expression, with β-actin acting as a loading control. Densitometry analysis of resulting western blots (N=3 minimum) was performed, with HIF-1α, BNIP3 and ANGPTL4 all being normalised to β-actin. Resulting ratios were then expressed as fold changes compared to control sample (DMSO) and plotted on graphs. Significance annotations above each bar on graph indicates significance of difference in foldchange between each condition and the control sample (DMSO). Statistical analysis of differences in foldchange of normalised protein relative to control was by student's t test. Significance denoted by: * = p <0.05, ** = p <0.01, *** = p< 0.001, NS = not significant. Bars represent standard error of the mean. Predicted running band size (kDa) of protein targets can be found in chapter 2, table 2.6.

According to densitometry analysis of the *Tsc2* −/− MEFs, only the more potent 2nd generation Ref-1 inhibitors resulted in a significant decrease in HIF-1α protein relative to the DMSO control (figure 4.9). This was also true for *TSC2* deficient AML cells (figure 4.10). Although APX2009 and APX2014 potently repressed HIF-1α expression in the MEF cell line, they were unable to decrease BNIP3 expression. In the AML cell line, higher concentrations of APX3330 and APX2009 and the lower concentration of APX2014 was sufficient to significantly decrease BNIP3 expression relative to the DMSO control (figure 4.10). For those Ref-1 inhibitors, at a

specified concentration, which resulted in a significant decrease in HIF-1α or BNIP3 expression, there was no significant difference compared to rapamycin. Within the AML line, treatment with rapamycin and treatment with the Ref-1 inhibitors at the lower/higher or both concentrations used significantly repressed ANGPTL4 expression relative to the DMSO control. 10 μM of APX2014 was sufficient to reduce ANGPTL4 expression to a point that was significantly lower than observed with rapamycin treatment (p=0.0151) (figure 4.10).

ELISA studies, shown in figure 4.11, were performed within the *TSC2* deficient AML cell line only. Rapamycin consistently repressed HGF and VEGFA expression relative to the DMSO. Treatment with Ku-0063794 only significantly repressed HGF expression within the whole cell lysate. Whilst Ku-0063794 treatment actually resulted in a small, but significant, increase in VEGFA expression. This finding was surprising as it was expected that that Ku-0063794 treatment should repress VEGFA protein expression to a greater extent than rapamycin within *TSC2* deficient AML cells owing to the differences in efficacy of these drugs to inhibit downstream mTORC1 substrates. eIF4E activity is thought to stimulate VEGFA protein expression more strongly than S6K1 activity. With Dodd et al. (2015) finding that expressing a dominant inhibitory mutant that blocks eIF4E's ability to promote protein expression (Richter and Sonenberg, 2005), resulted in a marked decrease in the protein expression of VEGFA. Conversely, expression of a constitutively active S6K1 mutant, only slightly increased VEGFA protein expression, which indicated VEGFA is driven primarily through eIF4E and not S6K1 activity. Indeed, VEGFA belongs to a subset of mRNAs whose translation is strongly stimulated by eIF4E (Graff *et al.* 2008). With Graff *et al.* (2007) finding targeting eIF4E with an anti-sense oligonucleotide preferentially inhibited the translation of such mRNAs, including VEGFA. Given eIF4E is inhibited by 4E-BP1, and Ku-0063794 has been shown to repress mTORC1 mediated phosphorylation of 4E-BP1 more robustly than rapamycin (Garcia *et al.* 2009), the increase in VEGFA protein expression on Ku-0063794 treatment was unexpected.

As shown in figure 4.11, Ref-1 inhibitors were ineffective at decreasing protein expression of HGF within whole cell lysates or conditioned media. And only APX3330 at 100 μM significantly decreased expression of VEGFA relative to the DMSO control within the AML line. Treatment of multiple pancreatic cancer cell lines with APX3330 has been shown to decrease transcriptional activity of HIF-1α and expression of the HIF-1α regulated *CA9* (carbonic anhydrase 9) in a dose dependent manner (Fishel *et al*. 2011 and Logsdon *et al.* 2016). Though it is not clear why the more potent 2$^{nd}$ generation Ref-1 inhibitors were ineffective at decreasing VEGFA expression.

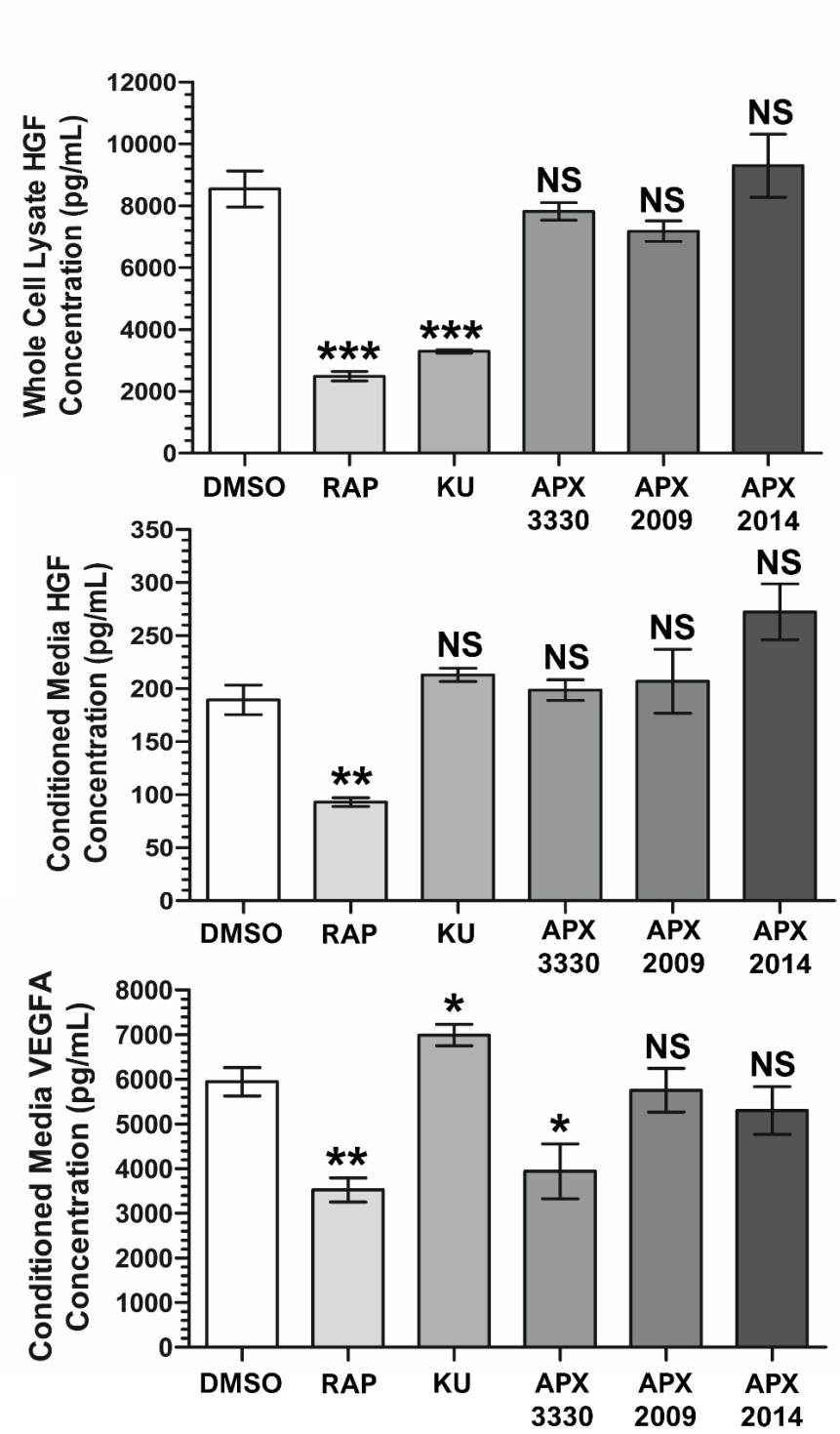


**Figure 4.11. Ref-1 inhibitors are largely ineffective compared to mTORC1 inhibitor rapamycin at decreasing protein expression of HGF and VEGFA in *TSC2* deficient AML cells.** *TSC2* deficient AML cells were cultured for 18 h in the presence of either DMSO, rapamycin (RAP) at 50 nM, Ku-0063794 (KU) at 1 µM, APX3330 at 100 µM, APX2009 at 10 µM or APX2014 at 10 µM. Conditioned media was then taken and assayed for VEGFA and HGF expression by way of ELISA or cells were lysed and whole cell lysates analysed for HGF expression by way of ELISA. N=4. Significance annotations above each bar on graph indicates significance of difference in HGF/VEGFA concentration between each condition and the control sample (DMSO). Statistical analysis of differences in protein concentration was by student's t test. Significance denoted by: * = p <0.05, ** = p <0.01, *** = p< 0.001, NS = not significant. Bars represent standard error of the mean.

### 4.2.7. Co-treatment with rapamycin and Ref-1 inhibitors are more effective in decreasing the protein expression of HIF-1α and BNIP3, but not ANGPTL4, HGF or VEGFA.

The next aim of the present chapter was to assess whether combinatorial treatment of Ref-1 inhibitors with rapamycin could elicit a more potent anti-angiogenic effect than either Ref-1 or mTORC1 inhibition alone. As seen from the blot panels and accompanying densitometry graphs in figures 4.12 and 4.13, inhibiting both Ref-1 and mTORC1 decreased HIF-1α and BNIP3 protein expression further when compared to single drug treatments. Inhibition of mTORC1 appeared consistent through treatment conditions, as seen by suppression of

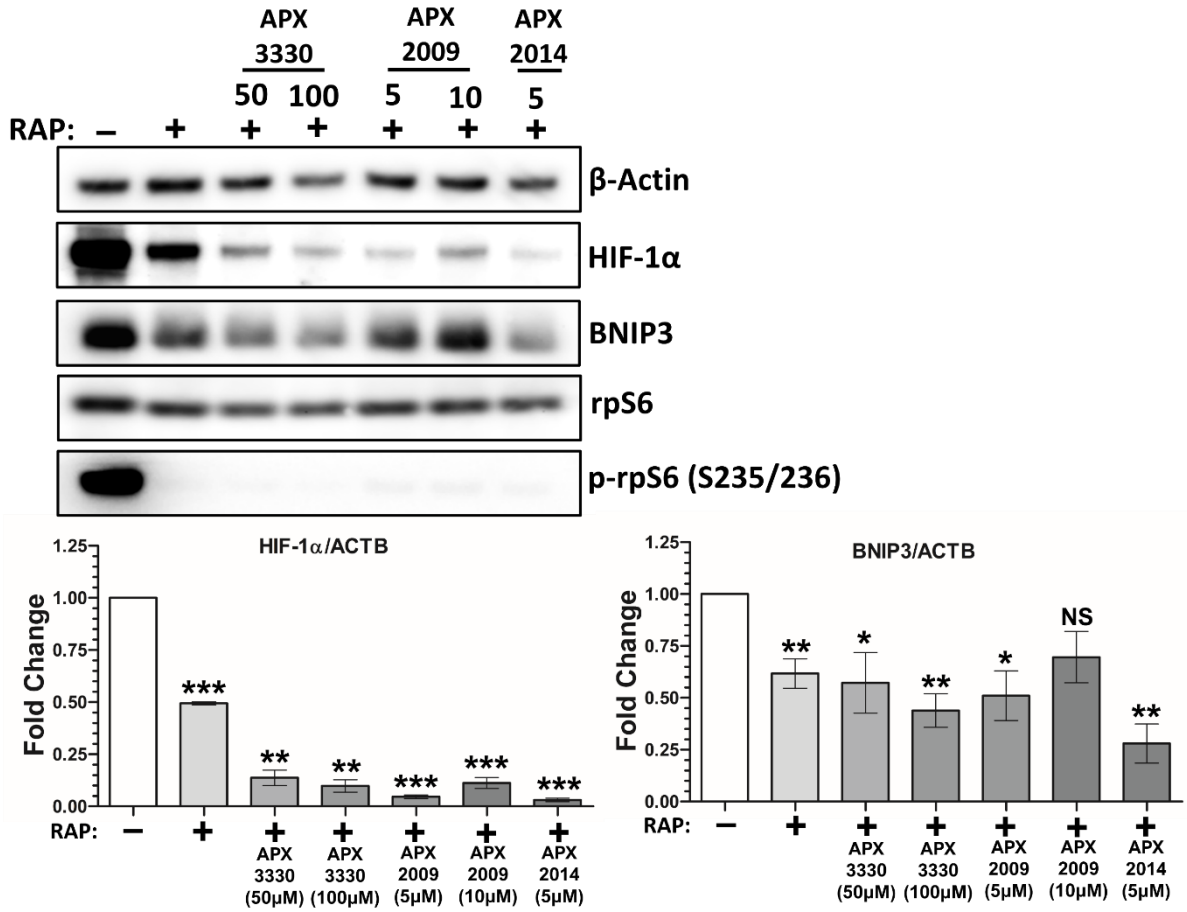


**Figure 4.12. Within *Tsc2* −/− MEF cells Ref-1 inhibitor and rapamycin co-treatment decreases HIF-1α protein expression further compared to rapamycin alone.** Representative western blots (N=3). *Tsc2* −/− MEF cells were cultured under hypoxia (1% $O_2$) for 18 h in the presence of either DMSO, rapamycin (RAP) at 50 nM, APX3330 at 50 μM or 100 μM, APX2009 at 5 μM or 10 μM or APX2014 at 5 μM alone or in combination. Through western blotting lysates were assayed for protein expression (N=3 minimum), with β-actin acting as a loading control. Densitometry analysis of resulting western blots (N=3 minimum) was performed, with HIF-1α and BNIP3 both being normalised to β-actin. Resulting ratios were then expressed as fold changes compared to control sample (DMSO) and plotted on graphs. Significance annotations above each bar on graph indicates significance of difference in foldchange between each condition and the control sample (DMSO). Statistical analysis of differences in foldchange of normalised protein relative to control was by student's t test. Significance denoted by: * = p <0.05, ** = p <0.01, *** = p< 0.001, NS = not significant. Bars represent standard error of the mean. Predicted running band size (kDa) of protein targets can be found in chapter 2, table 2.6.

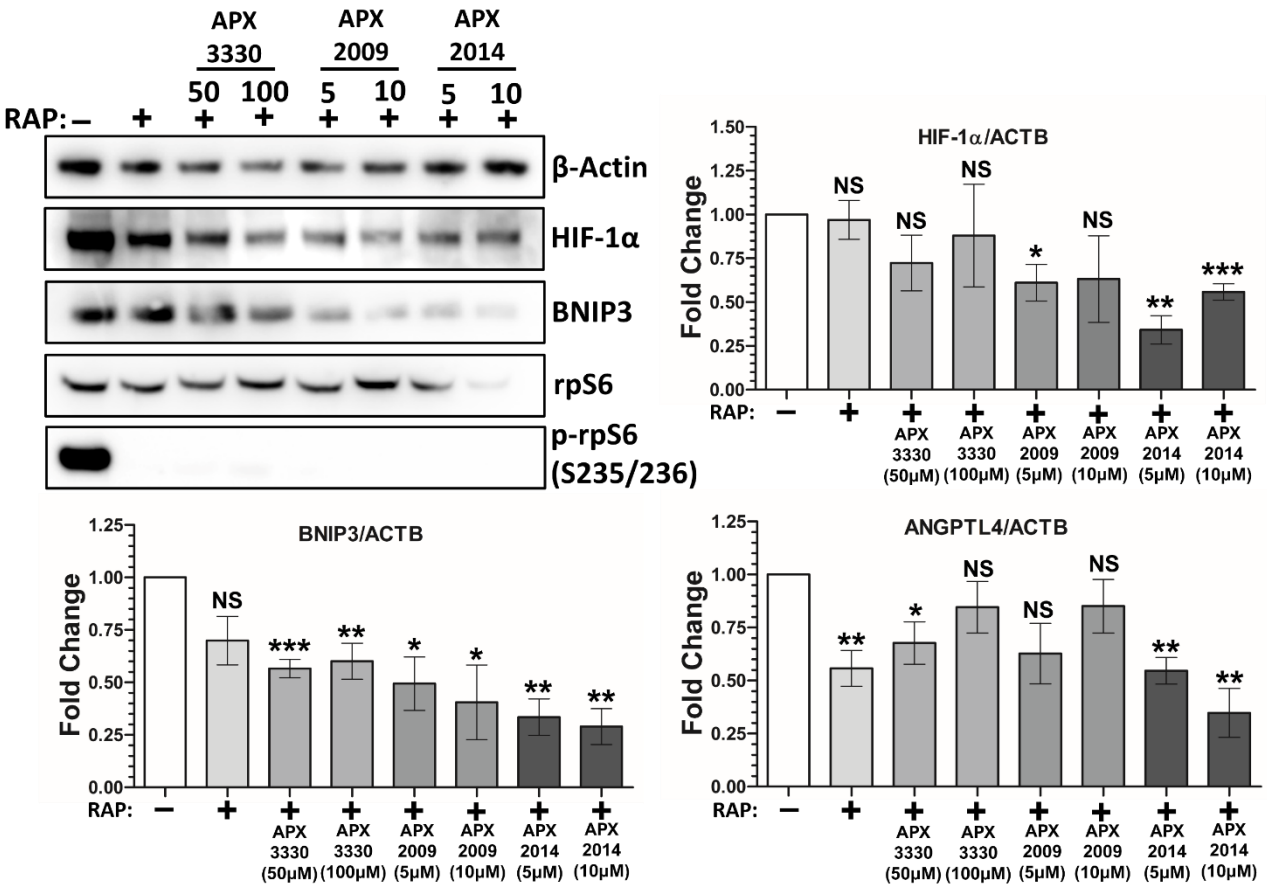


**Figure 4.13. Within *TSC2* deficient AML cells Ref-1 inhibitor and rapamycin co-treatment decreases HIF-1α and BNIP3 protein expression further compared to rapamycin alone.** Representative western blots (N=3). *TSC2* deficient AML cells were cultured under hypoxia (1% $O_2$) for 18 h in the presence of either DMSO, rapamycin (RAP) at 50 nM, APX3330 at 50 μM or 100 μM, APX2009 at 5 μM or 10 μM or APX2014 at 5 μM or 10 μM alone or in combination. Through western blotting lysates were assayed for protein expression, with β-actin acting as a loading control. Densitometry analysis of resulting western blots (N=3 minimum) was performed, with HIF-1α, BNIP3 and ANGPTL4 all being normalised to β-actin. Resulting ratios were then expressed as fold changes compared to control sample (DMSO) and plotted on graphs below blot panel. Significance annotations above each bar on graph indicates significance of difference in foldchange between each condition and the control sample (DMSO). Statistical analysis of differences in foldchange of normalised protein relative to control was by student's t test. Significance denoted by: * = p <0.05, ** = p <0.01, *** = p< 0.001, NS = not significant. Bars represent standard error of the mean. Predicted running band size (kDa) of protein targets can be found in chapter 2, table 2.6.

phosphorylation of rpS6 at S235/236. For the *Tsc2* −/− MEFs, densitometry analysis found that all treatment conditions significantly decreased HIF-1α expression relative to the DMSO control (figure 4.12). Furthermore, all Ref-1 inhibitors repressed HIF-1α expression more potently than rapamycin treatment alone (RAP FC=0.494, RAP+3330 (50 μM): FC=0.137 p=0.0108, RAP+3330 (100 μM): FC=0.098 p=0.0061, RAP+2009 (5 μM): FC=0.046, p=0.0007, RAP+2009 (10 μM): FC=0.113 p=0.0049, RAP+2014 (5 μM): FC=0.031 p=0.0006). For the *TSC2* deficient AML cells, whilst the blot panel clearly shows a decrease in HIF-1α protein expression relative to the DMSO control (when normalised to β-actin), only rapamycin in combination with APX2009 at 5 μM and APX2014 at 5 μM or 10 μM was sufficient to significantly decrease HIF-1α protein expression (figure 4.13). Overall, the decrease in HIF-1α protein expression from dual inhibition of Ref-1 and mTORC1 was more pronounced within the *Tsc2* −/− MEFs than in the AML cell line.

Within the *Tsc2* −/− MEF line Ref-1 inhibitors at all concentrations, except APX2009 at 10 μM, in concert with rapamycin significantly reduced BNIP3 expression (figure 4.12). Only with APX2014 at 5 μM with rapamycin was the reduction in expression of BNIP3 significantly different from that observed with rapamycin alone. For the *TSC2* deficient AML line, rapamycin treatment alone didn't significantly decrease BNIP3 expression relative to the DMSO control (figure 4.13). Co-treatment with Ref-1 inhibitors and rapamycin did however significantly repress BNIP3 expression relative to the DMSO control and rapamycin alone. Repression of ANGPTL4 protein expression on treatment with rapamycin and Ref-1 inhibitors was not consistent for all Ref-1 inhibitors used. Within *TSC2* deficient AML cells, only the more potent APX2014 resulted in a consistent and robust decrease in ANGPTL4 protein expression when used with rapamycin.

As seen in figure 4.14, co-treatment of *TSC2* deficient AML cells with Ref-1 inhibitors and rapamycin did significantly decrease protein expression of VEGFA and expression of HGF in the conditioned media and the whole cell lysate relative to the DMSO control. However, as a whole, differences in the protein expression of HGF or VEGFA observed on co-treatment with Ref-1 inhibitors and rapamycin was not significant compared to differences in the protein expression observed with rapamycin alone. Taken together with the ELISA data in figure 4.11, Ref-1 activity does not appear to drive elevated expression of HGF and VEGFA within *TSC2* deficient AML cells.

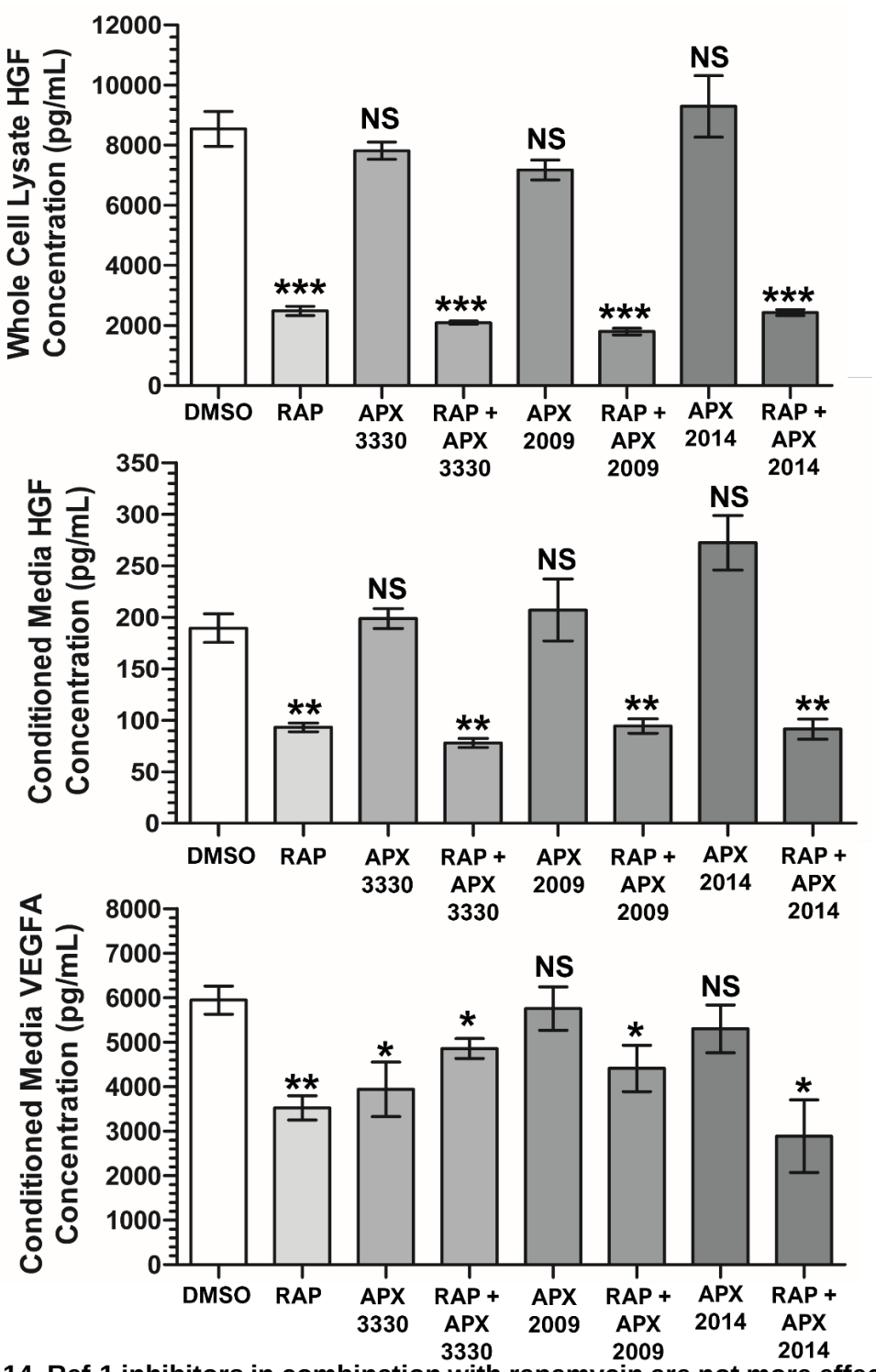


**Figure 4.14. Ref-1 inhibitors in combination with rapamycin are not more effective at decreasing expression of HGF and VEGFA than rapamycin alone in *TSC2* deficient AML cells.** *TSC2* deficient AML cells were cultured for 18 h in the presence of either DMSO, rapamycin (RAP) at 50 nM, APX3330 at 100 µM, APX2009 at 10 µM or APX2014 at 10 µM alone or in combination. Conditioned media was then taken and assayed for VEGFA and HGF expression by way of ELISA or cells were lysed and whole cell lysates analysed for HGF expression by way of ELISA. N=4. Significance annotations above each bar on graph indicates significance of difference in HGF/VEGFA concentration between each condition and the control sample (DMSO). Statistical analysis of differences in protein concentration was by student's t test. Significance denoted by: * = $p < 0.05$, ** = $p < 0.01$, *** = $p < 0.001$, NS = not significant. Bars represent standard error of the mean.

### 4.2.8 The STAT3 inhibitor C188-9 rapidly decreases protein expression of HIF-1α and BNIP3, and decreases expression of both HGF and VEGFA.

In diseases were HIF-1α and STAT3 both contribute to drive pathology; STAT3 is by and large considered to promote HIF-1α mRNA and protein expression, and/or target gene transcription. In various cell models, studies have found hyperactive STAT3 is able to drive *HIF1A* expression both under hypoxia (Niu *et al.* 2008) and normoxia (Demaria *et al.* 2010). More relevant to TSC, Dodd *et al.* (2015) showed mTORC1 induces transcription of *HIF1A* through STAT3, and that insulin induced mRNA expression of *HIF1A* within HEK293 cells could be repressed by treatment with rapamycin or the STAT3 inhibitor FLLL31. Whilst Pawlus *et al.* (2014) found within RCC4 cells that STAT3 activity was required for the efficient transcription of HIF-1α target genes. However, in various cancer cell lines with elevated activity of both STAT3 and HIF-1α, inhibiting STAT3 phosphorylation was not found to be associated with a decrease in *HIF1A* mRNA and/or protein expression (Adachi *et al.* 2012, Bai *et al.* 2014 and Pawlus *et al.* 2014). Inhibition of STAT3 was found to have no significant effect on *HIF1A* transcription (figure 4.6) within the *TSC2* deficient AML line, however C188-9 treatment repressed HIF-1α transcriptional activity in a dose dependent manner within *Tsc2* −/− MEF cells (figure 4.7). Therefore, whether C188-9 mediated repression of HIF-1α transcriptional activity (figure 4.7) was in part the result of decreased HIF-1α protein expression was assayed. As was the efficacy of STAT3 inhibition at repressing pro-angiogenic protein expression.

Additionally, in cancer cells, active STAT3 was reported to increase HIF-1α protein stability through preventing binding of the negative regulator of HIF-1α stability, pVHL (Jung *et al.* 2005 and Jung *et al.* 2008). This may be a mechanism by which STAT3 elevates HIF-1α protein levels within TSC cells, given STAT3 activity was found to be elevated within both *TSC2* deficient AML and MEF cells (see figure 3.1). To address this hypothesis, a C188-9 treatment time course was performed to assess how HIF-1α protein expression changed, if at all, over short term and long term inhibition of STAT3. Cells were treated under normoxia for this assay to remove the stabilising effect of hypoxia on HIF-1α (Majmundar *et al.* 2010) and avoid reoxygenation (from opening of hypoxic incubator door) affecting HIF-1α protein expression. As reperfusion of oxygen into previously hypoxic cells can rapidly increase reactive oxygen species (ROS) production (Korge *et al.* 2008), which was found to drive HIF-1α translation (Pagé *et al.* 2002).

As seen from the blot panel in figure 4.15, C188-9 treatment resulted in a rapid decrease in HIF-1α protein within both the *TSC2* deficient AML and MEF cells. Densitometry analysis found that within the *TSC2* deficient AML cells, the decrease in HIF-1α expression at every time point of C188-9 treatment relative to the DMSO control was significant. C188-9 treatment decreased HIF-1α protein expression at the shortest time point (0.5 h: FC=0.652 p=0.0371),

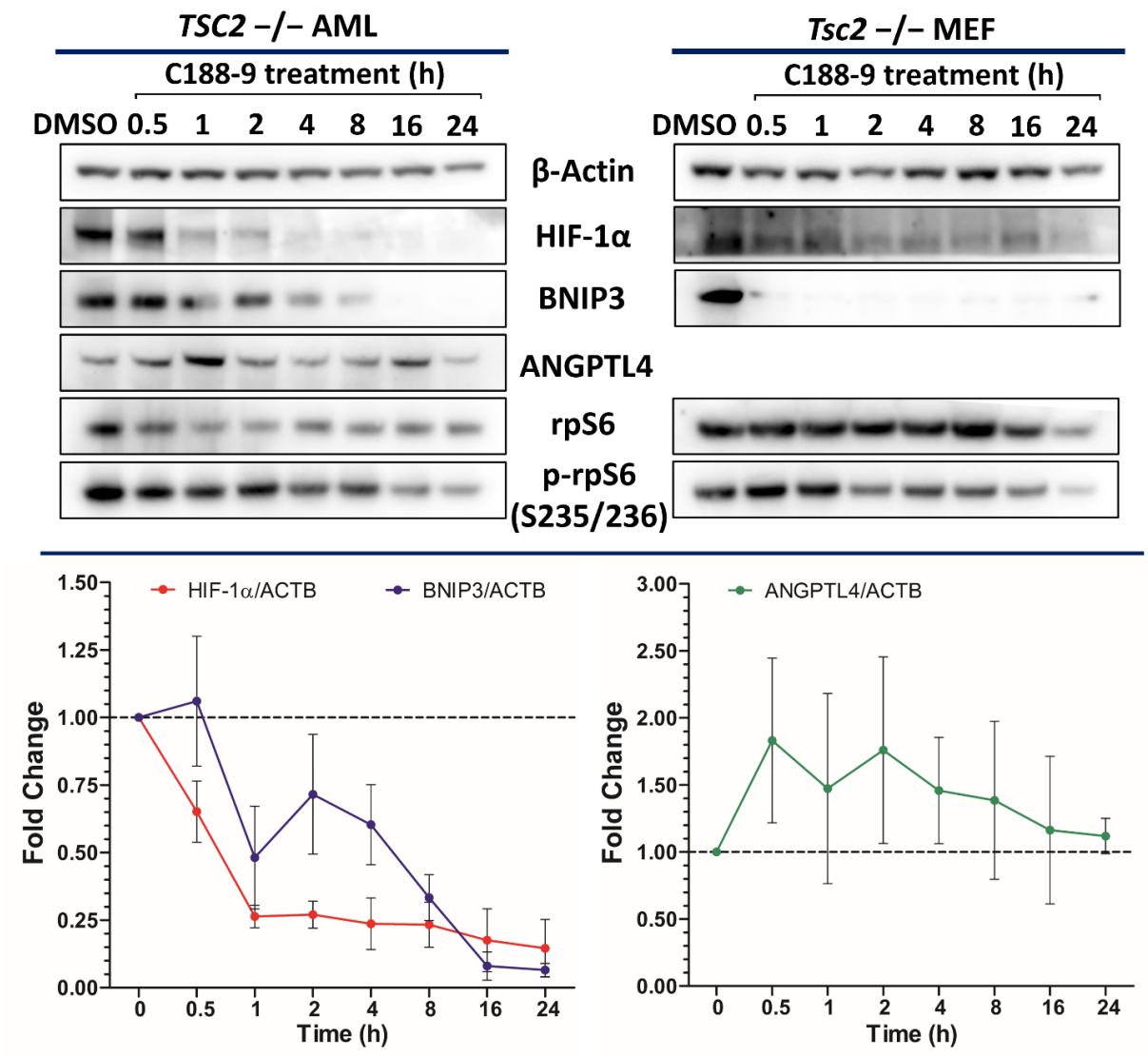


**Figure 4.15. STAT3 inhibition through C188-9 treatment rapidly decreases HIF-1α protein expression within both *TSC2* deficient AML and MEF cell lines.** Representative western blots (N=3). *TSC2* deficient AML or MEF cells were treated with either DMSO or C188-9 at 30 µM. Cells treated with DMSO (control) were lysed at time 0 h, whilst C188-9 treated cells were lysed at the time indicated. Through western blotting lysates were assayed for protein expression, with β-actin acting as a loading control. Densitometry analysis of resulting western blots (N=3 minimum) from the AML cell line was performed with HIF-1α, BNIP3 and ANGPTL4 all being normalised to β-actin. Resulting ratios were then expressed as fold changes compared to control sample (DMSO) at time 0 h and plotted to show change in fold change in protein expression during treatment time in respect to the control. Dotted line on graphs represents DMSO control sample fold change, i.e., 1.00. Bars represent the standard error of the mean. Predicted running band size (kDa) of protein targets can be found in chapter 2, table 2.6.

and by 1 h, was ~70% lower than HIF-1α expression within the DMSO control (1 h: FC=0.263 p=0.0001). By the final time point of C188-9 treatment, HIF-1α protein expression remained repressed (FC=0.146 p=0.0013) (figure 4.15). After 1 h C188-9 started to decrease BNIP3 protein expression with *TSC2* deficient AML cells. Which was longer into treatment time than

when HIF-1α protein expression was decreased. Which is in line with *BNIP3* being a known target of HIF-1α (Guo *et al.* 2001). C188-9 decreased BNIP3 protein expression earlier within the *Tsc2* −/− MEF cells, with BNIP3 barely detectable at 0.5 h of C188-9 treatment. BNIP3 protein expression remained depressed at the later time points of C188-9 treatment within both *TSC2* deficient cells.

In the *TSC2* deficient AML cells, ANGPTL4 protein expression over C188-9 treatment time was found to be hugely variable between repeats. ANGPTL4 protein expression appeared to peak within earlier time points of C188-9 treatment, before decreasing to a level comparable with the DMSO control at time 24 h (figure 4.15). The increased protein expression of ANGPTL4 observed aligns with the observed increase in *ANGPTL4* mRNA expression on C188-9 treatment (figure 4.6). In both *TSC2* deficient cell lines, overtime C188-9 treatment significantly decreased phosphorylation of rpS6 at S235/236. Suggesting C188-9 is inhibiting mTORC1. Longer term inhibition of STAT3 through C188-9 treatment, therefore could potentially repress HIF-1α expression further through inhibition of mTORC1 activity. The cross talk between STAT3 and mTORC1 signalling within TSC cells will be explored further in result chapter 5.

Consistent with previous ELISA assay results (figure 4.11), rapamycin was effective at significantly decreasing expression of both HGF and VEGFA. Unlike Ref-1 inhibitors, C188-9 and FLLL31, which repress STAT3 Y705 phosphorylation, decreased the protein expression of HGF and VEGFA within *TSC2* deficient AML cells (figure 4.16). Both FLLL31 and C188-9, at least at one of the concentrations used, significantly decreased protein expression VEGFA and HGF, in the whole cell lysate and conditioned media, relative to the DMSO control. C188-9 was observed to decrease HGF expression further than FLLL31. Whereas for VEGFA expression FLLL31 was the more effective STAT3 inhibitor. Given that in *TSC2* deficient AML cells C188-9 was better able to repress *VEGFA* mRNA expression than FLLL31 (figure 4.6), why FLLL31 treatment decreased VEGFA expression further than C188-9 is unclear. Comparisons of the efficacy of FLLL31 and C188-9 at inhibiting STAT3 activity will be examined within chapter 5.

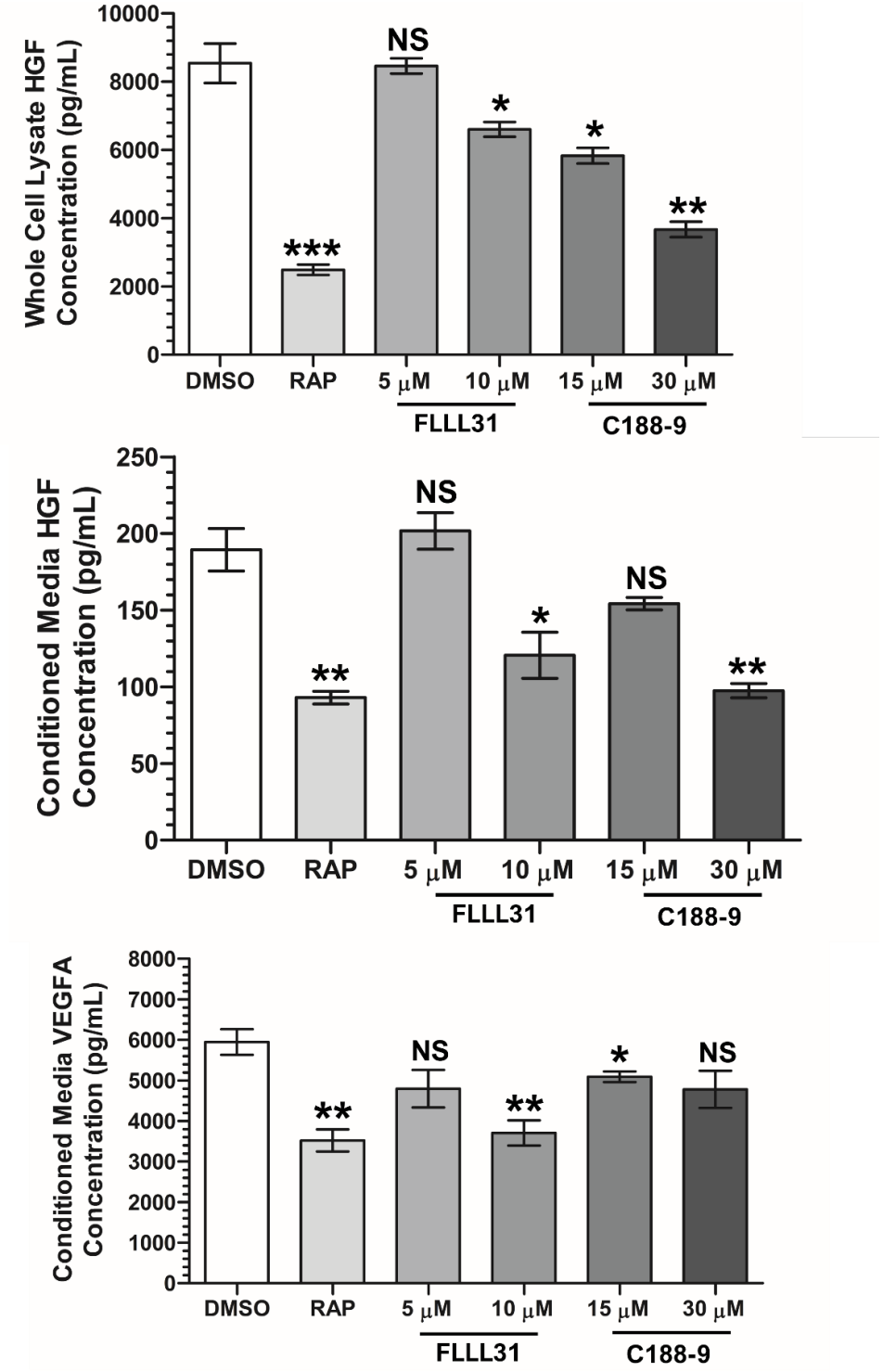


**Figure 4.16. The STAT3 inhibitors FLLL31 and C188-9 and the mTORC1 inhibitor rapamycin are all effective at significantly decreasing protein expression of HGF and VEGFA in *TSC2* deficient AML cells.** *TSC2* deficient AML cells were cultured for 18 h in the presence of either DMSO, rapamycin (RAP) at 50 nM, FLLL31 at 5 μM or 10 μM or C188-9 at 15 μM or 30 μM. Conditioned media was then taken and assayed for VEGFA and HGF expression by way of ELISA or cells were lysed and whole cell lysates analysed for HGF expression by way of ELISA. N=3 minimum. Significance annotations above each bar on graph indicates significance of difference in HGF/VEGFA concentration between each condition and the control sample (DMSO). Statistical analysis of differences in protein concentration was by student's t test. Significance denoted by: * = $p < 0.05$, ** = $p < 0.01$, *** = $p < 0.001$, NS = not significant. Bars represent standard error of the mean.

### 4.2.9 Effect of C188-9 and rapamycin co-treatment is largely not agonistic at decreasing expression of pro-angiogenic proteins elevated upon loss of *TSC2*.

Early studies found that HIF-1α protein stability was attenuated by rapamycin treatment within PC-3 cells (Hudson *et al.* 2002). A more recent study by Dodd *et al.* (2015) however found that within HEK293 cells, through a cycloheximide pulse-chase experiment, rapamycin treatment did not significantly affect the half-life of HIF-1α protein compared to untreated cells. Rather mTORC1 drives HIF-1α protein accumulation through upregulating translation of *HIF1A* mRNA (Düvel *et al.* 2010) (see chapter 1). Rapamycin has previously been shown to downregulate HIF-1α protein expression in murine cells lacking *TSC1/TSC2* (Brugarolas *et al.* 2003 and Düvel *et al.* 2010) or with mTORC1 hyperactivity (Dodd *et al.* 2015). Given that rapamycin treatment reduced HIF-1α in the *TSC2* deficient AML line (figure 4.10). Co-treatment of *TSC2* deficient AML cells with rapamycin and C188-9 may repress HIF-1α protein expression further if mTORC1 and STAT3 upregulate HIF-1α through distinct mechanisms within TSC. Therefore, the potential for greater repression of BNIP3, ANGPTL4, HGF and VEGFA protein expression was assessed by dual inhibition of STAT3 and mTORC1 by co-treating *TSC2* deficient AML cells with both rapamycin and C188-9.

Seen in figure 4.17, repression of rpS6 phosphorylation happened quicker with co-treatment of C188-9 with rapamycin, than C188-9 treatment alone. Of interest, a significant reduction in the expression of total rpS6 was observed with co-treatment of C188-9 and rapamycin within both *TSC2* deficient AML cells. The effects of C188-9 and rapamycin on surrogate markers of mTORC1 activity in *TSC2* deficient cells will be further explored within chapter 5. As seen from the densitometry graphs in figure 4.17 (previous densitometry from C188-9 long term treatment also plotted), the decrease in HIF-1α protein expression on co-treatment with rapamycin and C188-9 was not greater nor happened faster than the decrease in HIF-1α protein expression observed from C188-9 long term treatment alone. However, due to a difference in the antibody used to obtain the HIF-1α blots in figure 4.17, there is significant background signal. Which limited fair comparisons between the densitometry analyses of HIF-1α protein expression between treatment conditions. BNIP3 protein expression decreased on long-term co-treatment with C188-9 and rapamycin (figure 4.17), similar to C188-9 treatment alone (figure 4.15). Except the decrease in BNIP3 expression was observed later than that observed with C188-9 treatment alone. However, at no time point between 0.5-24 h was the expression of BNIP3 significantly different between the different treatment conditions. Changes in the protein expression of ANGPTL4 was observed to be less variable with co-treatment C188-9 and rapamycin than C188-9 treatment alone.

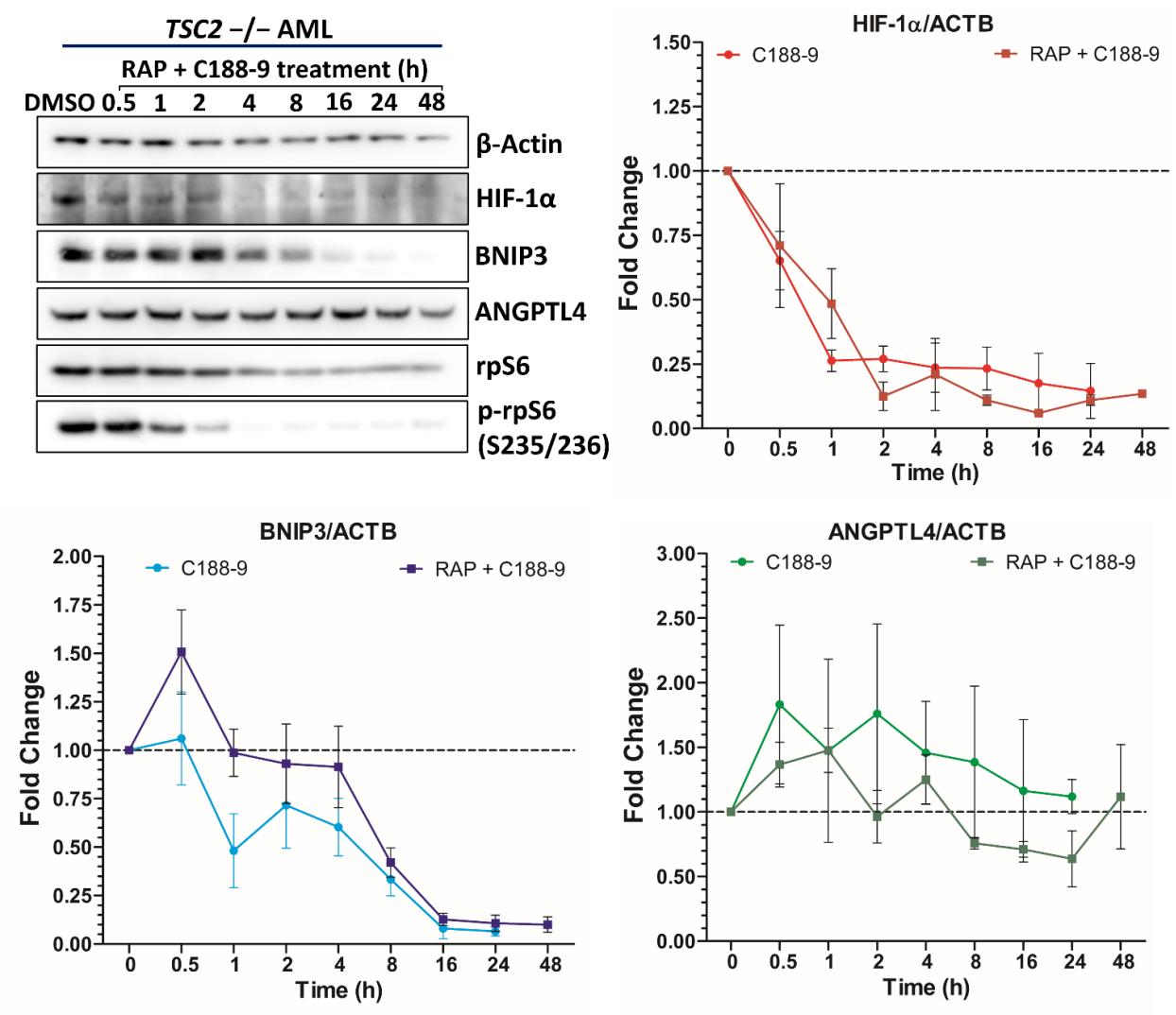


**Figure 4.17. Within *TSC2* deficient AML cells C188-9 and rapamycin co-treatment does not decrease HIF-1α or BNIP3 protein expression further than C188-9 treatment alone.** Representative western blots (N=3). *TSC2* deficient AML cells were treated with either DMSO or C188-9 at 30 μM in combination with rapamycin (RAP) at 50 nM. Cells treated with DMSO (control) were lysed at time 0 h, whilst RAP + C188-9 treated cells were lysed at the time indicated. Through western blotting lysates were assayed for protein expression, with β-actin acting as a loading control. Densitometry analysis of resulting western blots (N=3 minimum) from the AML cell line was performed with HIF-1α, BNIP3 and ANGPTL4 all being normalised to β-actin. Resulting ratios were then expressed as fold changes compared to control sample (DMSO) at time 0 h and plotted along with densitometry analysis of C188-9 treatment alone (as shown in figure 4.15) to show change in fold change in protein expression during treatment time in respect to the control. Dotted line on graphs represents DMSO control sample fold change, i.e., 1.00. Bars represent standard error of the mean. Predicted running band size (kDa) of protein targets can be found in chapter 2, table 2.6.

However, during the treatment time course, changes in the protein expression of ANGPTL4 observed under co-treatment with rapamycin and C188-9 was on average lower at each time point than observed with C188-9 alone. Therefore, co-treatment of rapamycin with C188-9 may help to limit the undesirable upregulation of ANGPTL4 protein expression observed with C188-9 treatment alone. Which is consistent with the effect of co-treatment with rapamycin and C188-9 on *ANGPTL4* mRNA expression that was observed (figure 4.6).

Co-treatment of *TSC2* deficient AML cells with rapamycin and the STAT3 inhibitors, FLLL31 or C188-9, significantly reduced the expression of HGF and VEGFA relative to the DMSO control (figure 4.18). However, the observed decrease in VEGFA expression and HGF expression within the whole cell lysate was not found to be significantly different from decreases observed with rapamycin treatment alone. The decrease in HGF within the conditioned media observed when co-treating with both rapamycin and C188-9 was significantly lower than that observed with rapamycin alone (RAP=93pg/mL RAP+C188-9=23 p=0.0016).

Taken together, the results indicate there is no agnostic effect of rapamycin and C188-9 together in reducing the protein expression of HIF-1α, BNIP3, HGF and VEGFA within *TSC2* deficient cells. Which indicates that the drug effects of C188-9 and rapamycin on pro-angiogenic protein expression may be working through similar mechanisms within *TSC2* deficient cells. However, as C188-9 was found to be more effective at repressing HIF-1α and BNIP3 protein expression, while rapamycin is better able to repress ANGPTL4, HGF and VEGFA protein expression. Dual targeting of mTORC1 and STAT3 activity, as a strategy to more robustly normalise pro-angiogenic protein expression, may still be a promising and valid therapeutic strategy for the treatment TSC.

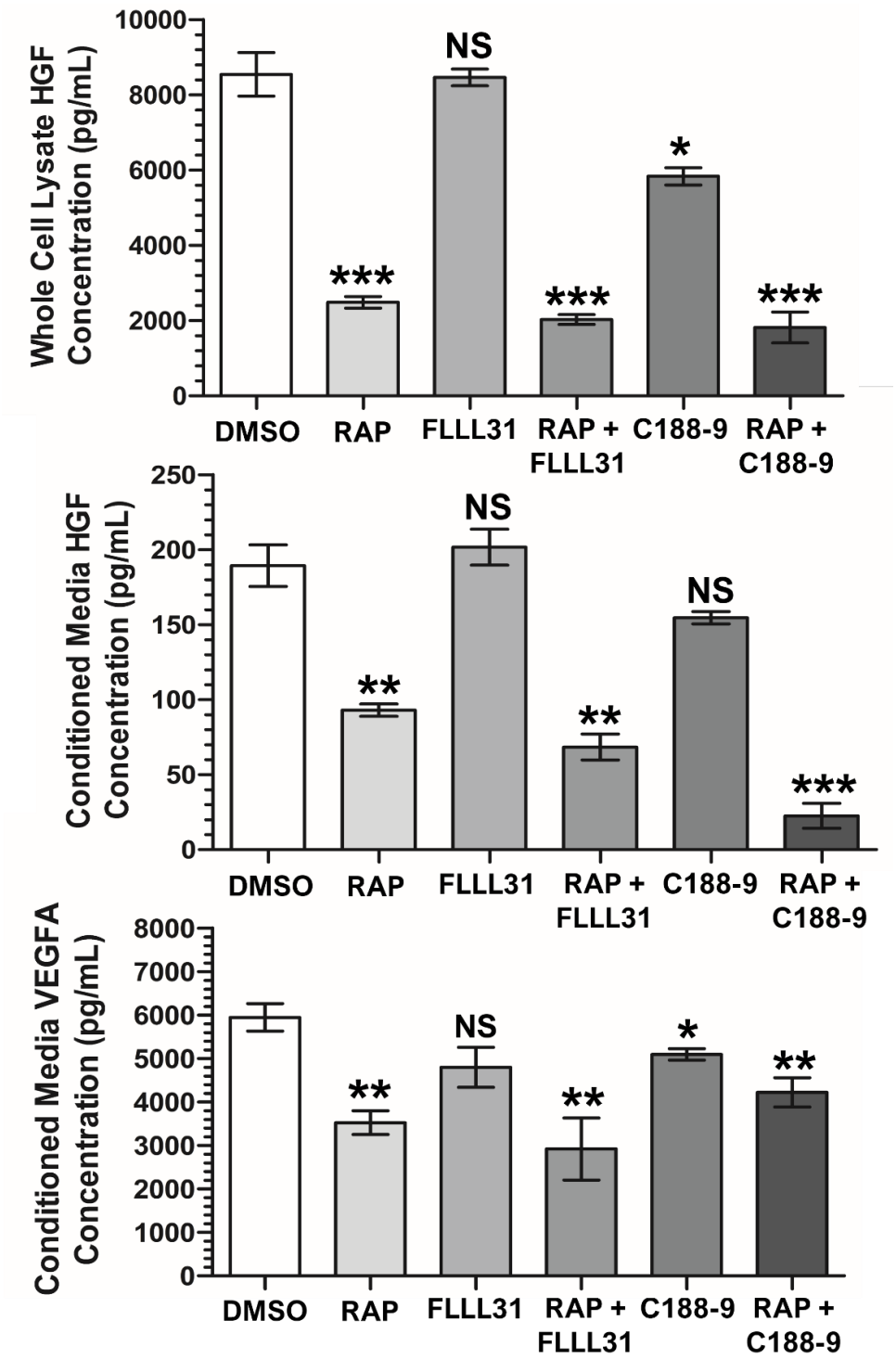


**Figure 4.18. STAT3 inhibitors in combination with rapamycin are not consistently more effective at decreasing expression of HGF and VEGFA than rapamycin alone in *TSC2* deficient AML cells.** *TSC2* deficient AML cells were cultured for 18 h in the presence of either DMSO, rapamycin (RAP) at 50 nM, FLLL31 at 5 μM or C188-9 at 15 μM alone or in combination. Conditioned media was then taken and assayed for VEGFA and HGF expression by way of ELISA or cells were lysed and whole cell lysates analysed for HGF expression by way of ELISA. N=3 minimum. Significance annotations above each bar on graph indicates significance of difference in HGF/VEGFA concentration between each condition and the control sample (DMSO). Statistical analysis of differences in protein concentration was by student's t test. Significance denoted by: * = $p < 0.05$, ** = $p < 0.01$, *** = $p < 0.001$, NS = not significant. Bars represent standard error of the mean.

### 4.2.10 Inhibition of mTORC1 or STAT3 has marked effect on HIF-1α transcriptome dysregulated on loss of *TSC2* within AML cells.

The present chapter has shown that both rapamycin and C188-9 treatment had marked effects on HIF-1α activity within both murine and human *TSC2* deficient cell lines. Given this, the final aim of this chapter was to assay the efficacy of rapamycin versus C188-9 treatment in normalising the expression of HIF-1α target genes shown to be dysregulated within *TSC2* deficient (621-102) AML cells (see figure 4.1). This was by way of an RNA sequencing experiment, comparing DMSO, rapamycin and C188-9 treated *TSC2* deficient AML cells under hypoxia. This RNA sequencing experiment was conducted by the Tee lab during (sequencing itself by Novogene) the course of research contained within this thesis. Full details of the sample origin and sequencing methodology for this RNA sequencing data set can be found in chapter 2, section 2.3.6. Hypoxia rather than normoxia was chosen for culture conditions, as expression of HIF-1α target genes on the whole was observed to be highest under hypoxia (see figure 4.1). The HIF-1α target gene set used for analysis was the same one used in subsection 4.1.

Volcano plots in figure 4.19 summarise HIF-1α target gene expression changes on rapamycin or C188-9 treatment relative to DMSO control within *TSC2* deficient AML cells cultured under hypoxia. 123 HIF-1α target genes were significantly differentially expressed between rapamycin and DMSO treated cells (figure 4.19 **A**), with 45 genes upregulated and 78 downregulated by rapamycin treatment. By and large, foldchanges of downregulated genes were greater than those observed for upregulated genes. 98 HIF-1α target genes were significantly differentially expressed between C188-9 and DMSO treated cells (figure 4.19 **B**), with an equal number of genes upregulated as downregulated by C188-9 treatment relative to the DMSO control. As with rapamycin, foldchanges of downregulated genes were greater than those observed for upregulated genes on C188-9 treatment. Comparing HIF-1α target gene expression between rapamycin and C188-9 treated cells (figure 4.19 **C**). 49 HIF-1α target genes were significantly differentially expressed, of which 40 were upregulated and 9 downregulated within the C188-9 treatment condition relative to the rapamycin condition. Comparing the fold change in expression of the HIF-1α target genes between rapamycin vs DMSO and C188-9 vs DMSO data sets, 133 genes were differentially expressed in the same direction (e.g., downregulated by rapamycin and C188-9), whilst 32 were differentially expressed in a different direction between the two data sets (e.g., downregulated by rapamycin, but upregulated by C188-9). Which indicates that rapamycin and C188-9 are by in large affecting the expression of HIF-1α target genes similarly relative to DMSO treatment. This is better highlighted by the heat map in figure 4.20, were FPKM (Fragments Per Kilobase Million per mapped reads) for each HIF-1α target gene assayed, for each repeat in each

condition is plotted. Whilst there are noticeable differences in FPKM for some genes between the rapamycin and C188-9 treatment conditions (seen by differing colour profiles), for most genes the FPKM values are more similar relative to the DMSO treatment condition.

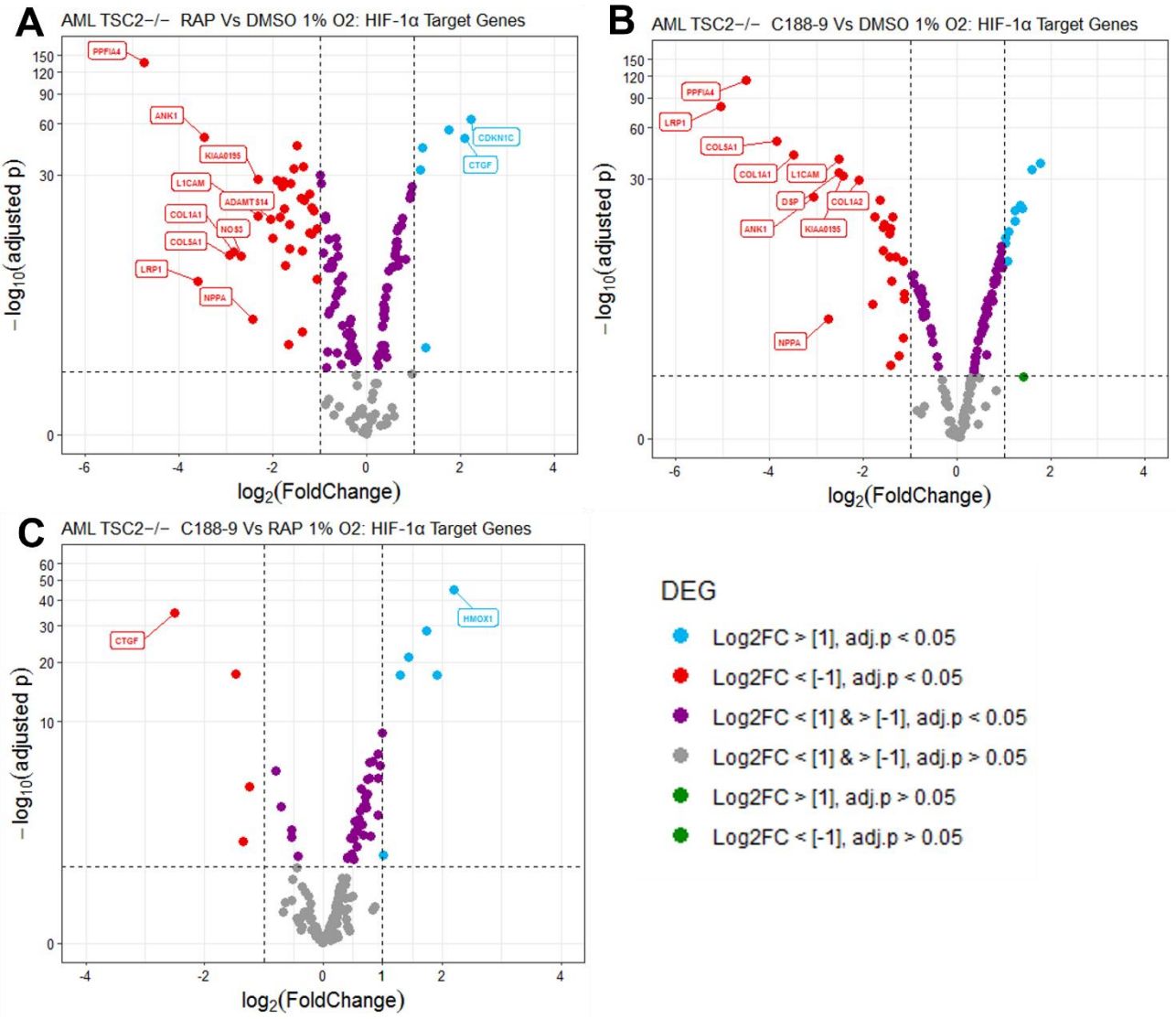


**Figure 4.19. Both rapamycin and C188-9 treatment are effective at decreasing HIF-1α target gene expression in *TSC2* deficient AML cells.** HIF-1α target gene set was collated from multiple publications (see methods and materials). Differential gene expression (DEG) comparison is annotated above each plot. AML *TSC2* deficient cells were cultured under hypoxia (1% $O_2$) for 8 h with either vehicle only (DMSO), rapamycin (RAP) at 50 nM or C188-9 at 15 μM (N=8). RNA purified from these samples was sequenced through Novogene. Expression levels were calculated and normalised from raw read counts as FPKM (Fragments Per Kilobase Million per mapped reads). Differential gene expression (DEG) analysis was through DEseq2 analysis and resulting p-values were corrected for multiple testing and false discovery by FDR method. For all volcano plots Log2 transformed fold change in expression of genes was plotted against their -log10 transformed FDR adjusted p-values. Dotted lines at x axis represent increase or decrease in foldchange of 2 or -2 respectively. Dotted line at y axis represents significance threshold of 0.05. Genes annotated had a Log2 fold change in expression greater or lower than 2 or -2 (i.e. four fold higher or lower in expression) respectively and an -log10 adjusted p-value greater than 3 (i.e. below 0.001 significance threshold).

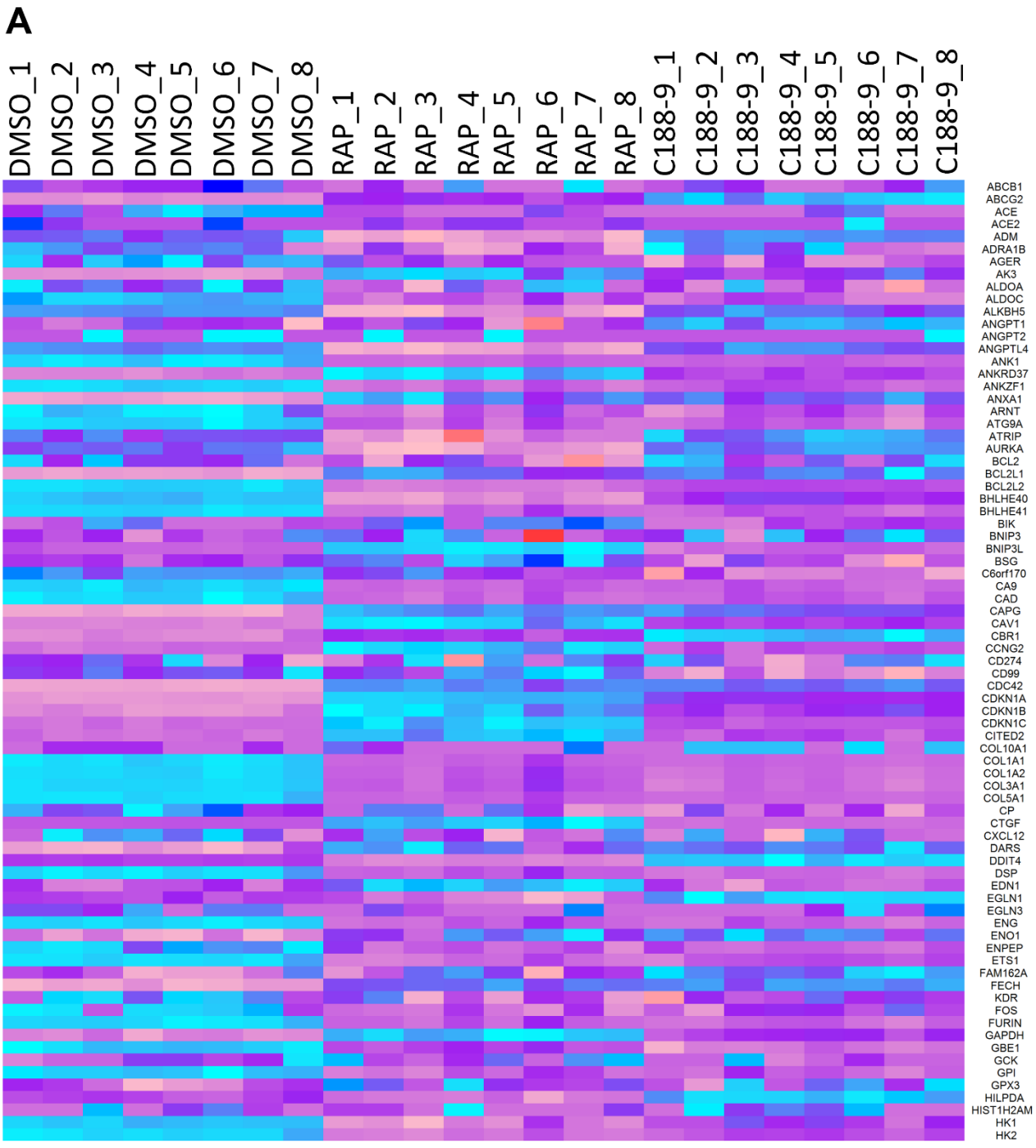
A
DMSO_1
DMSO_2
DMSO_3
DMSO_4
DMSO_5
DMSO_6
DMSO_7
DMSO_8
RAP_1
RAP_2
RAP_3
RAP_4
RAP_5
RAP_6
RAP_7
RAP_8
C188-9_1
C188-9_2
C188-9_3
C188-9_4
C188-9_5
C188-9_6
C188-9_7
C188-9_8
ABCB1
ABCG2
ACE
ACE2
ADM
ADRA1B
AGER
AK3
ALDOA
ALDOC
ALKBH5
ANGPT1
ANGPT2
ANGPTL4
ANK1
ANKRD37
ANKZF1
ANXA1
ARNT
ATG9A
ATRIP
AURKA
BCL2
BCL2L1
BCL2L2
BHLHE40
BHLHE41
BIK
BNIP3
BNIP3L
BSG
C6orf170
CA9
CAD
CAPG
CAV1
CBR1
CCNG2
CD274
CD99
CDC42
CDKN1A
CDKN1B
CDKN1C
CITED2
COL10A1
COL1A1
COL1A2
COL3A1
COL5A1
CP
CTGF
CXCL12
DARS
DDIT4
DSP
EDN1
EGLN1
EGLN3
ENG
ENO1
ENPEP
ETS1
FAM162A
FECH
KDR
FOS
FURIN
GAPDH
GBE1
GCK
GPI
GPX3
HILPDA
HIST1H2AM
HK1
HK2

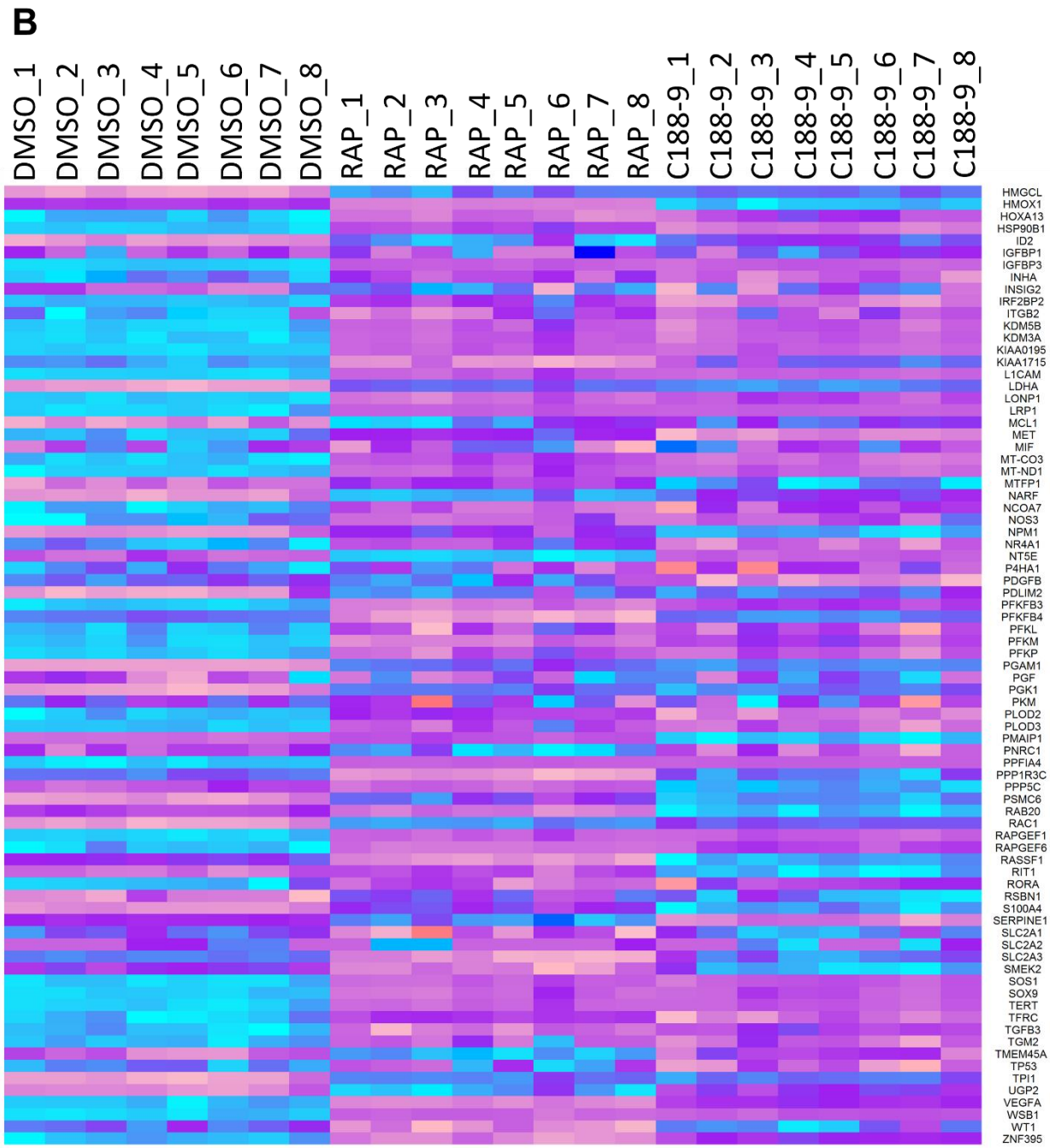


**Figure 4.20 Rapamycin and C188-9 treatment repress most of the same HIF-1α target genes compared to the DMSO control within *TSC2* deficient AML cells.** Panels **A** and **B** belong to the same heatmap comparing fold change in expression of HIF-1α target genes between AML cells treated for 8 h with either vehicle only (DMSO), rapamycin (RAP) at 50 nM or C188-9 at 15 μM (N=8) under hypoxia (1% $O_2$). FPKM (Fragments Per Kilobase Million per mapped reads) has been plotted for each gene with the HIF1-α target gene set for each sample. Gene names are shown on the right of the heatmap.

The efficacy of rapamycin vs C188-9 treatment in normalising dysregulated HIF-1α target gene expression observed upon *TSC2* loss (figure 4.1), can be assessed by comparing the rapamycin vs DMSO and C188-9 vs DMSO treatment RNA seq data sets to the *TSC2* deficient vs *TSC2* RE AML cells under hypoxia RNA seq data set. Under hypoxia 67 HIF-1α target genes are significantly upregulated within *TSC2* deficient AML cells relative to *TSC2* RE AML cells, whilst 53 are significantly downregulated. Out of the HIF-1α target genes found to be significantly differentially expressed upon *TSC2* loss under hypoxia, rapamycin appears to normalise dysregulated HIF-1α mediated gene expression more than C188-9 treatment (as seen by table 4.3). Out of the 67 HIF-1α target genes upregulated in *TSC2* deficient AMLs, rapamycin treatment significantly downregulates the expression of 37 genes relative to the DMSO control, whilst C188-9 treatment significantly downregulates the expression of 23 genes relative to the DMSO control. For the 53 HIF-1α target genes significantly downregulated in *TSC2* deficient AMLs, both rapamycin and C188-9 treatment upregulates the expression of 16 genes relative to the DMSO control. Some of the HIF-1α target genes whose expression was normalised were different under rapamycin or C188-9 treatment, as seen in table 4.3. Therefore, more robust normalisation of HIF-1α target genes whose expression is dysregulated upon loss of *TSC2* could be better achieved by dual targeting of mTORC1 and STAT3. Largely the effects of rapamycin and C188-9 are likely mediated by a reduction in HIF-1α protein expression. An important consideration however is that STAT3 itself is a transcription factor, which regulates its own set of target genes, some of those in common with HIF-1α. Therefore, changes in expression of assayed genes on C188-9 treatment, are likely not solely due to a reduction in HIF-1α protein.

**Table. 4.3 Comparison of the effect of Rapamycin (RAP) and C188-9 treatment on normalising HIF1-α target genes found to be significantly dysregulated upon loss of *TSC2* in AML cells cultured under hypoxia (1%$O_2$).** Genes in bold are those whose expression is significantly affected by rapamycin or C188-9 treatment, not both.

| **Genes downregulated in *TSC2* −/− AMLs upregulated on RAP treatment** | **Genes downregulated in *TSC2* −/− AMLs upregulated on C188-9 treatment** |
|---|---|
| ABCG2 | ABCG2 |
| AK3 | AK3 |
| ANKRD37 | ANKRD37 |
| **BIK** | **BCL2L2** |
| **BNIP3L** | CAV1 |
| CAV1 | CCNG2 |
| CCNG2 | CDKN1B |
| CDKN1B | DARS |
| **CTGF** | **FAM162A** |
| DARS | GPX3 |
| GPX3 | ID2 |
| ID2 | NARF |
| NARF | NPM1 |
| NPM1 | **PGK1** |
| **NT5E** | **PPP5C** |
| RSBN1 | RSBN1 |

| **Genes upregulated in *TSC2* −/− AMLs downregulated on RAP treatment** | | **Genes upregulated in *TSC2* −/− downregulated on C188-9 treatment** | |
|---|---|---|---|
| ADAMTS14 | HK2 | ADAMTS14 | PFKP |
| **ADM** | IRF2BP2 | ANKZF1 | PPFIA4 |
| **ANGPTL4** | ITGB2 | ATG9A | SOS1 |
| ANKZF1 | KDM5B | **BCL2L1** | |
| ATG9A | **KDR** | CAD | |
| **BCL2L2** | L1CAM | COL1A1 | |
| **BHLHE40** | LRP1 | COL1A2 | |
| CAD | **NCOA7** | CP | |
| COL1A1 | **PFKM** | DSP | |
| COL1A2 | PFKP | ENG | |
| **COL5A1** | **PLOD2** | ETS1 | |
| CP | PPFIA4 | FURIN | |
| **DDIT4** | **RASSF1** | HK2 | |
| DSP | **RORA** | IRF2BP2 | |
| ENG | **SLC2A3** | ITGB2 | |
| ETS1 | SOS1 | KDM5B | |
| FURIN | **VEGFA** | L1CAM | |
| **GBE1** | **WT1** | LRP1 | |
| **HK1** | | **PDGFB** | |

## 4.3 Discussion

The present chapter provided an expansive look at HIF-1α target gene expression within the human renal AML 621-102 line and MEFs upon loss of *TSC2*. The HIF-1α driven transcriptome is extensively dysregulated upon loss of *TSC2* (figures 4.1 and 4.2). And cross comparison with sequencing data from TSC associated lesions, reveals that many of the genes within the HIF-1α target genes set are differentially expressed in both the TSC lesions (figure 4.3) and *TSC2* deficient AML cells. However, cross comparison of DEG analyses of RNA sequencing data sets highlighted important differences as well. Not only was the expression of several HIF-1α target genes different among lesion type, which suggests the dependence on pro-angiogenic signalling pathways driving aberrant angiogenesis and neo-vascularisation may differ between TSC lesion type. Dysregulated HIF-1α genes in common between the AML line and TSC lesions, aren't always expressed in the same direction (e.g., upregulated/downregulated in both lesion and AML or not). For the present work and future work, these are important considerations for choosing a cell model or potential target for the study of angiogenesis within TSC. Expression of pro-angiogenic factors found to be elevated at the protein level within TSC associated lesions (Parker *et al.* 2011, Nguyen-Vu *et al.* 2001 and Mahimainathan *et al.* 2009) were also found to elevated within the AML 621-102 cell lines. This demonstrates that this cell line appears to be an appropriate model to test efficacy of mTORC1, Ref-1 and STAT3 inhibitors in normalising pathogenic and aberrant angiogenic signalling observed within TSC. Additionally, BNIP3 and ANGPTL4 were identified as new pro-angiogenic markers within cellular models of TSC. Hypoxia drove the expression of dysregulated HIF-1α target genes further within *TSC2* deficient AML cells (figure 4.1). But hypoxia was found to also affect the expression of many of the pro-angiogenic genes and proteins assayed. Whilst not driving *HIF1A* mRNA expression further, hypoxia did elevate protein expression and HIF-1α and BNIP3, as would be expected (Majmundar *et al.* 2010 and Guo *et al.* 2001). Furthermore, at least in the AML cell lines, hypoxia did not seem to impact protein expression of either HGF or VEGFA. Despite upregulating expression of the *VEGFA* gene.

Within the present work, the efficacy of mTORC1 inhibitors in normalising markers of pro-angiogenic signalling within our *TSC2* deficient cell lines was largely as expected. Within the *TSC2* deficient AML cells, rapamycin and Ku-0063794 were effective at decreasing the expression of the STAT3 and HIF-1α driven pro-angiogenic gene panel (*HGF*, *TNFRSF1A*, *VEGFA* and *ANGPTL4*) (figures 4.5 and 4.6) found to be elevated upon *TSC2* loss, particularly for *HGF*. However, mTORC1 inhibition did not alter *HIF1A* gene expression. Therefore, reduction in HIF-1α protein within *TSC2* deficient MEF and AML cells seen on treatment with

rapamycin and Ku-0063794 (figures 4.9 and 4.10), is mediated by a decrease in HIF-1α protein translation. Consistent with the current mechanism by which mTORC1 activity is thought to mediate elevation of HIF-1α protein. Through its effect on preferential translation of HIF-1α mRNA by action of downstream mTORC1 substrates (Land and Tee, 2007 and Dodd *et al*. 2015). Dodd *et al.* (2015) showed that neither rapamycin nor Ku-0063794 decreased HIF-1α protein stability. Within murine cell lines of TSC, rapamycin treatment decreased levels of HIF-1α protein elevated upon loss of *TSC1* or *TSC2* (Düvel *et al*. 2010 and Brugarolas *et al.* 2003). Aside from HIF-1α, within the *TSC2* deficient AML line, rapamycin treatment decreased the protein expression of ANGPTL4, HGF and VEGFA (figures 4.10, 4.13 and 4.11). Ku-0063794 treatment largely resulted in the same effects as rapamycin treatment. However, a slight, but significant, increase in VEGFA expression within the *TSC2* deficient AML cells was observed on Ku-0063794 treatment. This observation was surprising given Ku-0063794 inhibits mTORC1 more completely than rapamycin (García-Martínez *et al.* 2009). Zhang *et al.* (2013b) observed however that treatment of renal cell carcinoma cells with Temsirolimus, a rapamycin analogue, decreased VEGFA expression to a greater extent than KU-0063794. While Franz *et al.* (2012) found that whilst levels of many pro-angiogenic factors were lower in the plasma of TSC patients treated with Everolimus (rapamycin analogue) than placebo. Levels of VEGFA were elevated in Everolimus treated patients. Whilst the efficacy of rapamycin in decreasing angiogenesis in the context of TSC has been evaluated (Woodrum *et al.* 2010 and Yang *et al.* 2017 and Franz *et al.* 2012). The data presented in this chapter expands on the number of pro-angiogenic targets whose expression are successfully or unsuccessfully normalised by rapamycin treatment, at least within *in vitro* models of TSC.

The present work assayed the efficacy of Ref-1 and STAT3 inhibitors in decreasing expression of pro-angiogenic markers cited as elevated in TSC model cell lines and lesions within the literature. However, they are not equally effective for all targets assayed. Ref-1 inhibitors were not found to repress the transcription of HIF-1α target genes assayed by qPCR within *TSC2* deficient AML cells (figure 4.5). Within the *Tsc2* −/− MEFs, Ref-1 inhibitors have been found to decrease transcriptional activity of HIF-1α (Champion *et al.* 2022). With the Ref-1 inhibitor APX3330 being found effective at decreasing the expression of *CA9*, a HIF-1α target gene, within pancreatic cancer lines (Logsdon *et al.* 2016 and Logsdon *et al.* 2018). This suggests either *ANGPTL4* and *VEGFA* are not exclusively/strongly driven by HIF-1α activity within the AML cells or Ref-1's transactivation of HIF-1α may not be driving HIF-1α mediated transcription within the AML cells. Additionally, Ref-1 inhibition had no significant effect on mRNA expression of STAT3 driven pro-angiogenic genes assayed (figure 4.5). This is in spite of APX3330 treatment being found to be effective at decreasing transcriptional activity of STAT3 in both TSC and cancer cells (Champion *et al.* 2022 and Cardoso *et al.* 2012).

Expression of STAT3 driven pro-angiogenic gene was significantly affected by the STAT3 inhibitor C188-9 (figure 4.6). Which confirmed that the STAT3 pro-angiogenic genes chosen from the literature and the RNA seq. data presented in this chapter, were actually STAT3 driven within context of TSC. Or at least within the *TSC2* deficient AML line. The fact that Ref-1 inhibitors did not alter the mRNA expression of the pro-angiogenic gene panel suggests that transactivation of HIF-1α and STAT3 by Ref-1 does not substantially contribute to these gene regulation within *TSC2* deficient cells. Of interest was the observation that Ref-1 inhibitors effected STAT3 phosphorylation, but their effect was not consistent between treatment conditions and between cell lines (Supplemental figures S.4.2 and S.4.3). Whilst Ref-1 inhibitors do not target STAT3 phosphorylation directly, inhibition of STAT3 transcription could decrease STAT3 phosphorylation by blocking the positive feedback loop that reinforces STAT3 signalling through increased expression of STAT3 stimulatory cytokines.

The Ref-1 inhibitors, especially the more potent 2$^{nd}$ generation inhibitors, did however repress protein expression of HIF-1α within both the *TSC2* deficient MEF and AML cell line and ANGPTL4 in the AML cells (figures 4.9 and 4.10). The repression of HIF-1α protein expression was enhanced when Ref-1 inhibitors were used in combination with rapamycin (figure 4.12 and 4.13), which indicates that Ref-1 and mTORC1 activity within TSC are elevating HIF-1α expression through distinct mechanisms. The redox function of Ref-1 is mediated through transactivation of target transcription factors, promoting their activity and in turn the expression of those transcription factors target genes (Shah *et al.* 2017). However, Ref-1 inhibition did not repress *HIF1A* mRNA expression (figure 4.5) within *TSC2* deficient AML cells. Ref-1 target transcription factors have been found to regulate the *HIF1A* gene. Both STAT3 and NF-kB activity have been shown to promote *HIF1A* mRNA expression (Niu *et al* 2008 and BelAiba *et al.* 2007), and the Ref-1 inhibitor APX3330 was effective at repressing transcriptional activity of HIF-1α (Logsdon *et al.* 2018), STAT3 (Cardoso *et al.* 2012) and NF-kB (Fishel *et al.* 2011), not only within human cancer cells but also within murine *Tsc2* −/− cells (Champion *et al.* 2022). Thus, taking together the present work and what is known in the literature, it appears that repression of HIF-1α protein expression under hypoxia by Ref-1 inhibitors is not mediated through affecting the transcription of the *HIF1A* gene within *TSC2* deficient AML cells.

A potential mechanism by which Ref-1 inhibition is affecting HIF-1α expression within the *TSC2* deficient cell lines, is through Ref-1's effect on the redox environment of the cell, which in turn may affect HIF-1α protein stability or the stability/expression of HIF-1α's negative regulators. Multiple studies have found reactive oxygen species (ROS) affect HIF-1α protein stability (Chandel *et al.* 1998, Chandel *et al.* 2000, Mansfield *et al.* 2005, Lu *et al.* 2005, Pan *et al.* 2007 and Lee *et al.* 2016). And drug or siRNA targeting of Ref-1 has been found to affect the redox environment of cells (Champion *et al.* 2022 and Li *et al.* 2014 and Fishel *et al.* 2015).

However, further work is needed to establish whether HIF-1α stability/activity is impacted by the redox environment within *TSC2* deficient cells. Which will be addressed in chapter 6. Regardless of the mechanism, the present work shows that Ref-1 inhibitors, especially if used in combination with mTORC1 inhibitors, show promise in decreasing aberrant HIF-1α protein expression and downstream activity observed within TSC model cells (Düvel *et al*. 2010 and Brugarolas *et al.* 2003) and patient renal AMLs (Mahimainathan *et al.* 2009). As a concurrent decrease in the expression of BNIP3, which is strongly induced by HIF-1α activity (Guo *et al.* 2001), alongside HIF-1α was observed in both *TSC2* deficient cell lines on Ref-1 inhibitor treatment. Suggests HIF-1α activity is repressed within these cells. Ref-1 inhibitors were however, largely in effective at decreasing the protein expression of HGF and VEGFA (figure 4.11) within *TSC2* deficient AMLs. Therefore, beyond targeting HIF-1α, Ref-1 inhibitors efficacy at normalising pro-angiogenic factor expression within TSC, at the mRNA and protein level, maybe more limited.

Targeting STAT3 directly at its tyrosine phosphorylation site, i.e. the site necessary for STAT3 dimerization, appeared to be a better strategy for normalising pro-angiogenic signalling observed within TSC than targeting Ref-1. C188-9 treatment was more effective at decreasing the mRNA expression of the pro-angiogenic gene panel within *TSC2* deficient AML cells (figure 4.6). Whilst *CCL5* and *ANGPTL4* were upregulated on C188-9 treatment, co-treatment with rapamycin was able to block this undesirable increase in expression. Within cancer cells however, STAT3 inhibition was observed to decrease *ANGPTL4* expression in MDA-MB-231 cells (Pawlus *et al.* 2014). Suggesting *ANGPTL4* may be regulated differently by STAT3 within TSC. As observed with Ref-1 inhibitor treatment, the STAT3 inhibitors, FLLL31 or C188-9, did not decrease mRNA expression of *HIF1A* within *TSC2* deficient AML cells. Indicating the elevation of *HIF1A* expression observed upon the loss of *TSC2* (figure 4.6) may be independent of STAT3 within TSC. In cancers with hyperactive STAT3 and HIF-1α, inhibition of STAT3 does not always result in a decrease in *HIF1A* mRNA and protein expression. Pawlus *et al.* (2014) saw that reduction in STAT3 protein or phosphorylation at Y705, by way of siRNA knockdown of STAT3 or the inhibitor S3I-201, resulted in no or only a moderate decrease in *HIF1A* mRNA and protein expression within MDA-MB-231 cells or RCC4 cells. Similar observations have been made in other cancer cell lines (Bai *et al.* 2012 and Adachi *et al.* 2012). Within our TSC cell models however, C188-9 treatment did result in a rapid decrease in HIF-1α protein expression (figure 4.15). Whilst previous work has found that, constitutive STAT3 activity can drive mRNA expression of *HIF1A* (Niu *et al.* 2008 and Demaria *et al.* 2010). Given the present data (figures 4.5 and 4.6), the decrease in HIF-1α protein expression observed upon C188-9 treatment is unlikely to be mediated through repression of transcription

of the *HIF1A* gene. One possible mechanism by which STAT3 inhibition is rapidly decreasing HIF-1α expression is through active STAT3 stabilising HIF-1α protein. Jung *et al.* (2008) found overexpressing constitutively active STAT3 increased HIF-1α protein levels within COS7 cells in a dose dependent manner. The authors showed that this stabilising effect of STAT3 was mediated by active STAT3 binding with HIF-1α and preventing the binding of the negative regulator of HIF-1α stability pVHL, thereby decreasing poly-ubiquitination of HIF-1α and hence decreasing its proteasomal degradation. *TSC2* deficient AML and MEF cells were found to have constitutive STAT3 activity (figure 2.1). But further work is needed to elucidate whether active STAT3 stabilises HIF-1α within TSC. This could be tested using a pulse-chase cycloheximide based assay assessing HIF-1α protein expression in cell cultured with and without STAT3 inhibitors present.

Decreasing HIF-1α transcriptional activity was observed to be concurrent with decreasing phosphorylation of STAT3 at Y705 within *Tsc2* −/− MEFs treated with increasing dose of C188-9 (figure 4.7). This effect is likely the result of HIF-1α protein expression decreasing on C188-9 treatment (figure 4.15). Although within TSC this effect may also be mediated by active STAT3 co-operating with HIF-1α to promote HIF-1α driven transcription. Pawlus *et al.* (2014) showed within MDA-MB-231 and RCC4 cells through chromatin immunoprecipitation that inhibition of STAT3 blocked binding of the transcriptional coactivators, CBP and p300, as well as HIF-1α to HIF-1α target gene promoters. Regardless, C188-9 treatment was able to normalise expression of many HIF-1α target genes found to be dysregulated upon loss of *TSC2* within AML cells. Although it should be noted that many of the genes within the HIF-1α target gene set are also known STAT3 genes. Therefore, changes in expression of several genes are likely mediated through repression of STAT3 driven transcription. Overall rapamycin appeared to be better at normalising HIF-1α gene expression. STAT3 inhibitors were more effective at decreasing protein expression of angiogenic factors than Ref-1 inhibitors. Within *TSC2* deficient AML cells, C188-9 treatment markedly decreased levels of HGF (figure 4.16), expression previously shown to be elevated in TSC lesions (Parker *et al.* 2011). With regards to VEGFA expression, which again is an identified angiogenic biomarker within TSC lesions, STAT3 inhibitor treatment resulted in moderate decreases. The use of C188-9 as a treatment to normalise aberrant angiogenic signalling within TSC shows promise. Especially as an adjunct therapy with rapamycin. As decreases in the expression of assayed pro-angiogenic genes and proteins or the normalised HIF-1α target genes, did not completely overlap on treatment with either drug.

# Chapter 5: Characterisation of dysregulated STAT3 activity within *TSC2* deficient cells

## 5.1. Introduction

Aberrant STAT3 signalling has been described as feature of TSC for over two decades (Onda *et al.* 2002), with hyperactive STAT3 activity described in renal, pulmonary and brain manifestations of the disease (El-Hashemite and Kwiatkowski, 2005, Chan *et al.* 2004 and Goncharova *et al.* 2009). Targeting STAT3 has been shown to be effective at reducing tumorigenicity in pre-clinical models of TSC. Yang *et al.* (2016b) and Goncharova *et al.* (2009) showed that inhibiting STAT3 reduced proliferation and promoted apoptosis in *TSC1*/*TSC2* deficient cells. Furthermore, enhanced expression of STAT3 stimulatory cytokines/growth-factors have been found in *TSC1*- and *TSC2*- deficient cells, namely epidermal growth factor (EGF), hepatocyte growth factor (HGF) and interleukin-6 (IL-6) (Parker *et al.* 2011 and Wang *et al.* 2021a). Within murine models of TSC, studies have found that targeting these cytokines/growth-factors or their cognate receptors may be an effective strategy for decreasing dysregulated signalling and scores of tumorigenicity (Lesma *et al.* 2015 and Wang *et al.* 2021). It was also shown by Dodd *et al.* (2015) that mTORC1 co-operates with STAT3 to upregulate hypoxia-inducible factor 1-alpha (HIF-1α) and its downstream target vascular endothelial growth factor A (VEGFA), thereby increasing pro-angiogenic signalling. This study identified STAT3 as a potential driver of angiogenesis within TSC, that may contribute to the high vascularisation seen in TSC associated lesions (Arbiser *et al.* 2002); a significant cause of morbidity and mortality to TSC patients (Amin *et al.* 2015 and Zöllner *et al.* 2020). Despite this body of research highlighting aberrant STAT3 signalling as a driver of TSC pathology, much of our understanding of how the STAT3 pathway mechanistically functions within the context of TSC is still limited.

There is a lack of knowledge in how the STAT3 driven transcriptome is dysregulated upon loss of *TSC1* or *TSC*2 in cells, including the expression of negative modulators of the STAT3 signalling cascade. Also, how hyperactive STAT3 and mTORC1 signalling may influence one another within the context of TSC, and how this signalling crosstalk may further promote tumorigenesis. And lastly whether TSC cells promote their own constitutive STAT3 activity through an autocrine manner, as STAT3 regulated genes, such as *IL6*, in turn activate the STAT3 pathway. Such enhanced cytokine secretion may also further support development of the tumour microenvironment, by for example promoting inflammation or increasing dysregulated angiogenesis and neovascularisation.

The current work has previously shown that STAT3 inhibition is effective at reducing scores of tumorigenicity of *TSC2* deficient cells in tissue culture assays (chapter 3) and

downregulates the expression of HIF-1α and pro-angiogenic targets upregulated upon loss of *TSC2* (chapter 4). The main aims of the present chapter are as follows. Firstly, to better define how markers of active STAT3 signalling are expressed upon loss of *TSC2* at the protein and transcriptional level. Secondly, assess the effect of STAT3 and mTORC1 inhibition on markers of their own activity and each other. To better understand how STAT3 and mTORC1 signalling interplay within the context of TSC. Lastly to assess whether autocrine/paracrine signalling of TSC cells drives and maintains active STAT3 signalling in themselves and non-TSC cells.

## 5.2. Results

### 5.2.1 Loss of *TSC2* increases protein markers of active STAT3 signalling in AML and MEF cells.

The first aim of the present chapter was to determine whether constituents of the JAK2/STAT3 signalling cascade at the protein level were dysregulated in cells lacking *TSC2* through western blot analysis (figures 5.1 for AML cells and 5.2 for MEFs). With subsequent densitometry analysis normalising total proteins to β-Actin and phosphorylated proteins to their respective total proteins. Resulting ratios were then expressed as fold changes compared to a chosen control sample, *TSC2* RE (re-expressed) cells for AML lines and *TSC2* WT (wildtype) for MEF lines, and plotted.

As seen in the blot panels in figures 5.1 (**A**) and 5.2 (**A**), total STAT3 protein is elevated in both *TSC2* deficient AML and MEF cells compared to the *TSC2* RE and WT cells, respectively. The corresponding densitometry graphs show a significant fold change in the total STAT3 protein upon the loss of *TSC2* in both AML and MEF lines under normoxia (N) and hypoxia (H) conditions (figures 5.1 **B** and 5.2 **B**). Hypoxic culture conditions did not significantly affect total STAT3 protein expression relative to normoxic culture in either *TSC2* deficient AML or MEF cells. Phosphorylation of STAT3 at tyrosine 705 (Y705) and serine 727 (S727) (two post translation modifications that increase the transcriptional activity of STAT3, see main introduction) are elevated within both *TSC2* deficient cell lines, under either normoxia or hypoxia, compared to respective *TSC2* competent controls under either normoxia (figures 5.1 and 5.2). However only the enhanced level of pSTAT3(Y705)/STAT3 and pSTAT3(S727)/STAT3 in hypoxic cultured *TSC2* deficient AML cells relative to hypoxic cultured *TSC2* RE AML cells (figure 5.1 B) Which was not the case for the MEF cell lines. Densitometry analysis (figures 5.1 **B** and 5.2 **B**) found hypoxia did not induce the level of pSTAT3(Y705)/STAT3 and pSTAT3(S727)/STAT3 further in either the *TSC2* deficient AML or MEF cell lines. As differences in phosphorylated STAT3 between normoxia and hypoxia cultured *TSC2* deficient cells were not reported as significant. Oxygen availability was found

to significantly affect the level of pSTAT3(Y705)/STAT3 and pSTAT3(S727)/STAT3 in *TSC2* RE AML cells (figure 5.1 **B**), but not *Tsc2* +/+ MEF cells figure 5.2 **B**.

Regulators of activatory/inhibitory post translational modifications of STAT3 were also assayed by western blot, namely the activatory JAK2 and inhibitory SOCS3 and SIRT1 (see main introduction). As shown in the blot panels of figures 5.1 (**A**) and 5.2 (**A**), protein expression of total JAK2 was higher in both AML and MEF cell lines with *TSC2* relative to the *TSC2* deficient cells. Inversely, JAK2 phosphorylated at Y1007/1008 (pY1007/1008) is elevated within the *TSC2* deficient cell lines, but only reported as significant for the *TSC2* deficient AML cells cultured under normoxia or hypoxia (figure 5.1 **C**), not in the *Tsc2* −/− MEF cell lines figure 5.2 **C**. Likely due to variability in fold change of pJAK2 (Y1007/1008) in the

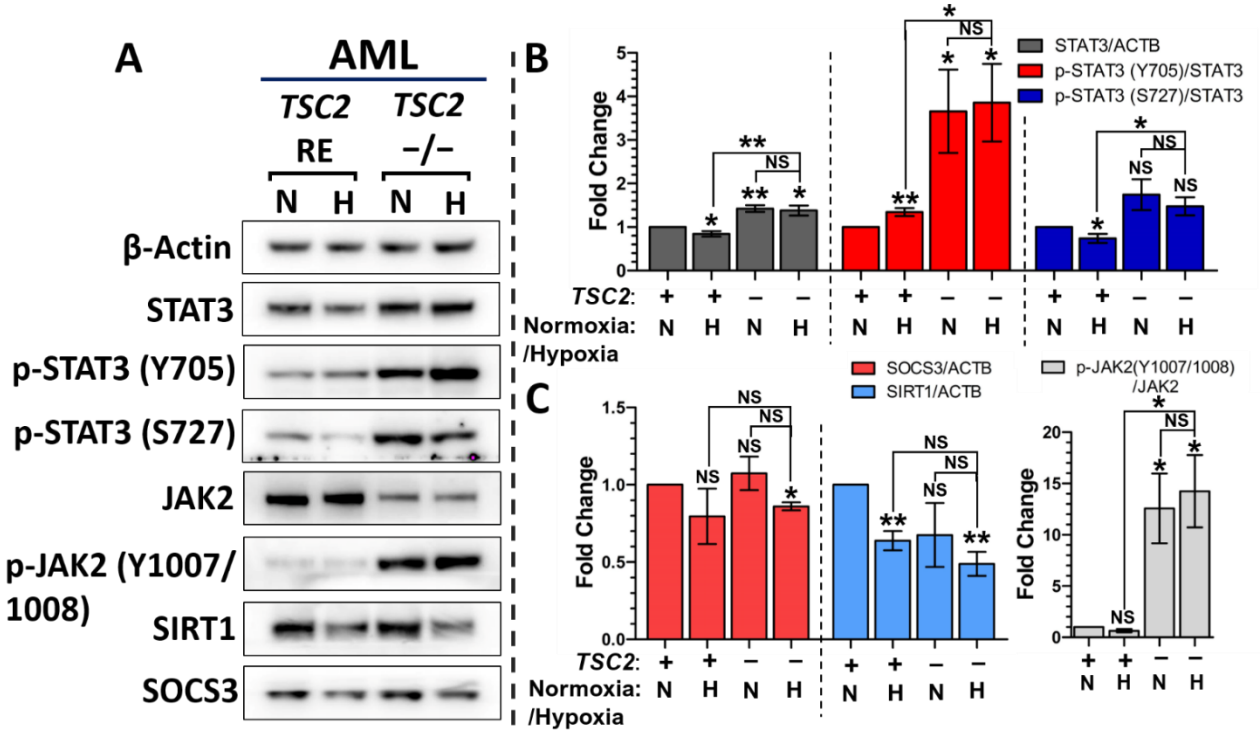


**Figure 5.1. Protein markers of STAT3 signalling are dysregulated upon loss of *TSC2* within AML cells.** Either under normoxia (**N**, 21% $O_2$) or hypoxia (**H**, 1% $O_2$), AML cells lacking *TSC2* (**TSC2 −/−**) or with *TSC2* re-expressed (***TSC2* RE**) were cultured overnight before being lysed. Through western blotting, protein lysates were then assayed for constituents of the STAT3 signalling pathway, with β-actin acting as a loading control. Panel **A** shows representative panel of the assayed protein targets in the AML cell lines (N=3 minimum). Densitometry analysis of resulting western blot (N=3 minimum) was performed (panels **B** & **C**) and total proteins (STAT3, SIRT1, SOCS3) were normalised to β-Actin and phosphorylated proteins were normalised to their respective total proteins. Resulting ratios were then expressed as fold changes compared to a designated control sample, in this case *TSC2* RE under normoxia. Statistical analysis of differences in foldchange was by student's t test. Significance annotations above each bar on graph indicates significance of difference in foldchange between each condition and *TSC2* RE cells under normoxia. Pairwise statistical comparisons between *TSC2* (−/−) cells under normoxia or hypoxia and between *TSC2* (−/−) and *TSC2* RE cells under hypoxia are also annotated. Significance denoted by: * = p <0.05, ** = p <0.01, *** = p< 0.001, NS = not significant. Bars represent standard error of the mean. Predicted running band size (kDa) of protein targets can be found in chapter 2, table 2.6.

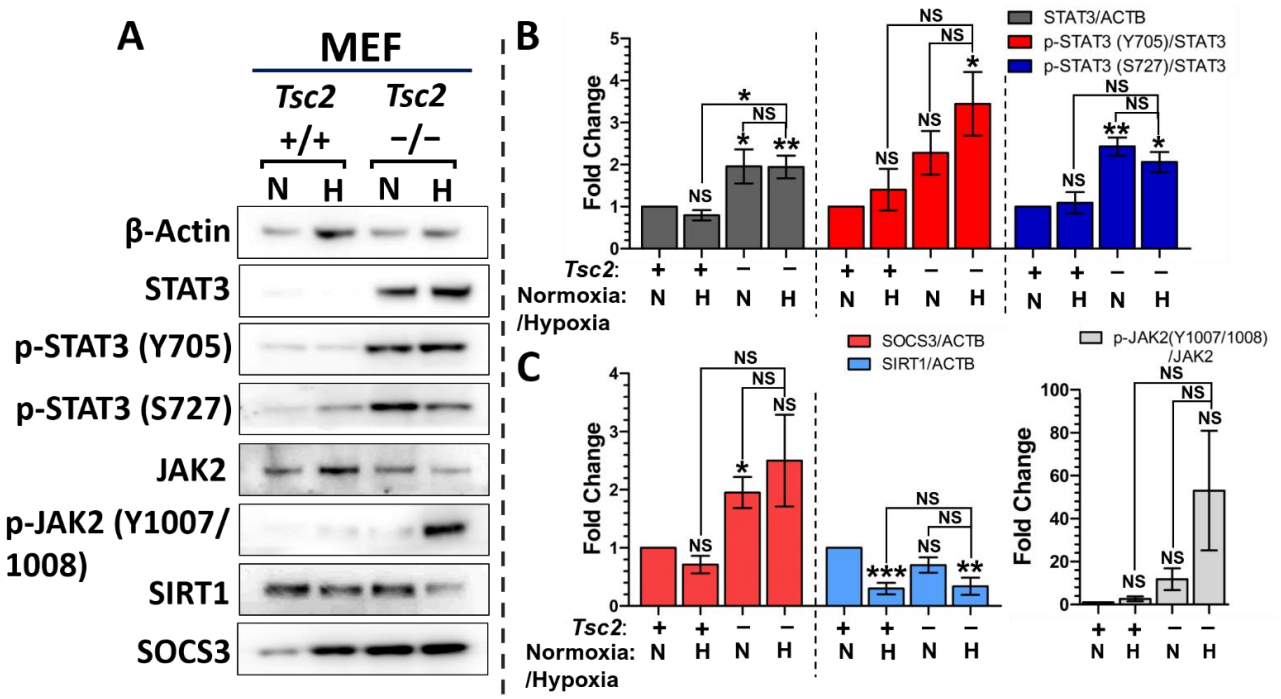


**Figure 5.2. Protein markers of STAT3 signalling are dysregulated upon loss of *Tsc2* within MEFs.** Either under normoxia (**N**, 21% $O_2$) or hypoxia (**H**, 1% $O_2$), MEF cells lacking *Tsc2* (***Tsc2-/-***) or with wildtype *Tsc2* (***Tsc2 +/+***) were cultured overnight before being lysed. Through western blotting protein lysates were then assayed for constituents of the STAT3 signalling pathway, with β-actin acting as a loading control. Panel **A** shows representative panel of the assayed protein targets in the MEF cell lines (N=3 minimum). Densitometry analysis of resulting western blot (N=3 minimum) was performed (panels **B** & **C**) and total proteins (STAT3, SIRT1, SOCS3) were normalised to β-actin and phosphorylated proteins were normalised to their respective total proteins. Resulting ratios were then expressed as fold changes compared to a designated control sample, in this case *Tsc2* +/+ under normoxia. Statistical analysis of differences in foldchange was by student's t test. Significance annotations above each bar on graph indicates significance of difference in foldchange between each condition and *Tsc2* +/+ cells under normoxia. Pairwise statistical comparisons between *Tsc2* −/− cells under normoxia or hypoxia and between *Tsc2* −/− and *Tsc2* +/+ cells under hypoxia are also annotated. Significance denoted by: * = p <0.05, ** = p <0.01, *** = p< 0.001, NS = not significant. Bars represent standard error of the mean. Predicted running band size (kDa) of protein targets can be found in chapter 2, table 2.6.

MEF cell lines. Hypoxia did not appear to elevate JAK2 phosphorylation further within the *TSC2* deficient AML line, whereas it did within the *Tsc2* −/− MEF line (figure 5.2 **A**). This increase in pJAK2 (Y1007/1008) was not found to be significant by densitometry analysis however (figure 5.2 **C**).

As can be seen by the western blot and densitometry analysis (figures 5.1 **C** and 5.2 **C**), only *Tsc2* −/− MEFs show elevated SOCS3 protein expression compared to the wildtype *Tsc2* +/+ MEFs, and only under normoxia was the difference in foldchange statistically significant by densitometry analysis. Hypoxia did not appear to significantly affect SOCS3 expression between either *TSC2* deficient/competent AML or MEF cell line. Densitometry analysis

showed decreased protein expression of SIRT1 within the *TSC2* deficient cells compared to their respective *TSC2* RE/WT cells cultured under normoxia (figures 5.1 **C** and 5.2 **C**), but the difference in foldchange was only reported as significant for *TSC2* deficient AML or MEF cells cultured under hypoxia relative to *TSC2* RE AML/*Tsc2* +/+ MEF cells cultured under normoxia. For *TSC2* RE AML and *Tsc2* +/+ MEF cells, hypoxia was found to significantly decrease SIRT1 expression relative to normoxia. Therefore, hypoxia but not loss of *TSC2* appears to downregulate protein expression of SIRT1 in AML and MEF cell lines.

### 5.2.2 Loss of *TSC2* within AML cells results in a gene expression pattern indicative of active STAT3 signalling.

The next aim of the present work was to assess whether hyperactive STAT3 signalling of *TSC2* deficient cells was reflected in gene expression changes. STAT3 can regulate the expression of a huge array of target genes. STAT3 target genes can differ markedly depending on the cell line and can be influenced by multiple physiological and pathogenic contexts (see chromatin immunoprecipitation sequencing studies: Synder *et al.* 2008, Durant *et al.* 2010 and McDaniel *et al.* 2017). Considering this variation of STAT3 regulated genes, expression of STAT3 gene targets that are key constituents of the STAT3 signalling pathway were assayed first. This panel of STAT3 signalling genes included *IL6R*, *PIAS3*, *SOCS3*, *STAT3* and *IL6*, which were assayed by qPCR within the AML cell lines.

As seen in figure 5.3, expression of *STAT3* and *IL6* is significantly upregulated upon loss of *TSC2*, irrespective of oxygen availability. Hyperactive STAT3 signalling is known to drive expression of *STAT3* and its associated regulatory genes, a mechanism to autoregulate its own expression and activation (Ichiba *et al.* 1998 and Narimatsu *et al.* 2001). STAT3 is known to drive *IL6* expression, one of its own activatory cytokines. STAT3 mediated IL6 expression is a well characterised feed-forward loop observed in cancers (Chang *et al.* 2013 and Yoon *et al.* 2012). With regards to the negative regulators of STAT3 signalling, *SOCS3* and *PIAS3*, their mRNA expression was found to be significantly upregulated in *TSC2* deficient AML cells cultured under normoxia or hypoxia relative to *TSC2* RE AML cells cultured under normoxia. However, neither *SOCS3* nor *PIAS3* mRNA expression in *TSC2* deficient AML cells was found to significantly different from *TSC2* RE AML cells cultured under hypoxia. Therefore, *TSC2* loss alone cannot be concluded to enhance mRNA expression of either *SOCS3* or *PIAS3*. Significantly upregulated expression of *SOCS3* upon loss of *TSC2* under normoxia is consistent with active STAT3 driven gene expression in these diseased cells however. *SOCS3* is a cytokine inducible gene, rapidly upregulated on STAT3 activation (Starr *et al.* 1997 and

Brender *et al.* 2001). Whilst *PIAS3* is thought of to be more constitutively expressed, its expression has been positively correlated with STAT3 activity (Borghouts *et al.* 2010).

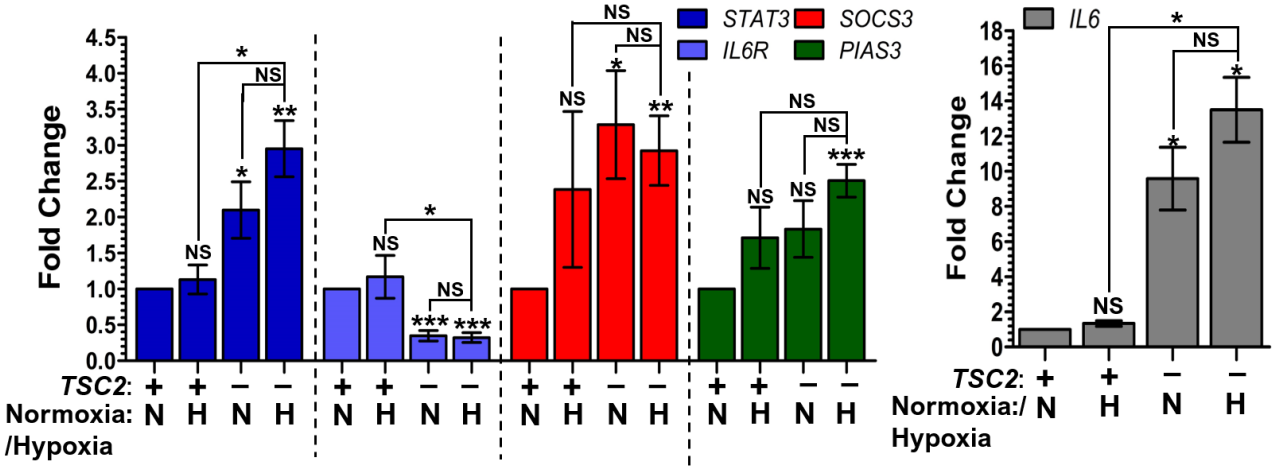


**Figure 5.3. Loss of *TSC2* in AML cells results in a gene expression pattern indicative of active STAT3 signalling.** Either under normoxia (**N**, 21% $O_2$) or hypoxia (**H**, 1% $O_2$), AML cells lacking *TSC2* (**TSC2 –**) or with *TSC2* re-expressed (***TSC2* +**) were cultured overnight before being lysed. Through qPCR, expression of target genes was quantified (N=3 minimum). Fold change in expression was calculated compared to a designated reference sample, in this case *TSC2* RE under normoxia. Fold changes of target genes were normalised to the housekeeping gene *HMBS*. Significance annotations above each bar on graph indicates significance of difference in foldchange between each condition and the reference sample (*TSC2* RE cells under normoxia). Pairwise statistical comparisons between *TSC2* deficient cells under normoxia or hypoxia and between *TSC2* deficient and *TSC2* RE cells under hypoxia are also annotated. Statistical analysis of differences in foldchange (N=3 minimum) was by student's t test. Significance denoted by: * = p <0.05, ** = p <0.01, *** = p< 0.001, NS = not significant. Bars represent standard error of the mean.

As seen in figure 5.3, expression of *IL6R* (IL6 receptor) was significantly downregulated upon loss of *TSC2*, irrespective of oxygen status. Normoxic versus hypoxic culture was found to have no significant effect on *IL6R* mRNA expression in either *TSC2* deficient AML or *TSC2* RE AML cells. Reduced expression of the activatory *IL6R* could be a compensatory mechanism by the *TSC2* deficient cells to dampen down hyperactive status of STAT3 signalling. This however would be in contrast to cancers were hyperactive STAT3 drives pathogenesis and has been correlated with increased *IL6R* expression (Tam *et al.* 2007 and Feng *et al.* 2016). Oxygen availability between *TSC2* deficient cells did not significantly affect the expression of genes assayed. Taken together, the expression pattern of these genes indicates increased STAT3 driven transcription within the *TSC2* deficient AML cells.

Looking more broadly at genes encoding constituents of STAT3 signalling beyond what was analysed by qPCR. The RNA sequencing data sets previously utilised in chapter 4, reveals the wider transcriptome of genes known to affect STAT3 activity are dysregulated within TSC

associated lesions and TSC model cells. That is genes whose products are STAT3 signalling cascade constituents, STAT3 stimulating cytokines/growth factors and their constituent receptors. This gene set (78 genes) was compiled through a literature search on STAT3 signalling component and regulatory genes and hence termed “STAT3 signalling genes”. As seen by volcano plots in figure 5.4 (**A** and **B**), for TSC associated brain lesions, that is subependymal nodules/ subependymal giant cell astrocytomas (SEN/SEGA) and cortical tubers (TUB), expression of “STAT3 signalling genes” are largely upregulated relative to normal brain tissue (NB). 37 of the 47 differentially expressed “STAT3 signalling genes” between SEN/SEGA and NB are upregulated. Less “STAT3 signalling genes” are upregulated within the TUB and NB. Of these 13 genes, 12 are upregulated in TUB relative to NB. Expression of “STAT3 signalling genes” appears less dysregulated within the renal AML lesions relative to normal kidney tissue (figure 5.4 **C**)., with 10 differentially expressed genes. Of those 6 are upregulated. The volcano plots in figure 5.5 show expression of “STAT3 signalling genes” is also largely upregulated upon loss of *TSC2* within AML (volcano plot **A**) and MEF (volcano plot **B**) cells. With the AML lines (cultured under normoxia) 26 of the 41 significantly differentially expressed “STAT3 signalling genes” are upregulated within *TSC2* −/− AML cells relative to AML cells in which *TSC2* has been re-expressed. Within the MEF lines, 23 of the 33 significantly differentially expressed “STAT3 signalling genes” are upregulated within *Tsc2* −/− MEF cells relative to *Tsc2* +/+ MEF cells. Therefore, if the protein expression data reflects what is seen within transcriptomic data, TSC cells within lesions and *TSC2* deficient cells may be propagating their own STAT3 signalling, through increased expression of STAT3 stimulatory cytokines for example.

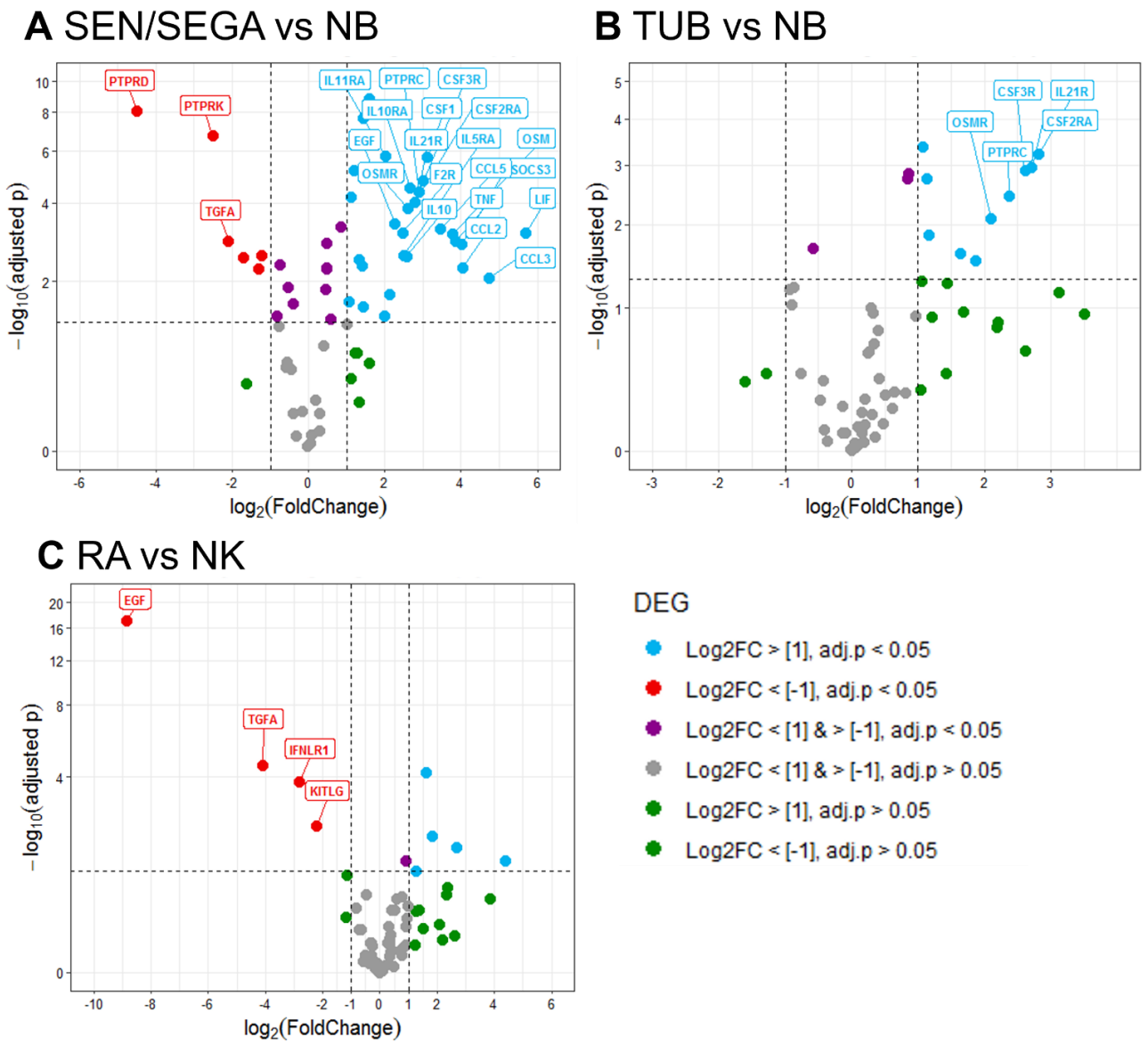


**Figure 5.4. Genes encoding constituents of the STAT3 signalling cascade, STAT3 activating cytokines/growth factors and their cognate receptors are dysregulated within TSC associated lesions.** Differential gene expression (DEG) comparison is annotated above each plot. Volcano plots were generated from previously published RNA sequencing data which Prof. Jeffrey MacKeigan kindly gave us access to. These data sets compare gene expression of donated TSC patient tumours samples versus non-TSC healthy tissue samples. In this case SEN/SEGA (Subependymal nodules/ Subependymal giant cell astrocytomas) (N=15) versus normal brain (N=8) (**A**), TUB (cortical tubers) (N=15) versus normal brain (N=8) (**B**) or renal AML (N=11) versus normal kidney (N=3) (**C**). See Martin *et al.* (2017) for methods on sample collection, data collection and DEG analysis. p-values from differential gene expression (DEG) analysis were corrected for multiple testing and false discovery by FDR method. Log2 transformed fold change in expression of genes was plotted against their -log10 transformed FDR adjusted p-values. Dotted lines at x axis represent increase or decrease in foldchange of 2 or -2 respectively. Dotted line at y axis represents significance threshold of 0.05.

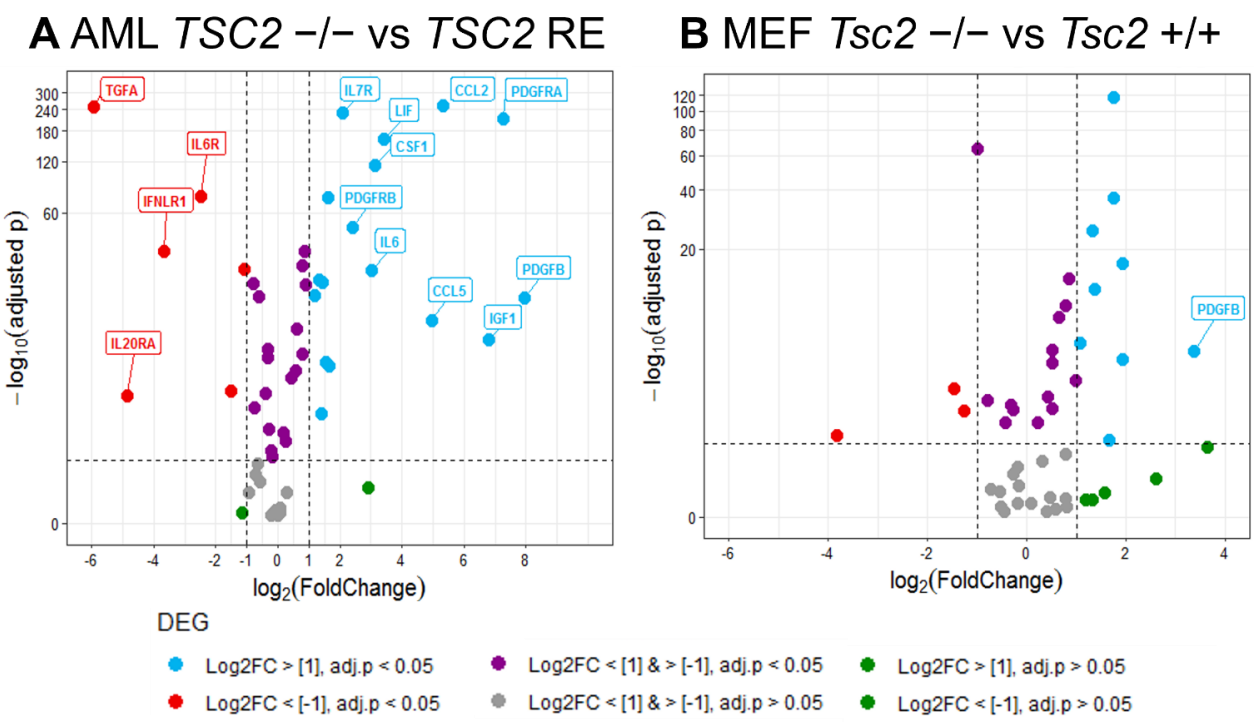


**Figure 5.5. Genes encoding constituents of the STAT3 signalling cascade, STAT3 activating cytokines/growth factors and their cognate receptors are dysregulated upon loss of *TSC2* in AML and MEF cells.** Volcano plots were generated from two separate RNA sequencing experiments conducted through Wales Gene Park, comparing either AML *TSC2* −/− and *TSC2* RE (re-expressed) (N=6) cells (**A**) or MEF *Tsc2*−/− and *TSC2* WT cells (N=3) (**B**). Expression levels were calculated and normalised from raw read counts as RPKM (Reads per Kilobase exon Model per million mapped reads). p-values from differential gene expression (DEG) analysis were corrected for multiple testing and false discovery by FDR method. Log2 transformed fold change in expression of genes (*TSC2* deficient cells against *TSC2* RE for AMLs or *Tsc2* WT for MEFs) was plotted against their -log10 transformed FDR adjusted p-values. Dotted lines at x axis represent increase or decrease in foldchange of 2 or -2 respectively. Dotted line at y axis represents significance threshold of 0.05.

### 5.2.3 STAT3 inhibitors in combination with rapamycin are more effective than each inhibitor alone in repressing STAT3 signalling related genes.

Following the finding that STAT3 signalling related genes were dysregulated between *TSC2* deficient and *TSC2* RE AML cells, the next aim of the present work was to examine how mTORC1 or STAT3 inhibition may alter gene expression of the STAT3 gene targets assayed in figure 5.3. Rapamycin was employed to inhibit mTORC1. Whilst FLLL31 and C188-9 were used to inhibit STAT3. STAT3 inhibitors were used as single drug treatments and then in combination with rapamycin.

mRNA expression of STAT3 target genes is graphed in figure 5.6, including *STAT3, IL6R, SOCS3, PIAS3* and *IL6*. In general, neither of the STAT3 inhibitor alone was sufficient to markedly change the expression of assayed STAT3 target genes. However, C188-9 treatment significantly downregulated the expression of *STAT3* mRNA and interestingly upregulated *IL6*

mRNA expression. FLLL31 alone, was ineffective at significantly affecting the expression of these known STAT3 regulated genes. mTORC1 inhibition, with rapamycin treatment, was observed to significantly downregulate *STAT3*, *IL6R* and *PIAS3* gene expression compared to the vehicle (DMSO) only control. Assuming these genes are still STAT3 driven within the context of TSC, then this effect could be due to a reduction in pS727 STAT3 (a known mTORC1 regulated phosphorylation site). It is known phosphorylation of STAT3 at S727 is required alongside phosphorylation at Y705 for fully transcriptionally active STAT3 (Wen *et al.* 1995). Furthermore, Dodd *et al.* (2015) demonstrated in the context of TSC that mTORC1 drives the transcription of *HIF1A* by directly phosphorylating STAT3 at S727. As seen in figure 5.6, *IL6* expression is substantially upregulated by treatment with C188-9 (fold change of 105). This marked foldchange of *IL6* gene expression might result from the relative increase of unphosphorylated STAT3 within the cell after C188-9 treatment. As it was observed that unphosphorylated STAT3 was able to drive expression of a subset of STAT3 regulated genes, including *IL6* (Yang *et al.* 2005 and Yang *et al.* 2007).

Directly inhibiting mTORC1 and STAT3 together, was found to be more effective at downregulating the expression of assayed genes in the *TSC2* deficient AML cells (figure 5.6).. Rapamycin in combination with C188-9 significantly downregulated *STAT3*, *IL6R, SOCS3* and *PIAS3* expression compared to the vehicle control and also to C188-9 alone in the case of *IL6*. One way ANOVA analysis reported significant overall differences in the expression of *STAT3, IL6R* and *IL6* between rapamycin, C188-9 and rapamycin + C188-9 treatments, but not for *SOCS3* or *PIAS3*. However, student's t tests reported the difference in the expression of *SOCS3* between rapamycin + C188-9 vs rapamycin treatments alone as being significant. Rapamycin in combination with FLLL31 significantly downregulated *STAT3*, *IL6R* and *PIAS3* expression compared to vehicle only control. One way ANOVA analysis showed significance in differences between STAT3 mRNA expression after treatment with rapamycin, FLLL31 and combined treatment with rapamycin and FLLL31 when compared to vehicle only control. Less stringent statistical analysis by student's t tests reported significance in expression of *IL6R* and *PIAS3* when comparing the combined treatment with rapamycin and FLLL31 versus the single drug treatment with FLLL31. Overall, efficacy of STAT3 inhibitors and rapamycin at significantly downregulating genes assayed appears to be greater with combination of drug treatments, perhaps due to repression of not only STAT3's S727 phosphorylation site by rapamycin, but also the Y705 phosphorylation site by either C188-9 or FLLL31.

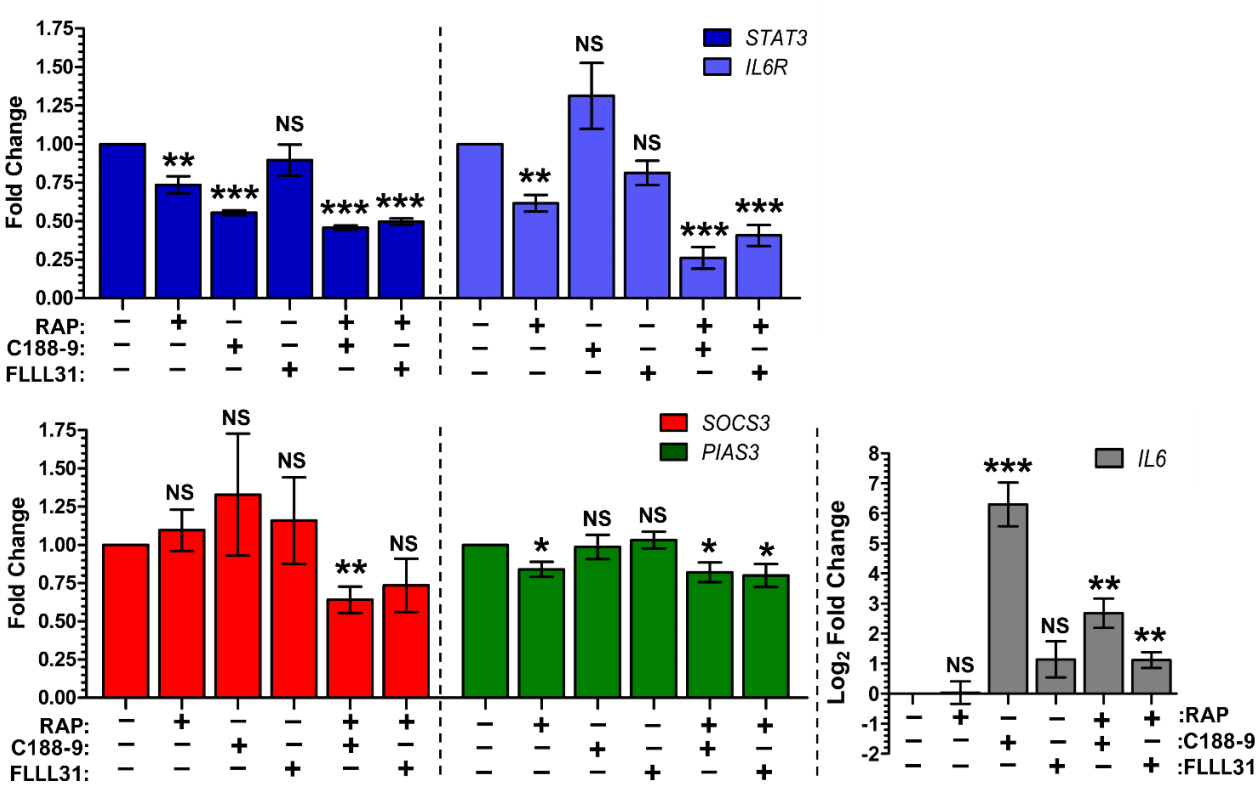


**Figure 5.6. qPCR reveals STAT3 and mTORC1 inhibition modulate dysregulated STAT3 signalling related genes within *TSC2* deficient AML cells.** *TSC2* deficient AML cells were cultured for 18 h in the presence of either DMSO, rapamycin (RAP) at 50 nM, C188-9 at 30 µM or FLLL31 10 µM alone or in combination before being lysed. Through qPCR, expression of target genes was quantified (N=3 minimum). Fold change in expression was calculated compared to a designated reference sample, in this *TSC2* deficient AML cells treated with vehicle (DMSO). Fold changes of target genes in samples were normalised to the housekeeping gene *IPO8*. Significance annotations above each bar on graph indicates significance of difference in foldchange between each condition and the reference sample (DMSO). Statistical analysis of differences in foldchange (N=3 minimum) was by student's t test. Significance denoted by: * = p <0.05, ** = p <0.01, *** = p< 0.001, NS = not significant. Bars represent standard error of the mean.

### 5.2.4. mTORC1 and STAT3 inhibition alter the amount of active nuclear STAT3 in *TSC2* deficient cells, but differentially between the AML and MEF cell lines.

As protein markers of STAT3 activity were found to be elevated upon loss of *TSC2*, the next aim of the present chapter was to assay whether this indication of increased STAT3 activity was reflected by an elevated level of STAT3 DNA binding. Figure 5.7 shows the results of experiments using the TransAM® STAT3 ELISA from Active motifs. These ELISA plates are coated in immobilised oligonucleotides containing STAT3 consensus sequences and therefore capture the transcriptionally active pool of STAT3 that can bind DNA in nuclear extracts. As expected from the increased presence of phosphorylated STAT3 at S727 and Y705 in *TSC2* deficient AML cells observed in figure 5.1 (**A**), the total amount of DNA bound STAT3 (nuclear active STAT3) is significantly higher in *TSC2* deficient AML cells when

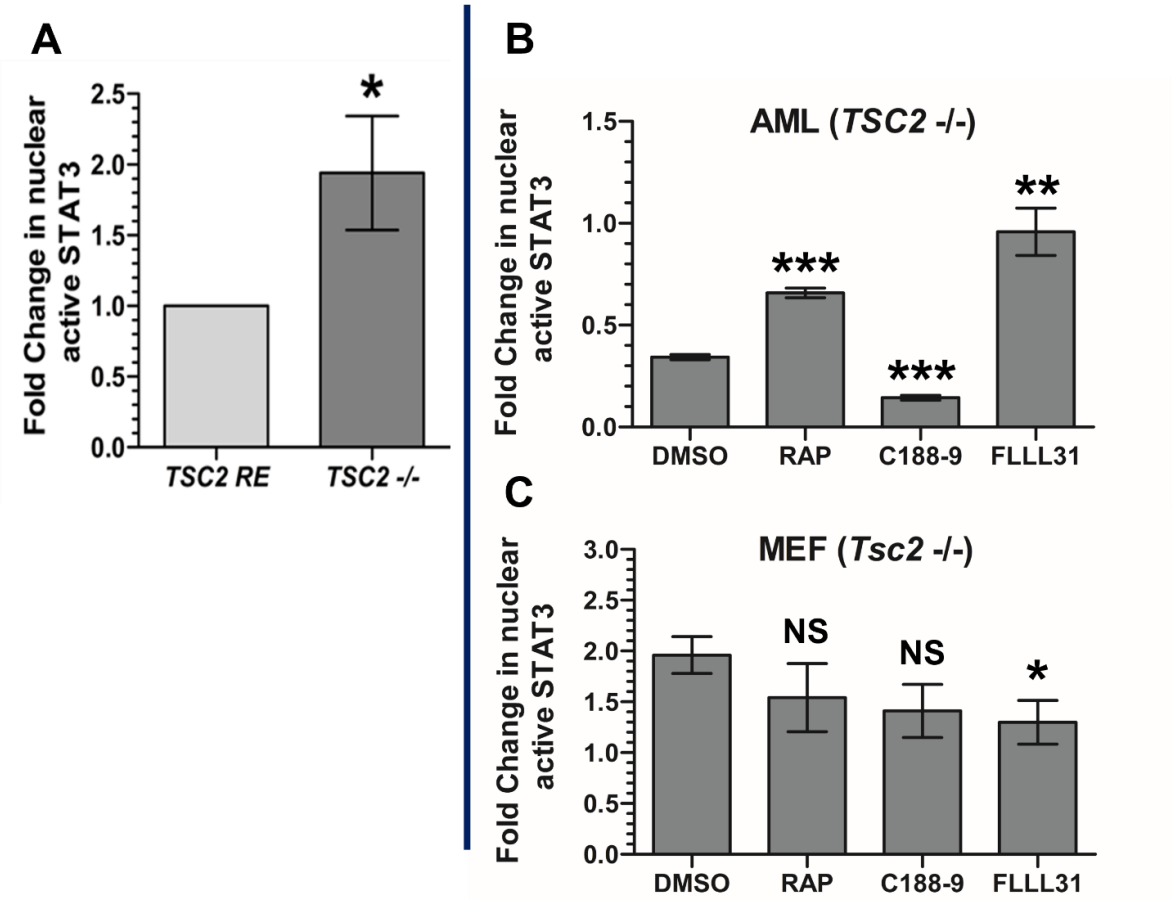


**Figure 5.7. Loss of *TSC2* increases active nuclear STAT3 within AML cells, whilst mTORC1 and STAT3 inhibition differentially effect the amount of nuclear active STAT3 within the *TSC2* deficient human and murine cell lines.** *TSC2* deficient (−/−) and *TSC2* RE cells were cultured overnight (**A**) or *TSC2*−/− AML (**B**) and *Tsc2* −/− MEF (**C**) cells were cultured in vehicle (DMSO), rapamycin (RAP) at 50 nM, C188-9 at 30 µM or FLLL31 at 5 µM for 16 h. Concentrated nuclear lysates were then generated and amount of DNA binding STAT3 (nuclear active STAT3) present in these extracts were assayed using Active Motifs TransAM® STAT3 ELISA. Graph **A** plots foldchange in nuclear active STAT3 of *TSC2* −/− cells compared to STAT3 *TSC2* RE cells (N=7). Graphs **B** and **C** plot foldchange in nuclear active STAT3 in treatment conditions compared to vehicle control (DMSO) (N=3). Significance annotations above each bar on graphs **B** & **C** indicates significance of difference in foldchange between each condition and the vehicle control (DMSO). Statistical analysis of differences in foldchange (**A** N=7, **B** and **C** N=3) was by student's t test. Significance denoted by: * = p <0.05, ** = p <0.01, *** = p< 0.001, NS = not significant. Bars represent standard error of the mean.

compared to the *TSC2* RE AML cells (figure 5.7 **A**). Treatment of *TSC2* deficient AML cells with rapamycin, didn't reduce nuclear active STAT3 relative to the vehicle only (DMSO) control, instead was observed to significantly increase nuclear active STAT3 (figure 5.7 **B**). Whilst within the *TSC2* deficient AML cells, the STAT3 inhibitors C188-9 and FLLL31 had opposing effects. C188-9 significantly reduced nuclear DNA bound STAT3, whilst FLLL31 surprisingly increased nuclear DNA bound STAT3 relative to the control. The opposing effects of C188-9 and FLLL31 on the amount of nuclear active STAT3 may reflect differences in drug

action on how they repress STAT3 activation in cells. mTORC1 and STAT3 inhibition in the *Tsc2* deficient MEF cells yielded different results (figure 5.7 **C**). The trend was for mTORC1 and STAT3 inhibition to reduce nuclear DNA bound STAT3. Statistical analysis showed that only FLLL31 treatment caused a significant reduction in nuclear DNA bound STAT3. As with the RNA sequencing analysis in section 5.2.3, these findings highlight there are distinct differences in aspects of STAT3 signalling and responsiveness to drug treatment in both the MEF and AML cell lines.

### 5.2.5 The STAT3 driven transcriptome is dysregulated within TSC associated lesions and *TSC2* deficient cells.

STAT3 target gene expression was also assayed on a transcriptomic level within RNA sequencing data sets previously utilised within chapter 4. Numerous studies have identified hundreds of experimentally validated STAT3 target genes (Mirzaei *et al*. 2021), with many more predicted based on presence of STAT3 binding consensus sequences within gene promoters. Therefore, the STAT3 target gene set used within the current work was manually compiled from well characterised STAT3 target genes and chromatin immunoprecipitation sequencing studies within the literature (see material and methods).

DEG analysis of RNA sequencing data comparing TSC lesions to non-TSC tissue, reveals many STAT3 target genes are differentially expressed in TSC associated lesions. This is most pronounced between SEN/SEGA lesions and non-TSC brain tissue, as shown by the volcano plot **A** in figure 5.8 and table 5.1. Over 66% of genes (138/207) within the STAT3 target gene set were significantly differentially expressed. Of those 138 significantly differentially expressed genes, 81 were upregulated and 57 were downregulated in SEN/SEGAs relative to normal brain tissue. As seen from table 5.1, and shown by volcano plots in supplemental figure S.5.1, far less genes within the STAT3 target gene set were dysregulated between cortical tubers/renal AML lesions and non-TSC tissue. 53 STAT3 target genes were significantly dysregulated within cortical tuber lesions, 36 upregulated and 17 downregulated, relative to normal brain tissue. 36 STAT3 target genes were significantly dysregulated within renal AML lesions, 16 upregulated and 21 downregulated. It should be quickly noted that expression was not detectable for all genes within the 214 gene STAT3 target gene set. Therefore, total number of detectable genes per comparison differs, as listed in table 5.1.

As with the TSC associated lesions, especially the SEN/SEGAs, AML cells deficient in *TSC2* showed dysregulated expression for majority of genes within the STAT3 target gene set. As can be seen from volcano blot **B** in figure 5.8. DEG analysis within the AML cell line RNA seq data reveals that over 71% of genes (124/174) within the STAT3 target gene set were significantly differentially expressed between *TSC2* −/− and *TSC2* RE AML cells. Of those 174

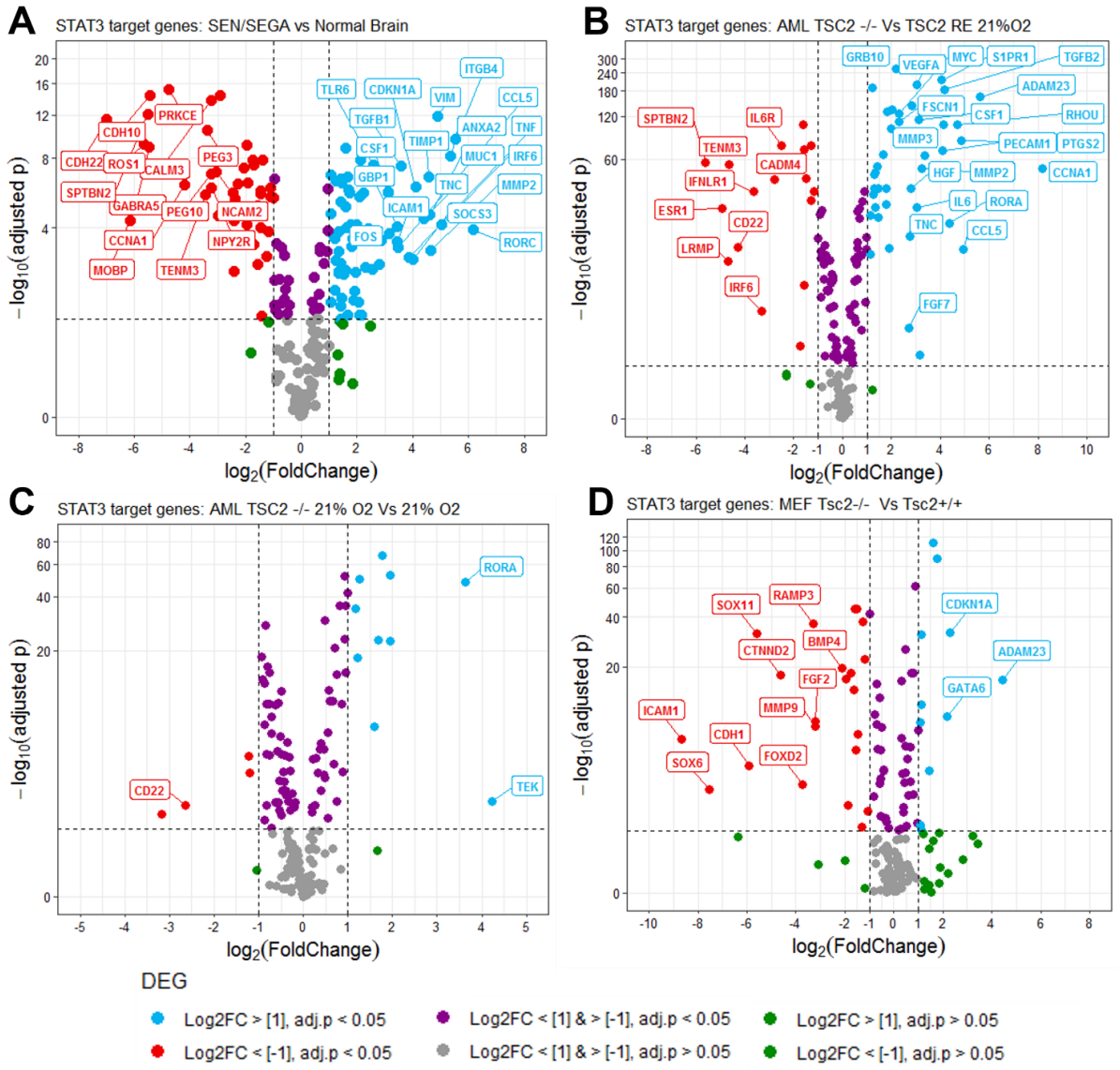


**Figure 5.8 Expression of STAT3 target genes are dysregulated in SEN/SEGA TSC lesions and within AML and MEF cells upon loss of *TSC2*.** Differential gene expression (DEG) comparison is annotated above each plot. Volcano plot **A** was generated from previously published RNA sequencing data which Prof. Jeffrey MacKeigan gave us access to. This data set compares gene expression of donated TSC patient tumours samples versus non-TSC healthy tissue samples. In this case SEN/SEGA (Subependymal nodules/ Subependymal giant cell astrocytomas) (N=15) versus normal brain (N=8). See Martin *et al*. (2017) for methods on sample collection, data collection and DEG analysis. Volcano plots **B** and **C** were generated from RNA sequencing data, comparing either AML *TSC2* deficient and *TSC2* RE (re-expressed) cells cultured under either normoxia (21% O2) or hypoxia (1% O2) (N=6). Volcano plot **D** was generated from RNA sequencing data comparing MEF *Tsc2* −/− and *Tsc2* +/+ (N=3) cells. RNA sequencing for volcano plots **B**, **C** and **D** was conducted through Wales Gene Park and expression levels were calculated and normalised from raw read counts as RPKM (Reads per Kilobase exon Model per million mapped reads) with DEG analysis generated through DEseq2 analysis and resulting p-values were corrected for multiple testing and false discovery by FDR method. For all volcano plots Log2 transformed fold change in expression of genes was plotted against their -log10 transformed FDR adjusted p-values. Dotted lines at x axis represent increase or decrease in foldchange of 2 or -2 respectively. Dotted line at y axis represents significance threshold of 0.05. Genes annotated had a Log2 fold change in expression greater or lower than 2 or -2 (i.e., fourfold higher or lower in expression) respectively and an -log10 adjusted p-value greater than 3 (i.e., below 0.001 significance threshold).

**Table 5.1 Comparison of STAT3 target gene DEG analysis between RNA sequencing data of TSC lesions vs non-TSC tissue, *TSC2* −/− AML vs TSC2 re-expressed (RE) AML cells and *Tsc2* −/− MEF vs *Tsc2* +/+ MEF cells**

| Comparison | Detectable genes (out of 214 genes) | Sig. differentially expressed genes | Sig. Upregulated (Log2FC = 0 – <1) | Sig. Upregulated (Log2FC = >1) | Sig. Downregulated (Log2 FC = >-1 – 0) | Sig. Downregulated (Log2 FC = <-1) |
|---|---|---|---|---|---|---|
| SEN/SEGA Vs normal brain | 207 | 138 | **11** | **70** | **15** | **42** |
| Cortical tuber Vs normal brain | 206 | 53 | **6** | **30** | **6** | **11** |
| Renal AML vs normal kidney | 207 | 36 | **1** | **15** | **2** | **19** |
| | | | | | | |
| *TSC2* −/− AML vs *TSC2* RE AML 21% $O_2$ | 174 | 124 | **32** | **41** | **34** | **17** |
| *TSC2* −/− AML vs *TSC2* RE AML 1% $O_2$ | 172 | 127 | **30** | **42** | **29** | **26** |
| *TSC2* −/− AML 1% $O_2$ vs 21% $O_2$ | 176 | 89 | **30** | **10** | **45** | **4** |
| | | | | | | |
| *Tsc2* −/− MEF vs *Tsc2* +/+ MEF 21% $O_2$ | 153 | 72 | **22** | **11** | **18** | **22** |

significantly differently expressed genes, 73 were upregulated and 51 were downregulated in *TSC2* −/− AML cells relative to AML cells in which *TSC2* was re-expressed. As shown by volcano plot **C** in figure 5.8, hypoxia does appear to affect STAT3 target gene expression within the *TSC2* −/− AML cells. As over 50% of genes (89/176) within the STAT3 target gene set are significantly differentially expressed between *TSC2* −/− AML cells cultured under normoxia (21% $O_2$) and hypoxia (1%$O_2$). With 40 genes upregulated and 49 genes downregulated in *TSC2* −/− AML cells cultured under hypoxia relative to those cultured under normoxia. However, as listed in table 5.1. Majority of those differentially expressed genes have $Log_2$ foldchanges between -1 and 1. Indicating that oxygen availability doesn't result in large sweeping changes to the STAT3 driven transcriptome within *TSC2* −/− AML cells. With the murine TSC cell model, the STAT3 driven transcriptome appears less dysregulated between *Tsc2* −/− and *Tsc2* +/+ MEFs than between the AML cell lines (volcano plot **D**, figure 5.8). Over 50% of the genes (89/176) within the STAT3 target gene set are still differentially expressed however. With 33 genes upregulated and 40 downregulated within the *Tsc2* −/− MEF cells relative to *Tsc2* +/+ MEF cells. However, comparatively less genes of those

significantly differentially expressed STAT3 target genes show $Log_2$ foldchanges >1 or <-1. Despite protein markers of STAT3 activity being elevated within both AML and MEF cell (figures 5.1 and 5.2). Regardless, STAT3 mediated transcription appears dysregulated upon *TSC2* loss in both AML and MEF cell lines, reflecting the dysregulated STAT3 mediated transcriptome observed in the clinically relevant SEN/SEGAs.

As shown in the heat map in figure 5.9, in which fold change in expression of STAT3 target genes that were significantly differentially expressed between *TSC2* −/− and *TSC2* RE AML cells (under either normoxia and hypoxia) and between at least one TSC lesion and corresponding non-TSC tissue, are displayed. The number of such genes 116, representing more than half the genes in the STAT3 target gene set. These STAT3 target genes dysregulated in common between *TSC2* deficient AML cells and TSC lesions are listed in table 5.2. Figure 5.9 does highlight however that there are variations in expression patterns of those genes among TSC associated lesions relative to their non-TSC tissue controls and crucially to this *in vitro* work, between TSC associated lesions and cellular models of TSC. Comparing the direction of fold changes (upregulated or downregulated) in STAT3 target genes between the *TSC2* −/− vs *TSC2* RE AML cells and SEN/SEGA vs NB data sets. With SEN/SEGA vs NB chosen for this comparison as this lesion data set is the one in which the most STAT3 target genes were differentially expressed. There are 85 significantly differentially expressed STAT3 target genes in common between both the *TSC2* −/− vs *TSC2* RE AML cells (normoxia) and SEN/SEGA vs NB data sets. Of these 85 genes, 49 are differentially expressed in the same direction (e.g., upregulated in both data sets), whilst 36 are differentially expressed in a different direction (e.g., upregulated in one data set, but downregulated in the other) between the two data sets. As for AML cells cultured under hypoxia, there are 90 significantly differentially expressed STAT3 target genes in common between both the *TSC2* −/− vs *TSC2* RE AML cells and SEN/SEGA vs NB data sets. Of these 90 genes, 48 are differentially expressed in the same, whilst 42 are differentially expressed in a different direction between the two data sets. Therefore *TSC2 −/−* cells cultured under hypoxia, are by in large, not more representative of the expression patterns observed in SEN/SEGA for STAT3 target genes.

Lastly, when comparing the *Tsc2* −/− vs *Tsc2* +/+ MEF cells to the SEN/SEGA vs NB data sets. There are 49 significantly differentially expressed STAT3 target genes in common between both the *Tsc2* −/− vs *Tsc2* +/+ MEF cells to the SEN/SEGA vs NB data set. Many less genes relative to the AML cells. Of those 49 genes, 21 are differentially expressed in the same direction, whilst 28 are differentially expressed in a different direction between the two data sets. The *Tsc2* −/− MEF cells therefore appear less representative of the dysregulated STAT3 driven gene expression seen in SEN/SEGA lesions than the *TSC2* −/− AML line. At

least for the genes assayed. Given the human and TSC patient origin of the AML lines, this is largely expected. These comparisons highlight that whilst STAT3 target gene expression appears dysregulated in both TSC lesions and TSC cell models, the *TSC2* deficient AML or MEF cells are not wholly representative of STAT3 driven transcriptome observed in patient lesions.

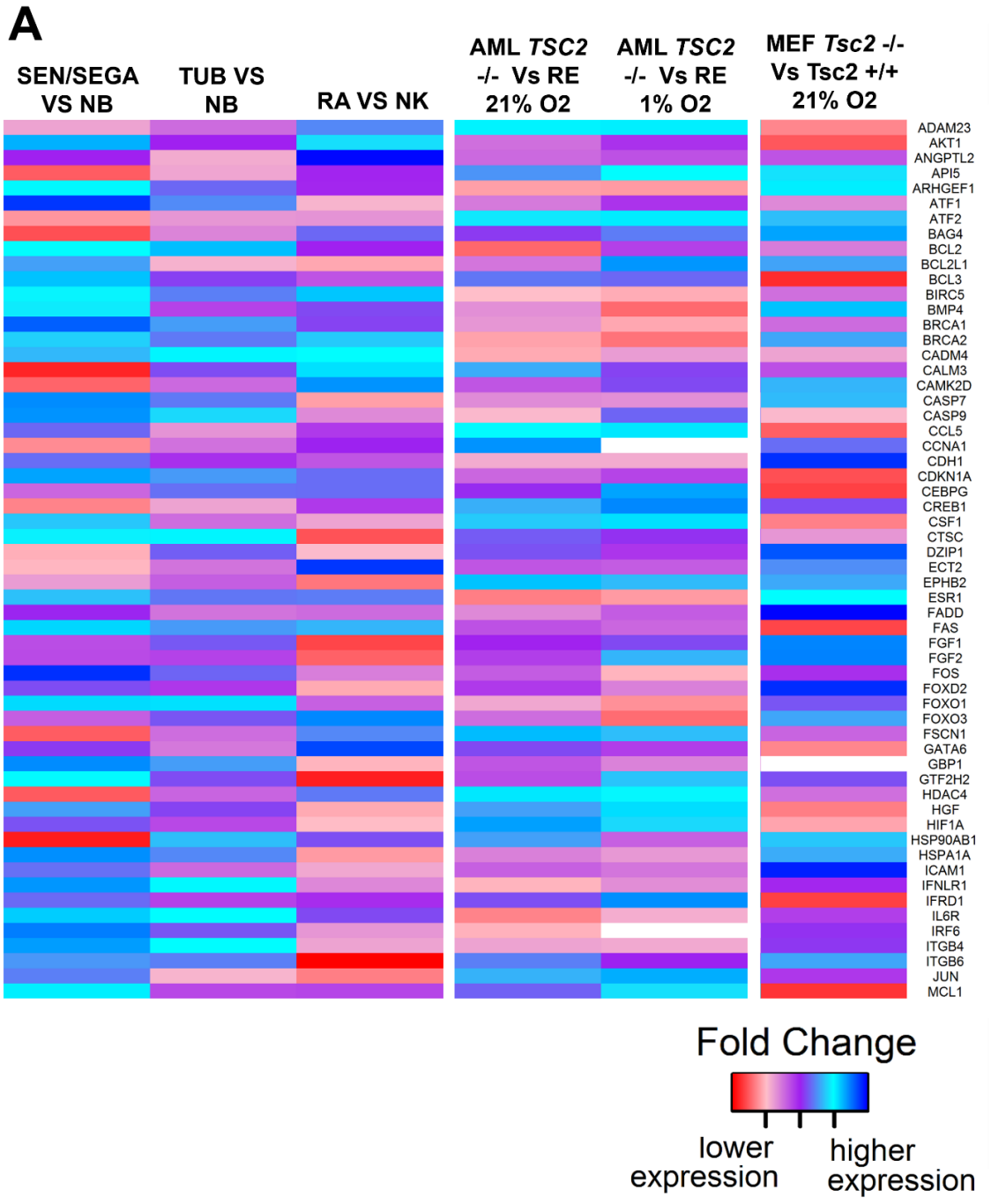


**Figure 5.9 STAT3 target gene set is differentially expressed between TSC tumour types, human and murine cell models lines of TSC.** Panels **A** and **B** belong to the same heatmap comparing fold change in expression of STAT3 target genes between either a TSC lesion and healthy tissue or a *TSC2* deficient cell line with a *TSC2* re-expressed (RE) (AML) or *Tsc2* +/+ (MEF) cell line. STAT3 target genes selected for the heatmap are those which are significantly differentially expressed between the *TSC2* −/− and *TSC2 RE* cell lines (under either oxygen conditions) and between at least one TSC lesion and healthy tissue. Differential gene expression (DEG) comparison is annotated above each column and the oxygen conditions, 21% $O_2$ (normoxia) or 1% $O_2$ (hypoxia), cell lines were cultured under is also denoted. White spaces within columns indicate that gene's expression was not detectable in that data set. Gene names are shown on the right of the heatmap. It should be noted these data sets are distinct and generated differently from one another (see methods and materials section). **SEN/SEGA** = subependymal nodule/Subependymal giant cell astrocytomas, **NB** = normal brain, **TUB** = TSC tuber, **RA** = renal angiomyolipoma, **NK** = normal kidney.

**Table 5.2. Many STAT3 target genes expression is dysregulated in both TSC lesions and in *TSC2* deficient AML cells.** STAT3 target genes below are those whose foldchange in expression between a lesion and its matched non-TSC tissue, or between *TSC2* deficient AML cells and *TSC2* expressed AML cells, were found significant.

| Dysregulated in TSC lesions only | | Dysregulated in cells only | | Dysregulated in both cells and at least one TSC lesion. | | | |
|---|---|---|---|---|---|---|---|
| *ADAM15* | *NF1* | *BATF* | *S1PR1* | *ADAM23* | *ECT2* | *MCM6* | *RBFOX2* |
| *ADAM8* | *NOS2* | *BATF2* | *SOX13* | *AKT1* | *EPHB2* | *MDM2* | *RORA* |
| *ANXA2* | *NPY2R* | *CCNA1* | *SRFBP1* | *ANGPTL2* | *ESR1* | *MMP2* | *RORC* |
| *BMP8A* | *PEG3* | *CCND1* | *TSG101* | *API5* | *FADD* | *MUC1* | *SIAH2* |
| *CCND2* | *POU2F1* | *CCND3* | | *ARHGEF1* | *FAS* | *MYC* | *SMAD5* |
| *CDH10* | *RAG1* | *CD22* | | *ATF1* | *FGF1* | *MYO5A* | *SMAD7* |
| *CDH2* | *ROS1* | *CDC25A* | | *ATF2* | *FGF2* | *NAV1* | *SMAD9* |
| *CDH22* | *SEMA3G* | *CDK1* | | *BAG4* | *FOS* | *NCAM2* | *SOCS3* |
| *CEBPA* | *SMAD1* | *CDON* | | *BCL2* | *FOXD2* | *NDRG3* | *SOX6* |
| *CTNNA2* | *SOX11* | *CLN6* | | *BCL2L1* | *FOXO1* | *NFKB1* | *SPTBN2* |
| *CTNND2* | *SOX2* | *CRTAM* | | *BCL3* | *FOXO3* | *NFKB2* | *STAT3* |
| *DNMT3A* | *TLR6* | *DNMT1* | | *BIRC5* | *FSCN1* | *NOTCH2* | *STMN1* |
| *FGFR1* | *TNF* | *FGF7* | | *BMP4* | *GATA6* | *PAXIP1* | *TCF12* |
| *FGFR1* | *TNFRSF1B* | *FOSL2* | | *BRCA1* | *GBP1* | *PCNT* | *TEK* |
| *FGL2* | *USP9X* | *GRB10* | | *BRCA2* | *GTF2H2* | *PDGFA* | *TENM3* |
| *FLT3* | | *HSP90AA1* | | *CADM4* | *HDAC4* | *PDIK1L* | *TGFB1* |
| *GABRA5* | | *IL1B* | | *CALM3* | *HGF* | *PECAM1* | *TGFB2* |
| *IGF2R* | | *IL6* | | *CAMK2D* | *HIF1A* | *PEG10* | *TGFBR3* |
| *IGHMBP2* | | *ITGA11* | | *CASP7* | *HSP90AB1* | *PIAS3* | *TIMP1* |
| *IL10* | | *JAK2* | | *CASP9* | *HSPA1A* | *PIK3R1* | *TNC* |
| *IL23A* | | *LRMP* | | *CCL5* | *ICAM1* | *PIM2* | *TNFRSF1A* |
| *IL23A* | | *MCM2* | | *CCNA1* | *IFNLR1* | *PORCN* | *TP53* |
| *INSM1* | | *MCM7* | | *CDH1* | *IFRD1* | *PRKACA* | *TWIST1* |
| *IRF4* | | *MMP1* | | *CDKN1A* | *IL6R* | *PRKCE* | *TXK* |
| *JUNB* | | *MMP3* | | *CEBPG* | *IRF6* | *PTGS2* | *VAV2* |
| *LTBP1* | | *NOTCH4* | | *CREB1* | *ITGB4* | *PTK2* | *VEGFA* |
| *MOBP* | | *PAWR* | | *CSF1* | *ITGB6* | *RAMP3* | *VIM* |
| *NCAM2* | | *PIM1* | | *CTSC* | *JUN* | *RASA3* | *XBP1* |
| *NDN* | | *RHOU* | | *DZIP1* | *MCL1* | *RB1* | *ZEB1* |

### 5.2.6. Phospho-markers of active STAT3 signalling fluctuate in *TSC2* deficient AML and MEF cells over the course of C188-9 and FLLL31 treatment.

Following on from section 5.3.4, whereby inhibiting STAT3 with either C188-9 or FLLL31 produced opposing effects on nuclear accumulation of STAT3 within *TSC2* deficient AML cells (figure 5.7 **B**), which wasn't reproduced in the *Tsc2* −/− MEF cells (figure 5.7 **C**), the effects of these inhibitors on markers of STAT3 activity over time within the two *TSC2* deficient cell lines was assayed. As can be seen from the blot panels and densitometry plots in figures 5.10 and 5.11, neither treatment with C188-9 or FLLL31 consistently repress the levels of phosphorylated STAT3 and JAK2 (pSTAT3 Y705, pSTAT3 S727 and pJAK2 Y1007/1008) throughout course of treatment in either cell line. Instead, not only do the relative amounts of these markers compared to the DMSO control tend to fluctuate over time with C188-9 or FLLL31 treatment, but the efficacy of these inhibitors at the concentrations used to repress each phospho-marker differs between cell lines.

As seen in figure 5.10 and 5.11, phosphorylation of STAT3 at Y705 is almost entirely abolished at 0.5 h in *TSC2* deficient AML and MEF cells treated with either C188-9 or FLLL31. It was observed that pY705 STAT3 started to recover under both C188-9 and FLLL31 treatments in both cell lines. By 8 h of C188-9 treatment in the AML line (figure 5.10 **B**) and 16 h in the MEF line (figure 5.11 **B**), the relative amount of pSTAT3 Y705/DMSO had enhanced to a level that was comparable to the DMSO control. As seen by blots for pSTAT3 Y705, at a longer duration of treatment with C188-9 at 24 h in both *TSC2* deficient cell lines, pSTAT3 Y705 was markedly reduced. This shows that C188-9 treatment has a bi-phasic drug response in both cell lines. Unlike with C188-9 treatment, densitometry analysis found at 24 h of FLLL31 treatment in both *TSC2* deficient cell lines (figures 5.10 **B** and 5.11 **B**), pSTAT3 Y705/STAT3 had enhanced to a level similar to the DMSO control. Despite the blots within the AML line showing a decreased level of pSTAT3 Y705 at 24 h (figure 5.10 **A**). For longer term inhibition of STAT3 phosphorylation at Y705, C188-9 does appear the more effective STAT3 inhibitor. These findings imply a difference in the sensitivity to STAT3 inhibition through FLLL31 and C188-9 between the AML and MEF models of TSC.

The relative amount of pJAK2 Y1007/1008 in both *TSC2* deficient cell lines isn't immediately repressed in either cell line, by either FLLL31 or C188-9. As seen by the blot panels, only after 4 h was FLLL31 treatment effective at blocking pJAK2 Y1007/1008 (figures 5.10 **A** and 5.11 **A**), which is surprising given that FLLL31 targets not only the SH2 domain of STAT3 but also JAK2 (Lin *et al.* 2010). Densitometry analysis found a longer duration of C188-9 treatment, 8 h, to reduce pJAK2 Y1007/1008/ACTB in both cell lines (figures 5.10 **B** and 5.11 **B**). It is therefore evident, that within *TSC2* deficient cells both STAT3 inhibitors require a longer treatment duration to establish a steady inhibition of the JAK2/STAT3 pathway.

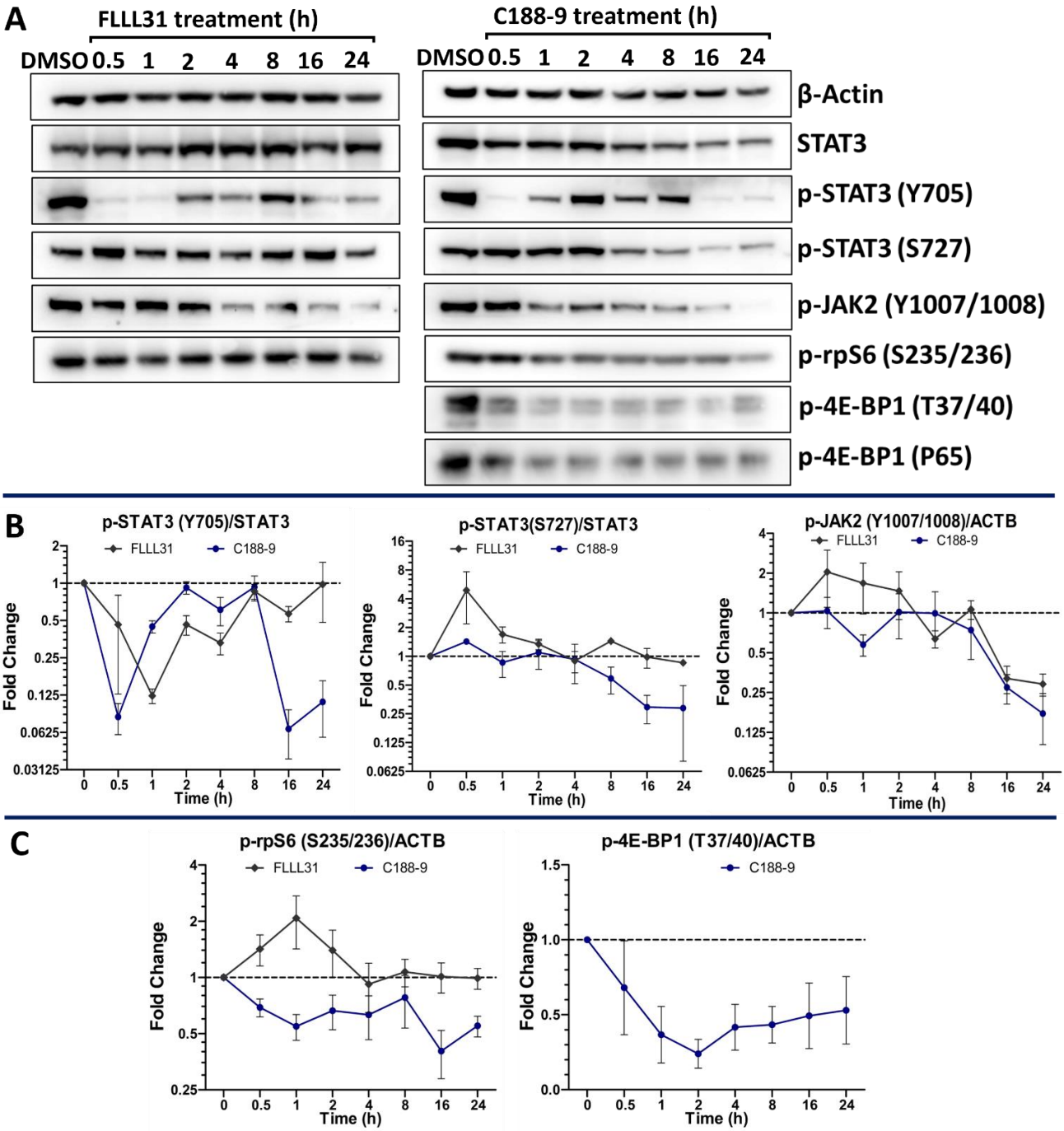


**Figure 5.10**. **FLLL31 and C188-9 differ in their ability to repress phospho-markers of active mTORC1 and STAT3 pathways over time in *TSC2* deficient AML cells.** *TSC2* deficient AML cells were treated with either vehicle (DMSO), C188-9 (30 μM) or FLLL31 (10 μM). Cells treated with DMSO (control) were lysed at time 0 h, whilst C188-9 and FLLL31 treated cells were lysed at the time indicated. Protein lysates were then assayed through western blotting (panel **A**) (N=3 minimum), with β-actin acting as a loading control. Densitometry analysis of resulting western blots (N=3 minimum) (**B** & **C**) was performed, phosphorylated STAT3 was normalised to total STAT3 and phosphorylated JAK2, rpS6 & 4E-BP1 were normalised to β-Actin. Resulting ratios were then expressed as fold changes compared to DMSO control and plotted, to show change in fold change during treatment time in respect to the control. Dotted line on graphs represents DMSO control fold change, i.e., 1.00. Bars represent standard error of the mean. Predicted running band size (kDa) of protein targets can be found in chapter 2, table 2.6.

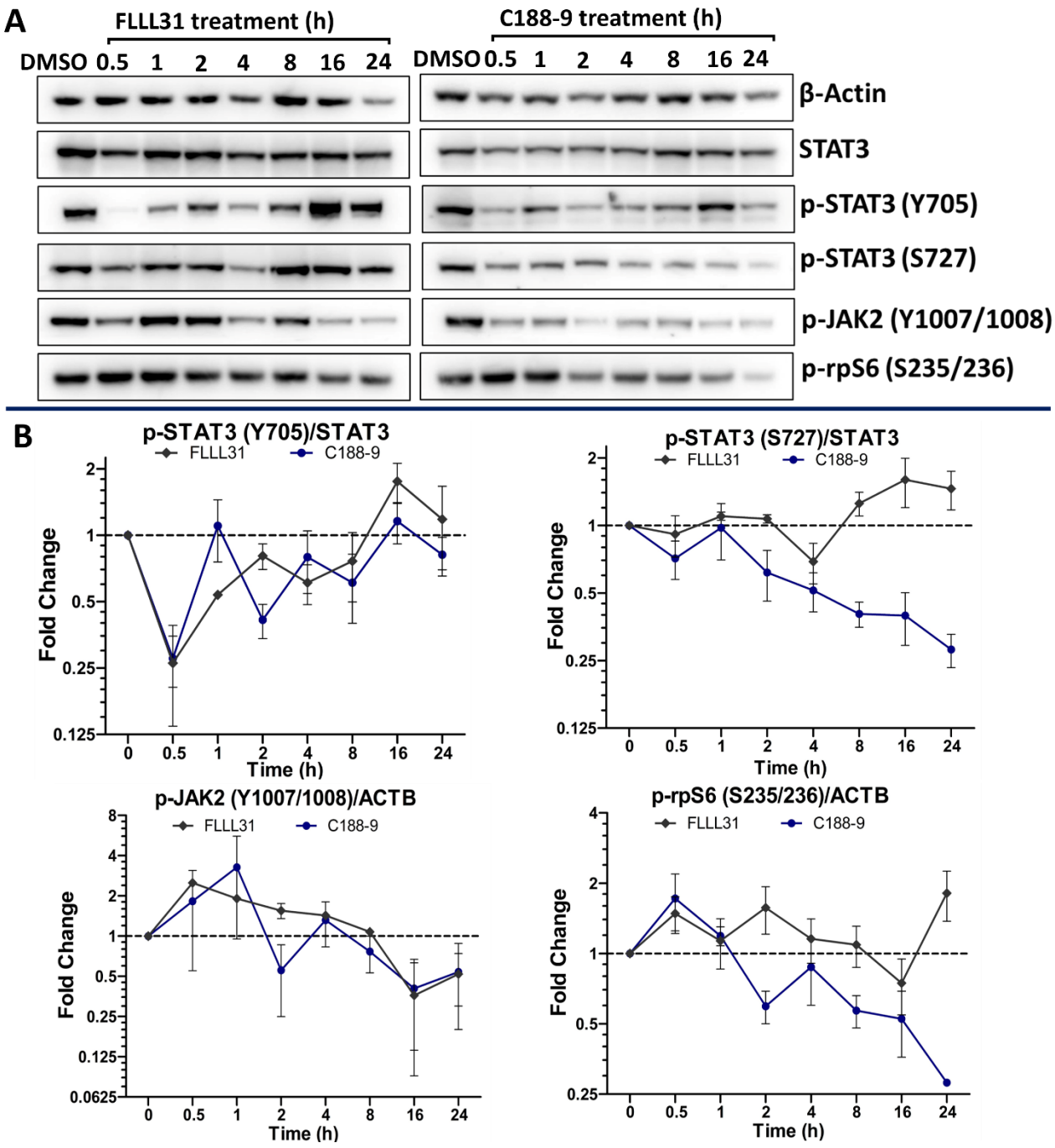


**Figure 5.11. FLLL31 and C188-9 differ in their ability to repress phospho-markers of active mTORC1 and STAT3 pathways over time in *Tsc2* −/− MEF cells.** *Tsc2* −/− MEF cells were treated with either vehicle (DMSO), C188-9 (30 µM) or FLLL31 (10 µM). Cells treated with DMSO (control) were lysed at time 0 h, whilst C188-9 and FLLL31 treated cells were lysed at the time indicated. Protein lysates were then assayed through western blotting (panel **A**) (N=3 minimum, with β-actin acting as a loading control. Densitometry analysis of resulting western blots (N=3 minimum) (**B**) was performed, phosphorylated STAT3 was normalised to total STAT3, phosphorylated JAK2 and rpS6 were normalised to β-Actin. Resulting ratios were then expressed as fold changes compared to DMSO control and plotted, to show change in fold change during treatment time in respect to the control. Dotted line on graphs represents DMSO control fold change, i.e., 1.00. Bars represent standard error of the mean. Predicted running band size (kDa) of protein targets can be found in chapter 2, table 2.6.

Over the treatment time, FLLL31 doesn't significantly reduce the level of pSTAT3 S727 in either cell line. Treatment with C188-9 was much more effective at later time points, causing a marked reduction in pSTAT3 S727. Densitometry analysis reveals reduction in levels of pSTAT3 S727/STAT3 relative to the DMSO control was not immediate (figures 5.10 **B** and 5.11 **B**). Occurring after 1 h in the MEF line and 4 h in the AML line. This suggests C188-9 isn't directly inhibiting this phospho-site. Which is consistent with how C188-9 targets STAT3, by binding the phosphotyrosine (pY) peptide binding site (Xu *et al.* 2009 and Redell *et al.* 2011), whilst the S727 site is located within the transactivation domain (Mishra *et al.* 2021). Instead, C188-9 may target the kinases responsible for phosphorylating STAT3 at S727, of which mTORC1 is one (Yokogami *et al.* 2000).

Consistent with the idea that C188-9 may be inhibiting mTORC1 is that C188-9, but not FLLL31, decreases the levels of phosphorylated rpS6 within both AML and MEF cell lines over the course of treatment (figures 5.10 **A/C** and 5.11 **A/B**). Phosphorylation of rpS6 at S235/236 is a marker of increased mTORC1 activity (Magnunson *et al.* 2012), as mTORC1 signalling activates rpS6's kinase; S6K1. In the AML line p-rpS6 (S235/236)/ACTB decreases immediately at 0.5 h of C188-9 treatment, remaining at a similar level throughout the course of treatment (figure 5.10 **A/C**). Whereas in the MEF line the level of p-rpS6 (S235/236)/ACTB decreases after 1 h, and then further decreases over the course of treatment (figures 5.11 **A**/**B**). At 1 h, the difference in the relative amount of p235/236 rpS6 between the C188-9 treated AML and MEF line is statistically significant (FC = 0.54 vs 1.19, p = 0.0186). This finding suggests that C188-9 may directly inhibit mTORC1 in *TSC2* deficient AML cells, but indirectly in *Tsc2* −/− MEF cells. Given the unexpected action of C188-9 to repress phosphorylation of rpS6. The effect of C188-9 treatment on 4E-BP1 phospho-markers of mTORC1 activity was assayed within the *TSC2* deficient AML cell line. Shown in figure 5.10 (**A**). As was the case with rpS6 phosphorylation, C188-9 treatment decreased the levels of both p4E-BP1 (T37/40) and p4E-BP1 (P65). As shown by the densitometry analysis (figure 5.10 **C**). Levels of p4E-BP1 (T37/40) decreased immediately on C188-9 treatment (0.5 h), reaching the lowest of point at 2 h. A complete N of 3 was not gathered for p4E-BP1 (P65) on C188-9 treatment, and therefore densitometry analysis was not performed. The decrease in not only rpS6 phosphorylation but that of 4E-BP1 on C188-9 treatment does indicate C188-9 is likely inhibiting mTORC1.

### 5.2.7. Long term treatment of *TSC2* deficient AML and MEF cells with rapamycin results in contrasting effects on S727 and Y705 phosphorylation of STAT3

Rapamycin is known to impact the mediators of the immune response (Arriola *et al.* 2016), generally depressing the immune system which was the rational for its use an immunosuppressant (Chang *et al.* 1991). In healthy individuals STAT3 is involved in regulating many normal immune and inflammatory processes within the body, but is also heavily implicated in driving pathogenesis in many cancers (Villarino *et al.* 2015); including through cross talk with the mTORC1 pathway (Wang *et al.* 2020a, He *et al.* 2014 and Morelli *et al.* 2021). Within the context of TSC, mTORC1 has been shown to promote STAT3 driven transcription of *HIF1A* through phosphorylating STAT3 at the S727 site (Dodd *et al.* 2015). From our previous findings, rapamycin treatment decreased STAT3 driven gene expression (section 5.2.3), especially in concert with C188-9, but increased nuclear accumulation of STAT3 (section 5.2.4). Given these opposing effects of rapamycin on two measures of active STAT3 signalling, how long term rapamycin treatment affected the phospho-markers of active STAT3 in the AML and MEF cell models of TSC was assayed.

Consistent with how phospho-markers of mTORC1 activity differ in their sensitivity to rapamycin, control blots (figure 5.12 **A**) of phosphorylated rpS6 and 4E-BP1 indicate rapamycin is inhibiting mTORC1 as predicted over long term treatment. That is rapamycin treatment results in rapid repression of mTORC1 regulated phosphorylation events: rpS6 phosphorylation at S235/236, 4E-BP1 phosphorylation and STAT3 phosphorylation at S727. Repression of these mTORC1 regulated sites was maintained over the 72 h duration of rapamycin treatment in both *TSC2* deficient lines. Phosphorylation of 4E-BP1 at T37/40 was much more resistant to rapamycin treatment, as seen in by densitometry analysis (figure 5.12 **C**), which has been previously reported (Choo *et al.* 2008). These blots confirm mTORC1 inhibition via rapamycin is consistent throughout the time course of treatment.

Over the entire course of treatment rapamycin did not significantly affect total STAT3 protein relative to the control in either the *TSC2* deficient AML or MEF cell lines (by densitometry analysis, N=3). As seen by the blot panels and accompanying densitometry plots in figure 5.12 (**B**), in both cell lines rapamycin treatment substantially increased the relative amount of pY705 STAT3 compared to the DMSO control. pY705 STAT3/STAT3 initially peaked at 2 h of rapamycin treatment for both cell lines and then reached a maximum at 16 h for the AML line and 24 h for the MEF lines. However, differences in the relative amount of pY705 STAT3 compared to the control between AML and MEF cell lines at 16 h and 24 h was not found to be significant. The relative amount of pY705 STAT3 doesn't increase in either cell line until after 1 h, which suggests this is a secondary effect of rapamycin treatment. Potentially through upregulating expression of an activatory protein that increases pY705 STAT3 in an autocrine

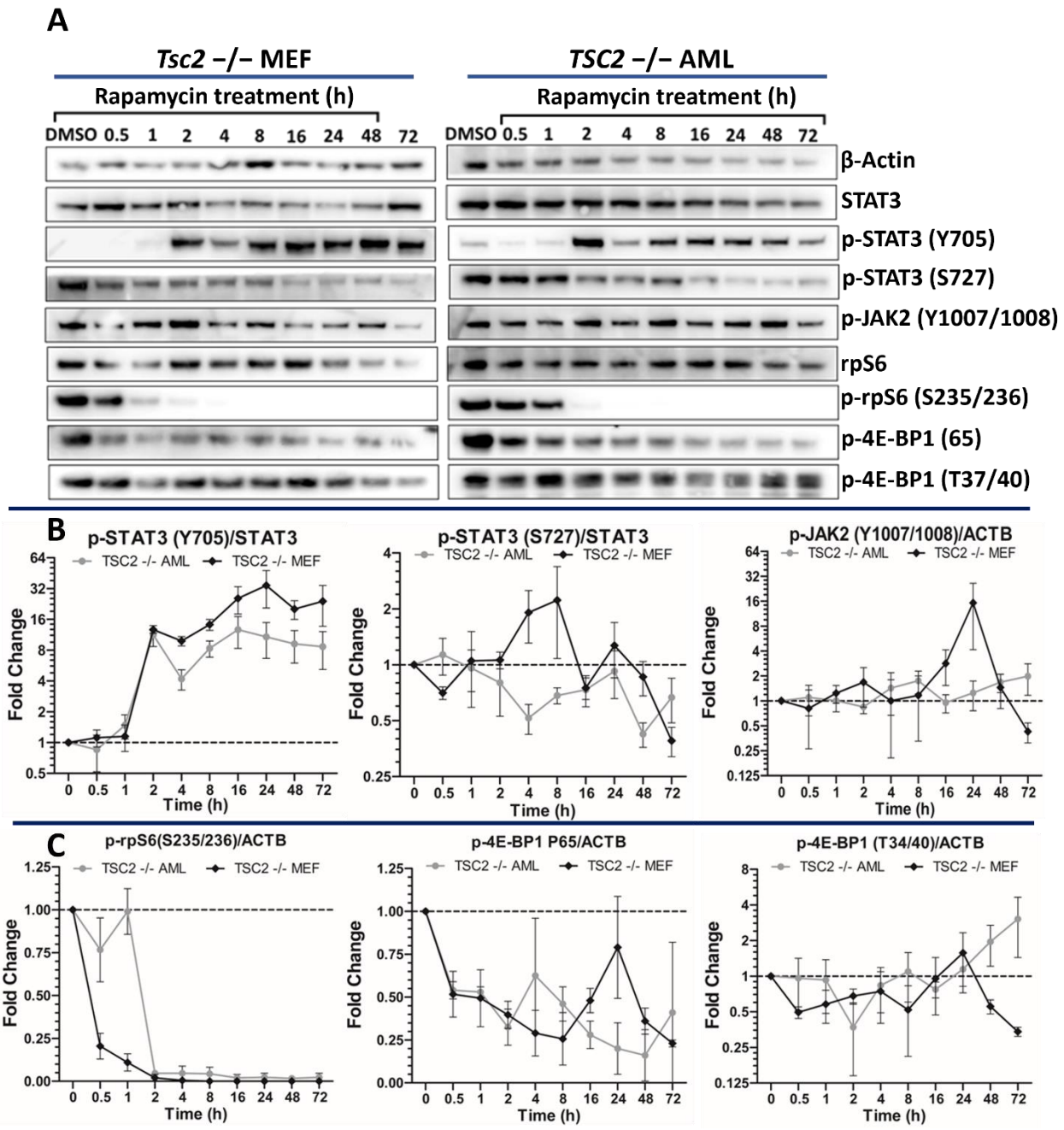


**Figure 5.12. Long term treatment of *TSC2* deficient AML and MEF cells with rapamycin results in contrasting effects on S727 and Y705 phosphorylation of STAT3.** Either *TSC2* deficient AML or MEF cells were treated with either vehicle (DMSO) or rapamycin (50 nM). Cells treated with DMSO (control) were lysed at time 0 h, whilst C188-9 and FLLL31 treated cells were lysed at the time indicated. Protein lysates were then assayed through western blotting (panel **A**) (N=3 minimum), with β-actin acting as a loading control. Densitometry analysis of resulting western blots (N=3 minimum) (**B** & **C**) was performed, phosphorylated STAT3 was normalised to total STAT3 and phosphorylated JAK2, rpS6 and 4E-BP1 were normalised to β-Actin. Resulting ratios were then expressed as fold changes compared to DMSO control sample and plotted, to show change in fold change during treatment time in respect to the control. Dotted line on graphs represents DMSO control sample fold change, i.e., 1.00. Bars represents standard error of the mean. Predicted running band size (kDa) of protein targets can be found in chapter 2, table 2.6.

manner. As seen from the blot panels in figure 5.12 (**A**), rapamycin results in immediate repression of phosphorylation of STAT3 at S727 in the MEF cells, and after 2 h in the AML cells. From the blots, pS727 remains low throughout rapamycin treatment course. However, when pS727 is normalised to total STAT3, the plots of the densitometry (figure 5.12 **B**) show pS727 fluctuates of time with rapamycin treatment. Especially in the MEF line, where the densitometry graph indicates phosphorylation of STAT3 at S727 is only repressed at time 2 and 72 h. How true this observation is within the MEF line is questionable, as mTORC1 is known to phosphorylate STAT3 at S727 (Yokogami *et al.* 2000) and mTORC1 is consistently inhibited by rapamycin throughout the treatment time course. Although other kinases modulating S727 phosphorylation of STAT3 beyond the scope of this work cannot be ruled out. Additionally, for the MEF cell lines in this experiment, N2 pS727 and total STAT3 blots were of low quality and in general different from N1 and N3, potentially skewing the normalisation of pS727 to total STAT3. The relative amounts of pJAK2 (Y1007/1008) remained comparable to the control throughout the majority of rapamycin treatment (figures 5.12 **A** and **B**). Increase in pY1007/1008 JAK2 at times 16 and 24 h with the MEF cell lines was not significant, nor was the change in pY1007/1008 JAK2 compared to the control at any other time aside from at 72 h in the MEF line. Therefore, treatment with rapamycin doesn't appear to influence levels of pJAK2 (Y1007/1008) in either *TSC2* deficient AML or MEF cells. In summary, mTORC1 inhibition through rapamycin does appear to affect STAT3 activity in *TSC2* deficient cells at the level of phosphorylation markers, reflecting the observations that mTORC1 inhibition effects the DNA binding of STAT3 also.

### 5.2.8 Co-treatment *TSC2* deficient cells with rapamycin and C188-9 limits the elevation of pSTAT3 Y705 seen on rapamycin treatment alone.

Treatment of either of the *TSC2* deficient AML or MEF cell lines with rapamycin elevated levels of STAT3 phosphorylated at Y705 (Y705 pSTAT3) (figure 5.13). And within the *TSC2* deficient AML cell line, rapamycin appeared to elevate the level of nuclear DNA bound STAT3 (figure 5.7 **B**). Rapamycin therefore appears to have some undesirable effects on markers of STAT3 activity. C188-9 treatment on the other hand largely repressed levels of pSTAT3 Y705 in *TSC2* deficient cells (figures 5.10. and 5.11). Therefore, the next aim of the present work was to assess, via western blotting, the effect of co-treating *TSC2* deficient cells with both rapamycin and C188-9 on phosphorylation markers of STAT3 activity. In particular assessing if co-treatment could control for increases in pSTAT3 Y705 observed when treating with rapamycin alone. Additionally, as C188-9 treatment appeared to decrease mTORC1 substrate phosphorylation. Whether co-treatment with both rapamycin and C188-9 further represses mTORC1 activity further than either inhibitor alone will be assayed.

As seen in figure 5.13 **A**, co-treatment with rapamycin and C188-9 decreases the expression of total STAT3 over time relative to the DMSO control within both the *TSC2* deficient MEF and AML cells. As with C188-9 treatment of the *TSC2* deficient AML line (figure 5.10 **B**), densitometry analysis found decreases in total STAT3 at later time points as not significant. However, blots for total STAT3 were consistent across biological repeats. As with rapamycin treatment and C188-9 treatment alone, co-treatment with C188-9 and rapamycin repressed phosphorylation of STAT3 at S727 (S727 pSTAT3) ((figure 5.13 **A**). With levels of S727

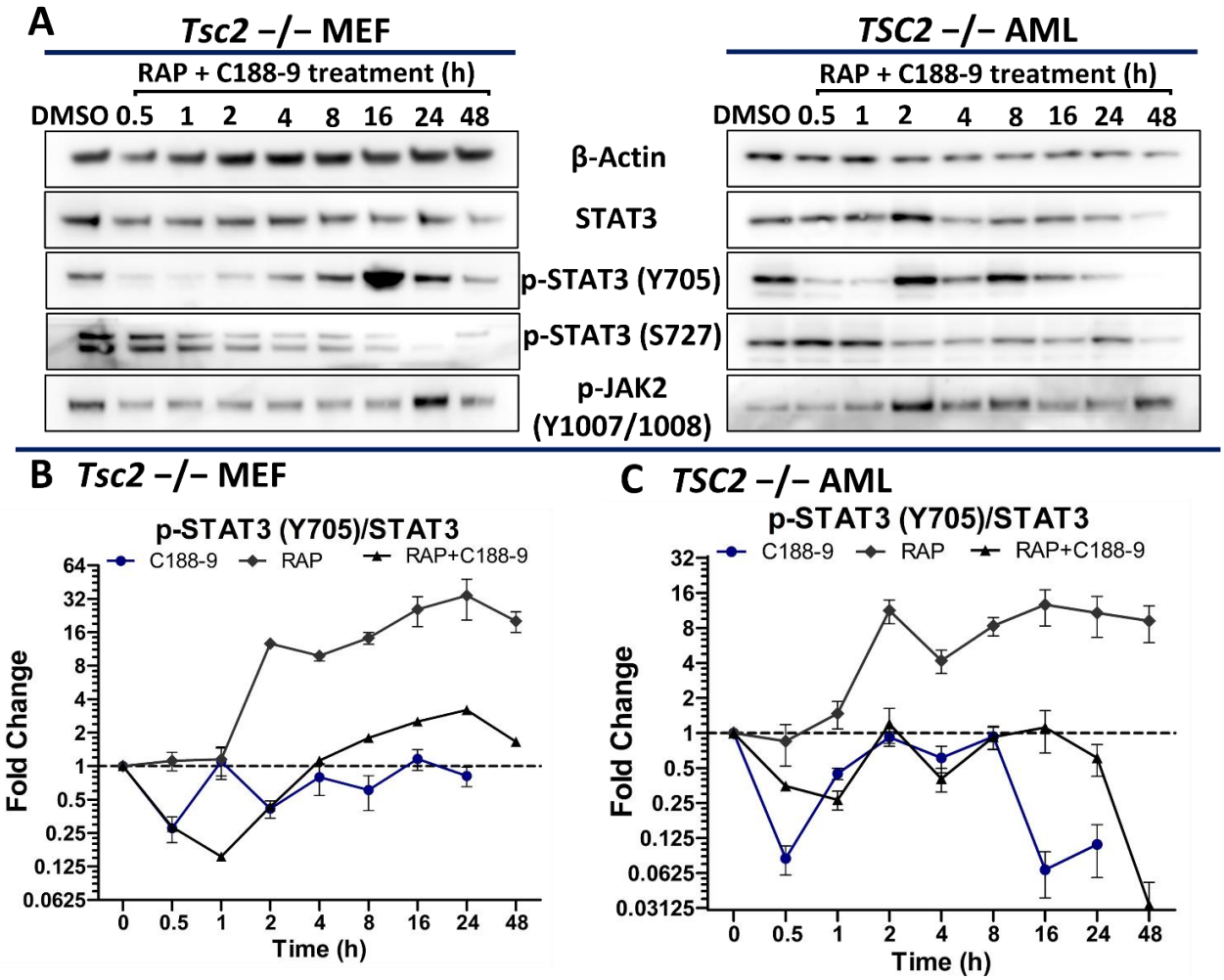


**Figure 5.13**. **Spike in levels of STAT3 phosphorylated at Y705 observed on rapamycin treatment is repressed by co-treatment with C188-9 within *TSC2* deficient AML cells and reduced within *Tsc2* −/− MEF cells.** *TSC2* deficient AML or MEF cells were treated with either vehicle (DMSO), or co-treated with C188-9 at 30 μM and rapamycin (RAP) at 50 nM. Cells treated with DMSO (control) were lysed at time 0 h, whilst C188-9 + RAP treated cells were lysed at the time indicated. Protein lysates were then assayed through western blotting (panel **A**) (N=3 minimum), with β-actin acting as a loading control. Densitometry analysis of resulting western blots (N=3 minimum) was performed, phosphorylated STAT3 was normalised to total STAT3 for blots from *TSC2* deficient MEF (**B**) and AML (**C**) cells. Resulting ratios were then expressed as fold changes compared to DMSO control and plotted, to show change in fold change during treatment time in respect to the control. Dotted line on graphs represents DMSO control fold change, i.e., 1.00. Bars represent standard error of the mean. Predicted running band size (kDa) of protein targets can be found in chapter 2, table 2.6.

pSTAT3 decreasing further over treatment time, being lowest at the end time point 48h. For blots of JAK2 phosphorylated at Y1007/1008 (pJAK2 1007/8), when normalising to β-actin during densitometry analysis, foldchanges in pJAK2 1007/8 during treatment time relative to the DMSO control were inconsistent. The trend within both *TSC2* deficient cell lines was for levels of pJAK2 1007/8 to increase during later time points. As can be seen from the blots in figure 5.13 (**A**) and accompanying densitometry graphs (**B** and **C**), co-treatment with both rapamycin and C188-9, decreases the level of Y705 pSTAT3 over treatment time relative to rapamycin treatment alone. At the earlier timepoints (0.5-2h) within both *TSC2* deficient cells lines, rapamycin and C188-9 co-treatment initially strongly decrease the level of Y705 pSTAT3/STAT3. Reaching a lowest level relative to the DMSO control with these earlier timepoints at 1 h for *Tsc2* −/− MEF cells (graph **B**) (FC=0.15, p=0.0001) and at 0.5 h for *TSC2* deficient AML cells (graph **C**) (FC=0.26, p=0.0001). Within both *TSC2* deficient cells lines, the level of Y705 pSTAT3/STAT3 relative to the DMSO control, starts to recover over time with rapamycin and C188-9 co-treatment (figure 5.13 **B/C**). As was the case C188-9 treatment alone. However, within the *Tsc2* −/− MEF cells this increase is not as large as seen with rapamycin treatment alone. Reaching a maximum at 24 h. As with C188-9 treatment alone, at the later time points of rapamycin and C188-9 co-treatment, levels of Y705 pSTAT3/STAT3 decrease again within the *TSC2* deficient AML line, albeit at 24 h not 16 h. Reaching the lowest level relative to the DMSO control at the end timepoint, 48 h (FC=0.03, $p=7.28x10^{-7}$). The reason for the differential response between the two *TSC2* deficient cell lines to C188-9, in terms of level of phosphorylation of STAT3 at Y705 is unclear. However, in both *TSC2* deficient AML and MEF cells, co-treating with C188-9 limits the increase in Y705 pSTAT3 seen when treating with rapamycin alone (figure 5.12).

Figure 5.14 (**A**) shows the effect of rapamycin and C188-9 co-treatment on mTORC1 substrates within *TSC2* deficient AML and MEF cells. Within both cell lines rpS6 phosphorylation at S235/236 decreases, as does both 4E-BP1 phosphorylation sites, over treatment time. Contrasting these blots with previous blots from long-term rapamycin treatment of both *TSC2* deficient cells (figure 5.12). In neither AMLs or MEFs is the level of phosphorylation of rpS6 or 4E-BP1 lower on co-treating with C188-9 (figure 5.14 **A**). Figure 5.14 **B** shows graphs of densitometry analysis of levels of phosphorylated rpS6 and 4E-BP1 relative to the DMSO control on co-treating *TSC2* deficient AML cells with rapamycin and C188-9. With previous densitometry analysis from rapamycin and C188-9 treatment alone also plotted. As shown by and large rapamycin and C188-9 co-treatment do not repress phosphorylation of these mTORC1 substrates further than either rapamycin or C188-9 alone. Therefore, in terms of inhibiting mTORC1 activity within TSC cells, there doesn't appear to be

an additional benefit in rapamycin and C188-9 co-treatment. At least for the markers of mTORC1 activity assayed here.

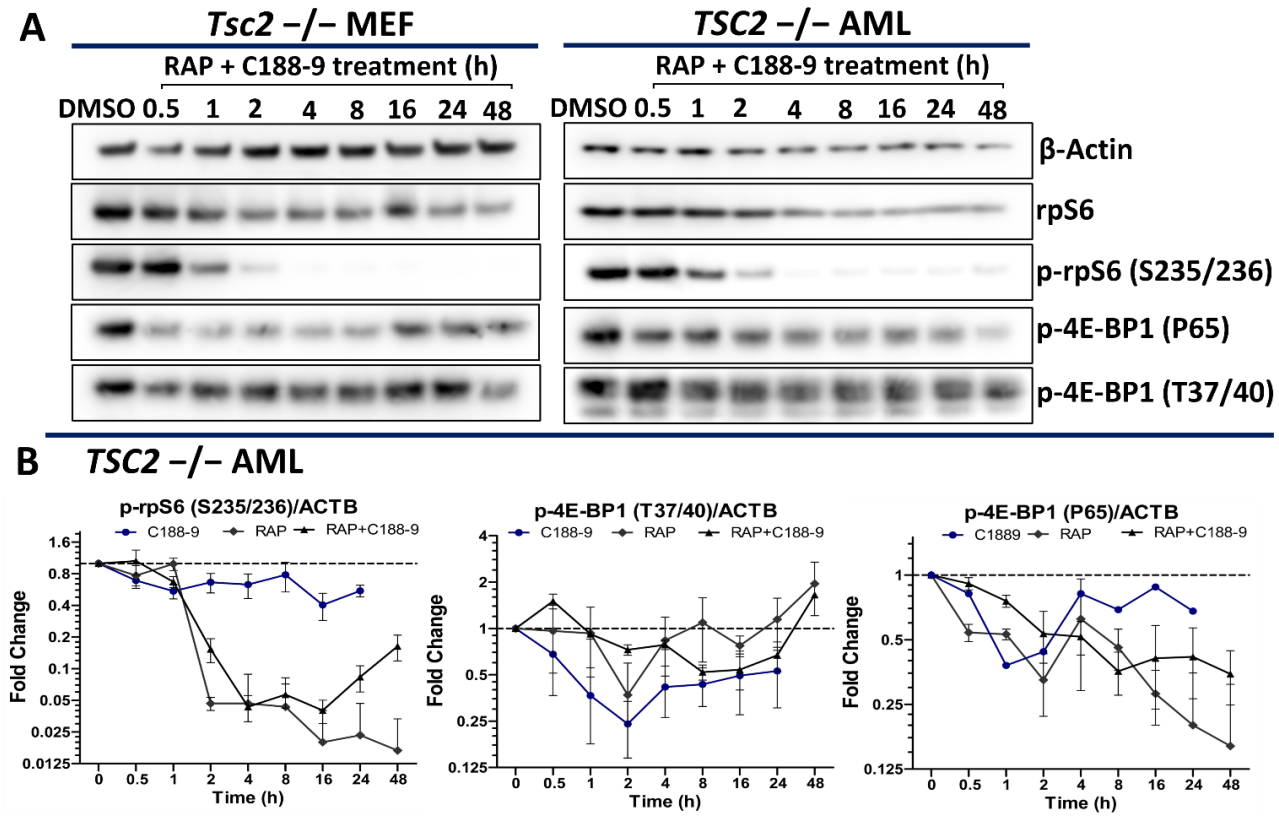


**Figure 5.14**. **Co-treatment of rapamycin and C188-9 does not repress markers of mTORC1 activity more than rapamycin alone within *TSC2* deficient AML or MEF cells.** *TSC2* deficient AML or MEF cells were treated with either vehicle (DMSO), or co-treated with C188-9 at 30 μM and rapamycin (RAP) at 50 nM. Cells treated with DMSO (control) were lysed at time 0 h, whilst C188-9 + RAP treated cells were lysed at the time indicated. Protein lysates were then assayed through western blotting (panel **A**) (N=3 minimum), with β-actin acting as a loading control. Densitometry analysis of resulting western blots from *TSC2* deficient AML cells (N=3 minimum) was performed (**B**), phosphorylated rpS6 and 4E-BP1 was normalised to β-actin. Resulting ratios were then expressed as fold changes compared to DMSO control and plotted, to show change in fold change during treatment time in respect to the control. Ratios of phosphorylated rpS6/ACTB and phosphorylated 4E-BP1/ACTB from previous densitometry analyses of long-term rapamycin and C188-9 treatment within *TSC2* deficient AML cells were also plotted. Dotted line on graphs represents DMSO control fold change, i.e., 1.00. Bars represent standard error of the mean. Predicted running band size (kDa) of protein targets can be found in chapter 2, table 2.6.

### 5.2.9 Both rapamycin and C188-9 treatment largely down regulate STAT3 target gene expression within *TSC2* deficient AML cells.

Given that C188-9 and rapamycin treatment had differing effects on phosphorylated STAT3 and JAK2 (figures 5.10, 5.11 and 5.12) within *TSC2* deficient cells. And opposing effects on the proportion of STAT3 able to bind STAT3 consensus sequences. The next aim of the present chapter was to assay how rapamycin and STAT3 inhibition would affect the dysregulated STAT3 driven transcriptome observed upon the loss of *TSC2* within the AML cells (figure 5.8). This was by way of analysis of the RNA sequencing data set comparing DMSO, rapamycin and C188-9 treated *TSC2* deficient AML cells under hypoxia utilised in chapter 4.

The volcano plots in figure 5.15 summarise STAT3 target gene expression changes on rapamycin (**A**) or C188-9 (**B**) treatment relative to DMSO control within *TSC2* −/− cells cultured under hypoxia. On rapamycin treatment, over 69% of the genes (128/184) within the STAT3 target gene set were significantly differentially expressed. Of those 128 significantly differentially expressed genes, 82 were downregulated whilst 46 were upregulated relative to the DMSO control. Therefore, despite rapamycin treatment increasing phosphorylation of STAT3 at Y705 (figure 5.15), majority of STAT3 target genes were downregulated by rapamycin treatment. Surprisingly on C188-9 treatment (figure 5.15 **B**), less STAT3 target genes were significantly differentially expressed relative to DMSO than rapamycin treatment. On C188-9 treatment over 63% of the genes (119/186) within the STAT3 target gene set were significantly differentially expressed. Of those 119 significantly differentially expressed genes, 67 were downregulated and 52 were upregulated relative to the DMSO control. Contrasting the effects of rapamycin and C188-9 treatment on STAT3 target gene expression, rapamycin appears to downregulate STAT3 target gene expression further on the whole. As seen from volcano plot **C** in figure 5.15. Of the 53 STAT3 target genes significantly differentially expressed between rapamycin and C188-9 treated *TSC2* −/− AML cells, 43 are downregulated on rapamycin treatment relative to C188-9 treatment. As both rapamycin and C188-9 treatment repress phosphorylation of STAT3 at S727 long term, perhaps the S727 phosphorylation site is more crucial for STAT3 mediated transcription within *TSC2* deficient cells.

The efficacy of rapamycin vs C188-9 treatment in normalising dysregulated STAT3 target gene expression upon *TSC2* loss, as seen in figure 5.15, can be assessed by comparing the rapamycin vs DMSO and C188-9 vs DMSO treatment RNA seq data sets to the *TSC2* −/− vs *TSC2* RE AML cells under hypoxia RNA seq data set. Under hypoxia 72 STAT3 target genes are significantly upregulated within *TSC2* −/− AML cells relative to *TSC2* RE AML cells, whilst 55 are significantly downregulated (see table 5.1). Out of the STAT3 target genes found to be

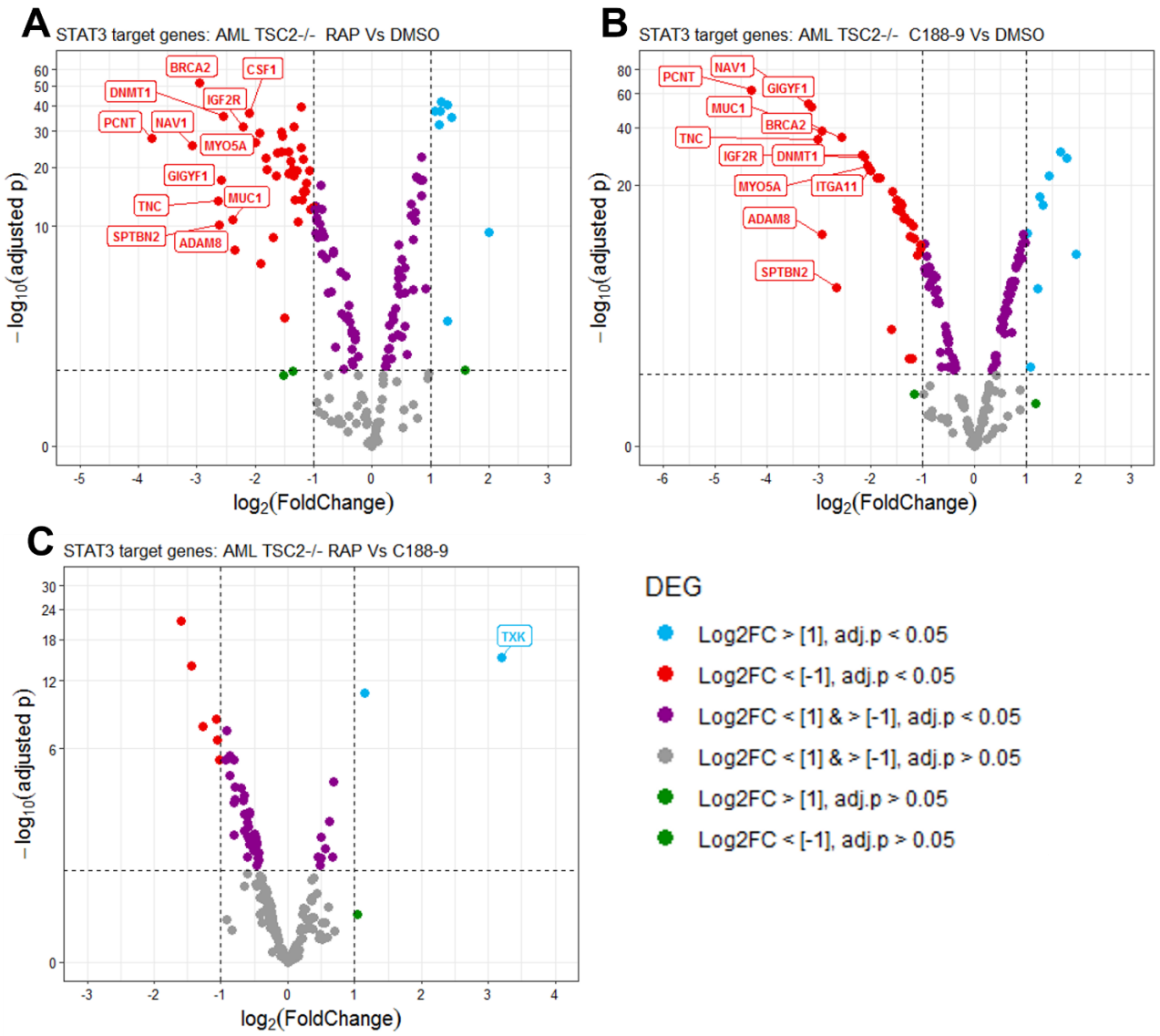


**Figure 5.15. Both rapamycin and C188-9 treatment are effective at decreasing STAT3 target gene expression in *TSC2* deficient AML cells.** STAT3 target gene set was collated from multiple publications (see methods and materials). Differential gene expression (DEG) comparison is annotated above each plot. AML *TSC2* −/− cells were cultured under hypoxia (1% $O_2$) for 8 h with either vehicle only (DMSO), rapamycin (RAP) at 50 nm or C188-9 at 15 µM (N=8). RNA purified from these samples was sequenced through Novogene. Expression levels were calculated and normalised from raw read counts as FPKM (Fragments Per Kilobase Million per mapped reads). Differential gene expression (DEG) analysis was through DEseq2 analysis and resulting p-values were corrected for multiple testing and false discovery by FDR method. For all volcano plots Log2 transformed fold change in expression of genes was plotted against their -log10 transformed FDR adjusted p-values. Dotted lines at x axis represent increase or decrease in foldchange of 2 or -2 respectively. Dotted line at y axis represents significance threshold of 0.05. Genes annotated had a Log2 fold change in expression greater or lower than 2 or -2 (i.e., four fold higher or lower in expression) respectively and an -log10 adjusted p-value greater than 3 (i.e., below 0.001 significance threshold).

significantly differentially expressed upon *TSC2* loss under hypoxia, rapamycin appears to normalise STAT3 target gene expression better than C188-9 treatment. Out of those 72 STAT3 target genes upregulated within the *TSC2* −/− AML cells, rapamycin treatment significantly downregulates expression of 33 genes relative to the DMSO control, whilst C188-9 treatment significantly downregulates 25 genes. Out of those 55 STAT3 target genes downregulated within the *TSC2* −/− AML cells, rapamycin treatment significantly upregulates expression 12 genes relative to the DMSO control, whilst C188-9 treatment significantly upregulates 9 genes. As seen from table 5.3, majority of the STAT3 target genes normalised on either rapamycin or C188-9 treatment are the same. This suggests that rapamycin and C188-9 are inhibiting STAT3 mediated transcriptome through similar mechanisms and to a similar extent within *TSC2* −/− AML cells. There are a few STAT3 target genes normalised by rapamycin but not by C188-9, and one gene normalised by C188-9 but not by rapamycin treatment. Highlighted in bold in table 5.3. Therefore, more robust normalisation of the STAT3 driven transcriptome within *TSC2* −/− AML cells may be achieved by co-treating with rapamycin and C188-9.

**Table. 5.3 Comparison of the effect of Rapamycin (RAP) and C188-9 treatment on normalising HIF1-α target genes significantly dysregulated upon loss of *TSC2* in AML cells cultured under hypoxia (1%$O_2$).** Genes in bold are those whose expression is significantly affected by rapamycin or C188-9 treatment, not both.

| Genes downregulated in *TSC2* −/− upregulated on RAP treatment | Genes downregulated in *TSC2* −/− upregulated on C188-9 treatment |
|---|---|
| BAG4 | BAG4 |
| BIRC5 | BIRC5 |
| BMP4 | BMP4 |
| CALM3 | CALM3 |
| ITGB6 | ITGB6 |
| MCM7 | MCM7 |
| **MDM2** | NOTCH4 |
| NOTCH4 | PAWR |
| PAWR | STMN1 |
| **PIM1** | |
| STMN1 | |
| **TXK** | |

| Genes upregulated in *TSC2* −/− downregulated on RAP treatment | | Genes upregulated in *TSC2* −/− downregulated on C188-9 treatment | |
|---|---|---|---|
| ADAM23 | NOTCH2 | ADAM23 | RASA3 |
| BCL3 | PDGFA | BCL3 | RBFOX2 |
| CCND1 | PIK3R1 | CCND1 | SMAD9 |
| CDON | **PRKCE** | CDON | STAT3 |
| CSF1 | RASA3 | CSF1 | **TGFB2** |
| EPHB2 | RBFOX2 | EPHB2 | TNC |
| FOSL2 | **RORA** | FOSL2 | VIM |
| HDAC4 | SMAD9 | HDAC4 | ZEB1 |
| **HGF** | **SRFBP1** | ICAM1 | |
| **HIF1A** | STAT3 | ITGA11 | |
| ICAM1 | **TCF12** | JUN | |
| **IFRD1** | **TGFBR3** | MMP2 | |
| ITGA11 | TNC | MYO5A | |
| JUN | **VEGFA** | NAV1 | |
| MMP2 | VIM | NOTCH2 | |
| MYO5A | ZEB1 | PDGFA | |
| NAV1 | | PIK3R1 | |

### 5.2.10 Genes encoding components of the mTORC1 and mTORC2 complexes are dysregulated on loss of *TSC2* and are sensitive to mTOR and STAT3 inhibition.

Given that C188-9 treatment of *TSC2* deficient cells repressed markers of mTORC1 activity, the next aim of the present work was to assess whether STAT3 transcriptionally regulated any of the genes encoding the components of mTORC1 and mTORC2 complexes. As such an effect of C188-9 would be beneficial in downregulating activity of mTORC1 in *TSC2* deficient cells. As can be seen from the volcano plot in figure 5.16 (**A**), genes encoding the components of mTORC1/2 complexes (see main introduction for detailed description of mTORC1/2 complex components) are dysregulated between *TSC2* −/− and *TSC2* RE AML cells. Of note *AKT1S1* (PRAS40) and *DEPTOR*, which both encode negative regulators of mTORC1 complex and mTORC1/2 complexes respectively (Sancak *et al.* 2007 and Peterson *et al.* 2009) are significantly downregulated in *TSC2* −/− AML cells. Conversely, *RICTOR* and *RPTOR*, which encode subunits of the mTORC1 and mTORC2 complexes respectively, are upregulated in *TSC2* −/− cells. *TELO2*, along with *TTI1*, both encode proteins that form a complex which helps to stabilise mTORC1/2 complexes (Kaizuka *et al.* 2010). *TTI1* is downregulated and *TELO2* is upregulated within *TSC2* −/− cells. Although the fold change in *TELO2* is relatively small, *TELO2* has a further role in promoting mTORC1 signalling, as Brown and Gromeier (2017) found MAPK-interacting kinase (MNK) signalling promotes TELO2 proteins association with mTORC1 and facilitates substrate binding to the complex. By in large hypoxia doesn't significantly alter expression of many of the genes encoding the components of mTORC1/2 within the *TSC2* −/− AML cells (figure 3.16 **B**). Of note however is that hypoxia reduces *MTOR* slightly and further decreases expression of mTORC1/2 complexes negative regulator *DEPTOR*. Suggesting hypoxia may further exacerbate hyperactive mTORC1 signalling if protein expression of DEPTOR matches the gene expression trend.

As can be seen from the volcano plots in figure 5.16 (**C** & **D**), treating AML cells with either rapamycin or C188-9 results in expression changes in the aforementioned genes. Rapamycin treatment (figure 3.16 **C**) downregulates not only the active kinase *MTOR* itself, but also *RPTOR*. In addition, the positive regulators of mTORC1 stability, *TELO2* and *TTI1*, are downregulated by rapamycin treatment, whilst the negative regulator of mTORC1/2 complexes *DEPTOR* is upregulated. C188-9 treatment (figure 5.16 **D**) produces similar changes in gene expression as rapamycin treatment. *MTOR* and *RPTOR* are downregulated, whilst *DEPTOR* is upregulated. C188-9 treatment doesn't however, downregulate *TELO2* and *TTI1*. From the volcano plots in figure 5.16 (**A**, **C** & **D**) rapamycin or C188-9 treatment appears to help restore dysregulated expression of *TSC2* −/− cells compared to *TSC2* RE cells, in that either treatment upregulates *DEPTOR*, whilst downregulating *RPTOR*. Additionally, if on

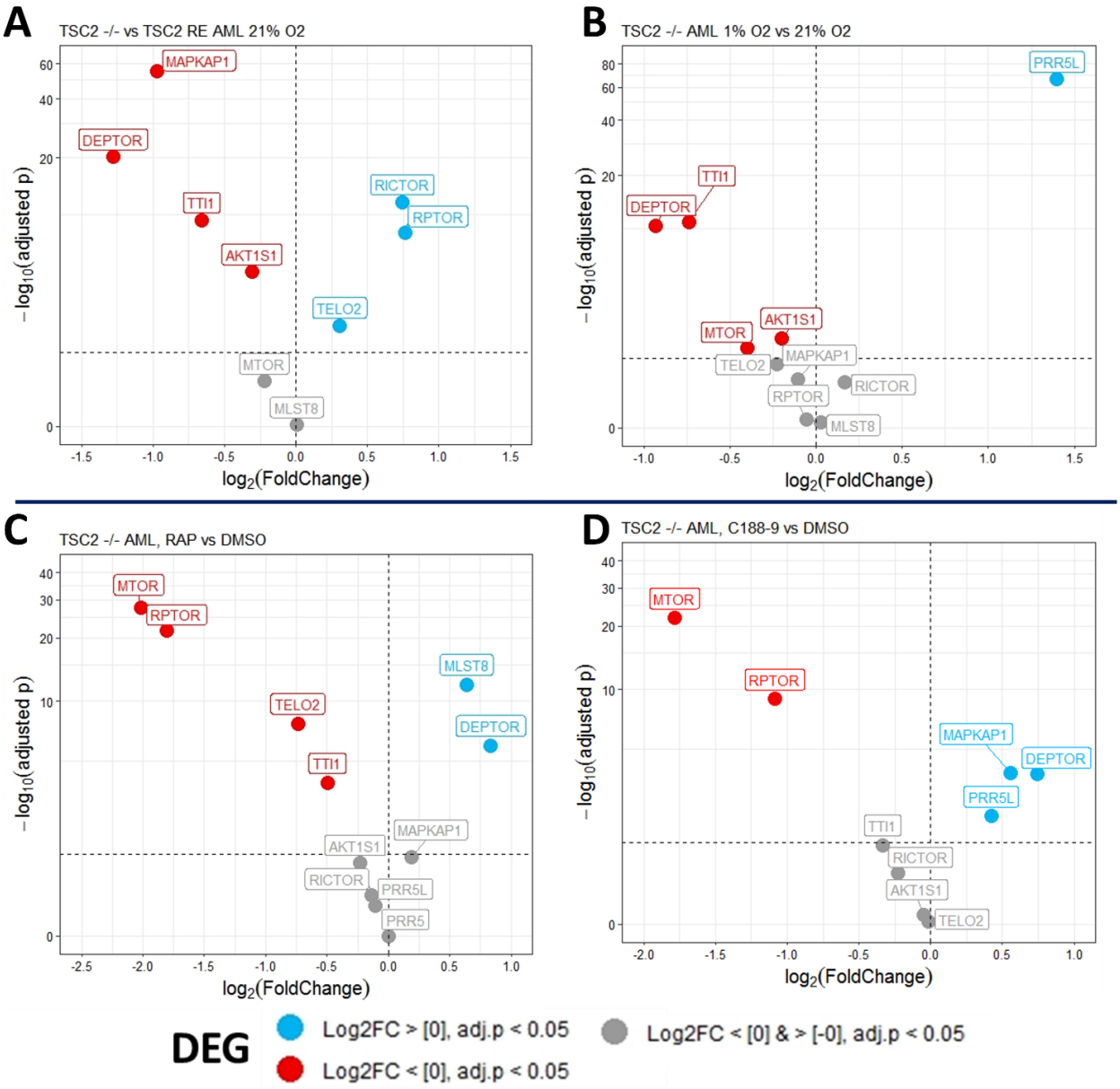


**Figure 5.16. Expression of genes encoding components of the mTORC1 and mTORC2 complexes are dysregulated between *TSC2* deficient and *TSC2* RE AML cells and are sensitive to mTOR and STAT3 inhibition.** Two separate RNA sequencing experiments were conducted. One through Wales Gene Park, comparing either AML *TSC2* deficient (*TSC2* −/−) and *TSC2* RE (re-expressed) cells cultured under either normoxia (21% $O_2$) or hypoxia (1% $O_2$) (**A** & **B**) (N=6). The other through Novogene comparing AML *TSC2* −/− cells cultured under hypoxia (1% $O_2$) treated for 8 h with either vehicle only (DMSO), rapamycin (RAP) at 50 nm or C188-9 at 15 µM (**B** & **C**) (N=8). Expression levels were calculated and normalised from raw read counts as RPKM (Reads per Kilobase exon Model per million mapped reads) (**A** & **B**) or FPKM (Fragments Per Kilobase Million per mapped reads) (**B** & **C**). Differential gene expression (DEG) analysis was through DEseq2 analysis and resulting p-values were corrected for multiple testing and false discovery by FDR method. Log2 transformed fold change in expression of genes (**A** = *TSC2* −/− vs *TSC2* RE AML cells under hypoxia, **B** = *TSC2* −/− AML cells 1% vs 21%, **C** = rapamycin treated vs DMSO treated *TSC2* −/− AML cells, **D** = C188-9 treated vs DMSO treated *TSC2* −/− AML cells) was plotted against their -log10 transformed FDR adjusted p-values. Dotted line at y axis represents significance threshold of 0.05.

rapamycin or C188-9 treatment protein expression of *MTOR*, *RPTOR* and *DEPTOR* (and *TELO2* and *TTI1* in the case of rapamycin) follows the trend in the transcription data, then either treatment could reduce mTORC1 signalling over time. By reducing the level of constituent subunits of mTORC1 overtime, whilst increasing one of its inhibitors (DEPTOR), within *TSC2* deficient AML cells. Furthermore, rapamycin and C188-9 treatments produced similar effect on the expression of *MTOR*, *RPTOR* and *DEPTOR* (figure 5.16 **C/D**). Implying a common transcriptional regulator is being affected. This common transcriptional regulator is likely STAT3, as both rapamycin and C188-9 repress phosphorylation of residues crucial in promoting STAT3's transcriptional activity; as shown in sections 5.2.7 (figure 5.13) and 5.2.6 (figures 5.10 and 5.11). Lastly, downregulation of *MTOR* on rapamycin treatment may represent another mode in which long term rapamycin treatment can inhibit mTORC2 complex. Aside from occluding newly synthesised mTOR protein from forming active mTORC2 complex (Sarbassov *et al.* 2006).

### 5.2.11 *TSC2* deficient cells autoactivate STAT3 by increasing pY705 STAT3 through autocrine signalling.

Our previous data showed not only that phospho-markers of STAT3 activity and nuclear active STAT3 are substantially elevated within *TSC2* deficient cells, but also that many genes encoding STAT3 stimulatory cytokines/growth factors and their cognate receptors are upregulated within the *TSC2* deficient AML cell line. Often in cancers, where hyperactive STAT3 drives pathogenesis (Avalle *et al.* 2017), dysregulated STAT3 drives its own activity in a feed-forward manner, by upregulating STAT3 stimulating cytokines/growth-factors. Such as the IL-6/JAK/STAT3 feedforward loop, shown to drive tumourigenesis in breast and pancreatic cancer (Chang *et al.* 2013 and Lesina *et al.* 2011). Therefore, the next aim of the present work was to assay whether *TSC2* deficient cells maintain constitutively active STAT3 through an autocrine mechanism.

Either *TSC2* deficient AML or MEF cells were serum starved to remove any cytokines/growth factors present, either in the serum or secreted by the cells (Levin *et al.* 2010). Whether oxygen status effects phospho-markers of STAT3 activity during this assay was assessed as well. As seen in figure 5.17, in both *TSC2* deficient cell lines, Y705 pSTAT3 Y705 spontaneously recovers and increases after initial repression by serum starvation at time 1 h. The induction of pSTAT3 Y705 reached a maximum at the 24 and 32 h timepoints. Densitometry analysis found that differences in relative pSTAT3 Y705 (normalised to STAT3 total) was not significant between normoxia cultured cells and hypoxia cultured cells at 24 and 32 h. Densitometry analysis found that pJAK2 Y1007/1008 did steadily increase over time in serum starvation for both *TSC2* deficient AML and MEF lines. However, in the MEF line, longer-term serum

starvation under hypoxia led to a decrease in pJAK2 Y1007/1008 at 24 and 32 h. Phosphorylation of rpS6 at S235/236 only decreased on serum starvation in the *Tsc2* −/− MEF cells, further repressed by hypoxia.

The spontaneous recovery of pSTAT3 Y705 and steady increase in pJAK2 1007/1008 under serum starvation implies *TSC2* deficient cells stimulate their own STAT3 activity through an autocrine mechanism. Results of a conditioned media experiment in figure 5.18, strongly supports this hypothesis. Large increases in pY705 STAT3 were seen in both *TSC2* deficient cell lines, when treated for 30 mins with conditioned media collected from the same *TSC2* deficient cell line cultured for 24 h under serum free (CM-SS) or serum containing (CM-FBS) media. Relative to respective controls (fresh media, SS & FBS). Densitometry analysis did not find the difference in relative pY705 STAT3 (normalised to STAT3 total) significant between CM-SS or CM-FBS treated cells for either cell line.

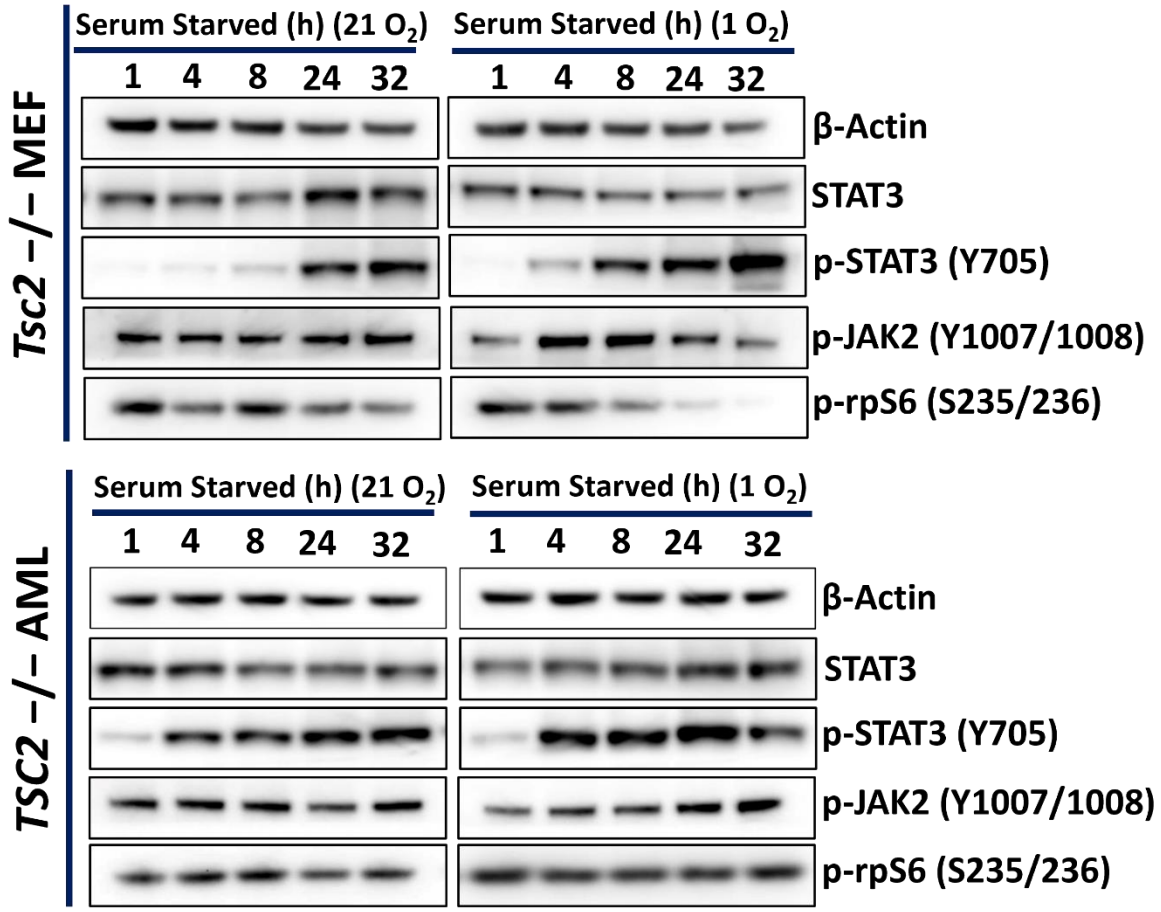


**Figure 5.17. *TSC2* deficient cells recover p-STAT3 phosphorylation over time after serum starvation.** Either *TSC2* deficient (*TSC2* −/−) AML or MEF cells were grown to confluency and then serum starved (0% FBS v/v) under either normoxia (21% $O_2$) or hypoxia (1% $O_2$). Cells were then lysed at the time indicated Through western blotting, protein lysates were then assayed for target proteins, with β-actin acting as a loading control. Blot panels show representative image for each protein target (N=3). Predicted running band size (kDa) of protein targets can be found in chapter 2, table 2.6.

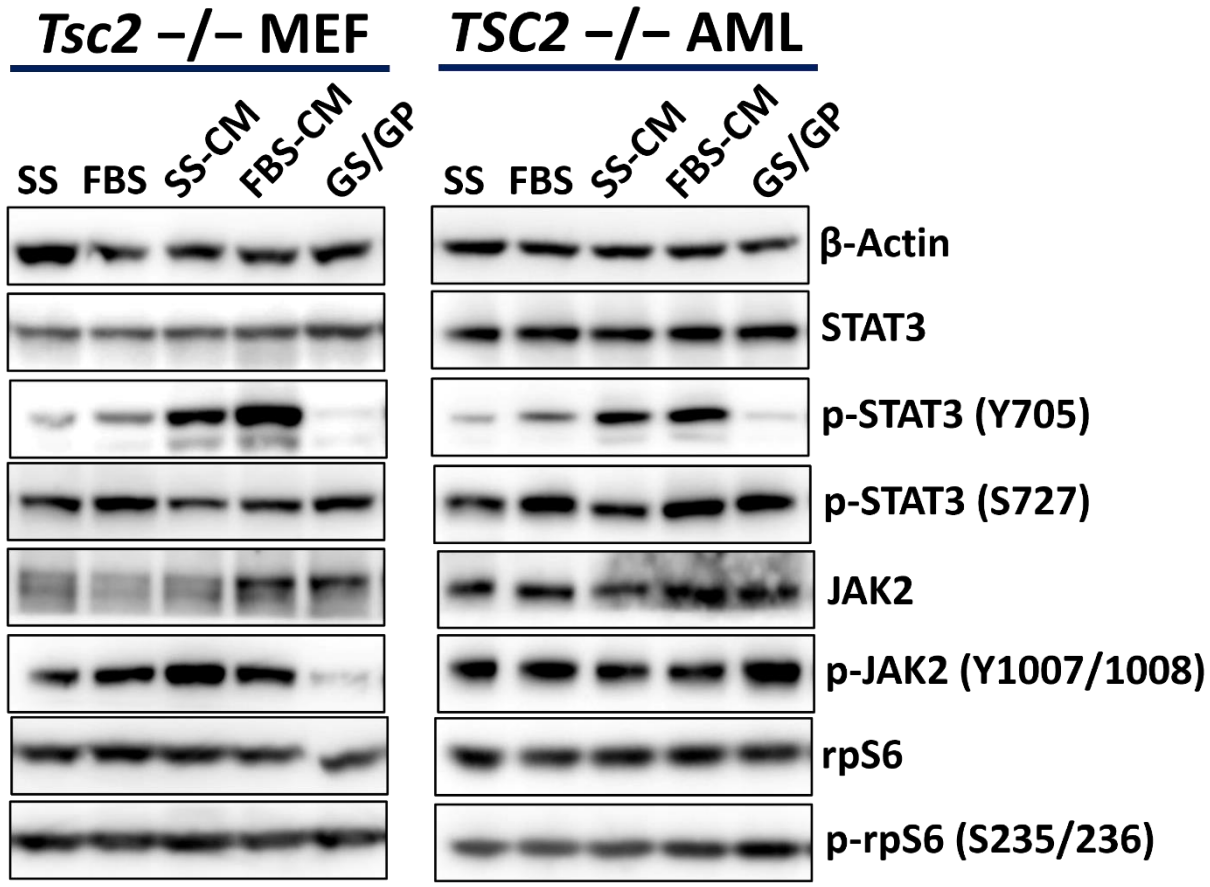


**Figure 5.18. *TSC2* deficient cells increase phosphorylation of STAT3 at Y705 through autocrine signalling.** Under normoxia, either *TSC2* deficient (*TSC2* −/−) AML or MEF cells were treated with either serum free media (**SS**), media containing serum at 10% v/v (**FBS**), conditioned media from *TSC2* deficient AML or MEFs respectively cultured for 24 h in either: serum free media (**SS-CM**), media containing serum at 10% v/v (**FBS-CM**) or media containing serum at 10% v/v and the protein transport inhibitors GolgiStop™ (at 0.66 µ/mL) and GolgiPlug™ (at 1.00µ/mL) (**GS/GP**). Cells were lysed after 30 min of treatment. Protein lysates were then assayed through western blotting, with β-actin acting as a loading control. Blots shown are representative of an N = 3. Predicted running band size (kDa) of protein targets can be found in chapter 2, table 2.6.

### 5.2.12 Effect of IL-6 stimulation on markers of STAT3 activity differ between *TSC2* −/− AML and MEF cells.

*IL6* expression and relative amounts of pJAK2 10007/1008 are several fold higher in unstimulated *TSC2* deficient AML cells compared to *TSC2* RE AML cells (sections 5.2.2 and 5.2.3 respectively). Furthermore, *TSC2* deficient cells spontaneously recover pSTAT3 Y705 after initial repression by serum starvation, which is likely mediated by secreted factors acting in an autocrine manner. Taken together, this data suggests IL-6 may be one of these secreted factors *TSC2* deficient cells express to constitutively activate STAT3 signalling. The next aim of the present work was therefore to assay how IL-6 treatment would affect phospho-markers of STAT3 activity and nuclear active STAT3 in *TSC2* deficient cell lines.

As seen in the blot panel of figure 5.19 (**A**), pSTAT3 Y705 increases upon IL-6 treatment in both *TSC2* deficient cell lines. Densitometry analysis (n=3) of blots found the increases in STAT3 Y705/STAT3 between the untreated control and all IL-6 treatments statistically significant in both cell lines (figure 5.19 **A**). With the level of STAT3 Y705/STAT3 peaking upon IL-6 treatment at 100 ng and 25 ng within the MEF and AML line respectively. In neither cell line did IL-6 treatment significantly affect levels of pSTAT3 S727/STAT3 or rpS6 phosphorylated at 235/236. Suggesting that in the short term, increased IL6/STAT3 signalling is unlikely to affect mTORC1 activity. However long term, increased STAT3 activity mediated by IL-6 may promote mTORC1 signalling by upregulating expression mTORC1/2 component genes found to be downregulated on C188-9 treatment (figure 5.16 **D**). pJAK2 Y1007/1008 only increases after IL-6 stimulation in the *Tsc2* −/− MEF cell line, not the AML line (figure 5.19 **A**). This suggests that JAK2 is already maximally phosphorylated within the AML lines. It should also be noted that JAK2 is not the only JAK family adaptor kinase responsible for IL-6R/gp130 receptor signalling transduction (O'shea *et al.* 2013). Both TYK2 and JAK1 can mediate IL-6 activation of STAT3 (Jiang *et al.* 2017 and Song *et al.* 2011).

Whilst IL-6 treatment increases pSTAT3 Y705 in both *TSC2* deficient cell lines, interestingly it has contrasting effects on the nuclear accumulation of DNA bound STAT3 between the AML and MEFs lines (figure 5.19 **B**). Within the MEF line, following the trend in increasing pSTAT3 Y705 with increasing IL-6 dose, the relative amount of nuclear DNA bound STAT3 also increases with higher IL-6 dose. Peaking at 2.5 fold higher on 100 ng of IL-6 treatment. However, whilst pY705 increases on IL-6 stimulation in the AML line, increasing doses of IL-6 appear to reduce the relative amount of nuclear active STAT3 compared to the untreated control, decreased by 0.68 fold on 100 ng of IL-6 treatment. Why IL-6 stimulation would have these contrasting effects on nuclear accumulation of active STAT3 between the two cell lines is unclear.

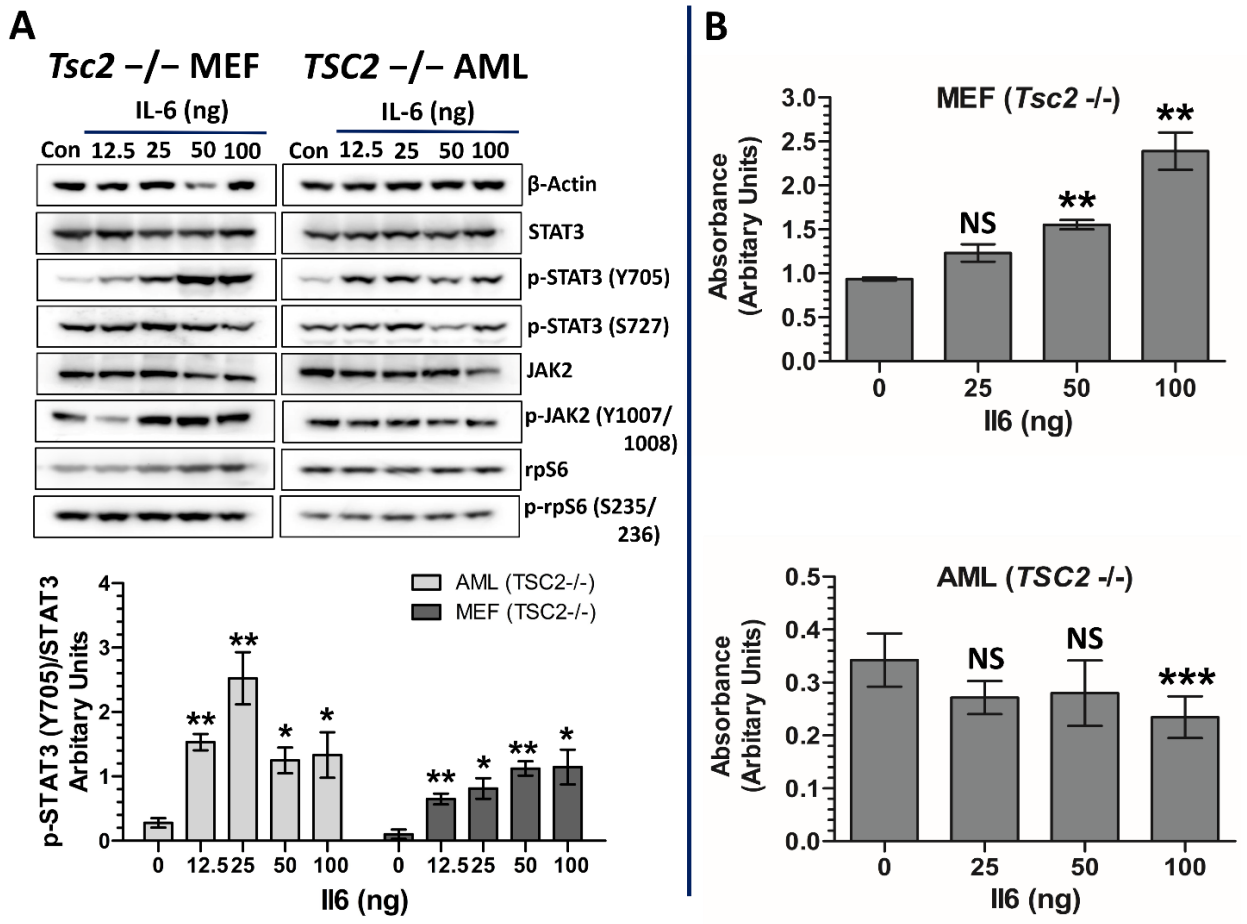


**Figure 5.19 Phospho-markers and nuclear accumulation of active STAT3 are affected by IL-6 stimulation differently in *TSC2* deficient AML and MEF cell lines.** *TSC2* deficient (*TSC2* −/−) MEF or AML cells were treated with dose of IL-6 specified for 45 min before either being: lysed with laemmli sample buffer and analysed through western blot (N=3) (**A**) or used to generate concentrated nuclear lysates which were assayed for amount of active DNA binding STAT3 (nuclear active STAT3) present using Active Motifs TransAM STAT3 ELISA (**B**). Densitometry analysis of resulting western blots (N=3 minimum) (**A**) was performed, phosphorylated STAT3 was normalised to total STAT3 and expressed as fold changes compared to untreated control sample (IL6 = 0 ng). Statistical analysis of differences in foldchange was by student's t test. Significance annotations above each bar on graph (**A**) indicates significance of difference in foldchange between each Il6 treated condition and untreated (0 Il6). Amount of nuclear active STAT3 in IL-6 treated conditions was expressed as fold changes compared to untreated control sample (**B**). Significance annotations above each bar on graphs (**B**) indicates significance of difference in foldchange between each Il6 treated condition and untreated (0 Il6). Statistical analysis (N=3 minimum) was by student's t test. Significance denoted by: * = p <0.05, ** = p <0.01, *** = p< 0.001, NS = not significant. Bars represent standard error of the mean. Predicted running band size (kDa) of protein targets can be found in chapter 2, table 2.6.

### 5.2.13 Upon loss of *TSC2,* protein expression of IL-6, but not IL-6/IL6R, is upregulated and expression of both IL-6 and IL-6/IL6R is further elevated by mTORC1 and STAT3 inhibitors.

Given pSTAT3 Y705 is elevated on IL-6 stimulation in *TSC2* deficient AML cells and that these cells show increased mRNA expression of the *IL6* gene. IL-6 protein expression within the AML cell lines was also assayed by ELISA. To assess whether enhanced IL-6 secretion upon

loss of *TSC2*, may be a mechanism by which these cells maintain hyperactive STAT3 signalling. Whether IL-6 protein expression is sensitive to mTORC1 or STAT3 inhibitors will also be assayed. Additionally, IL-6 has another mode of signalling. Whereby IL-6 binds with a soluble form of IL-6 receptor (IL-6/IL6R) and this complex can stimulate gp130 expressing cells (Rose-John, 2012). Therefore, secretion of IL-6/IL6R was assayed within the AML cell lines.

IL-6 protein expression was several fold higher in *TSC2* deficient AML cells than *TSC2* RE cells (figure 5.20 **A**), which matches the *IL6* mRNA expression data in section 5.3.2. Oxygen availability had no significant effect on IL-6 protein expression. Very little IL-6/IL6R was detected in the media of either AML cell line (figure 5.20 **B**) by the ELISA. IL6/IL6R was detectable in whole cell lysates, showing the complex is present within both cell lines. A decrease in IL-6/IL6R was observed in the *TSC2* deficient AML cells cultured under hypoxia and was significantly lower than that observed in *TSC2* deficient AML cells cultured under normoxia and *TSC2* RE cells cultured under normoxia or hypoxia (figure 5.20 **B**). Given such low secretion of IL-6/IL6R by *TSC2* deficient AML cells, secreted IL-6 is likely by far the main mediator of IL-6 autocrine and paracrine signalling by *TSC2* deficient AML cells. Both expression of secreted IL-6 and whole cell IL-6/IL6R are sensitive to mTORC1 and STAT3 inhibition (figure 5.20 **C** & **D**). Treatment with either mTORC1 inhibitor, rapamycin (RAP) and Ku-0063794 (KU), increased expression of IL-6 several fold relative to the DMSO only control (3.1 and 6.7 fold respectively) in *TSC2* deficient AML cells (figure 5.20 **C**). The larger increase in IL-6 expression under Ku-0063794 treatment compared to rapamycin treatment is significant and may result from the more complete inhibition of mTORC1 by this more potent mTORC1 inhibitor (García-Martíne *et al.* 2009). Treatment with the STAT3 inhibitors, FLLL31 and C188-9, have a similar effect in increasing IL-6 expression compared to the control (3.3 fold and 4.4 fold respectively). Combinatorial treatment of either STAT3 inhibitor with rapamycin appeared to elevate IL-6 expression even further than either FLLL31 or C188-9 treatment alone (figure 5.20 **C**). A one way ANOVA found the difference in IL-6 expression between RAP or C188-9 alone and in combination statistically significant ($p= 0.0004$), as was the difference between RAP or FLLL31 alone and in combination ($p= 6.44x10^{-6}$). Similar as the effect on IL-6 protein expression, rapamycin and C188-9 treatment increased IL-6/IL6R relative to the control within whole cell lysates of *TSC2* deficient AML cells (figure 5.20 **D**). A one way ANOVA reported the difference in IL-6/IL6R between RAP, C188-9 alone and in combination as not significant however. The modest increase in IL-6/IL6R within whole cell lysates of *TSC2* deficient AML cells upon rapamycin and C188-9 treatment may be due to the increase in IL-6 expression under these treatments, increasing the amount of secreted IL-6 in

the media able to bind IL6R. However, this was not seen under FLLL31 treatment, despite FLLL31 increasing IL-6 expression more than rapamycin or C188-9 treatment alone.

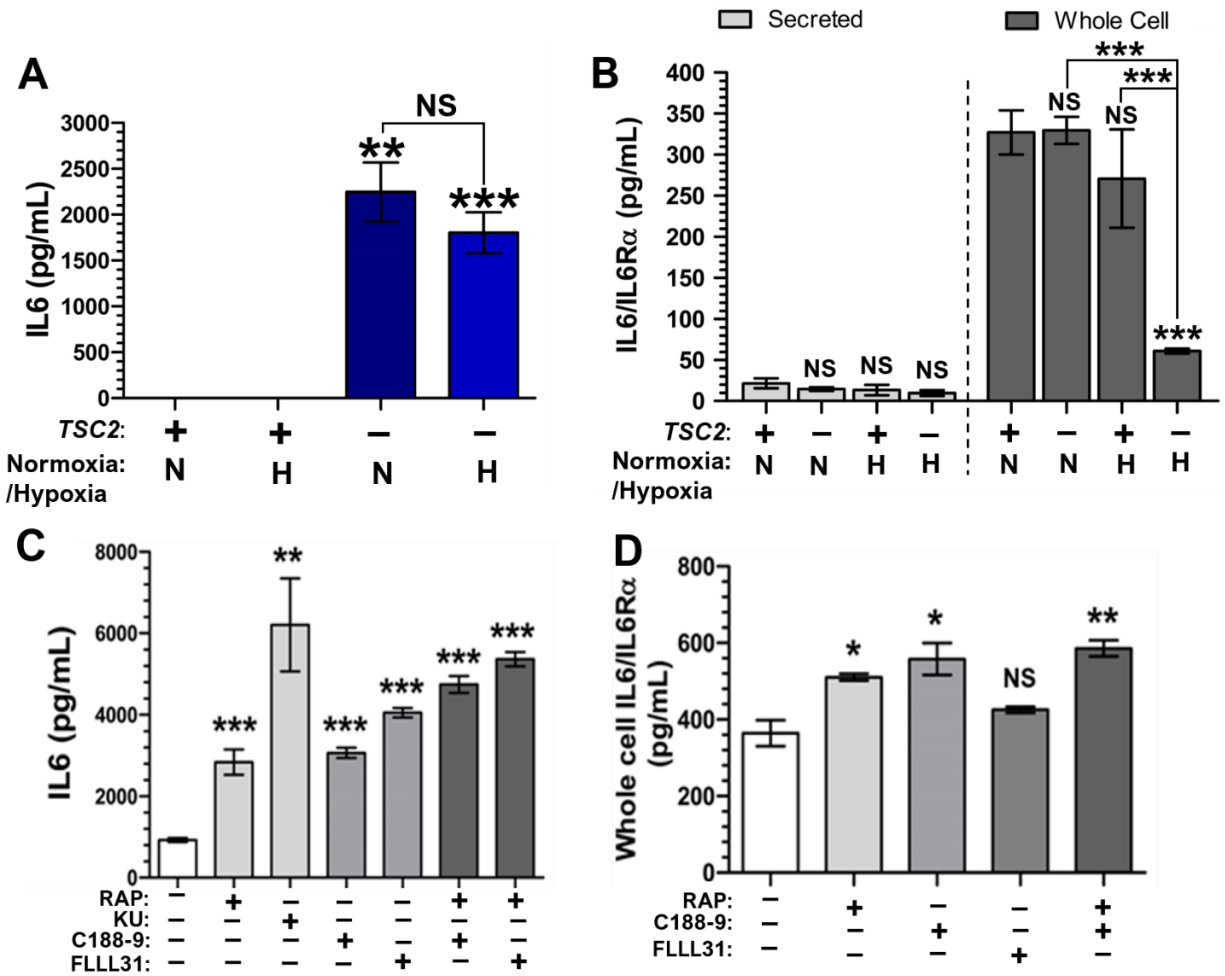


**Figure 5.20. Loss of *TSC2* within AMLs cells results in over-expression of IL-6 but not soluble IL6/ILRα, expression, expression of both is further upregulated by mTORC1 and STAT3 inhibition. A:** protein expression of IL-6 was assayed in culture media of *TSC2* deficient (*TSC2* −/−) and *TSC2* RE AML cells cultured for 24 h either under normoxia (N, 21% $O_2$) or hypoxia (H, 1% $O_2$) by way of ELISA (N=3). **B:** protein expression of IL-6 complexed with IL6Rα (IL6/IL6Rα) within culture media (secreted) or lysates (whole cell) of *TSC2* −/− and *TSC2* RE AML cells cultured for 24 h either under normoxia (N, 21% $O_2$) or hypoxia (H, 1% $O_2$) by way of ELISA (N=3). Statistical analysis of differences in foldchange was by student's t test. Significance annotations above each bar on graph indicates significance of difference in foldchange between each condition and *TSC2* RE cells under normoxia. Pairwise statistical comparisons between *TSC2* (−/−) cells under normoxia or hypoxia and between *TSC2* (−/−) and *TSC2* RE cells under hypoxia are also annotated. **C** & **D**: Effect of mTORC1 and STAT3 inhibition on protein expression of IL-6 and IL6/IL6Rα was assayed through assaying culture media/lysates of *TSC2* −/− AML cells cultured for 24 h under normoxia with either vehicle (DMSO) or specified inhibitor alone or in combination (N=3). Concentrations of inhibitors used were, rapamycin (RAP) at 50 nM, Ku-0063794 (KU) at 1 µM, C188-9 at 30 µM and FLLL31 at 10 µM. Significance annotations above each bar on graphs (**C** & **D**) indicates significance of difference in protein concentration between each condition and vehicle only treated cells (DMSO). Statistical analysis of differences in protein concentration (N=3 minimum) was by student's t test. Significance denoted by: * = p <0.05, ** = p <0.01, *** = p< 0.001, NS = not significant. Bars represent standard error of the mean.

### 5.2.14 Through paracrine signalling *TSC2* deficient AML cells upregulate STAT3 activity in non-TSC cells.

Hyperactive STAT3 signalling is implicated in the pathology of many cancers (Kamran *et al*. 2013), in which aberrant STAT3 signalling can reshape the tumour microenvironment to promote metastasis (Chang *et al.* 2013), immuno-suppression (Jing *et al.* 2020) and angiogenesis (Yang *et al.* 2013b). In turn, upregulated STAT3 signalling within the tumour micro-environment can reinforce hyperactive STAT3 signalling within the tumour cells themselves (Wu *et al.* 2017a). Therefore, the final aim of the present chapter is to assay whether *TSC2* deficient AML cells, through paracrine signalling, could promote hyperactive STAT3 activity in non-TSC cells. Namely HK2 and HEK293 (HEK), as these are of renal origin like the AML cell lines.

As can be seen from the blot panels in figure 5.21 (**A**), conditioned media from the *TSC2* deficient AML cells, increased pSTAT3 Y705 in the HEK cell line. Which from the pSTAT3 Y705 blots, appeared enhanced for treatment with conditioned media from hypoxic *TSC2* deficient AML cells. In the HK2 line, only treatment with conditioned media from *TSC2* deficient AMLs cultured under hypoxia significantly increased pSTAT3 Y705 relative to the fresh media control (figure 5.21 **B**). These findings indicate enhanced stimulation of STAT3 activity of non-TSC cells by *TSC2* deficient AML cells under conditions of low oxygen availability. Furthermore, densitometry analysis found treatment with conditioned media from the *TSC2* RE AML cells, caused a significant decrease in the levels of pSTAT3 Y705 within the HK2 cells relative to the control (figure 5.21 **B**). On treatment with conditioned media from *TSC2* deficient AML cells and *TSC2* RE AML cells (under hypoxia), the level of pJAK2 (Y1007/1008) relative to the control increased. Indicating cytokine/growth factor receptors are being activated in HK2 cells. The antibodies used could not detect JAK2 in HEK cell lysates. Interestingly, conditioned media from both cell lines resulted in decreased p-rpS6 (S235/236) relative to the control in both HEK and HK2 cell lines (figure 5.21). A larger decrease in p-rpS6 (S235/236) within HEK and HK2 cells was observed on treatment with conditioned media from *TSC2* deficient AMLs than *TSC2* RE AML cells and this difference was reported as significant by densitometry analysis in the HEK cell line.

As well as increasing markers of STAT3 activity at the protein level, conditioned media from AML cells promoted nuclear accumulation of DNA bound STAT3 relative to the control within the HK2 and HEK cell lines (figure 5.22 **A**). This was only significant for HK2 cells treated with conditioned media from the *TSC2* deficient and *TSC2* RE AML cells cultured under normoxia. Whereas within the HEK cell line, the increase in nuclear accumulation of DNA bound STAT3 was substantial on conditioned media treatment from *TSC2* deficient AML cells, far higher than conditioned media treatment from *TSC2* RE AML cells.

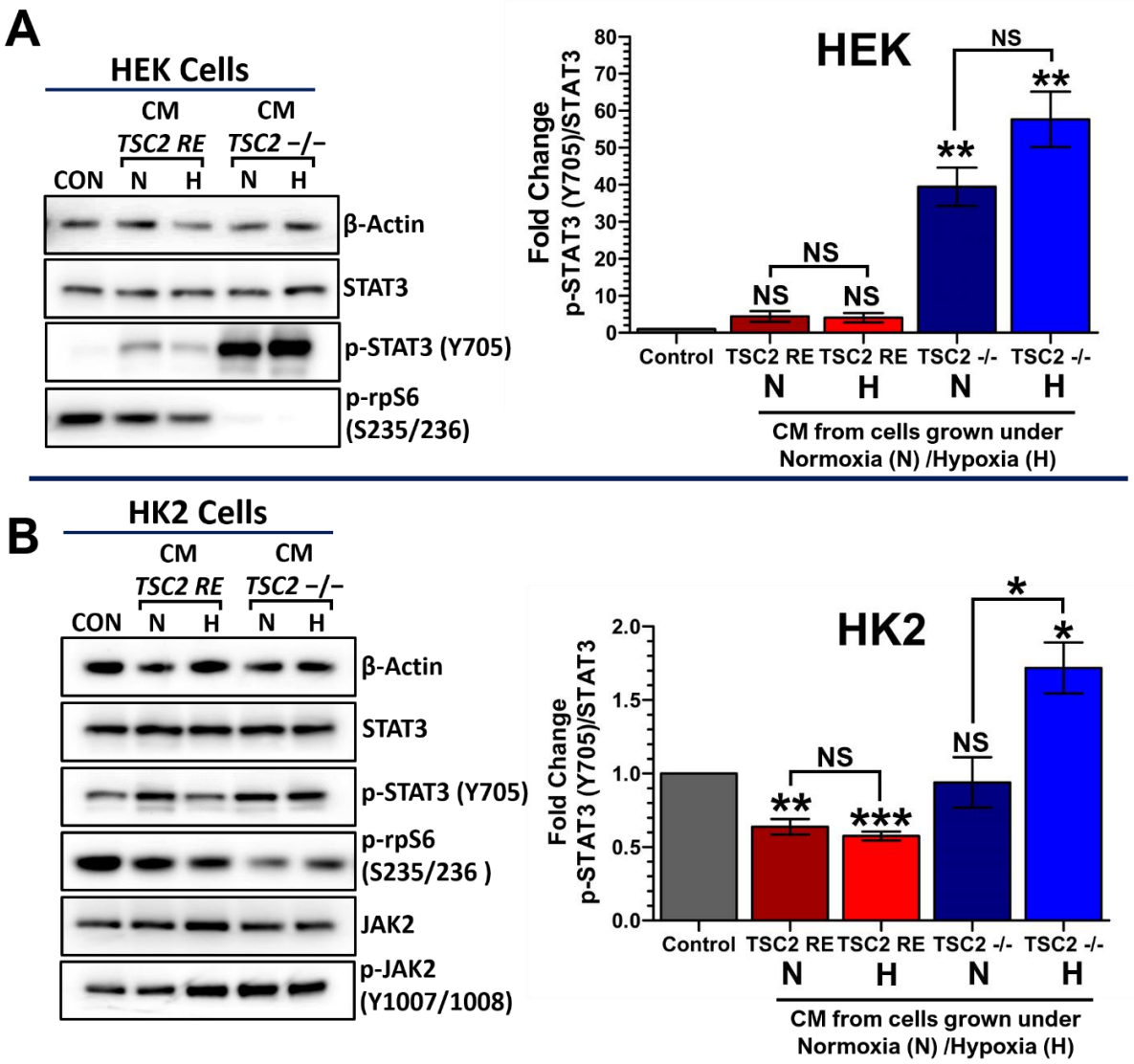


**Figure 5.21. Conditioned media from *TSC2* deficient AML cells increases pY705 STAT3 in HK2 and HEK cells.** Under normoxia, either HK2 (**A**) or HEK (**B**) cells were treated with fresh media (10% v/v FBS) (control) or conditioned media from *TSC2* deficient (*TSC2* −/−) or *TSC2* RE AML cells cultured for 24 h under either normoxia (N) or hypoxia (H). After 40 min of treatment HK2 and HEK cells were lysed and analysed through western blot. Densitometry analysis of resulting western blots (N=3 minimum) was performed, pSTAT3 Y705 was normalised to total STAT3 and expressed as fold changes compared to control sample. pSTAT3 Y705/STAT3 was normalised to cell number counts for *TSC2* −/− or *TSC2* RE AML cells from which conditioned media was taken. Significance annotations above each bar on graph indicates significance of difference in foldchange between each condition and HEK/HK2 cells treated with fresh media (control). Pairwise statistical comparisons between differences in foldchange between cells treated with conditioned media from *TSC2* deficient (*TSC2* −/−) under normoxia or hypoxia and between cells treated with conditioned media from *TSC2* RE AML cells under normoxia or hypoxia are also annotated. Statistical analysis (N=3 minimum) of differences in foldchange was by student's t test. Significance denoted by: * = p <0.05, ** = p <0.01, *** = p< 0.001, NS = not significant. Bars represent standard error of the mean. Predicted running band size (kDa) of protein targets can be found in chapter 2, table 2.6.

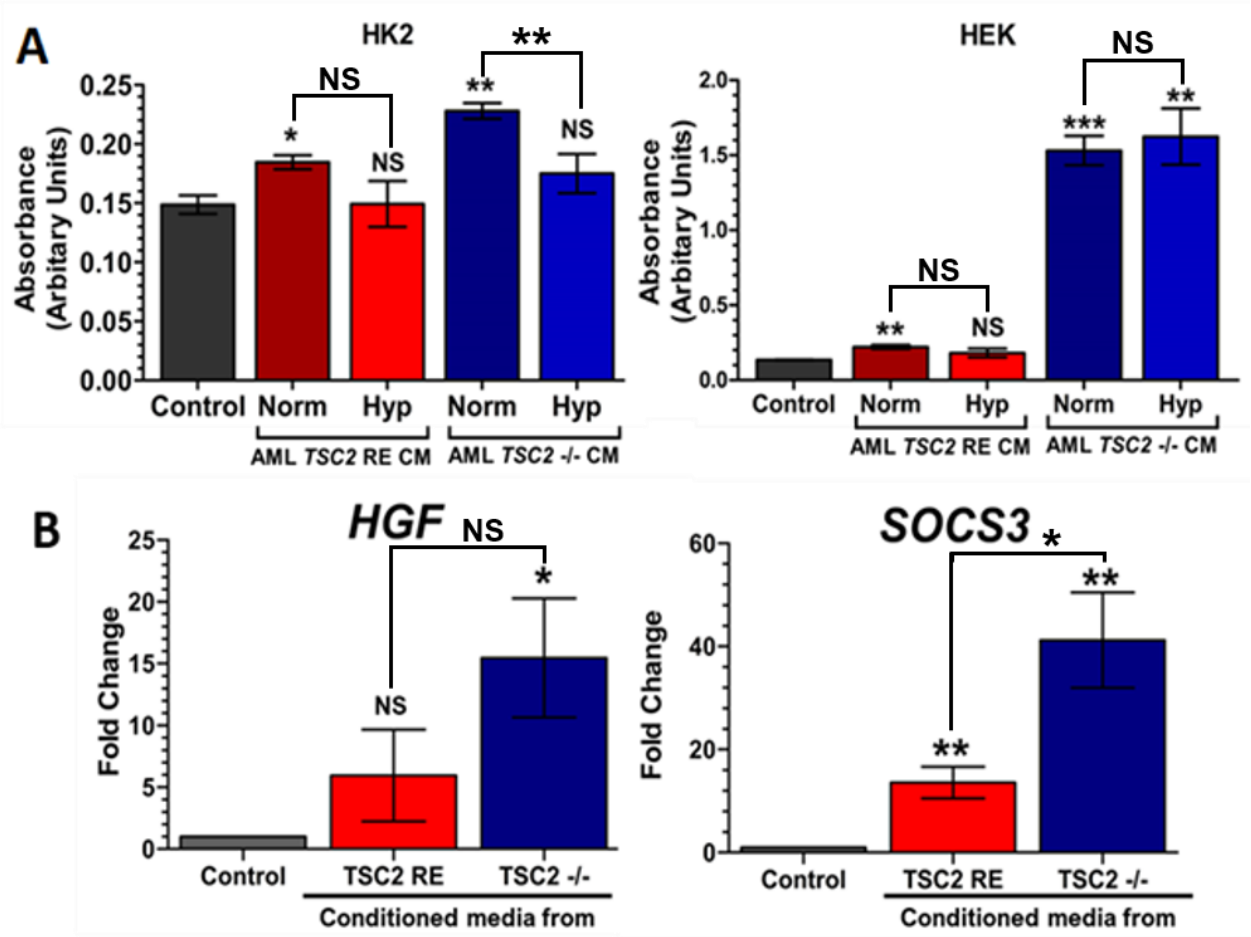


**Figure 5.22. Conditioned media from *TSC2* deficient AML cells increases nuclear accumulation of active STAT3 and upregulates expression of the STAT3 driven *HGF* and *SOCS3* in non-TSC cells. A:** Under normoxia, either HK2 or HEK cells were treated with fresh media (10% v/v FBS) (control) or conditioned media from *TSC2* deficient (*TSC2* −/−) or *TSC2* RE AML cells cultured for 24 h under either normoxia (Norm) or hypoxia (Hyp). After 40 min of treatment, concentrated nuclear lysates were generated from HK2 and HEK cells and then assayed for amount of active DNA binding STAT3 present using Active Motifs TransAM STAT3 ELISA. Significance annotations above each bar on graphs (A) indicates significance of difference in amount of active DNA binding STAT3 between cells treated with each conditioned media treatment and fresh media control. Pairwise statistical comparisons between differences in amount of active DNA binding STAT3 between cells treated with conditioned media from *TSC2* deficient (*TSC2* −/−) under normoxia or hypoxia and between cells treated with conditioned media from *TSC2* RE AML cells under normoxia or hypoxia are also annotated. Statistical analysis (N=3 minimum) of differences in amount of active DNA binding STAT3 was by student's t test. **B**: For 8 h HEK cells were treated with fresh media (10% v/v FBS) or conditioned media from *TSC2* deficient or *TSC2* RE AML cells cultured for 24 h under normoxia. Conditioned media was replenished 4 h into treatment. After treatment HEK cells were lysed and mRNA was purified from these lysates, converted to cDNA, and through qPCR, expression of target genes was quantified (N=4). Fold change in gene expression was calculated compared to a designated control sample. Fold changes of target genes were normalised to the housekeeping genes *HMBS* and *IPO8*. Significance annotations above each bar on graphs (**B**) indicates significance of difference in fold change between each conditioned media treatment and fresh media control. Pairwise statistical comparison between differences in foldchange in expression between conditioned media treated cells is also annotated. Statistical analysis (N=4) was by student's t test. Significance denoted by: * = p <0.05, ** = p <0.01, *** = p< 0.001, NS = not significant. Bars represent standard error of the mean.

Within the HEK cell line, conditioned media treatment from *TSC2* deficient cells substantially upregulated the expression of STAT3 driven genes (figure 5.22 **B**). *HGF* expression, as previously shown in chapter 4.2, was sensitive to STAT3 inhibition. HEK cells treated with conditioned media from *TSC2* deficient cells expressed *HGF* at 15 fold higher than the control. Increase in *HGF* expression within HEK cells treated with conditioned media from *TSC2* RE cells relative to the control was not reported as significant. *SOCS3*, an inhibitor of the STAT3 pathway rapidly upregulated on STAT3 activation (Starr *et al*. 1997 and Brender *et al*. 2001), was upregulated in the HEK cells treated with conditioned media from either cell line relative to the control. *SOCS3* expression is far higher in HEK cells treated with conditioned media from *TSC2* deficient cells than *TSC2* RE cells (41.5 fold vs 13.6 fold respectively) however (figure 5.22 **B**).. Which was reported as significant. Overall, these results show AML cells upon loss of *TSC2*, upregulate secreted factors that act in a paracrine manner to activate STAT3 signalling in non-TSC cells at the level of protein phosphorylation, subcellular location and target gene transcription.

## 5.3 Discussion

The data presented in the current chapter not only reinforces known aspects of STAT3 signalling within TSC, but elucidates new mechanisms of constitutive STAT3 activity. Elevated pY705 and pS727 STAT3 observed in *TSC2* deficient cells is consistent with constitutive phosphorylation of these sites previously demonstrated in both murine and human pre-clinical models of TSC (Onda *et al.* 2002, El-Hashemite and Kwiatkowski 2005 and Chan *et al.* 2004). Building on this work, the present work provides further evidence of hyperactive STAT3 signalling within *TSC2* deficient cells at the protein and mRNA level. Not only are phospho-markers of STAT3 activity (figures 5.1 and 5.2) upregulated on loss of *TSC2*, but so is the mRNA and protein expression of *STAT3* itself. Hyperactive STAT3 is likely driving its own expression within TSC cells, as *STAT3* is known to autoregulate its own expression (Ichiba *et al.* 1998 and Narimatsu *et al.* 2001). Genes encoding modulators of STAT3 signalling are also dysregulated on loss of *TSC2* in AML cells, with an expression signature indicative of hyperactive STAT3 signalling. That is upregulation of *STAT3, IL6, SOCS3* and *PIAS3* and downregulation of *IL6R* (figure 5.3). Whilst *SOCS3* expression is known to be rapidly increased on activation of STAT3 (Starr *et al.* 1997 and Brender *et al.* 2001) to dampen the STAT3 signalling. Interestingly however elevated SOCS3 protein expression was only observed within *Tsc2* −/− MEF cells, not AML cells. Potentially highlighting a disconnect in the autoregulating pathways within *TSC2* deficient AML cells that dampen STAT3 activity post stimulation. Within the AML lines, the amount of DNA binding STAT3 in nuclear cell fractions

was found to be almost two fold higher in AML cells deficient for *TSC2* relative to AML cells in which *TSC2* has been re-expressed (figure 5.7). This finding suggested a potential increase in STAT3 mediated transcription upon the loss of *TSC2*. This hypothesis was supported by the DEG analysis of STAT3 target genes in RNA sequencing data collected from TSC model cells and patient lesions. As the STAT3 driven transcriptome was found to be dysregulated in cells deficient for *TSC2* and patient lesions, especially SEN/SEGAs (figure 5.8). Additionally, many genes part of the STAT3 target gene set dysregulated in TSC lesions were significantly differentially expressed between the AML lines. Supporting the notion that dysregulated STAT3 mediated transcription is of clinical relevance within TSC. Whilst the present work provides the most detailed analysis of STAT3 driven transcription within TSC model cells, as could be told from the literature. STAT3 however has been shown to regulate the expression of many hundreds of genes within different settings and cell lines (Mirzaei *et al*. 2021). And therefore, an important limitation to the STAT3 target gene set compiled, is that for many of these genes it is not known if STAT3 mediates their expression in the context of TSC. Whilst beyond the scope of this work, chromatin immunoprecipitation sequencing of *TSC2* deficient and wildtype cells would help elucidate which dysregulated genes are STAT3 driven. Which would be key to understanding the transcriptional role of STAT3 in driving TSC pathogenesis.

At a broader transcriptional level, the transcriptome encoding STAT3 signalling components, STAT3 stimulatory cytokines and their cognate receptors were dysregulated upon loss of *TSC2* in cells and within TSC patient lesions (figures 5.4 and 5.5). Many cytokines/growth factors are known to stimulate STAT3 activity (Roca Suarez *et al.* 2018), some of which are already known to be upregulated in *TSC1* and *TSC2* deficient cells, such as HGF, EGF and IL-6 (Parker *et al.* 2011 and Wang *et al.* 2021a). DEG analysis of RNA sequencing data comparing *TSC2* −/− vs *TSC2* RE AMLs revealed that genes encoding STAT3 stimulatory cytokines/growth factors were also upregulated upon loss of *TSC2* in AML cells. Including *PDGFA/B*, *CCL2*, *CCL5, LIF, CSF1, IL12A* and *IL5*. mRNA expression of many of these cytokines/growth factors was elevated in TSC lesions, strengthening the clinical relevance of these findings. Fewer of these STAT3 stimulatory cytokines/growth factors were dysregulated between *Tsc2* −/− vs *Tsc2* +/+ MEF cells. However, conditioned media experiments showed that both *TSC2* deficient AML and MEF lines increase STAT3 activity in an autocrine manner, as judged by increases in pSTAT3 at Y705 (figures 5.17 and 5.18). And an increase over time in JAK2 phosphorylation at Y1007/1008 after serum starvation was observed within both *TSC2* deficient cell lines. Therefore, whilst the present work provides evidence that autocrine cytokine/growth-factor signalling to STAT3 is increased upon loss of *TSC2*, RNA sequencing analysis suggests that there may be a difference between the AML and MEF lines in which STAT3 stimulatory cytokines/growth-factors auto-activate STAT3 activity. Further work

analysing protein expression of such STAT3 stimulatory between the two cell lines is needed to further test this hypothesis however.

One of the original hypotheses of the present chapter, was that STAT3 activity would be elevated further under hypoxic conditions. Informed by the fact that many of the tissues affected by TSC, have hypoxic gradients across them (Northrup *et al*. 2013) and hypoxia has been shown to elevate STAT3 activity in certain cancers (Pawlus *et al*. 2014 and Soleymani Abyaneh *et al*. 2017). However, it was found that overall hypoxia did not have a significant effect on protein markers of STAT3 activity in *TSC2* deficient cells (figures 5.1 and 5.2) or mRNA expression of STAT3 regulated genes in *TSC2* deficient AML cells (figure 5.3). Additionally, whilst DEG analysis found many STAT3 target genes were significantly differentially expressed between *TSC2* deficient AML cells cultured under hypoxia relative to normoxia. The foldchange in expression for majority of these genes were relatively small however (figure 5.8). This data suggests within TSC cells hypoxia is not a main driver of STAT3 activity itself, except outside the context of angiogenesis (see chapter 4).

Cross-talk between the mTORC1 and STAT3 signalling pathways driving pathogenesis has been described in certain cancers (Li *et al,* 2020, Lin *et al.* 2021 and Zhou *et al.* 2007), with studies highlighting dual targeting of mTORC1 and STAT3 being effective at reducing scores of tumorigenicity in multiple cancer cell lines (Jin *et al.* 2014, Miyata *et al.* 2017 and Wang *et al.* 2021b). How aberrant mTORC1 and STAT3 signalling interplay to drive pathology within TSC is less well understood. Dodd *et al.* (2015) showed that mTORC1 drives *HIF1A* and its downstream target *VEGFA* through activating STAT3. Data in chapter 4 built on this finding and showed that dual inhibition of both mTORC1 and STAT3 was more effective at downregulating expression of pro-angiogenic targets that inhibiting either mTORC1 or STAT3 alone. Namely protein expression of HIF1A and HGF, and mRNA expression of *VEGFA* and *HGF*. Similarly, within the data forming the current chapter, it was observed dual inhibition of both mTORC1 and STAT3 more effective at downregulating STAT3 responsive genes. Namely, *STAT3, IL6R, SOCS3* and *PIAS3* within *TSC2* deficient AML cells (figure 5.6). Rapamycin treatment significantly downregulated expression of *STAT3*, *IL6R* and *SOCS3*. Whilst not transcriptionally active itself, mTORC1 has an extensive influence of gene expression through regulating the activity of target transcription factors (Laplante and Sabatini, 2013). Which include mTORC1s phosphorylation of STAT3 at S727 (Dodd *et al.* 2015), thought to be required for STAT3 to be fully transcriptionally active (Wen *et al.* 1995). Therefore, mTORC1 inhibition likely downregulates expression of these genes through a reduction in pS727 STAT3, as seen when *TSC2* deficient cells were treated with rapamycin (figure 5.12). Inhibition of phosphorylation of STAT3 at both the Y705 and S727 residues, by combinatorial treatment of rapamycin and C188-9 (figure 5.13) may explain the greater

reduction in target gene expression. However, despite rapamycin treatment elevating pSTAT3 Y705 in *TSC2* deficient cells (figure 5.12), rapamycin treatment alone by in large repressed STAT3 target gene expression (relative to DMSO) within *TSC2* deficient cells AML cells (figure 5.15). C188-9 treatment meanwhile repressed both the S727 and Y705 phosphorylation of STAT3 in *TSC2* deficient AMLs, but was found to be less effective at normalising STAT3 target gene expression found to be dysregulated in this cell line (figure 5.15 and table 5.3). These findings highlight that repression of the S727 phosphorylation site within TSC cells may be more important in decreasing STAT3 driven transcription than the Y705 phosphorylation site.

Interestingly RNA sequencing analysis of *TSC2* deficient AML cells treated with either rapamycin or C188-9 revealed these inhibitors normalised dysregulated expression of genes encoding components of the mTORC1/2 complexes. Both decreased the expression of the mTORC1 core component *RPTOR*, whilst upregulating the expression of the mTORC1/2 inhibitor *DEPTOR* (Peterson *et al.* 2009). Both had the additional effect of downregulating the expression of the active kinase itself, *MTOR*. Within the literature limited data on the effect of mTORC1/STAT3 inhibition on the expression of genes encoding the mTORC1 complex was found. Lee *et al.* (2020a) found siRNA inhibition of *STAT3* downregulated expression of *MLST8*, a component of the mTORC1 and mTORC2 complexes, and attenuated phosphorylation of 4E-BP1. Efficacy of targeting STAT3 to inhibit mTORC1 in TSC is further supported by the finding that inhibition of STAT3, through C188-9, over time reduced phosphorylation of rpS6 at S235/236 in both *TSC2* deficient cells and phosphorylation of 4E-BP1 at P65 and T37/40 in *TSC2* deficient cells AML cells (figures 5.13 and 5.14). However, the present work doesn't allow for the hypothesis that STAT3 inhibition represses mTORC1 to be firmly concluded. Firstly, the other STAT3 inhibitor used, FLLL31, wasn't effective at repressing phosphorylation of STAT3 at either Y705 and S727 within *TSC2* deficient cells. Despite FLLL31 previously being found by Dodd *et al.* (2015) to suppress CNTF and insulin mediated phosphorylation of STAT3 Y705 and S727, in non-TSC cells. Secondly co-treatment of *TSC2* deficient AML cells with rapamycin and C188-9 did not repress rpS6 and 4E-BP1 phosphorylation more than either inhibitor alone (figure 5.14). Therefore, more work with another more effective STAT3 inhibitor, or siRNA targeting of STAT3, must be performed to rule out C188-9 treatments repression of mTORC1 potentially being through off-target drug effects.

*TSC2* deficient AML cells express IL-6 protein and mRNA many fold higher than *TSC2* RE AML cells (figures 5.3 and 5.20). Whilst elevated IL-6 expression in pre-clinical models of TSC is not a novel finding, the present work found IL-6 protein expression is further increased under rapamycin, C188-9 and FLLL31 treatment. This contrasted with work by Wang *et al.* (2021a), which found rapamycin treatment decreased IL-6 secretion within the *Tsc2* −/− MEF line. The

increased IL-6 secretion within the *TSC2* deficient AML line on mTORC1/STAT3 inhibition maybe due to the dephosphorylation of STAT3 protein at Y705 and S727. Unphosphorylated STAT3 is able to regulate gene expression. As demonstrated by Yang *et al.* (2005), who found overexpressing a mutant of STAT3 incapable of being phosphorylated at Y705, resulted in increased expression of a subset of genes that included *IL6* and *CCL5* (previously shown to be upregulated under C188-9 treatment, chapter 4). The presence of unphosphorylated STAT3 may explain why IL-6 is elevated within *TSC2* deficient cells in the first place. Narimatsu *et al*. (2001) found that *STAT3* is upregulated by IL-6 treatment and Yang *et al.* (2005) and Yang *et al.* (2007) both found long term IL-6 treatment increases amount of unphosphorylated STAT3. The present data has shown not only that IL-6 expression is elevated within *TSC2* deficient AML cells, but that STAT3 protein and mRNA expression is enhanced upon loss of *TSC2* in both AML and MEF cells. Whilst levels of pSTAT3 Y705 increased in both cell lines on IL-6 stimulation (figure 5.19). Increased IL-6 expression within *TSC2* deficient AML cells treated with rapamycin may also help explain why on rapamycin treatment, levels of pSTAT3 Y705 increase. As IL-6 induces the phosphorylation of STAT3 at Y705 (Kaptein *et al*. 1996). Furthermore, increased IL-6 expression observed in *TSC2* deficient AML cells under C188-9 or FLLL31 treatment may be why phosphorylation of STAT3 at Y705 isn't consistently repressed by these inhibitors. As targeting of STAT3s SH2 domain by C188-9 or FLLL31 (Bharadwaj *et al*. 2016 and Lin *et al*. 2010) may only block part of increased signal transduction from activated receptors.

However, the presence of either phosphorylated or unphosphorylated STAT3 in *TSC2* deficient cells does not explain the differences observed in nuclear active STAT3 (DNA bound STAT3) on inhibition with rapamycin, C188-9 or FLLL31. Rapamycin appeared to increase the proportion of DNA binding STAT3, as did FLLL31 treatment, in *TSC2* deficient AMLs (figure 5.7). However, C188-9 treatment reduced the amount of DNA binding STAT3. The Active Motif ELISA kits used are coated with oligonucleotides containing consensus GAS (interferon γ-activated sequence) elements (Waitkus *et al.* 2013) for STAT3. Both tyrosine phosphorylated and unphosphorylated STAT3 have been shown to bind STAT3's GAS (interferon γ-activated sequence) motif (Tian *et al.* 1994 and Timofeeva *et a*l. 2012). Within the *TSC2* deficient AML cells, an increase in pSTAT3 Y705 phosphorylation on IL-6 treatments was observed with a decrease in the amount of DNA binding STAT3 (figure 5.19). Thus, if in the *TSC2* deficient AML cell line, repression of pSTAT3 Y705 on C188-9 treatment decreased the amount of DNA binding STAT3, then the inverse would be expected. In the *Tsc2* −/− MEF cell line, changes in amount of DNA binding STAT3 from stimulation or drug inhibition were as expected. That is mTORC1 and STAT3 inhibition decreased the amount of DNA binding STAT3, whilst increasing doses of IL-6 increased the amount of DNA binding STAT3. It should be noted

however that concentrations of IL-6 used for treatment were far in excess of the IL-6 concentration present in the media of *TSC2* deficient AML cells. Therefore, it is possible that increased negative regulatory signalling impacted the amount of DNA binding STAT3 within AML *TSC2* deficient cell line. The effect of treatments on phosphorylation of STAT3 at S727 may not play a role in our assays quantifying DNA binding STAT3. As Wen and Darnell Jr (1997) found no difference in the DNA binding capacity between wild type STAT3 and a mutant STAT3 in which the serine at residue position 727 had been substituted for an alanine. Lastly, as STAT3 nuclear import is thought to be constitutive and independent of its phosphorylation status (Liu *et al*. 2005), treatments used may not directly affect the nuclear localisation of either unphosphorylated or phosphorylated STAT3. But instead affect STAT3 DNA binding affinity.

The data gathered within this chapter strongly suggests that *TSC2* deficient cells, at least in part, maintain their constitutive STAT3 signalling through an autocrine mechanism. Previous studies have suggested that *TSC1/TSC2* deficient cells may autoregulate their STAT3 activity. Additionally, a recent study by Wang *et al.* (2021a) suggested *TSC2* deficient cells maintain their hyperactive STAT3 signalling in part through IL-6 secretion. They found that treating *TSC2* deficient cells with an anti-IL-6 antibody attenuated phosphorylation of STAT3 at Y705. And that the IL-6 receptor α was highly expressed in the membrane fraction of *Tsc2 −/−* MEF cells compared to *Tsc2* +/+ MEF cells. As mentioned, STAT3 stimulatory cytokines have been shown to be upregulated within *TSC2* deficient cells and TSC lesions (figures 5.4 and 5.5). The present work has also shown that *TSC2* deficient cells spontaneously recover Y705 STAT3 phosphorylation overtime in serum starvation (figure 5.17). Additionally short term treatment of *TSC2* deficient cells with conditioned media from separate cultures of *TSC2* deficient cells cultured for 24 h, massively elevated pSTAT3 Y705 relative to fresh media (figure 5.18). Even when cultured under serum starved conditions. The increase in pSTAT3 Y705 was not observed if conditioned media treatment was sourced from cells cultured in the presence of protein transport inhibitors. Therefore, strongly suggesting a secreted factor or factors are responsible for the elevation in pY705 STAT3. Lastly, not only do *TSC2* deficient cells maintain their own constitutive STAT3 signalling by autocrine signalling, they can stimulate STAT3 activity in non-TSC cells (HK2 and HEK293 cells). At the level of protein markers of STAT3 activity (figure 5.21), nuclear localisation of STAT3 (figure 5.22) and STAT3 driven gene expression. These findings highlight that *TSC2* deficient cells within TSC associated lesions likely influence the signalling of cells within their environment in ways which promote pathogenesis. Through activated STAT3 signalling for example. However, it should be noted that the HK2 and HEK293 cells utilised in this work are not heterozygous for *TSC2* or *TSC1*, as would be the case for most cells outside of TSC associated lesion in patients (Peron *et al.* 2018a).

# Chapter 6: Characterising the oxidative stress response of *TSC2* deficient cells

## 6.1. Introduction

In previous chapters, the activity and expression of HIF-1α, STAT3 and Ref-1 were shown to be elevated upon loss of *TSC2*. The activity of these transcription factors and regulators are positively impacted by oxidative stress. The ability of Ref-1 to transactivate HIF-1α and STAT3 (Shah *et al.* 2017) is dependent on the redox status of the cell (Xanthoudakis *et al.* 1992). Reactive oxygen species (ROS) are found to modulate the mRNA and protein expression of Ref-1 (Ramana *et al.* 1998, Pines *et al.* 2005, Jiang *et al.* 2015 and Hu *et al.* 2021). Multiple studies have found that mitochondria generated ROS stabilised HIF-1α protein and elevated its transcriptional activity (Chandel *et al.* 2000 and Mansfield *et al.* 2005). While studies reported that ROS enhanced HIF-1α protein stability by inhibiting prolyl hydroxylases that would consequently decrease proteasome targeted degradation of HIF-1α (Lu *et al.* 2005, Pan *et al.* 2007 and Lee *et al.* 2016). Treatment of multiple cancer cell lines with exogenous ROS or ROS scavengers modulated phosphorylation markers of STAT3 activity (Mohammed *et al.* 2020, Chen *et al.* 2016 and Yoon *et al.* 2010) and enhanced the DNA binding ability of STAT3 (Yoon *et al.* 2010 and Li *et al.* 2010).

Elevated levels of oxidative stress and ROS within TSC diseased cells may contribute to the observed pathogenic enhancement of HIF-1α, STAT3 and Ref-1 that is reported within this work. Several studies have previously suggested that loss of either *TSC1* or *TSC2* elevates oxidative stress. Chen *et al*. (2008) found that deletion of *TSC1* in hematopoietic stem cells increased ROS levels and mitochondrial biogenesis. Whilst Suzuki *et al.* (2008) showed that overexpression of *TSC2* mutants within COS-1 cells increased ROS levels. Elevated oxidative stress has also been observed in rodent neuronal models of TSC. Ebrahimi-Fakhari *et al.* (2016) found that either *TSC1*- or *TSC2*-deficient neuronal cells showed impaired mitophagy, enhanced mitochondrial load while impairing oxidative phosphorylation. Di Nardo *et al.* (2009) showed that *TSC2* deficient rat hippocampal neurons had elevated mitochondrial ROS. Murine cells deficient in *Tsc2* have also been shown to have increased levels of glutathione, a key endogenous antioxidant (Champion *et al.* 2022 and Torrence *et al.* 2021). Increased oxidative stress also appears to increase tumour burden in animal models of TSC. Habib *et al.* (2003) found a greater incidence of kidney tumours in Eker rats (a TSC model animal) on treatment a ROS inducing drug, TGHQ (2,3,5- tris -(glutathion- S -yl)hydroquinone). Furthermore, it was shown drug induced oxidative stress depleted the active glutathione pool and was selectively cytotoxic to *Tsc2* −/− MEF (Li *et al.* 2015) and *TSC2* deficient AML cells (Medvetz *et al.* 2015). Cytotoxicity observed in these studies was blocked by co-treatment with antioxidants. Research so far highlights that a better understanding of the redox sensitive

pathways within TSC is required, which might have therapeutic benefit for patients. Therefore, within the final result chapter, oxidative stress responses of *TSC2* deficient cells will be explored within three main aims. The first aim utilises RNA sequencing data sets used in prior chapters to explore oxidative stress response gene expression differences in *TSC2* deficient cells and TSC patient associated lesions. These include genes that restore redox homeostasis. The second aim was to assess the cytotoxicity and selectivity of ROS inducing agents in human and murine TSC model cells. Cytotoxicity of these agents was further tested when combined with inhibitors of mTORC1 or Nrf2. Nrf2 is the master regulator of the cells oxidative stress response (Tonelli *et al*. 2018). The third aim was to briefly examine the relationship between STAT3/HIF-1α activity and the redox status of *TSC2* deficient cells.

## 6.2 Results

### 6.2.1 Expression of Nrf2 target genes are upregulated in TSC associated lesions and *TSC2* deficient AML and MEF cells.

Nrf2 is a key regulator of the cell's response to oxidative stress (Tonelli *et al.* 2018). Nrf2 transcribes genes involved in detoxifying ROS, glutathione biosynthesis and iron metabolism. Immunohistochemical analysis of SEGA tissue by Malik *et al.* (2015) found increased expression of two Nrf2 target genes, *GCLC* and *HMOX1*. The authors showed that inhibition of GCLC, a key enzyme in the glutathione biosynthesis, raised the protein expression of Nrf2 further in SEGA derived cell lines. Therefore, the first aim of this result chapter was to examine whether loss of *TSC2* elicits a transcriptional response that is indicative of increased redox stress. Differentially expressed gene (DEG) analyses of Nrf2 target genes was carried out within RNA sequencing data of TSC model cell lines. To assess clinical relevance, Nrf2 target gene expression was then compared to RNA sequencing data from patient lesions. Additionally, the effect of hypoxia on Nrf2 target gene expression will be assayed as hypoxia can further promote the generation of ROS (Wang *et al.* 2007b and Kondoh *et al.* 2013).

DEG analysis of RNA sequencing data comparing TSC lesions to non-TSC tissue, reveals many Nrf2 target genes that are differentially expressed (figure 6.1). Findings were more pronounced within SEN/SEGA lesions, relative to the normal brain tissue, as shown by the volcano plot in figure 6.1 (**A**). Out of the 64 genes within the Nrf2 target gene set, 42 were significantly differentially expressed. The vast majority of Nrf2 target genes are significantly upregulated (39 genes), with only 3 genes significantly downregulated. With regards to the DEG analysis of other TSC lesions vs non-TSC tissue. Renal AMLs and cortical tubers have less Nrf2 target genes that are differentially expressed (see supplemental figure S.6.1). Out of the 64 genes within the Nrf2 target gene set, 20 significantly differentially expressed genes

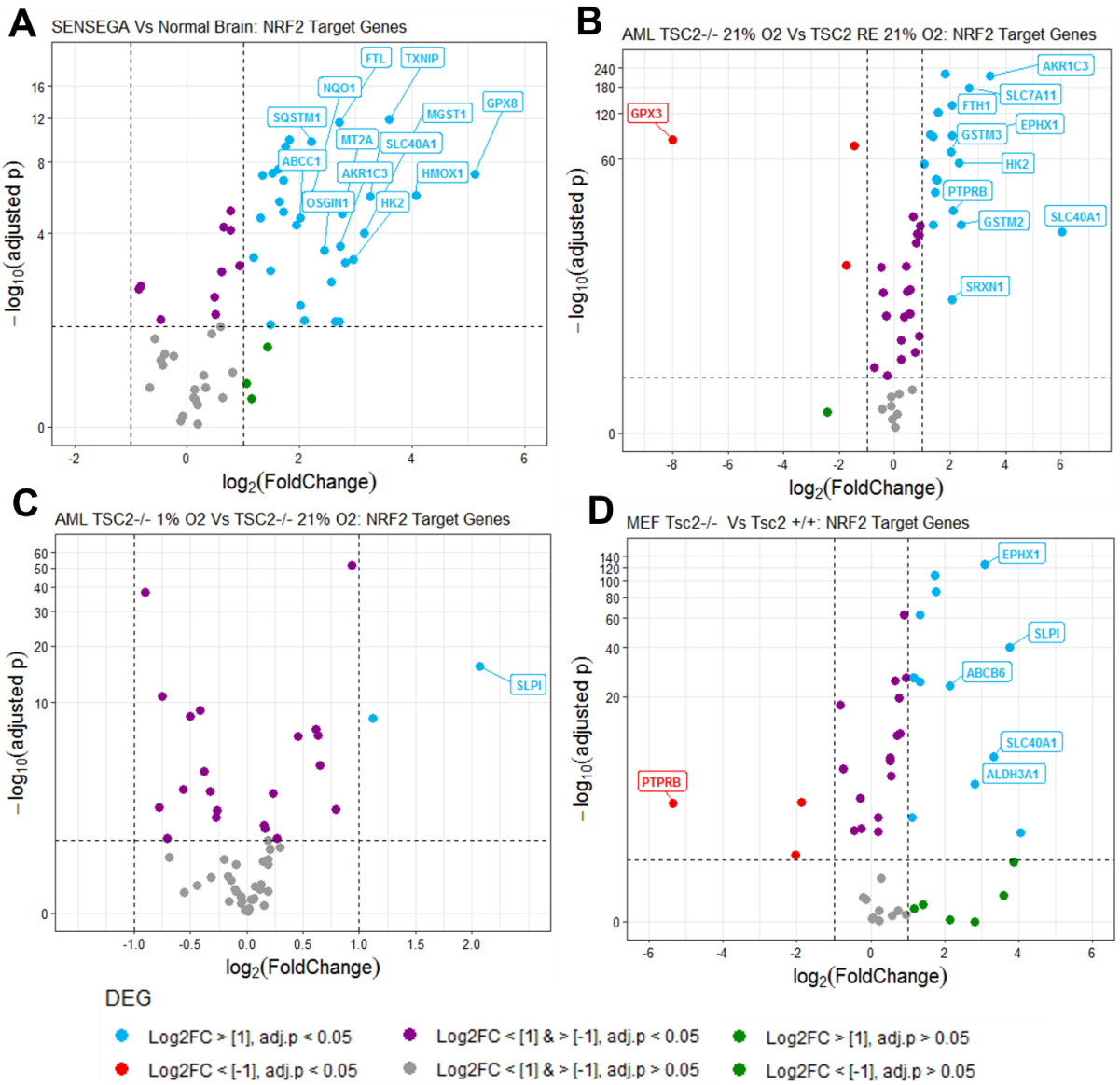


**Figure 6.1 Genes encoding NRF2 target genes are dysregulated upon loss of *TSC2* within patient tumours, and AML and MEF cell lines.** Differential gene expression (DEG) comparison is annotated above each plot. Volcano plot **A** was generated from previously published RNA sequencing data which Prof. Jeffrey MacKeigan gave us access to. This data set compares gene expression of donated TSC patient tumours samples versus non-TSC healthy tissue samples, in this case SEN/SEGA (Subependymal nodules/ Subependymal giant cell astrocytomas) (N=15) versus normal brain (N=8), see Martin *et al*. (2017). Volcano plots **B** and **C** were generated from RNA sequencing data, comparing either AML *TSC2* deficient and *TSC2* RE (re-expressed) cells cultured under either normoxia (21% O2) or hypoxia (1% O2) (N=6). Volcano plot **D** was generated from RNA sequencing data comparing MEF *Tsc2* −/− and *Tsc2* +/+ (N=3) cells. RNA sequencing for volcano plots **B**, **C** and **D** was conducted through Wales Gene Park and expression levels were calculated and normalised from raw read counts as RPKM (Reads per Kilobase exon Model per million mapped reads) with DEG analysis generated through DEseq2 analysis and resulting p-values were corrected for multiple testing and false discovery by FDR method. For all volcano plots Log2 transformed fold change in expression of genes was plotted against their -log10 transformed FDR adjusted p-values. Dotted lines at x axis represent increase or decrease in foldchange of 2 or -2 respectively. Dotted line at y axis represents significance threshold of 0.05. Genes annotated had a Log2 fold change in expression greater or lower than 2 or -2 (i.e. four fold higher or lower in expression) respectively and an -log10 adjusted p-value greater than 3 (i.e. below 0.001 significance threshold).

were upregulated within cortical tubers relative to normal brain tissue. Whereas renal AMLs relative to normal kidney tissue, 21 genes were significantly differentially expressed (11 upregulated and 10 downregulated). Within all three TSC lesions, the majority of Nrf2 target genes were upregulated, indicating elevated oxidative stress present within tumours associated with TSC.

As with TSC associated lesions, AML cells lacking *TSC2* showed elevated Nrf2 target gene expression relative to *TSC2* RE cells (figure 6.1 **B**). As can be seen by the cross comparisons of DEG analyses of Nrf2 target genes between RNA sequencing data sets in table 6.1. DEG analyses within the AML cell line RNA seq data set revealed that out of 53 Nrf2 target genes (expression of all 64 genes part of the full Nrf2 target gene set was not detectable), 44 were significantly differentially expressed. With 36 genes being upregulated and 8 being downregulated. As seen in figure 6.1 (**C**), hypoxia (1%$O_2$) doesn't have a pronounced impact on Nrf2 target gene expression within *TSC2* deficient AML cells. Under hypoxia, Nrf2 target gene expression had similar numbers of significantly differentially expressed genes. DEG analysis of another TSC model cell line, similarly finds elevation of Nrf2 target gene expression. On loss of *Tsc2* within MEFs, 32 out of the 48 Nrf2 target genes assayed were significantly differentially expressed (figure 6.1 **D**). Again, the majority of those differentially expressed genes were upregulated (24 genes) as opposed to downregulated (8 genes). As seen in table 6.1, findings from both TSC model cell lines demonstrate an upregulation of Nrf2 mediated gene transcription upon *TSC2* loss and suggests that there could be a higher level of oxidative stress.

Over half of the genes within the Nrf2 target gene set were differentially expressed between *TSC2* −/− AML and *TSC2* RE AML cells and between at least one TSC associated lesion and non-TSC tissue. Differential expression of these 39 genes between RNA sequencing is highlighted in the heatmap in figure 6.2. As shown, foldchange in expression of these Nrf2 genes varies between lesions relative to their matched non-TSC tissue. The same is the case comparing the human and murine TSC model cell lines under normoxia. However, comparing the SEN/SEGA vs NB and *TSC2* −/− vs *TSC2* RE AML cells DEG analyses, the majority of differentially expressed genes common in both analyses are expressed in the same direction (27 genes). That is for example, a gene being upregulated within the SEN/SEGAs and *TSC2* −/− AML cells as opposed to upregulated within the SEN/SEGAs but downregulated within the *TSC2* −/− AML cells. The trends are clear that there is an upregulation of Nrf2 mediated gene expression between data sets analysed in TSC associated lesions and TSC cell line models.

As part of the present analysis, an additional gene set was analysed. This gene set was termed "endogenous antioxidants" and composed of genes again involved in maintaining redox

homeostasis. This includes genes involved in the synthesis of glutathione, and families of enzymes that utilise the glutathione and thioredoxin systems to reduce harmful free radicals. As with the Nrf2 target gene set, expression of “endogenous antioxidant” genes were largely upregulated within TSC brain lesions and *TSC2* deficient cells. Volcano plots and a heatmap summarising analyses of the “endogenous antioxidants” gene set can be seen in supplemental figures S.6.1, S.6.2. and S.6.3.

**Table 6.1 Cross comparison of DEG analyses between data sets – NRF2 target genes**

| Comparison | Detectable genes / 67 | Sig. diff. expressed genes | Sig. Upregulated Log2FC = 0 – <1 | Sig. Upregulated Log2FC = >1 | Sig. Downregulated Log2 FC = >-1 – 0 | Sig. Downregulated Log2 FC = <-1 |
|---|---|---|---|---|---|---|
| SEN/SEGA Vs normal brain | 64 | 42 | **7** | **32** | **3** | **0** |
| Cortical tuber Vs normal brain | 64 | 20 | **9** | **11** | **0** | **0** |
| Renal AML vs normal kidney | 64 | 21 | **1** | **10** | **1** | **9** |
| | | | | | | |
| *TSC2* −/− AML vs *TSC2* RE AML 21% $O_2$ | 53 | 44 | **15** | **21** | **5** | **3** |
| *TSC2* −/− AML 1% $O_2$ vs 21% $O_2$ | 56 | 23 | **10** | **2** | **11** | **0** |
| | | | | | | |
| *TSC2* −/− MEF vs *TSC2* +/+ MEF 21% $O_2$ | 48 | 32 | **11** | **13** | **5** | **3** |

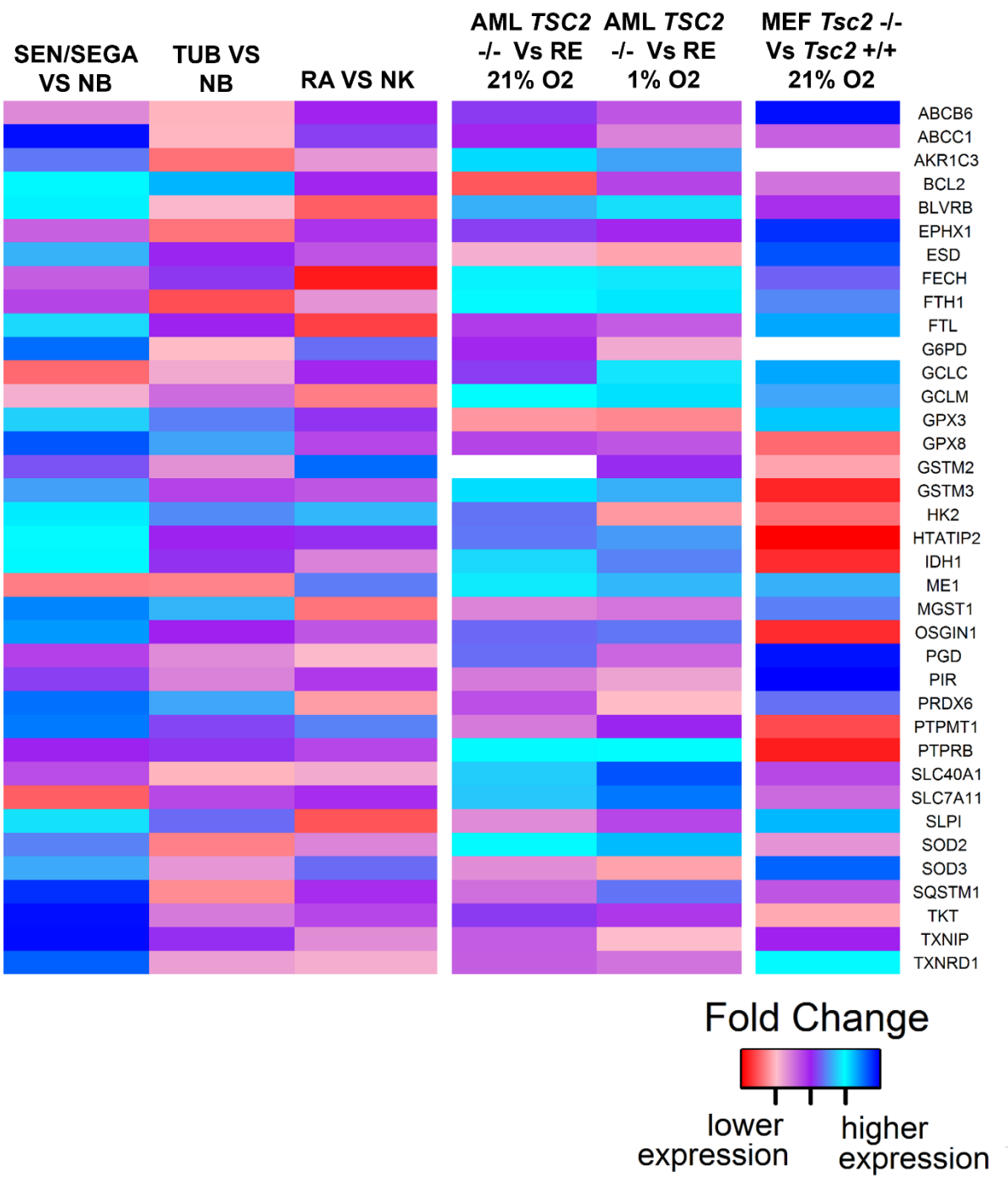


**Figure 6.2 NRF2 target genes are differentially expressed between TSC tumour types, human and murine cell models lines of TSC.** The above heatmap compares the fold change in expression of NRF2 target genes between either a TSC lesion and healthy tissue or a *TSC2* deficient (−/−) cell line with a *TSC2* re-expressed (RE) (AML) or *TSC2* +/+ (MEF) cell line. Genes selected for the heatmaps are those which are significantly differentially expressed between the *TSC2* −/− and *TSC2 RE* cell lines (under either oxygen conditions) and between at least one TSC lesion and healthy tissue. Differential gene expression (DEG) comparison is annotated above each column and the oxygen conditions, 21% $O_2$ (normoxia) or 1% $O_2$ (hypoxia), cell lines were cultured under is also denoted. White spaces within columns indicate that gene's expression was not detectable in that data set. Gene names are shown on the right of the heatmap. It should be noted these data sets are distinct, generated differently from one another (see methods and materials section). **SEN/SEGA** = subependymal nodule/Subependymal giant cell astrocytomas, **NB** = normal brain, **TUB** = TSC tuber, **RA** = renal angiomyolipoma, **NK** = normal kidney.

### 6.2.2 Loss of *TSC2*, but not hypoxia, elevates Nrf2 target gene expression within AML cells, and oxidative stress markers in AML and MEF cells.

The next aim was to validate expression of antioxidant genes by qPCR and protein expression by western blot. Oxygen availability has been linked to Nrf2 activity, so normoxia and hypoxia culture conditions were also compared. Hypoxia was found to elevate Nrf2 target gene expression in lung (Kim *et al.* 2007) and breast cancer (Syu *et al.* 2016) cell lines. It was found that silencing of Nrf2 in both colon and breast cancer cells suppressed the accumulation of HIF-1α, even under hypoxia (Kim *et al*. 2011c and Lee *et al.* 2019).

Nrf2 (*NFE2L2*) mRNA expression was substantially elevated upon loss of *TSC2* irrespective of oxygen availability (figure 6.3). Foldchange (FC) of which, relative to AML *TSC2* RE cells, is maximum under hypoxia (FC=3.22 p=0.0002). Hypoxia did not significantly alter expression of *NFE2L2* in either *TSC2* deficient or *TSC2* RE AML cells. Other genes assayed involve ROS detoxification at different compartments of the cell. *SOD3* encodes an extracellular protein, belonging to the superoxide dismutase family, that catalyses the dismutation of superoxide (Nguyen *et al.* 2020). *GPX4* and *GPX8* encode for glutathione peroxidases that prevent free radical formation from lipid hydroperoxides (Flohé *et al.* 2022). *MGST1* encodes an enzyme with broad substrate specificity and is localised primarily to the mitochondria where it conjugates electrophiles to glutathione (Kuang *et al.* 2021). *TXNRD1* gene product reduces and thereby replenishes active thioredoxin, which in turn can scavenge ROS (Cadenas *et al.* 2010).

Expression of all of these genes is elevated upon the loss of *TSC2*. Foldchange in mRNA expression of *SOD3*, *GPX8*, *MGST1* and *GPX4*, relative to AML *TSC2* RE cells, was highest under hypoxia (*SOD3*: FC=2.81 p= 0.0044, *GPX8*: FC=8.39 p=2.19x$10^{-5}$, *MGST1*: FC=1.85 p=0.0014 and *GPX4*: FC=1.76 p=0.0066) (figure 6.3). Whilst for *TXNRD1*, expression was highest under normoxia (FC=1.77 p=0.0002). mRNA expression for majority of the genes was found to be highest within *TSC2* deficient cells under hypoxia and significantly higher than observed in *TSC2* RE AML cells cultured under hypoxia. In addition, hypoxia did not significantly affect the mRNA expression of *SOD3*, *GPX8*, *MGST1*, *GPX4* or *TXNRD1* within *TSC2* deficient AML cells relative to normoxic culture conditions.

Genes related to ferroptosis, iron metabolism and storage were also upregulated upon loss of *TSC2*, as seen in figure 6.4. Iron is not only essential for oxygen transport but also as a cofactor in enzymatic catalysis and electron transfer within multiple cellular processes (Hentze *et al.* 2010). However, intracellular iron levels must be tightly regulated, as excess ferrous iron can generate highly reactive hydroxyl radicals through Fenton chemistry. Overwhelming of the glutathione antioxidant systems results in the non-apoptotic oxidative cell death termed ferroptosis (Kerins and Ooi, 2008). Ferroptosis is characterised by the iron dependent cell

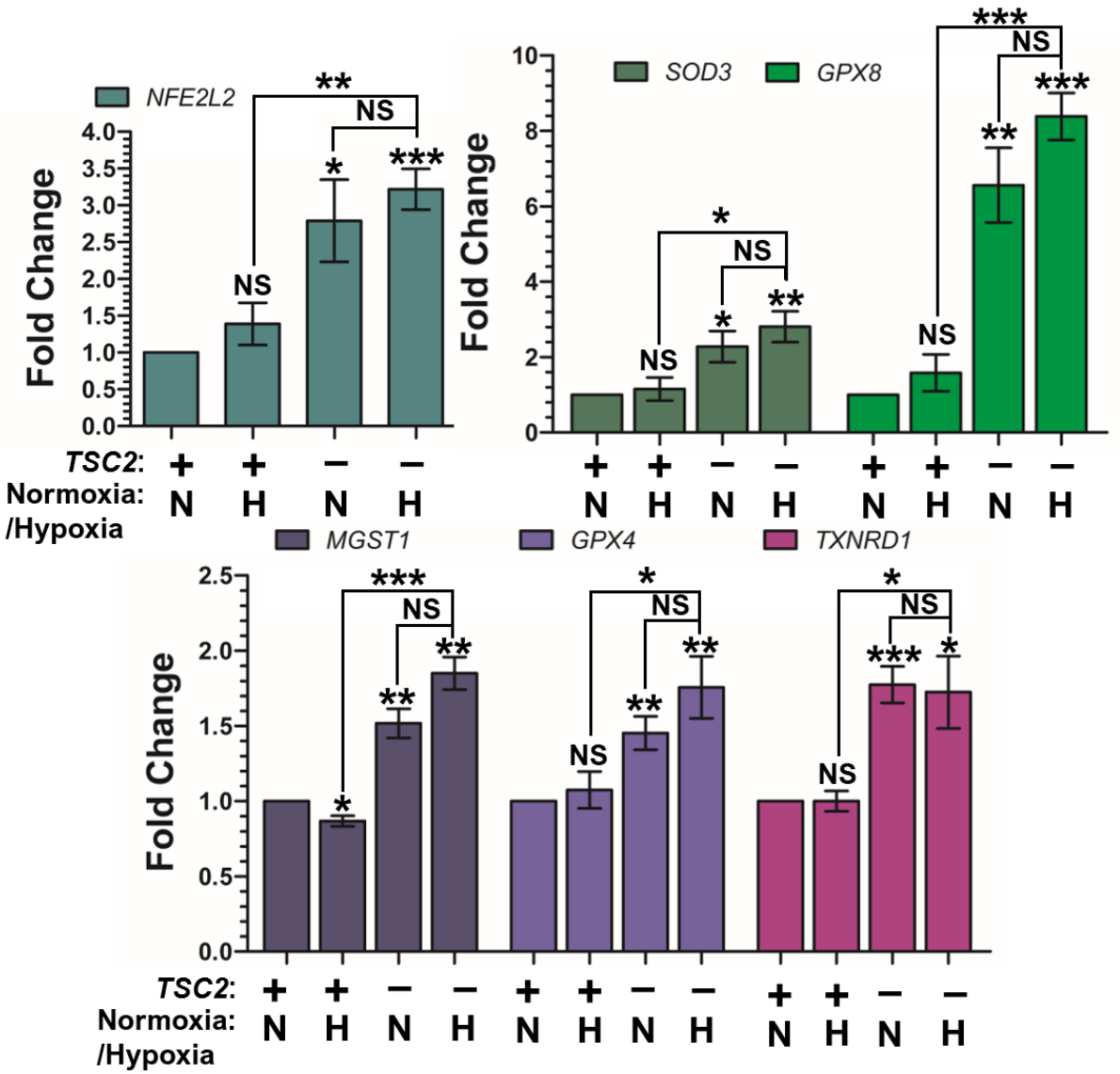


**Figure 6.3 Loss of *TSC2* in angiomyolipoma cells results in elevation of NFE2L2 (NRF2) and NRF2 target genes, with hypoxia not significantly effecting mRNA expression.** Either under normoxia (**N**, 21% $O_2$) or hypoxia (**H**, 1% $O_2$), AML cells lacking *TSC2* (***TSC2* –**) or with *TSC2* re-expressed (***TSC2* +**) were cultured overnight before being lysed. mRNA was purified from these lysates, converted to cDNA, and through qPCR the expression of target genes was quantified (N=3 minimum). Fold change in expression was calculated compared to a designated reference sample, in this case *TSC2* re-expressed under normoxia. Fold changes of target genes in samples were normalised to the housekeeping gene *HMBS*. Significance annotations above each bar on graph indicates significance of difference in foldchange between each condition and the reference sample (*TSC2* RE cells under normoxia). Pairwise statistical comparisons between *TSC2* deficient cells under normoxia or hypoxia and between *TSC2* deficient and *TSC2* RE cells under hypoxia are also annotated. Statistical analysis of differences in foldchange (N=3 minimum) was by student's t test. Significance denoted by: * = p <0.05, ** = p <0.01, *** = p< 0.001, NS = not significant. Bars represent standard error of the mean.

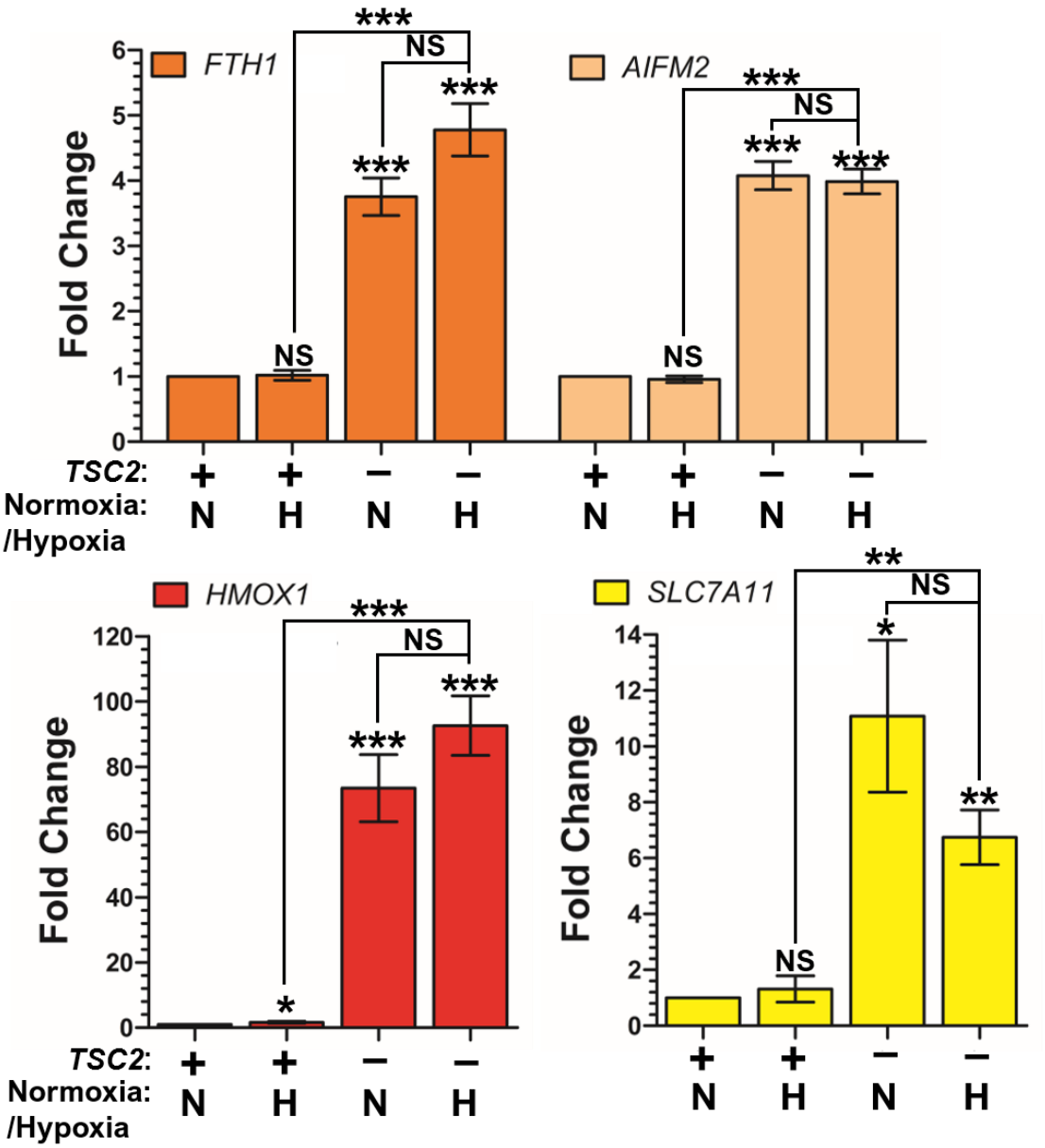


**Figure 6.4 Loss of *TSC2* in angiomyolipoma cells results in elevation in expression of ferroptosis related genes.** Either under normoxia (**N**, 21% $O_2$) or hypoxia (**H**, 1% $O_2$), AML cells lacking *TSC2* (***TSC2* –**) or with *TSC2* re-expressed (***TSC2* +**) were cultured overnight before being lysed. mRNA was purified from these lysates, converted to cDNA, and through qPCR the expression of target genes was quantified (N=3 minimum). Fold change in expression was calculated compared to a designated reference sample, in this case *TSC2* re-expressed under normoxia. Fold changes of target genes in samples were normalised to the housekeeping gene *HMBS*. Significance annotations above each bar on graph indicates significance of difference in foldchange between each condition and the reference sample (*TSC2* RE cells under normoxia). Pairwise statistical comparisons between *TSC2* deficient cells under normoxia or hypoxia and between *TSC2* deficient and *TSC2* RE cells under hypoxia are also annotated. Statistical analysis of differences in foldchange (N=3 minimum) was by student's t test. Significance denoted by: * = p <0.05, ** = p <0.01, *** = p< 0.001, NS = not significant. Bars represent standard error of the mean.

death that results from the accumulation of lipid peroxides. Oxidative stress, through Nrf2, can upregulate a number of genes linked to iron metabolism/storage and protect against ferroptosis (Duarte *et al.* 2021). This includes some genes shown in figure 6.4 (*FTH1*, *HMOX1* and *SLC7A11*) and *GPX4*. *FTH1* encodes a subunit of ferritin, the main iron storage protein (Theil *et al.* 2013) whereas *HMOX1* encodes an inducible heme oxygenase, which catalyses the breakdown of heme (Chau *et al.* 2015). Expression of *FTH1* and *HMOX1* was highest for *TSC2* deficient cells under hypoxia (*FTH1*: FC=4.78, *HMOX1*: FC=92.58) and relative to *TSC2* RE AML cells cultured under hypoxia was found to be significant (*FTH1* $p=1.57x10^{-5}$ , *HMOX1* p=0.0024) (figure 6.4). Difference in the mRNA expression of *FTH1* and *HMOX1* between normoxic cultured *TSC2* deficient and *TSC2* RE cells was reported as significant. Within the *TSC2* deficient AML cells, normoxic vs hypoxic culture did not significantly affect *FTH1* nor *HMOX1* expression. *AIFM2* encodes a protein which cooperates with GPX4 to inhibit ferroptosis by repressing lipid peroxidation (Doll *et al.* 2019). Whilst *SLC7A11* encodes the cysteine/glutamate antiporter, whose functions include importing cysteine, the rate limiting substrate in the biosynthesis of glutathione (Koppula *et al.* 2021). Indeed Champion *et al.* (2022) found cysteine was 1.7 fold higher within *Tsc2* −/− MEF cells than *Tsc2* +/+ MEF cells. Indicating either elevated synthesis and/or import of cysteine upon loss of *TSC2.* High cysteine pools likely contributes to the increased glutathione pool seen within *Tsc2* deficient murine cells (Torrence *et al.* 2021 and Champion *et al.* 2022). For *AIFM2* and *SLC7A11,* expression was highest for *TSC2* deficient cells under normoxia relative to *TSC2* RE cells cultured under normoxia (*AIFM2*: FC=4.08 $p=5.81x10^{-7}$, *SLC7A11*: FC=11.09 p=0.0100) (figure 6.4). Normoxic versus hypoxic culture had no significant effect on *AIFM2* nor *SLC7A11* mRNA expression in either *TSC2* deficient or *TSC2* RE AML cell lines. Expression of *AIFM2* and *SLC7A11* within hypoxic cultured *TSC2* deficient AML cells was found to be significantly higher than observed in hypoxic cultured *TSC2* RE AML cells.

Mitochondrial unfolded protein response (mtUPR) genes, *HSPE1*, *DNAJA3* and *LONP1,* were also examined (supplemental figure 6.4). The mtUPR is a stress response triggered by mitochondrial dysfunction (Shpilka *et al.* 2018) which in turn orchestrates a transcriptional programme that promotes mitochondrial recovery. Elevated mitochondrially generated ROS can trigger the mtUPR through damaging mitochondrial DNA and protein. Expression of *HSPE1* and *DNAJA3* was elevated upon loss of *TSC2*. Additionally, expression of *PPARGC1A,* the master regulator of mitochondrial biogenesis, was substantially elevated upon loss of *TSC2* within AML cells. *PPARGC1A* was expressed 46.94 fold higher in *TSC2* deficient AML cells. Higher expression of *PPARGC1A* would account for a higher mitochondrial load, a disease feature of TSC that has been previously reported in *TSC1*/*TSC2*

deficient murine neuronal cells (Ebrahimi-Fakhari *et al.* 2016). Higher numbers of mitochondria would further enhance ROS generation.

Antioxidant factors were elevated upon loss of *TSC2* with both AML and MEF cell lines at the protein level (figure 6.5). This included the ferroptosis inhibitor FSP1 (product of the *AIFM2* gene) and heme oxygenase 1 (HMOX1). Catalase, which is critical to a cell's antioxidant defence, by catalysing the decomposition of $H_2O_2$ (Tehrani and Moosavi-Movahedi, 2018), was only elevated in *Tsc2* −/− MEF cells. Changes in Thioredoxin-1 and -2 (TRX1 and TRX2) expression upon *TSC2* loss differed between the model cell lines. TRX1 was elevated within *TSC2* deficient AML cells, but TRX2 was not. Whereas the inverse was found for *Tsc2* −/− MEFs (figure 6.5). TRX1 and TRX2 have a cytoprotective role against oxidative stress, acting as electron donors to peroxidases in order for them to efficiently scavenge ROS (Lu and Holmgren, 2014). Within the AML cell line, cells deficient in *TSC2* had increased protein expression of glutathione peroxidase 8 (GPX8). Taken together the present data shows that expression of constituents of the cell's antioxidant defence are generally elevated upon loss of *TSC2*. This included increased expression of anti-ferroptosis/iron metabolising factors, enzymes utilising the glutathione or thioredoxin systems to neutralise ROS and proteins which contribute to biosynthesis of glutathione. This data indicates that TSC cells are under increased oxidative stress.

Assaying protein expression of Nrf2 within the AML and MEF cell lines by western blot was attempted. However, multiple banding was observed. Nrf2 has been observed to migrate by gel electrophoresis at multiple band sizes (Lau *et al.* 2013). As seen in supplemental figure 6.5, several bands for Nrf2 were observed in both cell lines, making accurate determination of protein expression difficult. However, of note within both *TSC2* deficient AML and MEF cells, a band at ~36 kDa was more strongly expressed compared to *TSC2* re-expressed and wildtype cells respectively. A literature search did not find mention of this lower resolving band or its potential biological function.

In Summary, the expression of antioxidant genes is elevated in *TSC2* deficient AML cells, a finding reflected in the increased protein expression for some of the antioxidant proteins in both the *TSC2* deficient AML and MEF cell lines. Indicating that upon loss of *TSC2* there is an enhanced response to oxidative stress.

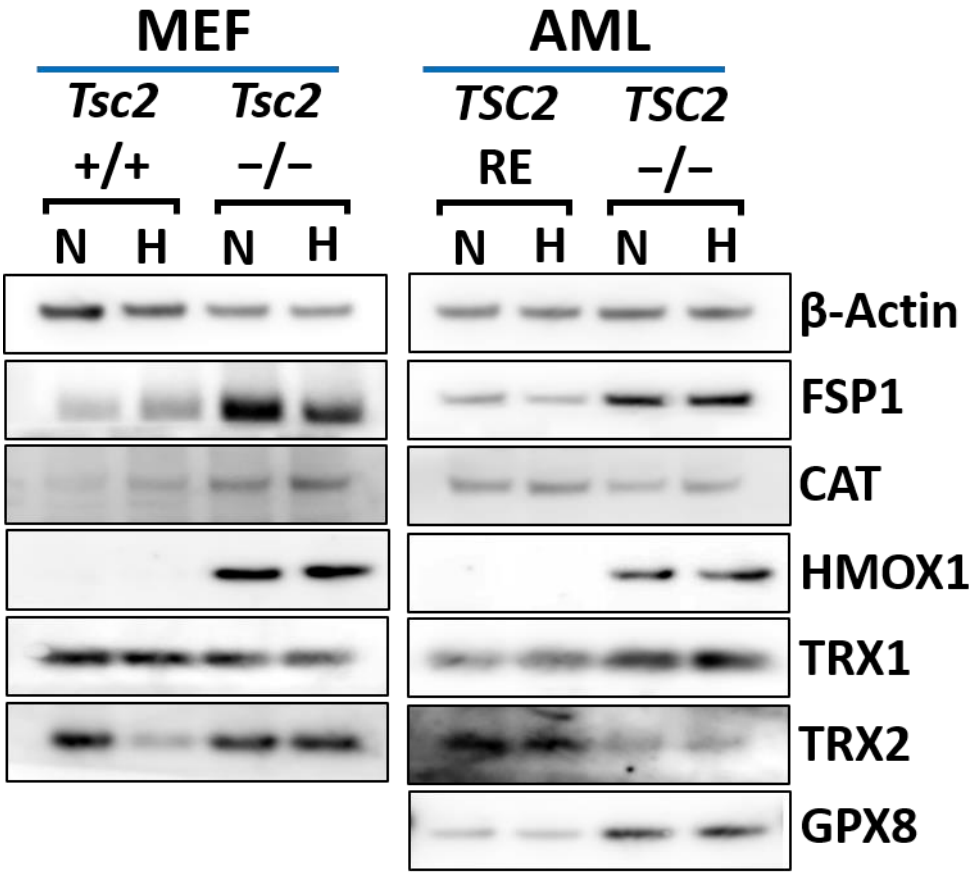


**Figure 6.5. Loss of *TSC2* within AML and MEF cell lines leads to elevated expression of oxidative stress related proteins.** AML cells lacking *TSC2* (*TSC2*−/−) or with *TSC2* re-expressed (*TSC2* RE) and MEF cells lacking *Tsc2* (−/−) or with wild type *Tsc2* (+/+), were cultured overnight under normoxia (**N**, 21% $O_2$) or hypoxia (**H**, 1% $O_2$) before being lysed. Through western blotting lysates were assayed for target protein expression (N=3), with β-actin acting as a loading control. Predicted running band size (kDa) of protein targets can be found in chapter 2, table 2.6.

### 6.2.3 Expression of the Nrf2 gene and Nrf2 target genes respond differently to agents affecting cellular redox status between *TSC2* deficient and *TSC2* RE cells

To confirm whether the elevated expression of antioxidant genes observed upon loss of *TSC2* were redox responsive in the AML cell lines and driven by Nrf2 activity, the next aim of the present chapter was to characterise how the expression of antioxidant defence genes in those cells changed in response to Nrf2 inhibitors, ROS inducing agents, and ROS quenching agents. *TSC2* RE and *TSC2* deficient AML cells were treated with either DMSO, the Nrf2 inhibitor ML385 (Singh *et al.* 2016), the ROS inducer DMNQ (Watanabe and Forman, 2003) or glutathione reduced ethyl ester (GLUT), a more cell permeable form of glutathione (Anderson *et al.* 1985) able to quench ROS. mRNA expression of *NFE2L2*, *HMOX1*, *FTH1* and *AIFM2* was then assayed by qPCR, as seen in figure 6.6. With foldchange in expression under treatment conditions normalised to DMSO controls (i.e. change in expression on a

treatment condition is in relation to the control for that cell line, *TSC2* RE or *TSC2 −/−*). Nrf2 has previously been reported to drive the anti-ferroptotic *FTH1* (Kwak et al. 2001) and pro-ferroptotic *HMOX1* (Alam *et al*. 1999). While Chorley *et al.* (2012) found through chromatin immunoprecipitation sequencing analysis that Nrf2 binds the *AIFM2* promoter in cells treated with the antioxidant sulphoraphane.

Upon Nrf2 inhibition in figure 6.6, the panel of ROS sensitive genes were all significantly repressed within *TSC2* RE and *TSC2* deficient AML cells, relative to their DMSO controls (apart from *HMOX1* within the *TSC2* RE AML line). Nrf2 (*NFE2L2*) expression was also downregulated, showing that Nrf2 autoregulates its own expression within the context of TSC. Antioxidant response element-like sequences have been reported within the *NFE2L2* promoter that could help explain this autoregulation (Kwak *et al.* 2002). Repression of *HMOX1*, *FTH1* and *AIFM2* expression relative to the DMSO control within *TSC2* deficient AML cells upon ML385 treatment (*HMOX1*: FC=0.66 p=0.0001, *FTH1*: FC=0.60 p=0.0001, *AIFM2*: FC=0.57 $p=3x10^{-5}$) identifies that Nrf2 is mediating transcription of these ROS sensitive genes (figure 6.6) and likely the other antioxidant genes shown to elevated upon loss of *TSC2* depicted in figure 6.1. The ROS inducer DMNQ significantly elevated expression of the antioxidant gene panel further in the *TSC2* RE AML line (*HMOX1*: FC=5.01 p=0.0006, *FTH1*: FC=1.83 p=0.0082, *AIFM2*: FC=1.99 p=0.0144) (figure 6.6). This data confirms that these genes are ROS induced within cells possessing functional TSC2. Of interest, DMNQ treatment did not further elevate the expression of the antioxidant genes assayed within *TSC2* deficient AML cells. Therefore, the ROS input to drive the expression of these genes appears to be already maximal (or a truncated response), which could possibly occur during long-term exposure to ROS. In line with this notion, excessive and chronic ROS can result in over-oxidation of Trx1 and its regenerative enzyme TrxR1, inhibiting both (reviewed in Cebula *et al*. 2015). Inhibition of the thioredoxin system has been shown to strongly stimulate Nrf2 activity in multiple settings (Suvorova *et al.* 2009, Patterson *et al.* 2013, Locy *et al*. 2012 and Burk *et al.* 2008). Therefore, stimulatory effect of ROS, through inhibiting redox systems such as the thioredoxin system, may already be at a maximal level. Possibly a reason why treatment with ROS inducing reagents does not elevate Nrf2 activity any further. As a possible method to further characterise this apparent saturated or truncated response to ROS, the redox status of the thioredoxin system components could be assayed under control and ROS insult conditions. This assay was beyond the scope of the present chapter. Interestingly, only the expression of *HMOX1* was significantly affected by the antioxidant glutathione. With mRNA expression significantly downregulated relative to the DMSO control within both *TSC2* RE (FC=0.62 p=0.038) and *TSC2* deficient AML (FC=0.77 p=0.0159) cells. Why glutathione treatment did not significantly repress *NFE2L2*, *FTH1* and *AIFM2* expression is uncertain

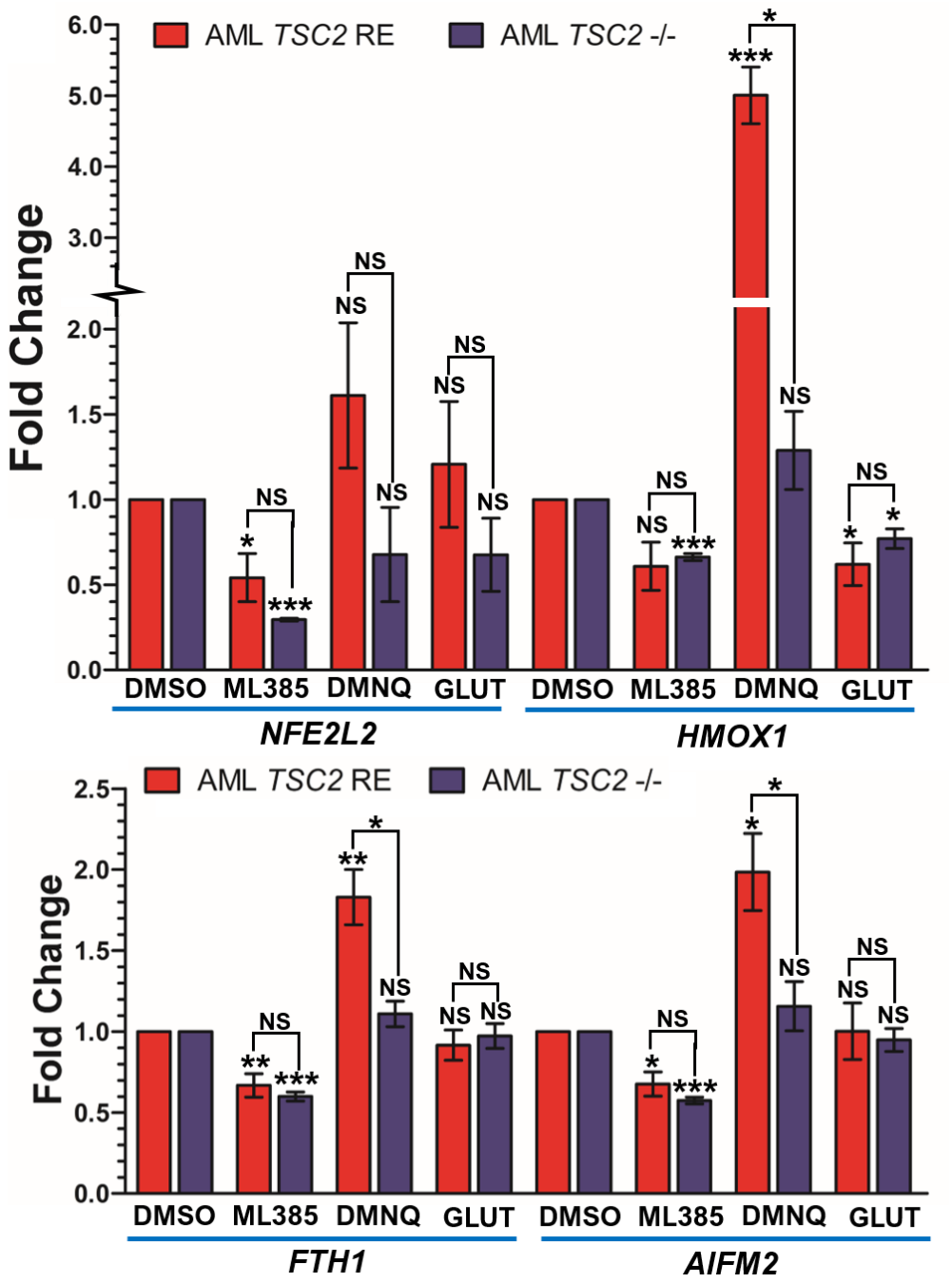


**Figure 6.6. In both *TSC2* RE and *TSC2* deficient AML cells expression of redox related genes are sensitive to NRF2 inhibition, but only in *TSC2* RE cells is expression significantly elevated by drug induced ROS.** *TSC2* RE or *TSC2* deficient (−/−) AML cells were cultured for 8 h in the presence of either DMSO, NRF2 inhibitor ML385 at 20 μM, ROS generating drug DMNQ at 5 μM or ROS scavenger glutathione at 1 mM before being lysed. mRNA was purified from these lysates, converted to cDNA, and through qPCR the expression of target genes was quantified (N=3). For each cell line, fold change in expression for treated conditions was calculated compared to a designated references sample, which was either *TSC2* RE or *TSC2* deficient AML cells treated with vehicle (DMSO). Fold changes of target genes in samples were normalised to the housekeeping gene *HMBS*. Significance annotations above each bar on graph indicates significance of difference in foldchange between each condition and the reference sample (DMSO treated *TSC2* RE/*TSC2* −/− cells). Pairwise comparisons of differences in foldchange between *TSC2* RE & *TSC2* −/− cells under each treatment condition is also annotated. Statistical analysis of differences in foldchange (N=3 minimum) between treated conditions and DMSO control was by student's t test. Significance denoted by: * = p <0.05, ** = p <0.01, *** = p< 0.001, NS = not significant. Bars represent standard error of the mean.

given their redox regulation. Glutathione is present within the cells at the millimolar concentration (Nordberg, J. and Arnér, 2001), and 1 mM was used for treatment. Therefore, a higher dose of treatment would be needed to be more effective. Additionally, other antioxidants can potently block *NFE2L2* and Nrf2 target gene expression. Such as N-acetyl cysteine (NAC) and palmitic acid. NAC can block exercise induced increase in *NFE2L2* expression within mouse skeletal muscle (Merry and Ristow, 2016) and palmitic acid induced Nrf2 target gene expression within Hepa1c1c7 cells (Lee *et al.* 2019). The inefficiency of glutathione to repress Nrf2 could be explained by Nrf2 stabilisation, which appears to be more strongly influenced by the thioredoxin system, rather than the glutathione antioxidant system (reviewed in Cebula *et al*. 2015).

### 6.2.4 The ROS inducing agents DMNQ, rotenone and RSL3 are selectively cytotoxic to cells with wildtype or re-expressed *TSC2* relative to *TSC2* deficient cells.

In this chapter, the data so far indicates redox stress and the concomitant antioxidant response may be maximally elevated upon loss of *TSC2.* A logical hypothesis is that further ROS induction might overwhelm the antioxidant defences and selectively kill *TSC2* deficient cells. Supporting this idea, therapeutic ROS inducing agents show anti-proliferative and pro-apoptotic properties in several cancer lines (Kuo *et al.* 2007, Cho *et al.* 2018, Tavsan and Kayali 2019 and Su *et al.* 2006). DMNQ, rotenone and RSL3 induce ROS through differing mechanisms and were used to assay cell viability on ROS insult in TSC cell models. DMNQ generates semiquinone radicals which that form ROS products, such as superoxide and hydroxyl radicals (Ishihara *et al.* 2006). Rotenone is a mitochondria toxin that inhibits complex I within the electron transport chain. Consequently, rotenone causes the incomplete electron transfer to oxygen that leads to the overproduction of ROS (Li *et al.* 2003). Whilst RSL3 is an inhibitor of the glutathione peroxidase GPX4 (Yang *et al.* 2014) which functions as an endogenous inhibitor of ferroptosis. Inhibition of GPX4 by RSL3 leads to accumulation of lipid ROS and activation of the ferroptosis pathway.

Cell viability was assayed using acridine orange/propidium iodide (AO/PI) and were carried out in either *TSC2* deficient and *TSC2* RE AML cells or *Tsc2* −/− and *Tsc2* +/+ MEFs (figure 6.7) with increasing doses of DMNQ, rotenone or RSL3. Surprisingly, all three ROS inducing reagents were selectively cytotoxic for the wildtype control cells (wildtype or re-expressed *TSC2*) relative to *TSC2* deficient cells. That said higher concentrations of DMNQ and RSL3 resulted in smaller differences in cell viability between the MEF lines. Whereas higher concentrations of RSL3 resulted in smaller differences in cell viability between AML the lines. RSL3 treatments were much more selectively cytotoxic to wildtype cells at lower concentrations (figure 6.7). Insensitivity of *TSC2* deficient cells to these agents might be due

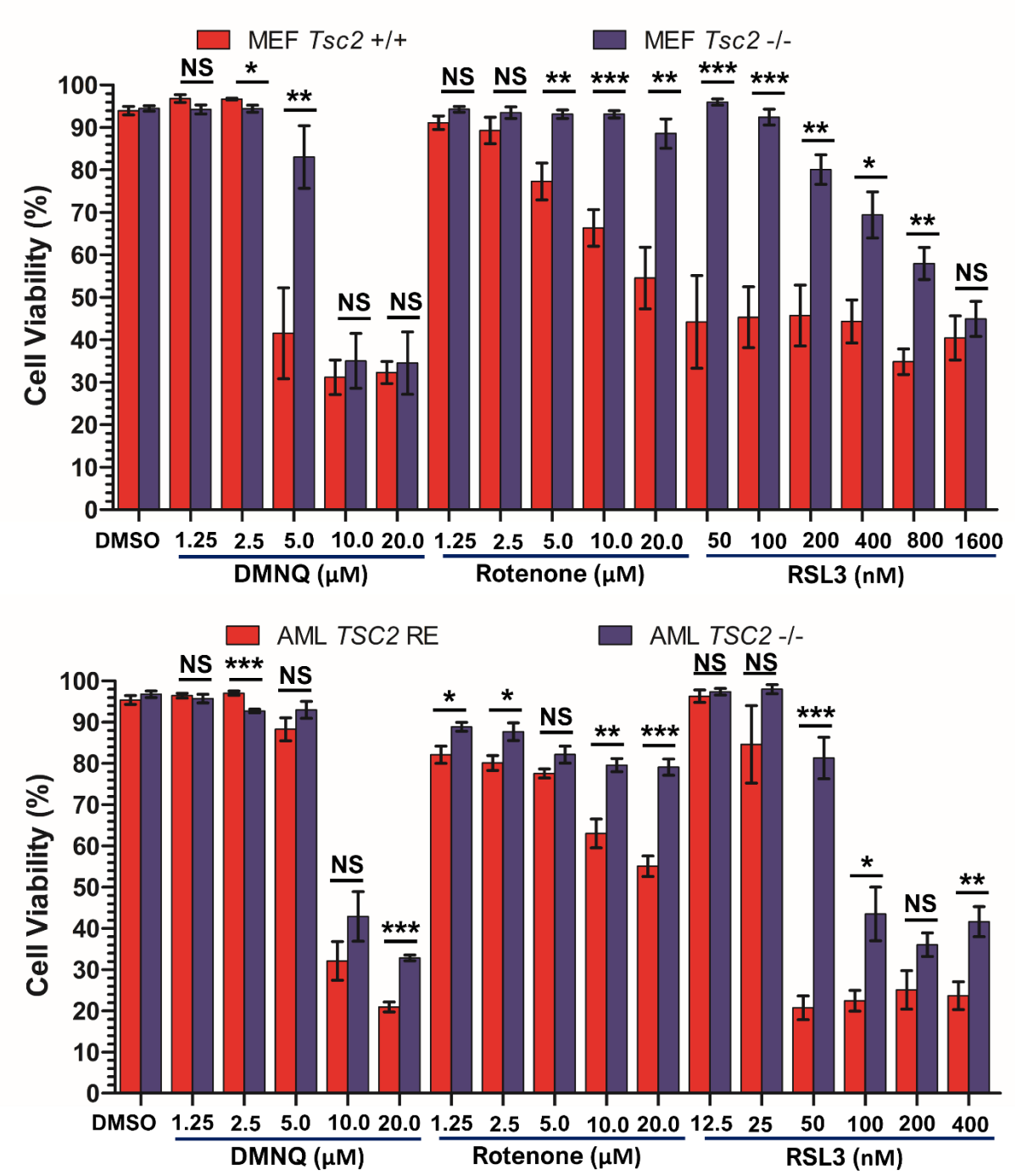


**Figure 6.7. Within both AML and MEF cell lines, loss of *TSC2* confers resistance to cytotoxicity of ROS inducing drugs.** *TSC2* RE and *TSC2* deficient AML cells and *Tsc2* +/+ or *Tsc2* −/−MEF cells were grown to ~80% confluency, before being treated with either DMSO or the ROS inducing drugs DMNQ, rotenone or RSL3 at the specified concentration for 24 h. Cells were then trypsinised and collected as were non-adherent cells within original drugged media and trypsin washes. Cells were spun down and fractions of cell suspensions were mixed with AO/PI stain. Viable/non-viable cells were then assayed on a dual-fluorescence cell counter. Average percentage of viable cells per condition (N=3 minimum) are plotted on the above graphs. The significance between differences in percentage of viable cells for each cell line under each drug condition was by student's t test and annotated on each graph. Significance denoted by: * = p <0.05, ** = p <0.01, *** = p< 0.001, NS = not significant. Bars represent standard error of the mean.

to the increased expression of antioxidant genes, better enabling them to handle further ROS insult. *Tsc2* −/− MEFs have been found to have a larger glutathione pool than *Tsc2* +/+ MEFs (Torrence *et al.* 2021 and Champion *et al.* 2022). Whilst co-treatment of AML and MEF lines with an antioxidant and DMNQ/rotenone/RSL3 was not undertaken to confirm cell death was mediated by increased ROS generation. The use of three drugs which induce ROS by separate mechanisms suggest selective cytotoxicity observed was likely due to increased ROS generation.

### 6.2.5 Nrf2 inhibition through ML385 sensitises *TSC2* deficient cells to DMNQ and RSL3 mediated cell death.

Improper Nrf2 activation, through mutation to *NFE2L2* or its negative regulator *KEAP1*, promotes tumorigenesis in cancer (Satoh *et al.* 2013 and Tao *et al.* 2017) and can increase resistance to chemotherapy (Jiang *et al.* 2010, Wang *et al.* 2008 and Singh *et al.* 2008). DeNicola *et al.* (2011) found that expression of oncogenic Kras, Braf and Myc within murine cells was sufficient to induce Nrf2 expression that lowered intracellular ROS. Given the observed increase of Nrf2 mediated transcription upon loss of *TSC2* (figure 6.1). Nrf2 is likely protecting these cells to drug induced cytotoxicity through ROS (figure 6.7). Therefore, inhibiting Nrf2 may re-sensitise *TSC2* deficient cells to ROS mediated cell death. Figure 6.8 shows the results of AO/PI cell viability assays in which either *TSC2* deficient and *TSC2* RE AML cells or *Tsc2* −/− and *Tsc2* +/+ MEF cells were co-treated with DMNQ, rotenone or RSL3 and increasing doses the NRF2 inhibitor, ML385. ML385 prevents Nrf2-MAFG (MAF BZIP Transcription Factor G) complex formation, thus impairing recognition of antioxidant response elements on Nrf2 target genes (Singh *et al.* 2016).

ML385 single drug treatments were carried out as a control. ML385 alone was not found to be cytotoxic at any of the concentrations used (1.25-20 µM). As seen in supplemental figure S.6.6. ML385 co-treatment did however sensitise both *TSC2* deficient cell lines to DMNQ and RSL3, causing a pronounced cytotoxic effect (figure 6.8). Co-treatment of DMNQ at 10 µM with increasing concentrations of ML385 resulted in a moderate but significant decrease in cell viability in the *TSC2* deficient cell lines. A maximum decrease in cell viability was seen with 5 µM of ML385 for *TSC2* deficient AML cells (41.1% vs 53.7% p=0.0131) and 20 µM of ML385 for *Tsc2* −/− MEF cells (57.0% vs 75.7% p=0.0156). With rotenone treatment, combined treatment with ML385 did not significantly alter the loss of cell viability, relative to rotenone treatment alone. Co-treatment of RSL3 with ML385 resulted in the largest decreases in *TSC2* deficient AML and MEF cell viability compared to any ROS inducing drug treatment alone. With the maximum decrease in viability relative to RSL3 treatment alone seen at 20 µM of ML385 for *TSC2* deficient AML cells (27.7% vs 57.8% p=0.0011) and *Tsc2* −/− MEF cells

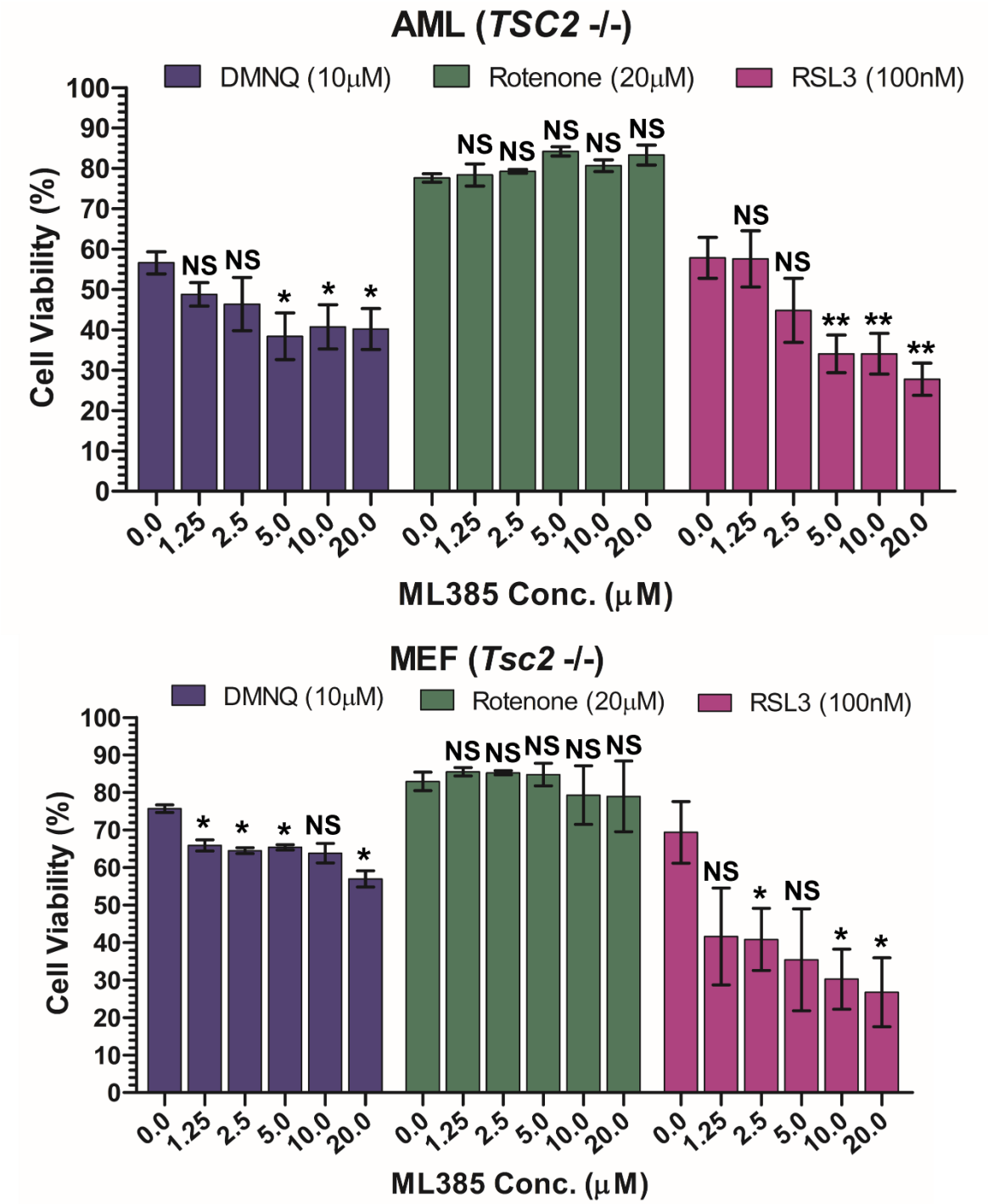


**Figure 6.8. Within both *TSC2* deficient AML and MEF cell lines, NRF2 inhibition sensitises cells to ROS inducing drug cytotoxicity.** *TSC2* deficient AML and *Tsc2* −/−MEF cells were grown to ~80% confluency, before being treated for 24 h with either DMNQ, rotenone or RSL3 alone or with the NRF2 inhibitor ML385 at the specified concentration. Cells were then trypsinised and collected with non-adherent cells within original drugged media and trypsin washes. Cells were spun down and fractions of cell suspensions were mixed with AO/PI stain. Viability of cells were then assayed on a dual-fluorescence cell counter. Average percentage of viable cells per condition (N=3 minimum) are plotted on the above graphs. Statistical analysis of differences in percentage of viable cells between ML385 and DMNQ/rotenone/RSL3 co-treated conditions and DMNQ/rotenone/RSL3 treated conditions was by student's t test and annotated on each graph. Significance denoted by: * = p <0.05, ** = p <0.01, *** = p< 0.001, NS = not significant. Bars represent standard error of the mean.

(26.8% vs 69.38% p=0.0135). Overall, this data reveals Nrf2 is a prominent antioxidant cell survival mechanism in the *TSC2* deficient cells.

In recent years cross talk between the mTORC1 and Nrf2 signalling pathways has been uncovered in disease progression. For example, drug inhibition or silencing of Nrf2 was found to decrease proliferation of cancer cell lines through inhibition of mTORC1 signalling (Jia *et al.* 2016 and Ji *et al.* 2022). Additionally, Nrf2 has been found to modulate transcription of *MTOR* (Bendavit *et al.* 2016), with the *MTOR* gene itself containing an antioxidant response element. In regard to TSC, Medvetz *et al.* (2015) found that Chelerythrines was selectively cytotoxic to *TSC2* deficient cells was antagonised by co-treatment with rapamycin. Chelerythrine, can partly induce apoptosis through ROS induction (Yamamoto *et al.* 2001 and Matkar *et al.* 2008). To assess whether mTORC1 activity upon *TSC2* loss can provide a degree of resistance to ROS inducing agents, another AO/PI cell viability assay was undertaken. Cells were treated with either a lower or higher concentration of DMNQ, rotenone or RSL3 alone or with 50nM of rapamycin. As shown in figure 6.9, co-treatment with rapamycin with 20 μM of rotenone significantly affected the viability of the *Tsc2* −/− MEFs. For rotenone at 10 μM and DMNQ or RSL3 at either the lower or higher concentration used, rapamycin co-treatment did not significantly affect cell viability. For *TSC2* deficient AML cells, rapamycin co-treatment with DMNQ, rotenone or RSL3 at either the lower or higher concentration used did not significantly affect cell viability when compared to DMNQ, rotenone or RSL3 alone (figure 6.9). This data reveals that mTORC1 inhibition is neither agonistic or antagonistic to drug induced ROS cytotoxicity. Overall, the data suggests that *TSC2* deficient cells protect themselves from ROS through Nrf2, rather than through mTORC1.

These results show mTORC1 inhibition through rapamycin is neither antagonistic or agonistic to cytotoxicity of the ROS inducers used. Which suggests that mTORC1 hyperactivity within *TSC2* deficient cells isn't driving the greater resistance of these cells to ROS inducing agents relative to cells with wildtype or re-expressed *TSC2*.

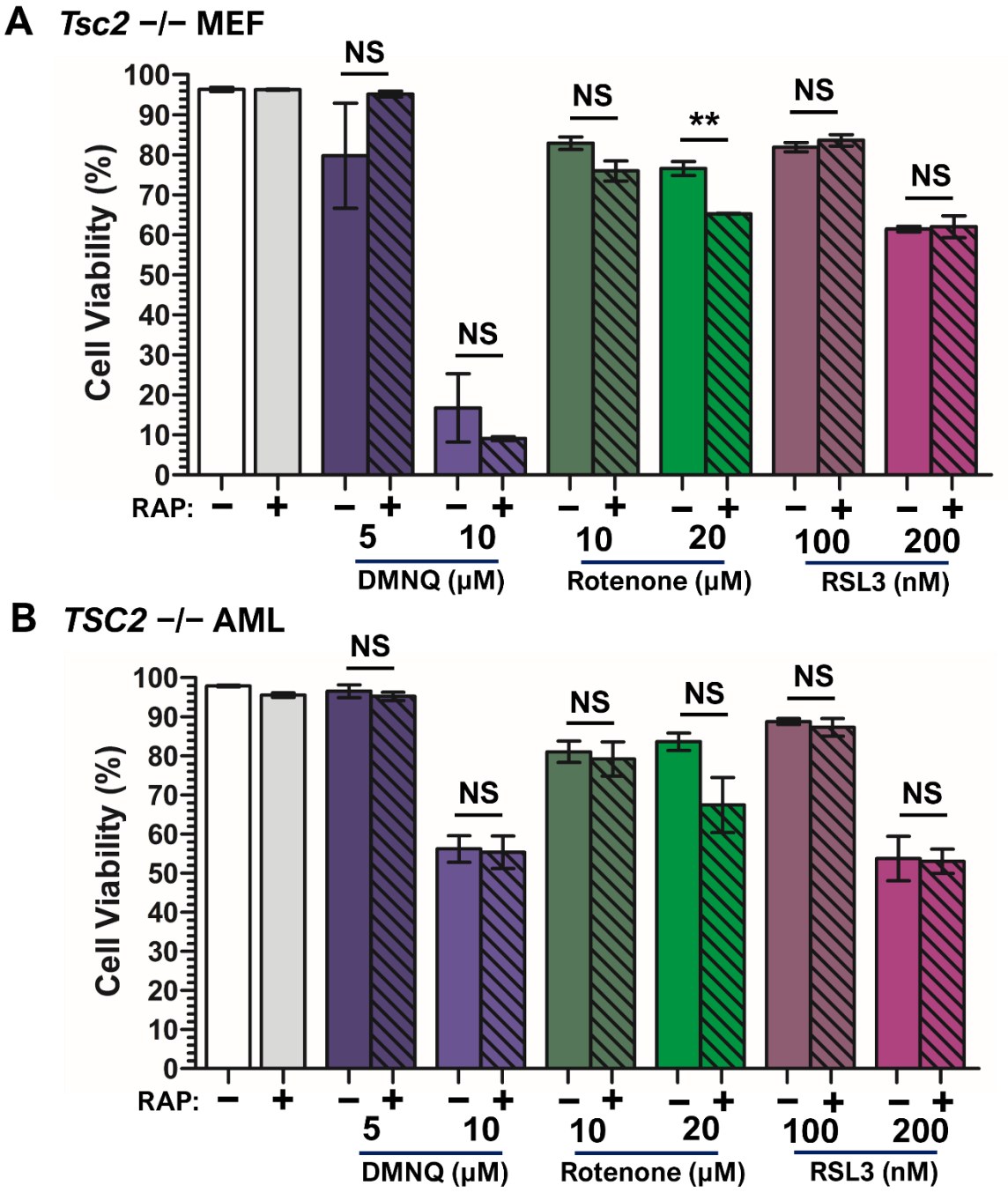


**Figure 6.9. Within both *TSC2* deficient AML and MEF cell lines, rapamycin does not sensitise cells to ROS inducing drug cytotoxicity.** *TSC2* RE and *TSC2* deficient AML cells and *Tsc2* +/+ or *Tsc2* −/− MEF cells were grown to ~80% confluency, before being treated for 24 h with either DMSO, rapamycin at 50 nM, DMNQ, rotenone or RSL3 alone at the specified concentration alone or with rapamycin at 50 nM. Cells were then trypsinised and collected as were non-adherent cells within original drugged media and trypsin washes. Cells were spun down and fractions of cell suspensions were mixed with AO/PI stain. Viability of cells were then assayed on a dual-fluorescence cell counter. Average percentage of viable cells per condition (N=3 minimum) are plotted on the above graphs. The significance between differences in percentage of viable cells for between each drug condition with or without rapamycin was by student's t test and annotated on each graph. Statistical analysis was by student's t test. Significance denoted by: * = $p < 0.05$, ** = $p < 0.01$, *** = $p < 0.001$, NS = not significant. Bars represent standard error of the mean.

### 6.2.6 mTORC1 and STAT3 inhibition modulate Nrf2 target gene expression within *TSC2* deficient AML cells.

Within cancer, STAT3 and Nrf2 signalling can drive tumourigenesis and drug resistance. STAT3 inhibition before cisplatin treatment was found to decrease protein expression of Nrf2 and GPX4 expression in osteosarcoma MG63 and Saos-2 cells (Liu and Wang, 2019). Paracrine IL6 activation of STAT3 was also found to induce *NFE2L2* (Nrf2) expression within pancreatic cancer cells, driving their increased proliferation and epithelial-mesenchymal transition (Wu *et al.* 2016 and Wu *et al.* 2017b). Furthermore, Kim *et al.* (2021) reported within basal-like breast cancer cells that STAT3 and Nrf2 physically interacted, forming a complex on the promoter of *IL23A*. As demonstrated in chapter 5, STAT3 activity was upregulated within both *TSC2* deficient cells. Therefore, the next aim of the present chapter was to assess whether STAT3 activity is a promoter of Nrf2 activity in TSC cell line models. As part of this study, the involvement of Ref-1 and mTORC1 was also investigated.

As seen in figure 6.10, only potent STAT3 inhibition with C188-9 had a significant effect on Nrf2 (*NFE2L2*) gene expression, which was slightly increased relative to the DMSO control (FC=1.27 p=0.016). Neither rapamycin nor co-treatment of C188-9 with rapamycin altered *NFE2L2* expression. mTORC1 inhibition affected one Nrf2 target gene's expression, *HMOX1*, which was moderately decreased with rapamycin (FC=0.1 p=0.0002). *APEX1* expression was also slightly reduced with rapamycin (FC=0.1 p=0.0002). Therefore, mTORC1 is unlikely to influence Nrf2 driven transcription within *TSC2* deficient AML cells. In figure 6.6, Nrf2 inhibition with ML385 reduced expression of *HMOX1*, but was not as potent as rapamycin. mTORC1 activity may therefore being affecting a different transcriptional regulator of *HMOX1*, such as HIF-1α.

C188-9 treatment resulted in a substantial upregulation of *HMOX1* expression relative to the DMSO control (FC=0.1 p=0.0002) (figure 6.10). There are conflicting reports of STAT3's regulation of *HMOX1* in the literature. In the breast cancer cell line MDA-MB-231, Lahiri *et al.* (2021) reported that STAT3 knock out decreased *HMOX1* mRNA expression. Conversely, Ferrer *et al.* (2021) found that STAT3 inhibitors, including C188-9 (at 30 μM), increased expression of *HMOX1*. Relative to the DMSO control, C188-9 also significantly upregulated expression of *GPX8* by 1.72 fold and *APEX1* by 1.32 fold. C188-9 treatment did not however significantly affect the expression of *FTH1* or *GPX4*. This data suggests that STAT3 activity within *TSC2* deficient cells is unlikely to act as a positive driver of Nrf2. Instead, significant upregulation of *NFE2L2*, *APEX1* and *GPX8* may result from another effect of STAT3 inhibition. Potentially, affecting oxidative stress. As STAT3 knockout within cancer cell lines has been reported to increase mitochondrial ROS (Garama *et al.* 2015 and Lahiri *et al.* 2021).

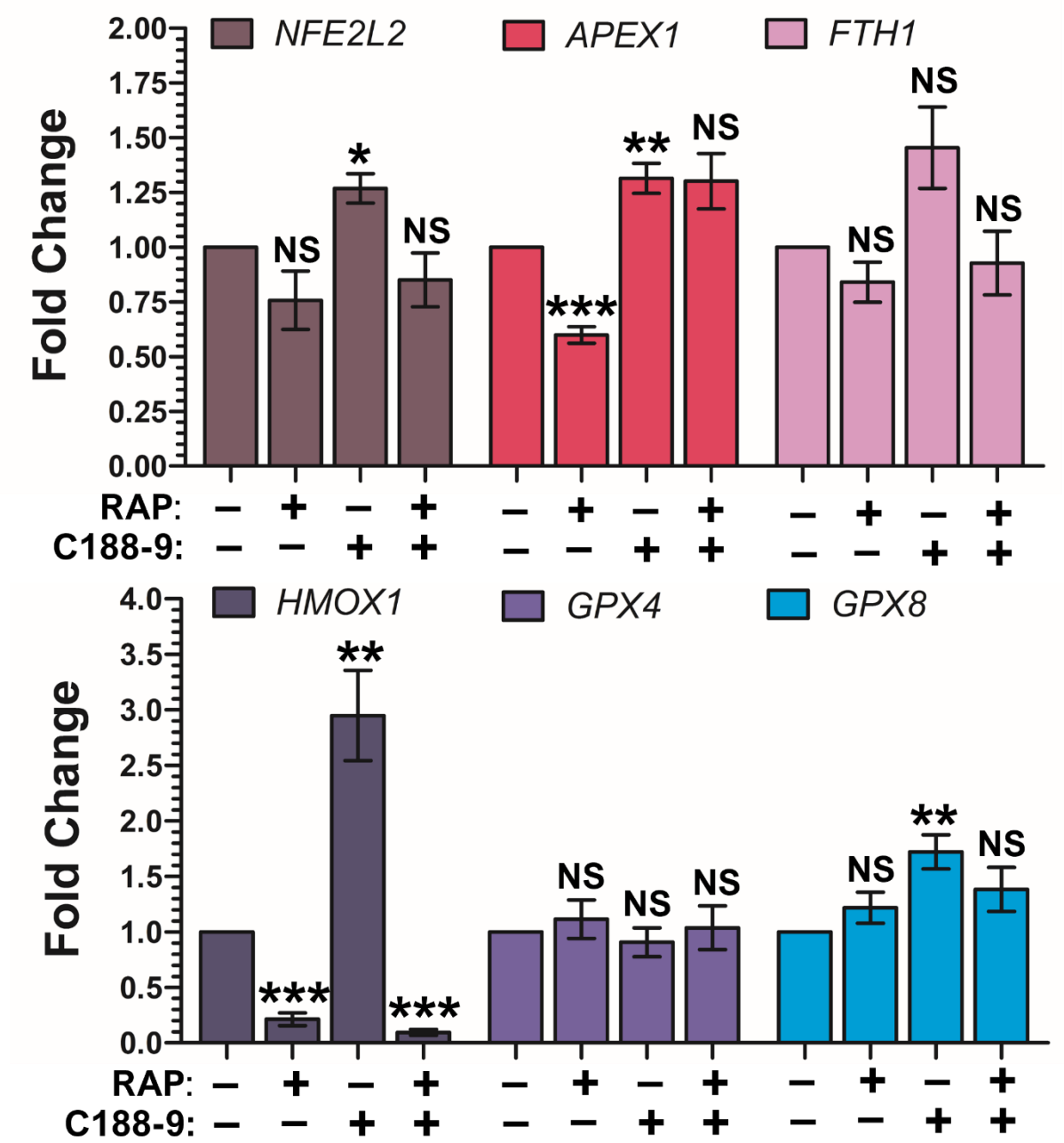


**Figure 6.10. qPCR analysis reveals rapamycin and C188-9 treatment regulates redox related genes in *TSC2* deficient AML cells.** *TSC2* deficient AML cells were cultured for 18 h in the presence of either DMSO, rapamycin (RAP) at 50 nM, C188-9 at 30 μM or FLLL31 10 μM alone or in combination before being lysed. mRNA was purified from these lysates, converted to cDNA, and through qPCR the expression of target genes was quantified (N=3). Fold change in expression was calculated compared to a designated reference sample, in this case *TSC2* deficient cells treated with vehicle (DMSO). Fold changes of target genes in samples were normalised to the housekeeping gene *IPO8*. Significance annotations above each bar on graph indicates significance of difference in foldchange between each condition and the reference sample (DMSO). Statistical analysis of differences in foldchange (N=3 minimum) was by student's t test. Significance denoted by: * = p <0.05, ** = p <0.01, *** = p< 0.001, NS = not significant. Bars represent standard error of the mean.

Volcano plots showing DEG analyses of Nrf2 target genes are shown in figure 6.11, comparing either rapamycin (figure 6.11 **A**) or C188-9 (figure 6.11 **B**) versus DMSO control of *TSC2* deficient AML cells. This data confirms that neither STAT3 nor mTORC1 are positive drivers of Nrf2. For instance, both rapamycin and C188-9 mostly increased the expression of Nrf2 target genes. Comparing rapamycin to DMSO, 49 Nrf2 target genes (out of 59) were significantly differentially expressed between conditions, with 13 being downregulated and 36 upregulated by rapamycin. Comparing, C188-9 to DMSO treatment, 50 Nrf2 target genes were significantly differentially expressed between conditions. C188-9 treatment appeared to upregulate a higher proportion of Nrf2 target genes. For instance, C188-9 upregulated the expression of 43 Nrf2 target genes. This data provides evidence that inhibition of either mTORC1 or STAT3 is not sufficient alone to normalise the higher levels of Nrf2 target gene expression that is observed in *TSC2* deficient cells. Therefore, the mechanisms that drive Nrf2 activity, and by extension the greater resistance to ROS insult, of *TSC2* deficient cells is unlikely to be mediated in large part by either STAT3 or mTORC1 hyperactivity.

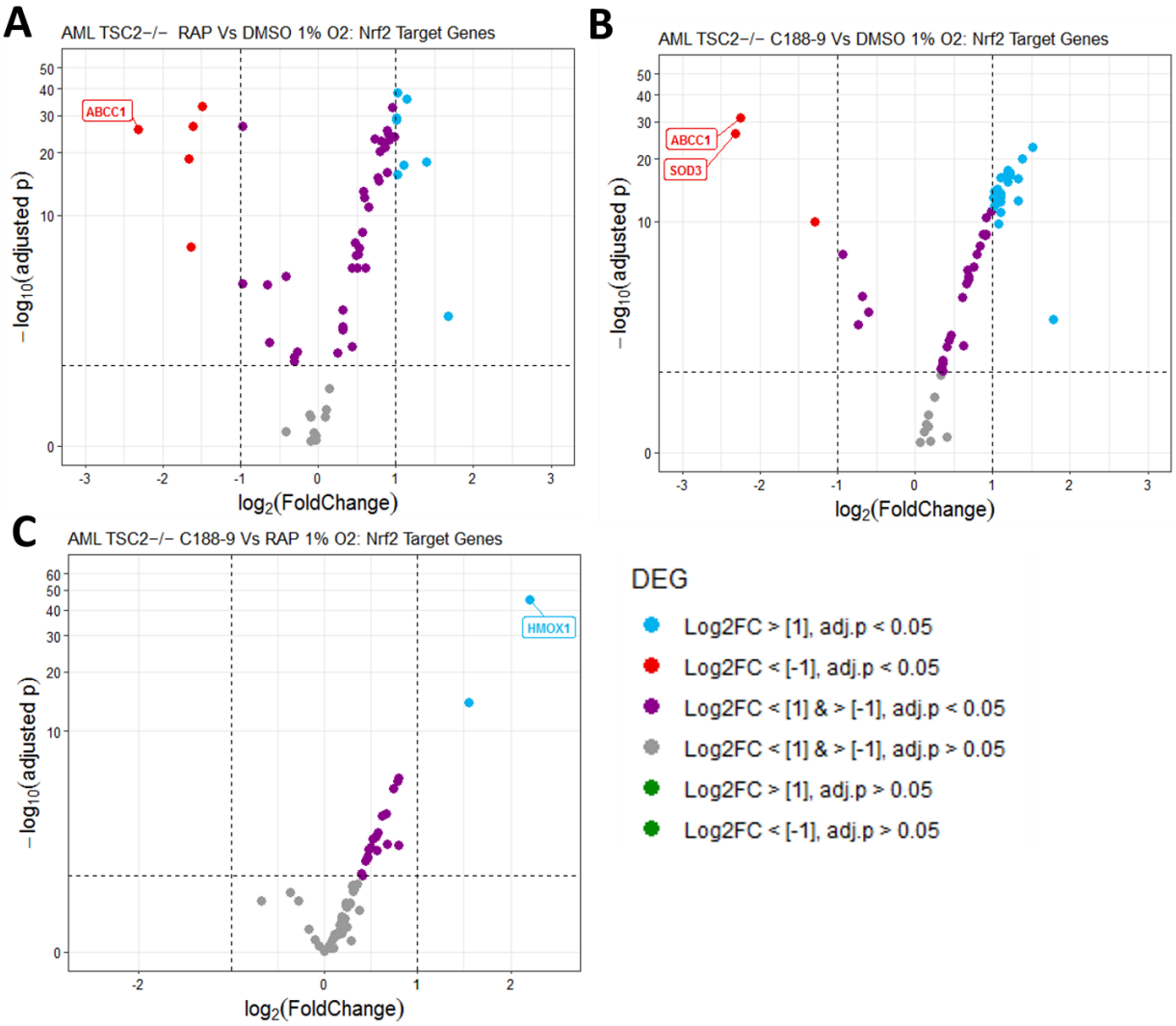


**Figure 6.11. Both rapamycin and C188-9 treatment upregulate Nrf2 target gene expression in *TSC2* deficient AML cells.** Nrf2 target gene set was collated from multiple publications (see methods and materials). Differential gene expression (DEG) comparison is annotated above each plot. AML *TSC2* deficient (−/−) cells were cultured under hypoxia (1% $O_2$) for 8 h with either vehicle only (DMSO), rapamycin (RAP) at 50 nM or C188-9 at 15 µM (N=8). RNA purified from these samples was sequenced through Novogene. Expression levels were calculated and normalised from raw read counts as FPKM (Fragments Per Kilobase Million per mapped reads). Differential gene expression (DEG) analysis was through DEseq2 analysis and resulting p-values were corrected for multiple testing and false discovery by FDR method. For all volcano plots Log2 transformed fold change in expression of genes was plotted against their -log10 transformed FDR adjusted p-values. Dotted lines at x axis represent increase or decrease in foldchange of 2 or -2 respectively. Dotted line at y axis represents significance threshold of 0.05. Genes annotated had a Log2 fold change in expression greater or lower than 2 or -2 (i.e., four fold higher or lower in expression) respectively and an -log10 adjusted p-value greater than 3 (i.e., below 0.001 significance threshold).

### 6.2.7 Treatment with the antioxidant trolox represses tyrosine phosphorylation of STAT3 and the level of DNA binding STAT3 within *TSC2* deficient cells.

While STAT3 activity appears not to drive dysregulated antioxidant gene expression in AML cells upon loss of *TSC2*, numerous studies have found that ROS can influence STAT3 activity within cancer cells. For instance, starvation or drug induced ROS has been found to increase phosphorylation of STAT3 at both the tyrosine 705 and serine 727 site (Mohammed *et al.* 2020, Chen *et al.* 2016 and Yoon *et al.* 2010), which was blocked with antioxidant treatment. Additionally, exogenous ROS or antioxidants can affect STAT3 mediated transcription and DNA binding (Yoon *et al.* 2010 and Li *et al.* 2010). The signalling interplay between oxidative stress and STAT3 is evidently complex and requires further investigation within the context of TSC. One of the final aims of this chapter was to assess whether markers of STAT3 activity was modulated by oxidative status of TSC cell line models.

To assess the impact of redox status on STAT3 activity within TSC cell models, *TSC2* deficient AML and MEF cells were treated with increasing concentrations of a ROS inducing drug (rotenone) or a ROS scavenger (trolox). Western blot analysis was carried out to examine STAT3 and Ref-1 (figure 6.12). Rotenone did not have a consistent or dose dependent effect on Y705 pSTAT3. Within the *TSC2* deficient AML and MEF cells, low doses of rotenone appeared to slightly, but significantly, decrease levels of Y705 pSTAT3 (figure 6.12 **B**). However, treatment with the antioxidant trolox markedly decreased STAT3 Y705 phosphorylation within both *TSC2* deficient cell lines. Within the *Tsc2* −/− MEF line, decrease in Y705 pSTAT3 on trolox treatment was more pronounced and showed a more obvious dose dependent response.

Rotenone increased the phosphorylation of STAT3 at S727 (S727 pSTAT3) relative to the DMSO control in both *TSC2* deficient cell lines (figure 6.12 **A**), but this finding was not reported as significant by densitometry analysis. Mohammed *et al.* (2020) had previously found that rotenone enhanced S727 phosphorylation of STAT3 in both HeLa and HEK cells. Similarly, trolox did not cause any significant differences to S727 phosphorylation of STAT3 when compared to DMSO. SOCS3 expression also was not affected with either rotenone or trolox treatment in either cell line. However, both rotenone and trolox treatments reduced the level of JAK2 phosphorylated at Y1007/1008 in *TSC2* deficient AML cells (figure 6.12 **A**). Whereas in the MEF line trolox appeared to enhance JAK2 phosphorylation at Y1007/1008. The reason for the differences in the effect of trolox on JAK2 phosphorylation between the two cell lines is unclear. Repeat blots, showed variability and densitometry analysis did not report significance, but the general trends for JAK2 phosphorylation observed on rotenone and trolox treatment appeared consistent.

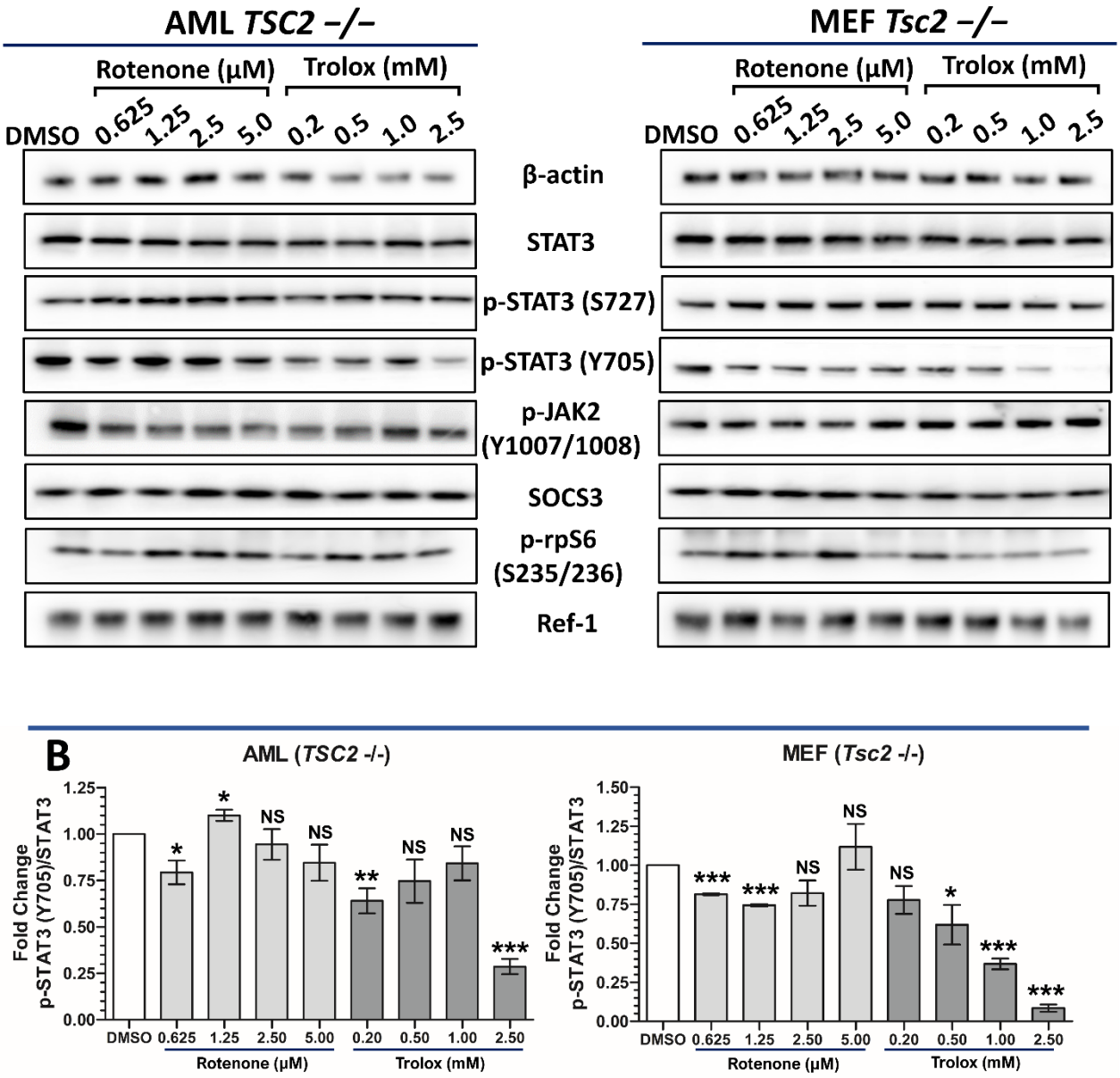


**Figure 6.12. The antioxidant Trolox decreases phosphorylation of STAT3 at Y705 in a concentration dependent manner within *TSC2* deficient AML and MEF cells.** Panel **A** shows representative western blots (N=3 minimum). *TSC2* deficient AML or MEF cells were cultured for 8 h in the presence of either DMSO, rotenone or trolox before lysis. Through western blotting lysates were assayed for protein expression, with β-actin acting as a loading control. **B.** Densitometry analysis of resulting western blots (N=3 minimum) was performed, with pSTAT3 Y705 being normalised to total STAT3. Resulting ratios of pSTAT3 Y705/STAT3 were then expressed as fold changes compared to control sample (DMSO) and plotted on accompanying graphs. Statistical analysis of differences in foldchange of normalised pSTAT3 (Y705) relative to DMSO control was by student's t test and annotated on graphs (**B**). Significance denoted by: * = p <0.05, ** = p <0.01, *** = p< 0.001, NS = not significant. Bars represent standard error of the mean. Predicted running band size (kDa) of protein targets can be found in chapter 2, table 2.6.

No significant changes to Ref-1 protein or rpS6 phosphorylation at S235/236 was observed with either rotenone or trolox treatment (figure 6.12 **A**). Given that rpS6 phosphorylation was unaltered, it is unlikely changes to the redox status of *TSC2* deficient cells by either rotenone or trolox is sufficient to affect mTORC1 activity. The main finding from this western blot analysis was potent reduction in Y705 STAT3 phosphorylation by trolox, which could indicate a reduction in STAT3 activity. Therefore, experiments were set up to examine the effect of the antioxidants NAC and trolox on transcriptionally active STAT3, using a TransAM® STAT3 ELISAs (figure 6.13). These ELISA assays measure the amount of nuclear STAT3 that is able to bind DNA in an active form (i.e., are 'transcriptionally active'). While NAC decreased STAT3 activity, (AML: FC=0.78, MEF: FC=0.72), this was not reported as significant. However, 2.5 mM trolox potently and significantly decreased the activity of STAT3, relative to the DMSO control, which is consistent with the observed decrease in Y705 STAT3 phosphorylation (figure 6.12). Within the *TSC2* deficient AML cells, trolox decreased transcriptionally active STAT3 by over 50% (FC=0.42 p= $2.69X10^{-8}$). As with the level of Y705 pSTAT3, trolox potently decreased transcriptionally active STAT3 in the *Tsc2* −/− MEF cells (FC=0.23 p= $2.13X10^{-6}$). These findings reveal that the oxidative status of *TSC2* deficient cells influences STAT3 at both the level of DNA binding and phospho-markers of activity.

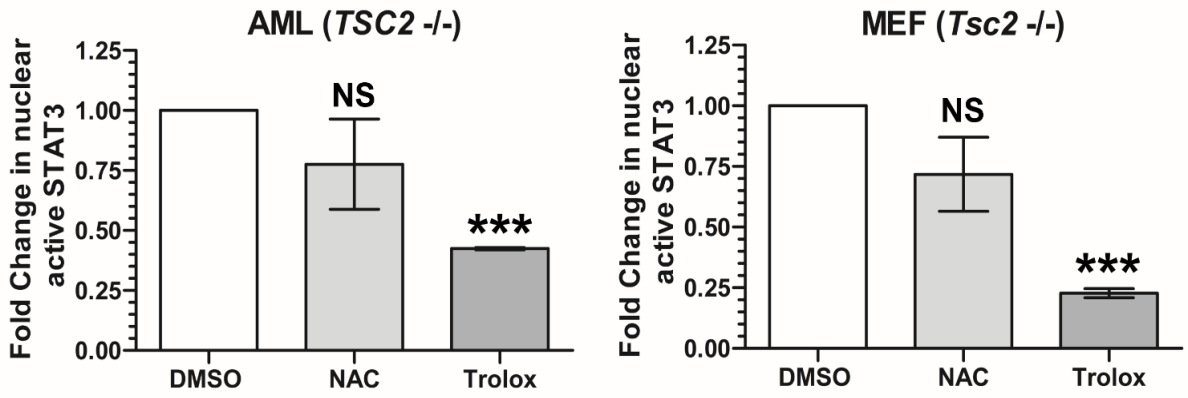


**Figure 6.13 The antioxidant trolox decreases nuclear accumulation of active STAT3 within *TSC2* deficient AML and MEF cells.** *TSC2*-deficient AML or MEF cells were treated with either DMSO, NAC at 2.5 mM or trolox at 2.5 mM for 8 h before either being used to generate concentrated nuclear lysates which were assayed for amount of active DNA binding STAT3 present using Active Motifs TransAM® STAT3 ELISA (N=3). Amount of nuclear active STAT3 in NAC and trolox treated conditions were expressed as fold changes compared to control sample (DMSO). Statistical analysis of differences in foldchange of nuclear active STAT3 relative to control was by student's t test and annotated on each graph. Significance denoted by: * = p <0.05, ** = p <0.01, *** = p< 0.001, NS = not significant. Bars represent a standard error of the mean.

### 6.2.8 Modulation of the intracellular redox environment by rotenone or trolox treatment modulates HIF-1α expression within *TSC2* deficient AML cells.

As described within this chapter's introduction, the expression and activity of HIF-1α can be modulated by oxidative stress in cancer cells. As markers of oxidative stress and elevated levels of HIF-1α were observed upon loss of *TSC2*, markers of HIF-1α and its activity was assessed with an inducer and quenchers of ROS in *TSC2* deficient AML cells. In this final aim, protein levels of HIF-1α and its downstream targets, BNIP3 and ANGPTL4 were examined.

Within *TSC2* deficient AML cells, it was found that HIF-1α protein was greatly enhanced by rotenone, while trolox reduced HIF-1α protein expression (figure 6.14). Densitometry analysis revealed that HIF-1α protein expression (normalised to β-actin expression) was markedly enhanced with all concentrations of rotenone, with the highest induction observed with 5 μM rotenone (FC=2.91 p= 0.0341). Decreases in HIF-1α protein levels at 1 and 2.5 mM were reported as significant, with the largest decrease in HIF-1α protein levels relative to the DMSO control observed at the maximum trolox dose (FC=0.55 p=0.0204). Rotenone did not appear to further enhance the protein expression of BNIP3 and ANGPTL4, while trolox was observed to decrease their protein expression. Whilst densitometry analysis only found the decreases in ANGPTL4 (normalised to β-actin expression) relative to the DMSO control significant. Blots from all three independent experiments showed the same trend in decreases in protein expression of BNIP3 and ANGPTL4 on trolox treatment. Overall, these results show, HIF-1α protein expression in *TSC2* deficient cells can be influenced by their oxidative status. With use of a ROS quencher, BNIP3 and ANPTL4 protein expression was reduced, that indicates a reduction in HIF-1α activity.

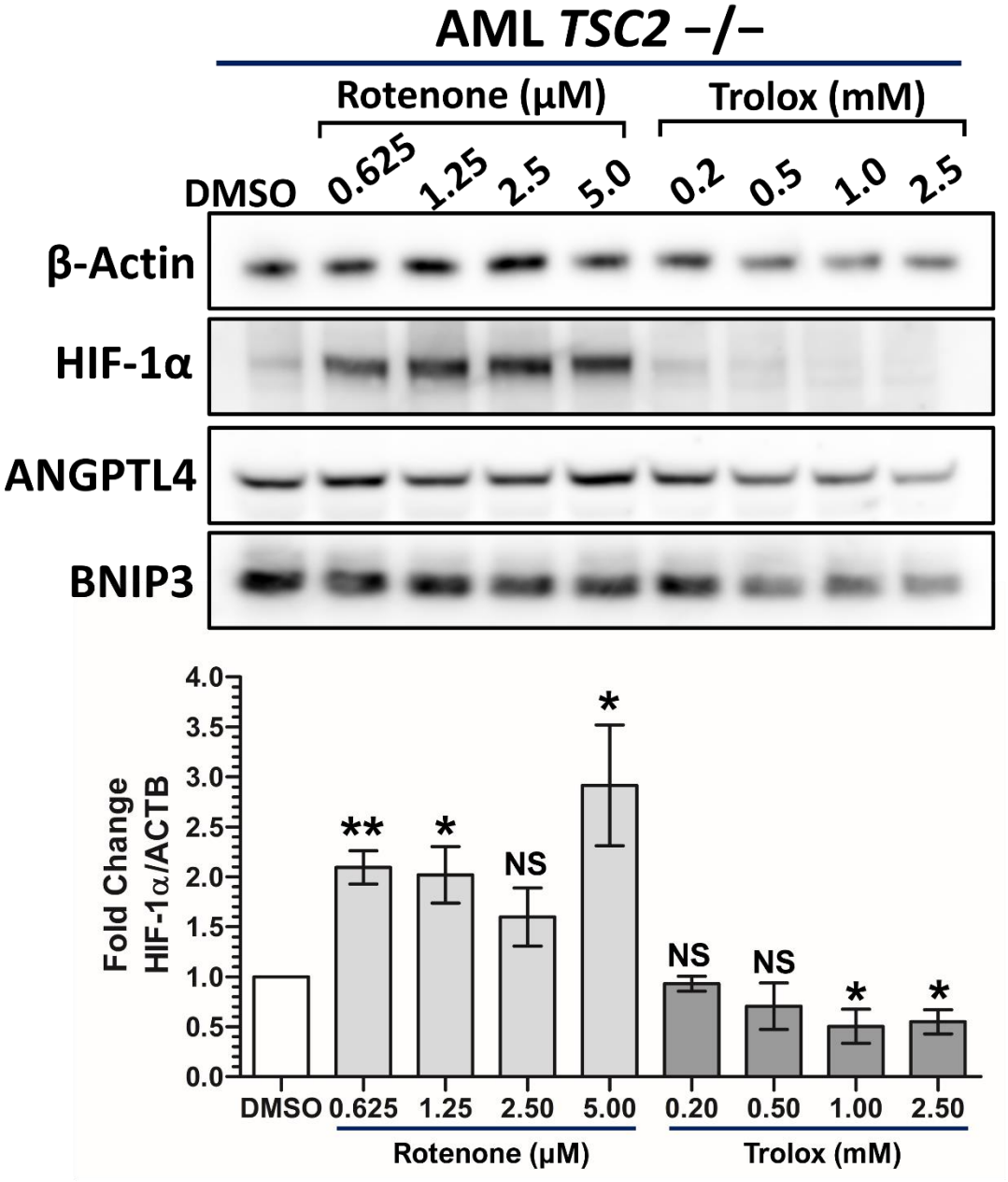


**Figure 6.14. Rotenone increases, whilst trolox decreases protein expression of HIF-1α and HIF-1α targets, ANGPTL4 and BNIP3, within *TSC2* deficient AML cells.** Representative western blots (N=3 minimum). *TSC2* deficient (−/−) AML cells were cultured for 8 h in the presence of either DMSO, rotenone or trolox before lysis. Through western blotting lysates were assayed for protein expression, with β-actin acting as a loading control. Densitometry analysis of resulting western blots (N=3 minimum) was performed, with HIF-1α being normalised to β-actin (ACTB). Resulting ratios HIF-1α/ACTB were then expressed as fold changes compared to control sample (DMSO) and plotted on accompanying graphs. Statistical analysis of differences in foldchange of normalised HIF-1α relative to control was by student's t test and annotated above bars on graph. Significance denoted by: * = p <0.05, ** = p <0.01, *** = p< 0.001, NS = not significant. Bars represent standard error of the mean. Predicted running band size (kDa) of protein targets can be found in chapter 2, table 2.6.

## 6.3. Discussion

Whilst several studies indicate that oxidative stress is elevated in TSC, appreciation for how ROS contributes towards TSC pathology is still relatively unknown. The data present within this chapter present several novel findings on how TSC model cells respond to oxidative stress and highlights the role Nrf2 activity may play in these responses.

The present work represents a comprehensive analysis of Nrf2 driven transcription in the context of TSC, an analysis that has not been previously carried out. Previous studies have been limited. It was found that Nrf2 protein expression was independent of *Tsc2* in MEFs (Zhang *et al.* 2014 and Lam *et* al. 2017). The present work finds that Nrf2 activity is elevated in TSC cell models and TSC-associated lesions (figure 6.1). The majority of Nrf2 target genes assayed were upregulated upon loss of *TSC2* within both AML and MEF cell lines and were also upregulated in at least one TSC associated lesion. This data highlights that Nrf2 activity likely has clinical relevance to TSC pathology. Within the *TSC2*-deficient AML cells, qPCR showed that expression of the Nrf2 gene itself was enhanced upon loss of *TSC2*. Nrf2 target gene products that function through multiple pathways to relieve oxidative stress were also markedly enhanced (figures 6.3 and 6.4). Western blotting (figure 6.5) confirmed expression of oxidative stress related markers at the protein level within *TSC2*-deficient AML and MEF cells. As previously described in subsection 6.2.2, Nrf2 activity has been shown to be modulated by oxygen availability (Cho *et al.* 2005, Kim *et al.* 2007 and Syu *et al.* 2016). However, within *TSC2* deficient AML cells, DEG analysis showed that hypoxia, by in large, did not further elevate Nrf2 target gene expression (figure 6.1). This finding was further confirmed by Nrf2 target gene expression assayed via qPCR (figures 6.3 and 6.4), in which hypoxia did not significantly elevate the expression of Nrf2 target genes. By in large, expression of protein oxidative stress markers was also unaffected by oxygen status (figure 6.5). In *TSC2* deficient AML cells, the basal protein expression of HIF-1α remains high even during normoxia (21% $O_2$), which is of interest. In a normal, untransformed cell, HIF-1α should remain low when oxygen is high. It is therefore likely that these AML cells are hardwired into HIF-1α signalling irrespective of oxygen status, a term that is referred to as pseudohypoxia. Pseudohypoxia is common in renal cancers, where these tumourigenic cells express low oxygen-associated proteins regardless of their oxygen status (Hayashi *et al.* 2019). So while oxygen availability is unlikely to be driving Nrf2- mediated transcriptome in these *TSC2* deficient AML cells, this might be because HIF-1α signalling and other low oxygen-associated factors appear to already be pathologically elevated.

Nrf2 activation within TSC cells has been proposed to be mediated by elevated expression of the autophagic substrate p62 (also known as sequestosome-1 (*SQSTM1*)) (Parkhitko *et al.* 2017). p62 sequesters Nrf2 from its negative regulator Keap1 to stabilise Nrf2 (Komatsu *et al.*

2010). In hepatocellular carcinoma, p62 regulation of Nrf2 is a known driving mechanism of tumourigenesis (Umemura *et al.* 2016 and Inami *et al.* 2011). Surprisingly, Lam *et al.* (2017) found that p62 knockdown with siRNA within *Tsc2* −/− MEFs had no effect on the protein levels of Nrf2. Instead, p62 knockdown decreased the intracellular pools of glutathione and expression of genes related to glutathione synthesis. Previously utilised RNA sequencing data showed elevated expression of the p62 gene (*SQSTM1*) within SEN/SEGA and renal AML tumours and within *TSC2* deficient AML and MEF cells. Rapamycin treatment also significantly upregulated Nrf2 target genes (figure 6.11). This was despite the known effect of rapamycin treatment to reduce p62 levels in *TSC2* deficient cells, but this is probably due to enhanced autophagy by inhibition of mTORC1, which is known to cause autosomal degradation of p62 (Jung *et al.* 2009). Evidently, p62 is not the main driver of Nrf2 activity within *TSC2*-deficient cells. Alternatively, increased Nrf2 expression is likely mediated by oxidative stress, a known disease facet of TSC (Chen *et al.* 2008, Suzuki *et al.* 2008 and Di Nardo *et a*l. 2009). Increased oxidative stress inactivates Keap1, a negative regulator of Nrf2 (Tonelli *et al.* 2018). Supporting this hypothesis is the finding that elevating oxidative stress increased the expression of Nrf2 targets within AML cells in which *TSC2* was re-expressed (figure 6.6). Nrf2 activity was not found to be promoted by STAT3 (figures 6.10 and 6.11). Interestingly STAT3 inhibition, through C188-9 treatment, increased Nrf2 target gene expression within these cells. The underlying reason for this is unclear. Although within the neuronal GT1-7 cell line, Ferrer *et al.* (2021) found that C188-9 increased intracellular ROS production. Therefore, C188-9 may be increasing oxidative stress within the *TSC2* deficient AML line, which would sequentially promote the activity of Nrf2.

Findings that ROS inducing reagents were selectively cytotoxic for wild-type AML and MEF cells relative to the *TSC2*-deficient cells (figure 6.7) is in conflict with the literature. Previous studies indicated that targeting the antioxidant capacity of TSC-diseased cells may have a therapeutic benefit. Malik *et al.* (2015) found that inhibition of GCLC, a rate-limiting enzyme in glutathione biosynthesis, increased death of SEGA-derived cells. Whilst a high-throughput drug screen by Medvetz *et al.* (2015) identified chelerythrine as a selective repressor of cell proliferation and inducer of cell death in *TSC2* deficient cells. An effect mediated by selective induction of ROS and depletion of the glutathione pool. Lastly, Li *et al.* (2015) found drug mediated depletion of glutathione and elevation of endoplasmic reticulum stress was selectively cytotoxic to *Tsc2* −/− MEFs. Increased resistance of *TSC2* deficient cells to ROS inducing reagents is likely the result of increased mRNA and protein expression of several Nrf2 target genes, observed upon loss of *TSC2* that protects them against oxidative stress (figures 6.3, 6.4 and 6.5). For example, the endogenous inhibitors of the ferroptotic pathway *GPX4* and *AIFM2* act to prevent peroxide mediated cell death (Kerins and Ooi, 2008).

Supporting this argument, Nrf2 inhibition through ML385 treatment decreased mRNA expression of Nrf2 and Nrf2 gene targets (figure 6.6). Nrf2 inhibitor co-treatment sensitised *TSC2* deficient cells to DMNQ- and RSL3-mediated cell death (figure 6.8), revealing Nrf2 is pivotal for cell survival upon escalating levels of ROS. Within cancer cells, targeting Nrf2 is an effective strategy to sensitise these cells to oxidative stressors that increase cellular ROS (Li *et al.* 2002, Niso-Santano *et al.* 2010 and Arlt *et al*. 2009).

Previous studies with TSC lesion derived cells (Malik *et al.* 2015) or *TSC2*-deficient cells (Medvetz *et al.* 2015 and Li *et al.* 2015) showed that there was increased cell death using drugs that targeted their antioxidant capacity. This involved depleting the glutathione pool. Indeed, levels of active glutathione have been shown to be elevated within *Tsc2* −/− MEFs (Torrence *et al*. 2021 and Champion *et al.* 2022). High glutathione levels may be a contributing factor to why *TSC2* deficient cells are resistant to ROS inducing agents that induce cell death. However, without having the direct measurement of the glutathione levels in cells, it is unclear to what degree the treatments of either DMNQ, rotenone or RSL3 could deplete the active glutathione pools. It is feasible that drugs that directly target glutathione synthesis, may instead selectively promote cytotoxicity in *TSC2* deficient cells, promoting even higher oxidative stress than is already indicated within these cells. It should be noted, however, that Nrf2 inhibitors alone were not cytotoxic to *TSC2* at any concentrations used (supplemental figure S.6.6). Nrf2 drives expression of target genes encoding proteins that promote glutathione biosynthesis, such as *GCLC*, *GCLM* and *SLC7A11* (Tonelli *et al.* 2018).

Whilst it has been that found that ROS increased phosphorylation STAT3 at Y705 (pSTAT3 Y705) within cancer cells (Chen *et al.* 2016 and Yoon *et al.* 2010), rotenone did not increase pSTAT3 Y705 in the *TSC2*-deficient AML or MEF cells. This may indicate that the higher levels of ROS within the *TSC2*-deficient cells is already maximally stimulating STAT3. Whilst ROS levels within the TSC cell line models used in this study were not successfully quantified in this present work, several studies did find elevated ROS upon loss of *TSC1*/*TSC2* (Chen *et al.* 2008, Suzuki *et al.* 2008 and Di Nardo *et al.* 2009). There is also elevated expression and activity of ROS generating enzymes in TSC. For example, Habib and Abboud (2016) found increased expression of several isoforms of NADPH-dependent oxidase (Nox) within *TSC2* deficient mouse and rat cells as well as within TSC renal lesion tissue. With cancer cell lines, targeting of Nox was effective at decreasing markers of STAT3 (Souza *et al.* 2009) and JAK2 activity (Lee *et al.* 2007).

Although, as seen in figure 6.12 and 6.13, within both *TSC2* deficient cell lines, treatment with the antioxidant trolox decreased phosphorylation of STAT3 at Y705 in addition to the amount of nuclear DNA binding STAT3. A novel finding within the context of TSC, showing that

oxidative status of the cell alters STAT3 activity. A similar effect of trolox on markers of STAT3 activity was observed by Ferrer *et al.* (2022) within neuronal GT1-7 cells. In which pre-treatment of these cells with trolox before methylmercury (MeHg) treatment (an inducer of cellular ROS) decreased MeHg induced STAT3 Y705 phosphorylation. Additionally, the antioxidant NAC was found to decrease ROS mediated phosphorylation of STAT3 at Y705 within cancer cells (Yu *et al.* 2015b and Yoon *et al.* 2010). The mechanism of how levels of pSTAT3 Y705 are regulated by ROS has not been determined within this work. But may be through decreasing STAT3 regulated expression of STAT3 activatory cytokines/growth factors. Within the previous chapter, *TSC2* deficient AML and MEF cells were found to activate their own STAT3 activity in an autocrine manner. With expression of cytokines/growth factors known to activate STAT3, including *IL6* were upregulated within *TSC2* deficient AML cells. As trolox treatment decreased levels of nuclear DNA binding STAT3 (figure 6.13), STAT3 driven transcription of such self-stimulatory factors may be repressed. Indeed, Yoon *et al.* (2010) found ROS generated by autophagy activated JAK2/STAT3 signalling within HeLa cells, enhancing the induction of *IL6* mRNA and protein expression, which was blocked by treatment with antioxidants. Serine phosphorylation of STAT3 (S727) was unaffected by either rotenone or trolox treatment. Within HeLa and HEK293 cells, Mohammed *et al.* (2020) observed rotenone induced STAT3 phosphorylation at the S727 site, but not the Y705 site. Therefore, the activity of mTORC1, or other kinases, responsible for S727 phosphorylation of STAT3 were likely unaffected by the ROS modulating treatments used. As observed by the lack of difference in phosphorylation of the mTORC1 substrate at S235/236 with trolox or rotenone. Exogenous and endogenous ROS has been found to repress phosphorylation of mTORC1 substrates 4E-BP1 and rpS6 (Alexander *et al.* 2010). However oxidative stress, including through p53, primarily signals mTORC1 through *TSC2* (Feng *et al.* 2005 and Budanov and Karin, 2008). Therefore, within *TSC2* deficient AML and *Tsc2* −/− *Tp53* −/− MEF cells, this mode of regulation is not functional.

Lack of change in Ref-1 protein levels on rotenone or trolox treatment was unexpected. However, on ROS insult, Ref-1 protein and mRNA expression has been found to be upregulated (Ramana *et al.* 1998 and Pines *et al.* 2005) and downregulated (Jiang *et al.* 2015 and Hu *et al.* 2021). Additionally, within this work sub-cellular localisation of Ref-1 was not assayed. Which was found to be functionally important to this protein's activity and responsive to ROS insult in non-TSC cells (Tell *et al*. 2000, Chen *et al.* 2010 and Li *et al.* 2010).

Although brief, the results from assaying the effect of ROS on HIF-1α expression are novel within the context of TSC. Within the *TSC2* deficient AML cell line the level of HIF-1α protein was found to be modulated by rotenone and trolox (figure 6.14). The increase in HIF-1α expression that was seen on rotenone treatment is consistent with the effect of ROS on HIF-

1α observed in non-TSC cells. Rotenone generates ROS at the mitochondria through inhibiting complex I of the electron transport chain (Li *et al.* 2003). Multiple studies have reported mitochondrially generated ROS promoting HIF-1α stability and transcriptional activity (Chandel *et al.* 1998 and Chandel *et al*. 2000 and Mansfield *et al.* 2005). Sanjuán-Pla *et al.* (2005) demonstrated that a mitochondrially targeted antioxidant, mitoubiquinone, potently repressed hypoxia induced HIF-1α protein expression and transcriptional activity within cancer cells. The decrease in BNIP3 and ANGPTL4 protein expression with trolox treatment within the *TSC2* deficient AML cells indicated a decrease in HIF-1α activity. The effect of ROS induction/quenching on STAT3 and HIF-1α within *TSC2* deficient AML cells suggests that increased oxidative stress may contribute to pathogenic activity of these transcription factors with the context of TSC. However, the data within this chapter does not allow a mechanism to be established. An important consideration is that within chapter 4, a decrease in HIF-1α expression was observed on C188-9 treatment within *TSC2* deficient cells. Trolox potently decreased repressed pSTAT3 Y705 (figure 6.12). The decrease in HIF-1-α protein may therefore result from a decrease in STAT3 activity. Alternatively, rotenone and trolox may have affected the negative regulators of HIF-1α protein stability. As ROS has been found to inactivate prolyl hydroxylases, by oxidising the ferrous iron required for these enzymes' catalytic mechanism (Lu *et al.* 2005 and Pan *et al.* 2007), or by promoting dimerization and subsequent inactivation of these enzymes (Lee *et al.* 2016).

# Chapter 7: General Discussion

## 7.1 Normalising tumourigenic outputs of *TSC2* deficient cells by Ref-1 and STAT3 inhibition

This study began by comparing the efficacy of inhibitors targeting Ref-1, STAT3 and NF-κB against mTORC1 inhibitors in reducing scores of tumorigenesis within TSC model cells *in vitro* (chapter 3). An improved therapeutic strategy for the treatment of TSC would be the use of a selectively cytotoxic agent, which induces death in cells with biallelic LoF *TSC1/TSC2* mutations, but not in cells heterozygous for LoF *TSC1/TSC2* mutations. Currently no such therapy is approved for the treatment of TSC. However *in vitro* studies have identified selectively cytotoxic compounds that target pathways other than mTORC1 signalling which are selectively cytotoxic to TSC cells. Such as Chelerythrine chloride which depletes glutathione levels/induces ROS production (Medvetz *et al.* 2015) and the combination of nelfinavir and bortezomib which induces endoplasmic reticulum stress while inhibiting proteasomal degradation (Johnson *et al.* 2018a). At low serum the AO/PI based viability assays found that generally concentrations of Ref-1, STAT3 or NF-κB inhibitors used within this work were well tolerated by both AML and MEF cells. However, these inhibitors, at the concentrations used, were not found to be selectively cytotoxic to either *TSC2* deficient AML or MEF cells as single agents. Additionally, *TSC2* deficient cell spheroids remained viable after long term treatment (14 days) with these inhibitors. Additionally, Ref-1, STAT3 or NF-κB inhibitors in combination with rapamycin failed to induce selective cell death in either *TSC2* deficient AML or MEF cells. Previous studies have found the combination of rapamycin and other compounds, especially autophagy inhibitors, such as chloroquine (Parkhitko *et al*. 2011) and resveratrol (Alayev *et al.* 2013), induced selective cell death in *TSC2* deficient cells. The findings of chapter 3 indicate the survival of *TSC2* deficient cells is unlikely to be mediated by Ref-1/STAT3/NF-κB signalling alone. And any potential therapeutic benefit for TSC patients of targeting Ref-1/STAT3/NF-κB signalling alone, or as an adjunct therapy with mTORC1 inhibition, is unlikely to be through inducing selective cell death.

The present work did however find drug inhibition of the Ref-1/STAT3/NF-κB signalling axis was effective at decreasing the growth of *TSC2* deficient spheroids and reducing *TSC2* deficient cell anchorage independent growth. Particularly effective inhibitors were APX2009, APX2014, and C188-9. Although these Ref-1/STAT3 inhibitors did not outperform the mTORC1 inhibitors, the anti-proliferative and anti-growth effect observed *in vitro* indicates these inhibitors may still be of clinical benefit for TSC patients. Especially when considering the limitations of current mTORC1 inhibitors. The cytostatic drug action of rapalogues means

that TSC symptoms are temporarily stabilised and if treatment with them is discontinued, for any reason, TSC lesions will regrow (Bissler 2008 and Franz *et al.* 2006). Continuous treatment with rapalogues is therefore necessary for the management of TSC, which exacerbates the adverse effects observed with these drugs (Bissler *et al.* 2013 and Franz *et al.* 2013). Furthermore, not all patients respond to treatment, as demonstrated in the EXIST trials for Everolimus, the most recently developed rapalogue which is clinically approved for the treatment of TSC. While several ATP-competitive mTOR inhibitors and mTOR/PI3K dual inhibitors have been developed over the years (reviewed in Chen and Zhou 2020) to overcome the incomplete inhibition of mTORC1 by rapalogues (Cho *et al*. 2008 and Thoreen and Sabatini, 2009). However, whilst pre-clinical studies within cancer showed great indications for these 2$^{nd}$ generation mTOR inhibitors, often these inhibitors showed marginal benefit to clinical trial participants and many showed significant toxicity (Naing *et al.* 2012, Carlo *et al.* 2016, Powles *et al.* 2016 and Graham *et al.* 2018). Therefore, alternatives to mTOR inhibitors are an unmet clinical need of TSC management. Aside from decreasing measures of proliferation, all Ref-1 and STAT3 inhibitors used within this work were able to potently block the vascular mimicry phenotype adopted by *TSC2* deficient cells grown on matrigel under hypoxia. Whereas rapamycin was ineffective. The term 'vasculature mimicry' typically describes a process within cancer by which tumorigenic cells form vascular like networks without endothelial cells (Dunleavey and Dudley, 2012). However, the contribution of the vasculature mimicry phenotype to TSC pathology currently remains unexplored and whether it is independent or dependent of the increased angiogenic signalling observed within TSC. Additionally, assays not included within this thesis, but formed part of a paper to which the current thesis contributed data, found the Ref-1 inhibitor APX3330 decreased *Tsc2* −/− MEF cell migration and invasion *in vitro* (Champion *et al.* 2022). Whereas rapamycin was ineffective. This study further bolsters the efficacy of Ref-1 inhibition in targeting rapamycin insensitive tumourigenic behaviour. At least in an *in vitro* setting.

Currently there are no studies investigating the efficacy of targeting Ref-1 in treating TSC, bar the recent paper which this thesis contributed data to (Champion *et al.* 2022). As for the efficacy of targeting STAT3, there is limited information within the literature. *Tsc2* −/− MEF cell proliferation was found to be repressed by treatment with an IL-6–neutralizing antibody (Wang *et al.* 2021a) or Huaier aqueous extract Yang *et al.* (2016b). Agents which decreased activation of STAT3. The Ref-1 and STAT3 inhibitors used within this work have currently not been approved for the management of disease. However, studies indicate they may be well tolerated by patients. The Ref-1 inhibitor APX3330 has been through a phase 1 clinical trial for the treatment of advanced solid tumours (Shahda *et al.* 2019) and phase 2 clinical trial for

the treatment of treatment of diabetic eye disease (Boyer *et al.* 2022). In both trials APX3330 was well tolerated and participants reported relatively mild adverse events. C188-9 (also called TTI-101) has been through several pre-clinical trials (Kettner *et al.* 2020, Kasembeli *et al.* 2021 and Robinson *et al.* 2022a) and is currently undergoing a phase 1 clinical trial within advanced cancers (Tsimberidou *et al.* 2021). However cautionary consideration for the potential use of STAT3 inhibitors for the treatment of TSC is that the efficacy of current drugs to actually inhibit STAT3 *in vivo* is very limited. Despite decades of research developing STAT3 inhibitors there is still no FDA approved direct STAT3 inhibitor (Liang *et al.* 2022 and Beebe *et al*. 2018).

The input of mTORC2 signalling into *TSC2* deficient AML and *Tsc2* −/− MEF cell growth, proliferation, and survival with the tumourigenic tissue cultures assays in chapter 3 was not assayed. mTORC2 activity can upregulate pro-survival and cell growth signalling pathways within cells (Szwed *et al.* 2021). Indeed, in *Tsc2* −/− MEF cells and *Tsc2* null Eker rat cells, Goncharova *et al.* (2011) found mTORC2 activity modulated cell survival and proliferation through RhoA GTPase and Bcl2 proteins. The authors observed siRNA knockdown of mTORC2 component *Rictor*, inhibited cell proliferation. Therefore, the inclusion of foetal bovine serum in the growing media of our tissue culture assays could increase growth factor PI3K signalling to mTORC2. Enhancing pro-survival and proliferation cell signalling pathways in the *TSC2* deficient AML and *Tsc2* −/− MEF cells. Indeed, in chapter 3, the dual mTORC1 and mTORC2 inhibitor Ku-0063794 (García-Martínez *et al.* 2009) was often more effective than rapamycin in tissue culture assays measuring cell proliferation and anchorage independent growth. However, this drug effect could be due to the greater repression of mTORC1 by Ku-0063794. Furthermore, in long term growth assays, such as the spheroid growth assay and anchorage independent growth assay, long term rapamycin treatment is likely to repress mTORC2 activity anyway. As long term rapamycin treatment can also inhibit mTORC2 signalling through decreasing mTORC2 complex assembly (Sarbassov *et al.* 2006).

Further studies highlight that mTORC2 is unlikely to be active within the TSC model cells utilised within this work. While there are conflicting reports on whether mTORC2 activity is enhanced or repressed in TSC cells and lesions (see chapter 1, section 1.6), two studies which utilised either the AML or MEF cell lines in their research found mTORC2 activity was decreased upon loss of *TSC2*. Düvel *et al*. (2010) observed the *Tsc2* −/− MEF cells showed depressed expression of the mTORC2 effector SGK1 and decreased mTORC2 dependent phosphorylation of Akt1 at S473 relative to the *Tsc2* +/+ MEF cells. While Li *et a*l. (2014b) observed that phosphorylation of Akt1 at S473 is decreased in the AML 621–102 cell line

(*TSC2* deficient) relative to the AML 621–103 cell line (*TSC2* re-expressed). Therefore, while the present work did not assay mTORC2 activity in either the AML or MEF cells, observations by Düvel *et al.* (2010) and Li *et al*. (2014b) in those same cell lines suggest mTORC2 activity was likely repressed in *TSC2* deficient AML and *Tsc2* −/− MEF cells. Furthermore, loss of *TSC2* itself has been shown to impair mTORC2 signalling and growth factor stimulation of mTORC2, outside the role of *TSC2* in regulating mTORC1. Huang *et al*. (2008) found the TSC1/TSC2 complex itself can physically associate with mTORC2 and positively regulate mTORC2 activity. The authors found endogenous mTORC2 immunoprecipitated from *Tsc2* −/− MEF cells showed decreased mTORC2 kinase activity towards exogenous Akt1 relative to mTORC2 immunoprecipitated from *Tsc2* +/+ MEF cells. Decreased mTORC2 kinase activity of *Tsc2* −/− MEF cells could be restored by reconstituting *Tsc2*. Furthermore, Huang *et al*. (2008) also observed that HeLa cells in which *TSC2* was knocked down, insulin stimulated increase in mTORC2 kinase activity was significantly blunted relative to that observed in control HeLa cells. These findings were substantiated in the *Tsc2* –/− MEF cells. The authors confirmed these findings were unlikely the result of feedback inhibition of mTORC2 by mTORC1 through the use of siRNA targeting of RAPTOR in *Tsc2* –/− MEF cells. RAPTOR knockdown did not restore the blunted kinase activity of mTORC2 in response to insulin stimulation within these cells. Further research by Huang *et al.* (2009) founds that several mTORC2 mediated phosphorylation events are disrupted in both *TSC2* deficient cells and lesions. Therefore, within both the *TSC2* deficient AML and *Tsc2* –/− MEF cell lines utilised by the present work, loss of *TSC2* itself likely hampers growth factor signalling to mTORC2 outside of the inhibitory role of mTORC1 hyperactivity to mTORC2.

## 7.2 Hypoxia and TSC Pathogenesis

One of the original hypotheses of this thesis was that hypoxia would enhance dysregulated signalling pathways within TSC, namely HIF-1α and STAT3 signalling. The rational for such a hypothesis was that within cancer cells, hypoxia can promote both HIF-1α and STAT3 mediated tumourigenesis (Pawlus *et al.* 2014 and Soleymani Abyaneh *et al.* 2017). Additionally, larger lesions are hypoxic environments by nature (Riffle and Hegde, 2017) and the tissues predominantly affected by TSC clinical manifestations have oxygen gradients across them (Northrup *et al.* 2013). Whilst aberrant HIF-1α and STAT3 signalling within TSC has been described for two decades (Brugarolas *et al.* 2003 and Onda *et al*. 2002). The investigation of the input of hypoxia into HIF-1α and STAT3 signalling within TSC model cells included within this thesis is a novel analysis in the context of TSC. The partial pressure of oxygen use for this work was set at 1% (hypoxia), which is at the lower extreme of oxygen tensions observed within tissues i.e. ‘physioxia’ (Carreau *et al.* 2011 and Carreau *et al*. 2014).

Greater efficacy of Ref-1/NF-κB/STAT3 inhibitors at repressing proliferation of *TSC2* deficient AML cells was observed under hypoxia (chapter 3). Indicating that, at least in part, Ref-1/NF-κB/STAT3 signalling mediated enhanced proliferation of *TSC2* deficient cells under hypoxia. Enhanced HIF-1α protein expression has previously been described within murine *Tsc2* −/− cells under both normoxia (Düvel *et al*. 2010) and hypoxia mimetic conditions (Brugarolas *et al.* 2003). Consistent with those studies elevated HIF-1α protein expression was detectable in *Tsc2* −/− MEFs cultured under normoxia and enhanced further under hypoxia (chapter 4). Dysregulated HIF-1α protein expression was only observed under hypoxia for *TSC2* deficient AMLs. Hypoxia was not found to be essential for driving dysregulated HIF-1α transcription with AML cells however. Under normoxia HIF-1α mediated transcription was found to be substantially elevated in AML cells upon the loss of *TSC2* (DEG analysis of RNA sequencing). Despite HIF-1α stabilisation and increased activity being an acute response to hypoxia within normal cells, with HIF-2α mediating hypoxic responses under chronic hypoxia (Löfstedt *et al.* 2007). Furthermore, the elevated protein expression of VEGFA, HGF and ANGPTL4 observed in *TSC2* deficient AMLs under normoxia was not induced further by hypoxia. Induction of VEGFA, HGF and ANGPTL4 expression by hypoxia has been reported within cancer cells (Ferrara *et al.* 2004, Shi *et al.* 2022 and Le Jan *et al.* 2003). In terms of HIF-1α signalling, this work further characterises *TSC2* deficient cells as 'psuedohypoxic', a term describing the phenomena of hypoxic-like signalling even under conditions of plentiful oxygen (Hayashi *et al.* 2019). The increased activity of other signalling pathways characterised within TSC supports the characterisation of TSC model cell lines as 'pseduohypoxic'. Upregulated expression of genes encoding glycolytic enzymes and increased glycolytic flux has been described in MEF cells upon the loss of *Tsc2* (Düvel *et al.* 2010). And the inhibition of glycolysis, alongside inhibition of mTORC1 or glutaminolysis has been shown to strongly repress the proliferation of *Tsc2* −/− MEF cells (Wang *et al.* 2020b and Jones *et al*. 2019). Despite not being necessary for HIF-1α activity, hypoxia was found to promote HIF-1α mediated transcription further in *TSC2* deficient AMLs. Stimulatory effect of hypoxia was also reflected within the luciferase data from the *Tsc2* −/− MEFs and the induction of the HIF-1α target BNIP3 (Guo *et al.* 2001). The enhanced expression and activity of HIF-1α within *TSC2* deficient cells observed under hypoxia, was likely through inhibition of the canonical oxygen sensitive pathways which negatively regulate HIF-1α protein stability (Majmundar *et al.* 2010). The data within this thesis therefore indicates that within TSC cells, hypoxia is likely a factor that exacerbates dysregulated HIF-1α signalling, but is not a prerequisite for HIF-1α signalling.

Within cells from multiple cancers, STAT3 activity has been found to mediate hypoxia dependent tumorigenesis and dysregulated signalling (Gray *et al.* 2005, Noman *et al.* 2009,

Pawlus *et al*. 2014 and Soleymani Abyaneh *et al*. 2017). Data within this thesis found that in the context of TSC, hypoxia doesn't appear to be a strong stimulus for the dysregulated STAT3 activity within *TSC2* deficient cells. Hypoxia has been found to promote the phosphorylation of STAT3 at both the Y705 site within glioma/glioblastoma (Almiron Bonnin *et al.* 2018 and Kang *et al.* 2010) and ovarian carcinoma cells (Selvendiran *et al.* 2009), and the S727 site within colorectal cancer cells (Li *et al.* 2017). However, in *TSC2* deficient AML and MEF cell, hypoxia did not enhance phosphorylation of STAT3 at either site (chapter 5). And while studies report that hypoxia increased STAT3 DNA binding (Oh *et al.* 2011) or transcriptional co-activator recruitment with STAT3 (Gray *et al.* 2005 and Pawlus *et al.* 2014) within cancer cells, hypoxia only had a moderate effect on STAT3 mediated transcription in *TSC2* deficient AML cells (as seen by RNA seq data in chapter 5). Transcription of the *STAT3* gene was not found to be significantly enhanced by hypoxia. The positive and negative regulators, IL-6 and SOCS3 respectively, of the JAK/STAT3 signalling pathway were unaffected by hypoxia. Within glioma/glioblastoma cells hypoxia has been found to activate STAT3 through either enhancing expression of IL-6 (Xue *et al.* 2016) or repressing expression of SOCS3 (Yokogami *et al.* 2013). mRNA and protein expression of neither IL-6 or SOCS3 was significantly impacted by hypoxia within *TSC2* deficient cells. While several reports highlight that hypoxia can be a strong stimulator of STAT3 activity within cancer cells, the data contained within this thesis indicate this is not the case for the *TSC2* deficient model cells used within this work.

### 7.3 Ref-1 signalling in TSC

Upregulation of Ref-1 expression and/or activity has been reported in multiple cancers (Thakur *et al.* 2014), and has been positively correlated with lower survival and chemo-/radiotherapy resistance (Yang *et al.* 2013, Mahjabeen *et al.* 2013 and Cao *et al.* 2020) and tumour grade (Bobola *et al.* 2001 and Al-Attar *et al*. 2010). Whilst now there is an increasing appreciation for the role of Ref-1 signalling in tumorigenesis, research into whether Ref-1 signalling contributes to TSC pathogenesis within this thesis is a novel contribution to TSC research. Whilst analysis of Ref-1 expression and regulation contained within this thesis was relatively basic, some novel observations were made. An obvious increase in the protein expression of Ref-1, upon the loss of *TSC2,* was only observed within the MEF cells not the AML cells (chapter 3). Additionally, mRNA expression of the Ref-1 gene (*APEX1*) was decreased in *TSC2* deficient cells relative to *TSC2* competent cells. Typically, in other human diseases where Ref-1 contributes to pathology, such as cancer, Ref-1 expression is elevated (Mahjabeen *et al.* 2013, Wang *et al.* 2019 and Cao *et al.* 2020). Typically, Ref-1 is expressed in the nucleus (Thakur *et al.* 2014), where it mediates both its BER and redox signalling function. Shuttling between the nucleus and cytoplasm however is an important part of Ref-1s

normal regulation (Tell *et al*. 2000 and Chen *et al.* 2010). Predominant subcellular localisation of Ref-1 at either the cytoplasm (Puglisi *et al.* 2001 and Di Maso *et al.* 2007) or nucleus (Koukourakis *et al.* 2001, Sak *et al.* 2005 and Al-Attar *et al.* 2010) has been observed for multiple cancers. As part of the research for this thesis, assaying the protein expression of Ref-1 in cytoplasmic and nuclear fractions of TSC model cell lines was attempted. Unfortunately, the repeats were highly variable and inconsistent. Therefore, whether patterns of Ref-1 subcellular localisation differ in cells upon the loss of *TSC2* or *TSC1* is an open question. Within chapter 4, expression of members of the thioredoxin system were upregulated within *TSC2* deficient AML cells. Namely protein expression of TRX1 and mRNA expression of *TRXND1*. Increased TRX1 and TRXND1 expression likely effects Ref-1 mediated redox signalling in TSC, as Ref-1 needs to be reduced in turn to reduce oxidised cysteines of target transcription factors to transactivate them (Karlenius and Tonissen, 2010). TRX1 and TRXND1 along with NADPH form a redox relay that regenerates reduced Ref-1. Multiple studies in non-TSC show Ref-1's expression is either enhanced (Ramana *et al.* 1998 and Pines *et al.* 2005) or repressed (Jiang *et al.* 2015 and Hu *et al*. 2021) on ROS insult. Within Chapter 4 however, Ref-1 protein expression in *TSC2* deficient cells was largely unaffected by modulation of the cell redox environment. At least by the use of rotenone and trolox. Which suggests Ref-1 expression is not regulated by oxidative status in *TSC2* deficient cell. Further work is needed to confirm these findings however.

Copy number of Ref-1 protein is not a true reflection of its redox signalling activity. As outlined in the main introduction (chapter 1, section 1.9), Ref-1 reduces oxidised cysteines within the target transcription factor DNA-binding or transactivation domains, typically increasing their DNA binding affinity/transcriptional activity (Shah *et al*. 2017). Ref-1 inhibitors have shown good efficacy in decreasing the transcriptional activity of HIF-1α (Fishel *et al.* 2011 and Logsdon *et al*. 2016) STAT3 (Cardoso *et al.* 2012 and Caston *et al.* 2021) and NF-κB (Nishi *et al*. 2002 and Fishel *et al.* 2011) within cancer cells. The paper this thesis contributed data to, analysed the efficacy of the Ref-1 inhibitors in repressing transcriptional activity of HIF-1α, STAT3 and NF-κB activity in *Tsc2* −/− MEFs by way of luciferase assays. Champion *et al.* (2022) found that the transcriptional activity of HIF-1α, STAT3 and NF-κB was enhanced within *Tsc2* −/− MEFs, but was repressed by the transfection of a wildtype *Tsc2* vector into these cells. The elevated transcriptional activity HIF-1α/STAT3/NF-κB was repressed by APX3330 in a dose-dependent manner. With the more potent Ref-1 inhibitor, APX2009, outperforming rapamycin in the repression of HIF-1α transcriptional activity. The findings of this study indicates that within *Tsc2* −/− MEFs, not only does Ref-1 promote the activity of HIF-1α/STAT3/NF-κB, but is an effective druggable target to normalise the dysregulated activity of

these transcription factors. As part of the planned research for this thesis, these findings were attempted to be recreated within the *TSC2* deficient AML cell line. However, AML cells proved incredibly resistant to transfection, despite the attempted testing of multiple transfection reagents. Furthermore, the Ref-1 inhibitors APX3330, APX2009 and APX2014, at the concentrations used within this work, were completely ineffective at decreasing the mRNA expression of genes that could be effectively targeted by either mTORC1 or STAT3 inhibitors. Such as *VEGFA, HGF* (chapter 4) and *STAT3* (chapter 5). Therefore, whilst Ref-1 drug inhibition shows promising therapeutic potential within murine TSC models, more research is needed to assess whether Ref-1 activity drives HIF-1α/STAT3/NF-κB transcriptional activity within human models of TSC. Or whether this a murine TSC model specific phenomena. As extrapolating drug efficacy findings from murine models to human models of disease can be famously misleading (Robinson *et al.* 2019b).

## 7.4 Targeting HIF-1α and pro-angiogenic signalling in *TSC2* deficient cells

Immunohistochemical analysis has confirmed enhanced protein expression of HIF-1α within the renal lesions TSC of *Tsc2*$^{+/-}$ mice (Dodd *et al.* 2015 and Yang *et al*. 2017b) and in both brain and renal lesions of TSC patients (Parker *et al.* 2011 and Mahimainathan *et al.* 2009). And it has previously been demonstrated that HIF-1α mediated transcription is elevated in murine TSC cell models. With 4 HIF-1α target genes identified by Brugarolas *et al*. (2003) and 26 HIF-1α target genes identified by Düvel *et al.* (2010) to be upregulated in *Tsc2* −/− in MEF cells relative to their wildtype *Tsc2* counterparts. Where this thesis makes a novel contribution to HIF-1α signalling within the context of TSC is through considerably expanding the known HIF-1α target genes dysregulated upon the loss of *TSC2* in both human and murine mouse models (chapter 4). Whilst this thesis does not contain the first reported RNA sequencing of the AML cell lines, as can be told from the literature. A considerable number of dysregulated HIF-1α target genes were identified within the *TSC2* deficient AML cell line. Cross comparison of these HIF-1α target genes to those dysregulated in the TSC associated lesions RNA sequencing data provided targets that are potentially clinically relevant and could be exploited by future therapeutic strategies or investigations into HIF-1α signalling within the context of TSC.

Data gathered from the *TSC2* deficient cells within this thesis indicate there may be other mechanisms driving elevated HIF-1α protein levels in TSC other than hyperactive mTORC1 signalling. The C188-9 treatment time courses of *TSC2* deficient cells in chapter 4, suggested phosphorylated STAT3 may enhance HIF-1α protein stability. A stabilising effect of STAT3 activity on HIF-1α protein expression has been observed within COS-1 cells, Caki-1 renal cell

carcinoma cells (Jung *et al.* 2005) and MCF-7 breast cancer cells (Xu *et al.* 2005). With further work by Jung *et al.* (2008) within COS-1 and Caki-1 cells finding phosphorylated STAT3 inhibited the association of HIF-1α with pVHL, thereby decreasing HIF-1α proteasomal degradation. Given the high expression of HIF-1α and constitutively phosphorylated STAT3 within *TSC2* deficient cells, such a mechanism may be relevant to the pathogenesis of TSC. However, given the short half-life of HIF-1α, cycloheximide based protein stability assays would need to be conducted in the presence of STAT3 inhibitors for any firm conclusions to be made. Work within chapter 6 showed HIF-1α protein levels in *TSC2* AML cells were induced by rotenone, whilst repressed by trolox treatment. With expression of the HIF-1α targets BNIP3 and ANGPTL4 also decreasing under ROS quenching conditions (Trolox). While oxidative status of cells has previously been shown to modulate HIF-1α protein expression in cancer cells (Sanjuán-Pla *et al.* 2005), the work within chapter 6 provides evidence that the redox environment of *TSC2* deficient cells may be important for the stabilisation of HIF-1α. Whilst further research beyond the basic analysis in this thesis is needed, studies within the literature show an enhancement of HIF-1α levels and activity by elevated ROS generation at the mitochondria (Chandel *et al.* 1998 and Chandel *et al*. 2000 and Mansfield *et al.* 2005). Previous studies have observed increased mitochondrial ROS generation upon the loss of either *TSC1* or *TSC2* (Chen *et al.* 2008 and Di Nardo *et al.* 2009). Lastly, within the *TSC2* deficient AML cell, enhanced expression of the *HIF1A* gene was insensitive to inhibitors of Ref-1, STAT3 or mTORC1 (chapter 4). Highlighting, that currently undefined dysregulated signalling pathways, independent of Ref-1/STAT3/mTORC1, are driving mRNA expression of *HIF1A* within TSC and therefore likely promoting pro-angiogenic signalling.

The status and function of mTORC2 activity was not evaluated within the current work. Therefore, it cannot be ruled out with certainty that increased HIF-1α and pro-angiogenic signalling, described in chapter 4, upon *TSC2* loss is not, in part, mTORC2 dependent. In renal cancer cells, mTORC2 signalling, as well as mTORC1 signalling, has been found to mediate HIF-1α expression. With Toschi *et al.* (2008) finding that siRNA depletion of the mTORC2 constituent Rictor decreased HIF-1α expression in RCC4 cells. The authors also observed that siRNA targeting of the mTORC2 substrate Akt3 decreased HIF-1α expression in RCC4 cells. Suggesting that mTORC2 activity may also be enhancing HIF-1α expression in *TSC2* deficient cells. In chapter 4, Ku-0063794 treatment did appear to result in modestly larger decreases in HIF-1α expression than rapamycin treatment in both *TSC2* deficient AML and *Tsc2* −/− MEF cells. Unlike rapamycin, Ku-0063794 can inhibit both mTORC1 and mTORC2 short term (García-Martínez *et al.* 2009). However, whether the greater capacity of Ku-0063794 treatment to repress HIF-1α expression is due to inhibition of both mTOR complexes or the more robust inhibition of mTORC1 cannot be concluded. mTORC2 activity

could also drive the expression of HIF-2α in the AML and MEF cell lines. HIF-2α expression or activity was not assayed as part of this work and studies into the potential role of HIF-2α in TSC pathology are severely lacking. Although Liu *et al*. (2003) observed that renal cell carcinoma cells from a *Tsc2* null Eker rat showed constitutively high HIF-2α expression. mTORC2 rather than mTORC1 appears to be the mTOR complex responsible for regulating expression of HIF-2α (Toschi *et al.* 2008 and Mohlin *et al.* 2015). And hypothetically, mTORC2 enhanced HIF-2α expression could contribute to the increased expression of pro-angiogenic factors, as those assayed in chapter 4. For instance, *VEGFA* is a HIF-2α target gene as well as a HIF-1α target gene (Holmquist-Mengelbier *et al.* 2006). However, in chapter 4, Ku-0063794 treatment by and large did not decrease the expression of pro-angiogenic genes further than rapamycin in *TSC2* deficient AML cells, including *VEGFA*. Therefore, given that Ku-0063794 has been shown to be an efficacious mTORC2 inhibitor (García-Martínez *et al.* 2009), the role of mTORC2 activity in pro-angiogenic gene expression of the *TSC2* deficient AML cell line appears minimal. At least for the genes assayed. Lastly, as described in section 7.1 of this chapter, observations by Düvel *et al.* (2010) and Li *et al.* (2014b) in the *TSC2* deficient AML and *Tsc2* −/− MEF cells suggest that mTORC2 activity was likely repressed in the same cell lines which were utilised in this work.

Chapter 4 provided new insights into targeting pro-angiogenic signalling within TSC. As can be told from the literature, this work is the first to assay the efficacy of Ref-1 and STAT3 inhibitors at targeting pro-angiogenic signalling within TSC model cells. ELISA assay results confirmed elevated expression of VEGFA and HGF within *TSC2* deficient AML, as previously observed within patient lesions (Parker *et al.* 2011 and Nguyen-Vu *et al.* 2001). Additionally, western blotting identified ANGPTL4 as a potentially pro-angiogenic biomarker within TSC. As previously observed (Brugarolas *et al*. 2003 and Dodd *et al.* 2015), enhanced VEGFA expression of *TSC2* deficient AML cells was not fully sensitive to repression by rapamycin. mRNA expression of the *VEGFA* gene was by in large insensitive to rapamycin treatment. New anti-angiogenic effects of rapamycin were uncovered however. Within *TSC2* deficient AML cells rapamycin was effective at decreasing ANGTPL4 expression and potently repressed HGF expression. Additionally, expanding on the work of Düvel *et al.* (2010), but in the human TSC cell model, RNA sequencing within the present work identified new rapamycin sensitive HIF-1α target genes. These findings in all, not only bolster the anti-angiogenic effects of rapamycin within the context of TSC, but may also have relevance to cancers where mTORC1 hyperactivity drives tumorigenesis.

Within both *TSC2* deficient cell lines, Ref-1 inhibitors were able to decrease HIF-1α protein expression. However, Ref-1's redox signalling function modulates transcription factor function and the Ref-1 inhibitors used did not decrease *HIF1A* mRNA in *TSC2* deficient AML cells. Information on the effect of Ref-1 on HIF-1α protein expression within the literature is currently lacking. Therefore, the mechanism of how Ref-1 inhibition downregulates HIF-1α protein expression is unclear. Ref-1 activity may be modulating the activity of regulators of HIF-1α protein stability and activity. A recent report by Kobayashi *et al.* (2020) found knock-down of Ref-1 within Hep3B, decreased expression of the negative regulators of HIF-1α, PHD2 and FIH1. However, the authors proposed Ref-1 regulated PHD2 and FIH1 through its effect on HIF-1α. Further work is needed to define the mechanism by which Ref-1 regulates HIF-1α within the context of TSC. Drug targeting of Ref-1 was found to decrease protein expression of the HIF-1α targets BNIP3 and ANGPTL4 in *TSC2* deficient cells. Consistent with the efficacy of Ref-1 inhibitors ability to target HIF-1α activity in other settings. Both Logsdon *et al.* (2016) and Fishel *et al.* (2011) found APX3330 decreased protein expression of the HIF-1α target gene carbonic anhydrase IX (CA9). More potent, repression of HIF-1α and BNIP3 was achieved when *TSC2* deficient cells were co-treated Ref-1 and rapamycin. Highlighting greater repression of dysregulated HIF-1α signalling within TSC may be achieved by the combination of these inhibitors.

Drug inhibition of STAT3 has been found to be effective at targeting pro-angiogenic signalling within cancers (Leong *et al*. 2009, Laird *et al.* 2003, Kukawski *et al.* 2008 and Xu *et al*. 2005). Including those with both hyperactive STAT3 and mTORC1, such as MPNTS cells, were STAT3 inhibitors have been shown to potently repress VEGFA expression (Rad *et al.* 2015). STAT3 inhibitors showed more promise than the Ref-1 inhibitors in targeting pro-angiogenic signalling within *TSC2* deficient cells. The expression of HIF-1α, BNIP3, HGF and VEGFA could be targeted by C188-9 treatment. Whilst not analysed on the same blot, C188-9 appeared to repress HIF-1α to a greater extent than rapamycin relative to untreated cells, especially in the *TSC2* deficient AML line. The observation that C188-9 repressed phosphorylation of downstream mTORC1 targets however, confounded elucidating whether individual pro-angiogenic targets expression was primarily driven by STAT3 activity or mTORC1 activity. This was illustrated by finding that the lists of HIF-1α target genes whose expression was able to be somewhat normalised on either rapamycin treatment or C188-9 treatment were largely the same. It possible the similar effects of rapamycin and C188-9 in repressing HIF-1α target gene expression is mediated more by inhibition of mTORC1. In chapter 5, repression of mTORC1 targets in *TSC2* deficient AMLs by C188-9 occurred ~1 h into treatment, a similar pattern was with rapamycin treatment. However, STAT3

phosphorylation at Y705 rebounded under C188-9 treatment for a period before being suppressed long term. AML cells used for the RNA sequencing data were treated for 8 h with either DMSO, rapamycin or C188-9 and this data set was generated before the C188-9 and rapamycin long term treatment time courses. More STAT3 dependent effects on HIF-1α target gene expression within the RNA sequencing data may have been observed if AML cells were treated for a longer period.

## 7.5 Dysregulation of STAT3 activity within TSC

Hyperactive STAT3 signalling within TSC has been described for over two decades with constitutive phosphorylation of STAT3 at both the S727 and Y705 sites reported in TSC cell models and lesions (Onda *et al.* 2002, Chan *et al*. 2004, El-Hashemite e*t al.* 2004, Weichhart *et al.* 2008 and Goncharova *et al.* 2009). However, relatively little work has been done to elucidate the mechanisms within TSC by which STAT3 activity is dysregulated. One of the major novel contributions of this work to the field of TSC research is the expansion of how constitutive STAT3 activity is promoted and maintained within *TSC2* deficient cells. This thesis proposes a model by which aberrant STAT3 activation is driven by multiple inputs to establish a positive feedforward signalling loop where STAT3 mediated transcription itself drives STAT3 activity.

Western blotting analysis within chapter 5 found phosphorylation of the S727 site in STAT3 was sensitive to mTORC1 inhibition through rapamycin. Consistent with reports identifying mTORC1 as a kinase responsible for this PTM (Yokogami *et al.* 2000 and Dodd *et al*. 2015). Within cells lacking *TSC2,* this may be the initial point of activation for STAT3. Within acute myeloid leukaemia cells, constitutive S727 and Y705 phosphorylation has been found to be driven by autocrine secretion IL-6 (Schuringa *et al.* 2000). IL-6 stimulation did not increase levels of pSTAT3 (S727) in *TSC2* deficient cells. Therefore, as *TSC2* deficient AML cells were found to secret high levels of IL-6, this work indicates either IL-6 mediated phosphorylation of STAT3 at S727 is already maximal within *TSC2* deficient AML cells or autocrine IL-6 signalling does not stimulate phosphorylation of STAT3 at S727. Elevated IL-6 expression has already been described within murine and human TSC model cells and lesions (Shu *et al.* 2010 and Wang *et al.* 2021a). Whilst autocrine activation and maintenance of constitutive STAT3 activity is a well-defined mechanism of tumorigenesis within cancer (Chang *et al.* 2013), the conditioned media experiments within chapter 5 provide evidence that such an autocrine mechanism is present within *TSC2* deficient cells. Likely mediated in part through IL-6 secretion, as both AML and MEF cells lines could be stimulated with exogenous IL-6. This conclusion was supported by the observation that JAK2 phosphorylation was already high

within unstimulated *TSC2* deficient cells, indicating enhanced growth factor/cytokine signalling. Total STAT3 is elevated in both *TSC2* deficient cell lines. This thesis shows this is likely in part mediated by the action of STAT3 itself, given C188-9 treatment downregulated *STAT3* mRNA expression. Consistent with *STAT3* autoregulating its own expression (Ichiba *et al.* 1998 and Narimatsu *et al.* 2001). Data within this thesis also suggests that unphosphorylated STAT3 (U-STAT3) transcriptional activity contributes towards the constitutive activation of STAT3 within *TSC2* deficient cells. C188-9 enhanced the expression of both *CCL5* and *IL6* (chapter 4 and 5), two genes strongly induced by U-STAT3 (Yang *et al.* 2007), likely through dephosphorylation of the large pool phosphorylated STAT3. Whilst the functional consequences of U-STAT3 within TSC are unknown, higher levels of nuclear U-STAT3 have been positively correlated with poor prognosis in glioblastoma patients (Rodrigues *et al.* 2016).

Within *TSC2* deficient cells, mRNA and protein expression of SOCS3, a negative regulator of STAT3 appears decoupled from STAT3 activity. SOCS3 expression is strongly induced by STAT3 activity (Starr *et al.* 1997 and Brender *et al.* 2001). mRNA expression of *SOCS3* was far higher in AML cells upon the loss of *TSC2*, but was not downregulated on STAT3 inhibition by C188-9 treatment. Furthermore, in chapter 6, trolox treatment repressed phosphorylation of STAT3 at Y705, but SOCS3 protein expression remained unchanged. In contrast, upregulation of *SOCS3* mRNA was concomitant with the increase in phosphorylation of STAT3 at Y705 in the non-TSC HEK cells on stimulation with conditioned media from *TSC2* deficient AML cells. Suppression of SOCS3 has been reported as a mechanism by which cancer cells maintain constitutive STAT3 activity (Pierconti *et al.* 2011 and Yu *et al*. 2015a). Lastly, data in chapter 6 implicates the cells redox environment as a regulator of STAT3 activity in *TSC2* deficient cells. Quenching ROS through trolox treatments decreased phosphorylation of STAT3 at Y705 but also the pool of nuclear STAT3 able to bind canonical GAS sequences within TSC deficient cells. Whilst ROS induction of STAT3 activity within cancer cell lines has been described (Yoon *et al.* 2010 and Chen *et al.* 2016), as far as can be told, the present work is the first to assess modulation of STAT3 activity by ROS within TSC model cells. Enhanced Nrf2 mediated transcription was observed within *TSC2* deficient cells and TSC associated lesions. Indicating that TSC cells are under increased oxidative stress, which may contribute to increased STAT3 activity observed within TSC. Further work is needed to conclude this hypothesis however and elucidate a potential mechanism.

The present work did not assess whether mTORC2 activity affected STAT3 signalling in the TSC model cell lines. Studies investigating the interplay between mTORC2 and STAT3 signalling have largely focused on the relationship between the two pathways in mediating immunity (Saleiro and Platanias, 2015) and pro-survival/drug resistance in cancer (Yadav *et*

*al.* 2013, Brown *et al.* 2016 and Chawsheen and Dash, 2021). One study did examine the relationship between mTORC2 activity and STAT3 activity in a TSC model cell. Ma *et al.* (2010) found that mTOR upregulated STAT3/p63/Notch signalling in *Tsc2* −/− MEF cells in a rapamycin sensitive manner. The authors found in *Tsc2* −/− MEFs, *Mtor* knockdown ablated STAT3/p63/Notch signalling, whereas *Rictor* knockdown did not affect phosphorylation of STAT3 at Y705 or downstream p63 or Notch signalling. Additionally, as previously described in this chapter, observations by Düvel *et al.* (2010) and Li *et al.* (2014b) indicate mTORC2 activity is likely repressed *TSC2* deficient AML and *Tsc2* −/− MEF cells. Whilst the present work did not assay mTORC2 activity, it is expected mTORC2 activity is by and large not driving constitutively active STAT3 signalling observed in chapter 5.

## 7.6 Drug inhibition of STAT3 within TSC

Often targeting phosphorylation of STAT3 at Y705 is the primary rational for STAT3 inhibitor design and is typically used as the metric within studies to assess inhibition of STAT3. The present work however indicates the S727 phosphorylation site may be more important a factor for the dysregulated STAT3 transcription observed in *TSC2* deficient cells than the Y705 site. And by extension, therefore the better target for therapeutic interventions within TSC. C188-9 and rapamycin treatment courses within *TSC2* deficient cells showed rapamycin and C188-9 having opposing effects on phosphorylation of STAT3 at Y705. While within the TransAM ELISA assays, rapamycin and C188-9 also had opposing effects on the amount of nuclear DNA binding STAT3. Treatment with either rapamycin or C188-9 however, resulted in similar effects on STAT3 and HIF-1α mediated transcription (chapters 5 and 4 respectively). One effect both inhibitors had in common is that they repressed phosphorylation of STAT3 at S727. Whilst S727 phosphorylation, in addition to Y705 phosphorylation, is thought to be necessary for maximal transcriptional activity of STAT3 (Wen *et al.* 1995 and Schuringa *et al.* 2001), constitutive phosphorylation of the serine site alone can drive the pathogenic activity of STAT3. As highlighted by several studies in cancer cells, in which constitutive phosphorylation of the S727 primarily promotes STAT3 mediated tumourigenesis (Qin *et al.* 2008, Aziz *et al.* 2010, Sakaguchi *et al.* 2012 and Tkach *et al.* 2013). Phosphorylation of the S727 site is has been shown to be key for p300/CBP recruitment to STAT3 target genes (Schuringa *et al.* 2001). Within the *TSC2* deficient cells, inhibition of p300/CBP recruitment by repressing phosphorylation of STAT3 at S727 may be how rapamycin and C188-9 primarily mediate their inhibitory effect on STAT3 transcription. As previously described the decrease in the phosphorylation of surrogate markers of mTORC1 activity by C188-9 does confound exact conclusions about the differing effects of rapamycin and C188-9.

The present work also informs on the strategy of targeting STAT3 within TSC. The other candidate STAT3 inhibitor, FLLL31, targets the SH2 domains of STAT3 and JAK2 (Lin *et al*. 2010). However, while in *TSC2* deficient cells FLLL31 treatment repressed phosphorylation of JAK2, repression of STAT3 phosphorylation at Y705 was short term only. Long term repression of JAK2 and STAT3 phosphorylation was observed with C188-9. Therefore, targeting single JAK family adaptor kinases only, may not be an appropriate strategy for targeting STAT3 activity within TSC. As more than one JAK family member can transduce signals from individual cytokine and growth factors, such as TYK2 and JAK1 in addition to JAK2, mediating IL-6 bound receptor activation of STAT3 (Jiang *et al.* 2017 and Song *et al.* 2011). Supporting this argument, was the observation that drug effects of FLLL31 were typically smaller in impact than those observed with C188-9 treatment in chapters 4 and 5. Given, autocrine activation of STAT3 observed within *TSC2* deficient cells, targeting STAT3 upstream, through the use of a cytokine receptor antagonist/cytokine blocking antibody may provide more robust repression of STAT3. This strategy has been found to be effective within multiple cancers (Garbers *et al.* 2015) and a recent report by Wang *et al*. (2021a) found treatment of *Tsc2* −/− MEFs with an IL-6 blocking antibody decreased phosphorylation of STAT3 at Y705.

## 7.7 Cross talk between STAT3 and mTORC1 signalling

In *TSC2* deficient cells, a decrease in phosphorylation markers of STAT3 activity were concomitant with a decrease in phosphorylation markers of mTORC1 activity on C188-9 treatment (chapter 5). Indicating that STAT3 inhibition decreased mTORC1 activity. However, as the other candidate STAT3 inhibitor, FLLL31, was ineffective at decreasing STAT3 phosphorylation longer term, it cannot be concluded that STAT3 activity drives mTORC1 activity within TSC cells. As C188-9's effect on mTORC1 activity may be an off target effect. A novel finding pertinent to the repression of hyperactive mTORC1 signalling in TSC, is that both rapamycin and C188-9 normalised, in part, the expression of some genes encoding constituents of the mTORC1 complex found to be dysregulated upon the loss of *TSC2* in AML cells. There is little literature on the effect of mTORC1/STAT3 inhibition on mTORC1 complex encoding genes, one study in cancer cells did however find inhibition of STAT3 downregulated expression of *MLST8* (Lee *et al*. 2020a). Other than the dual inhibitory effect of C188-9, a recent study found convallatoxin was able to repress both STAT3 phosphorylation and PI3K/AKT/mTOR activity within colorectal cancer cell lines, leading to decreased cell proliferation and markers of angiogenesis (Zhang *et al.* 2020). Autocrine signalling of IL-6

within TSC cells may also contribute to mTORC1 hyperactivity, as in non-TSC cells IL-6 has been found to stimulate PI3K/AKT signalling (Shi *et al.* 2002) and decrease expression of the mTORC1 inhibitor REDD1 (Pinno *et al.* 2016). These previous studies and the work within this thesis highlight that cross-talk between mTORC1 and STAT3 signalling is likely more extensive than appreciated within TSC. And targeting both mTORC1 and STAT3 is likely to show improved therapeutic advantages for TSC patients. In this vein, this thesis identifies C188-9 as a potential therapy for TSC patients, as dual inhibition of mTORC1 and STAT3 by this drug would be of clear clinical benefit if it was shown to be safe and efficacious within clinical trials.

## 7.8 Oxidative Stress in *TSC2* Deficient Cells

Briefly, data in chapter 6 expands on observations that oxidative stress is elevated with TSC (Chen *et al*. 2008, Suzuki *et al.* 2008 and Di Nardo *et al.* 2009). This thesis provides a novel and comprehensive analysis of Nrf2 mediated transcription within models of TSC, which further indicated loss of *TSC2* enhances oxidative stress within cells. Nrf2, but not mTORC1 activity, was also identified as a mediator of *TSC2* deficient cell survival in conditions of enhanced oxidative stress. Whilst Nrf2 inhibition alone was not cytotoxic to *TSC2* deficient cells, elevating oxidative stress further through inhibition of Nrf2 alongside inducing other forms of cell stress may provide selectivity to TSC cells. Selective cell death has been observed in *Tsc2* −/− deficient cells on enhancing metabolic stress (Johnson *et al.* 2018a) and also endoplasmic reticulum/protein homeostatic stress (Jones *et al*. 2019).

## 7.9 Limitations

Aside from the limitations already discussed, there are important limitations to this research that should be considered when interpreting the findings of this thesis.

The use of an AML line in which *TSC2* has been re-expressed as a control presents with some disadvantages. Firstly, these cells are not a true 'healthy' control, nor are they heterozygous for functional *TSC2,* as would typically be the case for cells from non-lesion tissue in TSC patients. Secondly, *TSC2* was over-expressed within these AML cells, and therefore expression of TSC2 protein likely does not reflect what would be expected in *TSC2* competent cells.

Whilst the FBS concentrations used for cell culture in the growth assays described in chapter 3 were deemed necessary for proliferation and growth of those cells, there are issues with including FBS in the experimental design. General problems with FBS include that FBS concentrations for optimal cell growth do not necessarily reflect the normal function or signalling environment for a given cell line. Additionally, the constituent signalling factors present in FBS, represent a black box, in that for example which growth factor and cytokines are present in the FBS and ay what concentrations is unknown. And therefore, it is very likely many signalling pathways are activated in the TSC model cell lines by the presence of FBS. Compounding this issue, is that given the animal origin of FBS, it is highly likely there was batch variability between FBS lots used for cell culture over the course of research for this thesis. Another problem with using FBS in regard to studying mTOR signalling, is there will be enhanced growth factor signalling to both mTORC1 and mTORC2 complexes and inhibition of the TSC1/TSC2 complex in *TSC2* competent cells. Activation of mTORC2 would likely enhance pro-survival and proliferation signalling pathways, which could have affected the findings through out the research for this thesis.

Another important limitation of the present work concerns the concentrations of drugs that were used. Drug titrations for the inhibitors used to target proteins in the specific cell lines used within this thesis, under the specific culture conditions, were not performed. The concentrations of rapamycin and Ku-0063794 that are effective in inhibiting mTORC1 in TSC model cell lines are well documented. This is not the case for the other inhibitors used. For example, while the concentrations of the STAT3 inhibitors FLLL31 and C188-9 chosen were informed by the $IC_{50}$ values and inhibitor constants determined by the papers that initially characterised their efficacy in inhibiting STAT3. This characterisation was not undertaken in the TSC model cell lines, nor under the same culture conditions that were utilised within the present work. Therefore, for the specific cell lines used within this thesis, the concentration of

inhibitors that maximally inhibit their target protein is unknown, nor whether that target protein is actually being maximally inhibited.

Within the present work mTORC2 activity was not assayed within the TSC cell lines. Inclusion of FBS in cell culture media likely would promote enhanced growth factor signalling, which could activate mTORC2, especially through the PI3K signalling pathway. mTORC2 therefore could be affecting cell signalling readouts and phenotypes within the AML and MEF cell lines. As described previously within this chapter, mTORC2 activity is likely repressed, and growth factor signalling to mTORC2 impaired, within the *TSC2* deficient AML and *Tsc2* −/− MEF cells. However, without downstream markers of mTORC2 activity, such as mTORC2 specific Akt1 and PKCα phosphorylation, the status of mTORC2 and therefore its impact on potential findings cannot be concluded with any degree of certainty.

There are issues with the compilation of the STAT3 target gene set. STAT3 is a highly pleotropic transcription factor, regulating many hundreds of genes under different contexts. The selection of STAT3 target genes bases on ChIP sequencing and microarray analysis in other cells lines, may not be entirely valid or appropriate. However, no such analysis of STAT3 target genes within TSC cells has been reported at the time of submission of this thesis. Furthermore, this thesis did not take into account cross talk between STAT3 and NF-κB signalling. Within cancer, STAT3 and NF-κB signalling have been found to reciprocally affect one another in both a positive and inhibitory manner. Given indications NF-κB activity may be elevated within TSC cells, some observations may result from induction or inhibition of NF-κB within *TSC2* deficient cells.

C188-9 appeared to be the much more effective STAT3 inhibitor, relative to FLLL31. Therefore, conclusions drawn based on the action of C188-9 are limited in their scope. As without a second effective STAT3 inhibitor, off-target effects of C188-9 being responsible for some findings cannot be ruled out. Potential off-target effects of C188-9 include the decrease in mTORC1 activity in *TSC2* deficient cells, as already discussed. Additionally, without experiments such as a cycloheximide based protein synthesis inhibition assay, conclusions about STAT3 and redox modulation of HIF-1α protein stability cannot be conclusively made.

Lastly, ROS species could not be successively measured within this work. Two different fluorescent dye based assays were attempted to quantify ROS in unstimulated TSC cell models and *TSC2* deficient cells treated with the ROS inducing drugs (DMNQ, rotenone and RSL3) and ROS quenching compounds (Trolox, NAC and glutathione monoethyl ester). Without actually quantifying ROS, treatment of *TSC2* deficient cells with the aforementioned compounds was assumed to modulate the redox environment of these cells, but was not firmly proven.

## 7.10 Future Directions

The work presented within this thesis provides a better understanding of Ref-1, HIF-1α and STAT3 signalling within TSC cell models and the potential efficacy of targeting Ref-1 and STAT3 as a therapeutic strategy for the treatment of TSC. This thesis is one of many steps taken towards elucidating mechanisms that drive the aetiology of TSC in the hope of providing better treatments for patients. As the causes and consequences of STAT3 dysregulation within TSC models are less studied, this thesis proposes future work should focus on elucidating more aspects of STAT3 signalling in TSC.

Selection of more effective candidate STAT3 inhibitors within *TSC2* deficient cells could be undertaken. This would allow key findings from this thesis dependent on the action of C188-9 to be supported or rejected. Additionally, assaying surrogate markers of mTORC1 activity within *TSC2* deficient cells, treated with effective STAT3 inhibitors, would allow a clearer and more definite understanding of whether STAT3 activity promotes mTORC1 activity within TSC.

To address the limitation regarding selecting STAT3 driven target genes to study within TSC, chromatin immunoprecipitation sequencing could be undertaken in unstimulated human and/or murine TSC cell models. This would allow for validation of which genes expression is dysregulated by the action of hyperactive STAT3 activity upon the loss of either *TSC1* or *TSC2.*

Majority of studies into STAT3 within diseases, such as cancers, focus on the S727 and Y705 phosphorylation sites of STAT3. However, as outlined within the main introduction there is a greater appreciation of how other STAT3 PTMs regulate this transcription factor's activity. As can be told form the literature, there is a complete lack of knowledge regarding other STAT3 PTMs within TSC models. Future work could first define whether activatory PTMs, aside from S727 and Y705, are constitutively present, or inhibitory PTMs repressed, within TSC models. Similarly, while SOCS3 and PIAS3 were explored within this thesis, the expression, activity and effect of protein tyrosine phosphatases on STAT3 signalling within TSC remains unexplored.

While this thesis indicated U-STAT3 may play a pathogenic role within TSC. This has not been conclusively proven, nor the consequences of U-STAT3 fully explored. In TSC models in which STAT3 has been silenced/knocked-out, constitutively phosphorylated or phosphorylation dead STAT3 mutants could be overexpressed. Sequencing of these cells would define which genes sub-sets are induced by phosphorylated STAT3 or U-STAT3.

## 7.11 Research Impact

It is the opinion of the author of this thesis that biomedical research into disease should not aim solely to elucidate how a disease arises mechanistically for its own sake. But should strive to improve treatment options and the lives of sufferers of that disease. This statement is especially true for TSC sufferers and their families, who currently have limited therapeutic options for managing this disease. Patients' lives have certainly been improved by the approval of mTOR inhibitors for the management of TSC symptoms. Similarly, the recent approval of cannabidiol for the management of TSC associated seizures has provided another avenue of treatment for TSC patients. However, these drugs do just that, manage the disease, they are not curative therapies. In addition, as can be told from the clinical trials, not all patients respond to mTOR inhibitors or cannabidiol. Therefore, curative drugs or better and alternative treatment options represent the core unmet clinical need for TSC patients. Aiming to help meet that unmet clinical need, the research presented by this thesis is one of many studies aiming to better elucidate the mechanisms which drive TSC pathology in the hope of identifying new candidate drugs.

Novel and impactful findings of this thesis on the field of TSC research include the appraisal of the efficacy of inhibitors of the Ref-1 and STAT3 signalling pathways on tumourigenic outputs and pro-angiogenic signalling of *TSC2* deficient cells *in vitro*. In this regard, both Ref-1 inhibition and STAT3 inhibition were effective, to different extents. Looking at the bigger picture, whilst not likely curative, agents that target Ref-1 or STAT3 could be beneficial in treating the angiogenic lesions of TSC patients. Which remain a high cause of morbidity and mortality for TSC patients, especially those not responsive to the currently approved mTOR inhibitors. Currently the Ref-1 inhibitors and the STAT3 inhibitor C188-9 are undergoing clinical trials. Whilst not for TSC, these trials will provide useful information on the efficacy of targeting these proteins *in vivo* and the safety profiles of these drugs. Which could inform their potential future use in TSC trials.

Additionally, whilst observations of increased STAT3 and HIF-1α signalling upon loss of *TSC2* are not novel contributions to the field of TSC research. The comprehensive bioinformatic analyses of STAT3 and HIF-1α target genes contained within this thesis expands the potential biomarkers and druggable targets of TSC. A useful tool for future work building on the presented research or in the area STAT3 and HIF-1α signalling. Additionally this research advanced the known mechanisms by which STAT3 activity is dysregulated and maintained within *TSC2* deficient cells. And built on the existing studies which examined the relationship between STAT3 and mTORC1 signalling in two TSC model cell lines. For example identifying autocrine signalling as a mechanism which potently enhances STAT3 activity in *TSC2* deficient cells, and an appreciation of the role, or lack of, that hypoxia plays in STAT3 activity.

Greater knowledge of such mechanisms and signalling interplay provides future research with signalling readouts that any novel therapy targeting the pathways in question should aim to be normalise. In this vein, the present work identifies C188-9 as a promising potential therapeutic agent which decreases *TSC2* deficient cell proliferation *in vitro* and hypothetically could target the enhanced activity of both mTORC1 and STAT3 in TSC patients. If safe and efficacious, C188-9 could represent a novel alternative for the treatment of lesions in patients which currently do not respond to mTORC1 inhibitors. Lastly, this thesis expands the known therapeutic effects of rapamycin, and by extension rapalogues, in targeting HIF-1α, STAT3 and pro-angiogenic signalling within TSC. Which in the future may be of use in the designing of more effective mTORC1 inhibitors, and importantly, defining what rapalogue based therapies cannot achieve in TSC model cells and by extension patients.

In conclusion, it is hoped that the research presented within this thesis will help expedite the search for better and alternate treatments for TSC, which meaningfully improve the lives of both TSC sufferers and the people that care for them.

# References


Abu-Sawwa, R., Scutt, B. and Park, Y. (2020). Emerging use of epidiolex (cannabidiol) in epilepsy. *The Journal of Pediatric Pharmacology and Therapeutics*, **25**: 485-499.

Adachi, M., Cui, C., Dodge, C.T., Bhayani, M.K. and Lai, S.Y. (2012). Targeting STAT3 inhibits growth and enhances radiosensitivity in head and neck squamous cell carcinoma. *Oral Oncology*, **48**: 1220-1226.

Al-Attar, A., Gossage, L., Fareed, K.R., Shehata, M., Mohammed, M., Zaitoun, A.M., Soomro, I. *et al.* (2010). Human apurinic/apyrimidinic endonuclease (APE1) is a prognostic factor in ovarian, gastro-oesophageal and pancreatico-biliary cancers. *British Journal of Cancer*, **102**: 704-709.

Alam, J., Stewart, D., Touchard, C., Boinapally, S., Choi, A.M. and Cook, J.L. (1999). Nrf2, a Cap'n'Collar transcription factor, regulates induction of the heme oxygenase-1 gene. *Journal of Biological Chemistry*, **274**: 26071-26078.

Alayev, A., Sun, Y., Snyder, R., Malka Berger, S., Yu, J. and Holz, M. (2014). Resveratrol prevents rapamycin-induced upregulation of autophagy and selectively induces apoptosis in TSC2-deficient cells. *Cell Cycle*, **13**: 371-382.

Alexander, A., Cai, S.L., Kim, J., Nanez, A., Sahin, M., MacLean, K.H., Inoki, K. *et al.* (2010). ATM signals to TSC2 in the cytoplasm to regulate mTORC1 in response to ROS. *Proceedings of the National Academy of Sciences*, **107**: 4153-4158.

Almiron Bonnin, D.A., Havrda, M.C., Lee, M.C., Liu, H., Zhang, Z., Nguyen, L.N., Harrington, L.X. *et al.* (2018). Secretion-mediated STAT3 activation promotes self-renewal of glioma stem-like cells during hypoxia. *Oncogene*, **37**: 1107-1118.

Amin, S., Lux, A., Calder, N., Laugharne, M., Osborne, J. and O'callaghan, F. (2017). Causes of mortality in individuals with tuberous sclerosis complex. *Developmental Medicine & Child Neurology*, **59**: 612-617.

Anderson, M.E., Powrie, F., Puri, R.N. and Meister, A. (1985). Glutathione monoethyl ester: preparation, uptake by tissues, and conversion to glutathione. *Archives Of Biochemistry and Biophysics*, **239**: 538-548.

Arany, Z., Huang, L.E., Eckner, R., Bhattacharya, S., Jiang, C., Goldberg, M.A., Bunn, H.F. *et al.* (1996). An essential role for p300/CBP in the cellular response to hypoxia. *Proceedings of the National Academy of Sciences*, **93**: 12969-12973.

Arbiser, J.L., Brat, D., Hunter, S., D'Armiento, J., Henske, E.P., Arbiser, Z.K., Bai, X., *et al*. (2002). Tuberous sclerosis-associated lesions of the kidney, brain, and skin are angiogenic neoplasms. *Journal of the American Academy of Dermatology*, **46**: 376-380.

Argaw, A.T., Zhang, Y., Snyder, B.J., Zhao, M.L., Kopp, N., Lee, S.C., Raine, C.S. *et al.* (2006). IL-1β regulates blood-brain barrier permeability via reactivation of the hypoxia-angiogenesis program. *The Journal of Immunology*, **177**: 5574-5584.

Arlt, A., Bauer, I., Schafmayer, C., Tepel, J., Müerköster, S.S., Brosch, M., Röder, C. *et al*. (2009). Increased proteasome subunit protein expression and proteasome activity in colon cancer relate to an enhanced activation of nuclear factor E2-related factor 2 (Nrf2). *Oncogene*, **28**: 3983-3996.

Aronica, E., Specchio, N., Luinenburg, M.J. and Curatolo, P. (2023). Epileptogenesis in tuberous sclerosis complex-related developmental and epileptic encephalopathy. *Brain*, **146**: 2694–2710.

Arriola Apelo, S.I., Neuman, J.C., Baar, E.L., Syed, F.A., Cummings, N.E., Brar, H.K., Pumper, C.P. *et al*. (2016). Alternative rapamycin treatment regimens mitigate the impact of rapamycin on glucose homeostasis and the immune system. *Aging Cell*, **15**: 28-38.

Au, K.S., Williams, A.T., Roach, E.S., Batchelor, L., Sparagana, S.P., Delgado, M.R., Wheless, J.W., (2007). Genotype/phenotype correlation in 325 individuals referred for a diagnosis of tuberous sclerosis complex in the United States. *Genetics in Medicine*, **9**: 88-100.

Auernhammer, C.J., Bousquet, C. and Melmed, S. (1999). Autoregulation of pituitary corticotroph SOCS-3 expression: characterization of the murine SOCS-3 promoter. *Proceedings of the National Academy of Sciences*, **96**: 6964-6969.

Avalle, L., Camporeale, A., Camperi, A. and Poli, V. (2017). STAT3 in cancer: A double edged sword. *Cytokine*, **98**: 42-50.

Avalle, L., Raggi, L., Monteleone, E., Savino, A., Viavattene, D., Statello, L., Camperi, A. *et al.* (2022). STAT3 induces breast cancer growth via ANGPTL4, MMP13 and STC1 secretion by cancer associated fibroblasts. *Oncogene*, **41**: 1456-1467.

Avgeris, S., Fostira, F., Vagena, A., Ninios, Y., Delimitsou, A., Vodicka, R., Vrtel, R. (2017). Mutational analysis of TSC1 and TSC2 genes in tuberous sclerosis complex patients from Greece. *Scientific Reports*, **7**: 1-9.

Aziz, M.H., Hafeez, B.B., Sand, J.M., Pierce, D.B., Aziz, S.W., Dreckschmidt, N.E. and Verma, A.K. (2010). Protein kinase Cε mediates Stat3Ser727 phosphorylation, Stat3-regulated gene expression, and cell invasion in various human cancer cell lines through integration with MAPK cascade (RAF-1, MEK1/2, and ERK1/2). *Oncogene*, **29**: 3100-3109.

Baba, K., Kitajima, Y., Miyake, S., Nakamura, J., Wakiyama, K., Sato, H., Okuyama, K. *et al.* (2017). Hypoxia-induced ANGPTL4 sustains tumour growth and anoikis resistance through different mechanisms in scirrhous gastric cancer cell lines. *Scientific Reports*, **7**: 1-13.

Bai, L., Yang, J.C., Ok, J.H., Mack, P.C., Kung, H.J. and Evans, C.P. (2012). Simultaneous targeting of Src kinase and receptor tyrosine kinase results in synergistic inhibition of renal cell carcinoma proliferation and migration. *International Journal of Cancer*, **130**: 2693-2702.

Baker, B.M. and Chen, C.S. (2012). Deconstructing the third dimension–how 3D culture microenvironments alter cellular cues. *Journal of Cell Science*, **125**: 3015-3024.

Barker-Haliski, M.L., Löscher, W., White, H.S. and Galanopoulou, A.S. (2017). Neuroinflammation in epileptogenesis: insights and translational perspectives from new models of epilepsy. *Epilepsia*, **58**: 39-47.

Becker, S., Groner, B. and Müller, C.W. (1998). Three-dimensional structure of the Stat3β homodimer bound to DNA. *Nature*, **394**: 145-151.

Beebe, J.D., Liu, J.Y. and Zhang, J.T. (2018). Two decades of research in discovery of anticancer drugs targeting STAT3, how close are we?. *Pharmacology & Therapeutics*, **191**, 74-91.

BelAiba, R.S., Bonello, S., Zähringer, C., Schmidt, S., Hess, J., Kietzmann, T. and Görlach, A. (2007). Hypoxia up-regulates hypoxia-inducible factor-1α transcription by involving phosphatidylinositol 3-kinase and nuclear factor κB in pulmonary artery smooth muscle cells. *Molecular Biology of the Cell*, **18**: 4691-4697.

Ben-Sahra, I., Howell, J.J., Asara, J.M. and Manning, B.D. (2013). Stimulation of de novo pyrimidine synthesis by growth signaling through mTOR and S6K1. *Science*, **339**: 1323-1328.

Bendavit, G., Aboulkassim, T., Hilmi, K., Shah, S. and Batist, G. (2016). Nrf2 transcription factor can directly regulate mTOR: linking cytoprotective gene expression to a major metabolic regulator that generates redox activity. *Journal of Biological Chemistry*, **291**: 25476-25488.

Benjamini, Y. and Hochberg, Y. (1995). Controlling the false discovery rate: a practical and powerful approach to multiple testing. *Journal of the Royal statistical society: series B (Methodological)*, **57**: 289-300.

Benvenuto, G., Li, S., Brown, S.J., Braverman, R., Vass, W.C., Cheadle, J.P., Halley, D.J. *et al.* (2000). The tuberous sclerosis-1 (TSC1) gene product hamartin suppresses cell growth and augments the expression of the TSC2 product tuberin by inhibiting its ubiquitination. *Oncogene*, **19**: 6306-6316.

Bernardi, R., Guernah, I., Jin, D., Grisendi, S., Alimonti, A., Teruya-Feldstein, J., Cordon-Cardo, C. *et al.* (2006). PML inhibits HIF-1α translation and neoangiogenesis through repression of mTOR. *Nature*, **442**: 779-785.

Betz, C. and Hall, M.N. (2013). Where is mTOR and what is it doing there?. *Journal of Cell Biology*, **203**: 563-574.

Betz, C., Stracka, D., Prescianotto-Baschong, C., Frieden, M., Demaurex, N. and Hall, M.N., (2013). mTOR complex 2-Akt signaling at mitochondria-associated endoplasmic reticulum membranes (MAM) regulates mitochondrial physiology. *Proceedings of the National Academy of Sciences*, **110**: 12526-12534.

Bhakat, K.K., Mantha, A.K. and Mitra, S. (2009). Transcriptional regulatory functions of mammalian AP-endonuclease (APE1/Ref-1), an essential multifunctional protein. *Antioxidants & Redox Signaling*, **11**: 621-637.

Bharadwaj, U., Eckols, T.K., Xu, X., Kasembeli, M.M., Chen, Y., Adachi, M., Song, Y. *et al.* (2016). Small-molecule inhibition of STAT3 in radioresistant head and neck squamous cell carcinoma. *Oncotarget*, **7**: 26307.

Bharadwaj, U., Kasembeli, M.M., Eckols, T.K., Kolosov, M., Lang, P., Christensen, K., Edwards, D.P. *et al.* (2014). Monoclonal antibodies specific for STAT3β reveal its contribution to constitutive STAT3 phosphorylation in breast cancer. *Cancers*, **6**: 2012-2034.

Bhaskar, P.T., Nogueira, V., Patra, K.C., Jeon, S.M., Park, Y., Robey, R.B. and Hay, N., (2009). mTORC1 hyperactivity inhibits serum deprivation-induced apoptosis via increased hexokinase II and GLUT1 expression, sustained Mcl-1 expression, and glycogen synthase kinase 3β inhibition. *Molecular and Cellular Biology*, **29**: 5136-5147.

Bi, Y.L., Min, M., Shen, W. and Liu, Y. (2018). Genistein induced anticancer effects on pancreatic cancer cell lines involves mitochondrial apoptosis, G0/G1cell cycle arrest and regulation of STAT3 signalling pathway. *Phytomedicine*, **39**: 10-16.

Bissler, J.J., Kingswood, J.C., Radzikowska, E., Zonnenberg, B.A., Frost, M., Belousova, E., Sauter, M. *et al.* (2013). Everolimus for angiomyolipoma associated with tuberous sclerosis complex or sporadic lymphangioleiomyomatosis (EXIST-2): a multicentre, randomised, double-blind, placebo-controlled trial. *The Lancet*, **381**: 817-824.

Bissler, J.J., McCormack, F.X., Young, L.R., Elwing, J.M., Chuck, G., Leonard, J.M., Schmithorst, V.J. et al. (2008). Sirolimus for angiomyolipoma in tuberous sclerosis complex or lymphangioleiomyomatosis. New England Journal of Medicine, 358: 140-151.

Bobola, M.S., Blank, A., Berger, M.S., Stevens, B.A. and Silber, J.R., (2001). Apurinic/apyrimidinic endonuclease activity is elevated in human adult gliomas. *Clinical Cancer Research*, **7**: 3510-3518.

Boer, K., Jansen, F., Nellist, M., Redeker, S., Van Den Ouweland, A.M.W., Spliet, W.G.M., van Nieuwenhuizen, O. *et al*. (2008). Inflammatory processes in cortical tubers and subependymal giant cell tumors of tuberous sclerosis complex. *Epilepsy Research*, **78**: 7-21.

Bonello, S., Zähringer, C., BelAiba, R.S., Djordjevic, T., Hess, J., Michiels, C., Kietzmann, T. *et al.* (2007). Reactive oxygen species activate the HIF-1α promoter via a functional NFκB site. *Arteriosclerosis, Thrombosis, and Vascular Biology*, **27**: 755-761.

Borghouts, C., Tittmann, H., Delis, N., Kirchenbauer, M., Brill, B. and Groner, B. (2010). The Intracellular Delivery of a Recombinant Peptide Derived from the Acidic Domain of PIAS3 Inhibits STAT3 Transactivation and Induces Tumor Cell DeathSTAT3 Peptide Inhibitor Derived from PIAS3. *Molecular Cancer Research*, **8**: 539-553.

Boulanger, M.J., Chow, D.C., Brevnova, E.E. and Garcia, K.C. (2003). Hexameric structure and assembly of the interleukin-6/IL-6 α-receptor/gp130 complex. *Science*, **300**: 2101-2104.

Boyer, D.S., Brigell, M., Kolli, A., Rahmani, K., Lazar, A., Sooch, M., Patel, R. *et al.* (2022). The safety of APX3330, an oral drug candidate for the treatment of diabetic eye disease, in the ongoing masked 24-week ZETA-1 Phase 2 clinical trial. *Investigative Ophthalmology & Visual Science*, **63**: 675-F0129.

Bracken, C.P., Fedele, A.O., Linke, S., Balrak, W., Lisy, K., Whitelaw, M.L. and Peet, D.J. (2006). Cell-specific regulation of hypoxia-inducible factor (HIF)-1α and HIF-2α stabilization and transactivation in a graded oxygen environment. *Journal of Biological Chemistry*, **281**: 22575-22585.

Braunstein, J., Brutsaert, S., Olson, R. and Schindler, C. (2003). STATs dimerize in the absence of phosphorylation. *Journal of Biological Chemistry*, **278**: 34133-34140.

Brender, C., Nielsen, M., Kaltoft, K., Mikkelsen, G., Zhang, Q., Wasik, M., Billestrup, N. *et al.* (2001). STAT3-mediated constitutive expression of SOCS-3 in cutaneous T-cell lymphoma. *Blood, The Journal of the American Society of Hematology*, **97**: 1056-1062.

Brown, M.C. and Gromeier, M. (2017). MNK controls mTORC1: substrate association through regulation of TELO2 binding with mTORC1. *Cell Reports*, **18**: 1444-1457.

Brown, R.E., Buryanek, J., Tammisetti, V.S., McGuire, M.F. and Csencsits-Smith, K. (2016). Morphoproteomics and biomedical analytics confirm the mTORC2/Akt pathway as a resistance signature and activated ERK and STAT3 as concomitant prosurvival/antiapoptotic pathways in metastatic renal cell carcinoma (RCC) progressing on rapalogs: pathogenesis and therapeutic options. *Oncotarget*, **7**: 41612.

Brugarolas, J., Lei, K., Hurley, R.L., Manning, B.D., Reiling, J.H., Hafen, E., Witters, L.A., Ellisen, L.W. and Kaelin, W.G. (2004). Regulation of mTOR function in response to hypoxia by REDD1 and the TSC1/TSC2 tumor suppressor complex. *Genes & Development*, **18**: 2893-2904.

Brugarolas, J.B., Vazquez, F., Reddy, A., Sellers, W.R. and Kaelin Jr, W.G. (2003). TSC2 regulates VEGF through mTOR-dependent and-independent pathways. *Cancer Cell*, ***4***: 147-158.

Brunn, G.J., Hudson, C.C., Sekulić, A., Williams, J.M., Hosoi, H., Houghton, P.J., Lawrence, J.C. *et al.* (1997). Phosphorylation of the translational repressor PHAS-I by the mammalian target of rapamycin. *Science*, **277**: 99-101.

Budanov, A.V. and Karin, M. (2008). p53 target genes sestrin1 and sestrin2 connect genotoxic stress and mTOR signaling. *Cell*, **134**: 451-460.

Burk, R.F., Hill, K.E., Nakayama, A., Mostert, V., Levander, X.A., Motley, A.K., Johnson, D.A. *et al.* (2008). Selenium deficiency activates mouse liver Nrf2–ARE but vitamin E deficiency does not. *Free Radical Biology and Medicine*, **44**: 1617-1623.

Busker, S., Qian, W., Haraldsson, M., Espinosa, B., Johansson, L., Attarha, S., Kolosenko, I. *et al.* (2020). Irreversible TrxR1 inhibitors block STAT3 activity and induce cancer cell death. *Science Advances*, **6**: 7945.

Butler, T.A., Paul, J.W., Chan, E.C., Smith, R. and Tolosa, J.M. (2019). Misleading westerns: common quantification mistakes in western blot densitometry and proposed corrective measures. *BioMed research international, 2019.*

Buttgereit, F. and Brand, M.D. (1995). A hierarchy of ATP-consuming processes in mammalian cells. *Biochemical Journal*, **312**: 163-167.

Butturini, E., Darra, E., Chiavegato, G., Cellini, B., Cozzolino, F., Monti, M., Pucci, P. *et al.* (2014). S-Glutathionylation at Cys328 and Cys542 impairs STAT3 phosphorylation. *ACS Chemical Biology*, **9**: 1885-1893.

Cadenas, C., Franckenstein, D., Schmidt, M., Gehrmann, M., Hermes, M., Geppert, B., Schormann, W. *et al.* (2010). Role of thioredoxin reductase 1 and thioredoxin interacting protein in prognosis of breast cancer. *Breast Cancer Research*, **12**: 1-15.

Cai, S.L., Tee, A.R., Short, J.D., Bergeron, J.M., Kim, J., Shen, J., Guo, R. *et al.* (2006). Activity of TSC2 is inhibited by AKT-mediated phosphorylation and membrane partitioning. *The Journal of Cell Biology*, **173**: 279-289.

Caldenhoven, E., van Dijk, T.B., Solari, R., Armstrong, J., Raaijmakers, J.A., Lammers, J.W.J., Koenderman, L. *et al.* (1996). STAT3β, a splice variant of transcription factor STAT3, is a dominant negative regulator of transcription. *Journal of Biological Chemistry*, **271**: 13221-13227.

Camposano, S.E., Greenberg, E., Kwiatkowski, D.J. and Thiele, E.A. (2009). Distinct clinical characteristics of tuberous sclerosis complex patients with no mutation identified. *Annals of human genetics*, **73**: 141-146.

Cao, L., Cheng, H., Jiang, Q., Li, H. and Wu, Z. (2020). APEX1 is a novel diagnostic and prognostic biomarker for hepatocellular carcinoma. *Aging*, **12**: 4573–4591.

Carbajo-Pescador, S., Ordoñez, R., Benet, M., Jover, R., García-Palomo, A., Mauriz, J.L. and González-Gallego, J. (2013). Inhibition of VEGF expression through blockade of Hif1α and STAT3 signalling mediates the anti-angiogenic effect of melatonin in HepG2 liver cancer cells. *British Journal of Cancer*, **109**: 83-91.

Cardoso, A.A., Jiang, Y., Luo, M., Reed, A.M., Shahda, S., He, Y., Maitra, A. *et al.* (2012). APE1/Ref-1 regulates STAT3 transcriptional activity and APE1/Ref-1–STAT3 dual-targeting effectively inhibits pancreatic cancer cell survival. *PLOS ONE*, **7**: 47462.

Carlo, M.I., Molina, A.M., Lakhman, Y., Patil, S., Woo, K., DeLuca, J., Lee, C.H. *et al.* (2016). A phase Ib study of BEZ235, a dual inhibitor of phosphatidylinositol 3-kinase (PI3K) and mammalian target of rapamycin (mTOR), in patients with advanced renal cell carcinoma. *The Oncologist*, **21**: 787-788.

Carpenter, R.L. and Lo, H.W. (2014). STAT3 target genes relevant to human cancers. *Cancers*, **6**: 897-925.

Carrero, P., Okamoto, K., Coumailleau, P., O'Brien, S., Tanaka, H. and Poellinger, L., (2000). Redox-regulated recruitment of the transcriptional coactivators CREB-binding protein and SRC-1 to hypoxia-inducible factor 1α. *Molecular and Cellular Biology*, **20**: 402-415.

Carreau, A., Hafny-Rahbi, B.E., Matejuk, A., Grillon, C. and Kieda, C. (2011). Why is the partial oxygen pressure of human tissues a crucial parameter? Small molecules and hypoxia. *Journal of Cellular and Molecular Medicine*, **15**: 1239-1253.

Carrera, S., Senra, J., Acosta, M.I., Althubiti, M., Hammond, E.M., de Verdier, P.J. and Macip, S. (2014). The role of the HIF-1α transcription factor in increased cell division at physiological oxygen tensions. *PloS One*, **9**: e97938.

Carriere, A., Romeo, Y., Acosta-Jaquez, H.A., Moreau, J., Bonneil, E., Thibault, P., Fingar, D.C. (2011). ERK1/2 phosphorylate Raptor to promote Ras-dependent activation of mTOR complex 1 (mTORC1). *Journal of Biological Chemistry*, **286**: 567-577.

Carson, R.P., Fu, C., Winzenburger, P. and Ess, K.C. (2013). Deletion of Rictor in neural progenitor cells reveals contributions of mTORC2 signaling to tuberous sclerosis complex. *Human Molecular Genetics*, ***22***: 140-152.

Carson, R.P., Van Nielen, D.L., Winzenburger, P.A. and Ess, K.C. (2012). Neuronal and glia abnormalities in Tsc1-deficient forebrain and partial rescue by rapamycin. *Neurobiology of Disease*, **45**: 369-380.

Cassavaugh, J.M., Hale, S.A., Wellman, T.L., Howe, A.K., Wong, C. and Lounsbury, K.M. (2011). Negative regulation of HIF-1α by an FBW7-mediated degradation pathway during hypoxia. *Journal of Cellular Biochemistry*, **112**: 3882-3890.

Caston, R.A., Shah, F., Starcher, C.L., Wireman, R., Babb, O., Grimard, M., McGeown, J. *et al.* (2021). Combined inhibition of Ref-1 and STAT3 leads to synergistic tumour inhibition in multiple cancers using 3D and in vivo tumour co-culture models. *Journal of Cellular and Molecular Medicine*, **25**: 784-800.

Cebula, M., Schmidt, E.E. and Arnér, E.S. (2015). TrxR1 as a potent regulator of the Nrf2-Keap1 response system. *Antioxidants & Redox Signaling*, **23**: 823-853.

Champion, J.D.; Dodd, K.M.; Lam, H.C.; Alzahrani, M.A.M.; Seifan, S.; Rad, E.; Scourfield, D.O. *et al.* (2022). Drug Inhibition of Redox Factor-1 Restores Hypoxia-Driven Changes in Tuberous Sclerosis Complex 2 Deficient Cells. *Cancers*, **14**, 6195.

Chan, J.A., Zhang, H., Roberts, P.S., Jozwiak, S., Wieslawa, G., Lewin-Kowalik, J., Kotulska, K. *et al.* (2004). Pathogenesis of tuberous sclerosis subependymal giant cell astrocytomas: biallelic inactivation of TSC1 or TSC2 leads to mTOR activation*. Journal of Neuropathology & Experimental Neurology*, **63**: 1236-1242.

Chandel, N.S., Maltepe, E., Goldwasser, E., Mathieu, C.E., Simon, M.C. and Schumacker, P. (1998). Mitochondrial reactive oxygen species trigger hypoxia-induced transcription. *Proceedings of the National Academy of Sciences*, **95**: 11715-11720.

Chandel, N.S., McClintock, D.S., Feliciano, C.E., Wood, T.M., Melendez, J.A., Rodriguez, A.M. and Schumacker, P.T. (2000). Reactive oxygen species generated at mitochondrial complex III stabilize hypoxia-inducible factor-1α during hypoxia: a mechanism of O2 sensing. *Journal of Biological Chemistry*, **275**: 25130-25138.

Chang, Q., Bournazou, E., Sansone, P., Berishaj, M., Gao, S.P., Daly, L., Wels, J. *et al.* (2013). The IL-6/JAK/Stat3 feed-forward loop drives tumorigenesis and metastasis. *Neoplasia*, **15**: 848-IN45.

Chang, J.Y., Sehgal, S.N. and Bansbach, C.C. (1991). FK506 and rapamycin: novel pharmacological probes of the immune response. *Trends in Pharmacological Sciences*, **12**: 218-223.

Chau, L.Y. (2015). Heme oxygenase-1: emerging target of cancer therapy. *Journal of Biomedical Science*, **22**: 1-7.

Chawsheen, M.A. and Dash, P.R. (2021). mTOR modulates resistance to gemcitabine in lung cancer in an MTORC2 dependent mechanism. *Cellular Signalling*, **81**: 109934.

Chen, B., Guan, D., Cui, Z.J., Wang, X. and Shen, X. (2010). Thioredoxin 1 downregulates MCP-1 secretion and expression in human endothelial cells by suppressing nuclear translocation of activator protein 1 and redox factor-1. *American Journal of Physiology-Cell Physiology*, **298**: 1170-1179

Chen, C., Liu, Y., Liu, R., Ikenoue, T., Guan, K.L., Liu, Y. and Zheng, P. (2008). TSC–mTOR maintains quiescence and function of hematopoietic stem cells by repressing mitochondrial biogenesis and reactive oxygen species. *The Journal of Experimental Medicine*, **205**: 2397-2408.

Chen, X., Liu, M., Tian, Y., Li, J., Qi, Y., Zhao, D., Wu, Z. *et al.* (2018). Cryo-EM structure of human mTOR complex 2. *Cell Research*, **28**: 518-528.

Chen, X., Tan, M., Xie, Z., Feng, B., Zhao, Z., Yang, K., Hu, C. *et al.* (2016). Inhibiting ROS-STAT3-dependent autophagy enhanced capsaicin–induced apoptosis in human hepatocellular carcinoma cells. *Free Radical Research*, **50**: 744-755.

Chen, J., Zheng, X. F., Brown, E. J. and Schreiber, S. L. (1995) Identification of an 11-kDa FKBP12-rapamycin-binding domain within the 289-kDa FKBP12-rapamycin-associated protein and characterization of a critical serine residue. *Proc. Natl. Acad. Sci. U.S.A*., **92**: 4947–4951

Chen, Y. and Zhou, X. (2020). Research progress of mTOR inhibitors. *European Journal of Medicinal Chemistry*, **208**: 112820.

Cheng, Q., Sandalova, T., Lindqvist, Y. and Arner, E.S. (2009). Crystal structure and catalysis of the selenoprotein thioredoxin reductase 1. *Journal of Biological Chemistry*, **284**: 3998-4008.

Cheng, G.Z., Zhang, W., Sun, M., Wang, Q., Coppola, D., Mansour, M., Xu, L. *et al.* (2008). Twist is transcriptionally induced by activation of STAT3 and mediates STAT3 oncogenic function. *Journal of Biological Chemistry*, **283**: 14665-14673.

Cherfils, J. and Zeghouf, M. (2013). Regulation of small gtpases by gefs, gaps, and gdis. *Physiological Reviews*, **93**: 269-309.

Chihi, M., Gembruch, O., Oppong, M.D., Chen, B., Dinger, T.F., Barthel, L., Pierscianek, D., *et al.* (2019). Intracranial aneurysms in patients with tuberous sclerosis complex: a systematic review*. Journal of Neurosurgery: Pediatrics*, **24**: 174-183.

Cho, H.D., Lee, J.H., Moon, K.D., Park, K.H., Lee, M.K. and Seo, K.I. (2018). Auriculasin-induced ROS causes prostate cancer cell death via induction of apoptosis. *Food and Chemical Toxicology*, **111**: 660-669.

Cho, H.Y., Reddy, S.P., DeBiase, A., Yamamoto, M. and Kleeberger, S.R. (2005). Gene expression profiling of NRF2-mediated protection against oxidative injury. *Free Radical Biology and Medicine*, **38**: 325-343.

Choo, A.Y., Yoon, S.O., Kim, S.G., Roux, P.P. and Blenis, J. (2008). Rapamycin differentially inhibits S6Ks and 4E-BP1 to mediate cell-type-specific repression of mRNA translation. *Proceedings of the National Academy of Sciences*, **105**: 17414-17419.

Chorley, B.N., Campbell, M.R., Wang, X., Karaca, M., Sambandan, D., Bangura, F., Xue, P. *et al.* (2012). Identification of novel NRF2-regulated genes by ChIP-Seq: influence on retinoid X receptor alpha. *Nucleic Acids Research*, **40**: 7416-7429.

Cimica, V., Chen, H.C., Iyer, J.K. and Reich, N.C. (2011). Dynamics of the STAT3 transcription factor: nuclear import dependent on Ran and importin-β1. *Plos One*, **6**: e20188.

Chu-Shore, C.J., Major, P., Montenegro, M. and Thiele, E. (2009). Cyst-like tubers are associated with TSC2 and epilepsy in tuberous sclerosis complex. *Neurology*, **72**: 1165-1169.

Chung, C.D., Liao, J., Liu, B., Rao, X., Jay, P., Berta, P. and Shuai, K. (1997). Specific inhibition of Stat3 signal transduction by PIAS3. *Science*, **278**: 1803-1805.

Cunningham, F., Allen, J.E., Allen, J., Alvarez-Jarreta, J., Amode, M.R., Armean, I.M., Austine-Orimoloye, O. *et al.* (2022). Ensembl 2022. *Nucleic Acids Research*, **50**: 988-995.

Curatolo, P., Bjørnvold, M., Dill, P.E., Ferreira, J.C., Feucht, M., Hertzberg, C., Jansen, A. *et al.* (2016). The role of mTOR inhibitors in the treatment of patients with tuberous sclerosis complex: evidence-based and expert opinions. *Drugs*, **76**: 551-565.

Curatolo, P., Moavero, R. and de Vries, P.J. (2015). Neurological and neuropsychiatric aspects of tuberous sclerosis complex. *The Lancet Neurology*, **14**: 733-745.

Dasgupta, M., Unal, H., Willard, B., Yang, J., Karnik, S.S. and Stark, G.R. (2014). Critical role for lysine 685 in gene expression mediated by transcription factor unphosphorylated STAT3. *Journal of Biological Chemistry*, **289**: 30763-30771.

Demaria, M., Giorgi, C., Lebiedzinska, M., Esposito, G., D'Angeli, L., Bartoli, A., Gough, D.J. *et al.* (2010). A STAT3-mediated metabolic switch is involved in tumour transformation and STAT3 addiction. *Aging*, **2**: 823-842.

Demple, B., Herman, T. and Chen, D.S. (1991). Cloning and expression of APE, the cDNA encoding the major human apurinic endonuclease: definition of a family of DNA repair enzymes. *Proceedings of the National Academy of Sciences*, **88**: 11450-11454.

Deng, X.S., Meng, X., Song, R., Fullerton, D. and Jaggers, J. (2016). Rapamycin decreases the osteogenic response in aortic valve interstitial cells through the Stat3 pathway. *The Annals of Thoracic Surgery*, **102**: 229-1238.

Dengler, V.L., Galbraith, M.D. and Espinosa, J.M. (2014). Transcriptional regulation by hypoxia inducible factors. *Critical Reviews in Biochemistry And Molecular Biology*, **49**: 1-15.

DeNicola, G.M., Karreth, F.A., Humpton, T.J., Gopinathan, A., Wei, C., Frese, K., Mangal, D., *et al.* (2011). Oncogene-induced Nrf2 transcription promotes ROS detoxification and tumorigenesis. *Nature*, **475**: 106-109.

DeYoung, M.P., Horak, P., Sofer, A., Sgroi, D. and Ellisen, L.W. (2008). Hypoxia regulates TSC1/2–mTOR signaling and tumor suppression through REDD1-mediated 14–3–3 shuttling. *Genes & Development*, **22**: 239-251.

Di Maso, V., Avellini, C., Crocè, L.S., Rosso, N., Quadrifoglio, F., Cesaratto, L., Codarin, E., *et al.* (2007). Subcellular localization of APE1/Ref-1 in human hepatocellular carcinoma: possible prognostic significance. *Molecular Medicine*, **13**: 89-96.

Di Nardo, A., Kramvis, I., Cho, N., Sadowski, A., Meikle, L., Kwiatkowski, D.J. and Sahin, M. (2009). Tuberous sclerosis complex activity is required to control neuronal stress responses in an mTOR-dependent manner. *Journal of Neuroscience*, **29**: 5926-5937.

Dibble, C.C. and Cantley, L.C. (2015). Regulation of mTORC1 by PI3K signaling. *Trends in Cell Biology*, **25**: 545-555.

Dibble, C.C., Elis, W., Menon, S., Qin, W., Klekota, J., Asara, J.M., Finan, P.M., *et al.* (2012). TBC1D7 is a third subunit of the TSC1-TSC2 complex upstream of mTORC1. *Molecular Cell*, **47**: 535-546.

Ding, Y., Wang, J., Zhou, S., Zhou, Y., Zhang, L., Yu, L. and Wang, Y. (2020). Genotype and Phenotype Analysis of Chinese Children With Tuberous Sclerosis Complex: A Pediatric Cohort Study. *Frontiers in Genetics*, **11**: 204.

Dodd, K.M., Yang, J., Shen, M.H., Sampson, J.R. and Tee, A.R. (2015). mTORC1 drives HIF-1α and VEGF-A signalling via multiple mechanisms involving 4E-BP1, S6K1 and STAT3. *Oncogene*, **34**: 2239-2250.

Doll, S., Freitas, F.P., Shah, R., Aldrovandi, M., da Silva, M.C., Ingold, I., Goya Grocin, A. *et al.* (2019). FSP1 is a glutathione-independent ferroptosis suppressor. *Nature*, **575**: 693-698.

Dombkowski, A.A., Cukovic, D., Bagla, S., Jones, M., Caruso, J.A., Chugani, H.T. and Chugani, D.C. (2019). TLR7 activation in epilepsy of tuberous sclerosis complex. *Inflammation Research*, **68**: 993-998.

Dorrello, N.V., Peschiaroli, A., Guardavaccaro, D., Colburn, N.H., Sherman, N.E. and Pagano, M. (2006). S6K1-and ßTRCP-mediated degradation of PDCD4 promotes protein translation and cell growth. *Science*, **314**: 467-471.

Duarte, T.L., Talbot, N.P. and Drakesmith, H. (2021). NRF2 and hypoxia-inducible factors: key players in the redox control of systemic iron homeostasis. *Antioxidants & Redox Signaling*, **35**: 433-452.

Dunleavey, J.M. and Dudley, A.C. (2012). Vascular mimicry: concepts and implications for anti-angiogenic therapy. *Current Angiogenesis*, **1**: 133-138.

Dunlop, E.A., Dodd, K.M., Seymour, L.A. and Tee, A.R. (2009). Mammalian target of rapamycin complex 1-mediated phosphorylation of eukaryotic initiation factor 4E-binding protein 1 requires multiple protein–protein interactions for substrate recognition. *Cellular Signalling*, **21**: 1073-1084.

Dunlop, E.A., Hunt, D.K., Acosta-Jaquez, H.A., Fingar, D.C. and Tee, A.R. (2011). ULK1 inhibits mTORC1 signaling, promotes multisite Raptor phosphorylation and hinders substrate binding. *Autophagy*, **7**: 737-747.

Durant, L., Watford, W.T., Ramos, H.L., Laurence, A., Vahedi, G., Wei, L., Takahashi, *et al.* (2010). Diverse targets of the transcription factor STAT3 contribute to T cell pathogenicity and homeostasis. *Immunity*, ***32***: 605-615.

Düvel, K., Yecies, J.L., Menon, S., Raman, P., Lipovsky, A.I., Souza, A.L., Triantafellow, E., *et al*. (2010). Activation of a metabolic gene regulatory network downstream of mTOR complex 1. *Molecular Cell*, **39**: 171-183.

Ebrahimi-Fakhari, D., Agricola, K.D., Tudor, C., Krueger, D. and Franz, D.N. (2020). Cannabidiol elevates mechanistic target of rapamycin inhibitor levels in patients with tuberous sclerosis complex. *Pediatric Neurology*, **105**: 59-61.

Ebrahimi-Fakhari, D., Meyer, S., Vogt, T., Pföhler, C. and Müller, C.S.L. (2017). Dermatological manifestations of tuberous sclerosis complex (TSC). *JDDG: Journal der Deutschen Dermatologischen Gesellschaft*, **15**: 695-700.

Ebrahimi-Fakhari, D., Saffari, A., Wahlster, L., Di Nardo, A., Turner, D., Lewis Jr, T.L., Conrad, C. *et al.* (2016). Impaired mitochondrial dynamics and mitophagy in neuronal models of tuberous sclerosis complex. *Cell Reports*, **17**: 1053-1070.

Edmondson, R., Broglie, J.J., Adcock, A.F. and Yang, L. (2014). Three-dimensional cell culture systems and their applications in drug discovery and cell-based biosensors. *Assay and Drug Development Technologies*, **12**: 207-218

Eijkemans, M.J., van der Wal, W., Reijnders, L.J., Roes, K.C., van Doorn, S.B.V.W., Pelletier, C., Magestro, M. (2015). Long-term follow-up assessing renal angiomyolipoma treatment patterns, morbidity, and mortality: an observational study in tuberous sclerosis complex patients in the Netherlands. *American Journal of Kidney Diseases*, **66**: 638-645.

El-Hashemite, N. and Kwiatkowski, D.J. (2005). Interferon-γ-Jak-Stat signaling in pulmonary lymphangioleiomyomatosis and renal angiomyolipoma: a potential therapeutic target. *American Journal of Respiratory Cell and Molecular Biology*, **33**: 227-230.

Ema, M., Hirota, K., Mimura, J., Abe, H., Yodoi, J., Sogawa, K., Poellinger, L. *et al.* (1999). Molecular mechanisms of transcription activation by HLF and HIF1α in response to hypoxia: their stabilization and redox signal-induced interaction with CBP/p300. *The EMBO Journal*, **18**: 1905-1914.

Epps, D.E., Raub, T.J., Caiolfa, V., Chiari, A. and Zamai, M. (1999). Determination of the affinity of drugs toward serum albumin by measurement of the quenching of the intrinsic tryptophan fluorescence of the protein. *Journal of Pharmacy and Pharmacology*, **51**: 41-48.

European Chromosome 16 Tuberous Sclerosis Consortium. (1993). Identification and characterization of the tuberous sclerosis gene on chromosome 16. *Cell*, **75**: 1305-1315.

Facchinetti, V., Ouyang, W., Wei, H., Soto, N., Lazorchak, A., Gould, C., Lowry, C. *et al.* (2008). The mammalian target of rapamycin complex 2 controls folding and stability of Akt and protein kinase C. *The EMBO Journal*, **27**: 1932-1943.

Falcon, B.L., Barr, S., Gokhale, P.C., Chou, J., Fogarty, J., Depeille, P., Miglarese, M. *et al.* (2011). Reduced VEGF production, angiogenesis, and vascular regrowth contribute to the antitumor properties of dual mTORC1/mTORC2 inhibitors. *Cancer Research*, **71**: 1573-1583.

Feldman, M.E., Apsel, B., Uotila, A., Loewith, R., Knight, Z.A., Ruggero, D. and Shokat, K.M., (2009). Active-site inhibitors of mTOR target rapamycin-resistant outputs of mTORC1 and mTORC2. *PLoS Bio*l, **7**: e1000038.

Feng, J., Witthuhn, B.A., Matsuda, T., Kohlhuber, F., Kerr, I.M. and Ihle, J.N. (1997). Activation of Jak2 catalytic activity requires phosphorylation of Y1007 in the kinase activation loop. Molecular and cellular biology, **17**: 2497-2501.

Feng, J., Yu, S.Y., Li, C.Z., Li, Z.Y. and Zhang, Y.Z. (2016). Integrative proteomics and transcriptomics revealed that activation of the IL-6R/JAK2/STAT3/MMP9 signaling pathway is correlated with invasion of pituitary null cell adenomas. *Molecular and Cellular Endocrinology*, **436**: 195-203.

Feng, Z., Zhang, H., Levine, A.J. and Jin, S. (2005). The coordinate regulation of the p53 and mTOR pathways in cells. *Proceedings of the National Academy of Sciences*, **102**: 8204-8209.

Ferrara, N. (2004). Vascular endothelial growth factor: basic science and clinical progress. *Endocrine Reviews*, **25**: 581-611.

Ferrer, B., Suresh, H., Santamaria, A., Rocha, J.B., Bowman, A.B. and Aschner, M. (2021). The antioxidant role of STAT3 in methylmercury-induced toxicity in mouse hypothalamic neuronal GT1-7 cell line. *Free Radical Biology and Medicine*, **171**: 245-259.

Fishel, M.L., Jiang, Y., Rajeshkumar, N.V., Scandura, G., Sinn, A.L., He, Y., Shen, C., *et al.* (2011). Impact of APE1/Ref-1 Redox Inhibition on Pancreatic Tumor GrowthAPE1/Ref-1 Redox Inhibition on Pancreatic Tumor Growth. *Molecular Cancer Therapeutics*, **10**: 1698-1708.

Fishel, M.L., Wu, X., Devlin, C.M., Logsdon, D.P., Jiang, Y., Luo, M., He, Y. *et al.* (2015). Apurinic/apyrimidinic endonuclease/redox factor-1 (APE1/Ref-1) redox function negatively regulates NRF2. Journal of Biological Chemistry, **290**: 3057-3068.

Fishel, M.L., Xia, H., McGeown, J., McIlwain, D.W., Elbanna, M., Craft, A.A., Kaimakliotis, H.Z. *et al.* (2019). Antitumor activity and mechanistic characterization of APE1/Ref-1 inhibitors in bladder cancer. *Molecular Cancer Therapeutics*, **18**: 1947-1960.

Flohé, L., Toppo, S. and Orian, L. (2022). The glutathione peroxidase family: Discoveries and mechanism. *Free Radical Biology and Medicine*, **187**: 113-122.

Flügel, D., Görlach, A., Michiels, C. and Kietzmann, T. (2007). Glycogen synthase kinase 3 phosphorylates hypoxia-inducible factor 1α and mediates its destabilization in a VHL-independent manner. *Molecular and Cellular Biology*, **27**: 3253-3265.

Fonseca, B.D., Smith, E.M., Yelle, N., Alain, T., Bushell, M. and Pause, A. (2014). The ever-evolving role of mTOR in translation. *In Seminars in Cell & Developmental Biology*: **36**: 102-112.

Foster, K.G., Acosta-Jaquez, H.A., Romeo, Y., Ekim, B., Soliman, G.A., Carriere, A., Roux, P.P. *et al.* (2010). Regulation of mTOR complex 1 (mTORC1) by raptor Ser863 and multisite phosphorylation. *Journal of Biological Chemistry*, **285**: 80-94.

Francescone III, R.A., Faibish, M. and Shao, R. (2011). A Matrigel-based tube formation assay to assess the vasculogenic activity of tumor cells. *Journal of Visualized Experiments: JoVE*: 55.

Franz, D.N., Belousova, E., Sparagana, S., Bebin, E.M., Frost, M., Kuperman, R., Witt, O. *et al.* (2013). Efficacy and safety of everolimus for subependymal giant cell astrocytomas associated with tuberous sclerosis complex (EXIST-1): a multicentre, randomised, placebo-controlled phase 3 trial. *The Lancet*, **381**: 125-132.

Franz, D.N., Kingswood, C., Jozwiak, S., Budde, K., Belousova, E., Sparagana, S., Zonnenberg, B.A. *et al.* (2012). Effect of everolimus on angiogenic biomarkers in patients with tuberous sclerosis complex (TSC): Results from EXIST-1 and EXIST-2. *Journal of Clinical Oncology* 30: 110619-10619.

Franz, D.N., Leonard, J., Tudor, C., Chuck, G., Care, M., Sethuraman, G., Dinopoulos, A., *et al.* (2006). Rapamycin causes regression of astrocytomas in tuberous sclerosis complex. *Annals of Neurology*, **59**: 490-498.

French, J.A., Lawson, J.A., Yapici, Z., Ikeda, H., Polster, T., Nabbout, R., Curatolo, P., *et al.* (2016). Adjunctive everolimus therapy for treatment-resistant focal-onset seizures associated with tuberous sclerosis (EXIST-3): a phase 3, randomised, double-blind, placebo-controlled study. *The Lancet*, **388**: 2153-2163.

Frost, P., Berlanger, E., Mysore, V., Hoang, B., Shi, Y., Gera, J. and Lichtenstein, A. (2013). Mammalian target of rapamycin inhibitors induce tumor cell apoptosis in vivo primarily by inhibiting VEGF expression and angiogenesis. *Journal of Oncology*, **2013**: 897025

Gan, X., Wang, J., Su, B. and Wu, D. (2011). Evidence for direct activation of mTORC2 kinase activity by phosphatidylinositol 3, 4, 5-trisphosphate. *Journal of Biological Chemistry*, **286**: 10998-11002.

Gao, Y., Gartenhaus, R.B., Lapidus, R.G., Hussain, A., Zhang, Y., Wang, X. and Dan, H.C. (2015). Differential IKK/NF-κB Activity Is Mediated by TSC2 through mTORC1 in PTEN-Null Prostate Cancer and Tuberous Sclerosis Complex Tumor CellsAkt-Mediated Differential Regulation of IKK/NF-κB by TSC2/mTORC1. *Molecular Cancer Research*, **13**: 1602-1614.

Gao, D., Inuzuka, H., Tan, M.K.M., Fukushima, H., Locasale, J.W., Liu, P., Wan, L. *et al.* (2011). mTOR drives its own activation via SCFβTrCP-dependent degradation of the mTOR inhibitor DEPTOR. *Molecular Cell*, **44**: 290-303.

Gao, P., Niu, N., Wei, T., Tozawa, H., Chen, X., Zhang, C., Zhang, J. *et al.* (2017). The roles of signal transducer and activator of transcription factor 3 in tumor angiogenesis. *Oncotarget*, **8**: 69139–69161.

Garama, D.J., Harris, T.J., White, C.L., Rossello, F.J., Abdul-Hay, M., Gough, D.J. and Levy, D.E. (2015). A synthetic lethal interaction between glutathione synthesis and mitochondrial reactive oxygen species provides a tumor-specific vulnerability dependent on STAT3. Molecular and cellular biology, **35**: 3646-3656.

Garami, A., Zwartkruis, F.J., Nobukuni, T., Joaquin, M., Roccio, M., Stocker, H., Kozma, S.C. (2003). Insulin activation of Rheb, a mediator of mTOR/S6K/4E-BP signaling, is inhibited by TSC1 and 2. *Molecular Cell*, **11**: 1457-1466.

Garbers, C., Aparicio-Siegmund, S. and Rose-John, S. (2015). The IL-6/gp130/STAT3 signaling axis: recent advances towards specific inhibition. *Current Opinion in Immunology*, **34**: 75-82.

Garcia, M., Juan, M., Mordan, J. and Clarke, R.G. (2009). Ku-0063794 is a specific inhibitor of the mammalian target of rapamycin (mTOR). *Portland Press*: Colchester, Vol. 421.

García-Martínez, J.M. and Alessi, D.R. (2008). mTOR complex 2 (mTORC2) controls hydrophobic motif phosphorylation and activation of serum-and glucocorticoid-induced protein kinase 1 (SGK1). *Biochemical Journal*, **416**: 375-385.

García-Martínez, J.M., Moran, J., Clarke, R.G., Gray, A., Cosulich, S.C., Chresta, C.M. and Alessi, D.R. (2009). Ku-0063794 is a specific inhibitor of the mammalian target of rapamycin (mTOR). *Biochemical Journal*, **421**: 29-42.

Gaultier, A., Arandjelovic, S., Niessen, S., Overton, C.D., Linton, M.F., Fazio, S., Campana, W.M., *et al.* (2008). Regulation of tumor necrosis factor receptor-1 and the IKK-NF-κB pathway by LDL receptor–related protein explains the antiinflammatory activity of this receptor. *Blood*, *The Journal of the American Society of Hematology*, **111**: 5316-5325.

Gebauer, F. and Hentze, M.W. (2004). Molecular mechanisms of translational control. Nature reviews *Molecular Cell Biology*, **5**: 827-835.

Gerber, S.A. and Pober, J.S. (2008). IFN-α induces transcription of hypoxia-inducible factor-1α to inhibit proliferation of human endothelial cells. *The Journal of Immunology*, **181**: 1052-1062.

Giannikou, K., Malinowska, I.A., Pugh, T.J., Yan, R., Tseng, Y.Y., Oh, C., Kim, J. *et al.* (2016). Whole exome sequencing identifies TSC1/TSC2 biallelic loss as the primary and sufficient driver event for renal angiomyolipoma development. *PLoS Genetics*, **12**: e1006242.

Gingras, A.C., Gygi, S.P., Raught, B., Polakiewicz, R.D., Abraham, R.T., Hoekstra, M.F., Aebersold, R. *et al.* (1999b). Regulation of 4E-BP1 phosphorylation: a novel two-step mechanism. *Genes & Development*, **13**: 1422-1437.

Gingras, A.C., Raught, B. and Sonenberg, N. (1999a). eIF4 initiation factors: effectors of mRNA recruitment to ribosomes and regulators of translation. *Annual Review of Biochemistry*, **68**: 913-963.

Goncharova, E.A., Goncharov, D.A., Damera, G., Tliba, O., Amrani, Y., Panettieri, R.A. and Krymskaya, V.P. (2009). Signal transducer and activator of transcription 3 is required for abnormal proliferation and survival of TSC2-deficient cells: relevance to pulmonary lymphangioleiomyomatosis. *Molecular pharmacology*, **76**: 766-777.

Goncharova, E.A., Goncharov, D.A., Li, H., Pimtong, W., Lu, S., Khavin, I. and Krymskaya, V.P. (2011). mTORC2 is required for proliferation and survival of TSC2-null cells. *Molecular and Cellular Biology*, **31**: 2484-2498.

Gorlach, A. (2009). Regulation of HIF-1α at the transcriptional level. *Current Pharmaceutical Design*, **15**: 3844-3852.

Gould, S.E., Junttila, M.R. and de Sauvage, F.J. (2015). Translational value of mouse models in oncology drug development. *Nature Medicine*, **21**: 431-439.

Graff, J.R., Konicek, B.W., Carter, J.H. and Marcusson, E.G. (2008). Targeting the eukaryotic translation initiation factor 4E for cancer therapy. *Cancer Research*, **68**: 631-634.

Graff, J.R., Konicek, B.W., Vincent, T.M., Lynch, R.L., Monteith, D., Weir, S.N., Schwier, P. *et al.* (2007). Therapeutic suppression of translation initiation factor eIF4E expression reduces tumor growth without toxicity. *The Journal of Clinical Investigation*, **117**: 2638-2648.

Graham, L., Banda, K., Torres, A., Carver, B.S., Chen, Y., Pisano, K., Shelkey, G. *et al.* (2018). A phase II study of the dual mTOR inhibitor MLN0128 in patients with metastatic castration resistant prostate cancer. *Investigational New Drugs*, **36**: 458-467.

Graham, F. L., Smiley, J., Russell, W. C., and Nairn, R. (1977) Characteristics of a human cell line transformed by DNA from human adenovirus type 5. *Journal of General Virology*, **36**: 59–74.

Grajkowska, W., Kotulska, K., Jurkiewicz, E. and Matyja, E. (2010). Brain lesions in tuberous sclerosis complex. Review. *Folia Neuropathologica*, **48**: 139-149

Gray, M. J., Zhang, J., Ellis, L. M., Semenza, G. L., Evans, D. B., Watowich, S. S., and Gallick, G. E. (2005). HIF-1alpha, STAT3, CBP/p300 and Ref-1/APE are components of a transcriptional complex that regulates Src-dependent hypoxia-induced expression of VEGF in pancreatic and prostate carcinomas. *Oncogene,* **24**: 3110–3120.

Grimes, D.R. and Currell, F.J. (2018). Oxygen diffusion in ellipsoidal tumour spheroids. *Journal of The Royal Society Interface*, **15**: 20180256.

Guba, M., von Breitenbuch, P., Steinbauer, M., Koehl, G., Flegel, S., Hornung, M., Bruns, C.J. *et al.* (2002). Rapamycin inhibits primary and metastatic tumor growth by antiangiogenesis: involvement of vascular endothelial growth factor. *Nature Medicine*, **8**: 128-135.

Guo, K., Searfoss, G., Krolikowski, D., Pagnoni, M., Franks, C., Clark, K., Yu, K.T. *et al.* (2001). Hypoxia induces the expression of the pro-apoptotic gene BNIP3. *Cell Death & Differentiation*, **8**: 367-376.

Gwinn, D.M., Shackelford, D.B., Egan, D.F., Mihaylova, M.M., Mery, A., Vasquez, D.S., Turk, B.E. *et al*. (2008). AMPK phosphorylation of raptor mediates a metabolic checkpoint. *Molecular Cell*, **30**: 214-226.

Haan, S., Kortylewski, M., Behrmann, I., Müller-Esterl, W., Heinrich, P.C. and Schaper, F. (2000). Cytoplasmic STAT proteins associate prior to activation. *Biochemical Journal*, **345**: 417-421.

Habib, S.L. and Abboud, H.E. (2016). Tuberin regulates reactive oxygen species in renal proximal cells, kidney from rodents, and kidney from patients with tuberous sclerosis complex. *Cancer Science*, **107**: 1092-1100.

Habib, S.L., Phan, M.N., Patel, S.K., Li, D., Monks, T.J. and Lau, S.S. (2003). Reduced constitutive 8-oxoguanine-DNA glycosylase expression and impaired induction following oxidative DNA damage in the tuberin deficient Eker rat. *Carcinogenesis*, **24**: 573-582.

Hagiwara, A., Cornu, M., Cybulski, N., Polak, P., Betz, C., Trapani, F., Terracciano, L. *et al.* (2012). Hepatic mTORC2 activates glycolysis and lipogenesis through Akt, glucokinase, and SREBP1c. *Cell Metabolism*, **15**: 725-738.

Han, Y., Ye, A., Bi, L., Wu, J., Yu, K. and Zhang, S. (2014). Th17 cells and interleukin-17 increase with poor prognosis in patients with acute myeloid leukemia. *Cancer Science*, **105**: 933-942.

Hanahan, D. and Weinberg, R.A. (2011). Hallmarks of cancer: the next generation. *Cell*, **144**: 646-674.

Hara, K., Yonezawa, K., Kozlowski, M.T., Sugimoto, T., Andrabi, K., Weng, Q.P., Kasuga, M. *et al.* (1997). Regulation of eIF-4E BP1 phosphorylation by mTOR. *Journal of Biological Chemistry*, **272**: 26457-26463.

Hara, K., Maruki, Y., Long, X., Yoshino, K.I., Oshiro, N., Hidayat, S., Tokunaga, C. *et al.* (2002). Raptor, a binding partner of target of rapamycin (TOR), mediates TOR action. *Cell*, **110**: 177-189.

Hardie, D.G., Ross, F.A. and Hawley, S.A. (2012). AMPK: a nutrient and energy sensor that maintains energy homeostasis. *Nature Reviews Molecular Cell Biology*, **13**: 251-262.

Harrington, L.S., Findlay, G.M., Gray, A., Tolkacheva, T., Wigfield, S., Rebholz, H., Barnett, J.*et al.* (2004). The TSC1-2 tumor suppressor controls insulin–PI3K signaling via regulation of IRS proteins. *The Journal of Cell Biology*, **166**: 213-223.

Hayashi, Y., Yokota, A., Harada, H. and Huang, G. (2019). Hypoxia/pseudohypoxia-mediated activation of hypoxia-inducible factor-1α in cancer. *Cancer Science*, **110**: 1510-1517.

Hazan-Halevy, I., Harris, D., Liu, Z., Liu, J., Li, P., Chen, X., Shanker, S. *et al.* (2010). STAT3 is constitutively phosphorylated on serine 727 residues, binds DNA, and activates transcription in CLL cells. *Blood, The Journal of the American Society of Hematology*, **115**: 2852-2863.

He, Z., He, X., Chen, Z., Ke, J., He, X., Yuan, R., Cai, Z. *et al.* (2014). Activation of the mTORC1 and STAT3 pathways promotes the malignant transformation of colitis in mice. *Oncology Reports*, **32**: 1873-1880.

Heinrich, P.C., Behrmann, I., Müller-Newen, G., Schaper, F. and Graeve, L. (1998). Interleukin-6-type cytokine signalling through the gp130/Jak/STAT pathway. *Biochemical Journal*, **334**: 297-314.

Heiss, E.H., Liu, R., Waltenberger, B., Khan, S., Schachner, D., Kollmann, P., Zimmermann, K. *et al.* (2016). Plumericin inhibits proliferation of vascular smooth muscle cells by blocking STAT3 signaling via S-glutathionylation. *Scientific Reports*, **6**: 20771.

Heitman, J., Movva, N.R. and Hall, M.N. (1991). Targets for cell cycle arrest by the immunosuppressant rapamycin in yeast. *Science*, **253**: 905-909.

Hemmann, U., Gerhartz, C., Heesel, B., Sasse, J., Kurapkat, G., Grötzinger, J., Wollmer, A., (1996). Differential activation of acute phase response factor/Stat3 and Stat1 via the cytoplasmic domain of the interleukin 6 signal transducer gp130: II. Src homology SH2 domains define the specificity of stat factor activation. *Journal of Biological Chemistry*, **271**: 12999-13007.

Hentze, M.W., Muckenthaler, M.U., Galy, B. and Camaschella, C. (2010). Two to tango: regulation of Mammalian iron metabolism. *Cell*, **142**: 24-38.

Ho, D.W., Chan, L.K., Chiu, Y.T., Xu, I.M., Poon, R.T., Cheung, T.T., Tang, C.N. *et al*. (2017). TSC1/2 mutations define a molecular subset of HCC with aggressive behaviour and treatment implication. *Gut*, **66**: 1496-1506.

Holmquist-Mengelbier, L., Fredlund, E., Löfstedt, T., Noguera, R., Navarro, S., Nilsson, H., Pietras, A. *et al.* (2006). Recruitment of HIF-1α and HIF-2α to common target genes is differentially regulated in neuroblastoma: HIF-2α promotes an aggressive phenotype. *Cancer Cell*, **10**: 413-423.

Hong, F., Larrea, M.D., Doughty, C., Kwiatkowski, D.J., Squillace, R. and Slingerland, J.M., (2008). mTOR-raptor binds and activates SGK1 to regulate p27 phosphorylation. *Molecular Cell*, **30**: 701-711.

Hong, C.H., Tu, H.P., Lin, J.R. and Lee, C.H. (2016). An estimation of the incidence of tuberous sclerosis complex in a nationwide retrospective cohort study (1997–2010). *British Journal of Dermatology*, ***174***: 1282-1289.

Hou, T., Ray, S., Lee, C. and Brasier, A.R. (2008). The STAT3 NH2-terminal domain stabilizes enhanceosome assembly by interacting with the p300 bromodomain. *Journal of Biological Chemistry*, **283**: 30725-30734.

Hresko, R.C. and Mueckler, M. (2005). mTOR· RICTOR is the Ser473 kinase for Akt/protein kinase B in 3T3-L1 adipocytes. *Journal of Biological Chemistry*, **280**: 40406-40416.

Hsieh, A.C., Liu, Y., Edlind, M.P., Ingolia, N.T., Janes, M.R., Sher, A., Shi, E.Y. *et al.* (2012). The translational landscape of mTOR signalling steers cancer initiation and metastasis. *Nature*, **485**: 55-61.

Hu, Z., Ding, X., Ji, Y., Liu, X. and Ding, Z. (2021). APEX1 protects against oxidative damage-induced cardiomyocyte apoptosis. *Biocell*, **45**: 745.

Huang, J., Dibble, C.C., Matsuzaki, M. and Manning, B.D. (2008). The TSC1-TSC2 complex is required for proper activation of mTOR complex 2. *Molecular and Cellular Biology*, **28**: 4104-4115.

Huang, J. and Manning, B.D. (2008). The TSC1–TSC2 complex: a molecular switchboard controlling cell growth. *Biochemical Journal*, **412**: 179-190.

Huang, J., Wu, S., Wu, C.L. and Manning, B.D. (2009). Signaling events downstream of mammalian target of rapamycin complex 2 are attenuated in cells and tumors deficient for the tuberous sclerosis complex tumor suppressors. *Cancer Research*, **69**: 6107-6114.

Hubbard, S.R. (1997). Crystal structure of the activated insulin receptor tyrosine kinase in complex with peptide substrate and ATP analog. *The EMBO journal*, **16**: 5572-5581.

Hudson, C.C., Liu, M., Chiang, G.G., Otterness, D.M., Loomis, D.C., Kaper, F., Giaccia, A.J. *et al.* (2002). Regulation of hypoxia-inducible factor 1α expression and function by the mammalian target of rapamycin. *Molecular and cellular biology*, ***22***: 7004-7014.

Huynh, H., Pierce Chow, K.H., Soo, K.C., Toh, H.C., Choo, S.P., Foo, K.F., Poon, D. *et al.* (2009). RAD001 (everolimus) inhibits tumour growth in xenograft models of human hepatocellular carcinoma. *Journal of Cellular and Molecular Medicine*, **13**: 1371-1380.

Ichiba, M., Nakajima, K., Yamanaka, Y., Kiuchi, N. and Hirano, T. (1998). Autoregulation of the Stat3 gene through cooperation with a cAMP-responsive element-binding protein. *Journal of Biological Chemistry*, **273**: 6132-6138.

Ikenoue, T., Inoki, K., Yang, Q., Zhou, X. and Guan, K.L. (2008). Essential function of TORC2 in PKC and Akt turn motif phosphorylation, maturation and signalling. *The EMBO Journal*, **27**: 1919-1931.

Inami, Y., Waguri, S., Sakamoto, A., Kouno, T., Nakada, K., Hino, O., Watanabe, S. *et al.* (2011). Persistent activation of Nrf2 through p62 in hepatocellular carcinoma cells. *Journal of Cell Biology*, **193**: 275-284.

Inoki, K., Li, Y., Xu, T. and Guan, K.L. (2003a). Rheb GTPase is a direct target of TSC2 GAP activity and regulates mTOR signaling. *Genes & Development*, **17**: 1829-1834.

Inoki, K., Ouyang, H., Zhu, T., Lindvall, C., Wang, Y., Zhang, X., Yang, Q., (2006). TSC2 integrates Wnt and energy signals via a coordinated phosphorylation by AMPK and GSK3 to regulate cell growth. *Cell*, **126**: 955-968.

Inoki, K., Zhu, T. and Guan, K.L. (2003b). TSC2 mediates cellular energy response to control cell growth and survival. *Cell*, **115**: 577-590.

Ishihara, Y., Shiba, D. and Shimamoto, N. (2006). Enhancement of DMNQ-induced hepatocyte toxicity by cytochrome P450 inhibition. *Toxicology and Applied Pharmacology*, **214**: 109-117.

Ivan, M., Kondo, K., Yang, H., Kim, W., Valiando, J., Ohh, M., Salic, A. *et al.* (2001). HIFα targeted for VHL-mediated destruction by proline hydroxylation: implications for O2 sensing. *Science*, **292**: 464-468.

Jacinto, E., Loewith, R., Schmidt, A., Lin, S., Rüegg, M.A., Hall, A. and Hall, M.N. (2004). Mammalian TOR complex 2 controls the actin cytoskeleton and is rapamycin insensitive. *Nature Cell Biology*, **6**: 1122-1128.

Jackson, R.J. and Wickens, M. (1997). Translational controls impinging on the 5′-untranslated region and initiation factor proteins. *Current Opinion in Genetics & Development*, **7**: 233-241.

Jayaraman, L., Murthy, K.G., Zhu, C., Curran, T., Xanthoudakis, S. and Prives, C. (1997). Identification of redox/repair protein Ref-1 as a potent activator of p53. *Genes & Development*, **11**: 558-570.

Jefferies, H.B., Reinhard, C., Kozma, S.C. and Thomas, G. (1994). Rapamycin selectively represses translation of the" polypyrimidine tract" mRNA family. *Proceedings of the National Academy of Sciences*, **91**: 4441-4445.

Jeon, D., Park, H.J. and Kim, H.S. (2018). Protein S-glutathionylation induced by hypoxia increases hypoxia-inducible factor-1α in human colon cancer cells. *Biochemical and Biophysical Research Communications*, **495**: 212-216.

Jewell, U.R., Kvietikova, I.V., Scheid, A.N., Bauer, C.H., Wenger, R.H. and Gassmann M. (2001). Induction of HIF–1α in response to hypoxia is instantaneous. *The FASEB Journal*, **15**: 1312-1314.

Ji, L., Moghal, N., Zou, X., Fang, Y., Hu, S., Wang, Y. and Tsao, M.S. (2022). The NRF2 antagonist ML385 inhibits PI3K-mTOR signaling and growth of lung squamous cell carcinoma cells. *Cancer Medicine*.

Ji, Z., He, L., Regev, A. and Struhl, K, (2019). Inflammatory regulatory network mediated by the joint action of NF-κB, STAT3, and AP-1 factors is involved in many human cancers. *Proceedings of the National Academy of Sciences*, **116**: 9453-9462.

Jia, Y., Wang, H., Wang, Q., Ding, H., Wu, H. and Pan, H. (2016). Silencing Nrf2 impairs glioma cell proliferation via AMPK-activated mTOR inhibition. Biochemical and biophysical research communications, **469**: 665-671.

Jiang, M., Chen, J., Zhang, W., Zhang, R., Ye, Y., Liu, P., Yu, W. *et al.* (2017). Interleukin-6 trans-signaling pathway promotes immunosuppressive myeloid-derived suppressor cells via suppression of suppressor of cytokine signaling 3 in breast cancer. *Frontiers in Immunology*, **8**: 1840.

Jiang, A., Gao, H., Kelley, M.R. and Qiao, X. (2011). Inhibition of APE1/Ref-1 redox activity with APX3330 blocks retinal angiogenesis in vitro and in vivo. *Vision Research*, **51**: 93-100.

Jiang, X., Takahashi, N., Matsui, N., Tetsuka, T. and Okamoto, T. (2003). The NF-κB activation in lymphotoxin β receptor signaling depends on the phosphorylation of p65 at serine 536. *Journal of Biological Chemistry*, **278**: 919-926.

Jiang, Y., Zhou, S., Sandusky, G.E., Kelley, M.R. and Fishel, M.L. (2010). Reduced expression of DNA repair and redox signaling protein APE1/Ref-1 impairs human pancreatic cancer cell survival, proliferation, and cell cycle progression. *Cancer Investigation*, **28**: 885-895.

Jiang, S., Zhu, L., Tang, H., Zhang, M., Chen, Z., Fei, J., Han, B. *et al.* (2015). Ape1 regulates WNT/β-catenin signaling through its redox functional domain in pancreatic cancer cells. *International Journal of Oncology*, **47**: 610-620.

Jiao, D., Wang, J., Lu, W., Tang, X., Chen, J., Mou, H. and Chen, Q.Y. (2016). Curcumin inhibited HGF-induced EMT and angiogenesis through regulating c-Met dependent PI3K/Akt/mTOR signaling pathways in lung cancer. *Molecular Therapy-Oncolytics*, **3**: 16018.

Jin, H.O., Lee, Y.H., Park, J.A., Kim, J.H., Hong, S.E., Kim, H.A., Kim, E.K. *et al.* (2014). Blockage of Stat3 enhances the sensitivity of NSCLC cells to PI3K/mTOR inhibition. *Biochemical and Biophysical Research Communications*, **444**: 502-508.

Jing, B., Wang, T., Sun, B., Xu, J., Xu, D., Liao, Y., Song, H. (2020). IL6/STAT3 Signaling Orchestrates Premetastatic Niche Formation and Immunosuppressive Traits in LungIL6 Promotes Lung Metastasis. *Cancer Research*, **80**: 784-797.

Johnson, C.E., Dunlop, E.A., Seifan, S., McCann, H.D., Hay, T., Parfitt, G.J., Jones, A.T. *et al.* (2018a). Loss of tuberous sclerosis complex 2 sensitizes tumors to nelfinavir− bortezomib therapy to intensify endoplasmic reticulum stress-induced cell death. *Oncogene*, **37**: 5913-5925.

Johnson, D.E., O'Keefe, R.A. and Grandis, J.R. (2018b). Targeting the IL-6/JAK/STAT3 signalling axis in cancer. *Nature Reviews Clinical Oncology*, **15**: .234-248.

Jones, A.T., Narov, K., Yang, J., Sampson, J.R. and Shen, M.H. (2019). Efficacy of Dual inhibition of glycolysis and glutaminolysis for therapy of renal lesions in Tsc2+/− mice. *Neoplasia*, **21**: 230-238.

Jozwiak, J., Kotulska, K., Grajkowska, W., Jozwiak, S., Zalewski, W., Oldak, M., Lojek, M., *et al.* (2007). Upregulation of the WNT pathway in tuberous sclerosis-associated subependymal giant cell astrocytomas. *Brain and Development*, **29**: 273-280.

Jung, C.H., Jun, C.B., Ro, S.H., Kim, Y.M., Otto, N.M., Cao, J., Kundu, M. *et al.* (2009). ULK-Atg13-FIP200 complexes mediate mTOR signaling to the autophagy machinery. *Molecular Biology of the Cell*, **20**: 1992-2003.

Jung, J.E., Kim, H.S., Lee, C.S., Shin, Y.J., Kim, Y.N., Kang, G.H., Kim, T.Y. *et al.* (2008). STAT3 inhibits the degradation of HIF-1α by pVHL-mediated ubiquitination. Experimental & molecular medicine, **40**: 479-485.

Jung, J.E., Lee, H.G., Cho, I.H., Chung, D.H., Yoon, S.H., Yang, Y.M., Lee, J.W. *et al.* (2005). STAT3 is a potential modulator of HIF-1-mediated VEGF expression in human renal carcinoma cells. *The FASEB Journal*, **19**: 1296-1298.

Kaidi, A., Williams, A.C. and Paraskeva, C. (2007). Interaction between β-catenin and HIF-1 promotes cellular adaptation to hypoxia. *Nature Cell Biology*, **9**: 210-217.

Kaizuka, T., Hara, T., Oshiro, N., Kikkawa, U., Yonezawa, K., Takehana, K., Iemura, S.I., *et al.* (2010). Tti1 and Tel2 are critical factors in mammalian target of rapamycin complex assembly. *Journal of Biological Chemistry*, **285**: 20109-20116.

Kajdaniuk, D., Marek, B., Foltyn, W. and Kos-Kudła, B. (2011). Vascular endothelial growth factor (VEGF)—part 2: in endocrinology and oncology. *Endokrynologia Polska*, **62**: 456-464

Kamran, M.Z., Patil, P. and Gude, R.P. (2013). Role of STAT3 in cancer metastasis and translational advances. *BioMed research international*, *2013*.

Kang, S.H., Yu, M.O., Park, K.J., Chi, S.G., Park, D.H. and Chung, Y.G. (2010). Activated STAT3 regulates hypoxia-induced angiogenesis and cell migration in human glioblastoma. *Neurosurgery*, **67**: 1386-1395.

Kaptein, A., Paillard, V. and Saunders, M. (1996). Dominant Negative Stat3 Mutant Inhibits Interleukin-6-induced Jak-STAT Signal Transduction (∗). *Journal of Biological Chemistry*, **271**: 5961-5964.

Karalis, V., Caval-Holme, F. and Bateup, H.S. (2022). Raptor downregulation rescues neuronal phenotypes in mouse models of Tuberous Sclerosis Complex. *Nature Communications*, **13**: 4665.

Karar, J. and Maity, A. (2011). PI3K/AKT/mTOR pathway in angiogenesis. *Frontiers in Molecular Neuroscience*, **4**: 51.

Karlenius, T.C. and Tonissen, K.F. (2010). Thioredoxin and cancer: a role for thioredoxin in all states of tumor oxygenation. *Cancers*, **2**: 209-232.

Kasembeli, M.M., Singhmar, P., Ma, J., Edralin, J., Tang, Y., Adams III, C., Heijnen, C.J. *et al.* (2021). TTI-101: A competitive inhibitor of STAT3 that spares oxidative phosphorylation and reverses mechanical allodynia in mouse models of neuropathic pain. *Biochemical Pharmacology*, **192**: 114688.

Kearney, A.L., Cooke, K.C., Norris, D.M., Zadoorian, A., Krycer, J.R., Fazakerley, D.J., Burchfield, J.G. *et al.* (2019). Serine 474 phosphorylation is essential for maximal Akt2 kinase activity in adipocytes. *Journal of Biological Chemistry*, **294**: 16729-16739.

Keith, B., Johnson, R.S. and Simon, M.C. (2012). HIF1α and HIF2α: sibling rivalry in hypoxic tumour growth and progression. *Nature Reviews Cancer*, **12**: 9-22.

Kent, W.J., Sugnet, C.W., Furey, T.S., Roskin, K.M., Pringle, T.H., Zahler, A.M. and Haussler, D. (2002). The human genome browser at UCSC. *Genome Research*, **12**: 996-1006.

Kerins, M.J. and Ooi, A. (2018). The roles of NRF2 in modulating cellular iron homeostasis. *Antioxidants & Redox Signaling*, **29**: 1756-1773.

Kelley, M.R., Wikel, J.H., Guo, C., Pollok, K.E., Bailey, B.J., Wireman, R., Fishel, M.L. *et al.* (2016). Identification and characterization of new chemical entities targeting apurinic/apyrimidinic endonuclease 1 for the prevention of chemotherapy-induced peripheral neuropathy. *Journal of Pharmacology and Experimental Therapeutics*, **359**: 300-309.

Kettner, N.M., Bui, T., Ha, M.J., Eckols, T.K., Tweardy, D.J., Meric-Bernstam, F., Hunt, K.K., *et al.* (2020). Abstract P6-04-12: STAT3 as a therapeutic target in estrogen receptor positive breast cancer patients refractory to CDK4/6 inhibition. *Cancer Research*, **80**: 6-04.

Kim, Y.J., Ahn, J.Y., Liang, P., Ip, C., Zhang, Y. and Park, Y.M. (2007). Human prx1 gene is a target of Nrf2 and is up-regulated by hypoxia/reoxygenation: implication to tumor biology. *Cancer Research*, **67**: 546-554.

Kim, H. and Baumann, H. (1997). The carboxyl-terminal region of STAT3 controls gene induction by the mouse haptoglobin promoter. *Journal of Biological Chemistry*, **272**: 14571-14579.

Kim, J. and Guan, K.L. (2019). mTOR as a central hub of nutrient signalling and cell growth. *Nature Cell Biology*, **21**: 63-71.

Kim, T.H., Hur, E.G., Kang, S.J., Kim, J.A., Thapa, D., Lee, Y.M., Ku, S.K., Jung, Y. and Kwak, M.K. (2011c). NRF2 blockade suppresses colon tumor angiogenesis by inhibiting hypoxia-induced activation of HIF-1α. *Cancer Research*, **71**: 2260-2275.

Kim, J.H., Kim, J.E., Liu, H.Y., Cao, W. and Chen, J. (2008b). Regulation of interleukin-6-induced hepatic insulin resistance by mammalian target of rapamycin through the STAT3-SOCS3 pathway. *Journal of Biological Chemistry*, **283**: 708-715.

Kim, E., Kim, M., Woo, D.H., Shin, Y., Shin, J., Chang, N., Oh, Y.T. *et al*. (2013). Phosphorylation of EZH2 activates STAT3 signaling via STAT3 methylation and promotes tumorigenicity of glioblastoma stem-like cells. *Cancer Cell*, **23**: 839-852.

Kim, M., Morales, L.D., Jang, I.S., Cho, Y.Y. and Kim, D.J. (2018). Protein tyrosine phosphatases as potential regulators of STAT3 signaling. *International Journal of Molecular Sciences*, **19**: 2708.

Kim, S.H., Park, Y.Y., Kim, S.W., Lee, J.S., Wang, D. and DuBois, R.N. (2011b). ANGPTL4 induction by prostaglandin E2 under hypoxic conditions promotes colorectal cancer progression. *Cancer Research*, **71**: 7010-7020.

Kim, S.J., Saeidi, S., Cho, N.C., Kim, S.H., Lee, H.B., Han, W., Noh, D.Y. *et al.* (2021). Interaction of Nrf2 with dimeric STAT3 induces IL-23 expression: Implications for breast cancer progression. *Cancer Letters*, **500**: 147-160.

Kim, D.H., Sarbassov, D.D., Ali, S.M., King, J.E., Latek, R.R., Erdjument-Bromage, H., Tempst, P. *et al.* (2002). mTOR interacts with raptor to form a nutrient-sensitive complex that signals to the cell growth machinery. *Cell*, **110**: 163-175.

Kim, E., Goraksha-Hicks, P., Li, L., Neufeld, T.P. and Guan, K.L (2008). Regulation of TORC1 by Rag GTPases in nutrient response. *Nature Cell Biology*, **10**: 935-945.

Kim, J., Kundu, M., Viollet, B. and Guan, K.L. (2011a). AMPK and mTOR regulate autophagy through direct phosphorylation of Ulk1. *Nature Cell Biology*, **13**: 132-141.

Kingswood, J.C., d'Augères, G.B., Belousova, E., Ferreira, J.C., Carter, T., Castellana, R., Cottin, V. *et al.* (2017). TuberOus SClerosis registry to increase disease Awareness (TOSCA)–baseline data on 2093 patients. *Orphanet Journal of Rare Diseases*, **12**: 2.

Kleinert, M., Parker, B.L., Fritzen, A.M., Knudsen, J.R., Jensen, T.E., Kjøbsted, R., Sylow, L. *et al.* (2017). Mammalian target of rapamycin complex 2 regulates muscle glucose uptake during exercise in mice. *The Journal of Physiology*, **595**: 4845-4855.

Kobayashi, Y., Oguro, A. and Imaoka, S. (2021). Feedback of hypoxia-inducible factor-1alpha (HIF-1alpha) transcriptional activity via redox factor-1 (Ref-1) induction by reactive oxygen species (ROS). *Free Radical Research*, **55**: 154-164.

Koivunen, P., Hirsilä, M., Remes, A.M., Hassinen, I.E., Kivirikko, K.I. and Myllyharju, J. (2007). Inhibition of hypoxia-inducible factor (HIF) hydroxylases by citric acid cycle intermediates: possible links between cell metabolism and stabilization of HIF. *Journal of Biological Chemistry*, **282**: 4524-4532.

Komatsu, M., Kurokawa, H., Waguri, S., Taguchi, K., Kobayashi, A., Ichimura, Y., Sou, Y.S. *et al*. (2010). The selective autophagy substrate p62 activates the stress responsive transcription factor Nrf2 through inactivation of Keap1. *Nature Cell Biology*, **12**: 213-223.

Kondoh, M., Ohga, N., Akiyama, K., Hida, Y., Maishi, N., Towfik, A.M., Inoue, N., Shindoh, M. and Hida, K. (2013). Hypoxia-induced reactive oxygen species cause chromosomal abnormalities in endothelial cells in the tumor microenvironment. *PloS One*, **8**: 80349.

Koong, A.C., Chen, E.Y. and Giaccia, A.J. (1994). Hypoxia causes the activation of nuclear factor κB through the phosphorylation of IκBα on tyrosine residues. *Cancer Research*, **54**: 1425-1430.

Koppula, P., Zhuang, L. and Gan, B. (2021). Cystine transporter SLC7A11/xCT in cancer: ferroptosis, nutrient dependency, and cancer therapy. *Protein & Cell*, **12**: 599-620.

Korge, P., Ping, P. and Weiss, J.N. (2008). Reactive oxygen species production in energized cardiac mitochondria during hypoxia/reoxygenation: modulation by nitric oxide. *Circulation Research*, **103**: 873-880.

Kotulska, K., Borkowska, J., Roszkowski, M., Mandera, M., Daszkiewicz, P., Drabik, K., Jurkiewicz, E. (2014). Surgical treatment of subependymal giant cell astrocytoma in tuberous sclerosis complex patients. *Pediatric Neurology*, **50**: 307-312.

Koukourakis, M.I., Giatromanolaki, A., Kakolyris, S., Sivridis, E., Georgoulias, V., Funtzilas, G., Hickson, I.D. *et al*. (2001). Nuclear expression of human apurinic/apyrimidinic endonuclease (HAP1/Ref-1) in head-and-neck cancer is associated with resistance to chemoradiotherapy and poor outcome. *International Journal of Radiation Oncology* Biology* Physics*, **50**: 27-36.

Kovacina, K.S., Park, G.Y., Bae, S.S., Guzzetta, A.W., Schaefer, E., Birnbaum, M.J. and Roth, R.A. (2003). Identification of a proline-rich Akt substrate as a 14-3-3 binding partner. *Journal of Biological Chemistry*, **278**: 10189-10194.

Kuang, F., Liu, J., Xie, Y., Tang, D. and Kang, R. (2021). MGST1 is a redox-sensitive repressor of ferroptosis in pancreatic cancer cells. *Cell Chemical Biology*, **28**: 765-775.

Kujawski, M., Kortylewski, M., Lee, H., Herrmann, A., Kay, H. and Yu, H. (2008). Stat3 mediates myeloid cell–dependent tumor angiogenesis in mice. *The Journal of Clinical Investigation*, **118**: 3367-3377.

Kurdi, M. and Booz, G.W. (2007). Evidence that IL-6-type cytokine signaling in cardiomyocytes is inhibited by oxidative stress: Parthenolide targets JAK1 activation by generating ROS. *Journal of Cellular Physiology*, **212**: 424-431.

Kuroki, M. and O'Flaherty, J.T. (1999). Extracellular signal-regulated protein kinase (ERK)-dependent and ERK-independent pathways target STAT3 on serine-727 in human neutrophils stimulated by chemotactic factors and cytokines. Biochemical Journal, 341: 691-696.

Kunz, J., Henriquez, R., Schneider, U., Deuter-Reinhard, M., Movva, N.R. and Hall, M.N. (1993). Target of rapamycin in yeast, TOR2, is an essential phosphatidylinositol kinase homolog required for G1 progression. *Cell*, **73**: 585-596.

Kuo, P.L., Chen, C.Y. and Hsu, Y.L. (2007). Isoobtusilactone A induces cell cycle arrest and apoptosis through reactive oxygen species/apoptosis signal-regulating kinase 1 signaling pathway in human breast cancer cells. *Cancer Research*, **67**: 7406-7420.

Kurian, A.W., Ward, K.C., Abrahamse, P., Bondarenko, I., Hamilton, A.S., Deapen, D., Morrow, M. *et al*. (2021). Time trends in receipt of germline genetic testing and results for women diagnosed with breast cancer or ovarian cancer, 2012-2019. *Journal of Clinical Oncology*, **39**: 1631.

Kwak, M.K., Itoh, K., Yamamoto, M., Sutter, T.R. and Kensler, T.W. (2001). Role of transcription factor Nrf2 in the induction of hepatic phase 2 and antioxidative enzymes in vivo

by the cancer chemoprotective agent, 3H-1, 2-dithiole-3-thione. *Molecular Medicine*, **7**: 135-145.

Kwak, M.K., Itoh, K., Yamamoto, M. and Kensler, T.W. (2002). Enhanced expression of the transcription factor Nrf2 by cancer chemopreventive agents: role of antioxidant response element-like sequences in the nrf2 promoter. *Molecular and Cellular Biology*, **22**: 2883-2892.

Kwiatkowski, D.J. (2003). Rhebbing up mTOR: new insights on TSC1 and TSC2, and the pathogenesis of tuberous sclerosis. *Cancer Biology & Therapy*, **2**: 471-476.

Kwiatkowski, D.J., Choueiri, T.K., Fay, A.P., Rini, B.I., Thorner, A.R., De Velasco, G., Tyburczy, M.E. *et al*. (2016). Mutations in TSC1, TSC2, and MTOR are associated with response to rapalogs in patients with metastatic renal cell carcinoma. *Clinical Cancer Research*, **22**: 2445-2452.

Kwon, T., Bak, Y., Park, Y.H., Jang, G.B., Nam, J.S., Yoo, J.E., Park, Y.N. *et al.* (2016). Peroxiredoxin II is essential for maintaining stemness by redox regulation in liver cancer cells. *Stem Cells*, **34**:1188-1197.

Lahiri, T., Brambilla, L., Andrade, J., Askenazi, M., Ueberheide, B. and Levy, D.E. (2021). Mitochondrial STAT3 regulates antioxidant gene expression through complex I-derived NAD in triple negative breast cancer. *Molecular Oncology*, **15**: 1432-1449.

Laird, A.D., Li, G., Moss, K.G., Blake, R.A., Broome, M.A., Cherrington, J.M. and Mendel, D.B. (2003). Src family kinase activity is required for signal tranducer and activator of transcription 3 and focal adhesion kinase phosphorylation and vascular endothelial growth factor signaling in vivo and for anchorage-dependent and-independent growth of human tumor cells. *Molecular Cancer Therapeutics*, **2**: 461-469.

Lam, H.C., Baglini, C.V., Lope, A.L., Parkhitko, A.A., Liu, H.J., Alesi, N., Malinowska, I.A. *et al.* (2017). p62/SQSTM1 cooperates with hyperactive mTORC1 to regulate glutathione production, maintain mitochondrial integrity, and promote tumorigenesis. *Cancer Research*, **77**: 3255-3267.

Lamalice, L., Le Boeuf, F. and Huot, J. (2007). Endothelial cell migration during angiogenesis. *Circulation Research*, **100**: 782-794.

Land, S.C. and Tee, A.R. (2007). Hypoxia-inducible factor 1α is regulated by the mammalian target of rapamycin (mTOR) via an mTOR signaling motif. *Journal of Biological Chemistry*, **282**: 20534-20543.

Lando, D., Peet, D.J., Whelan, D.A., Gorman, J.J. and Whitelaw, M.L. (2002). Asparagine hydroxylation of the HIF transactivation domain: a hypoxic switch. *Science*, **295**: 858-861.

Lang, R., Pauleau, A.L., Parganas, E., Takahashi, Y., Mages, J., Ihle, J.N., Rutschman, R. (2003). SOCS3 regulates the plasticity of gp130 signaling. *Nature Immunology*, **4**: 546-550.

Laplante, M. and Sabatini, D.M. (2013). Regulation of mTORC1 and its impact on gene expression at a glance. Journal of Cell Science, **126**: 1713-1719.

Lau, A., Tian, W., Whitman, S.A. and Zhang, D.D. (2013). The predicted molecular weight of Nrf2: it is what it is not. *Antioxidants & Redox Signaling*, **18**: 91-93.

Laughner, E., Taghavi, P., Chiles, K., Mahon, P.C. and Semenza, G.L. (2001). HER2 (neu) signaling increases the rate of hypoxia-inducible factor 1α (HIF-1α) synthesis: novel mechanism for HIF-1-mediated vascular endothelial growth factor expression. *Molecular and Cellular Biology*, **21**: 3995-4004.

Le Jan, S., Amy, C., Cazes, A., Monnot, C., Lamandé, N., Favier, J., Philippe, J. *et al.* (2003). Angiopoietin-like 4 is a proangiogenic factor produced during ischemia and in conventional renal cell carcinoma. *The American Journal of Pathology*, **162**: 1521-1528.

Lee, H., Chin, H., Kim, H., Jung, H. and Lee, D. (2020a) STAT3-mediated MLST8 gene expression regulates cap-dependent translation in cancer cells. *Molecular Oncology*, **14**: 1850-1867.

Lee, Y.H., Do, S.K., Lee, S.Y., Kang, H.G., Choi, J.E., Hong, M.J., Lee, J.H., *et al.* (2019). TSC2 genetic variant and prognosis in non-small cell lung cancer after curative surgery. *Thoracic Cancer*, **10**: 335-340.

Lee, J.K., Edderkaoui, M., Truong, P., Ohno, I., Jang, K.T., Berti, A., Pandol, S.J. *et al*. (2007). NADPH oxidase promotes pancreatic cancer cell survival via inhibiting JAK2 dephosphorylation by tyrosine phosphatases. *Gastroenterology*, **133**: 1637-1648.

Lee, M.Y., Joung, Y.H., Lim, E.J., Park, J.H., Ye, S.K., Park, T., Zhang, Z. *et al.* (2006). Phosphorylation and activation of STAT proteins by hypoxia in breast cancer cells. *The Breast*, **15**: 187-195.

Lee, D.H., Park, J.S., Lee, Y.S., Han, J., Lee, D.K., Kwon, S.W., Han, D.H. *et al.* (2020b). SQSTM1/p62 activates NFE2L2/NRF2 via ULK1-mediated autophagic KEAP1 degradation and protects mouse liver from lipotoxicity. *Autophagy*, **16**: 1949-1973.

Lee, P.S., Tsang, S.W., Moses, M.A., Trayes-Gibson, Z., Hsiao, L.L., Jensen, R., Squillace, R. *et al*. (2010). Rapamycin-insensitive up-regulation of MMP2 and other genes in tuberous sclerosis complex 2–deficient lymphangioleiomyomatosis-like cells. *American Journal of Respiratory Cell and Molecular Biology*, **42**: 227-234.

Lee, G., Won, H.S., Lee, Y.M., Choi, J.W., Oh, T.I., Jang, J.H., Choi, D.K. *et al.* (2016). Oxidative dimerization of PHD2 is responsible for its inactivation and contributes to metabolic reprogramming via HIF-1α activation. *Scientific Reports*, **6**: 1-12.

Leong, H., Mathur, P.S. and Greene, G.L. (2009). Green tea catechins inhibit angiogenesis through suppression of STAT3 activation. *Breast Cancer Research and Treatment*, **117**: 505-515.

Lesina, M., Kurkowski, M.U., Ludes, K., Rose-John, S., Treiber, M., Klöppel, G., Yoshimura, A. *et al.* (2011). Stat3/Socs3 activation by IL-6 transsignaling promotes progression of pancreatic intraepithelial neoplasia and development of pancreatic cancer. *Cancer Cell*, **19**: 456-469.

Lesma, E., Chiaramonte, E., Ancona, S., Orpianesi, E., Di Giulio, A.M. and Gorio, A. (2015). Anti-EGFR antibody reduces lung nodules by inhibition of EGFR-pathway in a model of lymphangioleiomyomatosis. *BioMed Research International*.

Li, X., Bao, C., Ma, Z., Xu, B., Ying, X., Liu, X. and Zhang, X. (2018). Perfluorooctanoic acid stimulates ovarian cancer cell migration, invasion via ERK/NF-κB/MMP-2/-9 pathway. *Toxicology Letters*, **294**: 44-50.

Li, L., Cheung, S.H., Evans, E.L. and Shaw, P.E. (2010). Modulation of Gene Expression and Tumor Cell Growth by Redox Modification of STAT3Redox Control of STAT3. *Cancer Research*, **70**: 8222-8232.

Li, J., Csibi, A., Yang, S., Hoffman, G.R., Li, C., Zhang, E., Yu, J.J. *et al.* (2015a). Synthetic lethality of combined glutaminase and Hsp90 inhibition in mTORC1-driven tumor cells. *Proceedings of the National Academy of Sciences*, **112**: 21-29.

Li, J., Lee, J.M. and Johnson, J.A. (2002). Microarray analysis reveals an antioxidant responsive element-driven gene set involved in conferring protection from an oxidative stress-induced apoptosis in IMR-32 cells. *Journal of Biological Chemistry*, **277**: 388-394.

Li, C., Lee, P.S., Sun, Y., Gu, X., Zhang, E., Guo, Y., Wu, C.L. *et al.* (2014). Estradiol and mTORC2 cooperate to enhance prostaglandin biosynthesis and tumorigenesis in TSC2-deficient LAM cells. *Journal of Experimental Medicine*, **211**: 15-28.

Li, Y., Liu, X., Zhou, T., Kelley, M.R., Edwards, P.A., Gao, H. and Qiao, X. (2014). Suppression of choroidal neovascularization through inhibition of APE1/Ref-1 redox activity. *Investigative Ophthalmology & Visual Science*, **55**: 4461-4469.

Li, N., Ragheb, K., Lawler, G., Sturgis, J., Rajwa, B., Melendez, J.A. and Robinson, J.P. (2003). Mitochondrial complex I inhibitor rotenone induces apoptosis through enhancing mitochondrial reactive oxygen species production. *Journal of Biological Chemistry*, **278**: 8516-8525.

Li, H., Rokavec, M., Jiang, L., Horst, D. and Hermeking, H. (2017). Antagonistic effects of p53 and HIF1A on microRNA-34a regulation of PPP1R11 and STAT3 and hypoxia-induced epithelial to mesenchymal transition in colorectal cancer cells. *Gastroenterology*, **153**: 505-520.

Li, Y., Wang, Y., Kim, E., Beemiller, P., Wang, C.Y., Swanson, J., You, M. *et al.* (2007). Bnip3 mediates the hypoxia-induced inhibition on mammalian target of rapamycin by interacting with Rheb. *Journal of Biological Chemistry*, **282**: 35803-35813.

Li, X., Yang, Z., Han, Z., Wen, Y., Ma, Z. and Wang, Y. (2018b). Niclosamide acts as a new inhibitor of vasculogenic mimicry in oral cancer through upregulation of miR-124 and downregulation of STAT3. *Oncology Reports*, **39**: 827-833.

Li, M., Yu, X., Li, W., Liu, T., Deng, G., Liu, W., Liu, H. *et al.* (2018a). Deguelin suppresses angiogenesis in human hepatocellular carcinoma by targeting HGF-c-Met pathway. *Oncotarget*, **9**: 152.

Li, J., Yuan, W., Jiang, S., Ye, W., Yang, H., Shapiro, I.M. and Risbud, M.V. (2015b). Prolyl-4-hydroxylase domain protein 2 controls NF-κB/p65 transactivation and enhances the catabolic effects of inflammatory cytokines on cells of the nucleus pulposus. *Journal of Biological Chemistry*, **290**: 7195-7207.

Li, T., Zhang, G., Wang, L., Li, S., Xu, X. and Gao, Y. (2020). Defects in mTORC1 Network and mTORC1-STAT3 Pathway Crosstalk Contributes to Non-inflammatory Hepatocellular Carcinoma. *Frontiers in Cell and Developmental Biology*, **8**: 225.

Li, M., Zhong, Z., Zhu, J., Xiang, D., Dai, N., Cao, X., Qing, Y. *et al.* (2010). Identification and characterization of mitochondrial targeting sequence of human apurinic/apyrimidinic endonuclease 1. *Journal of Biological Chemistry*, **285**: 14871-14881.

Liang, Z., Lei, F., Deng, J., Zhang, H., Wang, Y., Li, J., Shi, T., *et al.* (2022). Design, synthesis and bioactivity evaluation of novel evodiamine derivatives with excellent potency against gastric cancer. *European Journal of Medicinal Chemistry*, **228**: 113960.

Liang, S., Zhang, J., Yang, Z., Zhang, S., Cui, Z., Cui, J., Zhang, J. *et al*. (2017). Long-term outcomes of epilepsy surgery in tuberous sclerosis complex. *Journal of Neurology*, **264**: 1146-1154.

Libermann, T.A. and Baltimore, D. (1990). Activation of interleukin-6 gene expression through the NF-kappa B transcription factor. *Molecular and Cellular Biology*, **10**: 2327-2334.

Lim, C.P. and Cao, X. (1999). Serine phosphorylation and negative regulation of Stat3 by JNK. *Journal of Biological Chemistry*, **274**: 31055-31061.

Lim, C.P. and Cao, X. (2001). Regulation of Stat3 activation by MEK kinase 1. Journal of Biological Chemistry, 276: 21004-21011.

Lim, J.H., Lee, Y.M., Chun, Y.S., Chen, J., Kim, J.E. and Park, J.W. (2010). Sirtuin 1 modulates cellular responses to hypoxia by deacetylating hypoxia-inducible factor 1α. *Molecular Cell*, **38**: 864-878.

Lin, L., Hutzen, B., Zuo, M., Ball, S., Deangelis, S., Foust, E., Pandit, B. *et al.* (2010). Novel STAT3 Phosphorylation Inhibitors Exhibit Potent Growth-Suppressive Activity in Pancreatic and Breast Cancer CellsNovel Curcumin Analogues Target JAK2/STAT3. *Cancer research*, **70**: 2445-2454.

Lin, W., Wan, X., Sun, A., Zhou, M., Chen, X., Li, Y., Wang, Z., *et al.* (2021). RUNX1/EGFR pathway contributes to STAT3 activation and tumor growth caused by hyperactivated mTORC1. *Molecular Therapy-Oncolytics*, **23**: 387-401.

Liu, P., Begley, M., Michowski, W., Inuzuka, H., Ginzberg, M., Gao, D., Tsou, P. *et al.* (2014a). Cell-cycle-regulated activation of Akt kinase by phosphorylation at its carboxyl terminus. *Nature*, **508**: 541-545.

Liu, P., Gan, W., Inuzuka, H., Lazorchak, A.S., Gao, D., Arojo, O., Liu, D. *et al.* (2013). Sin1 phosphorylation impairs mTORC2 complex integrity and inhibits downstream Akt signalling to suppress tumorigenesis. *Nature Cell Biology*, **15**: 1340-1350.

Liu, P., Guo, J., Gan, W. and Wei, W. (2014c). Dual phosphorylation of Sin1 at T86 and T398 negatively regulates mTORC2 complex integrity and activity. *Protein & Cell*, **5**: 171-177.

Liu, L., McBride, K.M. and Reich, N.C. (2005). STAT3 nuclear import is independent of tyrosine phosphorylation and mediated by importin-α3. *Proceedings of the National Academy of Sciences*, **102**: 8150-8155.

Liu, M.Y., Poellinger, L. and Walker, C.L. (2003). Up-regulation of hypoxia-inducible factor 2α in renal cell carcinoma associated with loss of Tsc-2 tumor suppressor gene. *Cancer Research*, ***63***: 2675-2680.

Liu, Q. and Wang, K. (2019). The induction of ferroptosis by impairing STAT3/Nrf2/GPx4 signaling enhances the sensitivity of osteosarcoma cells to cisplatin. *Cell Biology International*, **43**: 1245-1256.

Liu, P., Wang, Z. and Wei, W. (2014b). Phosphorylation of Akt at the C-terminal tail triggers Akt activation. *Cell Cycle*, **13**: 2162-2164.

Locy, M.L., Rogers, L.K., Prigge, J.R., Schmidt, E.E., Arnér, E.S. and Tipple, T.E. (2012). Thioredoxin reductase inhibition elicits Nrf2-mediated responses in Clara cells: implications for oxidant-induced lung injury. *Antioxidants & Redox Signaling*, **17**: 1407-1416.

Löfstedt, T., Fredlund, E., Holmquist-Mengelbier, L., Pietras, A., Ovenberger, M., Poellinger, L. and Påhlman, S. (2007). Hypoxia inducible factor-2α in cancer. *Cell Cycle*, **6**: 919-926.

Logsdon, D.P., Grimard, M., Luo, M., Shahda, S., Jiang, Y., Tong, Y., Yu, Z. *et al.* (2016). Regulation of HIF1α under Hypoxia by APE1/Ref-1 Impacts CA9 Expression: Dual Targeting in Patient-Derived 3D Pancreatic Cancer ModelsDual-Targeting APE1/Ref-1 and CA9 in Hypoxic PDAC Cells. *Molecular Cancer Therapeutics*, **15**: 2722-2732.

Logsdon, D.P., Shah, F., Carta, F., Supuran, C.T., Kamocka, M., Jacobsen, M.H., Sandusky, G.E., Kelley, M.R. and Fishel, M.L., (2018). Blocking HIF signaling via novel inhibitors of CA9 and APE1/Ref-1 dramatically affects pancreatic cancer cell survival. Scientific reports, **8**: 1-14.

Long, X., Lin, Y., Ortiz-Vega, S., Yonezawa, K. and Avruch, J. (2005). Rheb binds and regulates the mTOR kinase. *Current Biology*, **15**: 702-713.

Lu, H., Dalgard, C.L., Mohyeldin, A., McFate, T., Tait, A.S. and Verma, A. (2005). Reversible inactivation of HIF-1 prolyl hydroxylases allows cell metabolism to control basal HIF-1. *Journal of Biological Chemistry*, **280**: 41928-41939.

Lu, J. and Holmgren, A. (2014). The thioredoxin antioxidant system. *Free Radical Biology and Medicine*, **66**: 75-87.

Lu, M., Wang, J., Ives, H.E. and Pearce, D. (2011). mSIN1 protein mediates SGK1 protein interaction with mTORC2 protein complex and is required for selective activation of the epithelial sodium channel. *Journal of Biological Chemistry*, **286**: 30647-30654.

Luo, M., Zhang, J., He, H., Su, D., Chen, Q., Gross, M.L., Kelley, M.R. *et al.* (2012). Characterization of the redox activity and disulfide bond formation in apurinic/apyrimidinic endonuclease. *Biochemistry*, **51**: 695-705.

Ma, Q. (2013). Role of nrf2 in oxidative stress and toxicity. *Annual Review of Pharmacology and Toxicology*, **53**, 401-426.

Ma, L., Chen, Z., Erdjument-Bromage, H., Tempst, P. and Pandolfi, P.P. (2005). Phosphorylation and functional inactivation of TSC2 by Erk: implications for tuberous sclerosisand cancer pathogenesis. *Cell*, **121**: 179-193.

Ma, J., Meng, Y., Kwiatkowski, D.J., Chen, X., Peng, H., Sun, Q., Zha, X. *et al.* (2010). Mammalian target of rapamycin regulates murine and human cell differentiation through STAT3/p63/Jagged/Notch cascade. *The Journal of Clinical Investigation*, **120**: 103-114.

Maemondo, M., Narumi, K., Saijo, Y., Usui, K., Tahara, M., Tazawa, R., Hagiwara, K. *et al.* (2002). Targeting angiogenesis and HGF function using an adenoviral vector expressing the HGF antagonist NK4 for cancer therapy. *Molecular Therapy*, **5**: 177-185.

Maes, H., Van Eygen, S., Krysko, D.V., Vandenabeele, P., Nys, K., Rillaerts, K., Garg, A.D *et al.* (2014). BNIP3 supports melanoma cell migration and vasculogenic mimicry by orchestrating the actin cytoskeleton. *Cell Death & Disease*, ***5***:1127-1127.

Mahimainathan, L., Ghosh-Choudhury, N., Venkatesan, B., Das, F., Mandal, C.C., Dey, N., Habib, S.L. *et al.* (2009). TSC2 deficiency increases PTEN via HIF1α. *Journal of Biological Chemistry*, **284**: 27790-27798.

Mahjabeen, I., Baig, R.M., Sabir, M. and Kayani, M.A. (2013). Genetic and expressional variations of APEX1 are associated with increased risk of head and neck cancer. *Mutagenesis*, **28**: 213-218.

Majmundar, A.J., Wong, W.J. and Simon, M.C. (2010). Hypoxia-inducible factors and the response to hypoxic stress. *Molecular Cell*, **40**: 294-309.

Malik, A.R., Liszewska, E., Skalecka, A., Urbanska, M., Iyer, A.M., Swiech, L.J., Perycz, M. *et al.* (2015). Tuberous sclerosis complex neuropathology requires glutamate-cysteine ligase. *Acta Neuropathologica Communications*, **3**: 1-13.

Magnuson, B., Ekim, B. and Fingar, D.C. (2012). Regulation and function of ribosomal protein S6 kinase (S6K) within mTOR signalling networks. *Biochemical Journal*, **441**: 1-21.

Mahimainathan, L., Ghosh-Choudhury, N., Venkatesan, B., Das, F., Mandal, C.C., Dey, N., Habib, S.L., *et al.* (2009). TSC2 deficiency increases PTEN via HIF1α. *Journal of Biological Chemistry*, **284**: 27790-27798.

Mak, B.C., Kenerson, H.L., Aicher, L.D., Barnes, E.A. and Yeung, R.S. (2005). Aberrant β-catenin signaling in tuberous sclerosis. *The American Journal of Pathology*, **167**: 107-116.

Maniotis, A.J., Folberg, R., Hess, A., Seftor, E.A., Gardner, L.M., Pe'er, J., Trent, J.M. *et al.* (1999). Vascular channel formation by human melanoma cells in vivo and in vitro: vasculogenic mimicry. *The American Journal of Pathology*, **155**: 739-752.

Mansfield, K.D., Guzy, R.D., Pan, Y., Young, R.M., Cash, T.P., Schumacker, P.T. and Simon, M.C. (2005). Mitochondrial dysfunction resulting from loss of cytochrome c impairs cellular oxygen sensing and hypoxic HIF-α activation. *Cell Metabolism*, **1**: 393-399.

Marimpietri, D., Brignole, C., Nico, B., Pastorino, F., Pezzolo, A., Piccardi, F., Cilli, M. *et al.* (2007). Combined therapeutic effects of vinblastine and rapamycin on human neuroblastoma growth, apoptosis, and angiogenesis. *Clinical Cancer Research*, **13**: 3977-3988.

Martin, K.R., Zhou, W., Bowman, M.J., Shih, J., Au, K.S., Dittenhafer-Reed, K.E., Sisson, K.A., *et al.* (2017). The genomic landscape of tuberous sclerosis complex. *Nature Communications*, **8**: 15816.

Martin, N., Zügge, K., Brandt, R., Friebel, D., Janssen, B. and Zimmerhackl, L.B. (2003). Discordant clinical manifestations in monozygotic twins with the identical mutation in the TSC2 gene. *Clinical Genetics*, **63**: 427-430.

Martina, J.A., Chen, Y., Gucek, M. and Puertollano, R. (2012). MTORC1 functions as a transcriptional regulator of autophagy by preventing nuclear transport of TFEB. *Autophagy*, **8**: 903-914.

Mascotti, K., McCullough, J. and Burger, S.R. (2000). HPC viability measurement: trypan blue versus acridine orange and propidium iodide. *Transfusion*, **40**: 693-696.

Masson, N., Willam, C., Maxwell, P.H., Pugh, C.W. and Ratcliffe, P.J. (2001). Independent function of two destruction domains in hypoxia-inducible factor-α chains activated by prolyl hydroxylation. *The EMBO Journal*, **20**: 5197-5206.

Masui, K., Tanaka, K., Ikegami, S., Villa, G.R., Yang, H., Yong, W.H., Cloughesy, T.F. *et al.* (2015). Glucose-dependent acetylation of Rictor promotes targeted cancer therapy resistance. *Proceedings of the National Academy of Sciences*, **112**: 9406-9411.

Matkar, S.S., Wrischnik, L.A. and Hellmann-Blumberg, U. (2008). Production of hydrogen peroxide and redox cycling can explain how sanguinarine and chelerythrine induce rapid apoptosis. *Archives of Biochemistry and Biophysics*, **477**: 43-52.

Maxwell, P.H., Wiesener, M.S., Chang, G.W., Clifford, S.C., Vaux, E.C., Cockman, M.E., Wykoff, C.C. *et al.* (1999). The tumour suppressor protein VHL targets hypoxia-inducible factors for oxygen-dependent proteolysis. *Nature*, **399**: 271-275.

Mazhab-Jafari, M.T., Marshall, C.B., Ishiyama, N., Ho, J., Di Palma, V., Stambolic, V. and Ikura, M. (2012). An autoinhibited noncanonical mechanism of GTP hydrolysis by Rheb maintains mTORC1 homeostasis. *Structure*, **20**: 1528-1539.

McCann, H.D., Johnson, C.E., Errington, R.J., Davies, D.M., Dunlop, E.A. and Tee, A.R. (2018). Energy stress-mediated cytotoxicity in tuberous sclerosis complex 2-deficient cells with nelfinavir and mefloquine treatment. *Cancers*, **10**: 375.

McDaniel, J.M., Varley, K.E., Gertz, J., Savic, D.S., Roberts, B.S., Bailey, S.K., Shevde, L.A., *et al.* (2017). Genomic regulation of invasion by STAT3 in triple negative breast cancer. *Oncotarget*, **8**: 8226.

McDougall, S.R., Anderson, A.R. and Chaplain, M.A. (2006). Mathematical modelling of dynamic adaptive tumour-induced angiogenesis: clinical implications and therapeutic targeting strategies. Journal of theoretical biology, **241**: 564-589.

McIlwain, D.W., Fishel, M.L., Boos, A., Kelley, M.R. and Jerde, T.J. (2018). APE1/Ref-1 redox-specific inhibition decreases survivin protein levels and induces cell cycle arrest in prostate cancer cells. *Oncotarget*, **9**: 10962.

Medvetz, D., Sun, Y., Li, C., Khabibullin, D., Balan, M., Parkhitko, A., Priolo, C., Asara, J.M., (2015). High-Throughput Drug Screen Identifies Chelerythrine as a Selective Inducer of Death in a TSC2-null SettingChelerythrine Induces Death in TSC2-null Cells. *Molecular Cancer Research*, **13**: 50-62.

Megeney, L.A., Perry, R.L., Lecouter, J.E. and Rudnicki, M.A. (1996). bFGF and LIF signaling activates STAT3 in proliferating myoblasts. *Developmental Genetics*, **19**: 139-145.

Menon, S. and Manning, B.D. (2008). Common corruption of the mTOR signaling network in human tumors. *Oncogene*, **27**: S43-S51.

Menon, S., Dibble, C.C., Talbott, G., Hoxhaj, G., Valvezan, A.J., Takahashi, H., Cantley, L.C. *et al.* (2014). Spatial control of the TSC complex integrates insulin and nutrient regulation of mTORC1 at the lysosome. *Cell*, **156**: 771-785.

Menon, D., Salloum, D., Bernfeld, E., Gorodetsky, E., Akselrod, A., Frias, M.A., Sudderth, J. *et al.* (2017). Lipid sensing by mTOR complexes via de novo synthesis of phosphatidic acid. *Journal of Biological Chemistry*, ***292***: 6303-6311.

Menrad, H., Werno, C., Schmid, T., Copanaki, E., Deller, T., Dehne, N. and Brüne, B. (2010). Roles of hypoxia-inducible factor-1α (HIF-1α) versus HIF-2α in the survival of hepatocellular tumor spheroids. *Hepatology*, **51**: 2183-2192.

Merry, T.L. and Ristow, M. (2016). Nuclear factor erythroid-derived 2-like 2 (NFE2L2, Nrf2) mediates exercise-induced mitochondrial biogenesis and the anti-oxidant response in mice. *The Journal of Physiology*, **594**: 5195-5207.

Meyuhas, O. (2000). Synthesis of the translational apparatus is regulated at the translational level. *European Journal of Biochemistry*, **267**: 6321-6330.

Minchinton, A.I. and Tannock, I.F. (2006). Drug penetration in solid tumours. *Nature Reviews Cancer*, **6**: 583-592.

Miricescu, D., Balan, D.G., Tulin, A., Stiru, O., Vacaroiu, I.A., Mihai, D.A., Popa, C.C. *et al.* (2021). PI3K/AKT/mTOR signalling pathway involvement in renal cell carcinoma pathogenesis*. Experimental and Therapeutic Medicine*, **21**: 1-7.

Mirzaei, S., Gholami, M.H., Mahabady, M.K., Nabavi, N., Zabolian, A., Banihashemi, S.M., Haddadi, A. *et al.* (2021). Pre-clinical investigation of STAT3 pathway in bladder cancer: paving the way for clinical translation. *Biomedicine & Pharmacotherapy*, **133**: 111077.

Mishra, S., Kumar, S., Choudhuri, K.S.R., Longkumer, I., Koyyada, P. and Kharsyiemiong, E.T., 2021. Structural exploration with AlphaFold2-generated STAT3α structure reveals selective elements in STAT3α-GRIM-19 interactions involved in negative regulation. *Scientific Reports*, **11**: 1-17.

Miyata, H., Ashizawa, T., Iizuka, A., Kondou, R., Nonomura, C., Sugino, T., Urakami, K., *et al.* (2017). Combination of a STAT3 inhibitor and an mTOR inhibitor against a temozolomide-resistant glioblastoma cell line. *Cancer Genomics & Proteomics*, **14**: 83-91.

Mohammed, F., Gorla, M., Bisoyi, V., Tammineni, P. and Sepuri, N.B.V. (2020). Rotenone-induced reactive oxygen species signal the recruitment of STAT3 to mitochondria. *FEBS letters*, **594**: 1403-1412.

Mohlin, S., Hamidian, A., von Stedingk, K., Bridges, E., Wigerup, C., Bexell, D. and Påhlman, S. (2015). PI3K–mTORC2 but not PI3K–mTORC1 Regulates Transcription of HIF2A/EPAS1 and Vascularization in Neuroblastoma. *Cancer Research*, **75**: 4617-4628.

Mole, D.R., Blancher, C., Copley, R.R., Pollard, P.J., Gleadle, J.M., Ragoussis, J. and Ratcliffe, P.J. (2009). Genome-wide association of hypoxia-inducible factor (HIF)-1α and HIF-2α DNA binding with expression profiling of hypoxia-inducible transcripts. *Journal of Biological Chemistry*, **284**: 16767-16775.

Moosavi, F., Giovannetti, E., Saso, L. and Firuzi, O., 2019. HGF/MET pathway aberrations as diagnostic, prognostic, and predictive biomarkers in human cancers. *Critical Reviews in Clinical Laboratory Sciences*, **56**: 533-566.

Morelli, A.P., Tortelli Jr, T.C., Mancini, M.C.S., Pavan, I.C.B., Silva, L.G.S., Severino, M.B., Granato, D.C. *et al.* (2021). STAT3 contributes to cisplatin resistance, modulating EMT markers, and the mTOR signaling in lung adenocarcinoma. *Neoplasia*, **23**: 1048-1058.

Morrison, P.J., Shepherd, C.H., Stewart, F.J. and Nevin, N.C. (1998). Prevalence of tuberous sclerosis in UK. *The Lancet*, **352**: 318-319.

Naing, A., Aghajanian, C., Raymond, E., Olmos, D., Schwartz, G., Oelmann, E., Grinsted, L., *et al.* (2012). Safety, tolerability, pharmacokinetics and pharmacodynamics of AZD8055 in advanced solid tumours and lymphoma. *British Journal of Cancer*, **107**: 1093-1099.

Narimatsu, M., Maeda, H., Itoh, S., Atsumi, T., Ohtani, T., Nishida, K., Itoh, M. (2001). Tissue-specific autoregulation of the stat3 gene and its role in interleukin-6-induced survival signals in T cells. *Molecular and cellular biology*, **21**: 6615-6625.

Nascimento, E.B., Snel, M., Guigas, B., van der Zon, G.C., Kriek, J., Maassen, J.A., Jazet, I.M., *et al.* (2010). Phosphorylation of PRAS40 on Thr246 by PKB/AKT facilitates efficient phosphorylation of Ser183 by mTORC1. *Cellular Signalling*, **22**: 961-967.

National Institute for Health and Care Excellence. (2023). Cannabidiol for treating seizures caused by tuberous sclerosis complex. [NICE Guideline TA873]. https://www.nice.org.uk/guidance/ta873

Naumov, G.N., Bender, E., Zurakowski, D., Kang, S.Y., Sampson, D., Flynn, E., Watnick, R.S., *et al.* (2006). A model of human tumor dormancy: an angiogenic switch from the nonangiogenic phenotype. *Journal of the National Cancer Institute*, **98**: 316-325.

Nguyen, N.H., Tran, G.B. and Nguyen, C.T. (2020). Anti-oxidative effects of superoxide dismutase 3 on inflammatory diseases. *Journal of Molecular Medicine*, **98**: 59-69.

Nguyen-Vu, P.A., Fackler, I., Rust, A., DeClue, J.E., Sander, C.A., Volkenandt, M., Flaig, M., *et al.* (2001). Loss of tuberin, the tuberous-sclerosis-complex-2 gene product is associated with angiogenesis. *Journal Of Cutaneous Pathology*, **28**: 470-475.

Nicholson, S.E., De Souza, D., Fabri, L.J., Corbin, J., Willson, T.A., Zhang, J.G., Silva, A. *et al.* (2000). Suppressor of cytokine signaling-3 preferentially binds to the SHP-2-binding site on the shared cytokine receptor subunit gp130. *Proceedings of the National Academy of Sciences*, **97**: 6493-6498.

Nishi, T., Shimizu, N., Hiramoto, M., Sato, I., Yamaguchi, Y., Hasegawa, M., Aizawa, S., *et al.* (2002). Spatial redox regulation of a critical cysteine residue of NF-κB in vivo. *Journal of Biological Chemistry*, **277**: 44548-44556.

Niso-Santano, M., González-Polo, R.A., Bravo-San Pedro, J.M., Gómez-Sánchez, R., Lastres-Becker, I., Ortiz-Ortiz, M.A., Soler, G. *et al.* (2010). Activation of apoptosis signal-regulating kinase 1 is a key factor in paraquat-induced cell death: modulation by the Nrf2/Trx axis. *Free Radical Biology and Medicine*, **48**: 1370-1381.

Niu, G., Briggs, J., Deng, J., Ma, Y., Lee, H., Kortylewski, M., Kujawski, M. *et al*. (2008). Signal transducer and activator of transcription 3 is required for hypoxia-inducible factor-1α RNA expression in both tumor cells and tumor-associated myeloid cells. *Molecular Cancer Research*, **6**: 1099-1105.

Nkansah, E., Shah, R., Collie, G.W., Parkinson, G.N., Palmer, J., Rahman, K.M., Bui, T.T., *et al.* (2013). Observation of unphosphorylated STAT3 core protein binding to target dsDNA by PEMSA and X-ray crystallography*. FEBS Letters*, **587**: 833-839.

Nobukuni, T., Joaquin, M., Roccio, M., Dann, S.G., Kim, S.Y., Gulati, P., Byfield, M.P. *et al.* (2005). Amino acids mediate mTOR/raptor signaling through activation of class 3 phosphatidylinositol 3OH-kinase. *Proceedings of the National Academy of Sciences*, **102**: 14238-14243.

Nojima, H., Tokunaga, C., Eguchi, S., Oshiro, N., Hidayat, S., Yoshino, K.I., Hara, K. *et al.* (2003). The mammalian target of rapamycin (mTOR) partner, raptor, binds the mTOR substrates p70 S6 kinase and 4E-BP1 through their TOR signaling (TOS) motif. *Journal of Biological Chemistry*, **278**: 15461-15464.

Noman, M.Z., Buart, S., Van Pelt, J., Richon, C., Hasmim, M., Leleu, N., Suchorska, W.M. *et al.* (2009). The cooperative induction of hypoxia-inducible factor-1α and STAT3 during hypoxia induced an impairment of tumor susceptibility to CTL-mediated cell lysis. *The Journal of Immunology*, **182**: 3510-3521.

Nordberg, J. and Arnér, E.S. (2001). Reactive oxygen species, antioxidants, and the mammalian thioredoxin system. *Free Radical Biology and Medicine*, **31**: 1287-1312.

Northrup, H., Krueger, D.A., Roberds, S., Smith, K., Sampson, J., Korf, B., Kwiatkowski, D.J. *et al.* (2013). Tuberous sclerosis complex diagnostic criteria update: recommendations of the 2012 International Tuberous Sclerosis Complex Consensus Conference. *Pediatric Neurology*, **49**: 243-254.

Oakley, F., Teoh, V., Ching–A–Sue, G., Bataller, R., Colmenero, J., Jonsson, J.R., Eliopoulos, A.G., (2009). Angiotensin II activates IκB kinase phosphorylation of RelA at Ser536 to promote myofibroblast survival and liver fibrosis. *Gastroenterology*, **136**: 2334-2344.

O'Callaghan, F.J., Shiell, A.W., Osborne, J.P. and Martyn, C.N. (1998). Prevalence of tuberous sclerosis estimated by capture-recapture analysis. *The Lancet*, **351**: 1490

Oeckinghaus, A. and Ghosh, S. (2009). The NF-κB family of transcription factors and its regulation. *Cold Spring Harbor Perspectives in Biology*, **1**: p.a000034.

Ohbayashi, N., Ikeda, O., Taira, N., Yamamoto, Y., Muromoto, R., Sekine, Y., Sugiyama, K., (2007). LIF-and IL-6-induced acetylation of STAT3 at Lys-685 through PI3K/Akt activation. *Biological and Pharmaceutical Bulletin*, **30**: 1860-1864.

Oh, M.K., Park, H.J., Kim, N.H., Park, S.J., Park, I.Y. and Kim, I.S. (2011). Hypoxia-inducible factor-1α enhances haptoglobin gene expression by improving binding of STAT3 to the promoter. *Journal of Biological Chemistry*, **286**: 8857-8865.

Ohh, M., Park, C.W., Ivan, M., Hoffman, M.A., Kim, T.Y., Huang, L.E., Pavletich, N. *et al.* (2000). Ubiquitination of hypoxia-inducible factor requires direct binding to the β-domain of the von Hippel–Lindau protein. *Nature Cell Biology*, **2**: 423-427.

Onda, H., Crino, P.B., Zhang, H., Murphey, R.D., Rastelli, L., Rothberg, B.E.G. and Kwiatkowski, D.J. (2002). Tsc2 null murine neuroepithelial cells are a model for human tuber giant cells, and show activation of an mTOR pathway. Molecular and Cellular Neuroscience, **21**: 561-574.

O'shea, J.J., Laurence, A. and McInnes, I.B. (2013). Back to the future: oral targeted therapy for RA and other autoimmune diseases. *Nature Reviews Rheumatology*, **9**: 173-182.

Oshiro, N., Takahashi, R., Yoshino, K.I., Tanimura, K., Nakashima, A., Eguchi, S., Miyamoto, T. *et al.* (2007). The proline-rich Akt substrate of 40 kDa (PRAS40) is a physiological substrate of mammalian target of rapamycin complex 1. *Journal of Biological Chemistry*, **282**: 20329-20339.

Pagé, E.L., Robitaille, G.A., Pouysségur, J. and Richard, D.E. (2002). Induction of hypoxia-inducible factor-1α by transcriptional and translational mechanisms. *Journal of Biological Chemistry*, **277**: 48403-48409.

Pal, R., Bondar, V.V., Adamski, C.J., Rodney, G.G. and Sardiello, M. (2017). Inhibition of ERK1/2 restores GSK3β activity and protein synthesis levels in a model of tuberous sclerosis. *Scientific Reports*, **7**: 4174.

Paltoglou, S. and Roberts, B.J. (2007). HIF-1α and EPAS ubiquitination mediated by the VHL tumour suppressor involves flexibility in the ubiquitination mechanism, similar to other RING E3 ligases. *Oncogene*, **26**: 604-609.

Pan, Y.R., Chen, C.C., Chan, Y.T., Wang, H.J., Chien, F.T., Chen, Y.L., Liu, J.L. *et al.* (2018). STAT3-coordinated migration facilitates the dissemination of diffuse large B-cell lymphomas. *Nature Communications*, **9**: 1-16.

Pan, Y., Mansfield, K.D., Bertozzi, C.C., Rudenko, V., Chan, D.A., Giaccia, A.J. and Simon, M.C. (2007). Multiple factors affecting cellular redox status and energy metabolism modulate hypoxia-inducible factor prolyl hydroxylase activity in vivo and in vitro. *Molecular and Cellular Biology*, **27**: 912-925.

Pang, X., Yi, Z., Zhang, J., Lu, B., Sung, B., Qu, W., Aggarwal, B.B. *et al.* (2010). Celastrol Suppresses Angiogenesis-Mediated Tumor Growth through Inhibition of AKT/Mammalian Target of Rapamycin PathwayCelastrol Inhibits Tumor Angiogenesis. *Cancer Research*, **70**: 1951-1959.

Papakonstantinou, E., Dionyssopoulos, A., Aletras, A.J., Pesintzaki, C., Minas, A. and Karakiulakis, G. (2004). Expression of matrix metalloproteinases and their endogenous tissue inhibitors in skin lesions from patients with tuberous sclerosis. *Journal of the American Academy of Dermatology*, **51**: 526-533.

Parker, W.E., Orlova, K.A., Heuer, G.G., Baybis, M., Aronica, E., Frost, M., Wong, M. (2011). Enhanced epidermal growth factor, hepatocyte growth factor, and vascular endothelial growth factor expression in tuberous sclerosis complex. *The American Journal of Pathology*, **178**: 296-305.

Parkhitko, A., Myachina, F., Morrison, T.A., Hindi, K.M., Auricchio, N., Karbowniczek, M., Wu, J.J. *et al*. (2011). Tumorigenesis in tuberous sclerosis complex is autophagy and p62/sequestosome 1 (SQSTM1)-dependent. *Proceedings of the National Academy of Sciences*, **108**: 12455-12460.

Parthasarathy, S., Mahalingam, R., Melchiorre, J., Harowitz, J. and Devinsky, O. (2021). Mortality in tuberous sclerosis complex. *Epilepsy & Behavior*, **121**: 108032.

Patel, P.H., Thapar, N., Guo, L., Martinez, M., Maris, J., Gau, C.L., Lengyel, J.A. *et al.* (2003). Drosophila Rheb GTPase is required for cell cycle progression and cell growth. *Journal of Cell Science*, **116**: 3601-3610.

Patterson, A.D., Carlson, B.A., Li, F., Bonzo, J.A., Yoo, M.H., Krausz, K.W., Conrad, M., (2013). Disruption of thioredoxin reductase 1 protects mice from acute acetaminophen-

induced hepatotoxicity through enhanced NRF2 activity. *Chemical Research In Toxicology*, **26**: 1088-1096.

Pawlus, M.R., Wang, L. and Hu, C.J. (2014). STAT3 and HIF1α cooperatively activate HIF1 target genes in MDA-MB-231 and RCC4 cells. *Oncogene*, **33**: 1670-1679.

Peña-Llopis, S. and Brugarolas, J. (2013). Simultaneous isolation of high-quality DNA, RNA, miRNA and proteins from tissues for genomic applications. *Nature Protocols*, **8**: 2240-2255.

Peron, A., Au, K.S. and Northrup, H. (2018a). September. Genetics, genomics, and genotype–phenotype correlations of TSC: Insights for clinical practice. *In American Journal of Medical Genetics Part C: Seminars in Medical Genetics*, **178**: 281–290.

Peron, A., Vignoli, A., La Briola, F., Morenghi, E., Tansini, L., Alfano, R.M., Bulfamante, G., Terraneo, S., Ghelma, F., Banderali, G. and Viskochil, D.H. (2018b). Deep phenotyping of patients with tuberous sclerosis complex and no mutation identified in TSC1 and TSC2. *European Journal of Medical Genetics*, **61**: 403-410.

Peterson, T.R., Laplante, M., Thoreen, C.C., Sancak, Y., Kang, S.A., Kuehl, W.M., Gray, N.S. *et al.* (2009). DEPTOR is an mTOR inhibitor frequently overexpressed in multiple myeloma cells and required for their survival. *Cell*, **137**: 873-886.

Pfaffl, M.W. (2001). A new mathematical model for relative quantification in real-time RT–PCR. *Nucleic Acids Research*, **29**: e45-e45.
Pierconti, F., Martini, M., Pinto, F., Cenci, T., Capodimonti, S., Calarco, A., Bassi, P.F. *et al.* (2011). Epigenetic silencing of SOCS3 identifies a subset of prostate cancer with an aggressive behavior. *The Prostate*, **71**: 318-325.

Pines, A., Bivi, N., Romanello, M., Damante, G., Kelley, M.R., Adamson, E.D., D'Andrea, P. *et al.* (2005). Cross-regulation between Egr-1 and APE/Ref-1 during early response to oxidative stress in the human osteoblastic HOBIT cell line: evidence for an autoregulatory loop. *Free Radical Research*, **39**: 269-281.

Pinno, J., Bongartz, H., Klepsch, O., Wundrack, N., Poli, V., Schaper, F. and Dittrich, A. (2016). Interleukin-6 influences stress-signalling by reducing the expression of the mTOR-inhibitor REDD1 in a STAT3-dependent manner. *Cellular Signalling*, **28**: 907-916.

Polivka Jr, J. and Janku, F. (2014). Molecular targets for cancer therapy in the PI3K/AKT/mTOR pathway. *Pharmacology & Therapeutics*, **142**: 164-175.

Powles, T., Wheater, M., Din, O., Geldart, T., Boleti, E., Stockdale, A., Sundar, S., *et al.* (2016). A randomised phase 2 study of AZD2014 versus everolimus in patients with VEGF-refractory metastatic clear cell renal cancer. *European Urology*, **69**: 450-456.

Puglisi, F., Aprile, G., Minisini, A.M., Barbone, F., Cataldi, P., Tell, G., Kelley, M.R. *et al.* (2001). Prognostic significance of Ape1/ref-1 subcellular localization in non-small cell lung carcinomas. *Anticancer Research*, **21**: 4041-4049.

Qin, J., Clore, G.M., Kennedy, W.P., Kuszewski, J. and Gronenborn, A.M. (1996). The solution structure of human thioredoxin complexed with its target from Ref-1 reveals peptide chain reversal. *Structure*, **4**: 613-620.

Qin, H.R., Kim, H.J., Kim, J.Y., Hurt, E.M., Klarmann, G.J., Kawasaki, B.T., Duhagon Serrat, M.A. *et al.* (2008). Activation of signal transducer and activator of transcription 3 through a phosphomimetic serine 727 promotes prostate tumorigenesis independent of tyrosine 705 phosphorylation. *Cancer Research*, **68**: 7736-7741.

Rad, E., Dodd, K., Thomas, L., Upadhyaya, M. and Tee, A. (2015). STAT3 and HIF1α Signaling Drives Oncogenic Cellular Phenotypes in Malignant Peripheral Nerve Sheath

TumorsSTAT3 and HIF1α Drive Malignancy in MPNSTs. *Molecular Cancer Research*, **13**: 1149-1160.

Ramana, C.V., Boldogh, I., Izumi, T. and Mitra, S. (1998). Activation of apurinic/apyrimidinic endonuclease in human cells by reactive oxygen species and its correlation with their adaptive response to genotoxicity of free radicals. *Proceedings of the National Academy of Sci*ences, **95**: 5061-5066.

Raught, B., Peiretti, F., Gingras, A.C., Livingstone, M., Shahbazian, D., Mayeur, G.L., Polakiewicz, R.D. *et al.* (2004). Phosphorylation of eucaryotic translation initiation factor 4B Ser422 is modulated by S6 kinases. *The EMBO Journal*, **23**: 1761-1769.

Ray, S., Boldogh, I. and Brasier, A.R. (2005). STAT3 NH2-terminal acetylation is activated by the hepatic acute-phase response and required for IL-6 induction of angiotensinogen. *Gastroenterology*, **129**: 1616-1632.

Raz, R., Durbin, J.E. and Levy, D.E. (1994). Acute phase response factor and additional members of the interferon-stimulated gene factor 3 family integrate diverse signals from cytokines, interferons, and growth factors. *Journal of Biological Chemistry*, **269**: 24391-24395.

Redell, M.S., Ruiz, M.J., Alonzo, T.A., Gerbing, R.B. and Tweardy, D.J. (2011). Stat3 signaling in acute myeloid leukemia: ligand-dependent and-independent activation and induction of apoptosis by a novel small-molecule Stat3 inhibitor. *Blood, The Journal of the American Society of Hematology*, **117**: 5701-5709.

Richter, J. D. and Sonenberg, N. (2005). Regulation of cap-dependent translation by eIF4E inhibitory proteins. *Nature*, **433**, 477-480.

Riffle, S. and Hegde, R.S. (2017). Modeling tumor cell adaptations to hypoxia in multicellular tumor spheroids. *Journal of Experimental & Clinical Cancer Research*, **36**: 1-10.

Rius, J., Guma, M., Schachtrup, C., Akassoglou, K., Zinkernagel, A.S., Nizet, V., Johnson, R.S. *et al.* (2008). NF-κB links innate immunity to the hypoxic response through transcriptional regulation of HIF-1α. *Nature*, **453**: 807-811.

Robinson, P., Hamana, L., Beretta, L., Kasembeli, M., Bharadwaj, U., Chun, Y.S., Wang, Y., *et al.* (2022). Abstract IA004: Targeting STAT3 with TTI-101, an oral small molecule, to prevent colorectal and hepatocellular cancer. *Cancer Prevention Research*, **1**: IA004-IA004.

Robinson, N.B., Krieger, K., Khan, F.M., Huffman, W., Chang, M., Naik, A., Yongle, R., *et al.* (2019b). The current state of animal models in research: A review. *International Journal of Surgery*, **72**: 9-13

Robinson, R.L., Sharma, A., Bai, S., Heneidi, S., Lee, T.J., Kodeboyina, S.K., Patel, N. *et al*. (2019a). Comparative STAT3-regulated gene expression profile in renal cell carcinoma subtypes. *Frontiers In Oncology*, **9**: 72.

Roca Suarez, A.A., Van Renne, N., Baumert, T.F. and Lupberger, J. (2018). Viral manipulation of STAT3: Evade, exploit, and injure. *PLoS Pathogens*, **14**: e1006839.

Roccio, M., Bos, J.L. and Zwartkruis, F.J.T. (2006). Regulation of the small GTPase Rheb by amino acids. *Oncogene*, **25**: 657

Rodrigues, B.R., Queiroz-Hazarbassanov, N., Lopes, M.H., Bleggi-Torres, L.F., Suzuki, S., Cunha, I.W., Sanematsu, P. *et al.* (2016). Nuclear unphosphorylated STAT3 correlates with a worse prognosis in human glioblastoma. *Pathology-Research and Practice*, **212**: 517-523.

Rogers Jr, G.W., Komar, A.A. and Merrick, W.C. (2002). eIF4A: the godfather of the DEAD box helicases. Nucleic Acid Research and Molecular Biology, **72**: 307–331

Rok, P., Kasprzyk-Obara, J., Domańska-Pakieła, D. and Jóźwiak, S. (2005). Clinical symptoms of tuberous sclerosis complex in patients with an identical TSC2 mutation. *Medical Science Monitor*, **11**: CR230-CR234.

Rose-John, S. (2012). IL-6 trans-signaling via the soluble IL-6 receptor: importance for the pro-inflammatory activities of IL-6. *International journal of biological sciences*, **8**: 1237.

Rosset, C., Vairo, F., Bandeira, I.C., Correia, R.L., De Goes, F.V., Da Silva, R.T.B., Bueno, L.S.M. *et al.* (2017). Molecular analysis of TSC1 and TSC2 genes and phenotypic correlations in Brazilian families with tuberous sclerosis. *PloS One*, **12**: e0185713

Roux, P.P., Ballif, B.A., Anjum, R., Gygi, S.P. and Blenis, J. (2004). Tumor-promoting phorbol esters and activated Ras inactivate the tuberous sclerosis tumor suppressor complex via p90 ribosomal S6 kinase. *Proceedings of the National Academy of Sciences*, **101**: 13489-13494.

Rozen, S. and Skaletsky, H. (2000). Primer3 on the WWW for general users and for biologist programmers. Methods Mol Biol., **132**: 365–86.

Ruppe, V., Dilsiz, P., Reiss, C.S., Carlson, C., Devinsky, O., Zagzag, D., Weiner, H.L. *et al.* (2014). Developmental brain abnormalities in tuberous sclerosis complex: a comparative tissue analysis of cortical tubers and perituberal cortex. *Epilepsia*, **55**: 539-550.

Ryan, M.J., Johnson, G., Kirk, J., Fuerstenberg, S.M., Zager, R.A. and Torok-Storb, B. (1994). HK-2: an immortalized proximal tubule epithelial cell line from normal adult human kidney. *Kidney International*, **45**: 48-57.

Sabatini, D.M., Erdjument-Bromage, H., Lui, M., Tempst, P. and Snyder, S.H. (1994). RAFT1: a mammalian protein that binds to FKBP12 in a rapamycin-dependent fashion and is homologous to yeast TORs. *Cell*, **78**: 35-43.

Sabers, C.J., Martin, M.M., Brunn, G.J., Williams, J.M., Dumont, F.J., Wiederrecht, G. and Abraham, R.T. (1995). Isolation of a protein target of the FKBP12-rapamycin complex in mammalian cells. *Journal of Biological Chemistry*, **270**: 815-822.

Saito, K., Araki, Y., Kontani, K., Nishina, H. and Katada, T. (2005). Novel role of the small GTPase Rheb: its implication in endocytic pathway independent of the activation of mammalian target of rapamycin. *Journal of Biochemistry*, **137**: 423-430.

Sak, S.C., Harnden, P., Johnston, C.F., Paul, A.B. and Kiltie, A.E. (2005). APE1 and XRCC1 protein expression levels predict cancer-specific survival following radical radiotherapy in bladder cancer. *Clinical Cancer Research*, **11**: 6205-6211.

Sakaguchi, M., Oka, M., Iwasaki, T., Fukami, Y. and Nishigori, C. (2012). Role and regulation of STAT3 phosphorylation at Ser727 in melanocytes and melanoma cells. Journal of *Investigative Dermatolog*y, **132**: 1877-1885.

Salceda, S. and Caro, J. (1997). Hypoxia-inducible factor 1α (HIF-1α) protein is rapidly degraded by the ubiquitin-proteasome system under normoxic conditions: its stabilization by hypoxia depends on redox-induced changes. *Journal of Biological Chemistry*, **272**: 22642-22647.

Saleiro, D. and Platanias, L.C. (2015). Intersection of mTOR and STAT signaling in immunity. *Trends in Immunology*, **36**: 21-29

Sancak, O., Nellist, M., Goedbloed, M., Elfferich, P., Wouters, C., Maat-Kievit, A., Zonnenberg, B. et al. (2005). Mutational analysis of the TSC1 and TSC2 genes in a diagnostic setting: genotype–phenotype correlations and comparison of diagnostic DNA techniques in tuberous sclerosis complex. *European Journal of Human Genetics*, **13**: 731-741.

Sancak, Y., Thoreen, C.C., Peterson, T.R., Lindquist, R.A., Kang, S.A., Spooner, E., Carr, S.A. *et al.* (2007). PRAS40 is an insulin-regulated inhibitor of the mTORC1 protein kinase. *Molecular Cell*, **25**: 903-915.

Sancak, Y., Peterson, T.R., Shaul, Y.D., Lindquist, R.A., Thoreen, C.C., Bar-Peled, L. and Sabatini, D.M. (2008). The Rag GTPases bind raptor and mediate amino acid signaling to mTORC1. *Science*, **320**: 1496-1501.

Sanchez-Correa, B., Bergua, J.M., Campos, C., Gayoso, I., Arcos, M.J., Bañas, H., Morgado, S. *et al.* (2013). Cytokine profiles in acute myeloid leukemia patients at diagnosis: survival is inversely correlated with IL-6 and directly correlated with IL-10 levels. *Cytokine*, **61**: 885-891.

Sarbassov, D.D., Ali, S.M., Sengupta, S., Sheen, J.H., Hsu, P.P., Bagley, A.F., Markhard, A.L. and Sabatini, D.M. (2006). Prolonged rapamycin treatment inhibits mTORC2 assembly and Akt/PKB. *Molecular Cell*, **22**: 159-168.

Sarbassov, D.D., Ali, S.M., Kim, D.H., Guertin, D.A., Latek, R.R., Erdjument-Bromage, H., Tempst, P. *et al.* (2004). Rictor, a novel binding partner of mTOR, defines a rapamycin-insensitive and raptor-independent pathway that regulates the cytoskeleton. *Current Biology*, **14**: 1296-1302.

Sarraf, M., Masoumi, A., Castro-Silva, F.J., Myers, J.B., Wilson, S.S. and Schrier, R.W. (2009). A case of tuberous sclerosis complex that progressed to end-stage renal disease. *Nature Reviews Nephrology*, **5**: 172-176.

Sasaki, A., Yasukawa, H., Suzuki, A., Kamizono, S., Syoda, T., Kinjyo, I., Sasaki, M. *et al.* (1999). Cytokine-inducible SH2 protein-3 (CIS3/SOCS3) inhibits Janus tyrosine kinase by binding through the N-terminal kinase inhibitory region as well as SH2 domain. *Genes to Cells*, **4**: 339-351.

Sato, T., Nakashima, A., Guo, L. and Tamanoi, F. (2009). Specific activation of mTORC1 by Rheb G-protein in vitro involves enhanced recruitment of its substrate protein. *Journal of Biological Chemistry*, **284**: 12783-12791.

Satoh, H., Moriguchi, T., Takai, J., Ebina, M. and Yamamoto, M. (2013). Nrf2 Prevents Initiation but Accelerates Progression through the Kras Signaling Pathway during Lung CarcinogenesisNrf2 in Kras-Mutant Lung Cancer. *Cancer Research*, **73**: 4158-4168.

Saxton, R.A. and Sabatini, D.M. (2017). mTOR signaling in growth, metabolism, and disease. Cell, **168**: 960-976.

Schaefer, T.S., Sanders, L.K. and Nathans, D. (1995). Cooperative transcriptional activity of Jun and Stat3 beta, a short form of Stat3. *Proceedings of the National Academy of Sciences*, **92**: 9097-9101.

Schuringa, J.J., Schepers, H., Vellenga, E. and Kruijer, W. (2001). Ser727-dependent transcriptional activation by association of p300 with STAT3 upon IL-6 stimulation. *FEBS Letters*, **495**: 71-76.

Schuringa, J.J., Wierenga, A.T., Kruijer, W. and Vellenga, E. (2000). Constitutive Stat3, Tyr705, and Ser727 phosphorylation in acute myeloid leukemia cells caused by the autocrine secretion of interleukin-6. Blood, *The Journal of the American Society of Hematology,* **95**: 3765-3770.

Sekiguchi, T., Hirose, E., Nakashima, N., Ii, M. and Nishimoto, T. (2001). Novel G proteins, Rag C and Rag D, interact with GTP-binding proteins, Rag A and Rag B. *Journal of Biological Chemistry*, **276**: 7246-7257.

Selvendiran, K., Bratasz, A., Kuppusamy, M.L., Tazi, M.F., Rivera, B.K. and Kuppusamy, P. (2009). Hypoxia induces chemoresistance in ovarian cancer cells by activation of signal transducer and activator of transcription 3. *International Journal of Cancer*, **125**: 2198-2204.

Semenza, G.L. (2000). HIF-1 and human disease: one highly involved factor. *Genes & Development*, **14**: 1983-1991.

Semenza, G.L. (2012). Hypoxia-inducible factors: mediators of cancer progression and targets for cancer therapy. Trends in Pharmacological Sciences, **33**: 207-214.

Semenza, G.L. and Wang, G.L. (1992). A nuclear factor induced by hypoxia via de novo protein synthesis binds to the human erythropoietin gene enhancer at a site required for transcriptional activation. *Molecular and Cellular Biology*, **12**: 5447-5454.

Serra, I., Scheldeman, C., Bazelot, M., Whalley, B.J., Dallas, M.L., De Witte, P.A. and Williams, C.M. (2019). Cannabidiol modulates phosphorylated rpS6 signalling in a zebrafish model of Tuberous Sclerosis Complex. *Behavioural Brain Research*, **363**: 135-144.

Shah, F., Logsdon, D., Messmann, R.A., Fehrenbacher, J.C., Fishel, M.L. and Kelley, M.R. (2017). Exploiting the Ref-1-APE1 node in cancer signaling and other diseases: from bench to clinic. *NPJ Precision Oncology*, **1**: 19.

Shah, O.J., Wang, Z. and Hunter, T. (2004). Inappropriate activation of the TSC/Rheb/mTOR/S6K cassette induces IRS1/2 depletion, insulin resistance, and cell survival deficiencies. *Current Biology*, **14**: 1650-1656.

Shahbazian, D., Roux, P.P., Mieulet, V., Cohen, M.S., Raught, B., Taunton, J., Hershey, J.W. (2006). The mTOR/PI3K and MAPK pathways converge on eIF4B to control its phosphorylation and activity. *The EMBO Journal*, **25**: 2781-2791.

Shahda, S., Lakhani, N.J., O'Neil, B., Rasco, D.W., Wan, J., Mosley, A.L., Liu, H. *et al.* (2019). A phase I study of the APE1 protein inhibitor APX3330 in patients with advanced solid tumors. *Journal of Clinical Oncology*, 37: 3097-3097.

Shepherd, C., Beard, M., Gomez, M.R., Kurland, L.T., and Whisnant, J.P. (1991a). Tuberous sclerosis complex in Olmsted County, Minnesota 1950–1989. *Archives of Neurology*, **48**: 400–402.

Shepherd, C.W., Gomez, M.R., Lie, J.T. and Crowson, C.S. (1991b). Causes of death in patients with tuberous sclerosis. *Mayo Clinic Proceedings*, **66**: 792-796.

Shen, Y., Schlessinger, K., Zhu, X., Meffre, E., Quimby, F., Levy, D.E. and Darnell Jr, J.E., (2004). Essential role of STAT3 in postnatal survival and growth revealed by mice lacking STAT3 serine 727 phosphorylation. *Molecular and Cellular Biology*, **24**: 407-419.

Shi, Y., Hsu, J.H., Hu, L., Gera, J. and Lichtenstein, A. (2002). Signal pathways involved in activation of p70S6K and phosphorylation of 4E-BP1 following exposure of multiple myeloma tumor cells to interleukin-6. *Journal of Biological Chemistry*, **277**: 15712-15720.

Shi, X., Wang, M., Zhang, Y., Guo, X., Liu, M., Zhou, Z., Zhao, Y. *et al.* (2022). Hypoxia activated HGF expression in pancreatic stellate cells confers resistance of pancreatic cancer cells to EGFR inhibition*. EBioMedicine*, **86**: 104352.

Shin, H.M., Kim, M.H., Kim, B.H., Jung, S.H., Kim, Y.S., Park, H.J., Hong, J.T. (2004). Inhibitory action of novel aromatic diamine compound on lipopolysaccharide-induced nuclear translocation of NF-κB without affecting IκB degradation. *FEBS Letters*, **571**: 50-54.

Shin, J., Lee, H.J., Jung, D.B., Jung, J.H., Lee, H.J., Lee, E.O., Lee, S.G. *et al.* (2011). Suppression of STAT3 and HIF-1 alpha mediates anti-angiogenic activity of betulinic acid in hypoxic PC-3 prostate cancer cells. *PloS One*, 6: p.e21492.

Shpilka, T. and Haynes, C.M. (2018). The mitochondrial UPR: mechanisms, physiological functions and implications in ageing. Nature reviews *Molecular Cell Biology*, **19**: 109-120.

Shuai, K., Horvath, C.M., Huang, L.H.T., Qureshi, S.A., Cowburn, D. and Darnell Jr, J.E., (1994). Interferon activation of the transcription factor Stat91 involves dimerization through SH2-phosphotyrosyl peptide interactions. *Cell*, **76**: 821-828.

Shu, H.F., Zhang, C.Q., Yin, Q., An, N., Liu, S.Y. and Yang, H. (2010). Expression of the interleukin 6 system in cortical lesions from patients with tuberous sclerosis complex and focal cortical dysplasia type IIb. Journal of Neuropathology & Experimental Neurology, **69**: 838-849.

Shweiki, D., Neeman, M., Itin, A. and Keshet, E. (1995). Induction of vascular endothelial growth factor expression by hypoxia and by glucose deficiency in multicell spheroids: implications for tumor angiogenesis. *Proceedings of the National Academy of Sciences*, **92**: 768-772.

Silvestro, S., Mammana, S., Cavalli, E., Bramanti, P. and Mazzon, E. (2019). Use of cannabidiol in the treatment of epilepsy: efficacy and security in clinical trials. *Molecules*, **24**: 1459.

Simon, A.R., Rai, U., Fanburg, B.L. and Cochran, B.H. (1998). Activation of the JAK-STAT pathway by reactive oxygen species. *American Journal of Physiology-Cell Physiology*, **275**: C1640-C1652.

Singh, A., Boldin-Adamsky, S., Thimmulappa, R.K., Rath, S.K., Ashush, H., Coulter, J., Blackford, A. *et al.* (2008). RNAi-mediated silencing of nuclear factor erythroid-2–related factor 2 gene expression in non–small cell lung cancer inhibits tumor growth and increases efficacy of chemotherapy. *Cancer Research*, **68**: 7975-7984.

Singh, A., Venkannagari, S., Oh, K.H., Zhang, Y.Q., Rohde, J.M., Liu, L., Nimmagadda, S. *et al*. (2016). Small molecule inhibitor of NRF2 selectively intervenes therapeutic resistance in KEAP1-deficient NSCLC tumors. *ACS Chemical Biology*, **11**: 3214-3225.

Slemc, L. and Kunej, T. (2016). Transcription factor HIF1A: downstream targets, associated pathways, polymorphic hypoxia response element (HRE) sites, and initiative for standardization of reporting in scientific literature. *Tumor Biology*, **37**: 14851-14861.

Snyder, M., Huang, X.Y. and Zhang, J.J. (2008). Identification of novel direct Stat3 target genes for control of growth and differentiation. *Journal of Biological Chemistry*, **283**: 3791-3798.

Sobotta, M.C., Liou, W., Stöcker, S., Talwar, D., Oehler, M., Ruppert, T., Scharf, A.N. *et al.* (2015). Peroxiredoxin-2 and STAT3 form a redox relay for H2O2 signaling. *Nature Chemical Biology*, **11**: 64-70.

Soleymani Abyaneh, H., Gupta, N., Radziwon-Balicka, A., Jurasz, P., Seubert, J., Lai, R. and Lavasanifar, A. (2017). STAT3 but not HIF-1α is important in mediating Hypoxia-Induced chemoresistance in MDA-MB-231, a triple negative breast cancer cell line. *Cancers*, **9**:137.

Song, L., Rawal, B., Nemeth, J.A. and Haura, E.B., 2011. JAK1 Activates STAT3 Activity in Non-Small–Cell Lung Cancer Cells and IL-6 Neutralizing Antibodies Can Suppress JAK1-STAT3 SignalingJAK1 Drives STAT3 in NSCLC. *Molecular Cancer Therapeutics*, **10**: 481-494.

Souza, V., del Carmen Escobar, M., Bucio, L., Hernández, E., Gómez-Quiroz, L.E. and Ruiz, M.C.G. (2009). NADPH oxidase and ERK1/2 are involved in cadmium induced-STAT3 activation in HepG2 cells. *Toxicology Letters*, **187**: 180-186.

Starr, R., Willson, T.A., Viney, E.M., Murray, L.J., Rayner, J.R., Jenkins, B.J., Gonda, T.J. *et al.* (1997). A family of cytokine-inducible inhibitors of signalling. *Nature*, **387**: 917-921.

Su, C.C., Lin, J.G., Li, T.M., Chung, J.G., Yang, J.S., Ip, S.W., Lin, W.C. *et al.* (2006). Curcumin-induced apoptosis of human colon cancer colo 205 cells through the production of ROS, Ca2+ and the activation of caspase-3. *Anticancer Research*, **26**: 4379-4389.

Suvorova, E.S., Lucas, O., Weisend, C.M., Rollins, M.F., Merrill, G.F., Capecchi, M.R. and Schmidt, E.E. (2009). Cytoprotective Nrf2 pathway is induced in chronically txnrd 1-deficient hepatocytes. *PloS One*, **4**: e6158.

Suzuki, T., Das, S.K., Inoue, H., Kazami, M., Hino, O., Kobayashi, T., Yeung, R.S. *et al.* (2008). Tuberous sclerosis complex 2 loss-of-function mutation regulates reactive oxygen species production through Rac1 activation. *Biochemical and Biophysical Research Communications*, **368**: 132-137.

Syu, J.P., Chi, J.T. and Kung, H.N. (2016). Nrf2 is the key to chemotherapy resistance in MCF7 breast cancer cells under hypoxia. *Oncotarget*, **7**: 14659–14672.

Szwed, A., Kim, E. and Jacinto, E. (2021). Regulation and metabolic functions of mTORC1 and mTORC2. *Physiological Reviews*, **101**: 1371-1426.

Tajima, M., Kurashima, Y., Sugiyama, K., Ogura, T. and Sakagami, H. (2009). The redox state of glutathione regulates the hypoxic induction of HIF-1. *European Journal Of Pharmacology*, **606**: 45-49.

Tam, L., McGlynn, L.M., Traynor, P., Mukherjee, R., Bartlett, J.M. and Edwards, J. (2007). Expression levels of the JAK/STAT pathway in the transition from hormone-sensitive to hormone-refractory prostate cancer. *British journal of cancer*, **97**: 378-383.

Tang, Y., Wallace, M., Sanchez-Gurmaches, J., Hsiao, W.Y., Li, H., Lee, P.L., Vernia, S. *et al.* (2016). Adipose tissue mTORC2 regulates ChREBP-driven de novo lipogenesis and hepatic glucose metabolism. *Nature Communications*, **7**: 11365.

Tao, S., Rojo de la Vega, M., Chapman, E., Ooi, A. and Zhang, D.D. (2018). The effects of NRF2 modulation on the initiation and progression of chemically and genetically induced lung cancer. Molecular carcinogenesis, **57**: 182-192.

Taylor, S.E., Bagnall, J., Mason, D., Levy, R., Fernig, D.G. and See, V. (2016). Differential sub-nuclear distribution of hypoxia-inducible factors (HIF)-1 and-2 alpha impacts on their stability and mobility. *Open Biology*, **6**: 160195.

Tavsan, Z. and Kayali, H.A. (2019). Flavonoids showed anticancer effects on the ovarian cancer cells: Involvement of reactive oxygen species, apoptosis, cell cycle and invasion. *Biomedicine & Pharmacotherapy*, **116**: 109004.

Tee, A.R., Anjum, R. and Blenis, J. (2003b). Inactivation of the tuberous sclerosis complex-1 and-2 gene products occurs by phosphoinositide 3-kinase/Akt-dependent and-independent phosphorylation of tuberin. *Journal of Biological Chemistry*, **278**: 37288-37296.

Tee, A.R., Fingar, D.C., Manning, B.D., Kwiatkowski, D.J., Cantley, L.C. and Blenis, J., (2002). Tuberous sclerosis complex-1 and-2 gene products function together to inhibit mammalian target of rapamycin (mTOR)-mediated downstream signaling. *Proceedings of the National Academy of Sciences*, **99**: 13571-13576.

Tee, A.R., Manning, B.D., Roux, P.P., Cantley, L.C. and Blenis, J. (2003a). Tuberous sclerosis complex gene products, Tuberin and Hamartin, control mTOR signaling by acting as a GTPase-activating protein complex toward Rheb. *Current Biology*, **13**: 1259-1268.

Tehrani, H.S. and Moosavi-Movahedi, A.A. (2018). Catalase and its mysteries. Progress in *Biophysics and Molecular Biology*, **140**: 5-12.

Teleanu, R.I., Chircov, C., Grumezescu, A.M. and Teleanu, D.M., (2019). Tumor angiogenesis and anti-angiogenic strategies for cancer treatment. *Journal of Clinical Medicine*, **9**: 84.

Tell, G., Zecca, A., Pellizzari, L., Spessotto, P., Colombatti, A., Kelley, M.R., Damante, G. *et al.* (2000). An 'environment to nucleus' signalling system operates in B lymphocytes: redox status modulates BSAP/Pax-5 activation through Ref-1 nuclear translocation. *Nucleic Acids Research*, **28**: 1099-1105.

Terada, N., Patel, H.R., Takase, K., Kohno, K., Nairn, A.C. and Gelfand, E.W. (1994). Rapamycin selectively inhibits translation of mRNAs encoding elongation factors and ribosomal proteins. *Proceedings of the National Academy of Sciences*, **91**: 11477-11481.

Thakur, S., Sarkar, B., Cholia, R.P., Gautam, N., Dhiman, M. and Mantha, A.K. (2014). APE1/Ref-1 as an emerging therapeutic target for various human diseases: phytochemical modulation of its functions. *Experimental & Molecular Medicine*, **46**: e106-e106.

Theil, E.C. (2013). Ferritin: the protein nanocage and iron biomineral in health and in disease. Inorganic chemistry, **52**: 12223-12233.

Thiele, E.A., Bebin, E.M., Bhathal, H., Jansen, F.E., Kotulska, K., Lawson, J.A., O'Callaghan, *et al*. (2021). Add-on cannabidiol treatment for drug-resistant seizures in tuberous sclerosis complex: a placebo-controlled randomized clinical trial. *JAMA Neurology*, **78**: 285-292.

Thiele, E.A., Bebin, E.M., Filloux, F., Kwan, P., Loftus, R., Sahebkar, F., Sparagana, S. and Wheless, J. (2022). Long-term cannabidiol treatment for seizures in patients with tuberous sclerosis complex: an open-label extension trial. *Epilepsia*, **63**: 426-439.

Thomas, G.V., Tran, C., Mellinghoff, I.K., Welsbie, D.S., Chan, E., Fueger, B., Czernin, J. *et al.* (2006). Hypoxia-inducible factor determines sensitivity to inhibitors of mTOR in kidney cancer. *Nature Medicine*, **12**: 122-127.

Thoreen, C.C., Chantranupong, L., Keys, H.R., Wang, T., Gray, N.S. and Sabatini, D.M. (2012). A unifying model for mTORC1-mediated regulation of mRNA translation. *Nature*, **485**: 109-113.

Thoreen, C.C., Kang, S.A., Chang, J.W., Liu, Q., Zhang, J., Gao, Y., Reichling, L.J. *et al*. (2009). An ATP-competitive mammalian target of rapamycin inhibitor reveals rapamycin-resistant functions of mTORC1. *Journal of Biological Chemistry*, **284**: 8023-8032.

Thoreen, C.C. and Sabatini, D.M. (2009). Rapamycin inhibits mTORC1, but not completely. *Autophagy*, **5**: 725-726.

Timofeeva, O.A., Chasovskikh, S., Lonskaya, I., Tarasova, N.I., Khavrutskii, L., Tarasov, S.G., Zhang, X. (2012). Mechanisms of unphosphorylated STAT3 transcription factor binding to DNA. *Journal of Biological Chemistry*, **287**: 14192-14200.

Tkach, M., Rosemblit, C., Rivas, M.A., Proietti Anastasi, C.J., Díaz Flaqué, M.C., Mercogliano, M.F., Beguelin, W. *et al.* (2013). p42/p44 MAPK-mediated Stat3 Ser727 phosphorylation is required for progestin-induced full activation of Stat3 and breast cancer growth. *Endocrine - Related Cancer*; **20**: 197-212

Tonelli, C., Chio, I.I.C. and Tuveson, D.A. (2018). Transcriptional regulation by Nrf2. *Antioxidants & Redox Signaling*, **29**: 1727-1745.

Toschi, A., Lee, E., Gadir, N., Ohh, M. and Foster, D.A. (2008). Differential dependence of hypoxia-inducible factors 1α and 2α on mTORC1 and mTORC2. *Journal of Biological Chemistry*, **283**: 34495-34499.

Toschi, A., Lee, E., Xu, L., Garcia, A., Gadir, N. and Foster, D.A. (2009). Regulation of mTORC1 and mTORC2 complex assembly by phosphatidic acid: competition with rapamycin. *Molecular and Cellular Biology*, **29**: 1411-1420.

Tsimberidou, A.M., de Achaval, S., Alibhai, I. and Kaseb, A.O. (2021). First-in-man phase I clinical trial evaluating TTI-101, an orally bioavailable, small molecule inhibitor of STAT3, in patients with advanced solid tumors. Journal of Clinical Oncology **39**: TPS3158.

Turkson, J. (2004). STAT proteins as novel targets for cancer drug discovery. *Expert Opinion on Therapeutic Targets*, **8**: 409-422.

Tyburczy, M.E., Dies, K.A., Glass, J., Camposano, S., Chekaluk, Y., Thorner, A.R., Lin, L., (2015). Mosaic and intronic mutations in TSC1/TSC2 explain the majority of TSC patients with no mutation identified by conventional testing. *PLoS Genetics*, 11: e1005637.

Umemura, A., He, F., Taniguchi, K., Nakagawa, H., Yamachika, S., Font-Burgada, J., Zhong, Z. *et al*. (2016). p62, upregulated during preneoplasia, induces hepatocellular carcinogenesis by maintaining survival of stressed HCC-initiating cells. *Cancer Cell*, **29**: 935-948.

Yadav, S.S., Buryanek, J., Brown, R.E., Ouyang, F. and Amato, R.J. (2013). Morphoproteomics of mTORC2 pathway as resistance signature and activated ERK and STAT3 prosurvival/antiapoptotic pathways in metastatic renal cell carcinoma (mRCC) progressing on rapalogs. *Journal of Clinical Oncology*, **31**:

van Slegtenhorst *et al.*, 1997 and European Chromosome 16 Tuberous Sclerosis Consortium, 1993.

van Slegtenhorst, M., de Hoogt, R., Hermans, C., Nellist, M., Janssen, B., Verhoef, S., Lindhout, D. *et al.* (1997). Identification of the tuberous sclerosis gene TSC1 on chromosome 9q34. *Science*, **277**: 805-808.

van Uden, P., Kenneth, N.S. and Rocha, S. (2008). Regulation of hypoxia-inducible factor-1α by NF-κB. *Biochemical Journal*, **412**: 477-484.

Vander Haar, E., Lee, S.I., Bandhakavi, S., Griffin, T.J. and Kim, D.H. (2007). Insulin signalling to mTOR mediated by the Akt/PKB substrate PRAS40. *Nature Cell Biology*, **9**: 316-323.

Yang, J., Kalogerou, M., Samsel, P.A., Zhang, Y., Griffiths, D.F., Gallacher, J., Sampson, J.R. *et al.* (2015). Renal tumours in a Tsc2+/− mouse model do not show feedback inhibition of Akt and are effectively prevented by rapamycin. Oncogene, **34**: 922-931.

Vella, A., D'Aversa, E., Api, M., Breveglieri, G., Allegri, M., Giacomazzi, A., Busilacchi, E.M. (2020). mTOR and STAT3 Pathway Hyper-Activation is Associated with evated Interleukin-6 Levels in Patients with Shwachman-Diamond Syndrome: Further Evidence of Lymphoid Lineage Impairment. *Cancers*, **12**: 597.

Villarino, A.V., Kanno, Y., Ferdinand, J.R. and O'Shea, J.J. (2015). Mechanisms of Jak/STAT signaling in immunity and disease. *The Journal of Immunology*, **194**: 21-27.

Vimalraj, S. (2022). A concise review of VEGF, PDGF, FGF, Notch, angiopoietin, and HGF signalling in tumor angiogenesis with a focus on alternative approaches and future directions. *International Journal of Biological Macromolecules*, **221**: 1428-1438

Vogt, M., Domoszlai, T., Kleshchanok, D., Lehmann, S., Schmitt, A., Poli, V., Richtering, W. (2011). The role of the N-terminal domain in dimerization and nucleocytoplasmic shuttling of latent STAT3. *Journal Of Cell Science*, **124**: 900-909.

von Ranke, F.M., Zanetti, G., e Silva, J.L.P., Neto, C.A.A., Godoy, M.C., Souza, C.A., Mançano, A.D. *et al.* (2015). Tuberous sclerosis complex: state-of-the-art review with a focus on pulmonary involvement. *Lung*, **193**: 619-627.

Vo Recklinghausen,F. (1862). Die Lymphelfasse und ihre Beziehung zum Bindegewebe (German). Berlin: A. Hirschwald.

Vollmer, S., Kappler, V., Kaczor, J., Flügel, D., Rolvering, C., Kato, N., Kietzmann, T. *et al.* (2009). Hypoxia-inducible factor 1α is up-regulated by oncostatin M and participates in oncostatin M signaling. *Hepatology*, **50**: 253-260.

Waitkus, M.S., Chandrasekharan, U.M., Willard, B., Haque, S.J. and DiCorleto, P.E. (2013). STAT3-mediated coincidence detection regulates noncanonical immediate early gene induction. *Journal of Biological Chemistry*, **288**: 11988-12003.

Walker, E.H., Perisic, O., Ried, C., Stephens, L. and Williams, R.L. (1999). Structural insights into phosphoinositide 3-kinase catalysis and signalling. *Nature*, **402**: 313-320.

Walker, L.J., Robson, C.N., Black, E., Gillespie, D. and Hickson, I.D. (1993). Identification of residues in the human DNA repair enzyme HAP1 (Ref-1) that are essential for redox regulation of Jun DNA binding. *Molecular And Cellular Biology*, **13**: 5370-5376.

Wang, R., Cherukuri, P. and Luo, J. (2005a). Activation of Stat3 sequence-specific DNA binding and transcription by p300/CREB-binding protein-mediated acetylation. *Journal of Biological Chemistry*, **280**: 11528-11534.

Wang, J., Filippakis, H., Hougard, T., Du, H., Ye, C., Liu, H.J., Zhang, L. *et al.* (2021a). Interleukin-6 mediates PSAT1 expression and serine metabolism in TSC2-deficient cells. *Proceedings of the National Academy of Sciences*, **118**: e2101268118.

Wang, L., Harris, T.E., Roth, R.A. and Lawrence, J.C. (2007a). PRAS40 regulates mTORC1 kinase activity by functioning as a direct inhibitor of substrate binding. *Journal of Biological Chemistry*, **282**: 20036-20044.

Wang, G.L., Jiang, B.H., Rue, E.A. and Semenza, G.L. (1995a). Hypoxia-inducible factor 1 is a basic-helix-loop-helix-PAS heterodimer regulated by cellular O2 tension. *Proceedings Of the National Academy of Sciences*, **92**: 5510-5514.

Wang, M., Kirk, J.S., Venkataraman, S., Domann, F.E., Zhang, H.J., Schafer, F.Q., Flanagan, S.W. *et al.* (2005b). Manganese superoxide dismutase suppresses hypoxic induction of hypoxia-inducible factor-1α and vascular endothelial growth factor. Oncogene, **24**: 8154-8166.

Wang, C., Leavenworth, J., Zhang, C., Liu, Z., Yuan, K.Y., Wang, Y., Zhang, G. *et al.* (2022). Epigenetic regulation of EIF4A1 through DNA methylation and an oncogenic role of eIF4A1 through BRD2 signaling in prostate cancer. *Oncogene*, **41**: 2778-2785.

Wang, X., Li, W., Williams, M., Terada, N., Alessi, D.R. and Proud, C.G. (2001). Regulation of elongation factor 2 kinase by p90RSK1 and p70 S6 kinase. *The EMBO Journal*, **20**: 4370-4379.

Wang, J., Lv, X., Guo, X., Dong, Y., Peng, P., Huang, F., Wang, P., Zhang, H., Zhou, J., Wang, Y. and Wei, B. (2021b). Feedback activation of STAT3 limits the response to PI3K/AKT/mTOR inhibitors in PTEN-deficient cancer cells. *Oncogenesis*, **10**: 1-12.

Wang, T., Niu, G., Kortylewski, M., Burdelya, L., Shain, K., Zhang, S., Bhattacharya, R. *et al.* (2004). Regulation of the innate and adaptive immune responses by Stat-3 signaling in tumor cells. *Nature Medicine*, **10**: 48-54.

Wang, G.L. and Semenza, G.L. (1995b). Purification and characterization of hypoxia-inducible factor 1 (∗). *Journal of Biological Chemistry*, **270**: 1230-1237.

Wang, X.J., Sun, Z., Villeneuve, N.F., Zhang, S., Zhao, F., Li, Y., Chen, W. *et al.* (2008). Nrf2 enhances resistance of cancer cells to chemotherapeutic drugs, the dark side of Nrf2. *Carcinogenesis*, **29**: 1235-1243.

Wang, Y.T., Tang, F., Hu, X., Zheng, C.X., Gong, T.J., Zhou, Y., Luo, Y. *et al.* (2020a). Role of crosstalk between STAT3 and mTOR signaling in driving sensitivity to chemotherapy in osteosarcoma cell lines. *IUBMB life*, **72**: 2146-2153.

Wang, Y., Tang, S., Wu, Y., Wan, X., Zhou, M., Li, H. and Zha, X. (2020b). Upregulation of 6-phosphofructo-2-kinase (PFKFB3) by hyperactivated mammalian target of rapamycin complex 1 is critical for tumor growth in tuberous sclerosis complex. *IUBMB Life*, **72**: 965-977.

Wang, Q.S., Zheng, Y.M., Dong, L., Ho, Y.S., Guo, Z. and Wang, Y.X. (2007b). Role of mitochondrial reactive oxygen species in hypoxia-dependent increase in intracellular calcium in pulmonary artery myocytes. *Free Radical Biology and Medicine*, **42**: 642-653.

Warfel, N.A., Dolloff, N.G., Dicker, D.T., Malysz, J. and El-Deiry, W.S. (2013). CDK1 stabilizes HIF-1α via direct phosphorylation of Ser668 to promote tumor growth. *Cell Cycle*, **12**: 3689-3701

Watanabe, N. and Forman, H.J. (2003). Autoxidation of extracellular hydroquinones is a causative event for the cytotoxicity of menadione and DMNQ in A549-S cells. *Archives of Biochemistry and Biophysics*, **411**: 145-157.

Watanabe, Y., Murdoch, C.E., Sano, S., Ido, Y., Bachschmid, M.M., Cohen, R.A. and Matsui, R. (2016). Glutathione adducts induced by ischemia and deletion of glutaredoxin-1 stabilize HIF-1α and improve limb revascularization. *Proceedings of the National Academy of Sciences*, **113**: 6011-6016.

Wei, D., Le, X., Zheng, L., Wang, L., Frey, J.A., Gao, A.C., Peng, Z., (2003). Stat3 activation regulates the expression of vascular endothelial growth factor and human pancreatic cancer angiogenesis and metastasis. *Oncogene*, **22**: 319-329.

Weichhart, T., Costantino, G., Poglitsch, M., Rosner, M., Zeyda, M., Stuhlmeier, K.M., Kolbe, T. *et al.* (2008). The TSC-mTOR signaling pathway regulates the innate inflammatory response. *Immunity*, **29**: 565-577.

Weinberg, F., Hamanaka, R., Wheaton, W.W., Weinberg, S., Joseph, J., Lopez, M., Kalyanaraman, B. (2010). Mitochondrial metabolism and ROS generation are essential for Kras-mediated tumorigenicity. *Proceedings of the National Academy of Sciences*, **107**: 8788-8793.

Wen, Z., Zhong, Z. and Darnell Jr, J.E. (1995). Maximal activation of transcription by Statl and Stat3 requires both tyrosine and serine phosphorylation. *Cell*, **82**: 241-250.

Wenger, R.H., Stiehl, D.P. and Camenisch, G. (2005). Integration of oxygen signaling at the consensus HRE. *Science's STKE*, **2005**: re12-re12.

West, M.J., Stoneley, M. and Willis, A.E. (1998). Translational induction of the c-myc oncogene via activation of the FRAP/TOR signalling pathway. *Oncogene*, **17**: 769-780.

Wiener, C.M., Booth, G. and Semenza, G.L. (1996). In vivoexpression of mRNAs encoding hypoxia-inducible factor 1. *Biochemical and Biophysical Research Communications*, **225**: 485-488.

Wirth, M., Joachim, J. and Tooze, S.A. (2013) Autophagosome formation-The role of ULK1 and Beclin1-PI3KC3 complexes in setting the stage. *Seminars in Cancer Biology*, **23**: 301-309

Woodrum, C., Nobil, A. and Dabora, S.L. (2010). Comparison of three rapamycin dosing schedules in A/J Tsc2+/-mice and improved survival with angiogenesis inhibitor or asparaginase treatment in mice with subcutaneous tuberous sclerosis related tumors. *Journal of Translational Medicine*, **8**: 1-18.

Wu, Y.S., Chung, I., Wong, W.F., Masamune, A., Sim, M.S. and Looi, C.Y. (2017a). Paracrine IL-6 signaling mediates the effects of pancreatic stellate cells on epithelial-mesenchymal transition via Stat3/Nrf2 pathway in pancreatic cancer cells. *Biochimica et Biophysica Acta (BBA)-General Subjects*, **1861**: 296-306.

Wu, Y.S., Looi, C.Y., Subramaniam, K.S., Masamune, A. and Chung, I. (2016). Soluble factors from stellate cells induce pancreatic cancer cell proliferation via Nrf2-activated metabolic reprogramming and ROS detoxification. *Oncotarget*, **7**: 36719.

Wu, X., Tao, P., Zhou, Q., Li, J., Yu, Z., Wang, X., Li, J. (2017b). IL-6 secreted by cancer-associated fibroblasts promotes epithelial-mesenchymal transition and metastasis of gastric cancer via JAK2/STAT3 signaling pathway. *Oncotarget*, **8**: 20741.

Xanthoudakis, S. and Curran, T. (1992). Identification and characterization of Ref-1, a nuclear protein that facilitates AP-1 DNA-binding activity. *The EMBO Journal*, **11**: 653-665.

Xanthoudakis, S., Miao, G.G. and Curran, T. (1994). The redox and DNA-repair activities of Ref-1 are encoded by nonoverlapping domains. *Proceedings of the National Academy of Science*s, **91**: 23-27.

Xia, Y., Cai, X., Fan, J., Zhang, L., Li, Z., Ren, J., Wu, G. and Zhu, F. (2017). RhoA/ROCK pathway inhibition by fasudil suppresses the vasculogenic mimicry of U2OS osteosarcoma cells in vitro. *Anti-Cancer Drugs*, **28**: 514-521.

Xia, Y., Cai, X.Y., Fan, J.Q., Zhang, L.L., Ren, J.H., Li, Z.Y., Zhang, R.G., Zhu, F. and Wu, G., (2019). The role of sema4D in vasculogenic mimicry formation in non-small cell lung cancer and the underlying mechanisms. *International Journal of Cancer*, **144**: 2227-2238.

Xia, X., Lemieux, M.E., Li, W., Carroll, J.S., Brown, M., Liu, X.S. and Kung, A.L. (2009). Integrative analysis of HIF binding and transactivation reveals its role in maintaining histone methylation homeostasis. Proceedings of the National Academy of Sciences, **106**: 4260-4265.

Xie, Y., Kole, S., Precht, P., Pazin, M.J. and Bernier, M. (2009). S-glutathionylation impairs signal transducer and activator of transcription 3 activation and signaling. *Endocrinology*, **150**: 1122-1131.

Xie, X., Xiao, H., Ding, F., Zhong, H., Zhu, J., Ma, N. and Mei, J, (2014). Over-expression of prolyl hydroxylase-1 blocks NF-κB-mediated cyclin D1 expression and proliferation in lung carcinoma cells. *Cancer Genetics*, **207**: 188-194.

Xu, Q., Briggs, J., Park, S., Niu, G., Kortylewski, M., Zhang, S., Gritsko, T. *et al.* (2005). Targeting Stat3 blocks both HIF-1 and VEGF expression induced by multiple oncogenic growth signaling pathways. *Oncogene*, **24**: 5552-5560.

Xu, X., Kasembeli, M.M., Jiang, X., Tweardy, B.J. and Tweardy, D.J., (2009). Chemical probes that competitively and selectively inhibit Stat3 activation. *PloS one*, **4**: e4783.

Xue, H., Yuan, G., Guo, X., Liu, Q., Zhang, J., Gao, X., Guo, X. *et al*. (2016). A novel tumor-promoting mechanism of IL6 and the therapeutic efficacy of tocilizumab: hypoxia-induced IL6 is a potent autophagy initiator in glioblastoma via the p-STAT3-MIR155-3p-CREBRF pathway. *Autophagy*, **12**: 1129-1152.

Yamakado, K., Tanaka, N., Nakagawa, T., Kobayashi, S., Yanagawa, M. and Takeda, K. (2002). Renal angiomyolipoma: relationships between tumor size, aneurysm formation, and rupture. *Radiology*, **225**: 78-82.

Yamamoto, S., Seta, K., Morisco, C., Vatner, S.F. and Sadoshima, J. (2001). Chelerythrine rapidly induces apoptosis through generation of reactive oxygen species in cardiac myocytes. *Journal of Molecular and Cellular Cardiology*, **33**: 1829-1848.

Yang, J., Chatterjee-Kishore, M., Staugaitis, S.M., Nguyen, H., Schlessinger, K., Levy, D.E. and Stark, G.R. (2005). Novel roles of unphosphorylated STAT3 in oncogenesis and transcriptional regulation. *Cancer research*, **65**: 939-947.

Yang, A., Fan, H., Zhao, Y., Zha, X., Zhang, H., Hu, Z. and Tu, P. (2016b). Huaier aqueous extract inhibits proliferation and metastasis of tuberous sclerosis complex cell models through downregulation of JAK2/STAT3 and MAPK signaling pathways. *Oncology Reports*, **36**: 1491-1498.

Yang, J., Huang, J., Dasgupta, M., Sears, N., Miyagi, M., Wang, B., Chance, M.R. *et al.* (2010a). Reversible methylation of promoter-bound STAT3 by histone-modifying enzymes. *Proceedings of the National Academy of Sciences*, **107**: 21499-21504.

Yang, H., Jiang, X., Li, B., Yang, H.J., Miller, M., Yang, A., Dhar, A. *et al.* (2017a). Mechanisms of mTORC1 activation by RHEB and inhibition by PRAS40. *Nature*, **552**: 368-373.

Yang, C., Lee, H., Pal, S., Jove, V., Deng, J., Zhang, W., Hoon, D.S., *et al.* (2013b). B cells promote tumor progression via STAT3 regulated-angiogenesis. *PloS One*, **8**: 64159.

Yang, J., Liao, X., Agarwal, M.K., Barnes, L., Auron, P.E. and Stark, G.R. (2007). Unphosphorylated STAT3 accumulates in response to IL-6 and activates transcription by binding to NFκB. *Genes & Development*, **21**: 1396-1408.

Yang, H., Rudge, D.G., Koos, J.D., Vaidialingam, B., Yang, H.J. and Pavletich, N.P. (2013a). mTOR kinase structure, mechanism and regulation. *Nature*, **497**: 217-223.

Yang, J., Samsel, P.A., Narov, K., Jones, A., Gallacher, D., Gallacher, J., Sampson, J.R *et al.* (2017). Combination of Everolimus with Sorafenib for Solid Renal Tumors in Tsc2+/− Mice Is Superior to Everolimus Alone. *Neoplasia*, **19**: .112-120.

Yang, W.S., SriRamaratnam, R., Welsch, M.E., Shimada, K., Skouta, R., Viswanathan, V.S., Cheah, J.H. *et al.* (2014). Regulation of ferroptotic cancer cell death by GPX4. *Cell*, **156**: 317-331.

Yang, H., Wang, J., Liu, M., Chen, X., Huang, M., Tan, D., Dong, M.Q. *et al.* (2016a). 4.4 Å Resolution Cryo-EM structure of human mTOR Complex 1. *Protein & Cell*, **7**: 878-887.

Yang, J., Yang, D., Cogdell, D., Du, X., Li, H., Pang, Y., Sun, Y. *et al.* (2010b). APEX1 gene amplification and its protein overexpression in osteosarcoma: correlation with recurrence, metastasis, and survival. *Technology In Cancer Research & Treatment*, **9**: 161-169.

Yang, F., Yang, L., Wataya-Kaneda, M., Yoshimura, T., Tanemura, A. and Katayama, I. (2018). Uncoupling of ER/Mitochondrial oxidative stress in mTORC1 hyperactivation-associated skin hypopigmentation. *Journal of Investigative Dermatology*, **138**: 669-678.

Yao, K.S., Xanthoudakis, S., Curran, T. and O'Dwyer, P.J. (1994). Activation of AP-1 and of a nuclear redox factor, Ref-1, in the response of HT29 colon cancer cells to hypoxia. Molecular and cellular biology, **14**: 5997-6003.

Ye, J., Coulouris, G., Zaretskaya, I., Cutcutache, I., Rozen, S. and Madden, T.L. (2012). Primer-BLAST: a tool to design target-specific primers for polymerase chain reaction. *BMC Bioinformatics*, **13**: 1-11.

Yokogami, K., Wakisaka, S., Avruch, J. and Reeves, S.A. (2000). Serine phosphorylation and maximal activation of STAT3 during CNTF signaling is mediated by the rapamycin target mTOR. *Current Biology*, **10**: 47-50.

Yokogami, K., Yamashita, S. and Takeshima, H. (2013). Hypoxia-induced decreases in SOCS3 increase STAT3 activation and upregulate VEGF gene expression. *Brain Tumor Pathology*, **30**: 135-143.

Yoon, S., Woo, S.U., Kang, J.H., Kim, K., Kwon, M.H., Park, S., Shin, H.J., (2010). STAT3 transcriptional factor activated by reactive oxygen species induces IL6 in starvation-induced autophagy of cancer cells. *Autophagy*, 6:1125-1138.

Yoshimura, S.H. and Hirano, T. (2016). HEAT repeats–versatile arrays of amphiphilic helices working in crowded environments?. *Journal of Cell Science*, **129**: 3963-3970.

Yu, J., Astrinidis, A., Howard, S. and Henske, E.P. (2004). Estradiol and tamoxifen stimulate LAM-associated angiomyolipoma cell growth and activate both genomic and nongenomic signaling pathways. *American Journal of Physiology-Lung Cellular and Molecular Physiology*, **286**: 694-L700.

Yu, H., Lee, H., Herrmann, A., Buettner, R. and Jove, R. (2014). Revisiting STAT3 signalling in cancer: new and unexpected biological functions. *Nature reviews Cancer*, **14**: 736-746.

Yu, Y., Li, S., Xu, X., Li, Y., Guan, K., Arnold, E. and Ding, J. (2005). Structural basis for the unique biological function of small GTPase RHEB. *Journal of Biological Chemistry*, **280**: 17093-17100.

Yu, H., Liu, Y., McFarland, B.C., Deshane, J.S., Hurst, D.R., Ponnazhagan, S., Benveniste, E.N. *et al*. (2015a). SOCS3 Deficiency in Myeloid Cells Promotes Tumor Development: Involvement of STAT3 Activation and Myeloid-Derived Suppressor CellsRole of STAT3/SOCS3 in MDSCs. *Cancer Immunology Research*, **3**: 727-740.

Yu, M.O., Park, K.J., Park, D.H., Chung, Y.G., Chi, S.G. and Kang, S.H. (2015b). Reactive oxygen species production has a critical role in hypoxia-induced Stat3 activation and angiogenesis in human glioblastoma. *Journal of Neuro-oncology*, **125**: 55-63.

Yuan, Z.L., Guan, Y.J., Chatterjee, D. and Chin, Y.E. (2005). Stat3 dimerization regulated by reversible acetylation of a single lysine residue. *Science*, **307**: 269-273.

Yu-Ting, T., Wu, A.C., Yang, W.B., Kao, T.J., Chuang, J.Y., Wen-Chang, C. and Hsu, T.I., (2019). ANGPTL4 Induces TMZ Resistance of Glioblastoma by Promoting Cancer Stemness Enrichment via the EGFR/AKT/4E-BP1 Cascade. International Journal of Molecular Sciences, **20**: 5625

Zeng, L.H., Xu, L., Gutmann, D.H. and Wong, M. (2008). Rapamycin prevents epilepsy in a mouse model of tuberous sclerosis complex. *Annals of Neurology: Official Journal of the American Neurological Association and the Child Neurology Society*, **63**: 444-453.

Zhang, M., An, C., Gao, Y., Leak, R.K., Chen, J. and Zhang, F. (2013c). Emerging roles of Nrf2 and phase II antioxidant enzymes in neuroprotection. Progress in neurobiology, **100**: 30-47.

Zhang, H., Berel, D., Wang, Y., Li, P., Bhowmick, N.A., Figlin, R.A. and Kim, H.L (2013b). A comparison of KU-0063794, a dual mTORC1 and mTORC2 inhibitor, and temsirolimus in preclinical renal cell carcinoma models. *PloS One*, **8**: e54918.

Zhang, X., Blenis, J., Li, H.C., Schindler, C. and Chen-Kiang, S. (1995). Requirement of serine phosphorylation for formation of STAT-promoter complexes. *Science*, **267**: 1990-1994.

Zhang, H., Cicchetti, G., Onda, H., Koon, H.B., Asrican, K., Bajraszewski, N., Vazquez, F., *et al*. (2003). Loss of Tsc1/Tsc2 activates mTOR and disrupts PI3K-Akt signaling through downregulation of PDGFR. *The Journal of Clinical Investigation*, **112**: 1223-1233.

Zhang, L., Feliciano, D.M., Huang, T., Zhang, S. and Bordey, A. (2016). Hypoxia-inducible factor-1a contributes to dendritic overgrowth in tuberous sclerosis. *Neuroscience Letters*, **612**: 43-47.

Zhang, J.G., Li, X.Y., Wang, Y.Z., Zhang, Q.D., Gu, S.Y., Wu, X., Zhu, G.H. *et al.* (2014b). ROCK is involved in vasculogenic mimicry formation in hepatocellular carcinoma cell line. *PloS One*, ***9***: 107661.

Zhang, Z.H., Li, M.Y., Wang, Z., Zuo, H.X., Wang, J.Y., Xing, Y., Jin, C. *et al.* (2020). Convallatoxin promotes apoptosis and inhibits proliferation and angiogenesis through crosstalk between JAK2/STAT3 (T705) and mTOR/STAT3 (S727) signaling pathways in colorectal cancer. *Phytomedicine*, **68**: 153172.

Zhang, H.H., Lipovsky, A.I., Dibble, C.C., Sahin, M. and Manning, B.D. (2006a). S6K1 regulates GSK3 under conditions of mTOR-dependent feedback inhibition of Akt. *Molecular Cell*, **24**: 185-197.

Zhang, S., Ma, J., Fu, Z., Zhang, Z., Cao, J., Huang, L., Li, W., *et al.* (2016). Promotion of breast cancer cells MDA-MB-231 invasion by di (2-ethylhexyl) phthalate through matrix metalloproteinase-2/-9 overexpression. *Environmental Science and Pollution Research*, **23**: 9742-9749.

Zhang, B., McDaniel, S.S., Rensing, N.R. and Wong, M. (2013a). Vigabatrin inhibits seizures and mTOR pathway activation in a mouse model of tuberous sclerosis complex. *PLoS One*, **8**: 57445.

Zhang, Y., Nicholatos, J., Dreier, J.R., Ricoult, S.J., Widenmaier, S.B., Hotamisligil, G.S., Kwiatkowski, D.J. *et al.* (2014a). Coordinated regulation of protein synthesis and degradation by mTORC1. *Nature*, **513**: 440-443.

Zhang, Q., Raghunath, P.N., Xue, L., Majewski, M., Carpentieri, D.F., Odum, N., Morris, S. *et al.* (2002). Multilevel dysregulation of STAT3 activation in anaplastic lymphoma kinase-positive T/null-cell lymphoma. *The Journal of Immunology*, **168**: 466-474.

Zhang, J.G., Zhou, H.M., Zhang, X., Mu, W., Hu, J.N., Liu, G.L. and Li, Q. (2020). Hypoxic induction of vasculogenic mimicry in hepatocellular carcinoma: role of HIF-1 α, RhoA/ROCK and Rac1/PAK signaling. *BMC Cancer*, **20**: 1-13.

Zhang, W., Zong, C.S., Hermanto, U., Lopez-Bergami, P., Ronai, Z.E. and Wang, L.H. (2006b). RACK1 recruits STAT3 specifically to insulin and insulin-like growth factor 1 receptors for activation, which is important for regulating anchorage-independent growth. *Molecular And Cellular Biology*, ***26***: 413-424.

Zhao, J., Du, P., Cui, P., Qin, Y., Hu, C.E., Wu, J., Zhou, Z. *et al.* (2018). LncRNA PVT1 promotes angiogenesis via activating the STAT3/VEGFA axis in gastric cancer. *Oncogene*, **37**: 4094-4109.

Zhao, M., Gao, F.H., Wang, J.Y., Liu, F., Yuan, H.H., Zhang, W.Y. and Jiang, B. (2011). JAK2/STAT3 signaling pathway activation mediates tumor angiogenesis by upregulation of VEGF and bFGF in non-small-cell lung cancer. *Lung Cancer*, **73**: 366-374.

Zheng, Y. and Jiang, Y. (2015). mTOR Inhibitors at a Glance. *Molecular And Cellular Pharmacology*, **7**: 15-20.

Zhong, L., Arnér, E.S. and Holmgren, A. (2000a). Structure and mechanism of mammalian thioredoxin reductase: the active site is a redox-active selenolthiol/selenenylsulfide formed from the conserved cysteine-selenocysteine sequence. Proceedings of the National Academy of Sciences, **97**: 5854-5859.

Zhong, H., Chiles, K., Feldser, D., Laughner, E., Hanrahan, C., Georgescu, M.M., Simons, J.W. *et al.* (2000). Modulation of hypoxia-inducible factor 1α expression by the epidermal growth factor/phosphatidylinositol 3-kinase/PTEN/AKT/FRAP pathway in human prostate

cancer cells: implications for tumor angiogenesis and therapeutics. *Cancer Research*, **60**: 1541-1545.

Zhong, Z., Wen, Z. and Darnell Jr, J.E. (1994). Stat3: a STAT family member activated by tyrosine phosphorylation in response to epidermal growth factor and interleukin-6. *Science*, **264**: 95-98.

Zhou, J., Wulfkuhle, J., Zhang, H., Gu, P., Yang, Y., Deng, J., Margolick, J.B., *et al.* (2007). Activation of the PTEN/mTOR/STAT3 pathway in breast cancer stem-like cells is required for viability and maintenance. *Proceedings of the National Academy of Sciences*, **104**: 16158-16163.

Ziel, K.A., Campbell, C.C., Wilson, G.L. and Gillespie, M.N. (2004). Ref-1/Ape is critical for formation of the hypoxia-inducible transcriptional complex on the hypoxic response element of the rat pulmonary artery endothelial cell VEGF gene. *The FASEB Journal*, **18**: 986-988.

Zinzalla, V., Stracka, D., Oppliger, W. and Hall, M.N. (2011). Activation of mTORC2 by association with the ribosome. *Cell*, **144**: 757-768.

Zöllner, J.P., Franz, D.N., Hertzberg, C., Nabbout, R., Rosenow, F., Sauter, M., Schubert-Bast, S., *et al.* (2020). A systematic review on the burden of illness in individuals with tuberous sclerosis complex (TSC). *Orphanet Journal of Rare Diseases*, **15**: 23.

Zong, C.S., Zeng, L., Jiang, Y., Sadowski, H.B. and Wang, L.H. (1998). Stat3 plays an important role in oncogenic Ros-and insulin-like growth factor I receptor-induced anchorage-independent growth. *Journal of Biological Chemistry*, **273**: 28065-28072.

Zordan, P., Cominelli, M., Cascino, F., Tratta, E., Poliani, P.L. and Galli, R. (2018). Tuberous sclerosis complex–associated CNS abnormalities depend on hyperactivation of mTORC1 and Akt. *The Journal of Clinical Investigation*, **128**: 1688-1706.

Zou, G.M., Karikari, C., Kabe, Y., Handa, H., Anders, R.A. and Maitra, A. (2009). The Ape-1/Ref-1 redox antagonist E3330 inhibits the growth of tumor endothelium and endothelial progenitor cells: therapeutic implications in tumor angiogenesis. *Journal of Cellular Physiology*, **219**: 209-218.

Zudaire, E., Gambardella, L., Kurcz, C. and Vermeren, S. (2011). A computational tool for quantitative analysis of vascular networks. *PloS One*, **6**: 27385.

# Supplementary Data

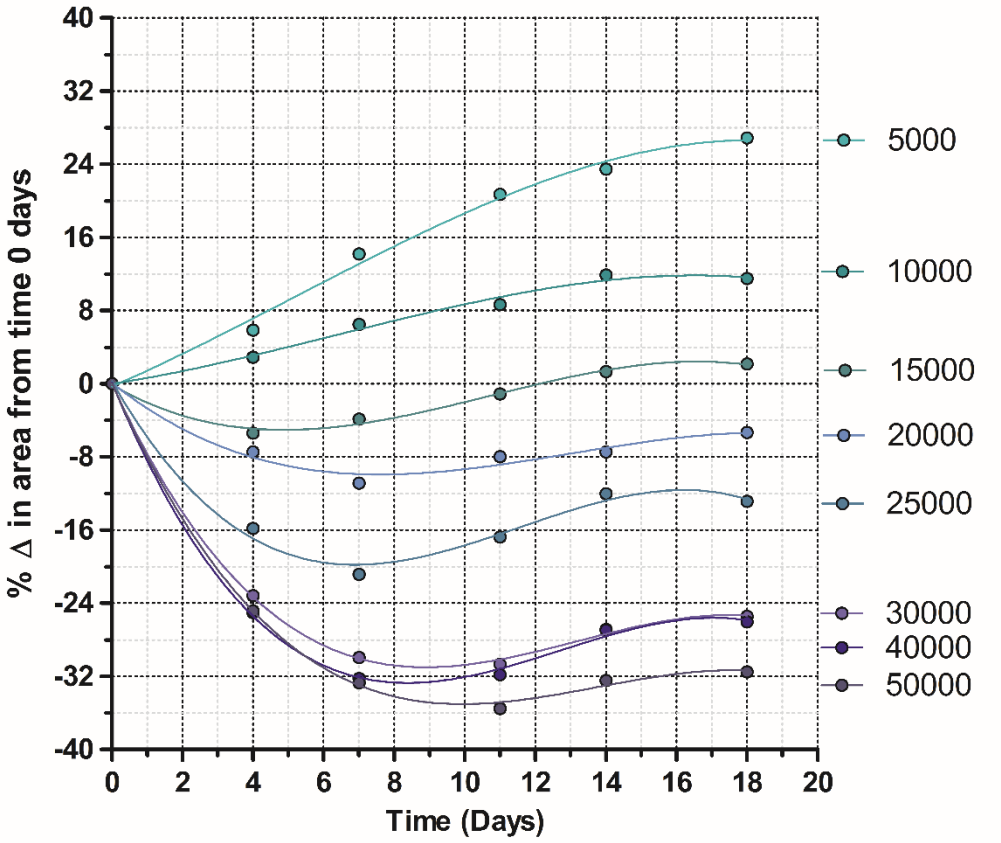


**Supplemental Figure S.3.1.** Cell seeding density calibration for determining seeding cell number for optimal growth of *TSC2* deficient (−/−) AML spheroids. AML cell seeding density per well is noted to the right on the graph. Spheroids were cultured as detailed in the materials and methods section (2.3.2.2)

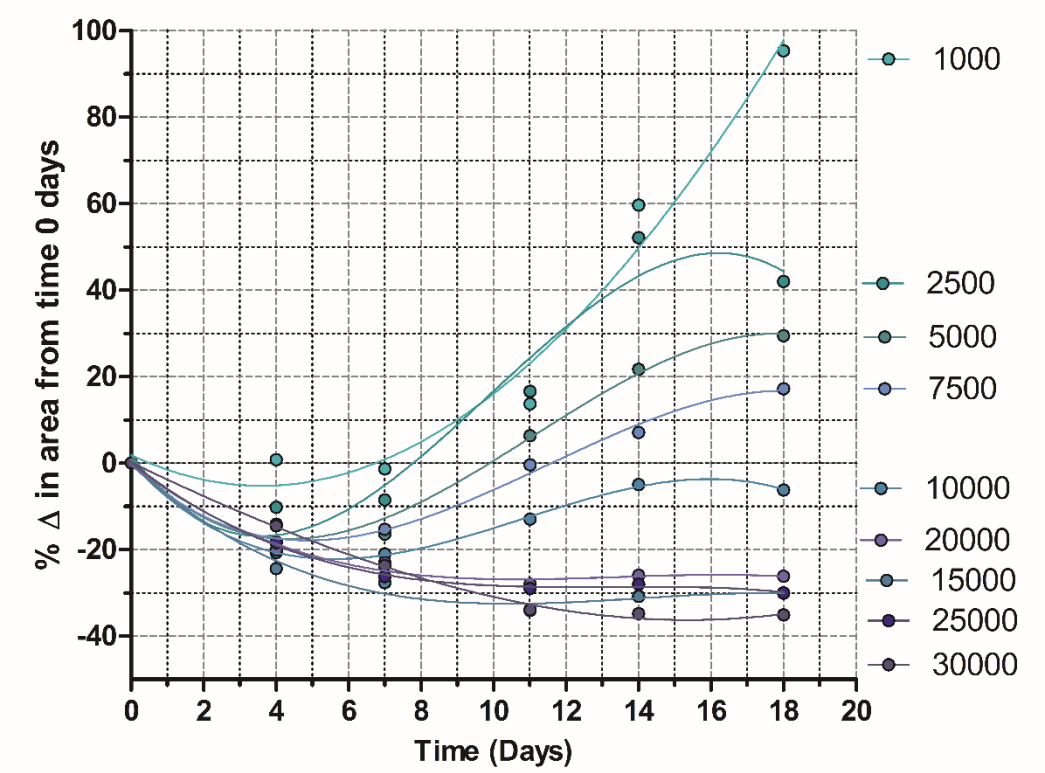


**Supplemental Figure S.3.2.** Cell seeding density calibration for determining seeding cell number for optimal growth of *Tsc2* −/− MEF spheroids. MEF cell seeding density per well is noted to the right on the graph. Spheroids were cultured as detailed in the materials and methods section (2.3.2.2)

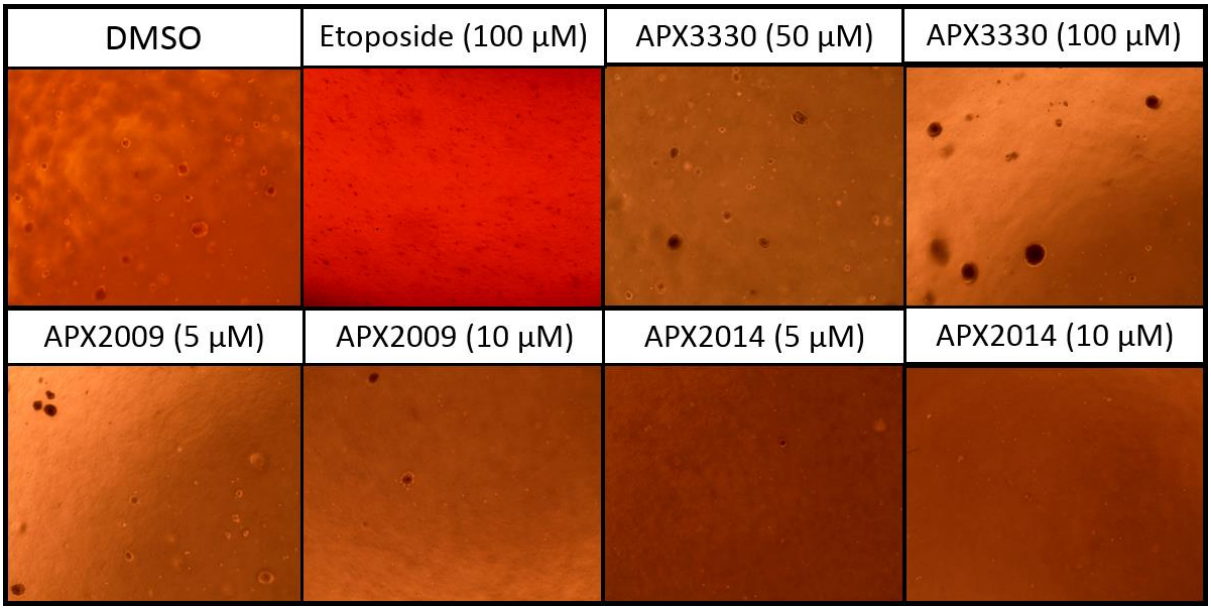


**Supplemental Figure S.3.3.** Panel shows representative images from anchorage independent growth assay of *TSC2* deficient (−/−) AML cells treated with the Ref-1 inhibitors APX3330, APX2009 and APX2014.

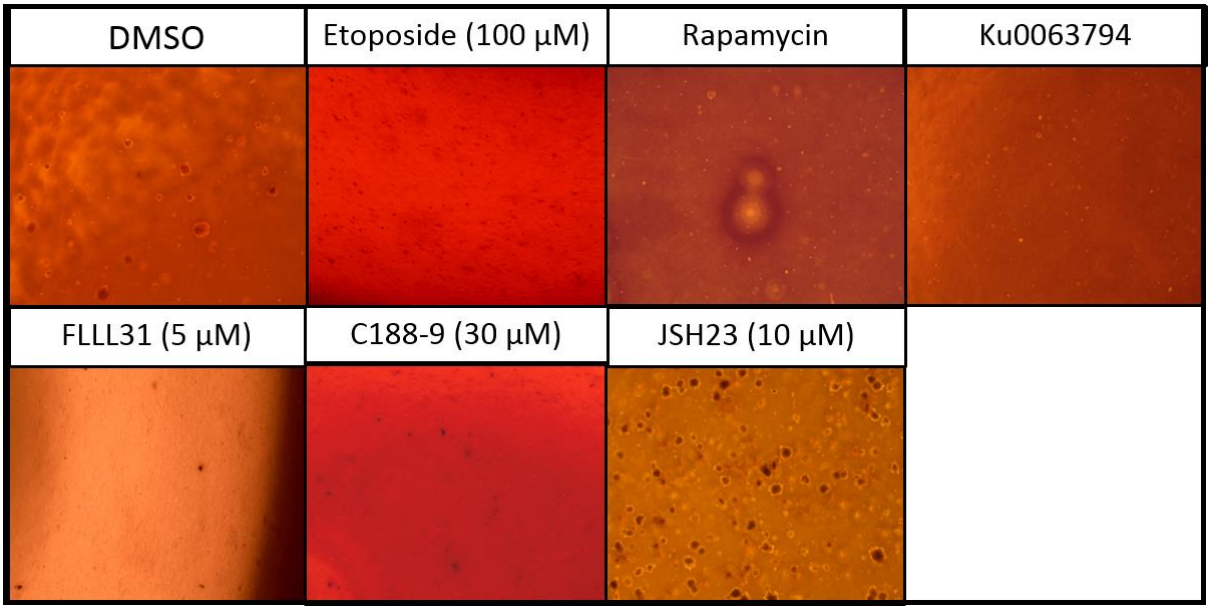


**Supplemental Figure S.3.4.** Panel shows representative images from anchorage independent growth assay of *TSC2* deficient (−/−) AML cells treated with the mTORC1 inhibitors rapamycin and Ku-0063794, the STAT3 inhibitors C188-9 and FLLL31, and the NF-κB inhibitor JSH23.

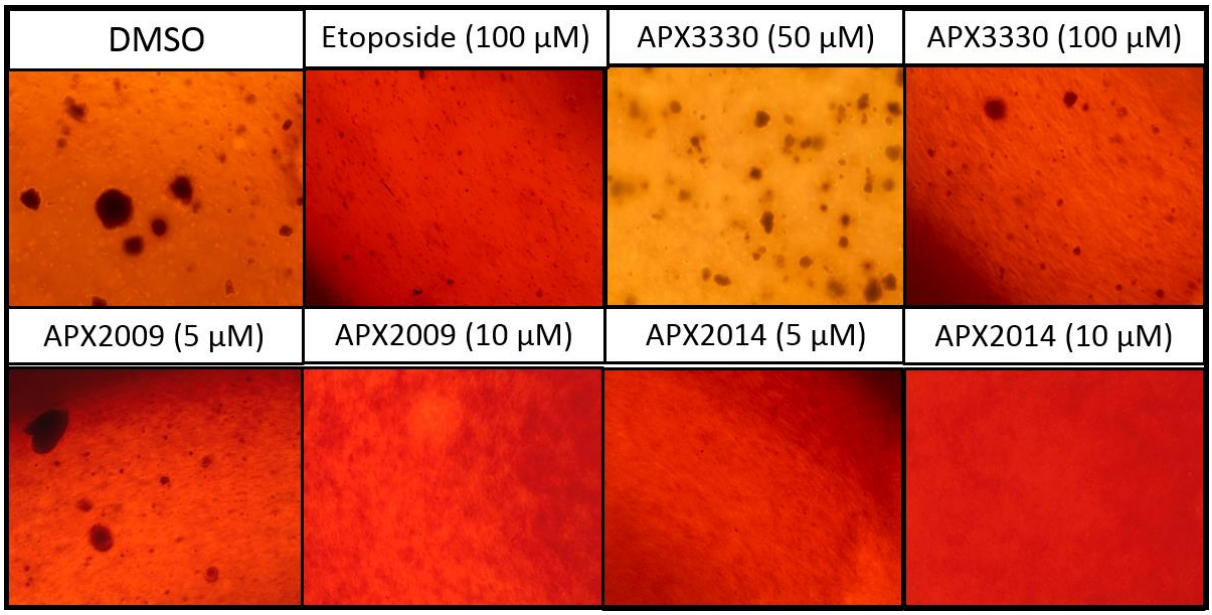


**Supplemental figure S.3.5.** Panel shows representative images from anchorage independent growth assay of *Tsc2* (−/−) MEF cells treated with the Ref-1 inhibitors APX3330, APX2009 and APX2014.

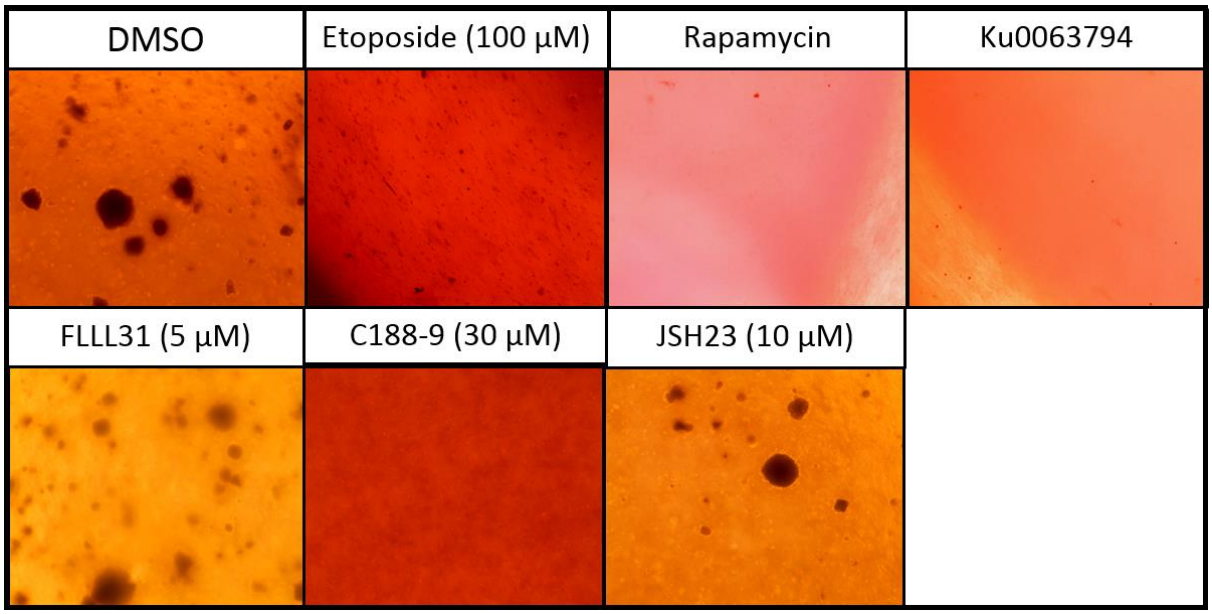


**Supplemental figure S.3.6.** Panel shows representative images from anchorage independent growth assay of *Tsc2* −/− MEF cells treated with the mTORC1 inhibitors rapamycin and Ku0063794, the STAT3 inhibitors C188-9 and FLLL31, and the NF-κB inhibitor JSH23.

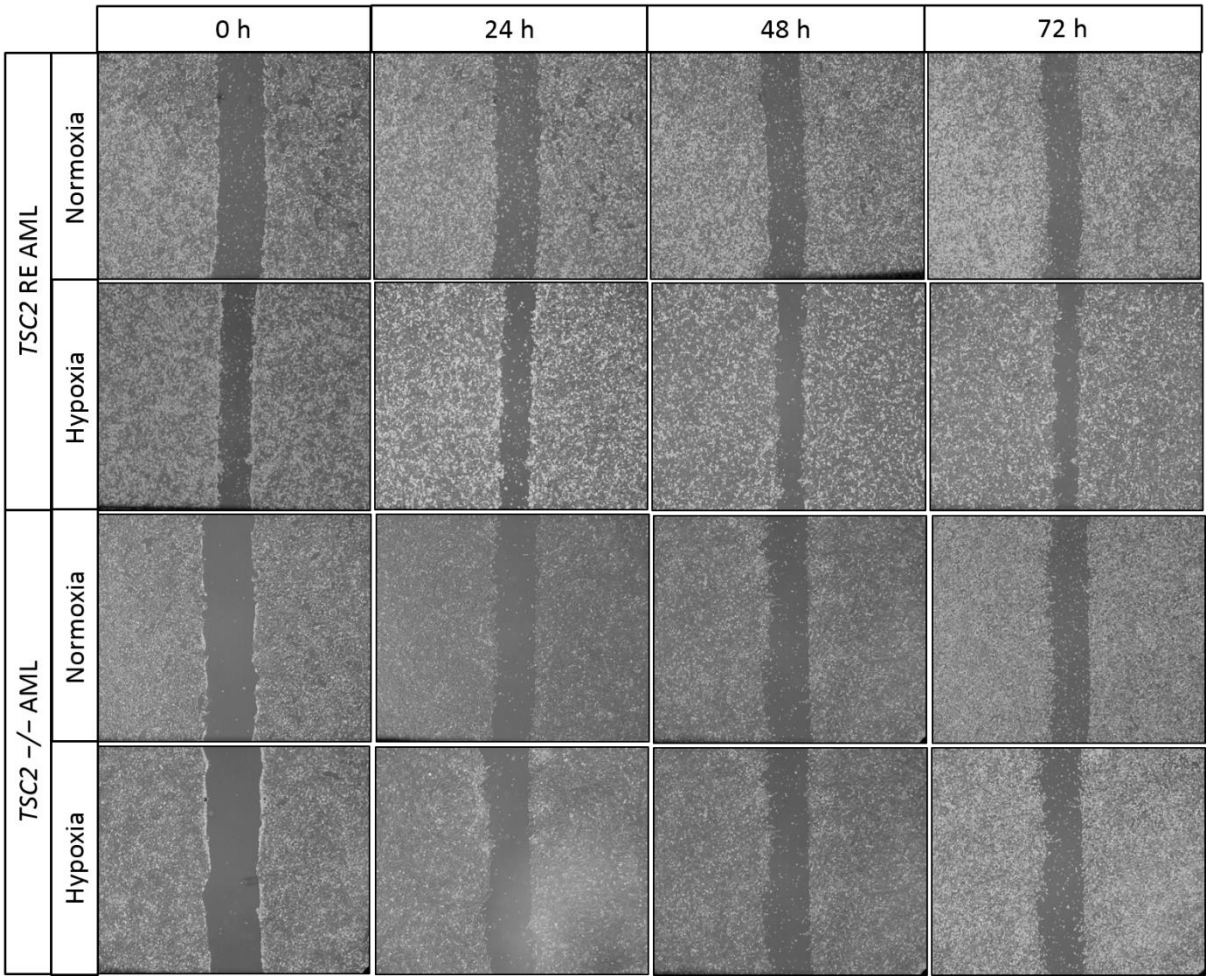


**Supplemental figure S.3.7.** Panel shows representative images from scratch wound healing assay of *TSC2* RE and *TSC2* deficient (−/−) AML cells under normoxia or hypoxia.

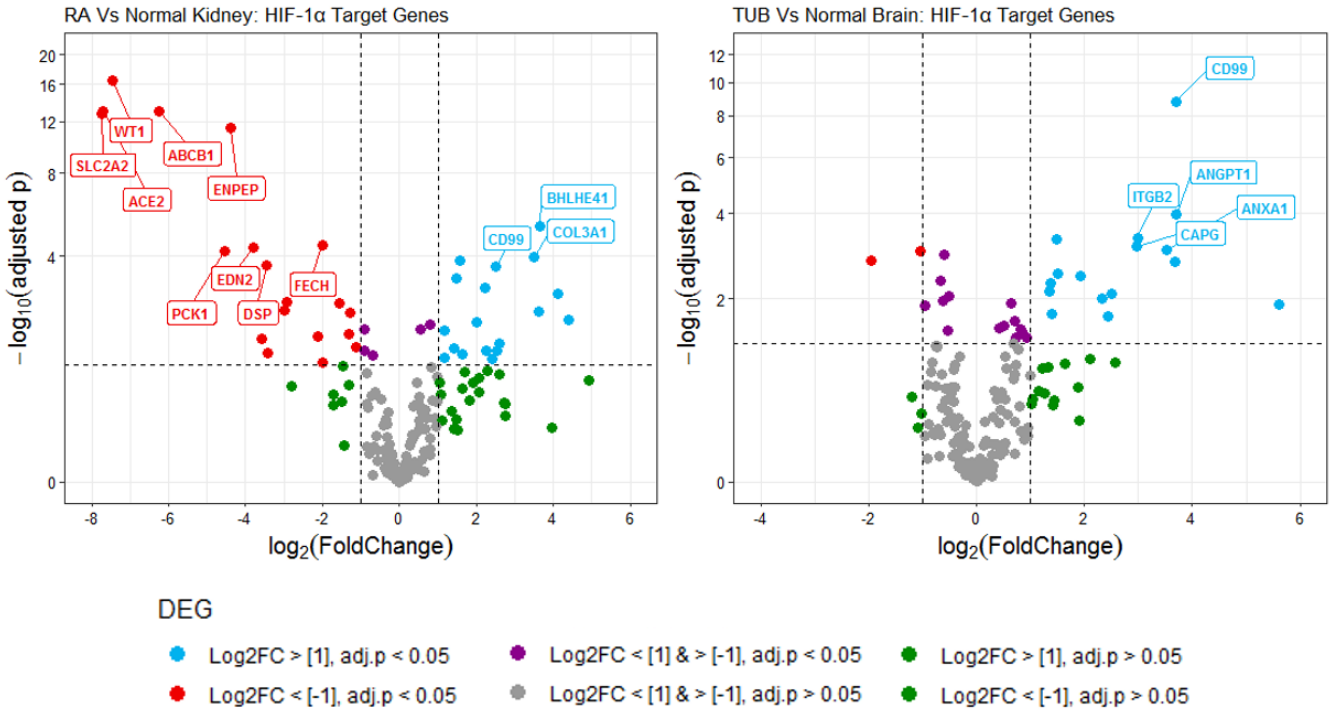


**Supplemental Figure S.4.1. HIF-1α target gene expression between renal angiomyolipomas and normal kidney or cortical tuber and normal brain.** Differential gene expression (DEG) comparison is annotated above each plot. The volcano plots were generated from previously published RNA sequencing data which Prof. Jeffrey MacKeigan kindly gave us access to. This data set compares gene expression of donated TSC patient tumours samples versus non-TSC healthy tissue samples. In this case TUB (cortical tubers) (N=15) versus normal brain (N=8) or renal AML (N=11) versus normal kidney (N=3). See Martin *et al*. (2017) for methods on sample collection, data collection and DEG analysis. For both volcano plots Log2 transformed fold change in expression of genes was plotted against their -log10 transformed FDR adjusted p-values. Dotted lines at x axis represent increase or decrease in foldchange of 2 or -2 respectively. Dotted line at y axis represents significance threshold of 0.05. Genes annotated had a Log2 fold change in expression greater or lower than 2 or -2 (i.e. four fold higher or lower in expression) respectively and an -log10 adjusted p-value greater than 3 (i.e. below 0.001 significance threshold).

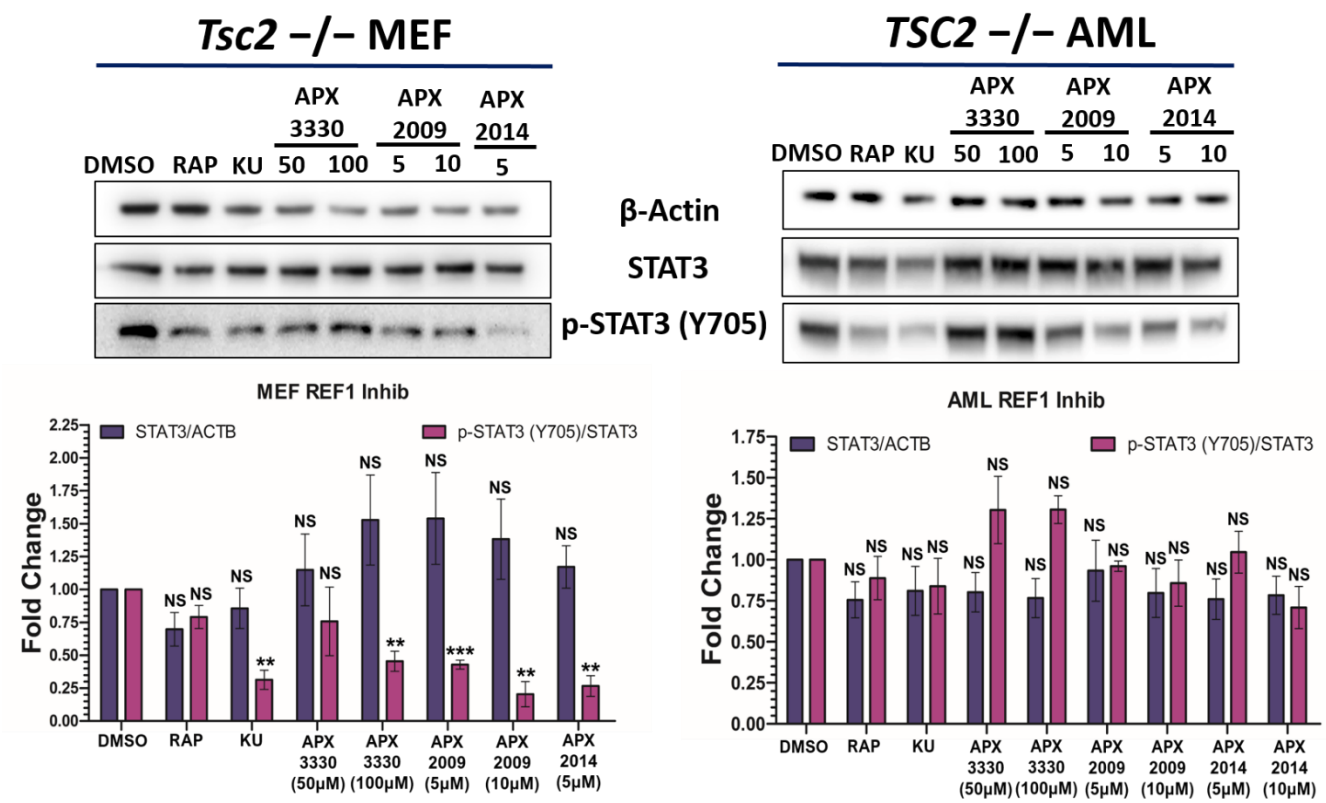


**Supplemental Figure S.4.2. Effect of Ref-1 inhibitors alone on Y705 STAT3 phosphorylation.** Representative western blots (N=3 minimum). *TSC2* deficient AML cells or *Tsc2* −/− MEF cells were cultured under hypoxia (1% $O_2$) for 18 h in the presence of either DMSO, rapamycin (RAP) at 50 nM, Ku-0063794 (KU) at 1 μM, APX3330 at 50 μM or 100 μM, APX2009 at 5 μM or 10 μM or APX2014 at 5 μM or 10 μM. Through western blotting lysates were assayed for protein expression, with β-actin acting as a loading control. Densitometry analysis of resulting western blots (N=3 minimum) was performed, with STAT3 being normalised to β-actin and p-STAT3 (Y705) being normalised to STAT3. Resulting ratios were then expressed as fold changes compared to control sample (DMSO) and plotted on graphs. Statistical analysis of differences in foldchange of normalised protein relative to control was by student's t test. Significance denoted by: * = $p < 0.05$, ** = $p < 0.01$, *** = $p < 0.001$, NS = not significant. Bars represent standard error of the mean.

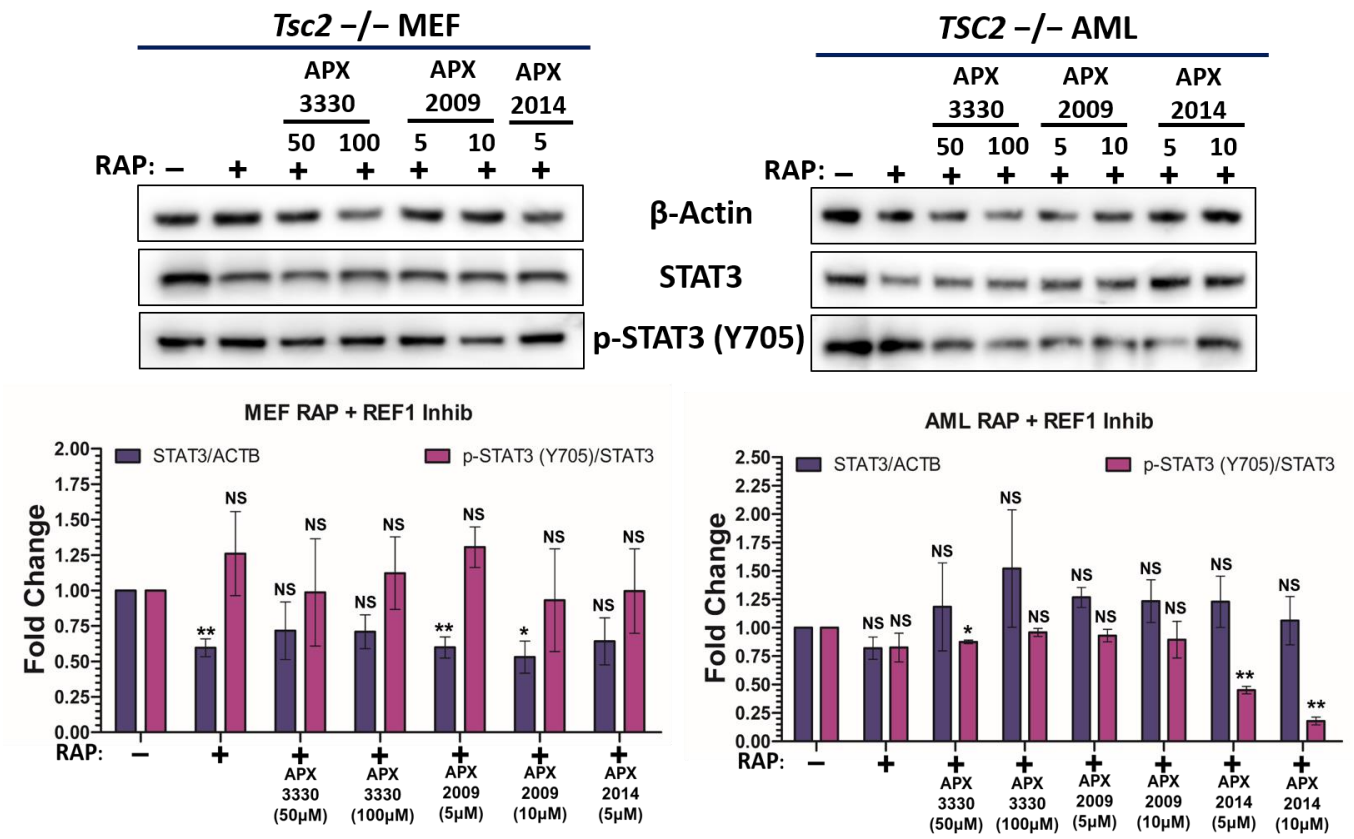


**Supplemental Figure S.4.2. Effect of Ref-1 inhibitors in combination with rapamycin on Y705 STAT3 phosphorylation.** Representative western blots (N=3 minimum). *TSC2* deficient AML cells or *Tsc2* −/− MEF cells were cultured under hypoxia (1% $O_2$) for 18 h in the presence of either DMSO, rapamycin (RAP) at 50 nM and APX3330 at 50 μM or 100 μM, APX2009 at 5 μM or 10 μM or APX2014 at 5 μM or 10 μM alone or in combination. Through western blotting lysates were assayed for protein expression, with β-actin acting as a loading control. Densitometry analysis of resulting western blots (N=3 minimum) was performed, with STAT3 being normalised to β-actin and p-STAT3 (Y705) being normalised to STAT3. Resulting ratios were then expressed as fold changes compared to control sample (DMSO) and plotted on graphs. Statistical analysis of differences in foldchange of normalised protein relative to control was by student's t test. Significance denoted by: * = p <0.05, ** = p <0.01, *** = p< 0.001, NS = not significant. Bars represent standard error of the mean.

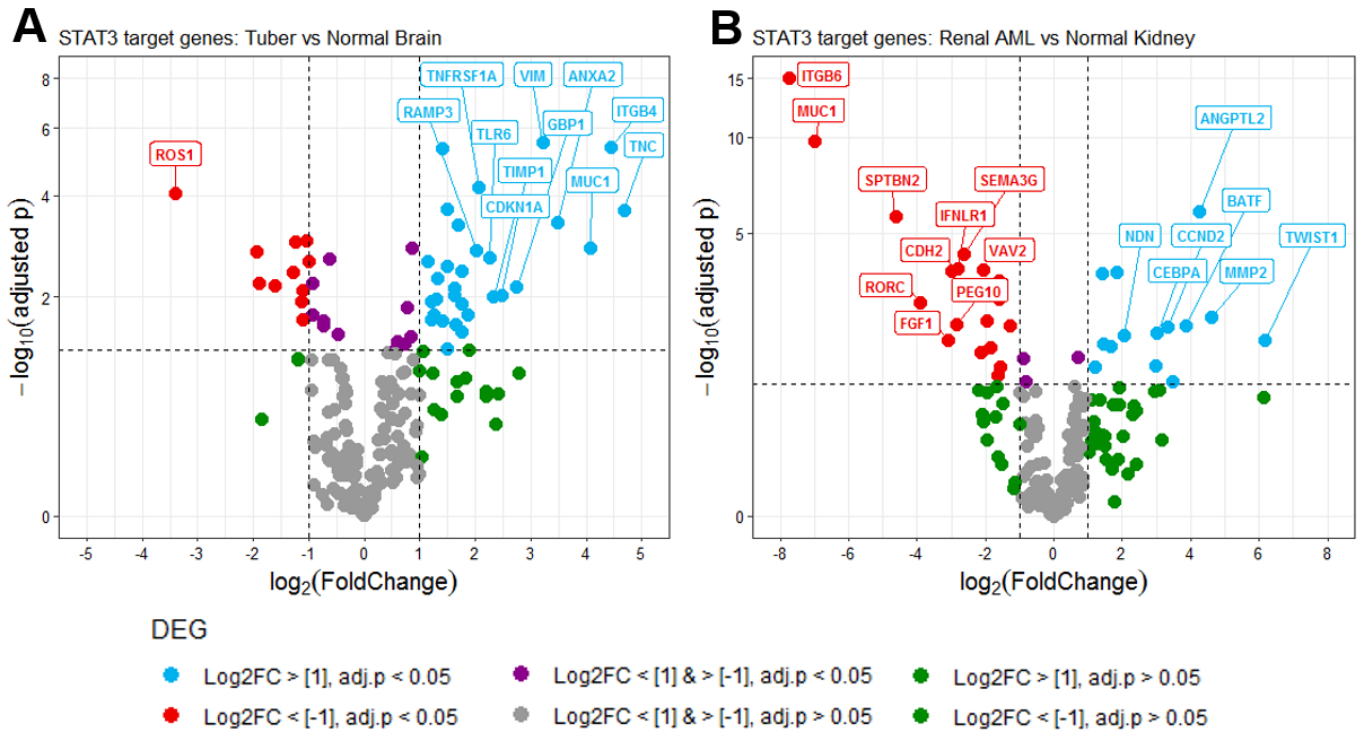


**Supplemental Figure S.5.1. STAT3 target gene expression within TSC associated lesions, renal AML and cortical tubers.** Differential gene expression (DEG) comparison is annotated above each plot. The volcano plots were generated from previously published RNA sequencing data which Prof. Jeffrey MacKeigan kindly gave us access to. This data set compares gene expression of donated TSC patient tumours samples versus non-TSC healthy tissue samples. In this case TUB (cortical tubers) (N=15) versus normal brain (N=8) or renal AML (N=11) versus normal kidney (N=3). See Martin *et al*. (2017) for methods on sample collection, data collection and DEG analysis. For both volcano plots Log2 transformed fold change in expression of genes was plotted against their -log10 transformed FDR adjusted p-values. Dotted lines at x axis represent increase or decrease in foldchange of 2 or -2 respectively. Dotted line at y axis represents significance threshold of 0.05. Genes annotated had a Log2 fold change in expression greater or lower than 2 or -2 (i.e. four fold higher or lower in expression) respectively and an -log10 adjusted p-value greater than 3 (i.e. below 0.001 significance threshold).

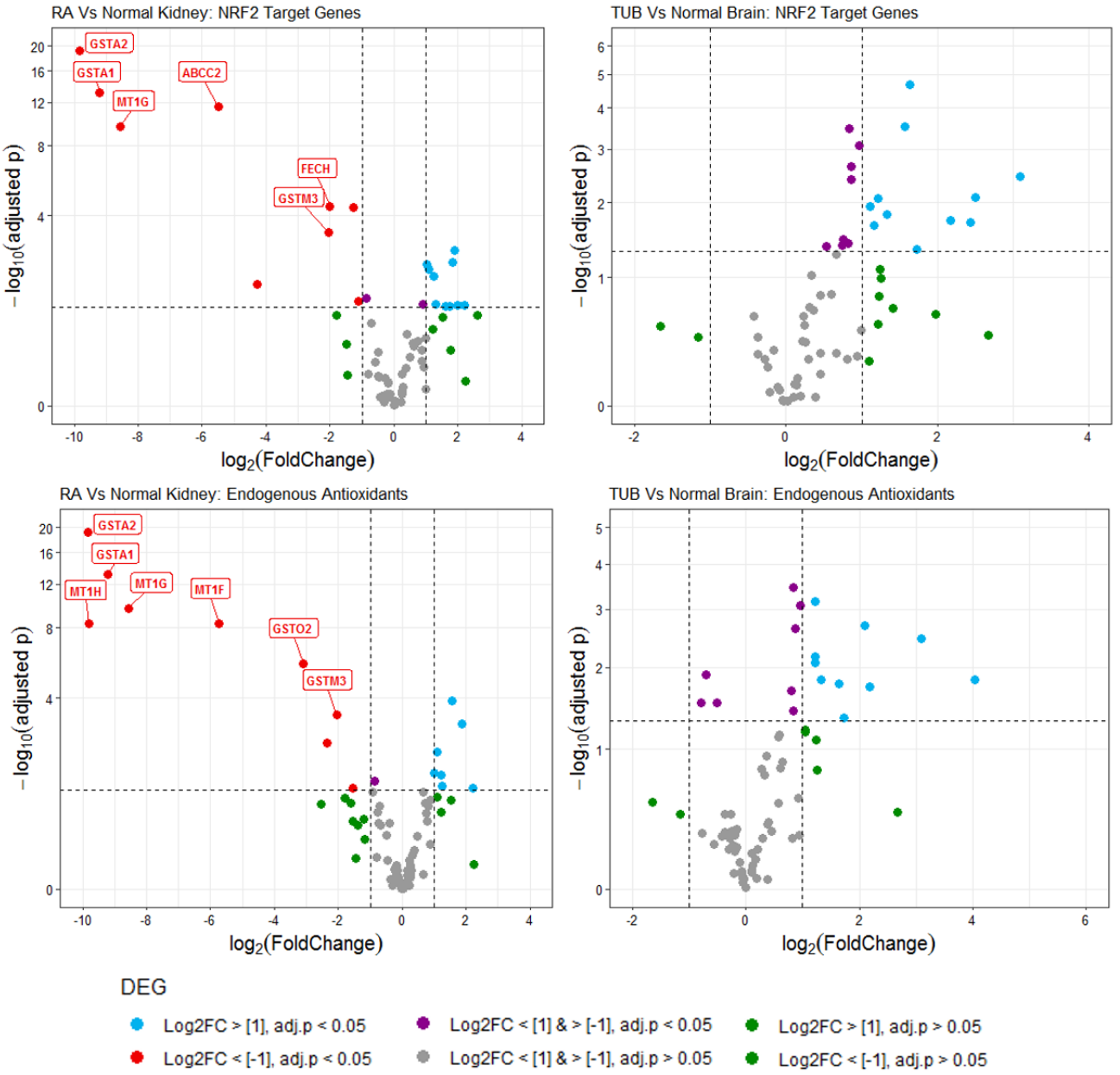


**Supplemental Figure S.6.1. Endogenous antioxidant and Nrf2 target gene set expression within TSC associated lesions, renal AML and cortical tubers.** Differential gene expression (DEG) comparison is annotated above each plot. The top-left volcano plot was generated from previously published RNA sequencing data which Prof. Jeffrey MacKeigan kindly gave us access to. This data set compares gene expression of donated TSC patient tumours samples versus non-TSC healthy tissue samples. In this case SEN/SEGA (Subependymal nodules/ Subependymal giant cell astrocytomas) (N=15) versus normal brain (N=8). See Martin *et al*. (2017) for methods on sample collection, data collection and DEG analysis. The top right and bottom left volcano plots were generated from RNA sequencing data, comparing either AML *TSC2* −/− and *TSC2* RE (re-expressed) cells cultured under either normoxia (21% $O_2$) or hypoxia (1% $O_2$) (N=6). The bottom right volcano plot was generated from RNA sequencing data comparing MEF *TSC2* −/− and *TSC2* +/+ (N=3) cells. RNA sequencing of AML and MEF cell lines was conducted through Wales Gene Park and expression levels were calculated and normalised from raw read counts as RPKM (Reads per Kilobase exon Model per million mapped reads) with DEG analysis generated through DEseq2 analysis and resulting p-values were corrected for multiple testing and false discovery by FDR method. For all volcano plots Log2 transformed fold change in expression of genes was plotted against their -log10 transformed FDR adjusted p-values. Dotted lines at x axis represent increase or decrease in foldchange of 2 or -2 respectively. Dotted line at y axis represents significance threshold of 0.05. Genes annotated had a Log2 fold change in expression greater or lower than 2 or -2 (i.e. four fold higher or lower in expression) respectively and an -log10 adjusted p-value greater than 3 (i.e. below 0.001 significance threshold).

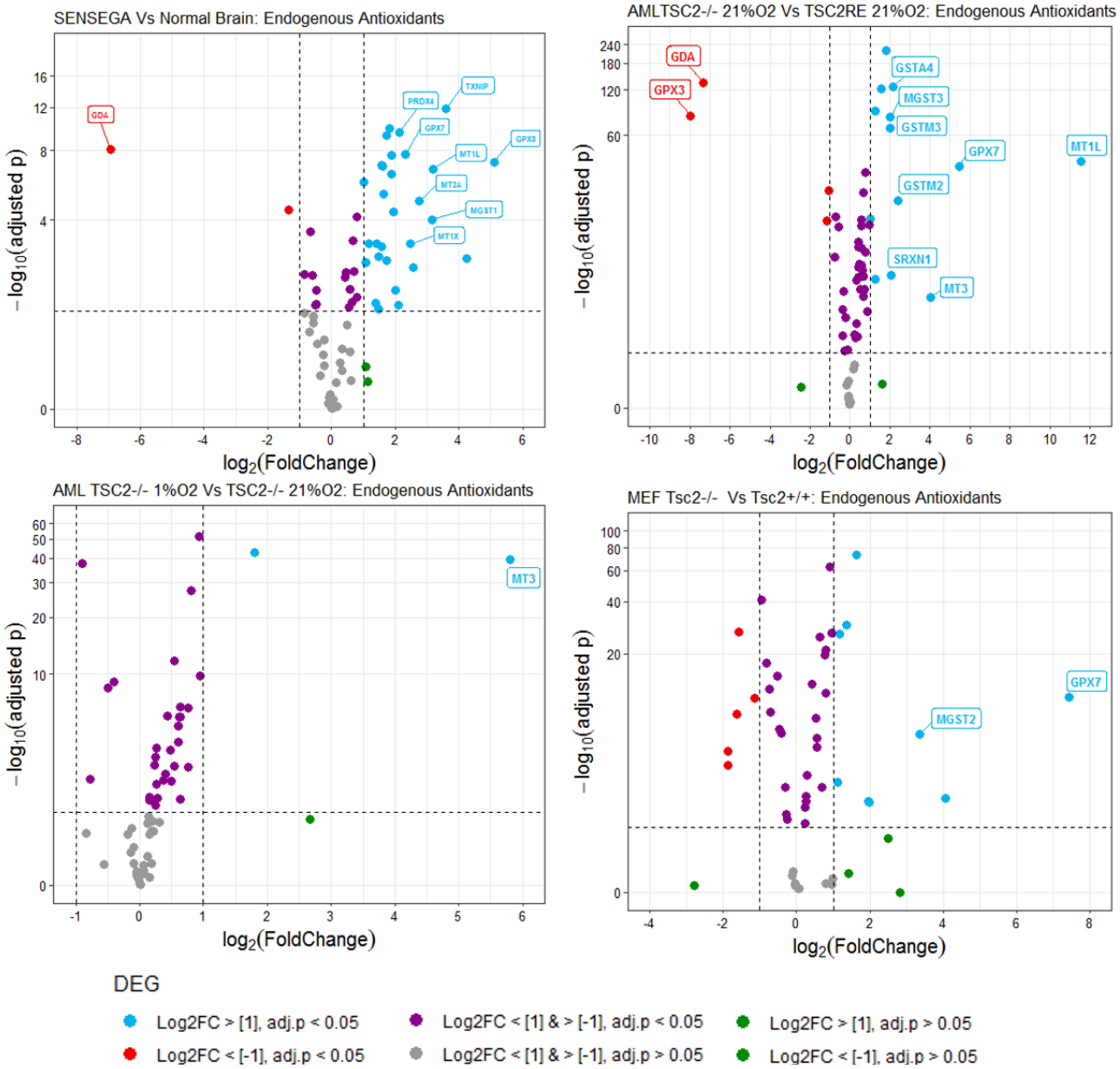


**Supplemental Figure S.6.2. Genes encoding endogenous antioxidants are dysregulated upon loss of *TSC2* within patient tumours, and AML and MEF cell lines.** Differential gene expression (DEG) comparison is annotated above each plot. The top-left volcano plot was generated from previously published RNA sequencing data which Prof. Jeffrey MacKeigan kindly gave us access to. This data set compares gene expression of donated TSC patient tumours samples versus non-TSC healthy tissue samples. In this case SEN/SEGA (Subependymal nodules/ Subependymal giant cell astrocytomas) (N=15) versus normal brain (N=8). See Martin *et al*. (2017) for methods on sample collection, data collection and DEG analysis. The top right and bottom left volcano plots were generated from RNA sequencing data, comparing either AML *TSC2* −/− and *TSC2* RE (re-expressed) cells cultured under either normoxia (21% $O_2$) or hypoxia (1% $O_2$) (N=6). The bottom right volcano plot was generated from RNA sequencing data comparing MEF *TSC2* −/− and *TSC2* +/+ (N=3) cells. RNA sequencing of AML and MEF cell lines was conducted through Wales Gene Park and expression levels were calculated and normalised from raw read counts as RPKM (Reads per Kilobase exon Model per million mapped reads) with DEG analysis generated through DEseq2 analysis and resulting p-values were corrected for multiple testing and false discovery by FDR method. For all volcano plots Log2 transformed fold change in expression of genes was plotted against their -log10 transformed FDR adjusted p-values. Dotted lines at x axis represent increase or decrease in foldchange of 2 or -2 respectively. Dotted line at y axis represents significance threshold of 0.05. Genes annotated had a Log2 fold change in expression greater or lower than 2 or -2 (i.e. four fold higher or lower in expression) respectively and an -log10 adjusted p-value greater than 3 (i.e. below 0.001 significance threshold).

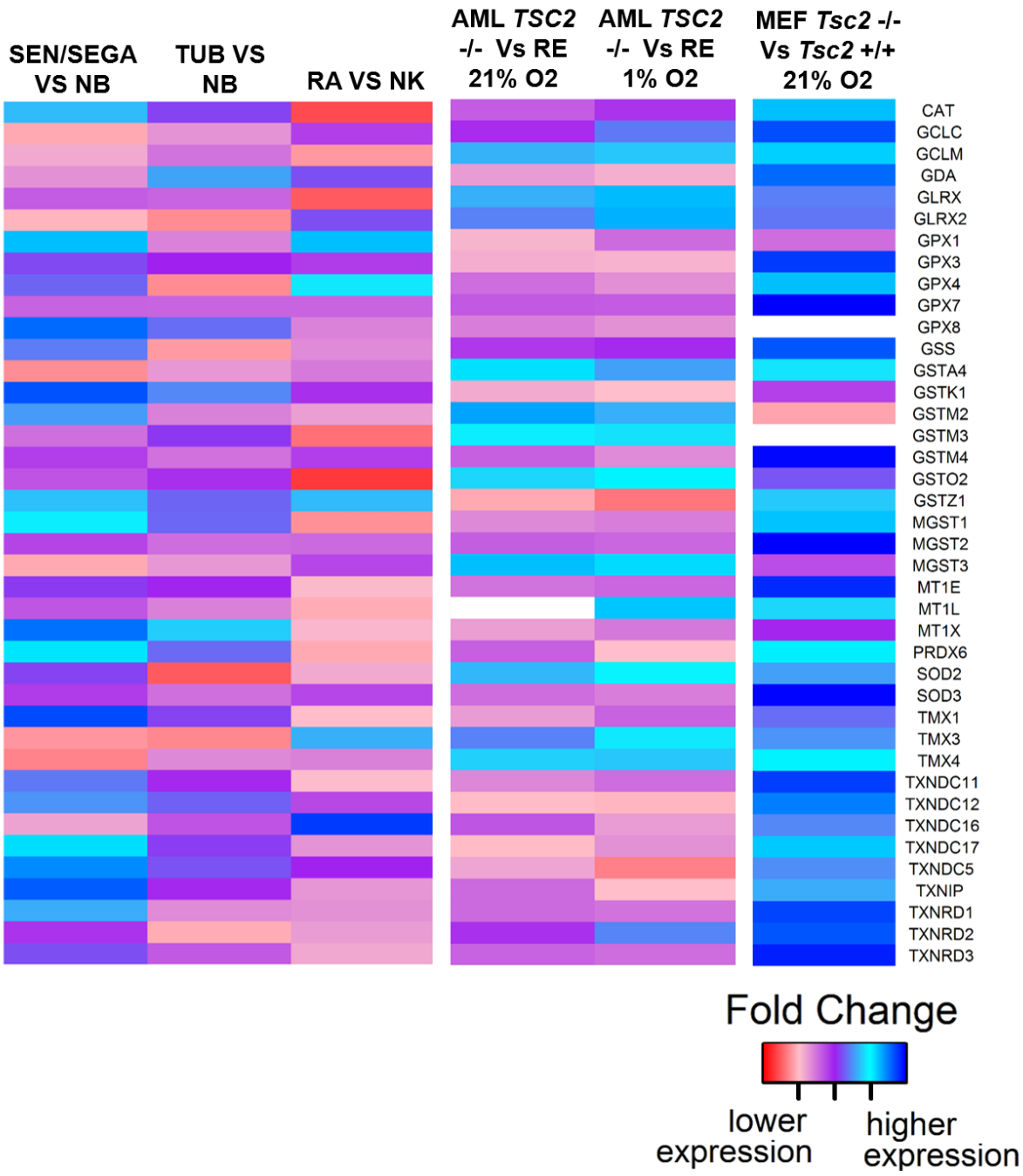


**Supplemental Figure S.6.3. Endogenous antioxidant genes are differentially expressed between TSC tumour types, human and murine cell models lines of TSC.** The above heatmap compares the fold change in expression of endogenous antioxidant genes between either a TSC lesion and healthy tissue or a *TSC2* −/− cell line with a *TSC2* re-expressed (RE) (AML) or *Tsc2* +/+ (MEF) cell line. Genes selected for the heatmaps are those which are significantly differentially expressed between the *TSC2* −/− and *TSC2 RE* cell lines (under either oxygen conditions) and between at least one TSC lesion and healthy tissue. Differential gene expression (DEG) comparison is annotated above each column and the oxygen conditions, 21% $O_2$ (normoxia) or 1% $O_2$ (hypoxia), cell lines were cultured under is also denoted. White spaces within columns indicate that gene's expression was not detectable in that data set. Gene names are shown on the right of the heatmap. It should be noted these data sets are distinct, generated differently from one another (see methods and materials section). **SEN/SEGA** = subependymal nodule/Subependymal giant cell astrocytomas, **NB** = normal brain, **TUB** = TSC tuber, **RA** = renal angiomyolipoma, **NK** = normal kidney.

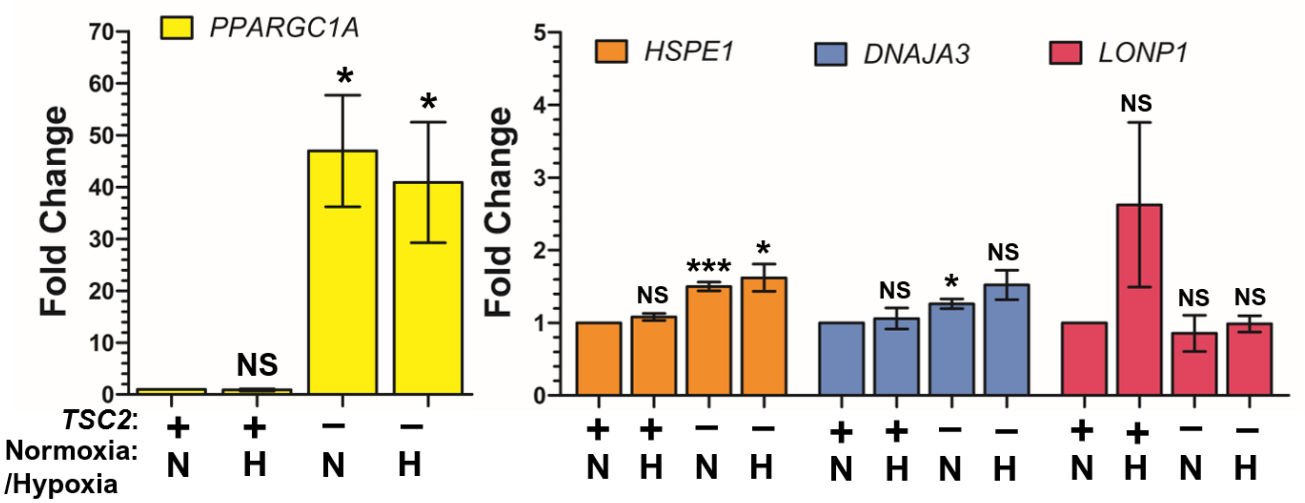


**Supplemental Figure S.6.4. Loss of *TSC2* in angiomyolipoma cells results in elevation of NFE2L2 (NRF2) and NRF2 target genes, with hypoxia not significantly effecting mRNA expression.** Either under normoxia (**N**, 21% $O_2$) or hypoxia (**H**, 1% $O_2$), AML cells lacking *TSC2* (***TSC2* –**) or with *TSC2* re-expressed (***TSC2* +**) were cultured overnight before being lysed. mRNA was purified from these lysates, converted to cDNA, and through qPCR the expression of target genes was quantified. Fold change in expression was calculated compared to a designated control sample, in this case *TSC2* re-expressed under normoxia. Fold changes of target genes in samples were normalised to the housekeeping gene *HMBS*. Statistical analysis of differences in foldchange (N=3 minimum) was by student's t test. Significance denoted by: * = p <0.05, ** = p <0.01, *** = p< 0.001, NS = not significant. Bars represent standard error of the mean.

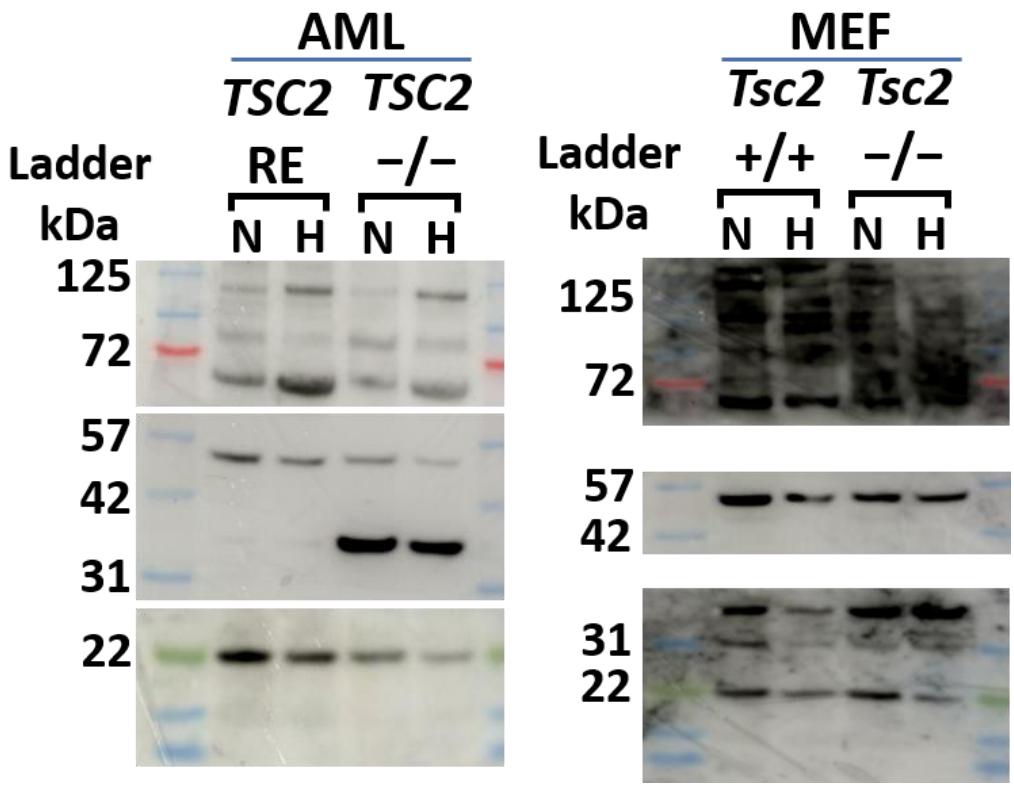


**Supplemental Figure S.6.5. Probing AML and MEF cell lines for Nrf2 expression by western blotting results in multiple bands of differing molecular weights are observed.** AML cells lacking *TSC2* (*TSC2*−/−) or with *TSC2* re-expressed (*TSC2* RE) and MEF cells lacking *Tsc2* (*TSC2*−/−) or with wild type *Tsc2* (*TSC2*+/+), were cultured overnight under normoxia (**N**, 21% $O_2$) or hypoxia (**H**, 1% $O_2$) before being lysed. Through western blotting lysates were assayed for protein expression, with β-actin acting as a loading control. Ladder band kDa is noted to the left of each blot panel. Individual blot images are from separate exposure times.

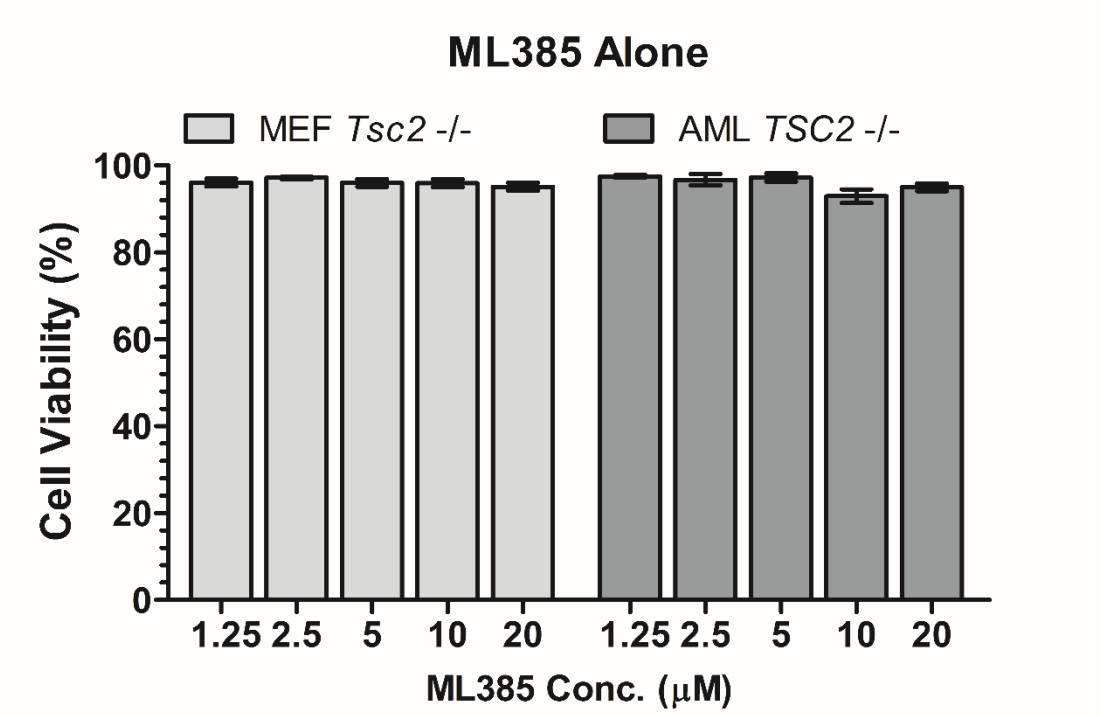


**Supplemental Figure S.6.6. The Nrf2 inhibitor is not cytotoxic to *TSC2* deficient AML and MEF cells between 1.25 μM and 20 μM.** *TSC2* deficient AML or MEF cells were grown to ~80% confluency, before being treated with ML385 at the specified concentration for 24 h. Cells were then trypsinised and collected as were non-adherent cells within original drugged media and trypsin washes. Cells were spun down and fractions of cell suspensions were mixed with AO/PI stain. Viable/non-viable cells were then assayed on a dual-fluorescence cell counter. Average percentage of viable cells per condition (N=3 minimum) are plotted on the above graphs. Statistical analysis was by student's t test. Significance denoted by: * = $p < 0.05$, ** = $p < 0.01$, *** = $p < 0.001$, NS = not significant. Bars represent standard error of the mean.

# Appendix

**Appendix Table 1. Human specific qPCR primer information**. Custom designed primers were ordered from either Merck or Eurofins. Pre-designed kiqstart primers were purchased from Merck, then validated for annealing temperature (Ann. Temp.) and primer efficiency.

| Target gene | Forward or Reverse Primer | Primer sequence (5' -> 3') | Ann. Temp. (°C) | Primer Efficiency % | Pre-designed or custom | Source |
|---|---|---|---|---|---|---|
| *AIFM2* | Forward | AAGAGGTCACTCTCATTCAC | 53.1 | 82 | Pre-designed | Merck |
| | Reverse | CTGCACTTTGATGTACTCTC | | | | |
| *ANGPTL4* | Forward | AGGCAGAGTGGACTATTTG | 56.4 | Not calculated | Pre-designed | Merck |
| | Reverse | CCTCCATCTGAGGTCATC | | | | |
| *APEX1* | Forward | GGATTAGATTGGGTAAAGGAAG | 56.4 | Not calculated | Pre-designed | Merck |
| | Reverse | TATTGATGAGAGAGTCCAGG | | | | |
| *CCL5* | Forward | CCTGCTGCTTTGCCTACATT | 56.4 | 89 | Custom | Eurofins |
| | Reverse | GACAAAGACGACTGCTGGGT | | | | |
| *DNAJA3* | Forward | GGCCTGTACGAGACGATCAA | 56.4 | 87 | Custom | Eurofins |
| | Reverse | TGTGGATGTAGTGGTCTCCG | | | | |
| *FTH1* | Forward | CAGGATATCAAGAAACCAGAC | 53.1 | 90 | Pre-designed | Merck |
| | Reverse | AGTTCCAGTAGTGACTGATTC | | | | |
| *GPX4* | Forward | CTTCACCAAGTTCCTCATCGAC | 58.4 | 87 | Custom | Merck |
| | Reverse | AGAAATAGTGGGGCAGGTCC | | | | |
| *GPX8* | Forward | ACTGAACCTCTTAGATCAC | 51.7 | 100 | Pre-designed | Merck |
| | Reverse | TACATTTTTGGCCATCTTCC | | | | |
| *HGF* | Forward | ACCACACGAACACAGCTTTT | 54.5 | 80 | Custom | Eurofins |
| | Reverse | ACTTCGTAGCGTACCTCTGG | | | | |
| *HIF1A* | Forward | CATAAAGTCTGCAACATGGAAGGT | 56.4 | 89 | Custom | Eurofins |
| | Reverse | ATTTGATGGGTGAGGAATGGGTT | | | | |
| *HMBS* | Forward | ATGGGCAACTGTACCTGACT | 58.4 | 96 | Custom | Eurofins |
| | Reverse | TCCTCAGGGCCATCTTCATG | | | | |
| *HMOX1* | Forward | CTTCAAGCTGGTGATGGCCT | 53.1 | 120 | Custom | Merck |
| | Reverse | GGAAGTAGACAGGGGCGAAG | | | | |
| *HSPE1* | Forward | GTTGAAAGGAGTGCTGCTGA | 56.4 | 84 | Custom | Eurofins |
| | Reverse | CCAACTTTCACGCTAACTGGT | | | | |
| *IL6* | Forward | CAGCCACTCACCTCTTCAGA | 56.4 | 100 | Custom | Eurofins |
| | Reverse | GCCTCTTTGCTGCTTTCACA | | | | |
| *IL6R* | Forward | AAGCCTCCCAGTGCAAGATT | 53.1 | 92 | Custom | Merck |
| | Reverse | GTCTTGCCTTCCTTCAGAGC | | | | |
| *IPO8* | Forward | ACTGTTGCACATTGTTAGAG | 51.7 | 85 | Pre-designed | Merck |
| | Reverse | ACTTTGCCAAATATCTCAGC | | | | |
| *LONP1* | Forward | AGTGGAGAAGGTGTTACGGA | 56.4 | 71 | Custom | Eurofins |
| | Reverse | CGGTGTCACGTCATACATGC | | | | |
| *MGST1* | Forward | CGAACAGATGACAGAGTAGAACG | 54.5 | 94 | Custom | Eurofins |
| | Reverse | GTCGGGACCACTCAAGGAAT | | | | |
| *NFE2L2* | Forward | GGTTGCCCACATTCCCAAAT | 56.4 | 102 | Custom | Eurofins |

| | | | | | | |
|---|---|---|---|---|---|---|
| | Reverse | GCCGAAGAAACCTCATTGTCA | | | | |
| *PIAS3* | Forward<br>Reverse | CAAGGAGAAATTGACTGCTG<br>GCTTCTTCTCATTCATCTGTAG | 53.1 | 86 | Pre-designed | Merck |
| *PPARGC1A* | Forward<br>Reverse | ACAGAACTGAGGGACCGTTT<br>TGCGTCCACAAAAGTACAGC | 54.5 | 81 | Custom | Eurofins |
| *RELA* | Forward<br>Reverse | GCTTGTAGGAAAGGACTGCC<br>GGAAGGGGTTGTTGTTGGTC | 54.5 | 84 | Custom | Eurofins |
| *SLC7A11* | Forward<br>Reverse | GGTTATTCTATGTTGCGTCTC<br>AATAACAGCTGGTAGAGGAG | 51.7 | 86 | Pre-designed | Merck |
| *SOCS3* | Forward<br>Reverse | CCTATTACATCTACTCCGGG<br>ACTTTCTCATAGGAGTCCAG | 51.7 | 98 | Pre-designed | Merck |
| *SOD3* | Forward<br>Reverse | CTCCATTTGTACCGAAACAC<br>AAGATCGTCAGGTCAAAGG | 53.1 | 102 | Pre-designed | Merck |
| *STAT3* | Forward<br>Reverse | TTCTACAGACTGCAGCCACT<br>AGATCCTGCACTCTCTTCCG | 56.4 | 94 | Custom | Eurofins |
| *TNFRSF1A* | Forward<br>Reverse | AGGAAATGGGTCAGGTGGAG<br>GGTGTTCTGTTTCTCCTGGC | 56.4 | 83 | Custom | Eurofins |
| *TXNRD1* | Forward<br>Reverse | AGACAGTTAAGCATGATTGG<br>AATTGCCCATAAGCATTCTC | 51.7 | 84 | Pre-designed | Merck |
| *VEGFA* | Forward<br>Reverse | TCTACCTCCACCATGCCAAG<br>GGTCTCGATTGGATGGCAGT | 56.4 | 85 | Custom | Eurofins |

**Appendix Table 2. Murine specific qPCR primer information**. Custom designed primers were ordered from either Merck or Eurofins. Pre-designed kiqstart primers were purchased from Merck, then validated for annealing temperature (Ann. Temp.) and primer efficiency.

| Target gene | Forward or Reverse Primer | Primer sequence (5' -> 3') | Ann. Temp. (°C) | Primer Efficiency % | Pre-designed or custom | Source |
|---|---|---|---|---|---|---|
| *Apex1* | Forward | CAAAGAAAACCGAGAAGGAG | 61.0 | Not calculated | Pre-designed | Merck |
| | Reverse | GCTTCTTCCTTTACCCAATC | | | | |
| *Hif1a* | Forward | CTGATCATCTGACCAAAACTC | 58.4 | Not calculated | Pre-designed | Merck |
| | Reverse | CGTGCTGAATAATACCACTTAC | | | | |
| *Hmbs* | Forward | TCTAAGATTGGAGAGAAGAGC | 58.4 | Not calculated | Pre-designed | Merck |
| | Reverse | AAAGACAACAGCATCACAAG | | | | |
| *Rela* | Forward | TGCAGAAAGAAGACATTGAG | 61.0 | Not calculated | Pre-designed | Merck |
| | Reverse | CATCAGCTTGAGAAAAGGAG | | | | |
| *Stat3* | Forward | CGTCTGGAAAACTGGATAAC | 58.4 | Not calculated | Pre-designed | Merck |
| | Reverse | TTAAGTTTCTGAACAGCTCC | | | | |

**Appendix Table 3.** Genes included within the "HIF-1α target gene set"

| | | | | |
|---|---|---|---|---|
| *ABCB1* | *CAV1* | *FURIN* | *NARF* | *SERPINE1* |
| *ABCG2* | *CBR1* | *GAPDH* | *NCOA7* | *SLC2A1* |
| *ACAN* | *CCNG2* | *GBE1* | *NOS2* | *SLC2A2* |
| *ACE* | *CD274* | *GCK* | *NOS3* | *SLC2A3* |
| *ACE2* | *CD99* | *GPI* | *NPM1* | *SMEK2* |
| *ADAMTS1* | *CDC42* | *GPX3* | *NPPA* | *SOS1* |
| *ADM* | *CDKN1A* | *HIG2* | *NR4A1* | *SOX9* |
| *ADRA1B* | *CDKN1B* | *HIST1H2AM* | *NT5E* | *TERT* |
| *AGER* | *CDKN1C* | *HK1* | *P4HA1* | *TF* |
| *AK3* | *CITED2* | *HK2* | *PCK1* | *TFF3* |
| *ALDOA* | *COL10A1* | *HMGCL* | *PDGFB* | *TFRC* |
| *ALDOC* | *COL1A1* | *HMOX1* | *PDLIM2* | *TGFB3* |
| *ALKBH5* | *COL1A2* | *HOXA13* | *PFKFB3* | *TGM2* |
| *ANGPT1* | *COL2A1* | *HSP90B1* | *PFKFB4* | *TMEM45A* |
| *ANGPT2* | *COL3A1* | *ID2* | *PFKL* | *TP53* |
| *ANGPTL4* | *COL5A1* | *IGFBP1* | *PFKM* | *TPI1* |
| *ANK1* | *COX4I2* | *IGFBP3* | *PFKP* | *UGP2* |
| *ANKRD37* | *CP* | *INHA* | *PGAM1* | *VEGFA* |
| *ANKZF1* | *CTGF* | *INSIG2* | *PGF* | *WSB1* |
| *ANXA1* | *CXCL12* | *IRF2BP2* | *PGK1* | *WT1* |
| *AQP1* | *CXCR4* | *ITGB2* | *PKM* | *ZNF395* |
| *ARNT* | *CYP2C11* | *JARID1B* | *PKM2* | |
| *ATG9A* | *DARS* | *JMJD1A* | *PLOD2* | |
| *ATRIP* | *DDIT4* | *KDM3A* | *PLOD3* | |
| *AURKA* | *DELEC1* | *KIAA0195* | *PMAIP1* | |
| *BCKDHA* | *DSP* | *KIAA1715* | *PNRC1* | |
| *BCL2* | *EDN1* | *L1CAM* | *PPFIA4* | |
| *BCL2L1* | *EDN2* | *LDHA* | *PPP1R3C* | |
| *BCL2L2* | *EGLN1* | *LEP* | *PPP5C* | |
| *BHLHE40* | *EGLN3* | *LOC401152* | *PSMA1* | |
| *BHLHE41* | *ENG* | *LONP1* | *PSMC6* | |
| *BIK* | *ENO1* | *LRP1* | *RAB20* | |
| *BNIP3* | *ENPEP* | *MCL1* | *RAC1* | |
| *BNIP3L* | *EPO* | *MET* | *RAPGEF1* | |
| *BSG* | *ETS1* | *MIF* | *RAPGEF6* | |
| *C3ORF28* | *FAM162A* | *MT1A* | *RASSF1* | |
| *C6ORF170* | *FECH* | *MT-CO3* | *RIT1* | |
| *CA9* | *FLK1* | *MT-ND1* | *RORA* | |
| *CAD* | *FLT1* | *MTP18* | *RSBN1* | |
| *CAPG* | *FOS* | *NA* | *S100A4* | |

**Appendix Table 4.** Genes included within the "STAT3 Signalling component, STAT3 stimulatory cytokine/growth factor and their cognate receptors gene set"

| | | | | |
|---|---|---|---|---|
| *ATR* | *IFNGR1* | *IL27* | *MPL* | *SRC* |
| *CCL2* | *IFNGR2* | *IL27RA* | *NDUFA13* | *STAT3* |
| *CCL3* | *IFNLR1* | *IL3RA* | *OSM* | *TGFA* |
| *CCL5* | *IGF1* | *IL5* | *OSMR* | *TNF* |
| *CNTF* | *IL10* | *IL5RA* | *PDGFA* | *TRIM28* |
| *CNTFR* | *IL10RA* | *IL6* | *PDGFB* | *TYK2* |
| *CSF1* | *IL10RB* | *IL6R* | *PDGFRA* | |
| *CSF2* | *IL11RA* | *IL6R* | *PDGFRB* | |
| *CSF2RA* | *IL12A* | *IL6ST* | *PIAS3* | |
| *CSF3* | *IL12B* | *IL7R* | *PTPN1* | |
| *CSF3R* | *IL15RA* | *IL9* | *PTPN2* | |
| *EGF* | *IL20RA* | *IL9R* | *PTPN9* | |
| *EGFR* | *IL20RB* | *JAK1* | *PTPRC* | |
| *F2R* | *IL21* | *JAK2* | *PTPRD* | |
| *F2RL3* | *IL21R* | *JAK3* | *PTPRK* | |
| *GHR* | *IL22* | *KITLG* | *SETD7* | |
| *IFNAR1* | *IL22RA1* | *LIF* | *SIRT1* | |
| *IFNG* | *IL22RA2* | *LIFR* | *SOCS3* | |

**Appendix Table 5.** Genes included within the "STAT3 target gene set"

| | | | | |
|---|---|---|---|---|
| *ADAM15* | *CLN6* | *HSPA1A* | *NCAM2* | *SIAH2* |
| *ADAM23* | *CREB1* | *ICAM1* | *NDN* | *SIN3B* |
| *ADAM8* | *CRP* | *IFNG* | *NDRG3* | *SMAD1* |
| *AKT1* | *CRTAM* | *IFNLR1* | *NF1* | *SMAD5* |
| *ANGPT2* | *CRX* | *IFRD1* | *NFKB1* | *SMAD7* |
| *ANGPTL2* | *CSF1* | *IGF2R* | *NFKB2* | *SMAD9* |
| *ANXA2* | *CTNNA2* | *IGFBP4* | *NOS2* | *SOCS3* |
| *API5* | *CTNND2* | *IGHMBP2* | *NOTCH2* | *SOX11* |
| *ARHGEF1* | *CTSC* | *IL10* | *NOTCH4* | *SOX13* |
| *ATF1* | *DNMT1* | *IL17A* | *NPY2R* | *SOX2* |
| *ATF2* | *DNMT3A* | *IL17F* | *PAWR* | *SOX6* |
| *BAG4* | *DZIP1* | *IL1B* | *PAX1* | *SPTBN2* |
| *BATF* | *ECT2* | *IL23A* | *PAX4* | *SRFBP1* |
| *BCL2* | *EPHB2* | *IL23R* | *PAXIP1* | *STAT1* |
| *BCL2L1* | *ESR1* | *IL6* | *PCNT* | *STAT3* |
| *BCL3* | *FADD* | *IL6R* | *PDAP1* | *STMN1* |
| *BIRC5* | *FAS* | *INSM1* | *PDGFA* | *SUPT5H* |
| *BMP4* | *FGF1* | *IRF4* | *PDIK1L* | *TCF12* |
| *BMP8A* | *FGF2* | *IRF6* | *PEG10* | *TEK* |
| *BRCA1* | *FGF7* | *ITGA11* | *PEG3* | *TENM1* |
| *BRCA2* | *FGFR1* | *ITGB4* | *PIAS3* | *TENM3* |
| *CADM4* | *FGL2* | *ITGB6* | *PIK3R1* | *TGFB1* |
| *CALM3* | *FLT3* | *JAK2* | *PIM1* | *TGFB2* |
| *CAMK2D* | *FOS* | *JUN* | *PIM2* | *TGFBR3* |
| *CASP7* | *FOSL2* | *JUNB* | *POMC* | *TIMP1* |
| *CASP9* | *FOXD2* | *LCN2* | *PORCN* | *TLR6* |
| *CCL5* | *FOXO1* | *LRMP* | *POU2F1* | *TNC* |
| *CCNA1* | *FOXO3* | *LTB* | *PRKACA* | *TNF* |
| *CCNB1* | *FOXP3* | *LTBP1* | *PRKCE* | *TNFRSF1A* |
| *CCND1* | *FSCN1* | *MCL1* | *PTGS2* | *TNFRSF1B* |
| *CCND2* | *GABRA5* | *MCM2* | *PTK2* | *TNFSF11* |
| *CCND3* | *GATA4* | *MCM6* | *RAG1* | *TNXB* |
| *CD22* | *GATA6* | *MCM7* | *RAMP3* | *TP53* |
| *CDC25A* | *GBP1* | *MDM2* | *RASA3* | *TSG101* |
| *CDH1* | *GIGYF1* | *MMP2* | *RB1* | *TWIST1* |
| *CDH10* | *GRB10* | *MMP3* | *RBFOX2* | *TXK* |
| *CDH2* | *GTF2H2* | *MMP9* | *RHOU* | *USP9X* |
| *CDH22* | *GTF2H4* | *MOBP* | *RORA* | *VAV2* |
| *CDK1* | *HDAC4* | *MUC1* | *RORC* | *VEGFA* |
| *CDKN1A* | *HGF* | *MYC* | *ROS1* | *VIM* |
| *CDON* | *HIF1A* | *MYO5A* | *S1PR1* | *XBP1* |
| *CEBPA* | *HSP90AA1* | *NANOG* | *SAA1* | *ZEB1* |
| *CEBPG* | *HSP90AB1* | *NAV1* | *SEMA3G* | |

***Appendix Table 6.*** Genes included within the "Nrf2 target gene set"

| | | | | |
|---|---|---|---|---|
| *ABCB6* | *ESD* | *GSTM2* | *NRF1* | *SOD3* |
| *ABCC1* | *FECH* | *GSTM3* | *OSGIN1* | *SQSTM1* |
| *ABCC2* | *FTH1* | *GSTP1* | *PARK7* | *SRXN1* |
| *ABCG2* | *FTL* | *GSTT1* | *PGD* | *TALDO1* |
| *ADH4* | *G6PD* | *HK2* | *PIR* | *TKT* |
| *AKR1A1* | *GCLC* | *HMOX1* | *PRDX1* | *TXN* |
| *AKR1B10* | *GCLM* | *HTATIP2* | *PRDX6* | *TXNIP* |
| *AKR1C1* | *GPX2* | *IDH1* | *PTPMT1* | *TXNRD1* |
| *AKR1C3* | *GPX3* | *ME1* | *PTPRB* | |
| *ALDH3A1* | *GPX8* | *MGST1* | *SLC40A1* | |
| *BCL2* | *GSR* | *MT1A* | *SLC7A11* | |
| *BLVRA* | *GSTA1* | *MT1G* | *SLPI* | |
| *BLVRB* | *GSTA2* | *MT2A* | *SOD1* | |
| *EPHX1* | *GSTM1* | *NQO1* | *SOD2* | |

**Appendix Table 7.** Genes included within the “Endogenous Antioxidant gene set”

| | | | | |
|---|---|---|---|---|
| *CAT* | *GSS* | *GSTZ1* | *PRDX1* | *TXN2* |
| *GCLC* | *GSTA1* | *MGST1* | *PRDX2* | *TXNDC11* |
| *GCLM* | *GSTA2* | *MGST2* | *PRDX3* | *TXNDC12* |
| *GDA* | *GSTA4* | *MGST3* | *PRDX4* | *TXNDC15* |
| *GLRX* | *GSTK1* | *MT1A* | *PRDX5* | *TXNDC16* |
| *GLRX2* | *GSTM1* | *MT1E* | *PRDX6* | *TXNDC17* |
| *GLRX3* | *GSTM2* | *MT1F* | *SOD1* | *TXNDC5* |
| *GLRX5* | *GSTM3* | *MT1G* | *SOD2* | *TXNDC9* |
| *GPX1* | *GSTM4* | *MT1H* | *SOD3* | *TXNIP* |
| *GPX2* | *GSTM5* | *MT1L* | *SRXN1* | *TXNRD1* |
| *GPX3* | *GSTO1* | *MT1M* | *TMX1* | *TXNRD2* |
| *GPX4* | *GSTO2* | *MT1X* | *TMX2* | *TXNRD3* |
| *GPX7* | *GSTP1* | *MT3* | *TMX3* | |
| *GPX8* | *GSTT1* | *NME9* | *TMX4* | |
| *GSR* | *GSTT2* | *PDIA6* | *TXN* | |